

INFORMATION TO USERS

This manuscript has been reproduced from the microfilm master. UMI films the text directly from the original or copy submitted. Thus, some thesis and dissertation copies are in typewriter face, while others may be from any type of computer printer.

The quality of this reproduction is dependent upon the quality of the copy submitted. Broken or indistinct print, colored or poor quality illustrations and photographs, print bleedthrough, substandard margins, and improper alignment can adversely affect reproduction.

In the unlikely event that the author did not send UMI a complete manuscript and there are missing pages, these will be noted. Also, if unauthorized copyright material had to be removed, a note will indicate the deletion.

Oversize materials (e.g., maps, drawings, charts) are reproduced by sectioning the original, beginning at the upper left-hand corner and continuing from left to right in equal sections with small overlaps. Each original is also photographed in one exposure and is included in reduced form at the back of the book.

Photographs included in the original manuscript have been reproduced xerographically in this copy. Higher quality 6" x 9" black and white photographic prints are available for any photographs or illustrations appearing in this copy for an additional charge. Contact UMI directly to order.

UMI

**A Bell & Howell Information Company
300 North Zeeb Road, Ann Arbor MI 48106-1346 USA
313/761-4700 800/521-0600**

University of Alberta

**Asphaltene Solubility and
Asphaltene Stabilized Water-in-Oil Emulsions**

by

Harvey William Yarranton



A thesis submitted to the Faculty of Graduate Studies and Research in partial fulfillment
of the requirements for the degree of Doctor of Philosophy.

Department of Chemical and Materials Engineering

Edmonton, Alberta

Fall, 1997



**National Library
of Canada**

**Acquisitions and
Bibliographic Services**

**395 Wellington Street
Ottawa ON K1A 0N4
Canada**

**Bibliothèque nationale
du Canada**

**Acquisitions et
services bibliographiques**

**395, rue Wellington
Ottawa ON K1A 0N4
Canada**

Your file *Votre référence*

Our file *Notre référence*

The author has granted a non-exclusive licence allowing the National Library of Canada to reproduce, loan, distribute or sell copies of this thesis in microform, paper or electronic formats.

The author retains ownership of the copyright in this thesis. Neither the thesis nor substantial extracts from it may be printed or otherwise reproduced without the author's permission.

L'auteur a accordé une licence non exclusive permettant à la Bibliothèque nationale du Canada de reproduire, prêter, distribuer ou vendre des copies de cette thèse sous la forme de microfiche/film, de reproduction sur papier ou sur format électronique.

L'auteur conserve la propriété du droit d'auteur qui protège cette thèse. Ni la thèse ni des extraits substantiels de celle-ci ne doivent être imprimés ou autrement reproduits sans son autorisation.

0-612-23096-1

University of Alberta

Library Release Form

Name of Author: Harvey William Yarranton


Title of Thesis: Asphaltene Solubility and Asphaltene Stabilized
Water-in-Oil Emulsions

Degree: Doctor of Philosophy

Year this Degree Granted: 1997

Permission is hereby granted to the University of Alberta Library to reproduce single copies of this thesis and to lend or sell such copies for private, scholarly, or scientific research purposes only.

The author reserves all other publication and other rights in association with copyright in the thesis, and except as hereinbefore provided, neither the thesis nor any substantial portion thereof may be printed or otherwise reproduced in any material form whatever without the author's prior written permission.



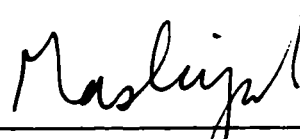
3723 Benton Dr. NW
Calgary, Alberta, T2L 1W7

August 1, 1997

University of Alberta

Faculty of Graduate Studies and Research

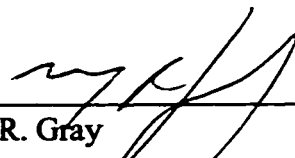
The undersigned certify that they have read, and recommend to the Faculty of Graduate Studies and research for acceptance, a thesis entitled *Asphaltene Solubility and Asphaltene Stabilized Water-in-Oil Emulsions* by Harvey William Yarranton in partial fulfillment of the requirements for the degree of Doctor of Philosophy.



Dr. J. H. Masliyah (supervisor)



Dr. F.F. Cantwell



Dr. M.R. Gray



Dr. A.E. Mather



Dr. T.G.M. van de Ven



Dr. S.E. Wanke

Date: August 25/97

Abstract

The oil industry is now developing small conventional reservoirs as well as heavy oil and oil sand reservoirs. Production problems such as the precipitation of asphaltenes and the formation of water-in-oil emulsions can be significant for such resources. Since asphaltenes are commonly identified as an emulsion stabilizer, their phase behavior and the means by which they stabilize emulsions are of great interest. To date, only partial success has been achieved in predicting asphaltene solubility. Furthermore, asphaltene stabilized emulsions are so little investigated that even the phase(s) of the asphaltenes that stabilizes water-in-oil emulsions is unknown.

In this thesis, asphaltene phase behavior and asphaltene stabilized emulsions are studied at low asphaltene concentrations. The concentrations are chosen so that the asphaltenes do not form micelles or colloids but exist as free molecules or precipitated solid particles. Asphaltene phase behavior is examined in toluene and hexane solvent mixtures. A thermodynamic model is developed to predict asphaltene solubility at low concentrations. Correlations are developed for the asphaltene molar volumes and solubility parameters required to employ the model. The thermodynamic model successfully fits the experimental data for the toluene/hexane solvent system and predicts asphaltene solubility in a variety of organic solvents. The thermodynamic model is a useful starting point for the development of a model to predict asphaltene solubility in crude oils at production conditions.

The asphaltene phase responsible for stabilizing water-in-toluene/hexane emulsions is determined by comparing the surface areas stabilized by different asphaltene subfractions. The asphaltene subfractions each have a different molar mass and form a different two phase mixture in a given toluene to hexane ratio. The comparisons indicate that asphaltenes stabilize emulsions as a molecular surfactant. The asphaltene stabilized emulsions are resistant to coalescence but do destabilize through a modified form of Ostwald ripening. The accelerating shrinkage of emulsion droplets that occurs with typical ripening is retarded perhaps because the asphaltenes adsorbed on the interface form a membrane. The membrane may become impermeable when the droplets shrink. Further investigation of the asphaltene membrane is recommended because it may affect the outcome of many emulsion treatments.

Acknowledgments

I first wish to thank Dr. J.H. Masliyah for his support and assistance throughout my doctoral program. Much of the work in this thesis has benefited from discussions with Dr. Masliyah and also with Drs. M.R. Gray, A.E. Mather, K. Nandakumar and S.E. Wanke. My colleagues in Rm.226 have also been a great help, in particular, Drs. Suddhasatwa Basu, Bill Eckert, Sean Sanders, Vilas Rewatkar and Nianxi Yan, and Mr. Artin Afacan. Cindy Heisler has often smoothed the troubled administrative waters and Bob Barton is indispensable to those of us who use computers.

Many others have contributed to this thesis. I would like to thank Darlene Mahlow for her help in analytical chemistry, Dr. Yadollah Maham for his assistance with physical property measurements and John Czuroski for his expertise in the dark room. The work of two summer students, Kristina Mannistu and Hisham Hussein was invaluable. I am also grateful to Syncrude Canada Ltd. and NSERC for their financial support. Apart from providing financial support, Jan Czarnecki, Bill Shelfantook and Bob Tipman of Syncrude were always glad to assist. Finally, I wish to thank my wife, Maureen Hurly, for her patience and support.

Table of Contents

| | | |
|------------------|--|-----------|
| Chapter 1 | Introduction to Asphaltene Solubility and Asphaltene Stabilized Emulsions | 1 |
| 1.1 | Introduction | 1 |
| 1.1.1 | Objectives | 3 |
| 1.1.2 | Thesis Outline | 4 |
| 1.2 | Basic Principles of Emulsions | 5 |
| 1.2.1 | Interfacial Properties | 6 |
| 1.2.2 | Forces Acting on Emulsion Droplets | 8 |
| 1.2.3 | Stability of Emulsions | 11 |
| 1.2.4 | Stability of Water-in-Oil Emulsions | 14 |
| 1.2.5 | Water-in-Oil Emulsion in Oil Sands Extraction | 15 |
| 1.3 | Asphaltene Chemistry | 17 |
| 1.3.1 | Classification of Petroleum Fractions | 17 |
| 1.3.2 | Characteristics of Bitumens | 20 |
| 1.3.3 | Asphaltene Composition, Structure and Molar Mass | 22 |
| 1.3.4 | Asphaltene Association | 28 |
| 1.3.5 | Asphaltene Solubility Models | 31 |
| 1.3.6 | Relevance of Asphaltene Chemistry to Emulsions | 38 |
| 1.4 | References | 38 |
| Chapter 2 | Molar Mass Distribution and Solubility Modeling of Asphaltenes | 64 |
| 2.1 | Introduction | 64 |
| 2.2 | Experimental Method | 66 |
| 2.2.1 | Terminology | 66 |
| 2.2.2 | Materials | 66 |
| 2.2.3 | Density Measurements | 67 |
| 2.2.4 | Interfacial Tension Measurements | 68 |

| | | |
|------------------|---|------------|
| 2.2.5 | Vapor Pressure Osmometry Measurements | 68 |
| 2.3 | Theory | 68 |
| 2.3.1 | Molar Mass from Interfacial Tension Measurements | 68 |
| 2.3.2 | Solubility | 69 |
| 2.4 | Results and Discussion | 71 |
| 2.4.1 | Solubility Data | 72 |
| 2.4.2 | Density | 73 |
| 2.4.3 | Interfacial Tension and Molar Mass | 76 |
| 2.4.4 | Molar Volume and Solubility Parameter Correlations | 80 |
| 2.4.5 | Solubility Model | 81 |
| 2.5 | Conclusions | 83 |
| 2.6 | References | 83 |
| Chapter 3 | Solubility Modeling of Asphaltenes in Organic Solvents | 98 |
| 3.1 | Introduction | 98 |
| 3.2 | Experimental Method | 99 |
| 3.3 | Theory | 100 |
| 3.4 | Results and Discussion | 103 |
| 3.4.1 | n-Alkane Homologous Series | 105 |
| 3.4.2 | Branched Alkanes | 106 |
| 3.4.3 | Aromatics | 107 |
| 3.4.4 | Cyclic Compounds | 107 |
| 3.4.5 | Dichloromethane and 1-Hexene | 108 |
| 3.4.6 | Polar Solvents | 108 |
| 3.5 | Conclusions | 109 |
| 3.6 | References | 110 |
| Chapter 4 | The Stabilization of Water-in-Oil Emulsions by Asphaltenes | 127 |
| 4.1 | Introduction | 127 |
| 4.2 | Experimental Method | 129 |

| | | |
|------------------|--|-----|
| 4.2.1 | Materials | 129 |
| 4.2.2 | Preparation of Emulsions | 130 |
| 4.3 | Theory | 130 |
| 4.4 | Results and Discussion | 133 |
| 4.4.1 | Experimental Design | 134 |
| 4.4.2 | Role of Solid Asphaltenes | 137 |
| 4.4.3 | Asphaltenes as a Molecular Surfactant | 139 |
| 4.4.4 | The Effect of the Hexane:Toluene Ratio | 143 |
| 4.5 | Conclusions | 147 |
| 4.6 | References | 148 |
| Chapter 5 | Ostwald Ripening of Asphaltene Stabilized Water-in-Toluene/Hexane Emulsions | 168 |
| 5.1 | Introduction | 168 |
| 5.2 | Experimental Method | 169 |
| 5.3 | Results and Discussion | 170 |
| 5.3.1 | Coalescence and Ostwald Ripening Theory | 171 |
| 5.3.2 | The Stability of Water-in-Hydrocarbon Emulsions | 176 |
| 5.3.3 | The Effect of Composition on Emulsion Stability | 178 |
| 5.3.4 | Modified Ostwald Ripening Models | 181 |
| 5.4 | Conclusions | 185 |
| 5.5 | References | 185 |
| Chapter 6 | Numerical Simulation of Ostwald Ripening in Emulsions | 197 |
| 6.1 | Introduction | 197 |
| 6.2 | Theory | 199 |
| 6.3 | Numerical Method | 202 |
| 6.3.1 | Ripening Equations | 202 |
| 6.3.2 | Critical Radius | 203 |
| 6.3.3 | Frequency Distribution | 205 |

| | |
|---|------------|
| 6.3.4 Numerical Procedure | 207 |
| 6.4 Results and Discussion | 209 |
| 6.4.1 Infinitely Dilute Case | 209 |
| 6.4.2 Infinitely Concentrated Case | 210 |
| 6.4.3 General Case | 211 |
| 6.4.4 Growth Rate Expression | 212 |
| 6.4.5 Approximate Method for Predicting Growth Rate | 214 |
| 6.5 Conclusions | 215 |
| 6.6 References | 216 |
| Chapter 7 Conclusions and Recommendations | 234 |
| 7.1 Asphaltene Solubility | 234 |
| 7.2 Asphaltenes on Water/Hydrocarbon Interfaces | 236 |
| 7.3 Stability of Water-in-Toluene/Hexane/Asphaltene Emulsions | 237 |
| 7.4 Implications for Treating the Oil Sands Emulsion | 238 |
| 7.4.1 Mechanical Treatments | 239 |
| 7.4.2 Chemical Treatments | 240 |
| 7.4.3 Recommended Treatments | 240 |
| 7.5 References | 241 |
| Appendix A Measurement of Asphaltene Physical Properties | 242 |
| A.1 Density | 242 |
| A.2 Interfacial Tension | 243 |
| A.3 Vapor Pressure Osmometry | 246 |
| A.4 Asphaltene Storage and Oxidation | 249 |
| A.5 UV Measurements of Asphaltene Concentration | 250 |
| A.6 References | 252 |

| | |
|---|-----|
| Appendix B Asphaltene Molar Mass Distribution and Solubility - Additional Material | 285 |
| B.1 Number Average Molar Mass | 285 |
| B.2 Solubility | 286 |
| B.3 Derivations | 288 |
| B.4 Computer Programs | 295 |
| B.5 References | 295 |
| | |
| Appendix C Asphaltene Molar Mass Distribution and Solubility - Additional Material | 313 |
| C.1 Drop Size Distributions | 313 |
| C.2 Ostwald Ripening Through an Interfacial Membrane | 314 |
| C.3 Computer Programs | 316 |
| C.4 References | 317 |

List of Tables

| | | |
|-------------------|--|-----|
| Table 1.1 | Order of magnitude of interaction forces between droplets. | 11 |
| Table 1.2 | UNITAR definition of heavy oils and bitumens. | 18 |
| Table 1.3 | Atomic H/C ratios for fuels. | 18 |
| Table 1.4 | Boiling ranges and uses of petroleum cuts. | 19 |
| Table 1.5 | Composition of petroleum, heavy oil/bitumen and residuum. | 19 |
| Table 1.6 | Properties of Alberta bitumens. | 20 |
| Table 1.7 | Elemental composition of various asphaltenes. | 22 |
| Table 1.8 | Elemental composition of Athabasca asphaltenes. | 23 |
| Table 1.9 | Ion resin fractionation of "Arabian" crude oil asphaltenes. | 26 |
| Table 1.10 | Production by pyrolysis of aromatics, non-aromatics and carbon residue from various Athabasca asphaltene fractions. | 26 |
| Table 1.11 | Asphaltene molar masses determined with various methods. | 27 |
| Table 1.12 | Measured range of asphaltene molar mass. | 28 |
| Table 2.1 | Molar masses calculated from interfacial tension data. | 78 |
| Table 3.1 | Physical properties of solvents. | 104 |
| Table 4.1 | A comparison of f_{sol}^c to f_{sol}^* at various hexane to toluene ratios. | 138 |
| Table 4.2 | Fitted estimates of f_a and C_a^{eq} at various hexane:toluene ratios. | 142 |
| Table 4.3 | The fraction of asphaltene-solids that stabilize water-in-toluene/hexane emulsions as a function of toluene content. | 147 |
| Table 5.1 | Fitted d_{10} and d_{32} for asphaltene stabilized water-in-toluene/hexane emulsions. | 179 |
| Table 5.2 | Interfacial tension, diffusivity and solubility of water in toluene and hexane. | 180 |
| Table 6.1 | Simulation input parameters | 208 |
| Table 6.2 | Growth rates of cobalt grains in liquid copper | 215 |

List of Plates and Figures

| | | |
|--------------------|---|------------|
| Plate 4.1 | Asphaltene stabilized water-in-toluene/hexane emulsions. | 150 |
| Figure 1.1 | Schematic of typical bitumen extraction plant. | 43 |
| Figure 1.2 | Some surfactant structures. | 44 |
| Figure 1.3 | Electrostatic and steric stabilization of emulsions. | 45 |
| Figure 1.4 | Potential energy curves between two droplets for (a) electrostatic and dispersion forces and (b) steric and dispersion forces. | 46 |
| Figure 1.5 | Simplified representation of separation of petroleum into six fractions. | 47 |
| Figure 1.6 | Examples of hydrocarbon groups in petroleum. | 48 |
| Figure 1.7 | Examples of sulfur and oxygen groups in petroleum. | 49 |
| Figure 1.8 | Examples of nitrogen and metal groups in petroleum. | 50 |
| Figure 1.9 | Example of condensed polynuclear model of an asphaltene molecule. | 51 |
| Figure 1.10 | Hypothetical representation of an average Athabasca asphaltene molecule. | 52 |
| Figure 1.11 | Molar mass of subfractions precipitated from Cold Lake bitumen. | 53 |
| Figure 1.12 | Atomic H/C ratio of subfractions precipitated from Cold Lake bitumen. | 54 |
| Figure 1.13 | Heteroatom content of subfractions precipitated from Cold Lake bitumen. | 55 |
| Figure 1.14 | Metal content of subfractions precipitated from Cold Lake bitumen. | 56 |
| Figure 1.15 | Interfacial tension of Cerro Negro asphaltene over water as a function of pH. | 57 |
| Figure 1.16 | Effect of solvent on asphaltene molar mass measured by vpo. | 58 |
| Figure 1.17 | Effect of asphaltene concentration on molar mass measured by vpo. | 59 |

| | | |
|--------------------|---|-----|
| Figure 1.18 | Pfeiffer-Saal model of an asphaltene-resin complex. | 60 |
| Figure 1.19 | Dickie-Yen model of an asphaltene colloid. | 61 |
| Figure 1.20 | Surface tension of solutions of asphaltene in pyridine over water. | 62 |
| Figure 1.21 | Solubility of asphaltenes precipitated by or redissolved in solutions of toluene and hexane. | 63 |
| Figure 2.1 | Mass fraction of solids in asphaltene-solids subfractions. | 86 |
| Figure 2.2 | The effect of asphaltene concentration on the solubility of asphaltene-solids in solutions of toluene and hexane. | 87 |
| Figure 2.3 | Theoretical solubility of a pure solute as a function of solute concentration. | 88 |
| Figure 2.4 | Dependence of asphaltene-toluene mixture specific volume on asphaltene concentration. | 89 |
| Figure 2.5 | Average density of asphaltene subfractions. | 90 |
| Figure 2.6 | Interfacial tension of asphaltene-solids in a toluene-hexane solution of 25 vol% toluene over water. | 91 |
| Figure 2.7 | Interfacial tension of solutions of asphaltene-solids in toluene over water. | 92 |
| Figure 2.8 | Molar mass of asphaltene subfractions determined by vapor pressure osmometry. | 93 |
| Figure 2.9 | Molar mass of asphaltene subfractions. | 94 |
| Figure 2.10 | PDMS molar mass frequency distribution of Athabasca bitumen. | 95 |
| Figure 2.11 | Enthalpy of vaporization of homologous series. | 96 |
| Figure 2.12 | Predicted and experimental solubility of asphaltenes in solutions of toluene and hexane. | 97 |
| Figure 3.1 | Solubility of asphaltenes in solutions of toluene and n-pentane. | 111 |
| Figure 3.2 | Solubility of asphaltenes in solutions of toluene and n-hexane. | 112 |
| Figure 3.3 | Solubility of asphaltenes in solutions of toluene and n-heptane. | 113 |
| Figure 3.4 | Solubility of asphaltenes in solutions of toluene and n-octane. | 114 |
| Figure 3.5 | Solubility of asphaltenes in solutions of toluene and n-decane. | 115 |
| Figure 3.6 | Solubility of asphaltenes in solutions of toluene and n-alkanes. | 116 |
| Figure 3.7 | Solubility of asphaltenes in solutions of toluene and isopentane. | 117 |

| | | |
|--------------------|--|-----|
| Figure 3.8 | Solubility of asphaltenes in solutions of toluene and isooctane. | 118 |
| Figure 3.9 | Solubility of asphaltenes in solutions of nitrobenzene and hexane. | 121 |
| Figure 3.10 | Solubility of asphaltenes in solutions of t-butylbenzene and hexane. | 122 |
| Figure 3.11 | Solubility of asphaltenes in solutions of decalin and hexane. | 123 |
| Figure 3.12 | Solubility of asphaltenes in solutions of cyclohexane and hexane. | 124 |
| Figure 3.13 | Solubility of asphaltenes in solutions of dichloromethane and hexane. | 125 |
| Figure 3.14 | Solubility of asphaltenes in solutions of toluene and 1-hexene. | 126 |
| Figure 3.15 | Solubility of asphaltenes in solutions of toluene and acetone. | 127 |
| Figure 3.16 | Solubility of asphaltenes in solutions of toluene and methanol. | 128 |
| Figure 4.1 | The fractionation of the asphaltene molar mass distribution by solubility. | 151 |
| Figure 4.2 | Drop size distribution of an asphaltene stabilized water-in-toluene/hexane emulsion measured 1.5 hr. after blending. | 152 |
| Figure 4.3 | Growth with time of the Sauter mean diameter of an asphaltene stabilized water-in-toluene/hexane emulsion. | 153 |
| Figure 4.4 | Change in the Sauter mean diameter of asphaltene stabilized water-in-toluene/hexane emulsions when the highest molar mass asphaltenes are removed before emulsification. ($\phi_H/\phi_T = 5$ and $\phi_W = 0.25$) | 154 |
| Figure 4.5 | Change in the Sauter mean diameter of asphaltene stabilized water-in-toluene/hexane emulsions when the highest molar mass asphaltenes are removed before emulsification. ($\phi_H/\phi_T = 3$ and $\phi_W = 0.25$, $C_A^0 = 1.00 \text{ kg/m}^3$) | 155 |
| Figure 4.6 | Change in the Sauter mean diameter of asphaltene stabilized water-in-toluene/hexane emulsions when the highest molar mass asphaltenes are removed before emulsification. ($\phi_H/\phi_T = 1.5$ and $\phi_W = 0.25$, $C_A^0 = 1.00 \text{ kg/m}^3$) | 156 |
| Figure 4.7 | Equilibrium relations between asphaltenes in an emulsion. | 157 |
| Figure 4.8 | Effect of water volume fraction and asphaltene concentration on the Sauter mean diameter of asphaltene stabilized water-in-toluene/hexane emulsions. ($\phi_H/\phi_T = 5$ and $f_{sol}^* = 0.63$) | 158 |

| | | |
|--------------------|--|-----|
| Figure 4.9 | Effect of f^*_{sol} on the Sauter mean diameter of asphaltene stabilized water-in-toluene/hexane emulsions. ($\phi_H/\phi_T = 5$ and $\phi_W = 0.25$) | 159 |
| Figure 4.10 | Predicted and experimental Sauter mean diameters of asphaltene stabilized water-in-toluene/hexane emulsions with a 5:1 volume ratio of hexane:toluene. | 160 |
| Figure 4.11 | Inverse Sauter mean diameter versus the concentration of soluble asphaltenes in asphaltene stabilized water-in-toluene/hexane emulsions with a 5:1 volume ratio of hexane:toluene. | 161 |
| Figure 4.12 | Inverse Sauter mean diameter versus the concentration of soluble asphaltenes in asphaltene stabilized water-in-toluene/hexane emulsions with a 3:1 volume ratio of hexane:toluene. | 162 |
| Figure 4.13 | Inverse Sauter mean diameter versus the concentration of soluble asphaltenes in asphaltene stabilized water-in-toluene/hexane emulsions with a 3:2 volume ratio of hexane:toluene. | 163 |
| Figure 4.14 | Inverse Sauter mean diameter versus the concentration of soluble asphaltenes in asphaltene stabilized water-in-toluene/hexane emulsions with a 1:1 volume ratio of hexane:toluene. | 164 |
| Figure 4.15 | Inverse Sauter mean diameter versus the concentration of soluble asphaltenes in asphaltene stabilized water-in-toluene/hexane emulsions with a 1:4 volume ratio of hexane:toluene. | 165 |
| Figure 4.16 | The effect of solvent composition on the mass ratio of surface active to soluble asphaltenes. | 166 |
| Figure 4.17 | The effect of the solvent on a hypothetical distribution of asphaltene adsorption coefficients. | 167 |
| Figure 5.1 | Effect of emulsion height on the measured Sauter mean diameter of an asphaltene stabilized water-in-toluene/hexane emulsion. ($\phi_H/\phi_T = 5$, $\phi_W = 0.40$, $C_A^o = 1.00 \text{ kg/m}^3$) | 187 |
| Figure 5.2 | The change over time of the self-preserving drop size distributions of an emulsion destabilizing through: a) coalescence, b) Ostwald ripening. | 188 |
| Figure 5.3 | Evolution of the drop size distribution for Ostwald ripening in emulsions with a two component dispersed phase. | 189 |

| | | |
|--------------------|--|-----|
| Figure 5.4 | Change in drop size distribution over time of an asphaltene stabilized water-in-toluene/hexane emulsion. ($\phi_H/\phi_T = 5$, $\phi_W = 0.25$, $C_A^o = 0.50 \text{ kg/m}^3$) | 190 |
| Figure 5.5 | Change in average drop diameters over time of an asphaltene stabilized water-in-toluene/hexane emulsion. ($\phi_H/\phi_T = 5$, $\phi_W = 0.25$, $C_A^o = 0.50 \text{ kg/m}^3$) | 191 |
| Figure 5.6 | Change in drop size distribution over time of an asphaltene stabilized water-in-toluene/hexane emulsion. ($\phi_H/\phi_T = 5$, $\phi_W = 0.25$, $C_A^o = 2.00 \text{ kg/m}^3$) | 192 |
| Figure 5.7 | Change in drop size distribution over time of an asphaltene stabilized water-in-toluene/hexane emulsion. ($\phi_H/\phi_T = 0$, $\phi_W = 0.40$, $C_A^o = 1.33 \text{ kg/m}^3$) | 193 |
| Figure 5.8 | Growth rate of the Sauter mean diameter of asphaltene stabilized water-in-toluene/hexane emulsions versus the toluene content of the continuous phase. ($\phi_W = 0.25$, $C_A^o = 1.00 \text{ kg/m}^3$) | 194 |
| Figure 5.9 | Change in drop size distribution over time of two asphaltene stabilized water-in-toluene/hexane emulsions: a) deionized water, b) deionized ultrafiltered water. ($\phi_H/\phi_T = 5$, $\phi_W = 0.40$, $C_A^o = 1.00 \text{ kg/m}^3$) | 195 |
| Figure 5.10 | Change in drop diameter over time of two asphaltene stabilized water-in-toluene/hexane emulsions: a) deionized water, b) deionized ultrafiltered water. ($\phi_H/\phi_T = 5$, $\phi_W = 0.40$, $C_A^o = 1.00 \text{ kg/m}^3$) | 196 |
| Figure 6.1 | Cell model of a dispersion. | 218 |
| Figure 6.2 | Discretization of number frequency interval. | 219 |
| Figure 6.3 | Number frequency distribution of drop radii for an infinitely dilute system. | 220 |
| Figure 6.4 | Cumulative number frequency distribution of drop radii for an infinitely dilute system. | 221 |
| Figure 6.5 | Cube of the mean radius versus τ for an infinitely dilute system. | 222 |
| Figure 6.6 | Number frequency distribution of drop radii for an infinitely concentrated system. | 223 |
| Figure 6.7 | Cumulative number frequency distribution of drop radii for an infinitely concentrated system. | 224 |

| | | |
|--------------------|---|-----|
| Figure 6.8 | Numerical and MR predictions of the cumulative number frequency of drop radii for an infinitely concentrated system. | 225 |
| Figure 6.9 | Square of the critical radius versus τ' for an infinitely concentrated system. | 226 |
| Figure 6.10 | Computed material balance error as a function of the critical radius. | 227 |
| Figure 6.11 | Comparison of numerically predicted and experimental cumulative frequency distributions. | 228 |
| Figure 6.12 | Growth rate for a system with a dispersed phase volume fraction of 0.50. | 229 |
| Figure 6.13 | System with a dispersed phase volume fraction of 0.5. a) half-separation distance versus critical radius, b) mean radius versus critical radius | 230 |
| Figure 6.14 | Growth rate, β' , for all dispersed phase volume fractions. | 231 |
| Figure 6.15 | Curve fits for: a) the growth rate, β ; b) the proportionality constant, b ; c) the proportionality constant, c . | 232 |
| Figure 6.16 | Growth rate correction factor for dispersed phase volume fractions less than 0.80. | 233 |

Nomenclature

| | |
|------------------|---|
| a | drop radius (m) |
| a_c | critical radius (m) |
| a_{10} | mean radius (m) |
| a_{21} | ratio of mean square radius to mean radius (m) |
| a_L | radius of largest drop (m) |
| a_p, b_p | linear fit parameters for density to molar mass correlation |
| \hat{a}_i | activity of component i |
| A, B | linear fit parameters for enthalpy of vaporization molar mass correlation |
| A_d, A_p, A_h | dispersion, polar and H-bonding component of linear fit parameter A |
| A_{dm}, B_{dm} | density meter calibration coefficients |
| A_H | Hamaker constant (J) |
| A_i | molar surface area (m ² /mol) |
| A_{uv} | ultraviolet absorbance |
| A_W | surface area on an emulsion (m ²) |
| b | ratio of half separation distance to critical radius |
| c | ratio of mean radius to critical radius |
| C | concentration (kg/m ³) |
| C_a^{eq} | concentration of surface active asphaltenes at equilibrium (kg/m ³) |
| C_A^o | concentration of asphaltenes in the continuous phase before emulsification |
| C_{ppt} | solubility limit (kg/m ³) |
| d | diameter (m) |
| d_{10} | mean diameter (m) |
| d_{30} | mean cubic diameter (m) |
| d_{32} | Sauter mean diameter (m) |
| D | diffusivity (m ² /s) |
| err | material balance error over a single time step |
| \hat{f} | cumulative number frequency |

| | |
|--------------------------|---|
| f_a | mass ratio of surface active to soluble asphaltenes |
| f_i | cumulative mass frequency up to the i^{th} asphaltene component |
| f_I^{max} | maximum mass ratio of interfacial to total asphaltene-solids |
| f_{insol} | mass ratio of insoluble asphaltene subfraction to total asphaltene fraction |
| f_{sol} | mass ratio of soluble asphaltene subfraction to total asphaltene fraction |
| f_I^* | mass ratio of asphaltenes adsorbed on the interface to total asphaltene-solids |
| f_{insol}^* | mass ratio of insoluble asphaltene-solids subfraction to total asphaltene-solids mixture |
| f_{sol}^* | mass ratio of soluble asphaltene-solids subfraction to total asphaltene-solids mixture |
| f_S^* | mass fraction of solids in asphaltene-solids mixture |
| f'_{insol} | mass ratio of insoluble to total asphaltenes at pretreatment conditions |
| f'_{sol} | mass ratio of soluble to total asphaltenes at pretreatment conditions |
| f^c_{sol} | critical mass ratio of soluble to total asphaltenes at pretreatment conditions |
| $f^{\circ L}$ | standard state fugacity in the liquid phase |
| $f^{\circ S}$ | standard state fugacity in the solid phase |
| \hat{F} | number frequency |
| g | gravitational acceleration (m/s^2) |
| $g(\alpha, \delta)$ | volume averaging function |
| \bar{G} | partial molar free energy of mixing (J/mol) |
| ΔG_{coal} | free energy barrier to coalescence (J) |
| h | separation distance between droplets (m) |
| $h(\alpha, \delta)$ | bridging function |
| H | molar enthalpy (J/mol) |
| \bar{H} | partial molar enthalpy of mixing (J/mol) |
| I | intercept |
| k | Boltzmann constant (J/K) |
| k_o | Ostwald ripening rate constant, defined as $D\phi_{\infty}\alpha$ (m^3/s) |
| k_{Ai} | interaction parameter between asphaltene molecule and solvent |
| k_B | collision rate constant (m^3/s) |

| | |
|------------------|---|
| k_c | threshold adsorption coefficient (m^3/kg) |
| k_i | adsorption coefficient of the i^{th} asphaltene component (m^3/kg) |
| K_i | equilibrium ratio of component i |
| K_{uv} | ultraviolet adsorption coefficient (m^3/kg) |
| K_{vpo} | vapor pressure osmometry calibration constant |
| m | mass (g) |
| M | molar mass (g/mol) |
| \bar{M} | number average molar mass (g/mol) |
| \bar{M}_m | mass average molar mass (g/mol) |
| n | moles (mol) |
| N | total number of drops |
| p_r | circumference of DeNouy ring tensiometer platinum ring (cm) |
| P | pressure (Pa) |
| r | mass transfer boundary radius |
| R | universal gas constant (J/mol K) |
| R_{dm} | density meter reading |
| ΔR_{vpo} | resistance in vapor pressure osmometer |
| S | slope |
| \bar{S} | partial molar entropy of mixing (J/mol K) |
| t | time (s) |
| t_A | thickness of an asphaltene molecule (nm) |
| T | temperature (K) |
| u | ratio of radius to critical radius |
| \bar{u} | velocity (m/s) |
| U | molar internal energy (J/mol) |
| \bar{U} | partial molar internal energy of mixing (J/mol) |
| \hat{U} | internal energy (J) |
| v | ratio of radius to mean radius |
| v_d | molar volume of dispersed phase (m^3/mol) |

| | |
|---------------------|---|
| v_i | molar volume of component i (m^3/mol) |
| V | volume (m^3) |
| V_{10} | mean volume (m^3) |
| \bar{V} | partial molar volume of mixing (m^3/mol) |
| x | mass fraction |
| \hat{x} | mole fraction |
| z | slope of the cumulative number frequency distribution of drop radii |
| \hat{z} | mole fraction of feed |
| α | defined as $2\sigma v_d/RT$ (m) |
| α_M, β_M | fit parameters for molar mass distribution |
| β | defined as $d(\delta^{\phi_d} a_c^{3-\phi_d})/d\tau$ |
| β' | defined as $da_{10}^3/d\tau$ |
| γ | activity coefficient |
| Γ | molar surface coverage (mol/m^2) |
| δ | half the average separation distance between drops |
| δ_i | solubility parameter of component i ($\text{MPa}^{1/2}$) |
| ε | dielectric constant |
| ε_{ij} | molecular interaction energy between components i and j (J/m^3) |
| ε_0 | permittivity of a vacuum (C/Vm) |
| η | correction factor to Ostwald ripening equation |
| θ | fractional excess volume fraction |
| θ_i | fractional surface coverage of the i^{th} asphaltene component |
| θ_T | fractional surface coverage |
| κ | inverse Debye length (m^{-1}) |
| μ | viscosity ($\text{mPa}\cdot\text{s}$) |
| μ_i | chemical potential of component i (J) |
| ξ_r | ratio of the radius of the tensiometer platinum ring to the radius of the wire |
| ρ | density (kg/m^3) |

| | |
|--------------|---|
| $\bar{\rho}$ | average density (kg/m ³) |
| σ | interfacial tension (mN/m) |
| σ_m | measured interfacial tension (mN/m) |
| τ | reduced time, defined as $k_o t$ (m ³) |
| τ' | reduced time, defined as $k_o t / \delta$ (m ²) |
| ϕ | volume fraction |
| ψ_1 | ratio of A_p to A_d |
| ψ_2 | ratio of A_h to A_d |
| ψ_s | surface potential (V) |

Subscripts

| | |
|----------------|--|
| <i>a</i> | surface active asphaltene |
| <i>A</i> | asphaltene |
| <i>b</i> | denotes drop that shrinks to radius a_i in a time step |
| <i>c</i> | continuous phase |
| <i>d</i> | dispersed phase |
| <i>F</i> | feed |
| <i>i</i> | i^{th} asphaltene component |
| <i>i,k,p,q</i> | frequency distribution interval designations |
| <i>insol</i> | insoluble |
| <i>H</i> | hexane |
| <i>I</i> | interface |
| <i>l</i> | liquid |
| <i>L</i> | smallest asphaltene molecule |
| <i>m</i> | solvent mixture |
| <i>mix</i> | mixing |
| <i>o</i> | infinitely concentrated |
| <i>O</i> | oil |
| <i>R</i> | resin |

| | |
|------------|-----------------------------|
| <i>s</i> | surface |
| <i>sol</i> | soluble |
| <i>sp</i> | solid precipitate |
| <i>S</i> | solids |
| <i>t</i> | total emulsion |
| <i>T</i> | toluene |
| <i>U</i> | largest asphaltene molecule |
| <i>W</i> | water |
| ∞ | infinitely dilute |

Superscripts

| | |
|------------|-------------------|
| <i>cr</i> | critical |
| <i>f</i> | fusion |
| <i>j</i> | time step counter |
| <i>l</i> | liquid phase |
| <i>o</i> | time zero |
| <i>s</i> | solid phase |
| <i>vap</i> | vaporization |

Chapter 1

INTRODUCTION TO ASPHALTENE SOLUBILITY AND ASPHALTENE STABILIZED EMULSIONS

1.1 Introduction

Oil and gas have powered the world economy for the past century and will likely continue to do so for at least the coming century. In the past, oil and gas have been produced from large easily developed pools. However, in the future, production must come from smaller more marginally economic reservoirs or from technologically challenging sources such as heavy oil and the oil sands. In either case, two problems which have faced the oil industry since its inception are likely to become more prominent. They are the precipitation of asphaltenes and the formation of stable water-in-oil emulsions.

Asphaltene precipitation in the reservoir can severely curtail productivity while precipitation during production and refining can foul equipment and add to operating costs. The formation of emulsions can also curtail production and add significantly to transportation and treating costs. Further, in the case of oceanic oil spills, the formation of emulsions can hinder clean up attempts and aggravate an already serious environmental problem. Asphaltenes are known to stabilize emulsions and there is some evidence that the stability of water-in-crude oil emulsions is related to the asphaltene precipitation point (1). Hence, the problems of asphaltene precipitation and emulsion formation may be linked.

There is increasing interest in asphaltene precipitation today from the conventional oil industry because precipitation or emulsion formation may tip the balance between a marginally economic producer or a shut-in well. In the case of heavy oils and the oil sands, the asphaltene content of the oil is high, up to 25% (2), and the precipitation of asphaltenes and the formation of emulsions is difficult to avoid. At present, the oil sands

operators seek means of treating a water-in-oil emulsion that is likely stabilized by asphaltenes. The water-in-oil emulsion encountered in the oil sands process shall be referred to here as the “oil sands emulsion”.

The oil sands currently mined for the production of synthetic crude consist of approximately 85% sand, silts and clays, 5% water and 10% bitumen as well as less than 1% particulate organic material that is insoluble in organic solvents (2,3). The formation water in some areas can be salty with chloride concentrations in the order of 300 ppm (3). During the extraction process, shown in Fig. 1.1, where bitumen is separated from the sand and water, a water-in-oil emulsion is formed containing many of the chlorides from the formation water. The water-in-oil emulsion is carried in the froth which consists of 60% bitumen, 10% solids and 30% water. The froth is then diluted with naphtha, centrifuged and distilled to recover the naphtha. The final coker feed bitumen product still contains 3-5% water and approximately 0.5% solids (3). The water in the diluted bitumen is in the form of water droplets approximately 2 microns in diameter. The chlorides content in the droplets is similar to that of the formation water. The water-in-oil emulsion travels through the downstream upgrading process and eventually brings the chlorides in contact with hot metal equipment. The chlorides form complexes with the iron from the equipment and corrode the metal.

In order to eliminate the potential corrosion problem, the oil sands operators wish to prevent the formation of the emulsion or remove it from the diluted bitumen. If the water is removed and sent to the tailings stream in the form of an emulsion, some bitumen will be trapped in the emulsion resulting in lost recovery and contamination of the tailings with bitumen. Therefore, it is necessary either to prevent the formation of the emulsion in the first place or to separate and break the emulsion to recover the entrained bitumen. In order to find an efficient method of treating the emulsion, it is first necessary to understand how the emulsion is stabilized.

As will be discussed in Section 1.2, water-in-oil emulsions can be stabilized by solid particles or high molar mass surfactants. Unfortunately, many bitumen components fit that description. Furthermore, bitumen is a complex mixture of many thousands of components and it is difficult to isolate the effect of any given agent(s) that may be responsible for stabilizing the emulsion. To avoid the difficulties inherent in studying a system as complex as bitumen, one can examine a simpler model system possessing the key characteristics of the original one. Circumstantial evidence suggests that asphaltenes are, most likely, the agent stabilizing the oil sands emulsion. Therefore, the model system will be designed to examine asphaltenes in emulsions. Asphaltenes may exist in bitumen as solid particles, colloids, micelles or non-associated molecules, as will be discussed in Section 1.3. Hence, the model system must also be designed to accommodate different asphaltene phases. The phase behavior of asphaltenes in toluene/hexane mixtures resembles that of asphaltenes in bitumen except that asphaltene-resin interactions are not accounted for. Therefore, water/toluene/hexane/asphaltenes was selected as the model system, keeping in mind that the effect of resins might need to be examined later.

1.1.1 Objectives

The purpose of the thesis is to study the nature of water-in-toluene/hexane emulsions stabilized by asphaltenes. The key to understanding a stable water-in-oil emulsion is to determine what is adsorbed on the interface. Hence, the main objective of the thesis is to determine in what state the asphaltenes adsorb on the interface: solid, colloidal, micellar or liquid. To address the question, it is necessary to study the solubility of asphaltenes in toluene/hexane mixtures. Since asphaltene precipitation is also of interest to the oil industry, a second objective of the thesis is to predict as well as measure asphaltene solubility. Finally, it is useful to assess the stability of the asphaltene stabilized emulsions over time for two reasons. First, the stability of the emulsion serves as a point of comparison with the water-in-bitumen emulsion. Second, the observed stability provides insights into the nature of the interface and the interaction between the emulsion droplets. Such insights may be useful in determining an effective treatment. Therefore,

the third objective of the thesis is to examine the stability of asphaltene stabilized emulsions. The three objectives are restated below:

1. Measure and predict the solubility of asphaltenes in toluene/hexane mixtures.
2. Determine what phase of the asphaltenes adsorb on the interface of water-in-hexane/toluene emulsions.
3. Examine the stability of water-in-hexane/toluene emulsions stabilized by asphaltenes.

1.1.2 Thesis Outline

Chapter 1 serves as a general introduction to the subject of asphaltene solubility and asphaltene stabilized emulsions. Emulsion principles are reviewed in Section 1.2. The review focuses on the factors controlling the stability of emulsions. Asphaltene chemistry is reviewed in Section 1.3. The review includes the composition, surface activity, phase behavior and solubility modeling of asphaltenes. Chapter 1 is intended to provide the background material necessary to put Section 1.1 and the subsequent Chapters in context.

The body of the thesis is set in paper format and is presented in Chapters 2 to 6.

Asphaltene solubility, the first thesis objective, is tackled in Chapters 2 and 3. In Chapter 2, the asphaltene physical properties necessary for solubility predictions are determined and asphaltene solubility in toluene/hexane mixtures is measured. The solubilities are measured in the regime where no micelles form. An appropriate thermodynamic solubility model is developed and the predictions compared with measured asphaltene solubility. In Chapter 3, the solubility model is tested on measured asphaltene solubilities in a variety of organic solvents. The chapter is intended to test the generality of the solubility model and is the first step in developing a model that could be applied to any solvent system or even crude oils.

The second thesis objective is dealt with in Chapter 4. The techniques developed in Chapter 2 are employed to obtain asphaltene subfractions of different molar mass and

different solubility in toluene/hexane mixtures. The surface areas of emulsions prepared with the different subfractions, and hence with different asphaltene phase mixtures, are measured and compared to determine what asphaltene phases participate in stabilizing the emulsions. Note that the experiments were conducted in the asphaltene phase region where no micelles exist. Only the effect of solid particles and free asphaltene molecules are considered. The emulsions created under these conditions are qualitatively similar to the oil sands emulsion.

The third thesis objective is considered in Chapters 5 and 6. In Chapter 5, the measured stability of water-in-toluene/hexane emulsions stabilized by asphaltenes is discussed. The emulsions cream but do not appear to coalesce. Rather, a form of Ostwald ripening takes place. The ripening process appears to be affected by a change in interfacial properties as the droplet surface area changes. To confirm this interpretation, an attempt was made to numerically model the ripening of the emulsions. A numerical approach was developed and tested for standard Ostwald ripening in Chapter 6. Extending the model to the asphaltene stabilized emulsions is left for future work.

Chapter 7 is a summary of Chapters 2-6 and includes a discussion of their relevance to asphaltene precipitation, the oil sands emulsion and emulsions in general. Implications for treating the oil sands emulsion are considered and recommendations for extending the work are made.

1.2 Basic Principles of Emulsions

An emulsion is a mixture of two immiscible liquids where one liquid is dispersed in the other in the form of droplets (4). If the droplets remain dispersed over time the emulsion is deemed stable. For commercial emulsion products and processes, it is vital to control the stability of the emulsion. For example, dairy products and cosmetics are emulsions that must be very stable to ensure long shelf life. Microencapsulated drug delivery systems must be stable everywhere except at the target organ where the microemulsion is designed to become unstable and release the drug. However, for the treatment of water-

in-crude oil emulsions, it is desired to decrease the stability of the emulsion in order to achieve rapid phase separation.

Emulsions may destabilize in several ways: creaming, flocculation, coalescence and Ostwald ripening (79). The form of instability that is manifested, if any, is a function of the forces acting between the droplets and the nature of the interface. Therefore, interfacial properties and the forces that occur between droplets will be reviewed before the destabilization mechanisms are discussed. The material in the following sections is intended as a brief review and the subjects are discussed in greater detail in several fine sources (5-11).

1.2.1 Interfacial Properties

In general, emulsions that consist solely of two pure, immiscible phases are unstable. The stability of the emulsion can be significantly altered by the addition of a third component particularly if that component is a surfactant. One way of measuring the effect of a surfactant and the stability of an emulsion is to examine the interfacial tension of the emulsion. The rheology of an adsorbed film of surfactant is also an important factor in the stability of emulsions. Surfactants, interfacial tension and interfacial rheology are discussed below.

Surfactants: A surfactant is a dual natured molecule in that part of the molecule, the head group(s), is hydrophilic and the remainder, the tail, is hydrophobic. For example, pentanol consists of a hydrophobic alkane tail and a hydrophilic hydroxyl head. A surfactant readily adsorbs on an oil/water interface because there the tail(s) can reside in the oil phase and the head(s) in the liquid phase, as shown in Fig. 1.2. An adsorbed surfactant is either ionic, e.g., a carboxylic acid, or nonionic, e.g., polyoxyethylenes. Ionic surfactants can be anionic, cationic or both (zwitterionic). The surfactants usually either ionize or attract ions from the aqueous phase so that there is a charge associated with the head group. As will be discussed in Section 1.2.2, the charge associated with the

surfactant head can act to stabilize an emulsion or, if the surfactant has a large tail, the tail can also stabilize an emulsion.

Surfactants can also self associate. Above a critical concentration, the critical micelle concentration or cmc, surfactant molecules collect in aggregates or micelles. In water, the surfactant molecules will aggregate in such a way that the head groups tend to align near the water and the tail groups tend to collect in the center of the structure away from the water, as shown schematically in Fig 1.2. The micellization is driven by the same forces that cause surfactants to adsorb on interfaces. The opposite effect is observed in oil and is called reverse micellization, also shown in Fig 1.2. An interesting feature of micellization is that every additional surfactant molecule above the cmc is incorporated into a micelle. Hence, the non-associated surfactant concentration is constant above the cmc.

Micelles are able to swell, that is, to retain oil in their internal structure. Likewise, reverse micelles can swell with water. The swollen structures form a microemulsion. Most emulsions are stabilized because the surface forces on the droplets prevent contact between the droplets, as will be discussed later. Microemulsions are a second phase and are thermodynamically stable. Therefore, microemulsions are fundamentally different from “standard” emulsions and it is important to determine which type of emulsion one is dealing with. Microemulsions generally consist of droplets of less than 1 micron in diameter. Standard emulsions are usually made up of droplets larger than 1 micron in diameter. The two types of emulsion can also be distinguished by measuring their interfacial tension. A “standard” emulsion has a finite interfacial tension while the interfacial tension drops to zero when a microemulsion forms.

Interfacial Tension: Interfacial tension can be visualized in several ways. It reflects the interactions of the molecules on the interface with the bulk phases on either side of the interface and is a measure of the free energy per unit area of the interface. In other words, interfacial tension is the reversible work at constant temperature and pressure required to

expand the interface by a given area. Another way to view interfacial tension is as half the reversible work required to separate two surfaces from complete contact to infinite separation. In either view, interfacial tension is a measure of the energy cost in maintaining an interface. For example, a hexane/water interface has a relatively high interfacial tension. The high tension reflects the high energy cost of holding water molecules in contact with hexane. Adding a surfactant lowers the interfacial tension because the surfactant adsorbs on the interface and reduces the net molecular interaction energy. In general, an emulsion with low interfacial tension is more stable than one with high interfacial tension. If the interfacial tension is reduced to zero, a thermodynamically stable microemulsion can form.

Interfacial tension measurements also provide a useful tool for detecting the presence of micelles. Interfacial tension is linearly related to the log concentration of non-associated surfactant. When micelles form, each additional surfactant molecule above the cmc becomes part of a micelle. Hence, above the cmc, the concentration of non-associated surfactant is constant and the interfacial tension is also constant. The cmc can be detected by looking for the point where the interfacial tension becomes constant on a plot of interfacial tension versus log surfactant concentration. This technique is discussed further in Chapter 2.

Interfacial Rheology: In many ways, an interface with adsorbed surfactant can be considered as a third phase having its own properties. Interfacial phases follow equations of state and undergo phase transitions analogous to bulk solid, liquid and vapor phase behavior. As with bulk phases, the interface has its own rheological properties which can affect how easily an interface is disrupted or displaced. Therefore, interfacial rheology has a significant impact on the breaking of emulsions.

1.2.2 Forces Acting on Emulsion Droplets

The following forces are important in the interaction between emulsion droplets: dispersion, electrostatic, steric, Brownian, viscous, inertial, and gravitational forces.

Dispersion, electrostatic and steric forces are the forces acting between droplets. Brownian, viscous, inertial and gravitational forces affect the movement of the droplets in the continuous phase. Each force is discussed briefly below.

Dispersion Forces: Consider two droplets of the same phase separated by a second continuous phase. At the atomic level, the spontaneous fluctuation in the electronic cloud in one droplet induces a corresponding fluctuation in the second droplet. In fact, the fluctuation is the cumulative effect of a vast number of induced dipoles. The fluctuations create an attractive force at the bulk level called the dispersion or London - van der Waals force. The surrounding medium also affects the force. For example, a conductive medium with a high dielectric constant can also respond to the electronic fluctuations and diminish the interaction between the droplets. Nonetheless, any two droplets of like phase have an attractive dispersion force between them with a magnitude in the order of $A_H a/h^2$ for $h \ll a$ (5). Here A_H is the Hamaker constant, a function of the dispersed and continuous phase properties, a is the radius of the droplet and h is the separation distance between the droplets.

Electrostatic Forces: Electrostatic forces in emulsions arise from a surface charge on the droplets. In a high dielectric medium, the droplets acquire a surface charge from adsorbed ions. More commonly, and in any medium, the adsorbed material is a third component in the system, usually a surfactant. The continuous phase also affects the nature of the electrostatic force. For example, consider oil droplets with an adsorbed surfactant dispersed in water. Counter ions from the water are attracted to the droplets and form a shell around them maintaining charge neutrality, as shown in Fig. 1.3a. The counter ions are free to diffuse through the surrounding medium. Hence, the shell of counter ions is not necessarily concentrated on the surface but may be quite diffuse depending on the dielectric constant of the medium. Therefore, the droplets can act as charged spheres at finite separation distances and when droplets approach each other an electrostatic repulsive force arises between them. The force can be derived from Coulomb's Law and is of the order $\epsilon \epsilon_0 \psi_s^2 \kappa a \exp(-\kappa h)$, where ϵ is the dielectric constant

of the continuous phase, ϵ_0 is the permittivity of a vacuum, ψ_s is the surface potential of the droplet and κ is the inverse Debye length (4,5). Generally, the electrostatic force is only significant for aqueous media, that is, oil-in-water emulsions.

Steric Forces: Consider the case where a polymer surfactant is adsorbed on the emulsion droplets, shown in Fig. 1.3b. When the droplets approach, the outermost layers of the polymers begin to overlap. A steric repulsive force usually arises because the polymer segments are forced into a more closely packed and entropically unfavorable arrangement. The steric force is short range and its magnitude is a complex function of the nature of the polymer and the solvent properties of the continuous phase (11).

Adsorbed solid particles, shown in Fig. 1.3c, also can give rise to a steric repulsion force because work is required to move them from the interface. Steric forces, in a sense, arise from a physical barrier between the droplets.

Brownian Force: If the emulsion droplets act as non-deformable particles, the thermal energy of the molecules in the continuous phase can influence their motion. The molecules of the continuous phase collide randomly with the droplets imparting momentum to the droplets. The net random motion is called Brownian motion. The Brownian force is approximately of order kT/a , where k is the Boltzmann constant and T is the temperature (5).

Viscous, Inertial and Gravitational Forces: Since the continuous phase has some viscosity, any movement of the droplets through the continuous phase generates a shear force acting against the direction of motion. This viscous force is of order $\mu \bar{u} a$, where μ is the viscosity of the continuous phase and \bar{u} is the velocity of the droplet. In addition, the movement of the droplets displaces the continuous phase giving rise to an opposing inertial force of order $\rho a^2 \bar{u}^2$, where ρ is the density of the continuous phase. The density difference between the continuous phase and the droplets, $\Delta\rho$, gives rise to a gravitational force on the droplets of order $a^3 g \Delta\rho$ (5).

The order of the various forces, except the steric force, are summarized in Table 1.1 along with estimates of their magnitude for a water-in-oil emulsion with droplets of 2 microns in diameter. The relative magnitude of the forces determines the stability of the emulsion, as will be discussed in Section 1.2.3.

Table 1.1: Order of magnitude of interaction forces between droplets in a non-aqueous medium (effective molarity 10^{-10} mol/L):
 $a = 10^{-6}$ m, $A_H = 10^{-21}$ J, $g = 9.81$ m/s², $h = 10^{-6}$ m, $k = 1.381 \cdot 10^{-23}$ J/K,
 $T = 300$ K, $\bar{u} = 10^{-6}$ m/s, $\varepsilon = 5$, $\varepsilon_0 = 8.85 \cdot 10^{-12}$ C/Vm, $\kappa = 10^5$ m⁻¹,
 $\rho = 10^3$ kg/m³, $\Delta\rho = 10^2$ kg/m³, $\mu = 10^{-3}$ Pa.s, $\psi_s = 0.05$ V. (Ref. 8,12)

| Force | Order of Magnitude Theoretical Expression | Order of Magnitude for Water-in-Oil Emulsion (N) |
|---------------|---|--|
| Dispersion | $A_H a / h^2$ | 10^{-15} |
| Electrostatic | $\varepsilon \varepsilon_0 \psi_s^2 \kappa a \exp(-\kappa h)$ | 10^{-15} |
| Brownian | kT/a | 10^{-15} |
| Viscous | $\mu \bar{u} a$ | 10^{-15} |
| Inertial | $\rho a^2 \bar{u}^2$ | 10^{-21} |
| Gravitational | $a^3 g \Delta\rho$ | 10^{-15} |

1.2.3 Stability of Emulsions

As mentioned previously, there are several ways an emulsion can destabilize: creaming, flocculation, coalescence and Ostwald ripening. Creaming and flocculation affect the dispersion of the droplets in the emulsion but do not affect the size distribution of the droplets. Coalescence and Ostwald ripening entail a change in the size distribution of the droplets but do not necessarily alter the dispersion of the droplets. Only coalescence and Ostwald ripening can lead to complete phase separation.

Creaming: If gravitational forces dominate, the droplets will rise or sink and collect at the top or bottom of the emulsion depending on the sign of the $\Delta\rho$ term (6). Clear continuous phase is left behind at the opposite end of the emulsion. In other words, some of the continuous phase separates from the original emulsion and the remaining emulsion

is concentrated. This process occurs when cream rises to the top of milk and hence is called creaming.

Flocculation: Flocculation depends on the relative magnitude of the attractive and repulsive forces acting between droplets. Both attractive dispersion forces and repulsive electrostatic or steric forces are present in most emulsions. The forces each arise from an energy potential. The combined potential energy or interaction energy between the droplets is a function of separation distance. The shape of the curve of potential energy versus separation distance determines the behavior of many emulsions. Several examples of potential energy curves (10,80) are given in Fig. 1.4. Types *A*, *B* and *C*, shown in Fig. 1.4a, result from electrostatic and dispersion forces. The relative magnitude of the dispersion force versus the electrostatic force increases from types *A* to *C*. Types *D* and *E*, shown in Fig. 1.4b, result from steric and dispersion forces. The relative magnitude of the dispersion force versus the steric force is greater for the type *E* curve.

Consider types *A* and *D* energy potential curves. There is a large positive, or repulsive, interaction energy at larger separation distances. Therefore the droplets resist approaching each other and will remain dispersed. Types *A* and *D*, then, are characteristic of stable dispersions.

Now consider a type *B* energy potential. The interaction energy is negative, or attractive, at large separation distances but is repulsive at intermediate separation distances. Consequently, a secondary energy minimum is formed. When droplets approach, there is a finite probability that they will be captured in the secondary energy minimum and stay together in a loose association or floc. Such an association is defined here as secondary flocculation. Secondary flocculation is slow and when it occurs the droplets group into many individual clusters. The flocculation is reversible and viscous, inertial and convective forces can break up the flocs. Generally, secondary flocculation is reversible under moderate mixing conditions.

Primary flocculation is here defined as the aggregation of particles in the primary energy minimum. Consider types *C* and *E* energy potential curves. The interaction energy is negative or attractive until the droplets reach the primary energy minimum. In this case, when droplets approach each other they are rapidly drawn together into close contact. Primary flocculation can also occur for type *B* energy potentials if the secondary minimum is shallow and the momentum of the particle is sufficient to carry it past the secondary energy minimum into the primary minimum. For electrostatic/dispersion systems, the primary energy minimum is a deep potential well and, therefore, primary flocculation is irreversible.

Coalescence: When droplets collide and flocculate, the continuous phase between the drops drains out until a thin layer or film remains between them (6). The film undergoes spontaneous thermal or mechanical fluctuations in thickness. The fluctuations can grow or dampen depending on the steric forces and film properties. If they dampen, the droplets remain flocculated but intact. If the fluctuations grow, the film ruptures and the droplets merge, that is, they coalesce. Coalescence always leads to an increase in drop size and eventually leads to complete phase separation.

Ostwald Ripening: Ostwald ripening occurs in emulsions with drops of different size and also results in a change in the drop size distribution. Ostwald ripening refers to mass transfer between particles of different curvature through their surrounding continuous medium (79). The concentration of the dispersed phase material at the surface of a drop is inversely related to the radius of curvature. Hence, a small drop has a high surface concentration relative to a large drop, giving rise to a concentration gradient of the dispersed phase material in the continuous phase. Mass transfer occurs along the concentration gradient from small drops to large drops, *i.e.*, small drops shrink and ultimately disappear while large drops grow at their expense, eventually leading to phase separation. Ostwald ripening is a slow process and generally is observed only in emulsions that do not coalesce.

1.2.4 Stability of Water-in-Oil Emulsions

For water-in-oil emulsions, electrostatic forces are usually relatively small. For example, the electrostatic force for the water-in-oil emulsion given previously in Table 1.1 is of a similar magnitude to the other forces acting on the emulsion droplets at a separation distance of 1 μm . At smaller separation distances, the dispersion force dominates the electrostatic force. Hence, electrostatic forces are unable to stabilize most water-in-oil emulsions. The steric force is also negligible unless a surfactant or solid particles are adsorbed on the interface. Therefore, a water-in-oil emulsion containing no surfactant or solids should flocculate and coalesce. The behavior of an emulsion stabilized by a surfactant or by solid particles depends on the size of the droplets and the potential energy curve between the particles.

The size of the droplets determines whether a cream will form. Gravity forces are proportional to the cube of the drop radius and dominate when the emulsion droplets are large. Brownian forces are inversely proportional to the drop radius and dominate for small droplets. The emulsion creams when gravity forces dominate and the emulsion remains dispersed when Brownian forces dominate. Hence, the larger the droplets, the more likely the emulsion will cream.

The droplets of a creamed emulsion may or may not be stable. The droplets are brought into closer contact as the emulsion creams. For a type *D* energy curve of Fig. 1.4b, the repulsive force acting between the droplets balances the gravitational force at a separation distance too great for coalescence to occur. The cream reaches a stable packing, does not coalesce but may undergo Ostwald ripening. For the type *E* energy curve, the creamed droplets flocculate. The flocculated cream may coalesce and break, undergo Ostwald ripening or remain stable.

A dispersed emulsion with a type *D* energy curve will remain dispersed. For a type *E* energy curve, the droplets will gradually flocculate as they collide forming many clusters or aggregates. The rate of aggregation depends on the balance between the Brownian

force and the strength of the primary minimum. If the Brownian forces are relatively strong, droplets may move away from the primary minimum and aggregates may break up as fast as they are formed. Hence, a dispersed emulsion with a type *E* energy curve may remain partly or wholly dispersed. If the aggregates are stable, they may coalesce, undergo Ostwald ripening or remain stable.

1.2.5 Water-in-Oil Emulsion in Oil Sands Extraction

At present, few facts are known about the water-in-oil emulsion formed in the oil sands extraction process. Some observations are given below. The droplets are 2-5 microns in diameter. The emulsion remains dispersed in aromatic solvents even when centrifuged at high speed but flocculates in aliphatic solvents and is easily settled. The flocculated emulsion is very stable. A variety of components have been identified in the continuous phase that may act as stabilizers including asphaltenes, clays and silica partially coated with organic material (3).

The stability of the emulsion and the fact that the continuous phase is non-aqueous indicate that the emulsion is sterically stabilized. The emulsion remains dispersed at normal gravity because the magnitude of the Brownian, viscous and inertial forces are larger or on par with the normal gravitational force for 2 micron diameter droplets. The magnitudes of the various forces were given in Table 1.1. The emulsion creams when centrifuged but does not break and it redisperses after centrifugation. The reversibility of the creaming emphasizes the strength of the steric stabilization.

The addition of a solvent can alter the stability of the emulsion. The emulsion remains dispersed in aromatic solvents. However, the water droplets flocculate and cream in aliphatic solvents. The creaming likely occurs because the flocs have a relatively large effective diameter. The change in aggregation behavior indicates a change in the interaction energy between the droplets. A change in interaction energy may occur because the dispersion forces are different in different solvents. Alternatively, the steric forces may change because the structure of the material on the interface depends on the

solvent. In any case, the flocculated emulsion does not coalesce, proving once again that a strong steric force is present. Hence, a strong surfactant membrane or particulate barrier exists on the interface.

The key to understanding the oil sands emulsion is to determine what material is on the interface preventing coalescence and stabilizing the emulsion. There are many potential surfactant and particulate emulsion stabilizers in bitumen including, asphaltenes, waxes, organic acids, clays, silica and acidic paraffinic solids (2). Organic acids are well known emulsifiers and waxes (13) and acidic paraffinic solids (14) have recently been shown to stabilize water-in-oil emulsions. However, only asphaltenes, clays and silica appear in the flocculated emulsion in sufficient quantities to account for the stability of the emulsion.

In general, asphaltenes are the most commonly identified emulsion stabilizer of water-in-crude oil emulsions. However, clays partially coated with asphaltenes have been shown to stabilize oil-in-water emulsions (15). Their ability to stabilize oil-in-water emulsions has yet to be investigated. Organically coated silica particles appear to be necessary to reconstitute a dispersed emulsion like the one observed in the extraction process (3). The organic material coating the particles is believed to be asphaltenic (16). Hence, asphaltenes can act as a stabilizer themselves and appear to be a factor in the other stabilization mechanisms.

Strong circumstantial evidence indicates that asphaltenes are involved in stabilizing the oil sands emulsion. First, the flocculation of the emulsion droplets as the aliphatic content of the solvent increases closely resembles the precipitation of asphaltenes. It is reasonable to assume that asphaltene coated water droplets act as asphaltene particles, precipitating or flocculating in a poor solvent. Second, the interface of the oil sands emulsion behaves differently in aromatic and aliphatic solvents. The interface appears to be mobile in toluene and immobile in hexane (17). A change in interfacial properties likely corresponds to a change in bulk phase properties. The asphaltenes in the bulk

phase undergo a phase change as the aliphatic content of the solvent increases. Thirdly, the interface acts like a membrane not a particle covered surface. The interface of a pendant water drop in diluted bitumen wrinkles and collapses when the contents of the drop are extracted (18). These three observations suggest that the asphaltenes form a membrane on the surface of the droplet. The membrane is a third phase whose properties depend on the surrounding solvent.

1.3 Asphaltene Chemistry

Asphaltenes are a complex mixture of molecular species and exhibit complex phase behavior. The state of the asphaltenes may be an important factor in their role as an emulsion stabilizer. Therefore, the asphaltene chemistry is reviewed with phase behavior in mind. Of course, the asphaltenes do not act in isolation and therefore some petroleum chemistry and, in particular, bitumen chemistry is reviewed first. The composition and structure of asphaltenes and asphaltene aggregates is then discussed followed by a review of asphaltene solubility modeling.

1.3.1 Classification of Petroleum Fractions

The following review of petroleum chemistry is drawn from several sources (2,19-21). Petroleums are mixtures of many thousands of components and it is impractical to classify them by composition. Consequently, several other criteria are employed to classify petroleums: physical properties, atomic H/C ratio, heteroatom content, boiling cut, and solubility class. An example of classification by physical properties is the UNITAR definition of oil grades by density and viscosity, provided in Table 1.2. The atomic hydrogen to carbon ratio of a petroleum is a good indicator of its type and of its heating and combustion properties. The H/C ratios for several fuels are listed in Table 1.3. Petroleums are also often compared according to their heteroatom content, that is, the elements present in the petroleum other than carbon and hydrogen, e.g., sulfur, nitrogen, oxygen, vanadium and nickel.

Table 1.2: UNITAR definition of oils and bitumens (19).

| Type | Viscosity (mPa.s) | Density (kg/m ³) |
|------------------|----------------------------------|------------------------------|
| Conventional Oil | < 10 ² | < 934 |
| Heavy Oil | 10 ² -10 ⁵ | 934-1000 |
| Bitumen | >10 ⁵ | >1000 |

Table 1.3: Atomic H/C ratios for fuels (19).

| Fuel | H/C Ratio |
|-------------|-----------|
| Methane | 4.0 |
| Gasoline | 1.9 |
| Light Crude | 1.8 |
| Bitumen | 1.4-1.6 |
| Coal | 0.5-0.8 |

A petroleum is also classified by the relative amounts of defined fractions of the oil. The fractions, or cuts, are defined by boiling range or by solubility/adsorption class.

Petroleum boiling cuts are given in Table 1.4 and solubility classes are shown in Fig. 1.5. Boiling ranges categorize the use of the petroleum cuts whereas solubility classes roughly subdivide the crude into classes of molecular species. The four most commonly used solubility classes are, in order of increasing polarity and H/C ratios: the asphaltenes, resins, aromatics and saturates. Crude petroleums from different sources have widely different proportions of each class but each class has many common properties.

Table 1.4: Boiling ranges and uses of petroleum cuts (19,20).

| Cut | Boiling Point Range (°C) | Use |
|-----------------|--------------------------|-------------------------------------|
| Light Naphtha | 1-150 | Gasoline, solvent |
| Gasoline | 1-180 | Gasoline |
| Heavy Naphtha | 150-205 | Reformed for gasoline |
| Kerosene | 205-260 | Jet fuel, solvent |
| Stove Oil | 205-290 | Fuel, solvent |
| Light Gas Oil | 260-315 | Diesel Fuel |
| Heavy Gas Oil | 315-425 | Catalytic or hydrocracker feed |
| Lubricating Oil | >400 | Lubricating oil |
| Vacuum Gas Oil | 425-600 | Catalytic or hydrocracker feed |
| Residuum | >600 | Asphalt, coker or hydrocracker feed |

Asphaltenes are defined as the fraction of a petroleum that is soluble in toluene but insoluble in an alkane solvent, usually pentane or heptane. As will be discussed later, asphaltenes are the highest molar mass solubility class in a petroleum. Therefore, asphaltenes have high boiling points and are always part of the residuum. Furthermore, asphaltenes have the greatest density of all the solubility classes. Therefore, the denser the petroleum, the higher the asphaltene content. The relationship of petroleum density to asphaltene content is illustrated in Table 1.5. For heavy oils and bitumens, the asphaltene content largely determines the properties of the oil.

Table 1.5: Composition of petroleum, heavy oil/bitumen and residuum (20).

| | Range of composition (wt%) | | |
|-------------------|----------------------------|--------|-------|
| | asphaltenes | resins | oils |
| Conventional Oil | 0-12 | 3-22 | 67-97 |
| Heavy Oil/Bitumen | 11-45 | 14-39 | 24-64 |
| Residuum | 11-29 | 29-39 | 32-49 |

1.3.2 Characteristics of Bitumens

This thesis is concerned with Alberta bitumens. The composition and properties of most Alberta bitumens fall into fairly narrow ranges and are summarized in Table 1.6.

Table 1.6: Properties of Alberta bitumens (2).

| <u>Composition (wt%)</u> | | <u>Solubility Class (wt%)</u> | |
|--------------------------|--|-------------------------------|-------|
| Carbon | 81-84 | Asphaltenes | 16-22 |
| Hydrogen | 10-11 | Resins | 29-49 |
| Nitrogen | 0.3-0.6 | Saturates | 15-21 |
| Oxygen | 0.8-1.6 | Aromatics | 18-32 |
| Sulfur | 4.6-5.6 | | |
| Nickel | 60-100 (mg/kg) | | |
| Vanadium | 160-300 (mg/kg) | | |
| Ash | 0.5-1.0 | | |
| | | | |
| H/C Atomic Ratio | 1.46-1.50 | | |
| Molar Mass | 490-620 g/mol | | |
| Density | 0.97-1.02 g/cm ³ | | |
| Viscosity | 10 ⁴ -10 ⁶ mPa.s @ 15 °C | | |
| Heat of Combustion | 41.0-42.6 MJ/kg | | |

Some representative molecular species found in bitumen are given in Figs. 1.6-1.8. The molecular composition of the Alberta bitumens is best discussed in terms of the solubility classes. The most easily described classes are the saturates and aromatics. The saturates fraction consists of alkyl cycloalkanes of 1 to 6 rings (17% of the bitumen). There are thousands of varieties of each alkyl cycloalkane and many of them are parts of homologous series. The aromatic fraction of the bitumens consists primarily of

monoaromatic (10% of the bitumen), and di- and trinuclear aromatic hydrocarbons (9% of the bitumen). The aromatic fraction contains a small amount (<1% of the bitumen) of sulfur and nitrogen heteroatoms in the form of benzothiophenes, alicyclic sulfides, alkylated benzoquinilines and carbazoles. Again many homologous series are observed. While both the saturates and the aromatics are complex mixtures and contain many unidentified components, each class contains distinct types of molecular species. Therefore, the two solubility classes are useful tools for separating groups of species with many common properties. In many cases, the properties of each class can be represented by lumped properties.

The resins are a mixture of heterocycles (40% of the bitumen) and a small amount (1-2% of the bitumen) of carboxylic acids. The carboxylic acids are a homologous series of tricyclic terpenoid acids, pentacyclic hopanoid acids and trace amounts of n-alkanoic acids. There are many heteroatom homologous series in the resins including benzofluorenones, cyclic sulfides, alkyl benzocarbozoles and alkyl benzoquinolines. The molecular species within the resins resemble the heteroatom species that make up 5% of the aromatics. However, the resin species have higher molar mass, greater polarity and lower H/C ratios. Hence, the difference between resins and aromatics is not as clear as that between saturates and aromatics.

The distinction between resins and asphaltenes is even less clear. The chemical species that make up each class are similar. Asphaltenes, on average, have higher molar mass, higher heteroatom content and lower H/C ratios than the resins (22). The resins and asphaltenes probably form a continuum of like chemical species with increasing average molar mass (23,24). Asphaltenes and resins can exhibit complex properties and phase behavior and cannot necessarily be treated as lumped components.

1.3.3 Asphaltene Composition, Structure and Molar Mass

Elemental Composition: The elemental composition of asphaltenes from sources throughout the world are remarkably similar considering the range of species included in the solubility class. The elemental compositions of various asphaltenes are compared in Table 1.7. The similarities in composition indicate that property correlations and predictions for one asphaltene may be applicable to other asphaltenes. For present purposes, only the properties of Athabasca asphaltenes are considered. The elemental composition and n.m.r. carbon type analysis for Athabasca asphaltenes are given in Table 1.8. Most of the metal and ash content of crude oils is concentrated in the asphaltenes (2). Ash is defined as the material insoluble in organic solvents and is comprised of clays and some associated organic material. The ash content in Athabasca asphaltenes is approximately 6-7%. The metals are primarily nickel, vanadium and iron. The nickel and vanadium are naturally occurring and mostly bound in porphyrin complexes. The iron is adsorbed from processing equipment and it and the remainder of the nickel and vanadium are held in non-porphyrin complexes (25,26).

Table 1.7: Elemental composition of various asphaltenes (27).

| Source | Precipitator | Carbon Content (wt%) | Atomic Ratios | | | |
|--------|--------------|----------------------|---------------|-------|-------|-------|
| | | | H/C | N/C | O/C | S/C |
| Canada | n-pentane | 79.5 | 1.21 | 0.013 | 0.036 | 0.035 |
| | n-heptane | 78.4 | 1.16 | 0.015 | 0.044 | 0.038 |
| Iran | n-pentane | 83.8 | 1.07 | 0.014 | 0.021 | 0.022 |
| | n-heptane | 84.2 | 1.00 | 0.016 | 0.012 | 0.026 |
| Iraq | n-pentane | 81.7 | 1.16 | 0.008 | 0.010 | 0.039 |
| | n-heptane | 80.7 | 1.06 | 0.010 | 0.014 | 0.016 |
| Kuwait | n-pentane | 82.4 | 1.14 | 0.009 | 0.014 | 0.034 |
| | n-heptane | 82.0 | 1.07 | 0.010 | 0.017 | 0.036 |

Table 1.8: Elemental composition of Athabasca asphaltenes (28).

| | |
|---|------------|
| Molar Mass | 3600 g/mol |
| <u>Elemental Analysis (normalized wt%)</u> | |
| Carbon | 79.9 |
| H | 8.3 |
| N | 1.2 |
| S | 7.6 |
| O | 3.2 |
| H/C | 1.24 |
| <u>Distribution of carbon atom types per 100 carbon atoms</u> | |
| C aliphatic | 58 |
| C aromatic | 42 |

Molecular Composition and Structure: While the elemental composition and aromatic nature of asphaltenes have been recognized since 1940 (29), there has been considerable debate over the structure of asphaltene molecules. Early interpretations of spectroscopic studies held that the an asphaltene molecule consists of a condensed polynuclear core carrying heteroatoms, alkyl chains and hydroaromatic ring systems (30-32). An example is given in Fig. 1.9. This interpretation resulted from an overestimate of the significance of the X-ray diffraction signal attributed to large aromatic disks and the failure, at that time, of instruments to detect naphthenic structural elements (33). In the 1970's, pyrolysis of asphaltenes produced only low molar mass non-aromatic and aromatic fragments (34) and mild thermolysis demonstrated that asphaltenes contain mostly mono to pentacyclic aromatic molecules (33,35,36). In pyrolysis techniques, the larger more complex molecules are converted to coke and their structure is not determined. Therefore, larger ring structures could pass undetected. However, other techniques have confirmed that asphaltenes are less condensed than previously believed (37-39). It is now generally accepted that asphaltenes contain aromatic clusters of at most 6 rings (22,25).

More recently, asphaltene researchers have attempted to determine some of the species and homologous series that comprise the asphaltenes. Using ruthenium-ion-catalyzed oxidation, Strausz and co-workers (33,40) identified many asphaltene elemental structures and constructed a hypothetical asphaltene molecule to illustrate their results. Their hypothetical structure is shown in Fig. 1.10. The structural elements incorporated into the molecule are listed below:

- a 2,5-n-alkyl thiolane and an oxide of it
- a 2,6 n-alkyl thiane
- 2,5-n-alkyl thiophenes
- 2,4-n-alkyl benzothiophenes
- 1,9-n-alkyl dibenzothiophenes
- a 4,9-n-alkyl fluorene
- o-di-n-alkyl benzenes
- an n-alkanoic acid ester
- a pentacyclic naphthenic ring system
- an n-alkyl pyridine
- an n-alkyl quinoline
- an o-di-n-alkyl naphthalene
- a decaline
- octahydrophenanthrenes, etc
- condensation products of some of the above mentioned aromatics
- a condensed deoxophyllerythroetioporphyrin
- biphenyl linkages

The elemental formula of their hypothetical asphaltene molecule is $C_{420}H_{496}N_6S_{14}O_4V$ with an H/C ratio of 1.18 and a molar mass of 6191 g/mol. This hypothetical molecule is illustrative only. The asphaltene solubility class appears to consist of a huge variety of molecular species each comprised of different proportions and arrangements of the structural elements listed above. Note that the structural elements found in the

asphaltenes are the same as those found in the resins. However, the asphaltene molecules contain a higher proportion of heteroatoms and possess a larger more polar structure.

Identifying the species that make up the asphaltenes gives some qualitative insight into asphaltene behavior. However, there are simply too many species to characterize the asphaltenes by their molecular composition. Instead, research has focused on identifying trends within the asphaltenes. Some trends in composition or properties may lead to a simple method of characterizing asphaltenes. For example, the asphaltene fraction appears to contain a range of molar masses from roughly 1000-10000 g/mol. The molar mass of asphaltenes is discussed in more detail later. Several studies have attempted to relate asphaltene characteristics to molar mass. Most research shows that as the asphaltene molar mass increases, heteroatom and metal content increases and the H/C ratio decreases (20,23,26,41). Some typical results are given in Figs. 1.11-1.14. The same correlations are evident in Table 1.7, bearing in mind that asphaltenes precipitated by n-heptane have higher average molar mass than asphaltenes precipitated by n-pentane.

It appears that the asphaltenes, the resins and some of the aromatics are part of a continuum of molecular species. The molar mass of the species increases from the aromatics through the resins to the asphaltenes. The molar mass continues to increase within the asphaltene solubility class. Heteroatom and metal content and aromaticity increase along with molar mass and the atomic H/C ratio decreases. If physical properties such as density and solubility can be correlated to any of these trends, then asphaltenes could be characterized simply by measuring the appropriate trend.

Surface Active Constituents: Asphaltenes have also been separated into acidic, basic, amphoteric and neutral constituents (20,41). These fractions are of interest when considering asphaltene stabilized emulsions because the non-neutral constituents are likely surface active. The non-neutral species are likely surface active because the sulfur, nitrogen and oxygen based acidic or basic groups are hydrophilic and the remaining large hydrocarbon structure of the molecules is hydrophobic. Asphaltenes in hydrocarbon

solvents have been shown to adsorb on hydrophilic surfaces, suggesting that some asphaltenes may be surface active (42,43). The relative proportions of the acid/base divisions are given in Table 1.9 and some characteristics of each fraction are given in Table 1.10. The existence of acid and basic asphaltene components is confirmed by interfacial tension experiments (44,45). The interfacial tension between water and asphaltene bearing oils decreases at both high and low pH values. The pH dependence at both ends of the pH scale indicates that both acid and base interactions occur at the interface. The change in interfacial tension with pH is shown in Fig. 1.15.

Table 1.9: Ion resin fractionation of “Arabian” crude oil asphaltenes (41,46):

| Fraction | wt% |
|-------------|-----|
| Acids | 7 |
| Bases | 55 |
| Amphoterics | 16 |
| Neutral | 22 |

Table 1.10: Production by pyrolysis of aromatics, non-aromatics and carbon residue from various Athabasca asphaltene fractions (20,47).

| Fraction | Atomic | Molar | Volatile Fractions | | Residue (wt%) |
|----------------|--------|-----------------|--------------------|--------|------------------|
| | H/C | Mass (g/mol) | aromatics | others | |
| Acids | 1.04 | 2350 | 51 | 49 | 63 |
| Bases | 1.06 | 2250 | 48 | 52 | 60 |
| Amphoterics | 1.23 | 1910 | 40 | 60 | 43 |
| Neutral Polars | 1.29 | 1420 | 33 | 65 | 38 |

Molar Mass: An very wide range of asphaltene molar masses has been measured with different experimental techniques. Some results are summarized in Table 1.11. The only

explanation for the variation in measured molar mass is that asphaltenes associate and in some, or all cases, the measured molar mass is the mass of an aggregate rather than a molecule. Today, the two most commonly used techniques are the ones that come closest to measuring the molar mass of an asphaltene molecule: gel permeation chromatography (gpc) and vapor pressure osmometry (vpo). The measured molar masses from both techniques are generally consistent with each other but are influenced by temperature, the solvent polarity and the asphaltene concentration. The effects of solvent polarity and asphaltene concentration on measured molar mass are shown in Figs. 1.16 and 1.17, respectively. The variation of molar mass with asphaltene concentration can be extrapolated to obtain values for infinitely dilute solutions of asphaltene. The molar mass found at infinitely dilute conditions is consistent in any one solvent. However, the measured molar mass varies from solvent to solvent indicating that some form of association between the asphaltene molecules or between the asphaltenes and the solvent is still occurring. Vpo measurements are generally accepted to set an upper limit on the number averaged asphaltene molar mass.

Table 1.11: Asphaltene molar masses determined with various methods (48-49).

| Method | Molar Mass (g/mol) |
|-------------------------------|--------------------|
| Ultracentrifuge | 20,000 - 300,000 |
| Osmotic Pressure | 20,000 - 80,000 |
| Monomolecular Film | 80,000 - 140,000 |
| X-ray Diffraction | 40,000 |
| Gel Permeation Chromatography | 20,000 - 60,000 |
| Dynamic Light Scattering | 20,000 - 100,000 |
| Ebullioscopic | 2500 - 4000 |
| Cryoscopic | 600 - 6000 |
| Viscosity Determination | 1000 - 4000 |
| Vapor Pressure Osmometry | 1000 - 5000 |
| Equal Vapor Pressure | 2000 - 3000 |

The number average molar mass determined by vpo for Athabasca asphaltenes in benzene is approximately 3600 g/mol (2). However, the average value disguises the fact that there is a broad range of molar masses within the asphaltene fraction. Some ranges measured for asphaltene molar masses are given in Table 1.12. The measurements suggest that asphaltene molar masses range from approximately 1000 to 10,000 g/mol. In addition, plasma mass desorption spectroscopy measurements of Athabasca bitumen in THF (51) indicate a range of molar masses up to 5000 g/mol. Mass spectroscopy tends to fragment higher molar mass material and therefore the range of molar masses is reasonably consistent with the vpo measurements. Nonetheless, it must be kept in mind that the molar mass distribution may be affected by the nature of the solvent.

Table 1.12: Measured range of asphaltene molar mass.

| Asphaltene Source | Technique | Molar Mass Range (g/mol) |
|-------------------|-----------|--------------------------|
| Unspecified (20) | vpo | 4000-12000 |
| Cold Lake (74) | gpc | 800-8000 |
| Cold Lake (26) | vpo | 1000-6000 |
| Athabasca (25) | gpc | 1000-17000 |
| Athabasca (50) | vpo | 1500-7000 |

1.3.4 Asphaltene Association

The variation in observed asphaltene molar masses demonstrates that asphaltenes self associate. Perhaps the most debated issue in asphaltene research is the nature of the self-association. The self association may be brought about by H-bonding through the heteroatoms, π - π bonding between aromatic rings, and charge transfer or van der Waals complexation between the rings and Lewis acid or base groups (2). The number of possible interactions allows for complex behavior and for a proliferation of association

models. However, the proposed models fall into two main categories, the *colloidal* model and the *micelle* model. Note that the terms colloid and micelle are often used interchangeably in the literature but here they are given distinct definitions.

Colloidal Model: The first models for asphaltene association were colloidal models where polynuclear aromatic asphaltenes were believed to form a dense core peptized or stabilized by resins and maltenes (29,52). An example of one such model is given in Fig. 1.18. It was assumed that resins were needed to stabilize the asphaltenes because many asphaltenes only redissolve in crude oils containing the original resins fraction (53,54). However, asphaltenes can form stable aggregates in a variety of organic solvents without the presence of resins or maltenes (55). Therefore, specific asphaltene-resin interactions are not a necessary part of the model.

The perception of the asphaltene core was modified based on x-ray diffraction (xrd) data that suggested that solid phase asphaltenes are composed of agglomerated stacks, with each stack consisting of up to 6 molecules (56). The stacks are held together by π - π bonding and physical constraints prevent larger stacks from forming. The same stacks are believed to form in solution, creating a colloid with a diameter in the order of 3 nm. The colloid can be dispersed by a variety of solvents. A model of the colloid is shown in Fig. 1.19.

Small angle neutron scattering (SANS) and small angle x-ray scattering studies (SAXS) have found spherical or disk-like structures in the order of 10 nm in diameter in asphaltene/solvent solutions (57,58). Rheological studies have confirmed the existence of spherical structures of the same diameter (59). In the colloidal model, the structures are interpreted as aggregates of asphaltene stacks. The aggregation of the stacks arises through H-bonding or complexation and the degree of association is expected to be a function of the concentration of the colloid and the relative strength of the colloid-colloid and colloid-solvent interactions. However, SANS measurements show that, in many

cases, the size of the aggregates is independent of asphaltene concentration or the polarity of the solvent. The apparent size limit has been attributed to packing constraints (59).

Asphaltene precipitation increases at higher concentrations, lower temperatures and in less polar solvents. The precipitated asphaltenes are visible to the naked eye and form flocs up to hundreds of microns in diameter (74). In the colloidal model, the precipitation is interpreted as the flocculation of aggregated stacks. In other words, there are at least three levels of asphaltene association: stacking, aggregation, and flocculation. The flocculation is driven by the relative magnitude of the aggregate-aggregate and aggregate-solvent forces. The aggregate-aggregate forces are weaker than the colloid-colloid forces because the functional groups giving rise to the forces are distributed differently. However, the details of the molecular arrangements have yet to be elucidated.

Micelle Model: The micelle model resembles the colloidal model except that it does not include asphaltene stacking. There is no direct proof that asphaltenes stack in solution and a consensus is forming that asphaltenes are dispersed as molecules rather than colloidal stacks (60). In this view, the resins in the natural crude do not peptize colloidal asphaltene but solvate asphaltene molecules. The asphaltenes are modeled as surfactants and the structures observed with SANS are believed to be micelles (23). Interfacial tension and vpo molar mass measurements of asphaltenes in pyridine show a cmc transition, supporting the idea that asphaltenes form micelles at higher concentrations. A plot of interfacial tension versus asphaltene concentration is shown in Fig. 1.20. The interfacial tension measurements (59) show a change in slope at an asphaltene concentration of approximately 0.05 wt%. The change in slope indicates the formation of micelles. The molar mass measurements were shown in Fig. 1.16. The measured molar masses (49) increase linearly over the range of experimental data from asphaltene concentrations of 2-7 wt%. The presence of micelles causes a linear increase of measured molar mass with solute concentration. The effect of micelles on measured molar mass is discussed in greater detail in Appendix A. Similar evidence indicating the existence of asphaltene micelles in 1,2-dichlorobenzene is also presented in Appendix A.

In the micelle model, the precipitation of asphaltenes is interpreted as a solid-liquid phase transition. However, the phase transition is not necessarily straight forward if micelles are present. Further complicating the problem is the fact that not all the asphaltenes may act as surfactants and participate in the micellization. Finally the model must address the different molar masses measured for asphaltenes in different solvents. The micelle model is a recent concept and there is an opportunity to contribute to the model in its early stages of development.

1.3.5 Asphaltene Solubility Models

There are two main groups of solubility models, the *steric-colloidal* and the *thermodynamic* model (61). The two models correspond to the two views of asphaltene aggregation, the *colloidal* and the *micelle* model. To illustrate the principles involved, the thermodynamic model is first reviewed in some detail. The difference in approach for the steric-colloidal model is briefly reviewed afterwards and the current issues in solubility modeling are discussed.

Thermodynamic Model: In the thermodynamic model, the precipitation of the asphaltenes is viewed as a phase transition and, as with all phase transitions, the derivation begins with the equilibrium condition for the chemical potential of a given component in the two phases.

$$\mu_i^l = \mu_i^s \quad (1.1)$$

where μ_i^l and μ_i^s are the chemical potentials of component i in the liquid and solid phases respectively. Eq. 1.1 can be expanded by relating chemical potential to bulk phase properties (62). The expanded equation is given by

$$\hat{x}_i^l \gamma_i^l f_i^{ol} \exp\left\{\int \frac{\Delta v dP}{RT}\right\} = \hat{x}_i^s \gamma_i^s f_i^{os} \quad (1.2)$$

Here, \hat{x}_i^l and \hat{x}_i^s are the mole fractions, γ_i^l and γ_i^s are the activity coefficients, and f_i^{ol} and f_i^{os} are the pure component standard state fugacities of component i in the liquid and solid phases, respectively. The exponential term accounts for the effect of pressure on the liquid phase fugacity as the pressure departs from the standard state. Here, P is pressure, R is the universal gas constant, T is temperature and v is molar volume. The ratio of the standard state fugacities is given by

$$\frac{f_i^{ol}}{f_i^{os}} = \exp\left\{\frac{\Delta H_i^f}{RT}\left(1 - \frac{T}{T_i^f}\right)\right\} \quad (1.3)$$

where ΔH_i^f is the molar heat of fusion and T_i^f is the melting point of component i . Eq. 1.3 is substituted into Eq. 1.1 to obtain an expression for the equilibrium ratio of component i , K_i ,

$$K_i = \frac{\hat{x}_i^s}{\hat{x}_i^l} = \frac{\gamma_i^l}{\gamma_i^s} \exp\left\{\frac{\Delta H_i^f}{RT}\left(1 - \frac{T}{T_i^f}\right) + \int \frac{\Delta v dP}{RT}\right\} \quad (1.4)$$

Once the equilibrium ratios are known, the amounts and composition of the solid-liquid mixture can be calculated in the same manner as a flash calculation. The only other required data is the feed composition. The equilibrium calculation is discussed in greater detail in Appendix B.

Nearly all thermodynamic models use some variation of Eq. 1.4. The models differ in the treatment of the asphaltenes in the feed composition and in the calculation of the activity coefficients. Note that the effect of micelles is not accounted for in Eq. 1.4 and, in fact, almost all of the existing thermodynamic models only apply to situations where no micelles have formed.

The first thermodynamic model (63) treated asphaltenes as a single lumped fraction of the oil and used Scatchard-Hildebrand solubility theory together with a Flory-Huggins entropy of mixing term to calculate the activity coefficient of the asphaltenes in the liquid phase. The precipitated asphaltenes were assumed to be a pure pseudo-liquid polymer phase with an activity coefficient of unity. The heat of fusion term was neglected because, for a two liquid phase system, the ratio of the standard state fugacities given in Eq. 1.3 is unity and hence the heat of fusion term is zero. The derivation of the expression for the activity coefficient is performed in Appendix B and applies to low concentrations of asphaltenes. The activity coefficient is given by

$$\gamma_A^l = \exp \left\{ 1 - \frac{v_A^l}{v_m^l} + \ln \frac{v_A^l}{v_m^l} + \frac{v_A^l}{RT} (\delta_A^l - \delta_m^l)^2 \right\} \quad (1.5)$$

Here, v_A^l and v_m^l are the molar volumes and δ_A^l and δ_m^l are the solubility parameters of the asphaltenes and the solvent mixture, respectively, all in the liquid phase. The molar volumes and the solubility parameters of each constituent are usually calculated from equations of state (64). The molar volume is an implicit function of temperature and pressure in any equation of state. Heats of vaporization, ΔH_i^{vap} , can also be determined from an equation of state and are employed to calculate the solubility parameter. The solubility parameter is defined as

$$\delta_i^l = \left(\frac{\Delta H_i^{vap} - RT}{v_i^l} \right)^2 \quad (1.6)$$

This type of model successfully predicts wax precipitation when the wax is treated as a solid phase and the heat of fusion term is included (65). The model (excluding the heat of fusion term) predicts the onset of asphaltene precipitation with some success but does not accurately predict the amount of precipitated material.

The thermodynamic model was improved by recognizing that asphaltenes are not a uniform material but include a range of molar masses. With this approach, the asphaltenes are treated as collection of subfractions of different molar mass each with its own equilibrium ratio. In some cases, the equilibrium ratio was calculated using Eq. 1.5 (66). In others cases, different equations describing the solubility parameter term (the last term in Eq. 1.5) have been attempted (67). For example, the following equation accounts for an interaction energy between the asphaltenes and the solvent that departs from the geometric mean of the pure component interaction energies.

$$\gamma'_A = \exp \left\{ 1 - \frac{v'_A}{v'_m} + \ln \frac{v'_A}{v'_m} + \frac{v'_A}{RT} \left[(\delta'_A - \delta'_m)^2 + 2k_{Ai} \delta'_A \delta'_m \right] \right\} \quad (1.7)$$

Here, k_{Ai} , is an interaction parameter between the asphaltenes and the solvent. The basis of Eq. 1.7 is discussed in Appendix B. Yet another model also accounts for a distribution of asphaltene molar masses and assumes that the precipitate is a true solid phase (75). In this case, Eq. 1.5 is employed together with the heat of fusion term from Eq. 1.3. One potential drawback of the above approaches is that the asphaltenes are assumed to precipitate as a relatively pure phase where the “solid” phase activity coefficients do not vary significantly from unity.

Solid phase activity coefficients have been developed to predict wax precipitation (68) and have been tested on asphaltene solubility (69). The solid and liquid phase coefficients were combined as follows

$$\frac{\gamma'_i}{\gamma^s_i} = \exp \left\{ \frac{v'_i}{RT} (\delta'_i - \delta'_m)^2 - \frac{v^s_i}{RT} (\delta^s_i - \delta^s_m)^2 \right\} \quad (1.8)$$

Eq. 1.8 does not include the entropic effects of mixing large molecules, that is, the Flory-Huggins term. In effect, it is assumed that all the molecular interactions are between like sized molecules. This implicit assumption is nearly true of the “solid” phase if the phase

consisted only of asphaltenes but it is certainly not true of most liquid oil phases. Furthermore, if the “solid” phase consisted only of asphaltenes, with their broadly similar chemical nature, the solid phase activity coefficients are not likely to depart significantly from unity. Hence, solid phase activity coefficients are only likely to play a significant role if the solid phase includes solvent, that is, if the “solid” phase is really another liquid phase.

A model has been developed that treats the precipitate as a liquid or highly solvated solid (23,70). In this model, the solvent is assumed to be a nearly pure phase with an activity coefficient near unity. Instead of using Eq. 1.4, the asphaltene volume fraction in the “solid” phase, ϕ_A^s , is determined from the equilibrium condition of the solvent in the liquid and solid phases. A variation of the Scatchard-Hildebrand/Flory-Huggins approach is used to solve for the solid phase activity coefficient and the following expression is found

$$\ln(1 - \phi_A^s) + \left(1 - \frac{v_m^s}{v_A^s}\right)\phi_A^s + \frac{v_m^s}{RT}(\delta_A^s - \delta_m^s)^2(\phi_A^s)^2 = 0 \quad (1.9)$$

In this case, the asphaltenes are treated as a lumped component and any effect of the variation of molar mass is ignored.

The variety of the thermodynamic approaches reflects the long-standing limited understanding of asphaltene behavior. None of the above approaches includes the effect of micelles and still there is little agreement on the nature of the precipitating phase. The nature of the precipitating phase can have a significant impact on the model predictions. If the precipitating phase is a pure “pseudo-liquid”, the existing thermodynamic models are adequate for the non-micelle regime. The only difficulty in applying the model is to determine the molar mass, molar volume and solubility parameter of the asphaltenes. However, if the precipitating phase is a second liquid phase, it is a mixture of asphaltenes and solvent. Hence, a “solid” phase activity coefficient may be required. If the asphaltenes precipitate as a true solid, the heat of fusion term must be included.

The omission of micelle thermodynamics can also be significant. For example there is often a significant difference between the amount of asphaltenes that precipitates from a crude oil in a given volume of solvent and the amount that will redissolve in the same volume of solvent (71). The hysteresis shown in Fig. 1.21 may well be caused by the presence of asphaltene micelles or possibly colloids. None of the existing thermodynamic models are capable of predicting the hysteresis. In short, while the thermodynamic models show promise there is considerable work to be done in determining the nature of the precipitating phase and the effect of micelles.

Steric-Colloidal Model: In the steric-colloidal model, a colloidal aggregate of asphaltene molecules is stabilized by resins or some other polar molecules (72). When there are insufficient resins to cover all the colloids, the colloids flocculate and precipitate. Hence, the precipitation is governed by the chemical potential of the resins rather than the asphaltenes. The expression for the chemical potential of the resins is the same as that for the asphaltenes,

$$\Delta\mu_R^l = RT \left[\ln\{\phi_R^l\} - \left(\frac{v_R^l}{v_m^l} - 1 \right) (1 - \phi_R^l) + \frac{v_R^l}{RT} (1 - \phi_R^l)^2 (\delta_R^l - \delta_m^l)^2 \right] \quad (1.10)$$

The expression as given is valid for all resin concentrations. In contrast, the simplified expression used for the asphaltene activity coefficient is valid only at low asphaltene concentrations. To determine the onset of asphaltene precipitation it is also necessary to find the critical chemical potential for the resins, $\Delta\mu_R^{cr}$, where the amount of resins adsorbed on the asphaltenes is just sufficient to stabilize the asphaltenes. When $\Delta\mu_R^l > \Delta\mu_R^{cr}$, the asphaltenes are stabilized and, when $\Delta\mu_R^l < \Delta\mu_R^{cr}$, the asphaltenes precipitate. In order to determine $\Delta\mu_R^{cr}$, it is necessary to predict the adsorption of resins on the asphaltene colloids and develop a flocculation model. A fractal aggregation model has been developed to handle the flocculation aspects of the steric-colloidal model (61,73).

The complexity of the steric-colloidal model renders it difficult to implement and the number of parameters involved raises questions as to its utility. To date, the predictive power of the model has not been tested and the underlying parameters have not been experimentally verified (23). Nonetheless, if asphaltenes are colloidal rather than micellar, the steric-colloidal model is the most likely route to understanding asphaltene phase behavior. And if asphaltenes are micellar, some aspects of the steric-colloidal model may yet prove useful, for example, the flocculation theory. Hence both thermodynamic and steric-colloidal models may be required to predict asphaltene solubility.

Issues in Solubility Modeling: There is strong evidence that asphaltenes associate into either colloids or micelles. Until it is discovered which structure is correct, solubility models are at best educated guesses. Nonetheless, a few points can be made about the existing models. Most existing thermodynamic models require few parameters and are relatively easy to implement. However, they are only valid in situations where micelles or colloids have not formed. To predict the effect of micelles, some ideas from the steric-colloidal model may need to be incorporated into the thermodynamic model. In fact, some models already combine aspects of the thermodynamic and steric-colloidal models (74,75). Unfortunately, steric-colloidal models require a large number of parameters many of which are difficult to evaluate experimentally. Therefore, the models are cumbersome and of limited utility.

The first priority for solubility models must be to determine the nature of the asphaltene aggregates. Then, it may be necessary to refine the existing steric-colloidal models or to develop hybrid micellar models. Either approach will likely produce unwieldy multiparameter models only useful as a bridge to understanding the mechanisms of asphaltene aggregation. An alternative may be to seek simplified models that only capture some asphaltene behavior but nonetheless give good predictions over given ranges of composition, temperature and pressure.

1.3.6 Relevance of Asphaltene Chemistry to Emulsions

The overall view of asphaltenes that emerges from the above summary is that asphaltenes are a mixture of hundreds or thousands of homologous series each containing 1 to 6 aromatic rings, several short alkyl chains and a variety of heteroatoms. The asphaltene mixture includes acidic, basic, amphoteric and neutral species and the molar masses of the various species range from 1000 to 10000 g/mol. Not surprisingly, given the range of molecular species encompassed in the asphaltene solubility class, asphaltenes exhibit complex and poorly understood phase behavior and may exist in an oil as solid particles, colloids, micelles or non-associated molecules.

It is not known which asphaltene phase is responsible for stabilizing emulsions. There are several equally likely possibilities: asphaltene particles, precipitation point asphaltenes, or asphaltene surfactants. Rheological studies of the interfaces of water-in-oil emulsions stabilized by asphaltenes appear to show the presence of solid particles (76,77). Electron micrography also indicates the presence of particles on the interface, although the particles may form during the freezing of the sample (78). The material on the interface could be asphaltene colloids, micelles or solid particles. However, there is evidence that emulsion stability is related to the asphaltene precipitation point (1) and hence asphaltene molecules on the verge of precipitation may act as emulsion stabilizers. Asphaltenes near the precipitation point are more likely to adsorb strongly on an interface and form a long lasting barrier to coalescence. Finally, the acidic, basic and amphoteric asphaltene species are capable of acting as surfactants and hence can potentially stabilize water-in-oil emulsions. Therefore, the first question in examining asphaltene stabilized emulsions should be: what phase of the asphaltenes is acting as a stabilizer?

1.4 References

1. Eley, D.D., Hey, M.J., and Symonds, J.D., *Colloids Surfaces.*, **32**, (1988), 87.
2. Strausz, O.P., in "AOSTRA Technical Handbook of Oil Sands, Bitumen and Heavy Oils", Ed. L.G. Hepler and C. Hsi, AOSTRA Technical Publications Series #6, Edmonton, 1989.

3. Long, Y., Tipman, R.N., Tran, T., "Studies on Froth Water and Solids Removal from Froth to Enhance Diluted Bitumen Quality", Syncrude Internal Report, Edmonton, Nov., 1994.
4. Israelachvili, J., *Colloids Surfaces*, **91**, (1994), 1.
5. Masliyah, J.H., "Electrokinetic Transport Phenomena", AOSTRA Technical Publication Series #12, Alberta Oil Sands Information Services, Calgary 1994.
6. Tadros, T.F., and Vincent, B., in "Encyclopedia of Emulsion Technology", Vol.1, Ed. P. Becher, Marcel Dekker Inc., New York, 1983, p. 129.
7. Israelachvili, J., "Intermolecular & Surface Forces", 2nd Ed., Academic Press, London, 1992.
8. Russel, W.B., Saville, D.A., and Schowalter, W.R., "Colloidal Dispersions", Cambridge University Press, Cambridge, 1989.
9. Adamson, A.W., "Physical Chemistry of Surfaces", 2nd Ed., Interscience Publishers, John Wiley & Sons, New York, 1967.
10. Ross, S., and Morrison, I.D., "Colloidal Systems and Interfaces", John Wiley & Sons, New York, 1988.
11. Hiemenz, P.C., "Principles of Colloid and Surface Chemistry", 2nd Ed., Marcel Dekker, Inc., New York, 1986.
12. Sanders, R.S.S., "Deposition of Emulsions in an Impinging Jet Cell", PhD Thesis, University of Alberta, 1997.
13. Sjöblom, J., Mingyuan, H., Höiland, H, and Johansen, E.J., *Colloids Surfaces*, **46**, (1990), 127.
14. Puskás, S., Balázs, J., Farkas, A., Regdon, I., Berkesi, O., Dékány, I., *Colloids Surfaces A*, **113**, (1996), 279.
15. Yan, N., Masliyah, J.H., *Colloids Surfaces A*, **96**, (1995), 229.
16. Shelfantook, W.E., Syncrude Canada Ltd., private communication, 1997.
17. Dabros, T., Western Research Centre, Canada Centre for Mineral and Energy Technology (CANMET), private communication, 1997.
18. Yeung, T., Department of Chemical and Materials Engineering, University of Alberta, private communication, 1997.
19. Gray, M.R., "Upgrading Petroleum Residues and Heavy Oils", Marcel Dekker, Inc., New York, N.Y., 1994.
20. Speight, J.G., in "Asphaltenes and Asphalts, 1", Ed. T.F. Yen and G.V. Chilingarian, Elsevier Science, Amsterdam, 1994, p. 7.

21. Speight, J.G., *The Chemistry and Technology of Petroleum*, Marcel Dekker, New York, N.Y., 1980.
22. Koots, J.A., and Speight, J.G., *Fuel*, **54**, (1975), 179.
23. Cimino, R., Corraera, S., Del Bianco, A., in "Asphaltenes Fundamentals and Applications", Ed. E.Y. Sheu and O.C. Mullins, Plenum Press, New York, 1995, p. 97.
24. Christy, A.A., Dahl, B., Kvalheim, M., *Fuel*, **68**, (1989), 430.
25. Semple, K.M., Cyr, N., Fedorak, P.M., and Westlake, D.W.S., *Can. J. Chem.*, **68**, (1990), 1092.
26. Brons, G., *Energy Fuels*, **9**, 1995, 641.
27. Speight, J.G., *Alberta Res. Counc. Inf. Ser.*, No. 81, 1978.
28. Cyr, N., McIntyre, D.D., Toth, G., and Strausz, O.P., *Fuel*, **66**, (1987), 1709.
29. Pfeiffer, J.Ph., and Saal, R.N.J., *J. Phys. Chem.*, **44**, (1940), 139.
30. Speight, J.G., *Applied Spectroscopic Reviews*, **5**, (1972), 211.
31. Yen, T.F., *Preprints, Div. Petr. Chem., ACS*, **17**(4), (1972), F102.
32. Speight, J.G., *Preprints, Div. Petr. Chem., ACS*, **24**, (1979), 910.
33. Strausz, O.P., Mojelsky, T.W., Lown, E.M., *Fuel*, **71**, (1992), 1355.
34. Speight, J.G., *Preprints, Div. Petr. Chem., ACS*, **34**, (1989), 321.
35. Ignaziak, T.M., Kemp-Jones, A.V., and Stausz, O.P., *J. Org. Chem.*, **42**, (1977), 312.
36. Rubenstein, I., and Strausz, O.P., *Geochim. Cosmochim. Acta*, **43**, (1979), 1887.
37. Ritchie, R., Roche, R.S., and Steedman, W., *Fuel*, **58**, (1979), 523.
38. El-Mohammed, S., Ackard, M.A., Hardouin, F., and Gasparoux, H., *Fuel*, **65**, (1986), 1501.
39. Yokota, T., Scriven, F., Montgomery, D.S., and Strausz, O.P., *Fuel*, **65**, (1986), 1142.
40. Mojelsky, T.W., Montgomery, D.S., and Strausz, O.P., *AOSTRA J. Res.*, **2**, (1986), 177.
41. Bestougeff, M.A., Byramjee, R.J., in "Asphaltenes and Asphalts, 1", Ed. T.F. Yen and G.V. Chilingarian, Elsevier Science, Amsterdam, 1994, p. 67.
42. Kokal, S., Tang, T., Schramm, L., and Sayegh, S., *Colloids Surfaces*, **94**, (1995), 253.

43. González, G., and Moriera, M.B.C., in "Asphaltenes and Asphalts, 1", Ed. T.F. Yen and G.V. Chilingarian, Elsevier Science, Amsterdam, 1994, p. 207.
44. Acevedo, S., Escobar, G., Gutiérrez, L.B., and Rivas, H., *Fuel*, **71**, (1992), 619.
45. Sheu, E.Y., De Tar, M.M., and Storm, D.A., *Fuel*, **71**, (1992), 1277.
46. Kiselow, V., *Neftekhimiya*, **19**, (1979), 714.
47. Speight, J.G., *Preprint, Div. Petr. Chem., ACS*, **31**, (1986), 818.
48. Yen, T.F., in "Asphaltenes and Asphalts, 1", Ed. T.F. Yen and G.V. Chilingarian, Elsevier Science, Amsterdam, 1994, p. 111.
49. Moschopedis, S.E., Fryer, J.F., and Speight, J.G., *Fuel*, **55**, (1976), 227.
50. Champagne, P.J., Manolakis, E., and Ternan, M., *Fuel*, **64**, (1985), 423.
51. Larsen, J.W., and Li, S., *Energy Fuels*, **9**, (1995), 760.
52. Nellensteyn, F.J., *J. Inst. Pet. Technol.*, **10**, (1924), 311.
53. Swanson, J., *J. Chem. Phys.*, **46**, (1942), 141.
54. Witherspoon, P.A., and Munir, Z.A., *Prod. Mon.*, **25**, (1960), 20.
55. Sheu, E.Y., De Tar, M.M., Storm, D.A., and DeCanio, S.J., *Fuel*, **71**, (1992), 299.
56. Dickie, J.P., and Yen, T.F., *Anal. Chem.*, **39**, (1967), 1847.
57. Sheu, E.Y., Storm, D.A., De Tar, M.M., *J. Non-Crystalline Solids*, **131-133**, (1991), 341.
58. Xu, Y., Koga, Y., Strausz, O.P., *Fuel*, **74**, (1995), 960.
59. Sheu, E.Y., and Storm, D.A., in "Asphaltenes Fundamentals and Applications", Ed. E.Y. Sheu and O.C. Mullins, Plenum Press, New York, 1995, p. 1.
60. Speight, J.G., and Long, R.B., *Fuel Sci. Technol. Intl.*, **14**, (1996), 1.
61. Park, S.J., Escobedo, J., Mansoori, G.A., in "Asphaltenes and Asphalts, 1", Ed. T.F. Yen and G.V. Chilingarian, Elsevier Science, Amsterdam, 1994, p. 179.
62. Prausnitz, J.M., Lichtenthaler, R.N., and de Azevedo, E.G., "Molecular Thermodynamics of Fluid-Phase Equilibria", 2nd Ed., Prentice Hall, Englewood Cliffs, NJ, 1986.
63. Hirschberg, A., deJong, N.J., Schipper, B.A., and Meijer, J.G., *SPE J.*, **24**, (1984), 283.
64. Rassamdana, H., Dabir, B., Nematy, M., Farhani, M., and Sahimi, M., *AIChE J.*, **42**, (1996), 10.
65. Lira-Galeana, C., Firoozabadi, A., and Prausnitz, J.M., *AIChE J.*, **42**, (1996), 239.

66. Ferworn, K.A., and Svrcek, W.Y., *Proc. Can. Chem. Eng. Conf.*, Calgary, Oct. 1994.
67. Kawanaka, S.S., Park, S.J., and Mansoori, G.A., *SPE Res. Eng.*, **5**, (1991), 185.
68. Won, K.W., *Fluid Phase Equilibria*, **30**, (1986), 265.
69. Thomas, F.B., Bennion, D.B., Bennion, D.W., and Hunter, B.E., *J. Can. Pet. Technol.*, **31**(1), (1992), 22.
70. Cimino, R., Corraera, S., Sacomani, P.A., Spa, E., and Carniani, C., SPE 28993, *SPE Intl. Symp. Oilfield Chem.*, San Antonio, Feb. 1995.
71. Andersen, S.I., and Stenby, E.H., "Hysteresis in Asphaltene Precipitation and Redissolution", *Proc. Can. Chem. Eng. Conf.*, Calgary, Oct. 1994.
72. Leonaritis, K.J., and Mansoori, G.A., *SPE 16258, Proc. 1987 SPE Symp. Oilfield Chem.*, Richardson, Tex., (1987).
73. Islam, M.R., in "Asphaltenes and Asphalts, 1", Ed. T.F. Yen and G.V. Chilingarian, Elsevier Science, Amsterdam, 1994, p. 249.
74. Victorov, A.I., and Firoozabadi, A., *AIChE J.*, **42**, (1996), 1753.
75. Ferworn, K.A., "Thermodynamic and Kinetic Modelling of Asphaltene Precipitation from Heavy Oils and Bitumens", PhD Thesis, University of Calgary, 1995.
76. Eley, D.D., Hey, M.J., and Lee, M.A., *Colloids Surfaces A*, **24** (1987), 173.
77. Acevedo, S., Escobar, G., Gutiérrez, L.B., and Rivas, H., *Colloids Surfaces A*, **71** (1993), 65.
78. Eley, D.D., Hey, M.J., and Symonds, J.D., and Willison, J.H.M., *J. Colloid Interface Sci.*, **54**, (1976), 462.
79. Kabal'nov, A.S., and Shchukin, E.D., *Adv. Colloid Interface Sci.*, **38**, (1992), 69.
80. Sanders, S., and Masliyah, J., "Characteristics and Demulsification of Solids-Stabilized Emulsions: A Literature Survey and Summary", Report to OSLO Project Group, Department of Chemical Engineering, University of Alberta, 1990.

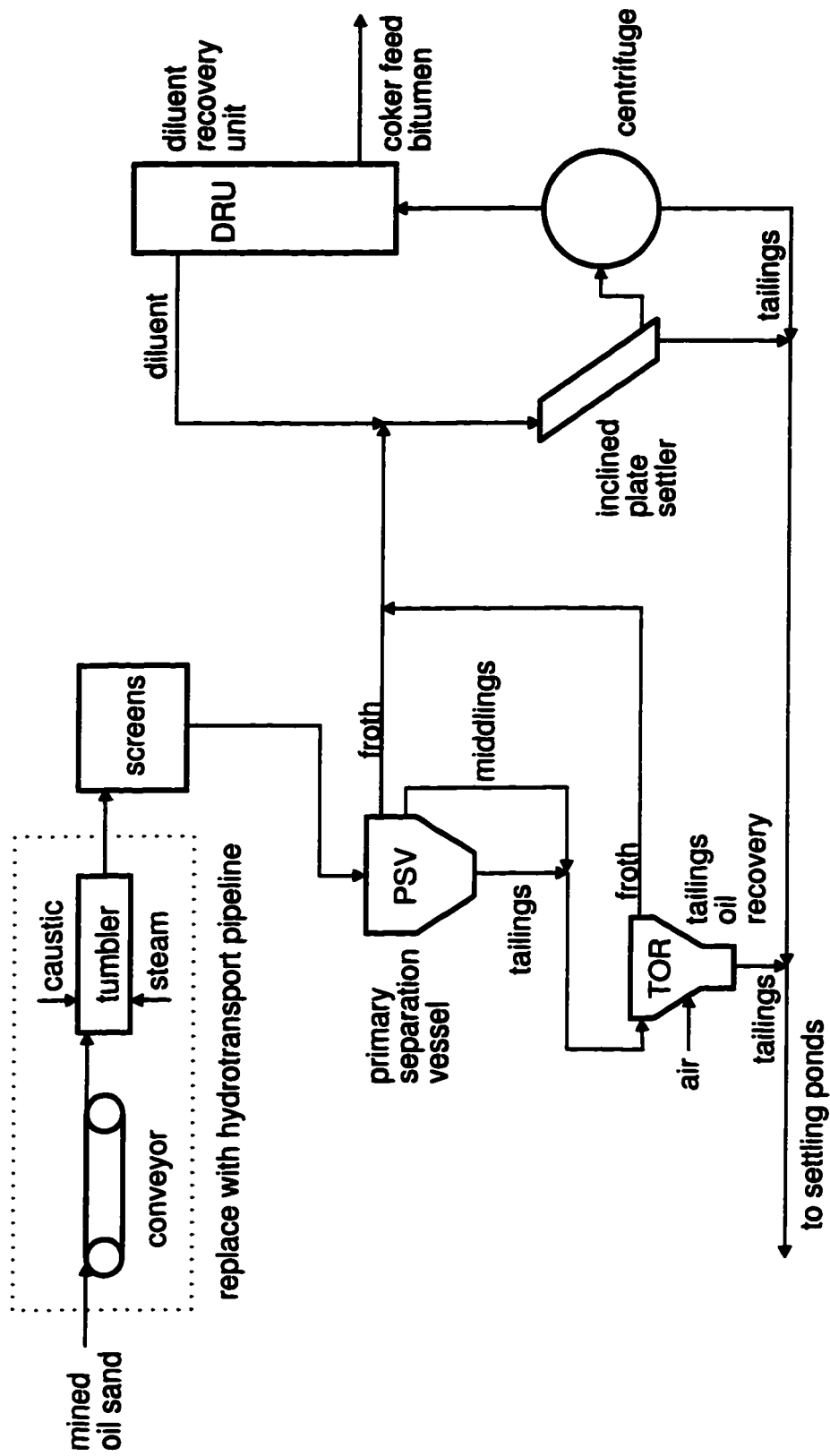


Figure 1.1: Schematic of typical bitumen extraction plant.

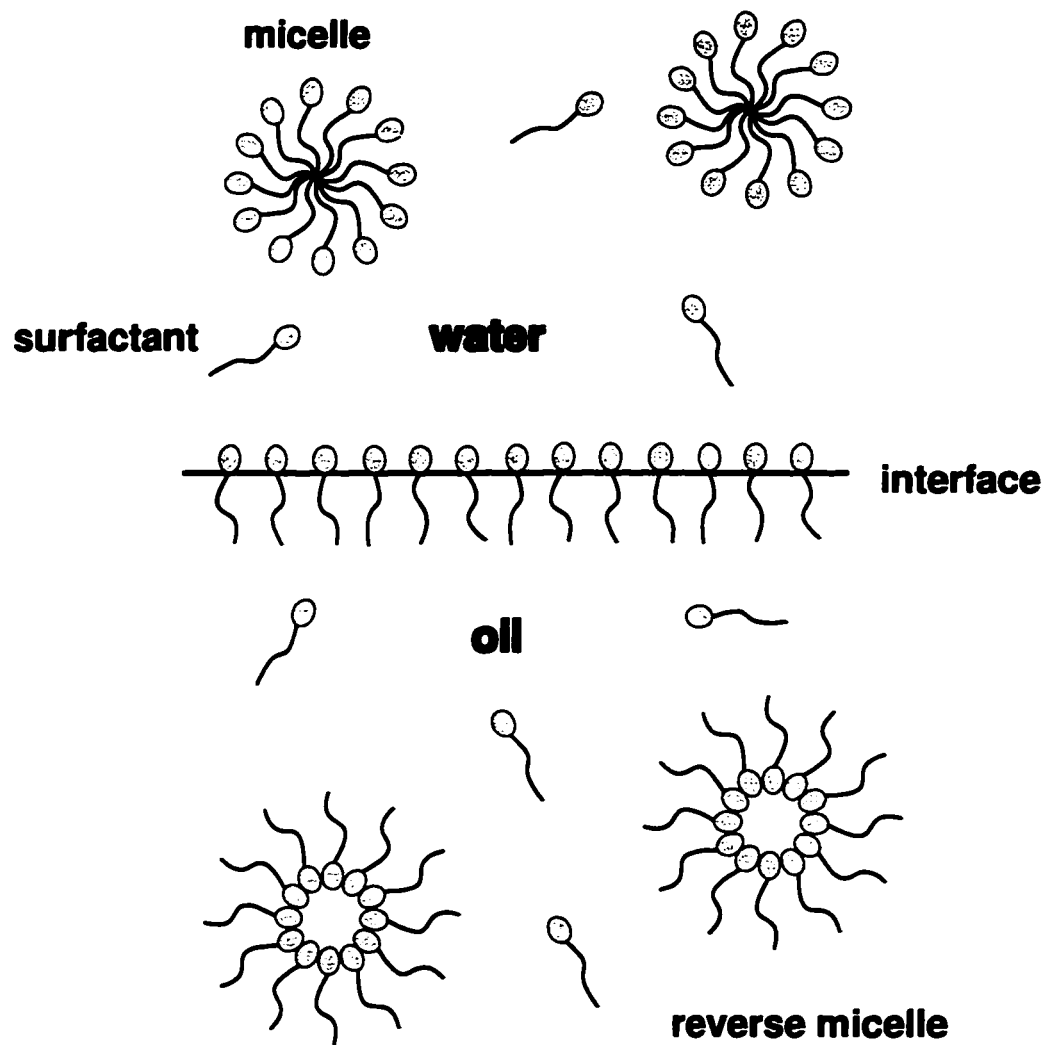
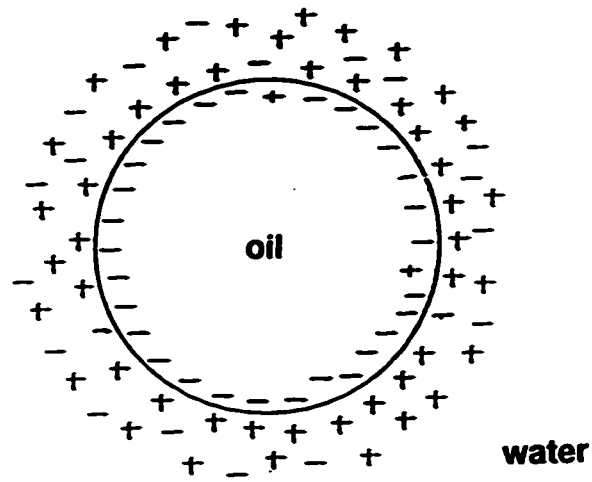
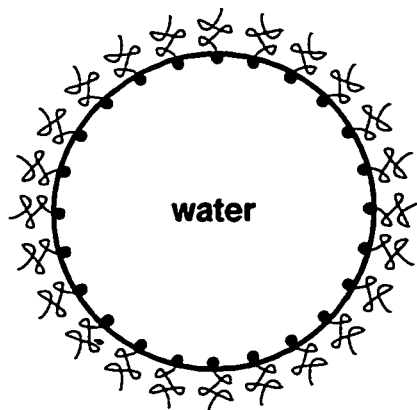


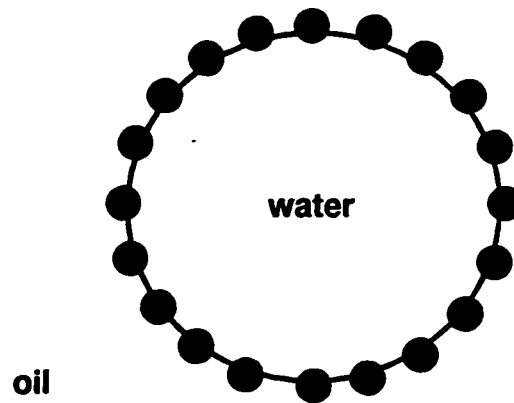
Figure 1.2: Some surfactant structures.



a) *Electrostatic Stabilization*



b) *Steric Stabilization
(Adsorbed Surfactant)*



c) *Steric Stabilization
(Adsorbed Solids)*

Figure 1.3: Electrostatic and steric stabilization of emulsions.

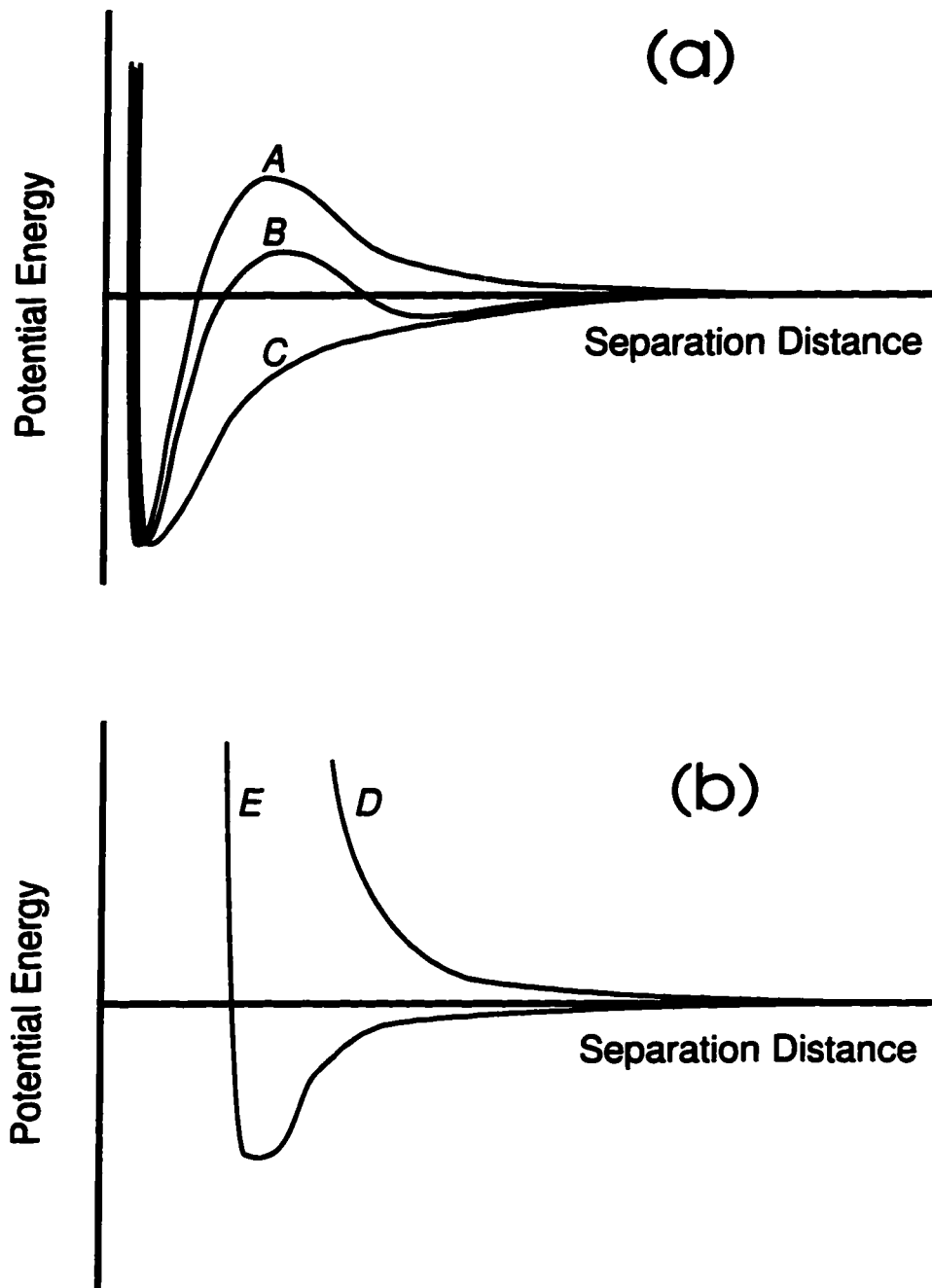


Figure 1.4: Potential energy curves between two droplets for (a) electrostatic and dispersion forces and (b) steric and dispersion forces (10,80).

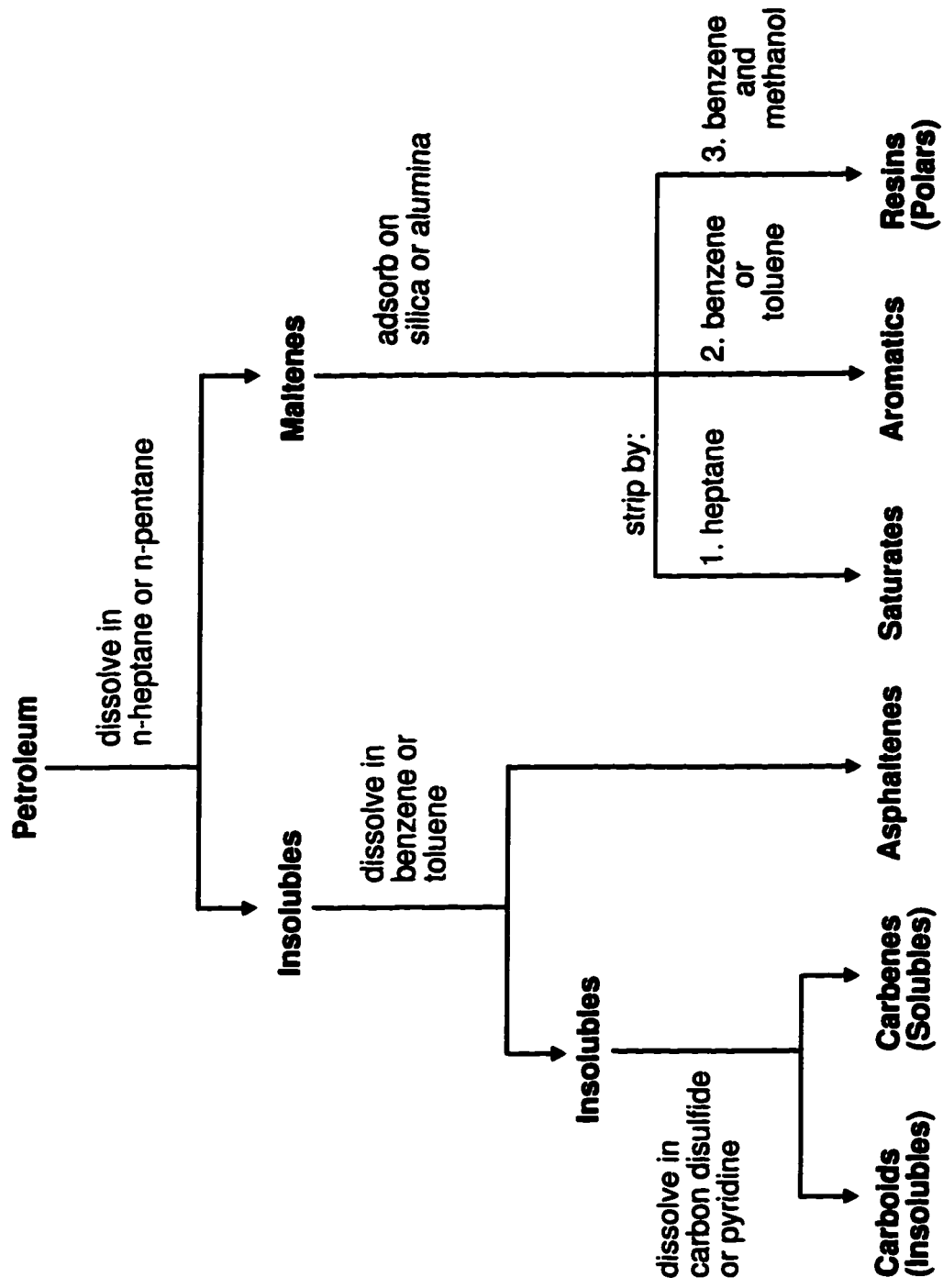
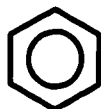
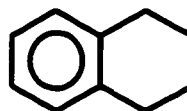
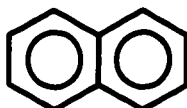
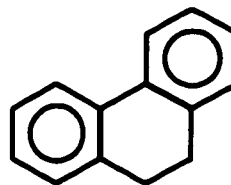
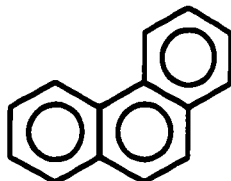
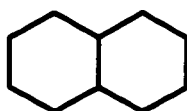
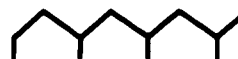
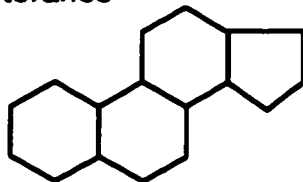


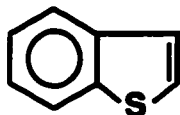
Figure 1.5: Simplified representation of separation of petroleum into six fractions (20).

Benzene**Tetralin
(1,2,3,4-tetrahydronaphthalene)****Naphthalene****9,10-Dihydrophenanthrene****Phenanthrene****a) Aromatics****b) Hydroaromatics****Decalin
(Decahydronaphthalene)****Isoprenoids****Steranes****Branched Alkanes****c) Naphthenes (Cyclics)****d) Paraffins****Figure 1.6:** Examples of hydrocarbon groups in petroleum.

Thiophene



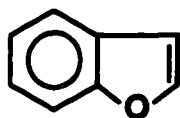
Benzothiophene



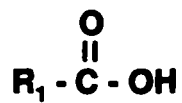
Thiol or Mercaptan



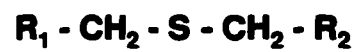
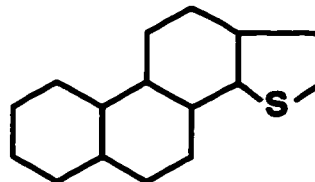
Benzofuran



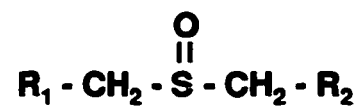
Carboxylic Acid



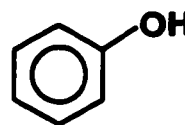
Sulfides or Thioethers



Sulfoxide



Phenol



Ketone

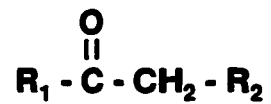
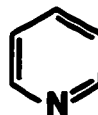


Figure 1.7: Examples of sulfur and oxygen groups in petroleum.

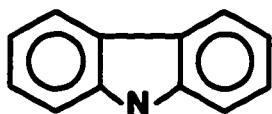
Pyrrole



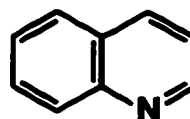
Pyridine



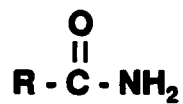
Carbazole



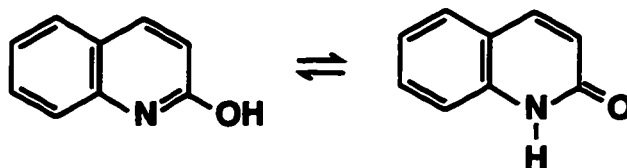
Quinoline



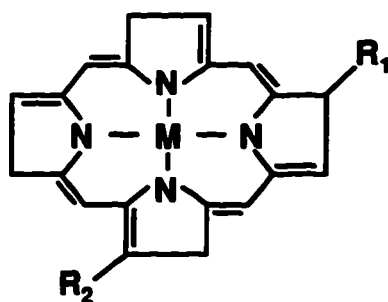
Amide



Quinolone



Porphyrin

**Figure 1.8:** Examples of nitrogen and metal groups in petroleum.

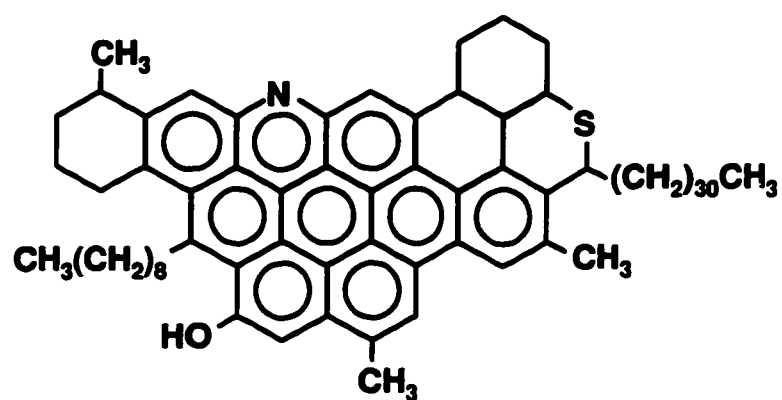


Figure 1.9: Example of condensed polynuclear model of an asphaltene molecule (34).

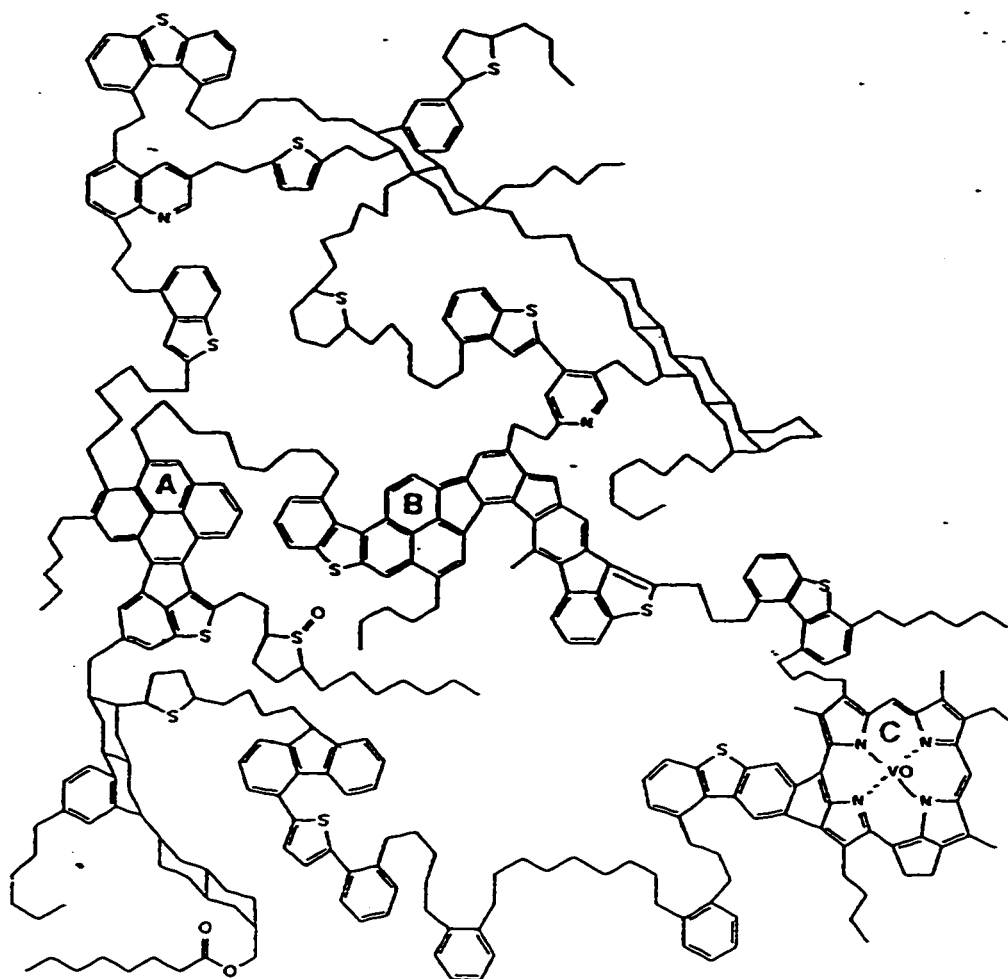


Figure 1.10: Hypothetical representation of an average Athabasca asphaltene molecule (33).

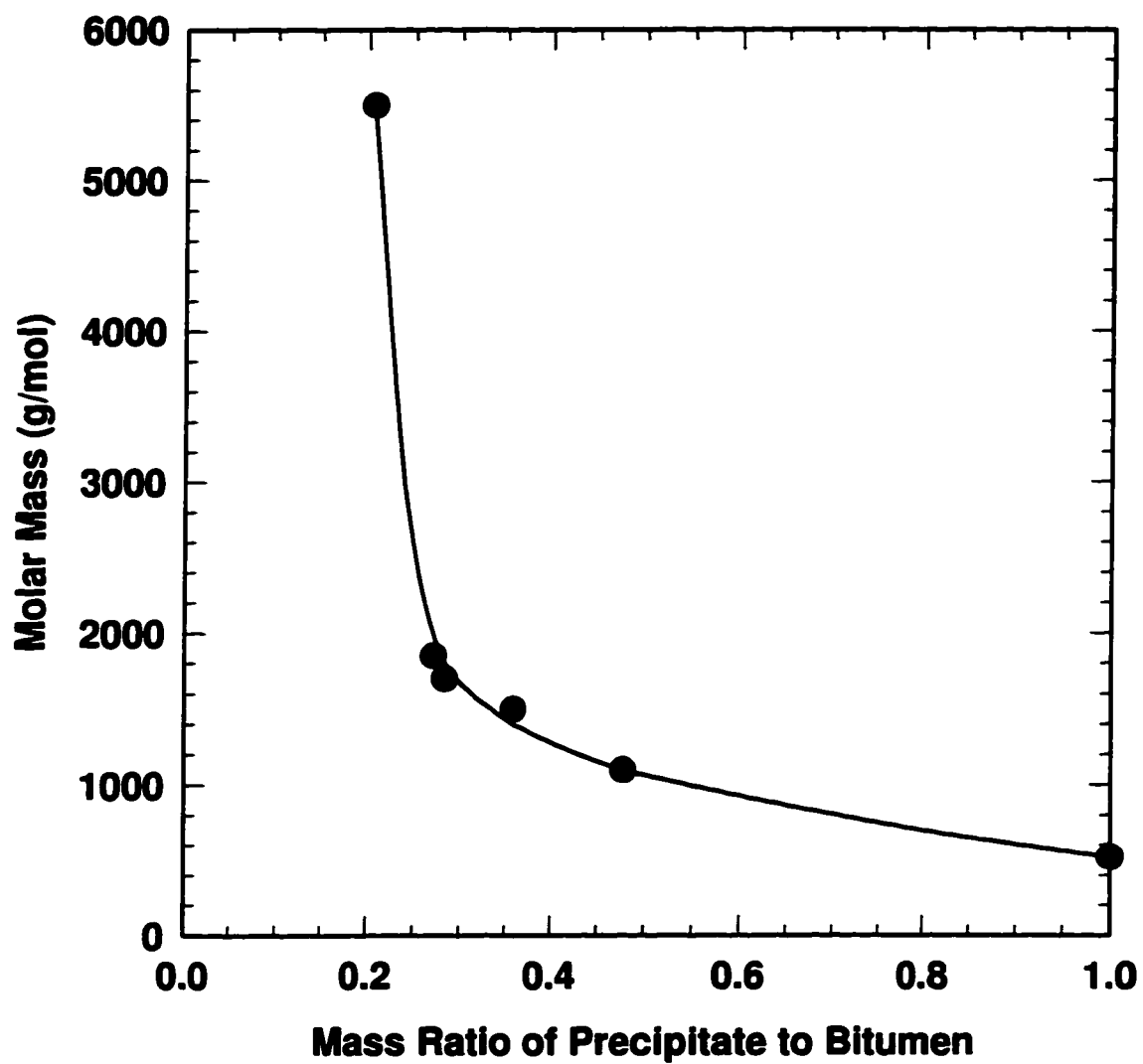


Figure 1.11: Molar mass of subfractions precipitated from Cold Lake bitumen (26).

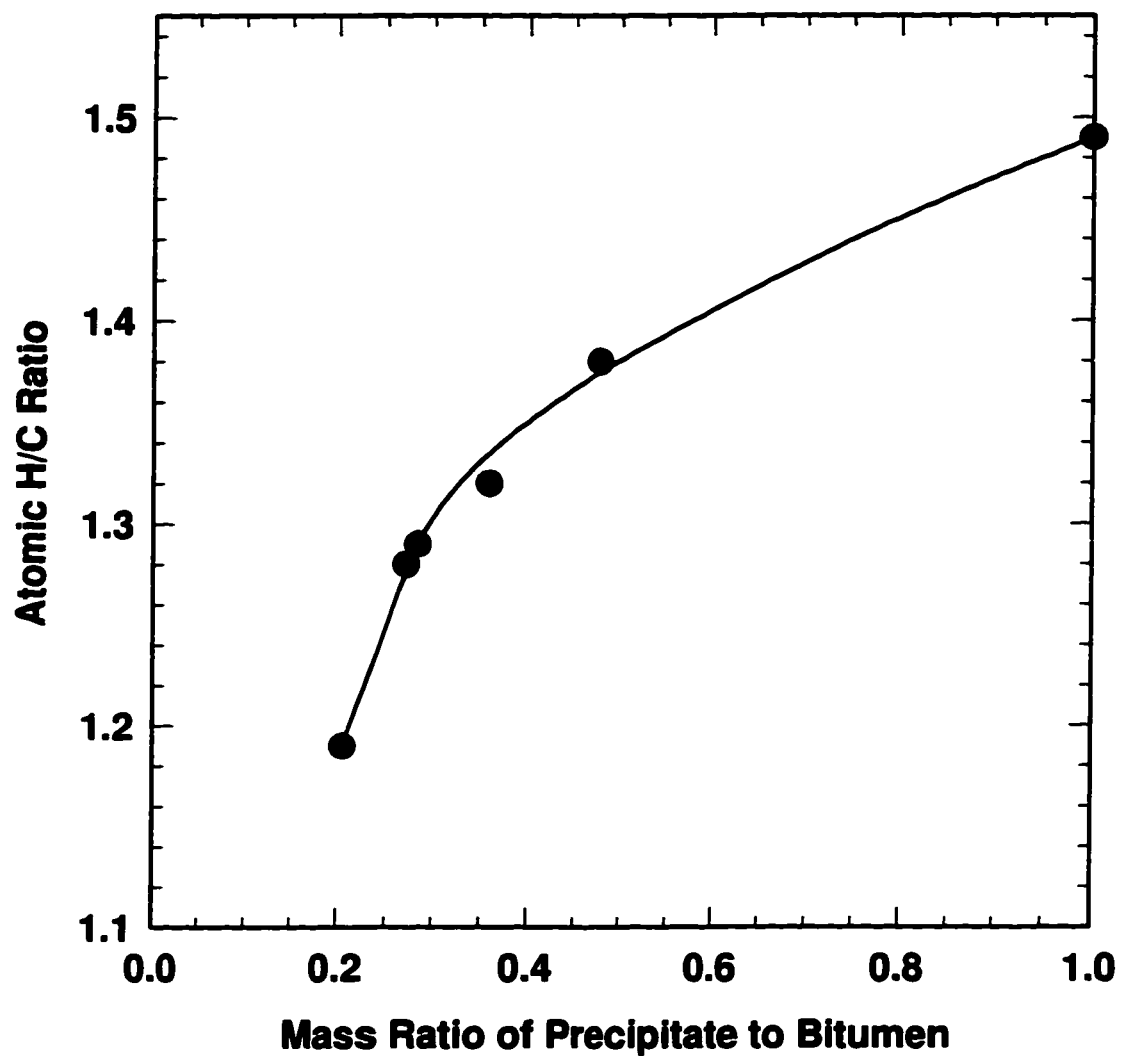


Figure 1.12: Atomic H/C ratio of subfractions precipitated from Cold Lake bitumen (26).

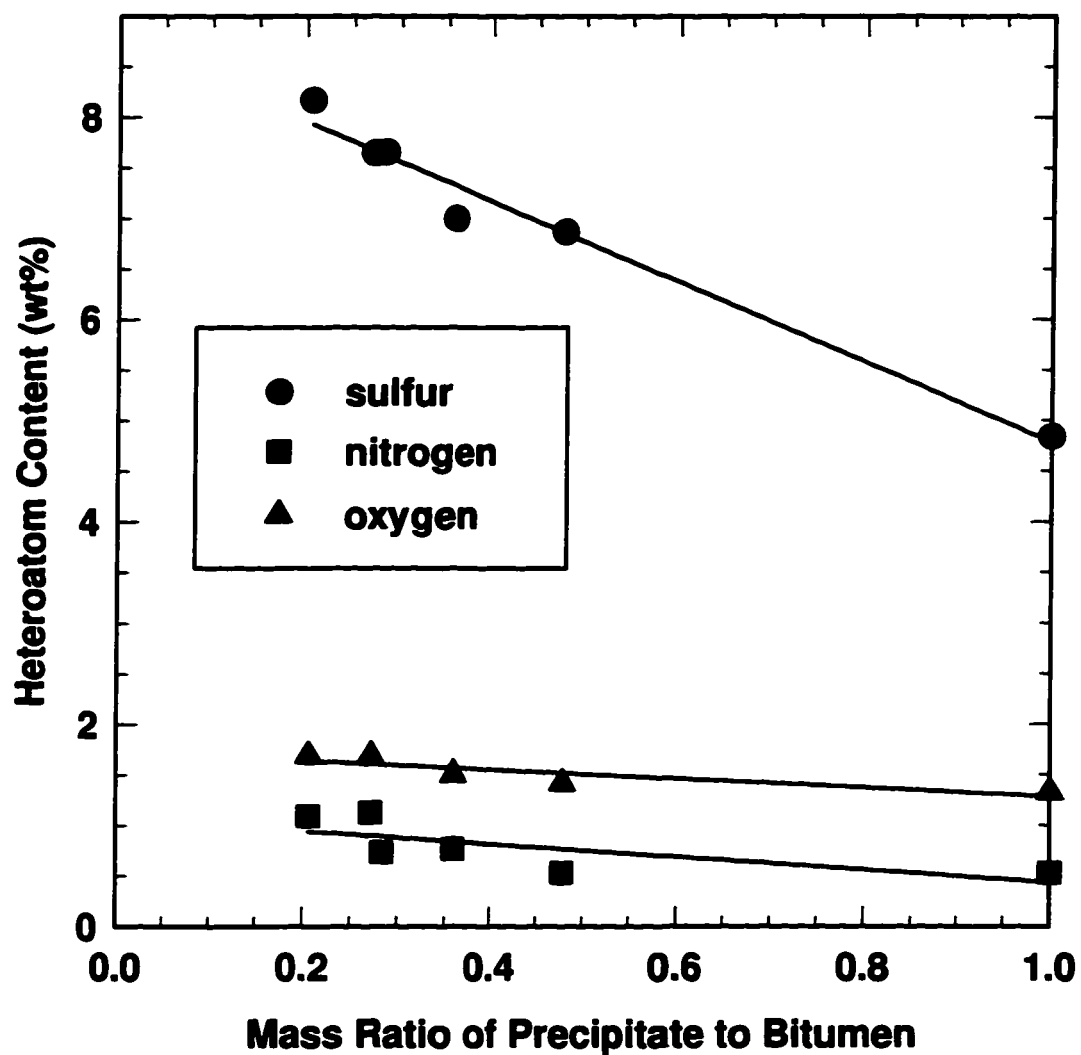


Figure 1.13: Heteroatom content of subfractions precipitated from Cold Lake bitumen (26).

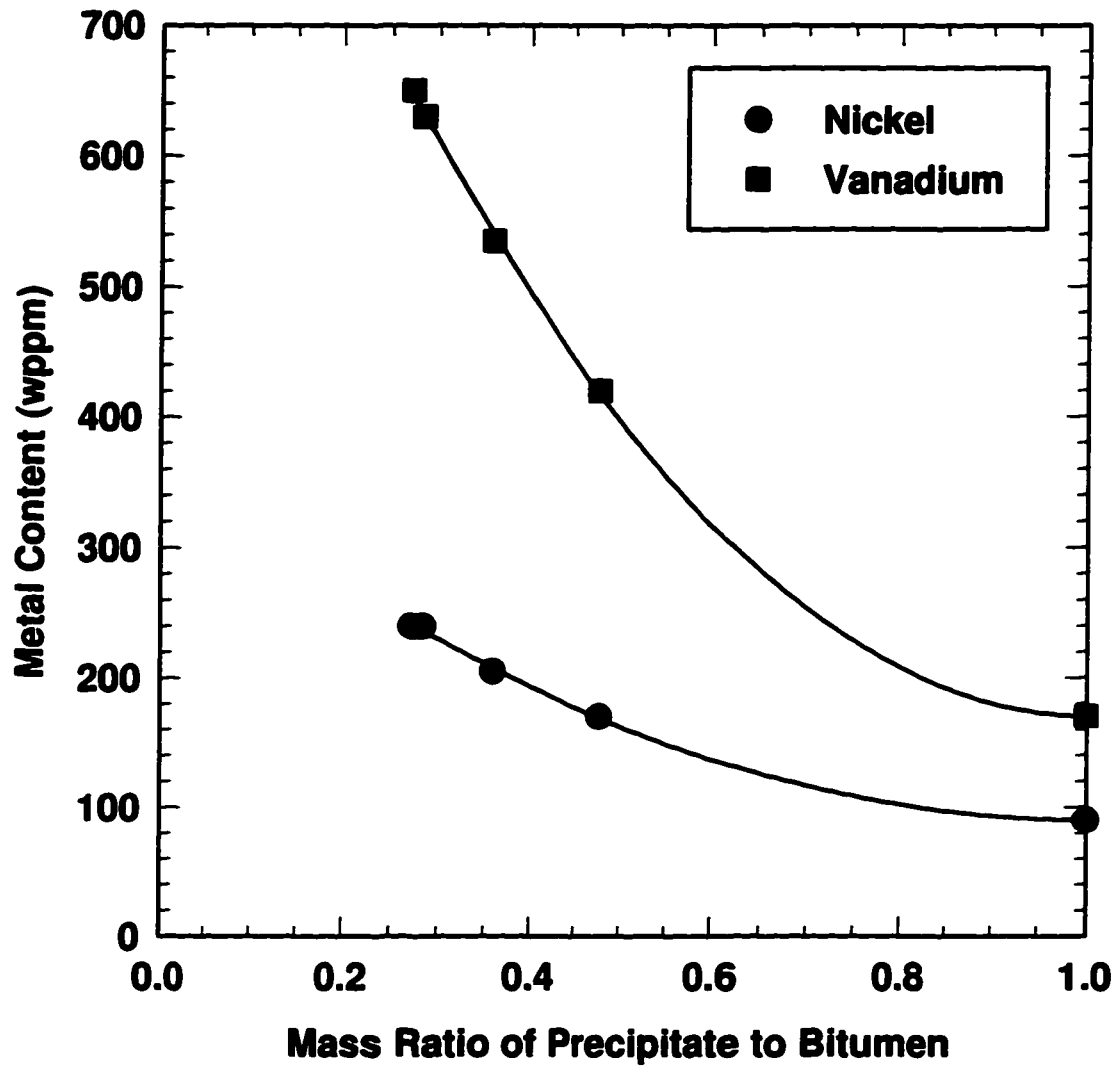


Figure 1.14: Metal content of subfractions precipitated from Cold Lake bitumen (26).

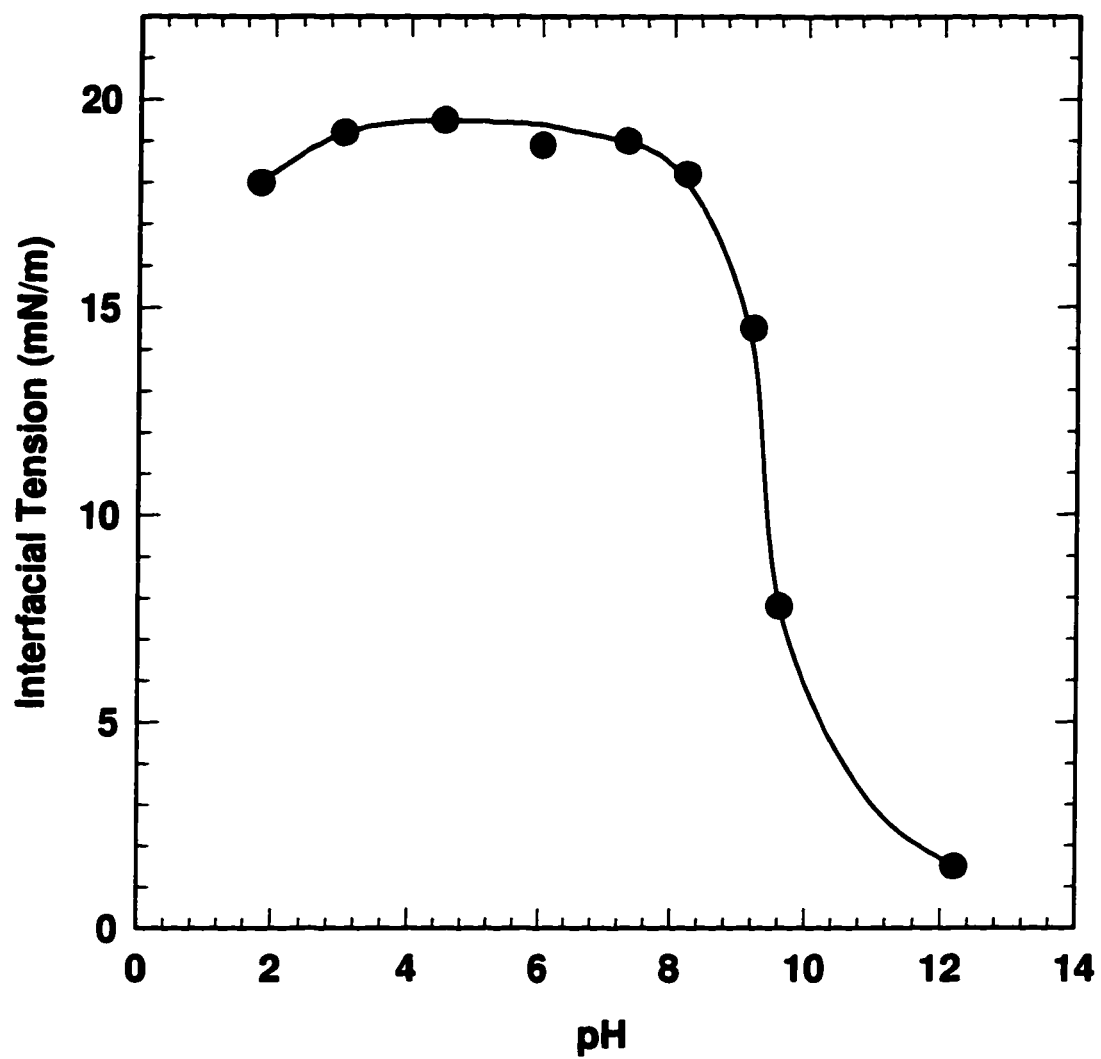


Figure 1.15: Interfacial tension of Cerro Negro asphaltene over water as a function of pH (44).

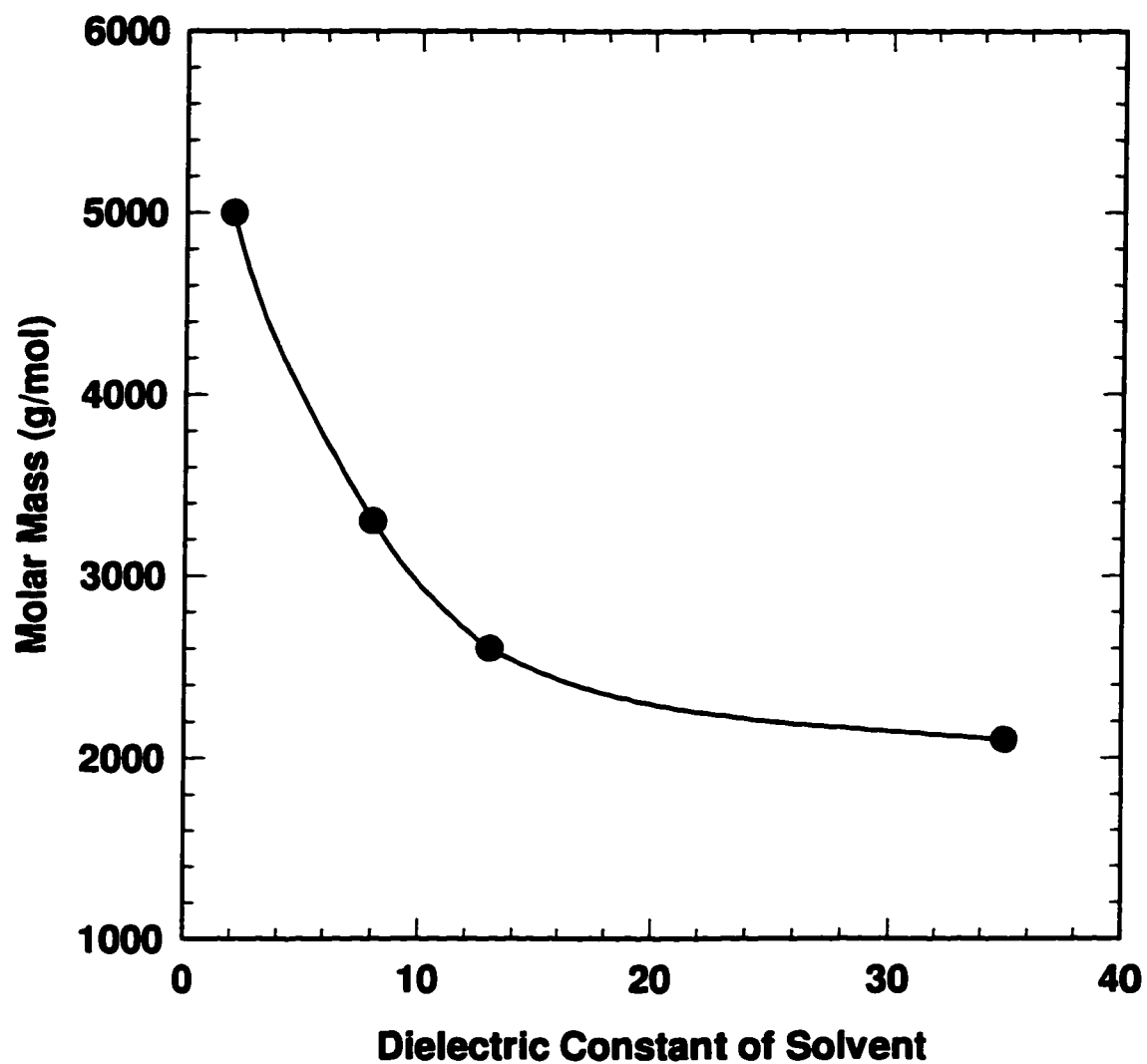


Figure 1.16: Effect of solvent on asphaltene molar mass measured by vpo (49).

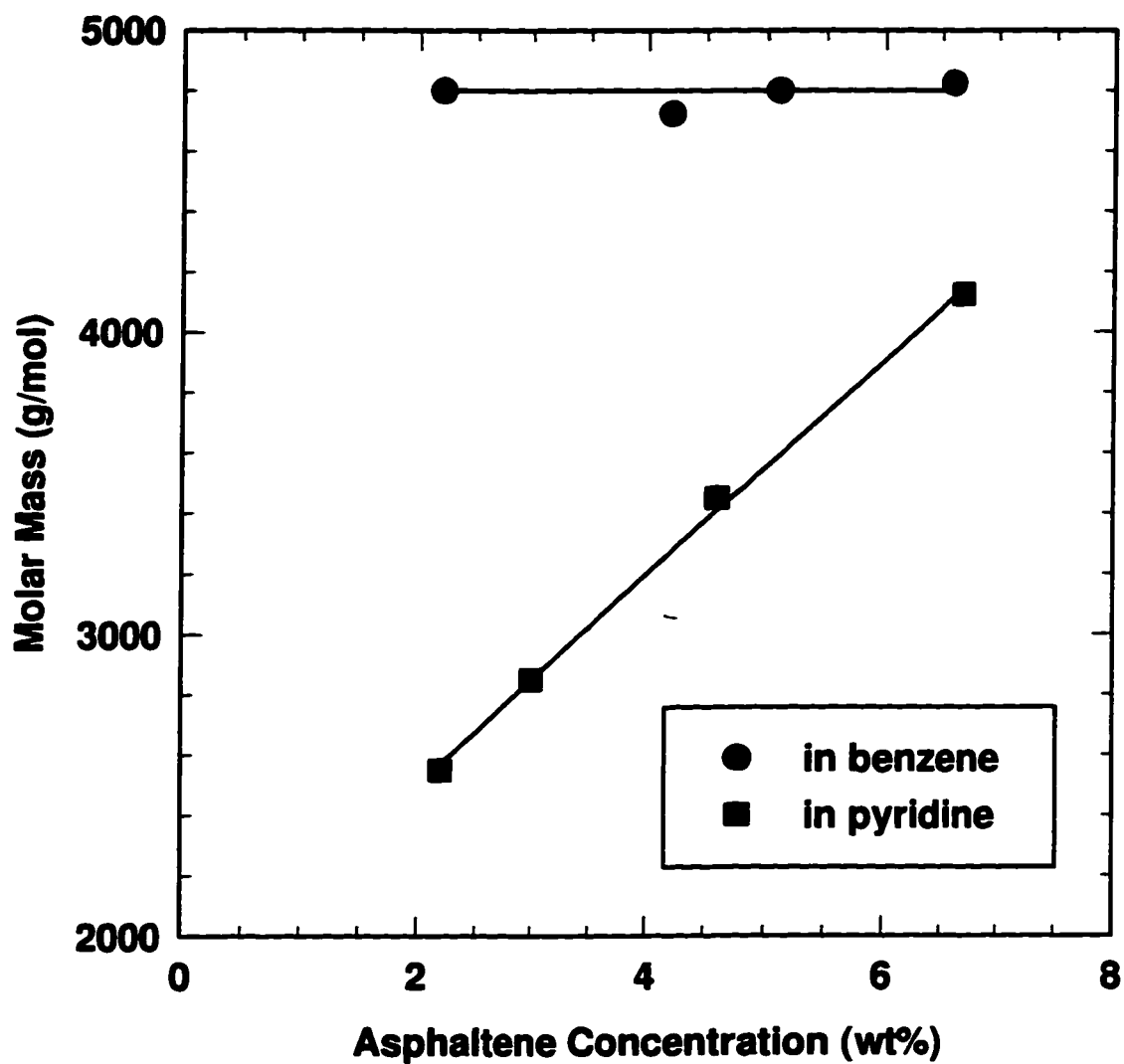


Figure 1.17: Effect of asphaltene concentration on molar mass measured by vpo (49).

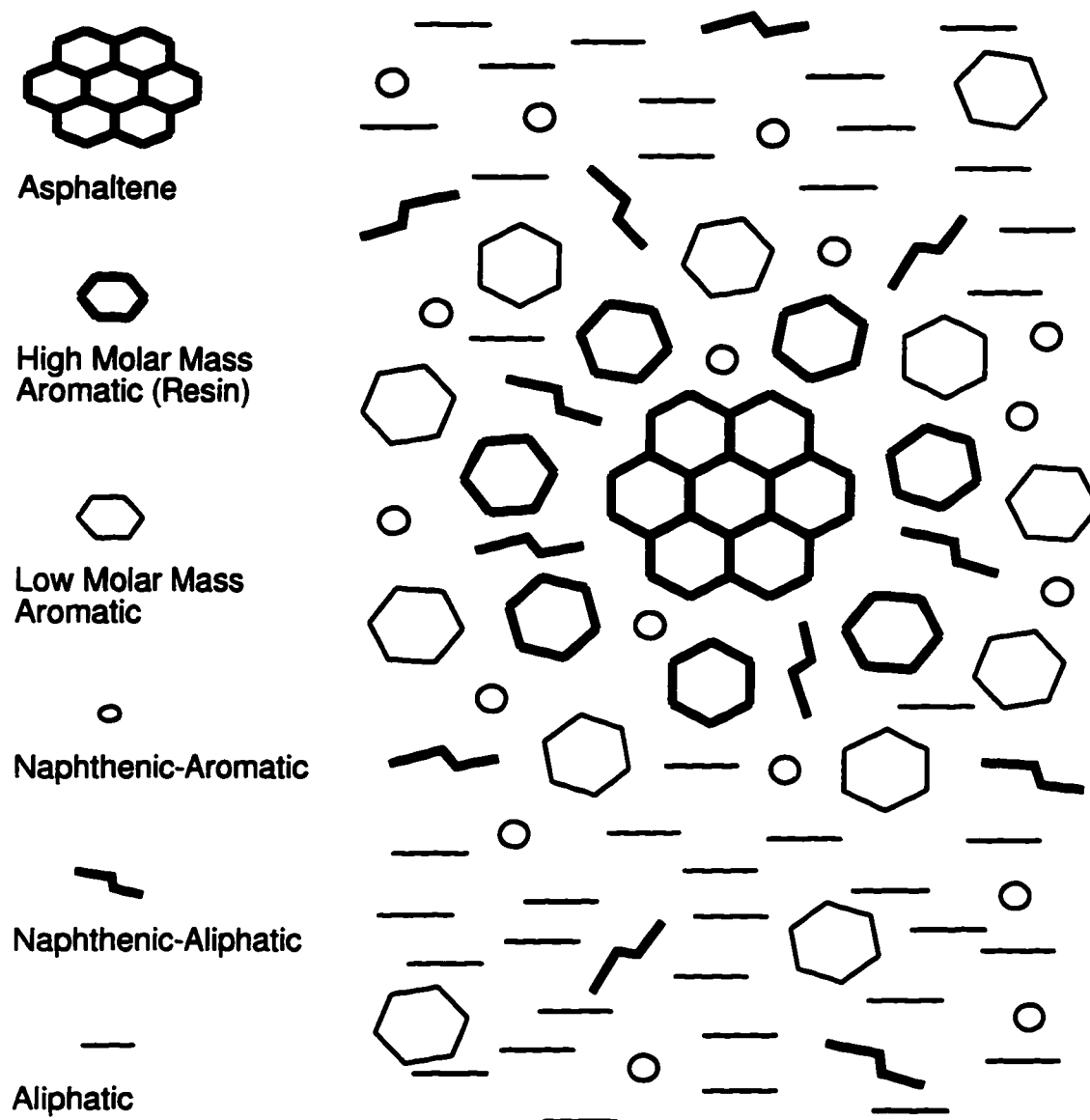


Figure 1.18: Pfeiffer-Saal model of an asphaltene-resin complex (59).

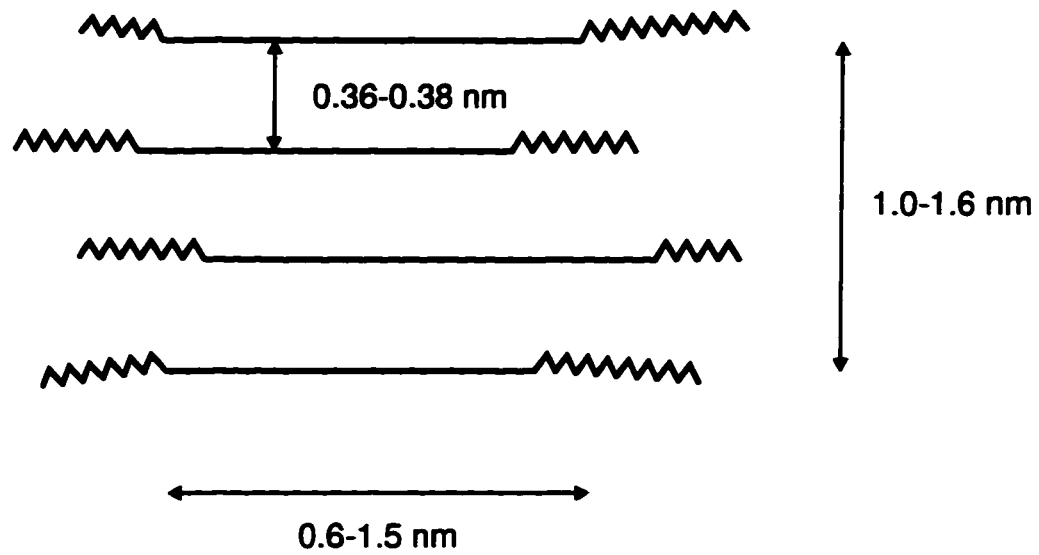


Figure 1.19: Dickie-Yen model of an asphaltene colloid (59).

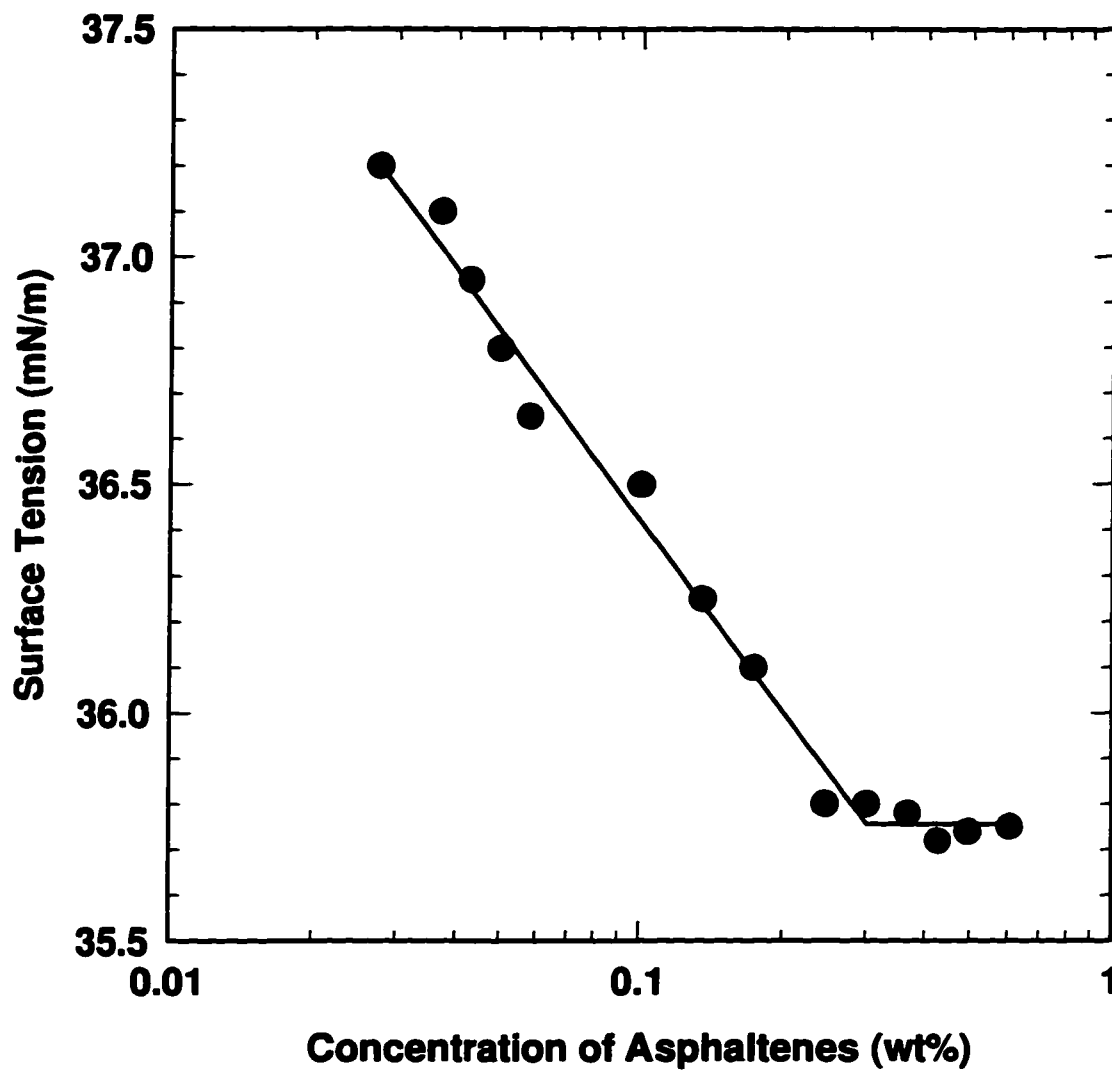


Figure 1.20: Surface tension of solutions of asphaltene in pyridine over water (59).

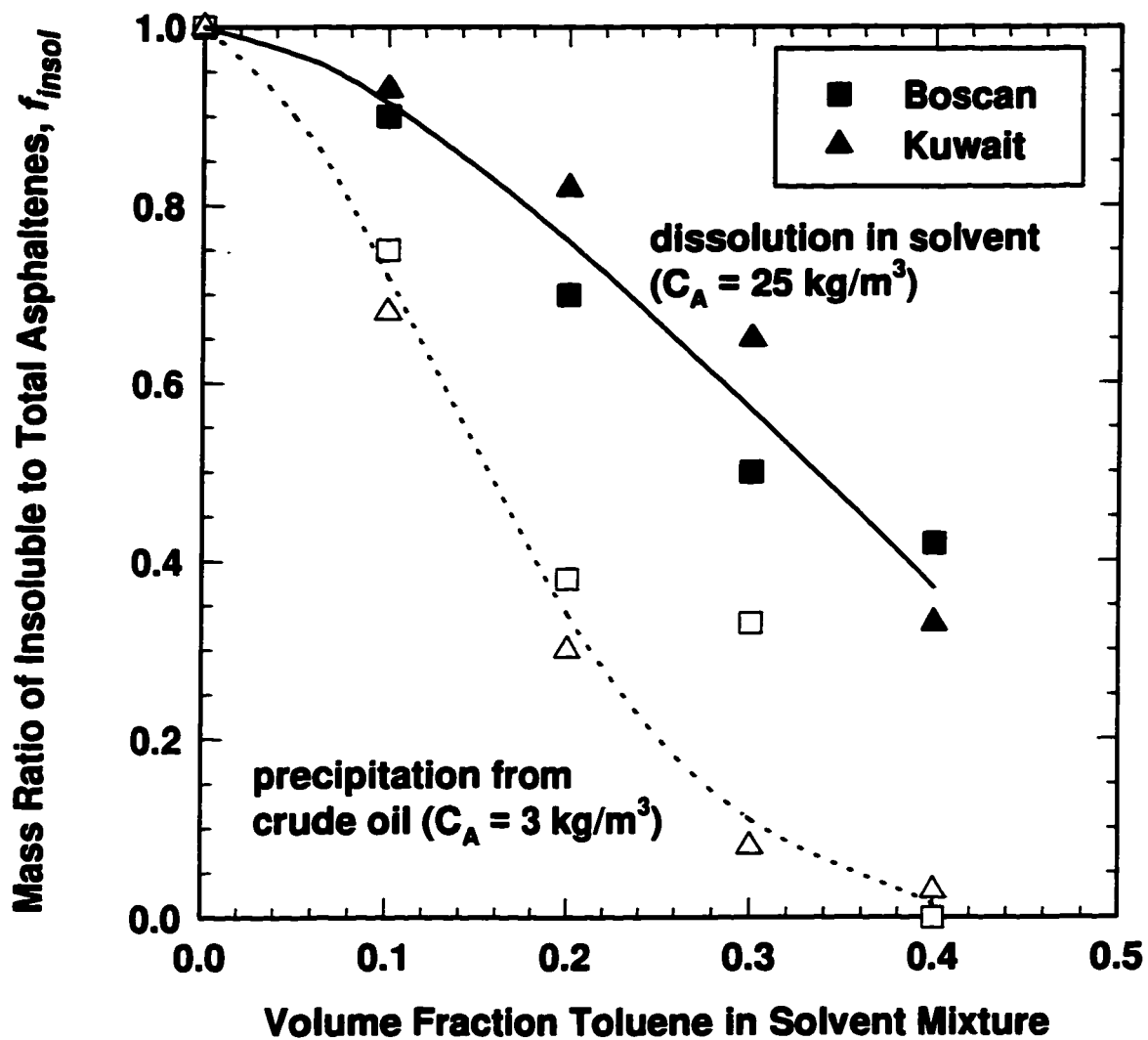


Figure 1.21: Solubility of asphaltenes precipitated by or redissolved in solutions of toluene and heptane (71).

Chapter 2

MOLAR MASS DISTRIBUTION AND SOLUBILITY MODELING OF ASPHALTENES [†]

2.1 Introduction

Crude oils are a complex mixture of hydrocarbons which, for convenience, are divided into several classes of material. In order of increasing polarity, the classes are: saturates, aromatics, resins and asphaltenes. Asphaltenes are the fraction of an oil that is soluble in toluene and insoluble in an alkane, typically pentane or heptane. Asphaltenes are of interest in many aspects of oil production because they tend to precipitate under producing conditions and because they can stabilize water-in-oil emulsions. However, since they are defined as a solubility class which consists of a large variety of molecules, they are difficult to characterize.

Asphaltenes are generally considered to be polyaromatic hydrocarbons, consisting primarily of aromatic and aliphatic groups (approximately 89% by mass) along with a variety of associated functional groups, including acids, thiophenes, pyridines and porphyrins (1,2). Recent work has demonstrated that, while there is a broad range of molar masses in the asphaltene fraction, roughly from 1000 to 10000+ g/mol, the functionality of the molecules does not vary significantly (3, 4), although there is some evidence that the functional groups tend to concentrate slightly at the upper end of the molar mass distribution (5). In most cases, the aromaticity of the asphaltenes was found to increase with increasing molar mass. To summarize, asphaltenes can be approximated as a series of polyaromatic hydrocarbons of increasing molar mass and aromaticity with a variety of associated functional groups randomly distributed on a mass basis.

[†] Published in part: Yarranton, H.W., and Masliyah, J.H., *AIChE J.*, **42**, (1996), 3533.

In attempting to describe the solubility of asphaltenes, most approaches have adopted some form of Scatchard-Hildebrand solubility theory (6), although in many cases the asphaltenes have been treated as a uniform material (7). While these models have successfully predicted the precipitation point, they have been less successful in predicting the amount of precipitated material. Lately, it has been shown that more accurate results can be obtained when the ranges of molar volume and solubility parameter are accounted for with a solid-liquid equilibrium method (8,9). The last approach has been particularly successful with wax precipitation where the physical properties of the wax are reasonably well known (10). However, because the physical properties of the asphaltenes are difficult to measure they are generally approximated using equations of state (11,12). Hence, the usefulness of solubility theory is limited by the accuracy of the molar volume and solubility parameter estimates.

The necessary experimental data to determine molar volume of the asphaltenes are the molar mass and density distributions. Historically, measuring the molar mass distribution has been problematic because asphaltenes self-associate to different degrees in different solvents. Hence, many methods have measured molar masses of asphaltene “micelles” rather than asphaltene molecules. Reasonably good results have been obtained with vapor pressure osmometry (VPO) (13) and, recently, plasma desorption mass spectrometry (PDMS) (14). However, in the former case, the error is sufficiently high that it is difficult to obtain an accurate distribution from a set of asphaltene subfractions. In the latter case, specialized equipment is required and, while the relative distribution seems reasonable, there remains some question as to the absolute value of the molar mass.

In the following study, a series of mass subfractions of Athabasca asphaltene is obtained by solvent extraction. The molar masses of the subfractions are determined from interfacial tension data and compared with VPO values. The resulting distribution is compared with PDMS measurements from the literature and used as the basis for a solid-liquid equilibrium model for the asphaltenes. Asphaltene densities are determined

indirectly from measurements of asphaltene-toluene solution densities. Correlations based on molar mass are developed from the experimental molar mass and density data for the two key model parameters, molar volume and solubility parameter. The model is tested on solubility measurements in toluene-hexane mixtures.

2.2 Experimental Method

2.2.1 Terminology

Asphaltenes are defined as the crude oil constituents that are insoluble in an alkane but soluble in toluene. When asphaltenes are precipitated from a crude oil some other material also precipitates. This other material, the “solids”, includes ash, fine clays and some adsorbed hydrocarbons and is insoluble in toluene. The mixture of asphaltenes and solids that first precipitates shall be referred to as “asphaltene-solids”. A superscript * will be added to symbols that apply to asphaltene-solids to distinguish them from symbols applying to solids-free asphaltenes. The asphaltene-solids precipitated directly from the bitumen will be referred to as the asphaltene-solids fraction. Any material separated from the asphaltene-solids fraction will be designated an asphaltene-solids subfraction. Hence, during a precipitation, the asphaltene-solids fraction is separated into a soluble subfraction and an insoluble subfraction. Whenever asphaltenes are referred to without the “-solids” modifier, it means that the asphaltenes are free of solids.

2.2.2 Materials

Asphaltene-solids were extracted from Syncrude coker feed Athabasca bitumen (bitumen that has been treated to remove sand and water and is ready for upgrading) with a 40:1 volume ratio of heptane:bitumen. The mixture was stirred for 4 hours and left to settle overnight. Then the supernatant liquid was removed and the remaining precipitate further diluted with heptane at a 4:1 volume ratio heptane:bitumen. After 4 hours, the final mixture was filtered and the remaining asphaltene-solids precipitate dried at ambient conditions until there was no further change in mass. The drying usually required one week. The asphaltene-solids recovered with this method made up 14.5 wt% of the original bitumen. Reagent grade toluene, hexane and heptane were purchased from Fisher Scientific.

Demineralized water produced by reverse osmosis was used for all interfacial tension measurements.

Asphaltene-solids subfractions were obtained with solvent extraction in two ways: by solubility and by precipitation. For the solubility method, asphaltene-solids were added to a premixed known ratio of hexane and toluene. The solution was stirred in a sonic mixer for 10 minutes (20 minutes at high asphaltene concentrations), left for 24 hours and then centrifuged at 3400 rpm on a desktop centrifuge (1300 g) for 5 minutes. The supernatant liquid was poured off and the undissolved asphaltene-solids subfraction dried until there was no further change in mass. For the precipitation method, the procedure was identical except that the asphaltene-solids were dissolved in toluene before the hexane was added. In the first case, the undissolved portion of the asphaltene-solids was recovered and in the second case, the precipitated portion.

When it was necessary to measure solids-free asphaltene properties, the solids were removed with the following procedure. The asphaltene-solids were dissolved in toluene and centrifuged at 1300 g for 5 minutes. The supernatant liquid was recovered and evaporated until only dry asphaltene remained. In the case of asphaltene subfractions, the supernatant liquid was used in the precipitation solvent extraction method described above.

2.2.3 Density Measurements

Densities were measured with an Anton Paar DMA 45 density meter calibrated with demineralized water and toluene. Density measurements with this instrument are generally accurate to $\pm 0.03 \text{ kg/m}^3$. All measurements were made at $25.7 \pm 0.05 \text{ }^\circ\text{C}$. Asphaltene densities were calculated indirectly from the densities of mixtures of known concentration of asphaltene in toluene. The density measurements are discussed in greater detail in Appendix A.

2.2.4 Interfacial Tension Measurements

Interfacial tensions of oil over demineralized water were measured with a Fisher deNouy ring tensiometer accurate to ± 0.5 mN/m. For each measurement, the platinum ring was placed in the water, the organic phase was added dropwise to the water surface and the two phase system left to equilibrate for one hour before the ring was pulled through the interface. Before each measurement, the surface tension of the water was checked and, after each measurement, the ring was cleaned in toluene and any traces of hydrocarbon burned off. All measurements were corrected for the solvent density using the Harkins and Jordan tables (15). Details of the interfacial tension measurements are provided in Appendix A.

2.2.5 Vapor Pressure Osmometry Measurements

The principles of vapor pressure osmometry are reviewed in Appendix A. Molar masses were determined with a Westcan Instrument Inc. Model 232A vapor pressure osmometer calibrated with benzil. Measurements in toluene and 1,2-dichlorobenzene were made at 50 and 120 °C respectively. Asphaltene molar masses in toluene were determined over a range of 1.5 to 4.5 gram asphaltene per liter solvent. There was no trend of molar mass versus concentration, so the reported values are an average of two or three measurements. It has been shown previously that asphaltene VPO molar mass is independent of concentration in 1,2-dichlorobenzene at 120 °C (13). Therefore, in that solvent, only one measurement was taken for each sample.

2.3 Theory

2.3.1 Molar Mass from Interfacial Tension Measurements

It has already been noted that an estimate of molar mass can be obtained from surface tension data (16). In a dilute solution, the area that a solute molecule occupies on the interface can be obtained from a plot of surface tension or interfacial tension, σ , versus the logarithm of solute concentration, C_i as follows:

$$\frac{d\sigma}{d \ln C_i} = -RT\Gamma_i = -\frac{RT}{A_i} \quad (2.1)$$

where R is the gas constant, T is temperature, Γ is molar surface coverage and A_i is molar surface area of the solute. When the solute concentration is sufficient to saturate the interface, the molar surface area is constant and can be determined from the slope of a plot of interfacial tension versus the log of the solute concentration. A molecular geometry must be assumed to calculate a molar volume from the molar surface area and then molar mass is found from the density and the molar volume. The molecular geometry is unknown but can be approximated as spherical or cylindrical. Both geometries give reasonable results but, in this study, the best results were obtained by assuming a cylindrical geometry. Accordingly, molar mass is expressed by:

$$M_i = \rho_i t_A \left\{ \frac{-4RT}{\pi \left(\frac{d\sigma}{d \ln C_i} \right)} \right\} \quad (2.2)$$

where M_i and ρ_i are the molar mass and density of component i , respectively. Here it is also assumed that the molar surface area represents the cross-section of the cylindrical molecule. Accordingly, t_A is the height of the cylinder; *i.e.* the thickness of the molecule. The value of t_A also accounts for any error introduced by the geometry assumptions. Since t_A is unknown, the interfacial tension method can be used to determine the shape of the asphaltene molar mass distribution but not the absolute value. Hence, the results must be compared with a second method such as VPO to calculate a value for t_A . Then, a realistic molar mass distribution can be obtained for use in solubility modeling.

2.3.2 Solubility

Asphaltenes are a mixture of molecules and their solubility can be determined in a manner analogous to a multicomponent flash calculation. In this case, it is a solid-liquid equilibrium and the appropriate equilibrium ratio is given by $K_i = \hat{x}_i^s / \hat{x}_i^l$ where \hat{x}_i^s and \hat{x}_i^l

are the solid phase and liquid phase mole fractions of component i , respectively. As discussed elsewhere (9), the equilibrium ratio can be determined at low pressure by equating the fugacities in each phase and neglecting pressure effects.

$$\hat{x}_i^l \gamma_i^l f_i^{ol} = \hat{x}_i^s \gamma_i^s f_i^{os} \quad (2.3)$$

Here γ_i^l and γ_i^s are the activity coefficients of component i in the liquid and solid phase respectively and f_i^{ol} and f_i^{os} are the standard state fugacities in the same respective phases. For solid-liquid equilibria, the ratio of the standard state fugacities can be approximated by (17):

$$\frac{f_i^{ol}}{f_i^{os}} = \exp\left\{\frac{\Delta H_i^f}{RT} \left(1 - \frac{T}{T_i^f}\right)\right\} \quad (2.4)$$

where ΔH_i^f is the enthalpy of fusion and T_i^f is the melting point temperature of component i . For low asphaltene concentrations, the activity coefficients can be estimated using Scatchard-Hildebrand solubility theory. With large molecules like asphaltenes, it is necessary to use the Flory-Huggins term for the entropy of mixing molecules with largely different sizes. The resulting expression is given here for the liquid phase activity coefficient.

$$\gamma_i^l = \exp\left\{1 - \frac{v_i^l}{v_m} + \ln\left(\frac{v_i^l}{v_m}\right) + \frac{v_i^l}{RT}(\delta_m - \delta_i^l)^2\right\} \quad (2.5)$$

where v_i^l and v_m are the liquid phase molar volumes of component i and the solvent respectively, and δ_i^l and δ_m are the solubility parameters for the same respective constituents. The solubility parameter is defined as follows:

$$\delta_i^l = \left(\frac{\Delta U^{vap}}{v_i^l} \right)^{1/2} \quad (2.6)$$

where ΔU^{vap} is the internal energy of vaporization. Note that for asphaltenes, the activity coefficients in the solid phase are near unity especially for the fractions nearest the point of incipient precipitation. Therefore, assuming a value of unity for the solid phase activity coefficients does not introduce significant error. When Eqs 2.4 and 2.5 are substituted into Eq. 2.3, the resulting expression for the K-value of component i becomes:

$$K_i = \exp \left\{ \frac{\Delta H_i^f}{RT} \left(1 - \frac{T}{T_i^f} \right) + 1 - \frac{v_i^l}{v_m} + \ln \left(\frac{v_i^l}{v_m} \right) + \frac{v_i^l}{RT} (\delta_m - \delta_i^l)^2 \right\} \quad (2.7)$$

The properties of most solvents are already known. In order to apply the equilibrium model, it remains to determine the molar volume and solubility parameters of the asphaltenes and to consider the enthalpy of fusion term. Scatchard-Hildebrandt theory and solid-liquid equilibria are reviewed in greater detail in Appendix B.

2.4 Results and Discussion

It is important to recognise that the asphaltenes precipitated from bitumen contain some other insoluble material, the “solids”, and that this material can affect measurements of asphaltene properties. The amount of solids in the asphaltene-solids subfractions is shown in Fig. 2.1. The solids make up 6.3% of the asphaltene-solids fraction or 0.9% of the coker feed bitumen. The same total amount of solids precipitates with each asphaltene-solids subfraction and, therefore, the relative fraction of solids increases as the size of the subfraction decreases. Consequently, the solids can introduce significant error in measurements of the properties of the smallest subfractions. Note that the raw data for the density, interfacial tension and vapor pressure osmometry measurements are given in Appendix A and the raw data for the asphaltene solubility measurements are given in Appendix B.

2.4.1 Solubility Data

The solubility of the asphaltene-solids was measured in hexane-toluene solutions of 20, 25, 33, 40 and 50 vol% toluene. Both the solubility and the precipitation methods give similar results except at low asphaltene concentrations, as shown in Fig. 2.2. At low concentrations, the insoluble subfraction from the precipitation method is smaller probably because flocculation is limited under these conditions. Note, that when used for asphaltene property correlations, the mass fractions in Fig. 2.2 must be adjusted to remove the solids contribution.

Fig. 2.2 also illustrates that the fraction of asphaltene-solids that precipitates at a given volume fraction of toluene is virtually independent of asphaltene concentration from concentrations of 1.76 to 17.6 kg/m³. It is interesting to compare Fig. 2.2 with the solubility curve of a pure component given in Fig. 2.3. The solute concentration in Fig. 2.3 is normalized to the precipitation point concentration. Fig. 2.3 shows that at normalized concentrations greater than 10, the insoluble mass fraction is greater than 0.85. Returning to Fig. 2.2, the precipitation point concentration is unknown but, since precipitation occurred at all concentrations, it must be less than the lowest experimental asphaltene concentration, 1.76 kg/m³. Hence, the highest experimental asphaltene concentration of 17.6 kg/m³ corresponds to a normalized concentration of at least 10. If the asphaltenes acted as a pure component, the insoluble mass fraction at 17.6 kg/m³ of asphaltene should be greater than 0.85. This is not the case and therefore asphaltenes cannot be considered as a uniform solubility class but must rather be treated as a range of molecular species.

Now, as will be shown, the higher the asphaltene molar mass, the less soluble it is. Also, by definition, all the asphaltenes are soluble in toluene but insoluble in hexane. Therefore, the higher the toluene/hexane ratio, the less asphaltene precipitates and the higher the molar mass and density of the precipitated subfraction. Consequently, the series of increasing toluene/hexane ratios yields a series of asphaltene subfractions with increasing molar mass and density from which the desired molar mass and density distributions can be calculated.

2.4.2 Density

Densities were measured for solutions of asphaltene in toluene at asphaltene concentrations of 0 to 1.14 wt%. Experiments were carried out on the entire asphaltene fraction and on the insoluble subfractions precipitated from hexane-toluene solutions of 20, 25 and 33 vol% toluene. Fractions with and without the solids were examined.

At low concentration, regular solution behavior can generally be assumed. Consequently, the asphaltene density can be determined indirectly from a plot of the inverse mixture density versus asphaltene mass fraction, as follows:

$$\frac{1}{\rho_m} = \frac{1}{\rho_T} + \left(\frac{1}{\rho_A} - \frac{1}{\rho_T} \right) x_A \quad (2.8)$$

hence

$$\rho_A = \frac{1}{S + I} \quad (2.9)$$

where ρ_m , ρ_T and ρ_A are the mixture, toluene and average asphaltene densities, respectively, and x_A is the asphaltene mass fraction. S and I are the slope and intercept of the inverse mixture density plot, respectively. Similarly, if the density of the solids is known, the average density of the asphaltenes can be estimated from a plot of inverse mixture density versus mass fraction of the asphaltene-solids:

$$\rho_A = \frac{1}{\frac{S^*}{1 - f_S^*} + (1 + f_S^*)I^* - \frac{f_S^*}{\rho_S}} \quad (2.10)$$

where ρ_S is the density of the solids, f_S^* is the mass fraction of solids in the asphaltene-solids mixture. S^* and I^* are the slope and intercept of the inverse mixture density versus mass fraction asphaltenes-solids plot.

A typical mixture density plot is given in Fig. 2.4. The calculated average asphaltene densities are shown in Fig. 2.5. Corrected values from the asphaltene-solids data were obtained using Eq. 2.10 and a solids density of 1550 kg/m^3 . This value is consistent with the expectation that the solids are comprised of ash, clay fines and adsorbed hydrocarbons. The average density varies only 5% for $0.35 < f_{insol} \leq 1.0$. Such a narrow change in density contributes to the apparent scatter in Fig. 2.5 even though the deviation is within 1%. Although, the density data are scattered, a downwards trend is evident. Therefore, a constant density or zero order density model is inappropriate. However, the density determinations are not accurate enough to justify fitting the data with more than a first order model. Consequently, we assume that asphaltene density increases linearly with molar mass. As will be discussed later, molar mass is related to the mass frequency distribution as follows:

$$\frac{df_i}{dM_i} = \text{constant} \left(1 + \alpha_M \exp\{-\beta_M M_i\} \right) \quad (2.11)$$

where α_M and β_M have values of 50.63 and 0.00165 mol/g, respectively and are used to fit the molar mass distribution. M_i is the molar mass of the i^{th} asphaltene component and f_i is the cumulative mass frequency up to the i^{th} asphaltene component. Eq. 2.11 can be integrated to find the cumulative mass frequency, given in Eq. 2.12:

$$\int_{M_L}^{M_i} \left(\frac{df_i}{dM_i} \right) dM_i = f_i = f_{sol} = \frac{M_i - M_L - \alpha_M \left(\exp\{-\beta_M M_i\} - \exp\{-\beta_M M_L\} \right)}{M_U - M_L - \alpha_M \left(\exp\{-\beta_M M_U\} - \exp\{-\beta_M M_L\} \right)} \quad (2.12)$$

Here f_{sol} is the mass ratio of the lightest asphaltene subfraction to the total asphaltene fraction. f_{sol} is expected to be equivalent to f_i . M_L and M_U are the molar masses of the smallest and largest asphaltene components, respectively. Now, the average density of the insoluble asphaltene subfraction in terms of f_i is given by:

$$\bar{\rho}_{insol} = \frac{\int_{f_{sol}}^1 df_i}{\int_{f_{sol}}^1 \frac{df_i}{\rho_i}} \quad (2.13)$$

However, Eq. 2.13 is more easily solved in terms of molar mass. Given that

$$\rho_i = a_p M_i + b_p \quad (2.14)$$

the average density of the insoluble subfraction may be expressed as follows:

$$\bar{\rho}_{insol} = \frac{M_U - M_i - \frac{\alpha_M}{\beta_M} (\exp\{-\beta_M M_U\} - \exp\{-\beta_M M_i\})}{\int_{M_i}^{M_U} \left(\frac{1 + \alpha_M \exp\{-\beta_M M_i\}}{a_p M_i + b_p} \right) dM_i} \quad (2.15)$$

Similarly, the average density of the soluble subfraction is given by:

$$\bar{\rho}_{sol} = \frac{M_i - M_L - \frac{\alpha_M}{\beta_M} (\exp\{-\beta_M M_i\} - \exp\{-\beta_M M_L\})}{\int_{M_L}^{M_i} \left(\frac{1 + \alpha_M \exp\{-\beta_M M_i\}}{a_p M_i + b_p} \right) dM_i} \quad (2.16)$$

Here, ρ_i is the density of the i^{th} asphaltene component and $\bar{\rho}_{insol}$ and $\bar{\rho}_{sol}$ are the average densities of the insoluble (high molar mass) and soluble (low molar mass) asphaltene subfractions, respectively. a_p and b_p are the linear fit coefficients of the asphaltene density to molar mass. Values of 0.017 and 1080 for a_p and b_p respectively were estimated to provide the best fit of the solubility data later on. As will be discussed later, values of 2000 and 8500 g/mol were determined for M_L and M_U , respectively. To compare calculated average densities with experimental data, Eq. 2.12 was used to determine the M_i that corresponds to a given f_{sol} . Then Eq. 2.15 was solved numerically with M_i serving as the

lower integration limit. Average densities predicted from Eq. 2.15 are compared with experimental data in Fig. 2.5.

The scatter in the density determinations illustrates the difficulty in obtaining asphaltene density distributions and may explain why there is little data on asphaltene densities in the literature. However, a value of 1158 kg/m^3 was predicted by Mehrotra et al. (18) for a fraction of Athabasca bitumen making up 20 wt% of the bitumen and containing the densest constituents. Their value of 1158 kg/m^3 compares well with our experimental average density of $1162 \pm 20 \text{ kg/m}^3$ for the entire asphaltene fraction, which comprises 14.5 wt% of the bitumen.

2.4.3 Interfacial Tension and Molar Mass

The near independence of solubility on asphaltene concentration, demonstrated in Fig. 2.2, proved useful for the interpretation of the interfacial tension data. For a solution where only part of the asphaltenes is soluble, the slope in Eq. 2.1 can be expressed as:

$$\frac{d\sigma}{d \ln C_i^{sol}} = \frac{d\sigma}{d \ln(f_{sol}^* C_i)} \quad (2.17)$$

where C_i^{sol} is the concentration of the soluble fraction of the asphaltene. As long as f_{sol}^* is constant, Eq. 2.17 is equivalent to the slope used in Eq. 2.1. Therefore, a plot of interfacial tension versus the concentration of asphaltene-solids mixture gives the correct slope for use in Eq. 2.2.

It is also necessary to determine if the precipitated asphaltenes affect the interfacial tension measurements. Measurements with and without the precipitated material are compared in Fig. 2.6. The presence of precipitated asphaltenes has no effect on the results at concentrations below 2 kg/m^3 . Above 2 kg/m^3 , the precipitate leads to higher interfacial tension values. At high concentrations, the precipitate may change the local density and lead to errors in the deNouy ring density correction or perhaps mechanically strengthen the

interface. Note in Fig. 2.6 that, for the purpose of comparison, the concentration of asphaltene prior to the removal of precipitate was used.

Interfacial tensions were measured for asphaltenes in toluene-hexane solutions of 20, 25, 33, 40, 50 and 100 vol% toluene. The following properties were calculated from the interfacial tension data and are listed in Table 2.1: the slope for Eq. 2.1, molecular cross section, molar mass. The mass ratios of the soluble subfractions to the entire asphaltene fraction given in Table 2.1 were corrected to account for the contribution of the solids. The asphaltene densities given in Table 2.1 apply to the soluble portion of the asphaltenes and were calculated numerically from Eq. 2.16. Molecular cross sections are the ratio of molar surface area to Avogadro's number. A value of 1.18 nm was estimated for t_A and it will be discussed later. The molecular cross-sections are in good agreement with those calculated from surface tension data (16,19). The calculated molar mass decreases from 3900 g/mol for the entire asphaltene fraction to 2600 g/mol for the smallest soluble subfraction. A question arises: do the molar mass values represent the average of the molecules in solution or only of the highest molar mass, possibly most surface active, fraction still soluble?

To answer the question, the interfacial area of a high molar mass subfraction must be compared with that of the entire asphaltene fraction, each in a solvent where both are fully soluble. If the interface is dominated by the highest molar mass molecules still in solution, the measured molar surface area should be the same in both cases. If the interface is covered by a representative mixture of molecules, the molar surface areas should reflect the average molar mass of the subfractions. A high molar mass asphaltene fraction was precipitated from bitumen with the procedure described in the materials section except that a 4:1 volume ratio of heptane to bitumen was used instead of a 40:1 ratio. The resulting fraction made up 10.0% of the bitumen by mass and 69% of the fraction precipitated at the 40:1 ratio. Accounting for the solids, the 4:1 fraction contains 65% of the asphaltene in the 40:1 fraction. Interfacial tensions were measured for the 4:1 fraction in toluene and compared with the results for the 40:1 fraction as shown in Fig. 2.7 and Table 2.1. The calculated molar mass of the 4:1 fraction is 70% greater than that of the 40:1 sample.

Hence, the measured molar surface area and the corresponding molar mass more closely reflect the average properties of the molecules in solution rather than the properties of a particular subfraction.

Table 2.1: Molar masses calculated from interfacial tension data

| vol% toluene in solvent | f_{sol} (mass%) | $\frac{d\sigma}{d \ln C_A}$ (mN/m) | molecular cross- section (nm) ² | average density (kg/m ³) | average molar mass (g/mol) |
|-------------------------------|----------------------|---------------------------------------|---|--|----------------------------------|
| 20 | 0.29 | -1.2487 | 3.26 | 1123 | 2600 |
| 25 | 0.42 | -1.1468 | 3.55 | 1129 | 2850 |
| 33 | 0.65 | -1.0125 | 4.02 | 1141 | 3260 |
| 40 | 0.84 | -0.9178 | 4.43 | 1152 | 3630 |
| 50 | 0.96 | -0.9134 | 4.45 | 1159 | 3670 |
| 100 | 1.00 | -0.8569 | 4.75 | 1162 | 3920 |
| 100 | 0.35* | -0.5258 | 7.75 | 1202 | 6620 |

* Asphaltene from the 4:1 precipitation contains 65% of the highest molar mass material from the 40:1 precipitation. Hence, the 4:1 fraction is equivalent to an f_{sol} of 0.35 for the 40:1 sample.

Also of interest here is that in none of the interfacial tension measurements was the asphaltene critical micelle concentration, cmc, reached. Above the cmc, interfacial tension is independent of the surfactant concentration. Thus, the cmc for Athabasca asphaltenes is above 44 kg/m³ in toluene and 18 kg/m³ in a toluene-hexane mixture of 25 vol% toluene. All the measurements reported in this paper are taken below the cmc and, therefore, are not influenced by the presence of micelles. In particular, the VPO results in toluene are expected to reflect the molar mass of molecules rather than micelles.

VPO molar masses were obtained for the insoluble asphaltene-solids subfractions precipitated in toluene-hexane solutions of 0, 20, 25, and 33 vol% toluene. The VPO measurements were made with toluene and 1,2-dichlorobenzene as a solvent as shown in Fig. 2.8. The values in 1,2-dichlorobenzene are 2.2 times lower than those in toluene. This is somewhat greater than the ratio of 1.6 reported elsewhere (13) but ratios as high as 3.6 have been observed with similar solvents (20). The difference in the apparent asphaltene molar mass in different solvents has been attributed to different degrees of molecular stacking (21). Given that the apparent molar mass does not vary with concentration in either case, it may be that asphaltene stacking depends only on the properties of the solvent. For present purposes, the results in toluene will be accepted.

To check on the effect of the solids, VPO measurements using toluene as the solvent were conducted on solids-free samples. As is observed in Fig. 2.8, the asphaltene molar masses are roughly 25% lower than the asphaltene-solids samples. Hence the solids introduce a 25% error. The asphaltene and corrected asphaltene-solids VPO molar masses are compared with the interfacial tension results in Fig. 2.9.

A good estimate of the shape of the Athabasca bitumen molar mass distribution has been obtained from PDMS (14) and is given in Fig. 2.10. We assume that the molar mass distribution of the extracted asphaltenes has the same shape as the portion of the bitumen distribution greater than 400 g/mol. Therefore, the fitting parameters α_M and β_M used in Eq. 2.11 can be obtained directly from the experimental data in Fig. 2.10 and are 50.63 and 0.00165 mol/g respectively. It remains to determine the range of molar masses present in the asphaltene distribution; i.e. the values of M_L and M_U .

The average molar masses for the soluble (lowest molar mass end of distribution) and insoluble (highest molar mass end) subfractions within the asphaltene can be calculated in the same manner as was the average asphaltene density:

$$\bar{M}_{sol} = \frac{M_i - M_L - \frac{\alpha_M}{\beta_M} (\exp\{-\beta_M M_i\} - \exp\{-\beta_M M_L\})}{\int_{M_L}^{M_i} \left(\frac{1 + \alpha_M \exp\{-\beta_M M_i\}}{M_i} \right) dM_i} \quad (2.18)$$

and

$$\bar{M}_{insol} = \frac{M_U - M_i - \frac{\alpha_M}{\beta_M} (\exp\{-\beta_M M_U\} - \exp\{-\beta_M M_i\})}{\int_{M_i}^{M_U} \left(\frac{1 + \alpha_M \exp\{-\beta_M M_i\}}{M_i} \right) dM_i} \quad (2.19)$$

Here, \bar{M} is the average molar mass. Values of 2000 and 8500 \pm 500 g/mol for M_L and M_U were found to best fit the VPO and interfacial tension based estimates of average molar mass as shown in Fig. 2.9. A molecular thickness of 1.18 nm was used in Eq. 2.2 to scale the molar masses calculated from the interfacial tension data to those from VPO experiments. A thickness of 1.18 nm is consistent with molecular dimensions.

2.4.4 Molar Volume and Solubility Parameter Correlations

Molar volume is the ratio of molar mass to density. As discussed previously, density was related to molar mass as follows:

$$\rho_i = 0.017M_i + 1080 \quad (2.20)$$

and therefore:

$$v_i = \frac{1000M_i}{0.017M_i + 1080} \quad (2.21)$$

The solubility parameter can also be correlated to molar mass with the use of Eq. 2.6. To the extent that the asphaltenes are a series of polyaromatic hydrocarbons with smoothly increasing aromaticity and with randomly distributed associated functional groups, they can be treated as a homologous series. For a homologous series, the enthalpy of vaporization is

a linear function of molar mass as is shown in Fig. 2.11. Assuming such a linear function for asphaltenes, the solubility parameter may be expressed as follows:

$$\delta'_i = \left(\frac{\Delta H_i^{\text{vap}} - RT}{v_i} \right)^{1/2} = \left(\frac{AM_i + B - RT}{M_i / \rho_i} \right)^{1/2} \quad (2.22)$$

where ΔH_i^{vap} is the molar enthalpy of vaporization, and A and B are the linear fit parameters for the enthalpy of vaporization versus molar mass. For high molar mass material such as asphaltenes, the term “ $B - RT$ ” has a magnitude in the order of -3 kJ/mol compared with a minimum value of 400 kJ/mol for the “ AM_i ” term. Therefore, the “ $B - RT$ ” term can be neglected and the following expression results from Eq. 2.22:

$$\delta'_i \cong (A\rho_i)^{1/2} \quad (2.23)$$

While A is a physically meaningful parameter, its value is not known and must be determined indirectly from solubility data. However, given that asphaltene aromaticity increases with increasing molar mass, one expects the value of A to be nearer that of the naphthalenes, 398 J/g than the alkanes, 270 J/g..

2.4.5 Solubility Model

Solid-liquid equilibrium calculations were performed using equilibrium ratios determined from Eq. 2.7. The ratio of the standard state fugacities, Eq. 2.4, was assumed to be near unity for asphaltenes in toluene-hexane mixtures. The assumption is based on two observations. First, the asphaltenes do not appear to precipitate in a crystalline form but rather as an amorphous, highly solvated, solid. Indeed, the solid material takes several days to dry out, and seems to crystallize only after most of the solvent has evaporated. The enthalpy of fusion at the point of precipitation may well be small in such circumstances. Secondly, good solubility predictions are obtained when the standard state fugacity ratio is

assumed to be near unity and the first term in the exponent of Eq. 2.7 is neglected. The computer programs employed to solve the solid-liquid equilibrium calculation are given in Appendix B.

Solvent solubility parameters of 18.25 for toluene and 14.9 for hexane were obtained from Barton's 1983 Handbook (22). The mixture solubility parameter is the volume average of the solvent parameters. Densities, molar volumes and solubility parameters were estimated with Eqs 2.20, 2.21 and 2.23 respectively based on the molar mass distribution obtained in Eq. 2.12. As discussed previously, the parameter A in Eq. 2.23 was adjusted until the predicted fractional solubilities agreed with experimental data. A value of 367 J/g was found to give the best results. As expected, this value is quite close to the naphthalene value of 398 J/g. Furthermore, the calculated solubility parameters ranged in value from 20 for the smallest asphaltene molecule to 21 for the largest, in good agreement with literature values near 20 (23). Model predictions are compared with experimental results at an asphaltene concentration of 8.8 kg/m³ in Fig. 2.12.

In order to illustrate the significance of the first order density correlation, a zero order prediction was made assuming a constant asphaltene density of 1162 kg/m³ with the results shown in Fig. 2.12. The use of constant density introduces significant errors in the prediction of both the precipitation point and the amount of precipitated material. Using the zero order density model is equivalent to using a constant value for the asphaltene solubility parameter. Hence, the comparisons in Fig. 2.12 indicate that a small variation in the solubility parameter with molar mass can significantly affect the accuracy of solubility calculations. A density correlation of at least first order is essential to predict the solubility of asphaltenes with acceptable accuracy.

The first order model agrees reasonably well with the experimental data and predicts fractional precipitation to within 0.02 except near the precipitation point. The precipitation point is underestimated by 0.07. Similar accuracy is obtained for an asphaltene-solids concentration range of 1.76 to 17.6 kg/m³ as shown in Fig. 2.2. Considering the

assumptions used to obtain the correlations employed in the model, this level of agreement is fairly good.

2.5 Conclusions

For the purpose of solubility calculations, the chemistry of asphaltenes can be estimated by treating asphaltenes as a series of polyaromatic hydrocarbons with randomly distributed associated functional groups. The molar mass distribution for asphaltenes can be obtained with interfacial tension measurements together with VPO data and PDMS data. Molar volume and the solubility parameter for the asphaltenes can be correlated to molar mass. Solubility can be modeled using a solid-liquid equilibrium calculation with K-values derived from Scatchard-Hildebrand solubility theory incorporating the Flory-Huggins entropy of mixing.

The resulting multicomponent equilibrium calculation was tested on solutions of toluene and hexane. In this case there was one estimated parameter, the rate at which the asphaltene enthalpy of vaporization changes with molar mass. The value of the parameter used in the model was within 10% of that for the naphthalenes. The solubility model predicted the precipitation point to within 0.07 of the hexane volume fraction required and predicted the fractional amount of precipitate to within 0.05 across a broad range of concentrations and toluene/hexane ratios. The small variation in asphaltene solubility parameter with molar mass resulted in significantly improved predictions compared with a constant solubility parameter model. The correlations used here need to be tested for their robustness on asphaltenes from other sources and with different solvents.

2.6 References

1. Strausz, O.P., Mojelsky, T.W., and Lown, E.M., "The Molecular Structure of Asphaltene: an Unfolding Story", *Fuel*, **71**, (1992), 1355.
2. Speight, J.G., Moschopedis, S.E., "Some Observations on the Molecular Nature of Petroleum Asphaltenes", *Preprints, Div. of Fuel Chem., ACS*, **24**, (1979), 910.

3. Cyr, N., G. McIntyre, Toth, G., and Strausz, O.P., "Hydrocarbon Structural Group Analysis of Athabasca Asphaltene and its G.P.C. Fractions by ^{13}C N.M.R.", *Fuel*, **66**, (1987), 1709.
4. Andersen, S.I., "Effect of Precipitation Temperatures on the Composition of N-Heptane Asphaltenes", *Fuel Sci. Technol. Intl.*, **12**(12), (1994), 51.
5. Brons, G., "Solvent Deasphalting Effects on Whole Cold Lake Bitumen", *Energy & Fuels*, **9**, (1995), 641.
6. Cimino, R., Corraera, S., Sacomani, E., and Carniani, C., "Thermodynamic Modelling for Prediction of Asphaltene Deposition in Live Oils", *SPE Intl. Symp. Oilfield Chemistry*, San Antonio (Feb. 1995).
7. Hirschberg, A., deJong, L.N.J., Schipper, B.A., and Meijer, J.G., "Influence of Temperature and Pressure on Asphaltene Flocculation", *SPEJ*, **24**, (1984), 283.
8. Kawanaka, S., Park, S.J., and Mansoori, G.A., Organic Deposition from Reservoir Fluids: A Thermodynamic Predictive Technique", *SPE Res. Eng.*, **5**, (1991), 185.
9. Ferworn, K.A. and Svrcek, W.Y., "Thermodynamic and Kinetic Studies of Asphaltene Deposition from Bitumens", *Proc. 44th Cnd. Chem. Eng. Conf.*, Calgary (Oct. 1994)
10. Lira-Galeana, C., Firoozabadi, A., and Prausnitz, J.M., "Thermodynamics of Wax Precipitation in Petroleum Mixtures", *AIChE J.*, **42**, (1996), 239.
11. Thomas, F.B., Bennion, D.B., and Bennion, D.W., "Experimental and Theoretical Studies of Solids Precipitation from Reservoir Fluid", *J. Cnd. Petr. Tech.*, **31**(1), (1992), 22.
12. Rassamdana, H., Dabir, B., Nematy, M., Farhani, M., and Sahimi, M., "Asphalt Flocculation and Deposition: I. The Onset of Precipitation", *AIChE J.*, **42**, (1996), 10.
13. Moschopedis, S.E., Fryer, J.F., and Speight, J.G., "Investigation of Asphaltene Molecular Weights", *Fuel*, **55**, (1976), 227.
14. Larsen, J.W., and Li, S., "Determination of Bitumen Molecular Weight Distributions Using ^{252}Cf Plasma Desorption Mass Spectrometry", *Energy & Fuels*, **9**, (1995), 760.
15. Harkins, W.D., and Jordan, H.F., "A Method for the Determination of Surface and Interfacial Tension from the Maximum Pull on a Ring", *J. Am. Chem. Soc.*, **52**, (1930), 1751.
16. Taylor, S.E., "Use of Surface Tension Measurements to Evaluate Aggregation of Asphaltenes in Organic Solvents", *Fuel*, **71**, (1992), 1338.
17. Prausnitz, J.M., Lichtenthaler, R.N. and de Azevedo, E.G., "Molecular Thermodynamics of Fluid-Phase Equilibria", 2nd Ed., Prentice-Hall, Inc., Englewood Cliffs, New Jersey (1986).

18. Mehrotra, A.K., Sarkar, M., and Svrcek, W.Y., "Bitumen Density and Gas Solubility Predictions Using the Peng-Robinson Equation of State", *AOSTRA J. Res.*, **1**(4), (1985), 215.
19. Sheu, E.Y., De Tar, M.M., and Storm, D.A., "Interfacial Properties of Asphaltenes", *Fuel*, **71**, (1992), 1277.
20. Acevedo, S., Escobar, G., Gutierrez, L., and Rivas, H., "Isolation and Characterization of Natural Surfactants from Extra Heavy Crude Oils, Asphaltenes and Maltenes. Interpretation of their Interfacial Tension-pH Behavior in Terms of Ion Pair Formation", *Fuel*, **71**, (1992), 619.
21. Brandt, H.C.A., Hendriks, E.M., Michels, M.A.J., and Visser, F., "Thermodynamic Model of Asphaltene Stacking", *J. Phys. Chem.*, **99**, (1995), 10430.
22. Barton, A.M.F., "CRC Handbook of Solubility Parameters and Other Cohesion Parameters", CRC Press, Boca Raton, FL. (1983).
23. Andersen, S.I., "Hysteresis in Precipitation and Dissolution of Petroleum Asphaltenes", *Fuel Sci. Technol. Intl.*, **10**(10), (1992), 1743.
24. Weast, R.C., "CRC Handbook of Chemistry and Physics", 59th Ed., CRC Press, Boca Raton, FL. (1978-79).
25. Daubert, T.E., and Danner, R.P., "Data Compilation Tables of Properties of Pure Compounds", AIChE, New York, NY (1985).

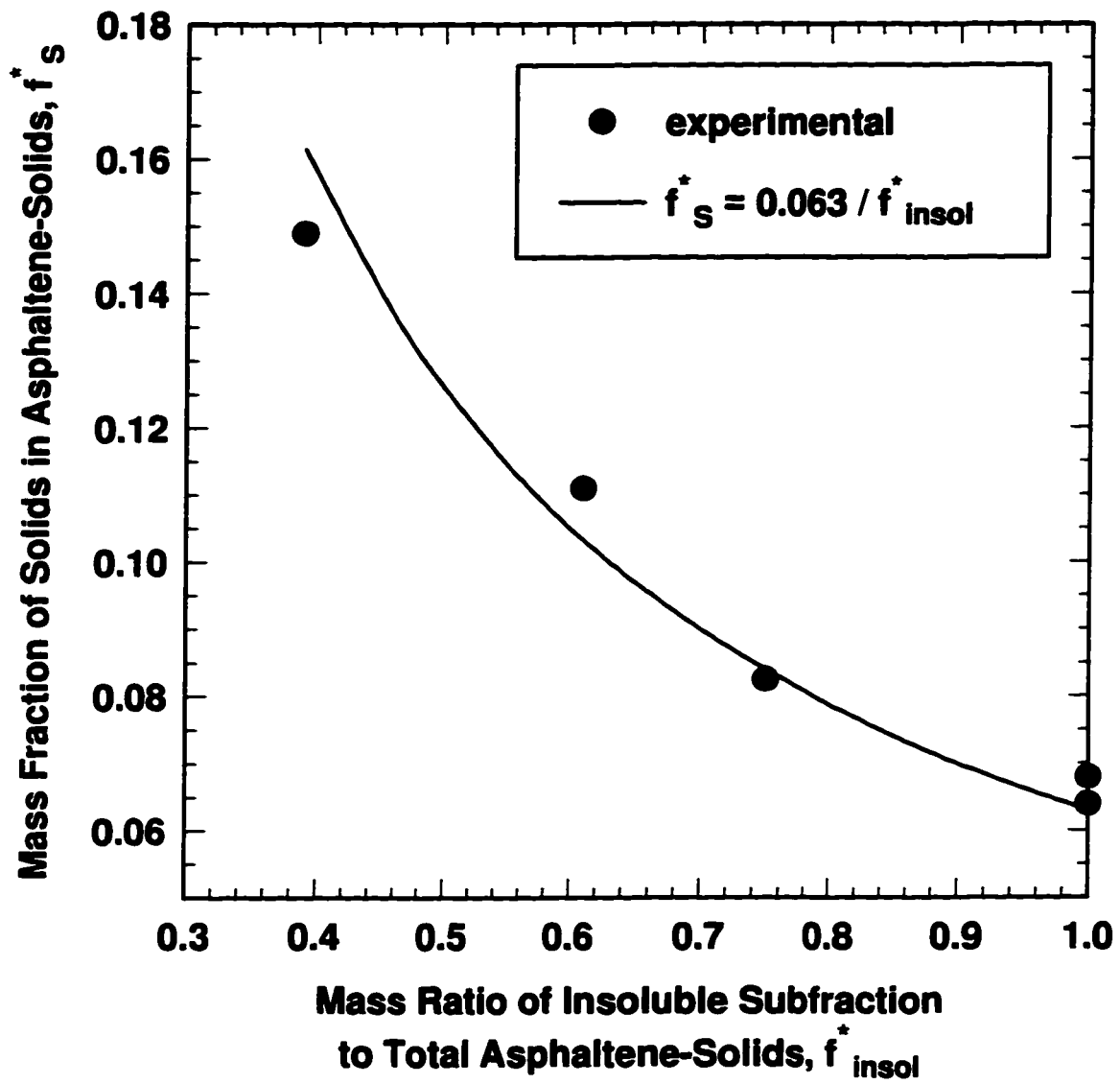


Figure 2.1: Mass fraction of solids in asphaltene-solids subfractions.

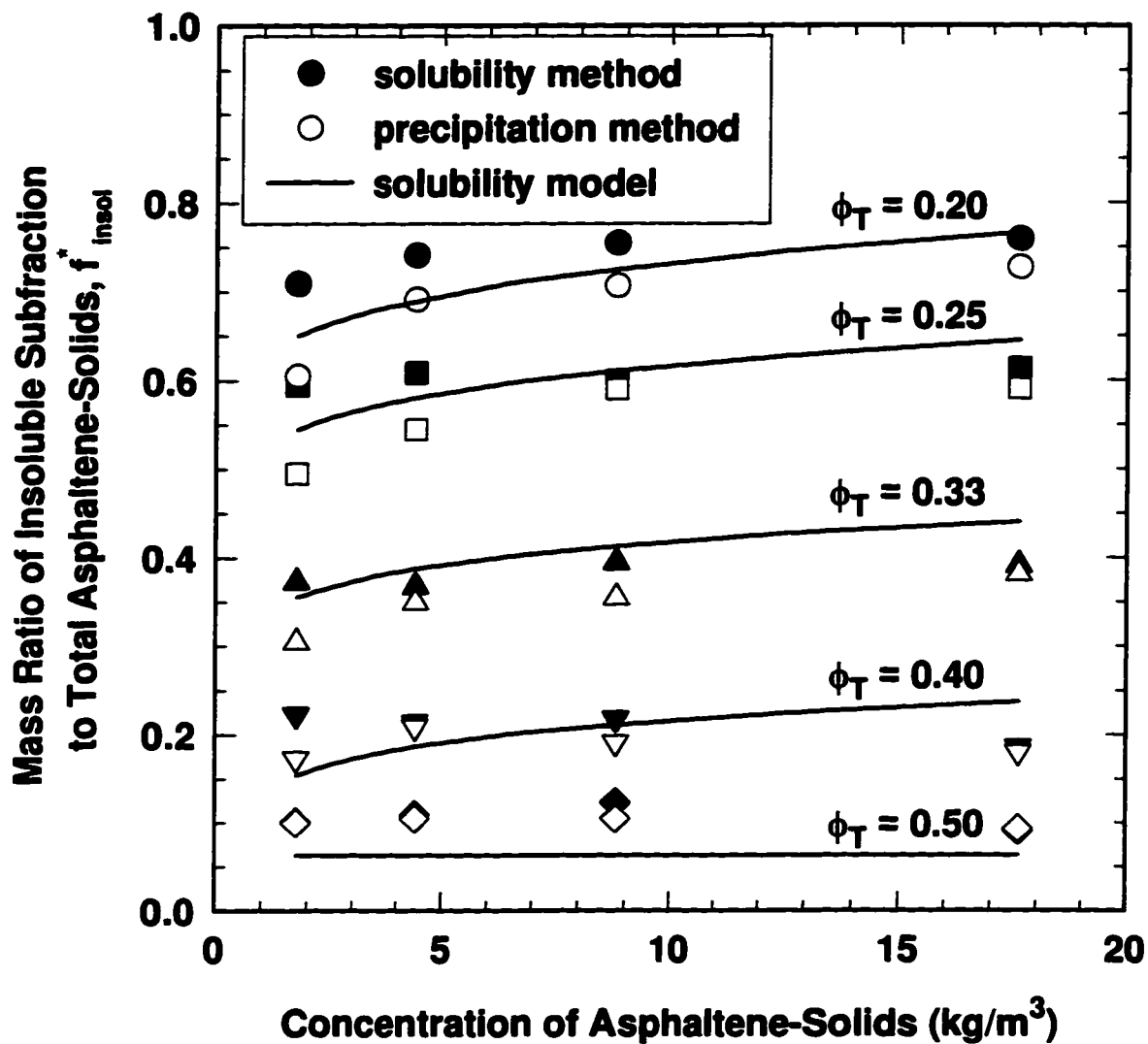


Figure 2.2: The effect of asphaltene concentration on the solubility of asphaltene-solids in solutions of toluene and hexane.

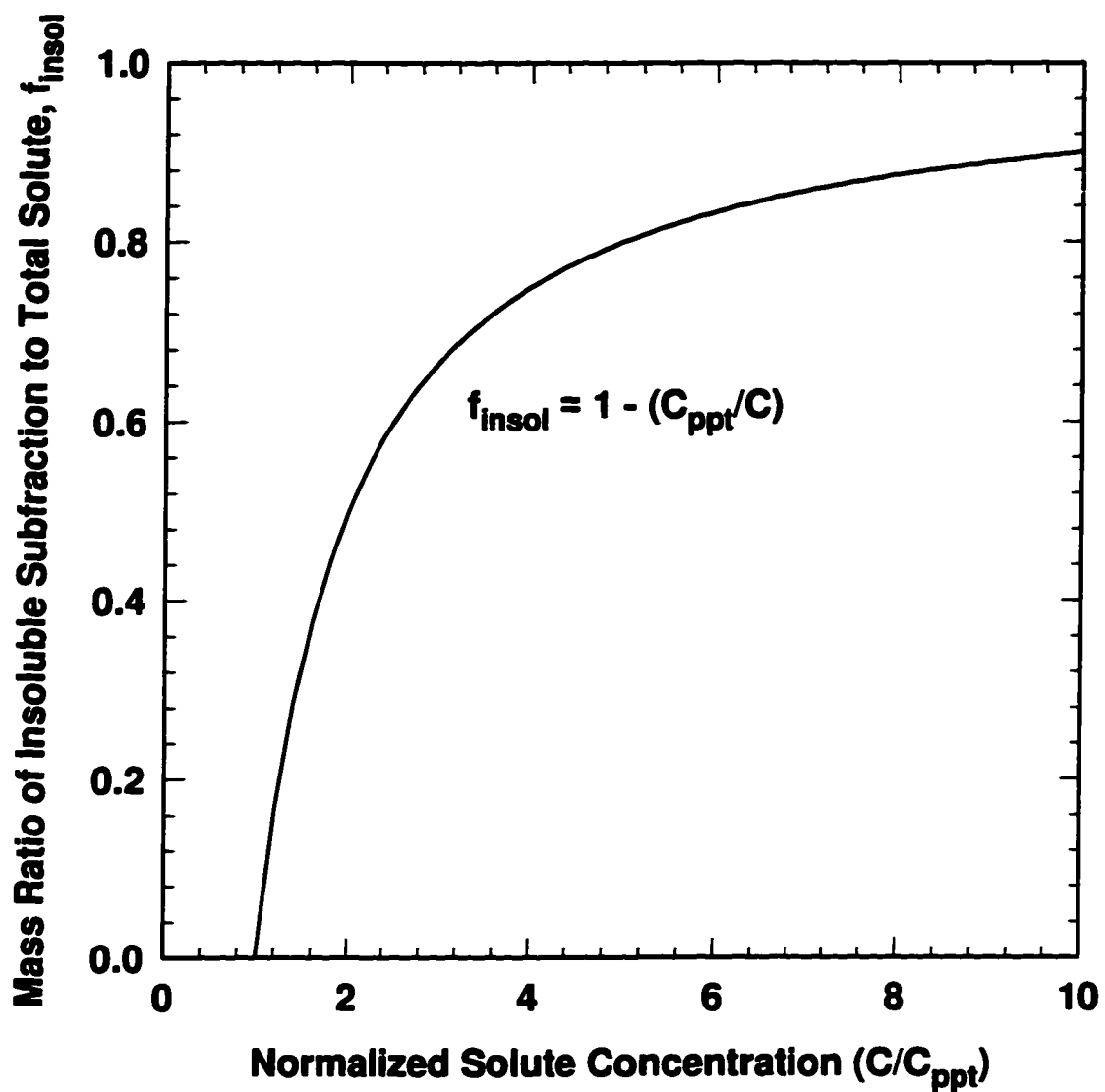


Figure 2.3: Theoretical solubility of a pure solute as a function of solute concentration.

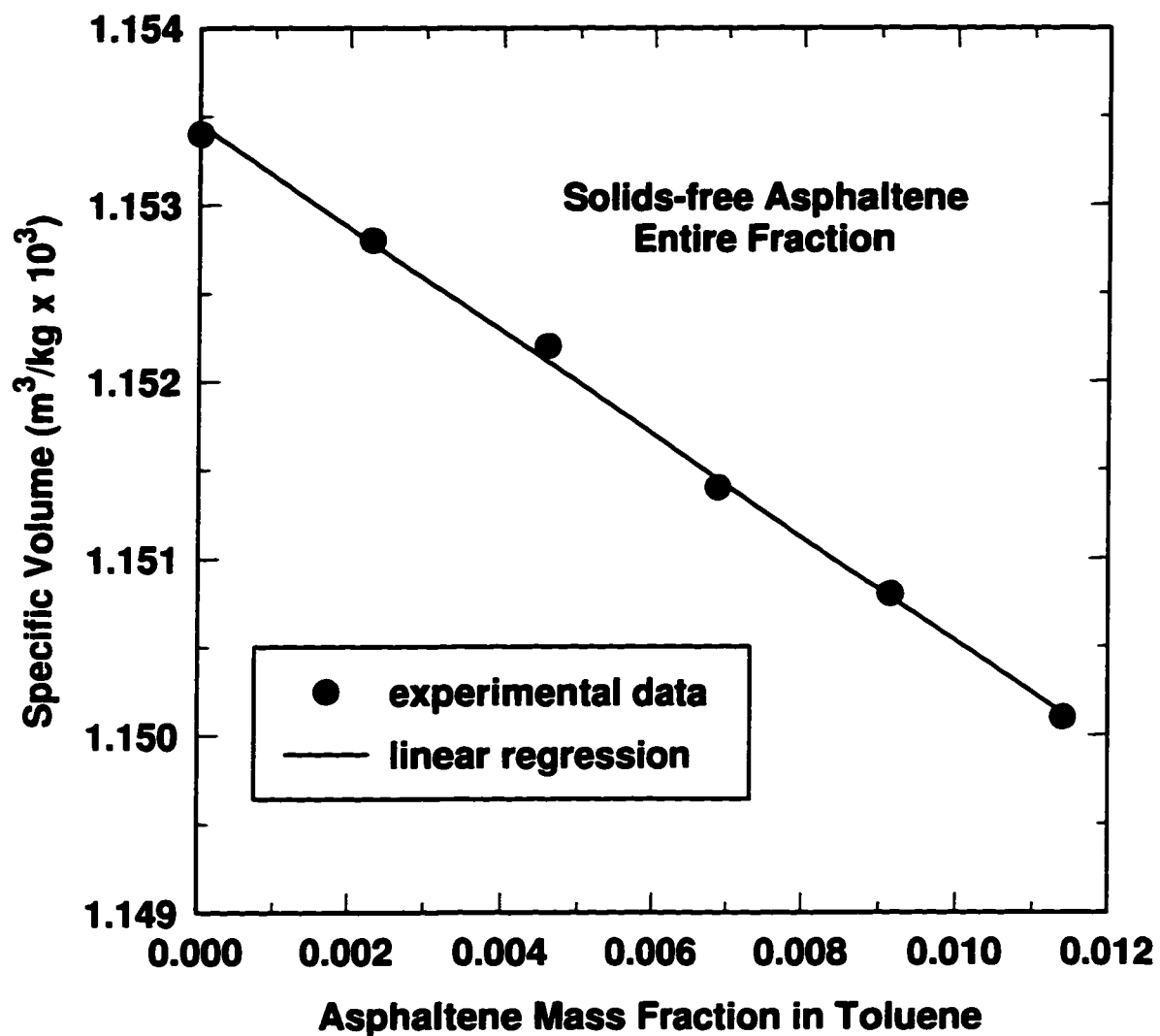


Figure 2.4: Dependence of asphaltene-toluene mixture specific volume on asphaltene concentration.

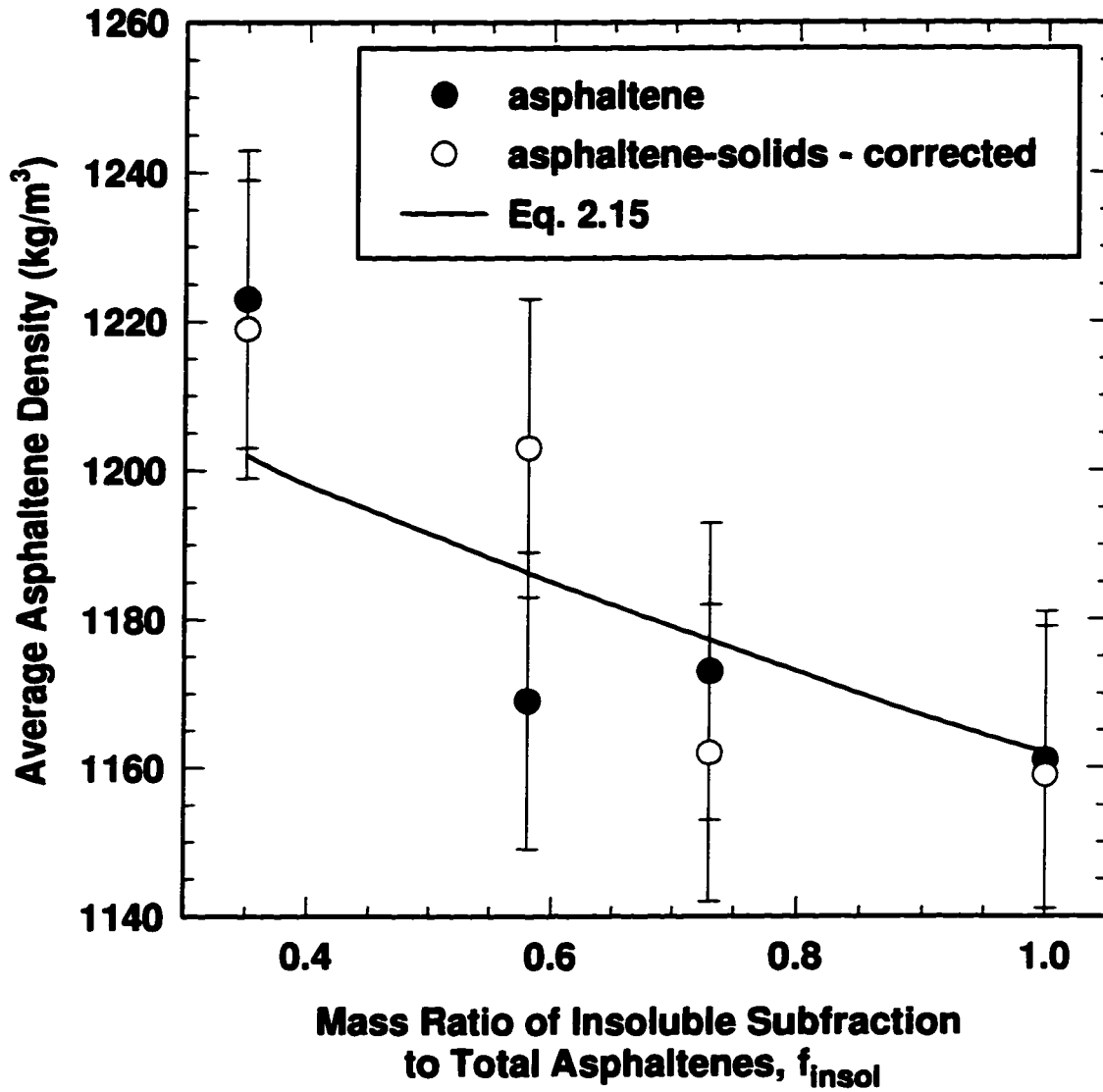


Figure 2.5: Average density of asphaltene subfractions.

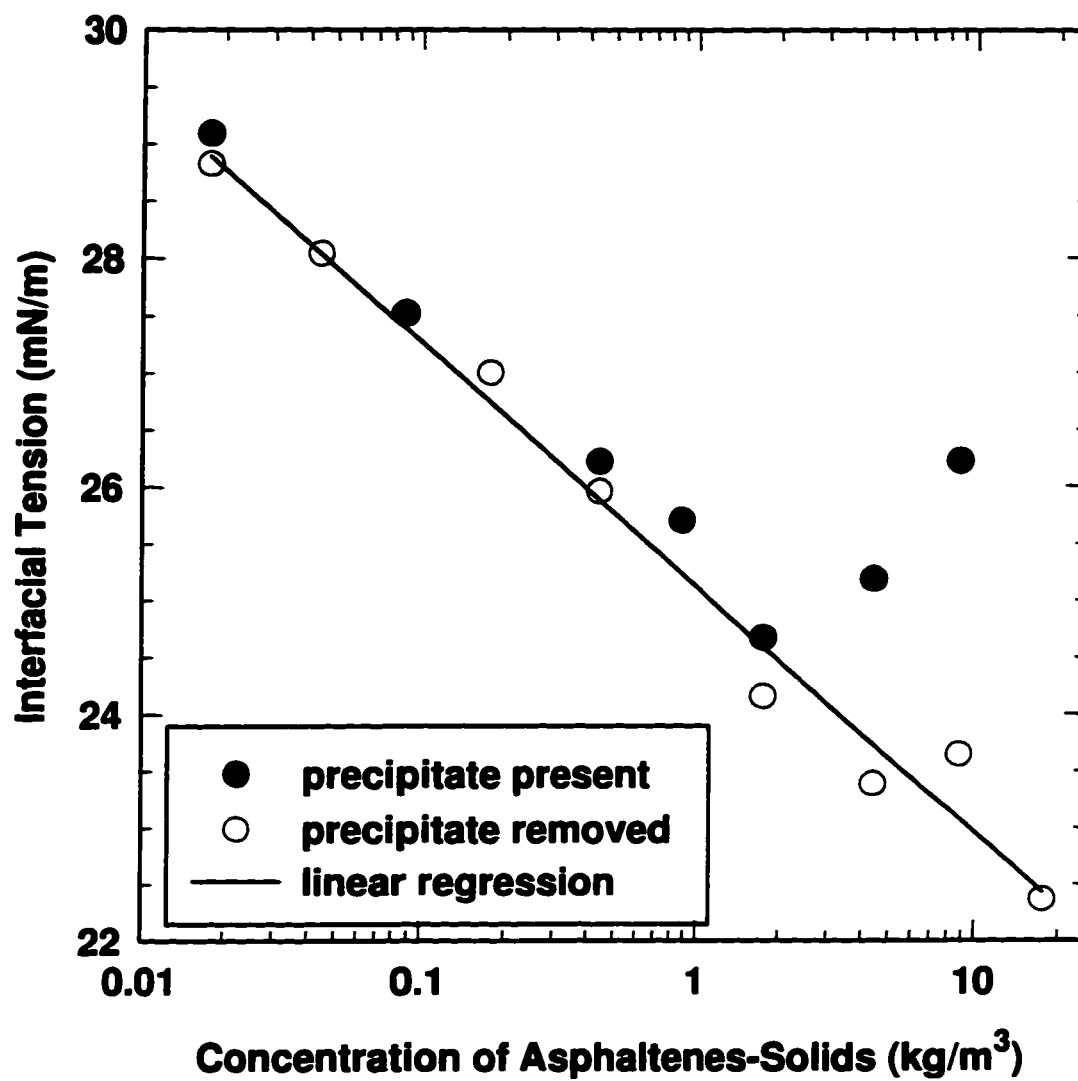


Figure 1.6: Interfacial tensions of asphaltene-solids in a toluene-hexane solution of 25 vol% toluene over water.

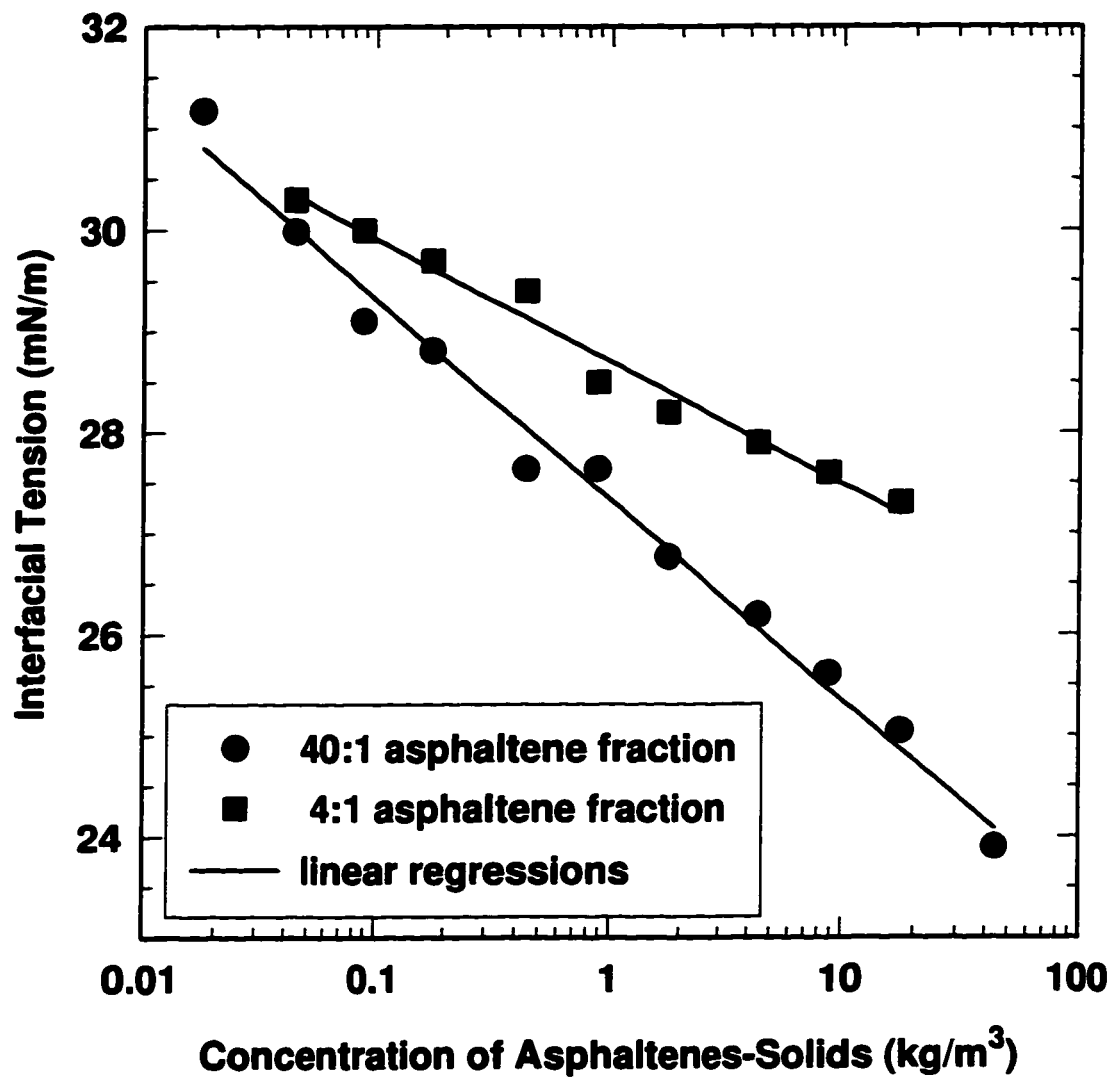


Figure 2.7: Interfacial tension of solutions of asphaltene-solids in toluene over water.

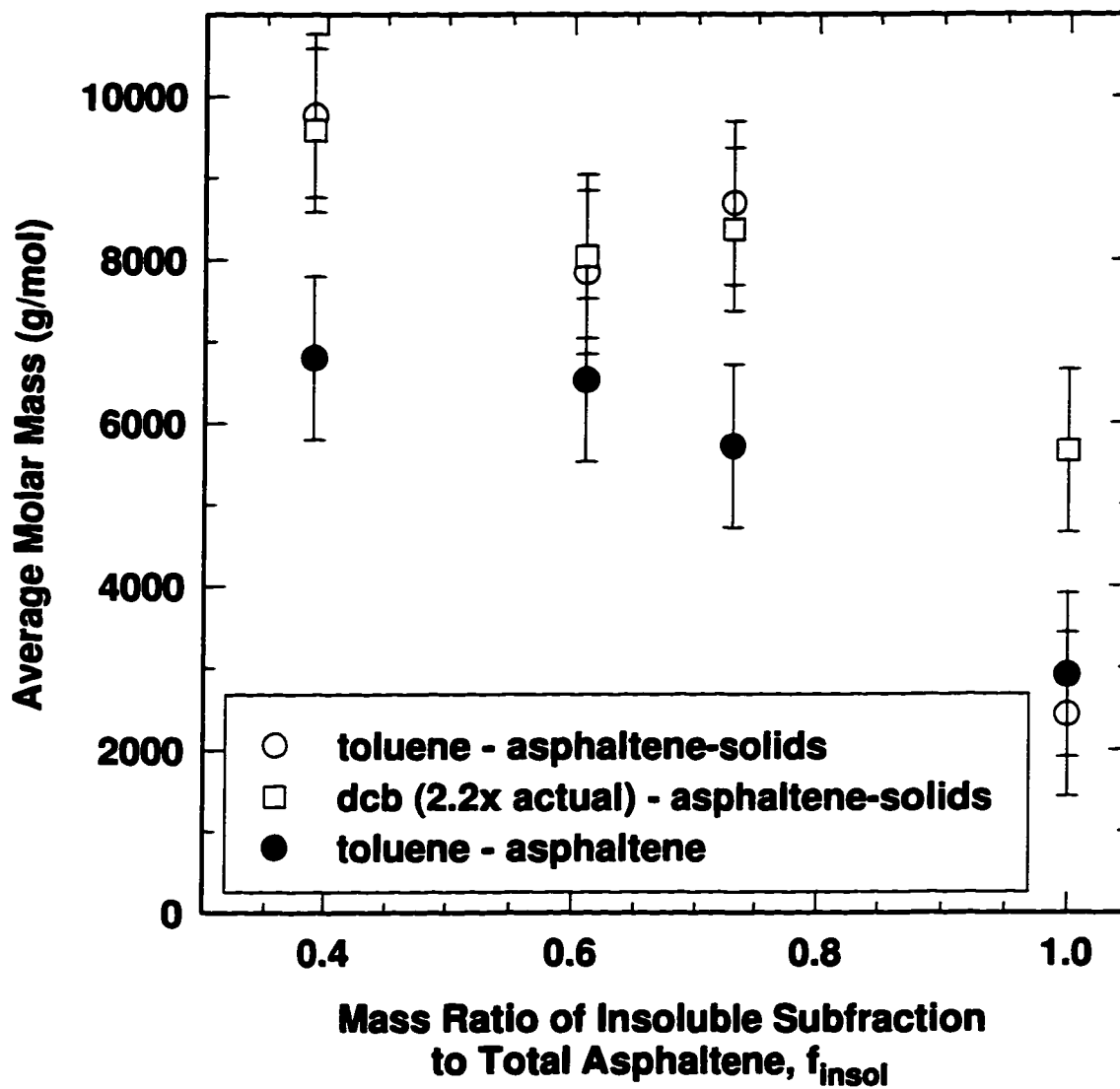


Figure 2.8: Molar mass of asphaltene subfractions determined by vapor pressure osmometry.

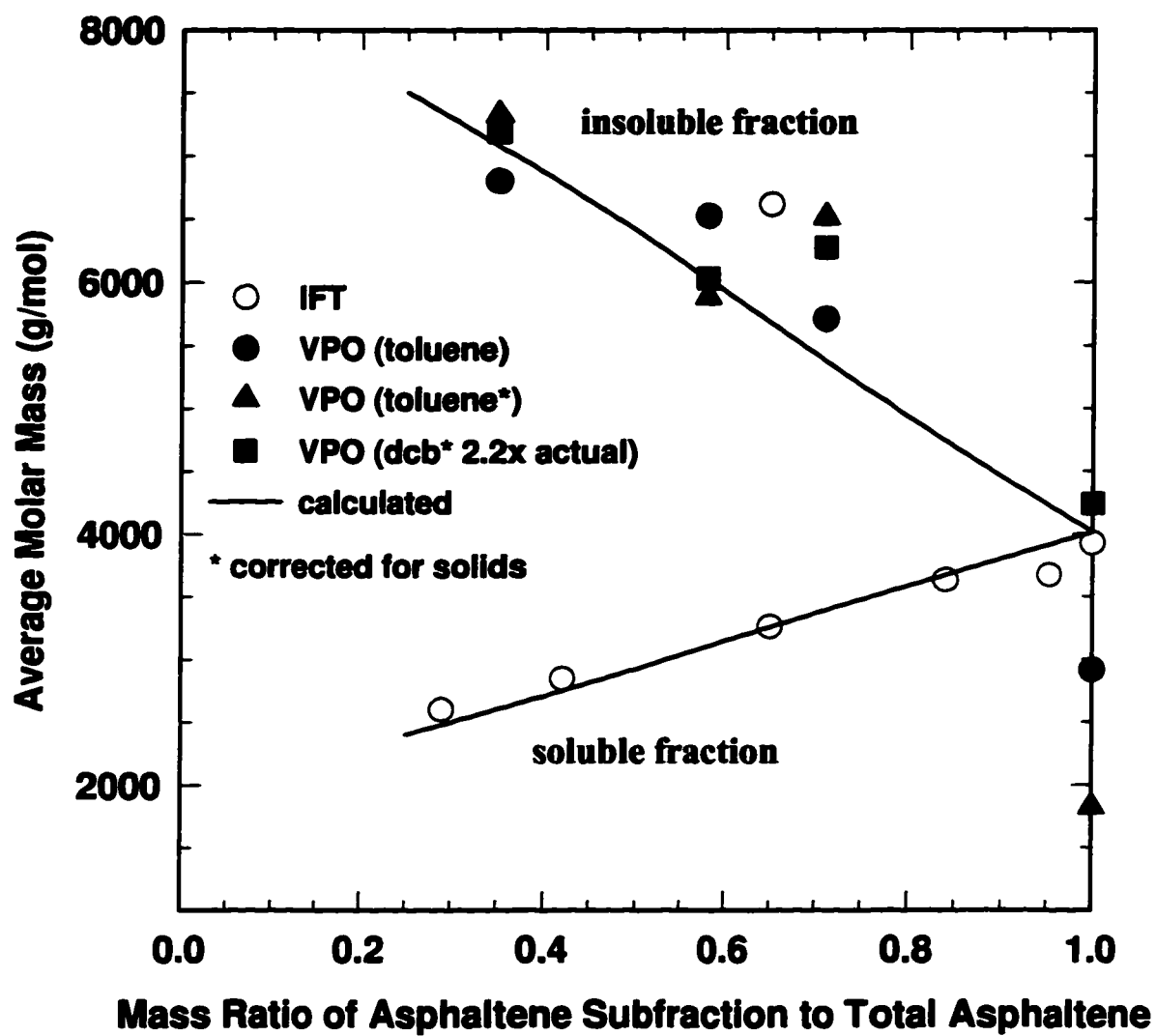


Figure 2.9: Molar mass of asphaltene subfractions.

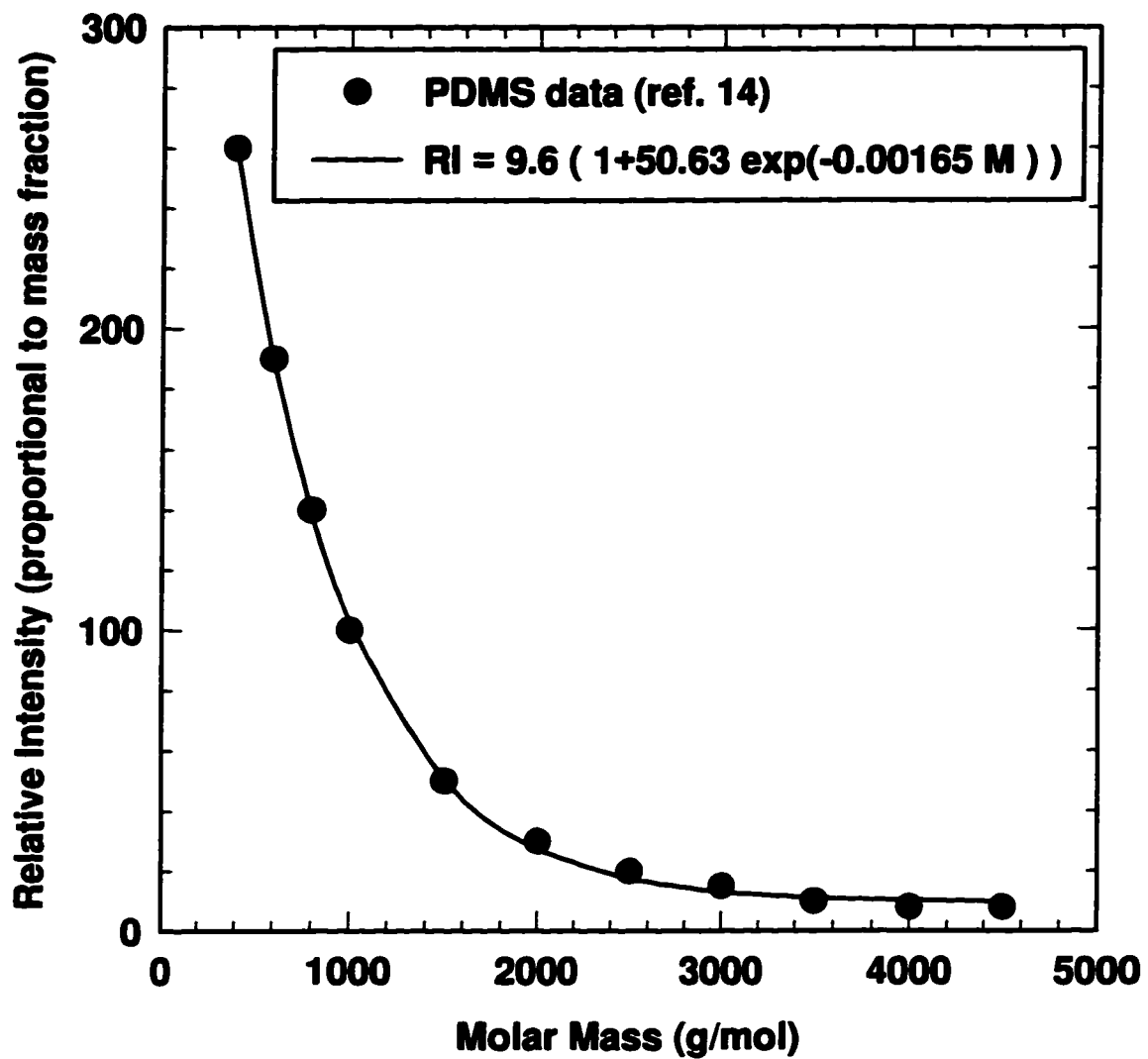


Figure 2.10: PDMS molar mass frequency distribution of Athabasca bitumen.

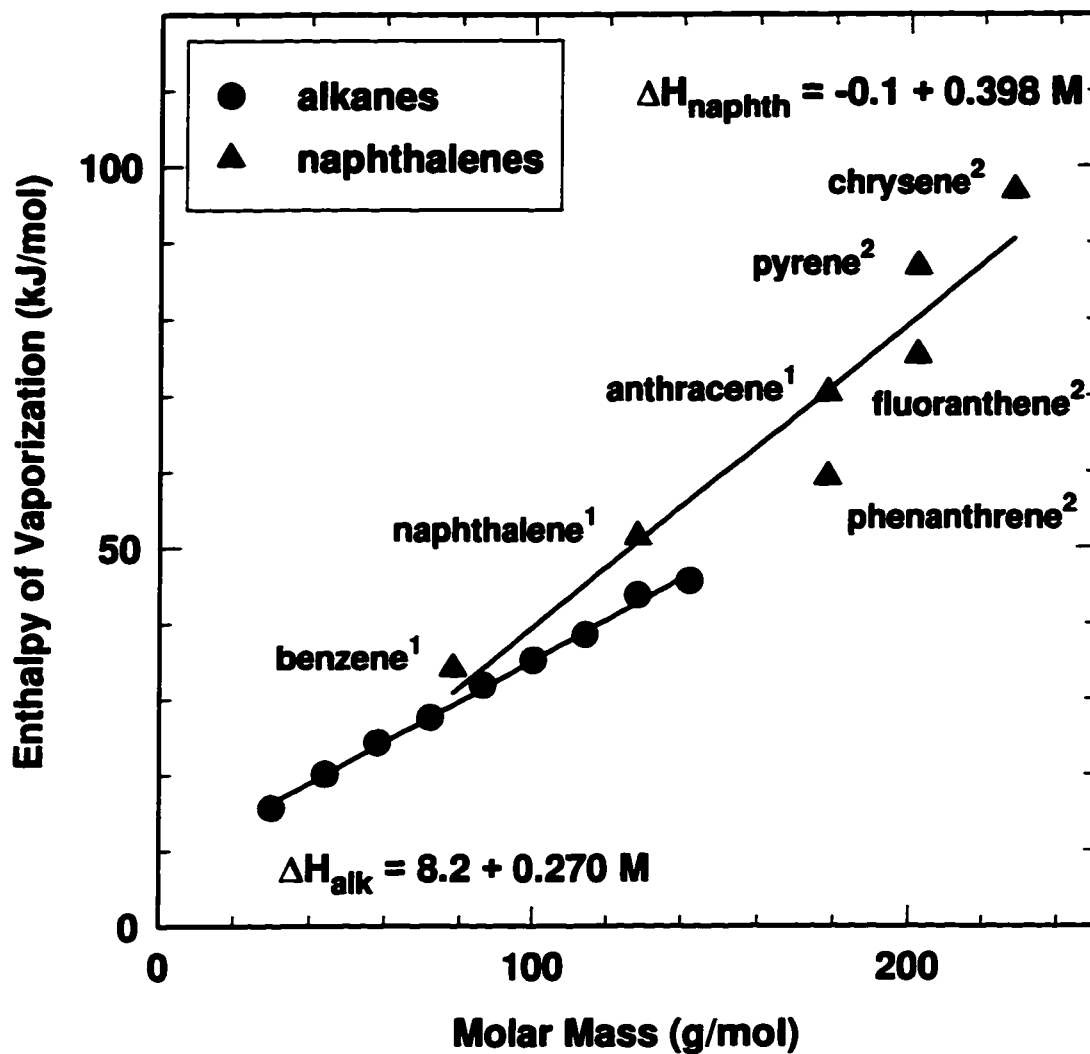


Figure 2.11: Enthalpy of vaporization of homologous series. (1. ref. 24; 2. ref. 25)

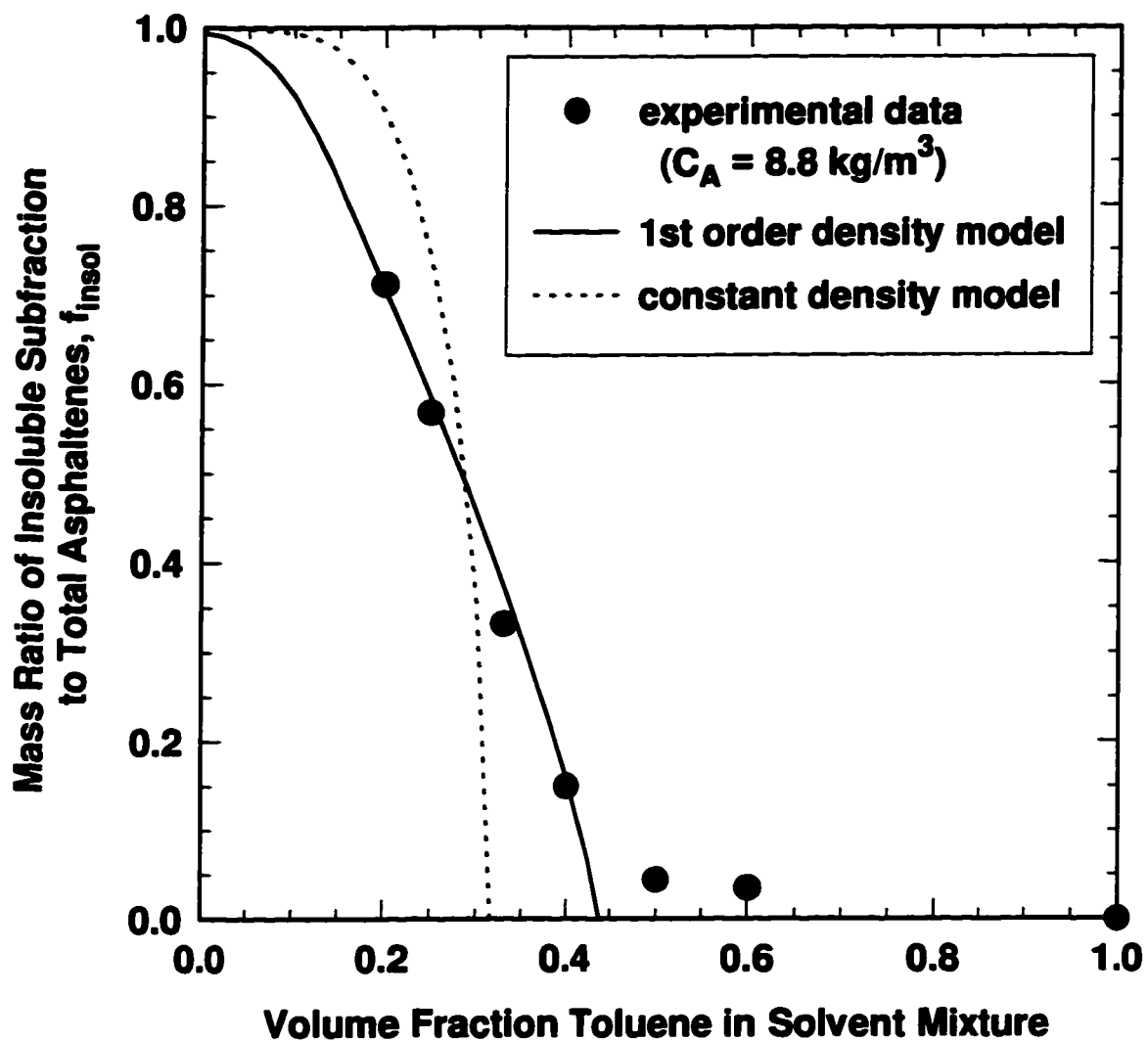


Figure 2.12: Predicted and experimental solubility of asphaltenes in solutions of toluene and hexane.

Chapter 3

SOLUBILITY MODELING OF ASPHALTENES IN ORGANIC SOLVENTS [†]

3.1 Introduction

There are two approaches to modeling asphaltene solubility. In the first approach, asphaltene micelles are assumed to be stabilized by resins and precipitation to be caused by the flocculation of the micelles. In the second approach, asphaltenes are assumed to exist as free molecules that precipitate in a conventional manner. In both cases, Scatchard-Hildebrand solubility theory with a Flory-Huggins entropy of mixing term forms the heart of the model (1). There is some evidence that the micelle model is appropriate for some asphaltenes, *e.g.*, Boscan asphaltenes (2). However, the research study presented here deals with Athabasca asphaltenes at relatively low concentrations, below 2 wt %. In the case of Athabasca asphaltenes, there is no evidence of micellization at asphaltene concentrations below 18 kg/m³ (2 wt %) in solutions of toluene and hexane, as discussed in Chapter 2. Therefore, the Athabasca asphaltenes are modeled as non-associated molecules.

When the solubility theory for non-associated asphaltenes was first developed, the asphaltenes were treated as a uniform material (3). With this assumption, good predictions of the asphaltene precipitation point were obtained but predictions of the amount of precipitated material were poor. Recently, more accurate results were obtained when the asphaltenes were treated as a multicomponent mixture with a variety of physical properties (4,5). However, because the physical properties of the asphaltenes are difficult to measure, they are generally approximated using equations of state (6,7). Hence, the usefulness of the theory is limited by the accuracy of the physical property estimates.

[†] Printed in part: Mannistu, K.D., Yarranton, H.W., and Masliyah, J.H., *Energy & Fuels*, 11, (1997), 615.

In Chapter 2, the molar mass distribution of the Athabasca asphaltenes was measured and correlations were developed for the physical properties required for the solubility calculation: molar volume and the solubility parameter. Using the correlations and Scatchard-Hildebrand solubility theory with a Flory-Huggins entropy of mixing term, the precipitation point and the amount of precipitated asphaltenes in solutions of toluene and hexane were successfully predicted at ambient conditions. Studies on the precipitation of asphaltenes from bitumen in different solvents indicate that it should be possible to generalize a solubility model based on Scatchard-Hildebrand theory to any solvent system provided there is no micellization (8). However, the prediction method had yet to be tested with solvents other than toluene and hexane.

In this chapter, the solubility of Athabasca asphaltenes is measured in fifteen solvent systems. The systems include branched, halogenated, and n-alkanes, cyclic alkanes, alcohols, ketones, and various aromatics. Predictions based on Scatchard-Hildebrand theory including the Flory-Huggins entropy of mixing term and the previously developed correlations are compared with the experimental results for each system. Predictions using single component and Hansen three component solubility parameters are examined.

3.2 Experimental Method

The asphaltenes used in the experiments were extracted from Syncrude coker feed Athabasca bitumen (bitumen that has been treated to remove sand and water and is ready for upgrading). As discussed in Chapter 2, these asphaltenes contain “solids” which make up 6.3 wt % of the asphaltenes. The “solids”, which include fine clays, ash and some adsorbed hydrocarbons, are insoluble in toluene. The “solids” form part of the first material to precipitate and hence are always part of the insoluble portion of the asphaltenes-solids mixture. For all the results presented here, the mass ratios of insoluble asphaltenes to total asphaltenes are reported on a “solids”-free basis.

The solubility of the asphaltenes in different solvent systems was determined by solubility and by precipitation, as described in Section 2.2.2. All of the reagents were of at least 98

% purity. Toluene, heptane, octane, isopentane, isooctane, dichloromethane, and decalin were purchased from Fisher Scientific. 1-hexene and t-butylbenzene were purchased from Aldrich Chemicals. Cyclohexane, pentane, and decane were purchased from Caledon. Nitrobenzene, hexane, methanol, and acetone were purchased from BDH Chemicals.

3.3 Theory

As discussed previously, the asphaltenes are assumed to be a mixture of non-associated molecules. The precipitation of the asphaltenes can then be predicted with a multicomponent equilibrium calculation. To perform the equilibrium calculation the following data are required: feed composition and equilibrium ratios for each component. To determine the equilibrium ratios, the molar volume and solubility parameter for each component are needed.

To obtain the feed composition, the molar mass distribution of the asphaltenes must be measured. The Athabasca asphaltenes precipitated with the method described in Chapter 2 were found to range in molar mass from 2000-8500 g/mol with the following molar mass distribution

$$\frac{df_i}{dM_i} = \text{constant}(1 + \alpha_M \exp\{-\beta_M M_i\}) \quad (2.11)$$

where f_i is the cumulative mass frequency up to the i^{th} asphaltene component, M_i is the molar mass (g/mol) of the i^{th} asphaltene component, and α_M and β_M have values of 50.63 and 0.00165 mol/g, respectively. The integrated form of Eq. 2.11 that is used to solve for the mass ratio of the insoluble subfraction to total asphaltenes is given by

$$\int_{M_i}^{M_U} \left(\frac{df_i}{dM_i} \right) dM_i = 1 - f_i = \frac{M_U - M_i - \alpha_M (\exp\{-\beta_M M_U\} - \exp\{-\beta_M M_i\})}{M_U - M_L - \alpha_M (\exp\{-\beta_M M_U\} - \exp\{-\beta_M M_L\})} \quad (2.12)$$

where $M_L=2000$ g/mol and $M_U=8500$ g/mol. Solubility theory predicts that the highest molar mass asphaltene molecules precipitate first and therefore $1-f_i = f_{insol}$. where f_{insol} is the mass ratio of the insoluble subfraction of asphaltenes to total asphaltenes.

For a mixture of high molar mass molecules like asphaltene, the expression for the equilibrium ratio ($K_i = \hat{x}_i^s / \hat{x}_i^l$ where \hat{x}_i^s and \hat{x}_i^l are the solid and liquid phase mole fractions of component i , respectively) was developed in Chapter 2 and is given by

$$K_i = \exp \left\{ 1 - \frac{v_i^l}{v_m} + \ln \left(\frac{v_i^l}{v_m} \right) + \frac{v_i^l}{RT} (\delta_i^l - \delta_m)^2 \right\} \quad (2.7)$$

Here, R is the universal gas constant (J/mol K), T is temperature (K) and v_i^l and v_m are the liquid phase molar volumes (cm^3/mol) of component i and the solvent, respectively. δ_i^l and δ_m are the solubility parameters ($\text{MPa}^{1/2}$) for the same respective constituents. The solvent mixture properties, v_m and δ_m , are calculated using published values for the properties of the mixture components. The solubility parameter of a mixture is the volume average of the individual component solubility parameters. For the asphaltene properties, the following correlations were developed in Chapter 2:

$$v_i^l = \frac{1000M_i}{0.017M_i + 1080} \quad (2.21)$$

$$\delta_i^l = [A(0.017M_i + 1080)]^{1/2} \quad (2.22)$$

where A is the change in the heat of vaporization of asphaltene with a change in molar mass. A value of 367 J/g for A gives the best prediction of asphaltene solubility in toluene/hexane solutions. The prediction is shown in Fig. 3.2.

The solubility parameter is the square root of the cohesive energy density of component i and represents the total molecular interaction energy which includes dispersion, polar, and hydrogen bonding interaction energies. A single component solubility parameter is expected to work well when dispersion forces dominate but may not accurately represent polar solvents where polar and hydrogen bonding forces approach the dispersion forces in significance. Two component solubility parameters accounting for the dispersion and polar interaction energies have been evaluated previously for asphaltenes. (9) However, a three component (Hansen) solubility parameter accounting for the different contributions of each interaction energy was developed earlier (10) and there are extensive published data available for the three component solubility parameters of many solvents. To determine K_i using Hansen parameters, Eq. 2.7 is modified as follows,

$$K_i = \exp \left\{ 1 - \frac{v_i'}{v_m} + \ln \left(\frac{v_i'}{v_m} \right) + \frac{v_i'}{RT} \left[(\delta_{di} - \delta_{dm})^2 + b \left[(\delta_{pi} - \delta_{pm})^2 + (\delta_{hi} - \delta_{hm})^2 \right] \right] \right\} \quad (3.1)$$

where δ_d , δ_p and δ_h are the dispersion, polar and hydrogen bonding solubility parameters, respectively. The variable b is a weighting factor, a property of component i , with a recommended value of 0.25 (10). The Hansen parameters represent the dimensions of a solubility “sphere” for a given component. The expression in Eq. 3.1 containing the squared differences of the solubility parameters is the distance between the solvent solubility “sphere” and the solubility “sphere” of asphaltene component i . The closer the two spheres, the more likely the asphaltene is to be dissolved. Although Eq. 3.1 is less theoretically justified than Eq. 2.7, the predictions from Eq. 3.1 were shown to be more accurate for more polar solvents than those from Eq. 2.7 (10). When dispersion forces dominate, *i.e.* for nonpolar solvents, Eq. 3.1 reduces to Eq. 2.7 and the predictions are expected to coincide. To use the three component parameters, correlations for each component of the asphaltene solubility parameter must be developed.

To approximate the asphaltene solubility parameters it is assumed that all three are related to molar mass in the same manner as the single component parameter given in Eq. 3.1.

$$\delta_{ji} = (A_j(0.017M_i + 1080))^{1/2} \quad j = d, p, h \quad (3.2)$$

Hence the respective values of A can be related as follows,

$$\psi_1 = \left(\frac{A_p}{A_d} \right) = \left(\frac{\delta_{pi}}{\delta_{di}} \right)^2 \quad (3.3a)$$

$$\psi_2 = \left(\frac{A_h}{A_p} \right) = \left(\frac{\delta_{hi}}{\delta_{pi}} \right)^2 \quad (3.3b)$$

A value of 4 is assumed for ψ_2 because this is the ratio for the known compounds most similar to asphaltenes: ethylbenzene and naphthalene. Values of 355 J/g and 0.01 for A_d and ψ_1 respectively, give the best prediction for the toluene/hexane system. The prediction is shown in Fig. 1b. The corresponding values of A_p and A_h are 3.55 and 14.2 J/g, respectively. At the average asphaltene molar mass of 3920 g/mol, the three components of the asphaltene solubility parameter are 20.2, 2.0 and 4.0 MPa^{1/2} for δ_d , δ_p and δ_h respectively, with a total solubility parameter, δ_r , of 20.7 MPa^{1/2}. These values are comparable to those of naphthalene given in Table 1. The total solubility parameter is in good agreement with published values for asphaltene of about 20 (11).

3.4 Results and Discussion

Solubility calculations are made using a multicomponent equilibrium calculation. The asphaltene feed composition is determined from Eq. 2.12. Equilibrium ratios are calculated from Eq. 2.7 for the single component solubility parameter model (δ_1 model) and from Eq. 3.1 for the three component solubility parameter model (δ_3 model). Asphaltene molar volumes are estimated using Eq. 3.2 and the single and three component solubility parameters are estimated from Eqs. 2.22 and 3.2 respectively. Solvent molar volumes and solubility parameters are calculated from the constituent

properties given in Table 3.1. The computer programs employed for the solubility calculations are given in Appendix B.

Table 3.1: Physical properties of solvents

| Solvent | Molar Mass (g/mol) ^a | Density (kg/m ³) ^a | Solubility Parameters (MPa) ^{1/2} ^b | | | | |
|-----------------------------|---------------------------------------|--|---|------------|------------|------------|------------|
| | | | δ | δ_d | δ_p | δ_h | δ_t |
| Pentane | 72.2 | 626 | 14.3 | 14.3 | 0 | 0 | 14.3 |
| Hexane | 86.2 | 655 | 14.9 | 14.9 | 0 | 0 | 14.9 |
| Heptane | 100.2 | 684 | 15.3 | 15.3 | 0 | 0 | 15.3 |
| Octane | 114.2 | 699 | 15.5 | 15.5 | 0 | 0 | 15.5 |
| Decane | 142.3 | 730 | 15.8 | 15.8 | 0 | 0 | 15.8 |
| Isopentane | 72.2 | 620 | 13.8 | 13.7 | 0 | 0 | 13.7 |
| Isooctane | 114.2 | 688 | 14.0 | 14.3 | 0 | 0 | 14.3 |
| Cyclohexane | 84.2 | 779 | 16.8 | 16.8 | 0 | 0 | 16.8 |
| Decalin ^c | 138.3 | 883 | 18.4 | 18.4 | 0 | 0 | 18.4 |
| Benzene | 78.1 | 877 | 18.8 | 18.4 | 0 | 2.0 | 18.6 |
| Toluene | 92.1 | 867 | 18.25 | 18.0 | 1.4 | 2.0 | 18.2 |
| Ethylbenzene | 106.2 | 867 | 17.8 | 17.8 | 0.6 | 1.4 | 17.8 |
| t-Butylbenzene ^d | 134.2 | 867 | 17.4 | 17.4 | 0 | 1.0 | 17.4 |
| Naphthalene | 128.2 | 1025 | 20.3 | 19.2 | 2.0 | 3.9 | 20.3 |
| Nitrobenzene | 123.1 | 1204 | 21.7 | 20.0 | 8.6 | 4.1 | 22.2 |
| Dichloromethane | 84.9 | 1327 | 19.8 | 18.2 | 6.3 | 6.1 | 20.3 |
| 1-Hexene | 84.2 | 673 | 15.0 | 15.1 | 1.9 | 0 | 15.2 |
| Methanol | 32.0 | 791 | 29.6 | 15.1 | 12.3 | 22.3 | 29.6 |
| Acetone | 58.1 | 790 | 20.0 | 15.5 | 10.4 | 7.0 | 20.0 |

Note:

- a) Source: ref. 14
- b) Source: ref. 10
- c) Density and solubility parameters for decalin are a volume average assuming that decalin is 50 vol% in the cis configuration and 50 vol% in the trans configuration.
- d) The three component solubility parameter was estimated from the single component value in ref. 8 and from the Hansen values for benzene and ethylbenzene in ref. 10.

The solvents chosen to test the models were selected to provide a broad range of molar masses, functional groups and solubility parameters. In each case, a poor solvent, or

precipitator, is paired with a good solvent and experiments and predictions performed for the entire composition range of solvents. Paired solvents allow a more rigorous test of the model because the exact points of full solubility and zero solubility can be located. Since the model was tuned to the toluene/hexane system, all poor solvents are paired with the good solvent, toluene, and all good solvents are paired with hexane. In all cases, the asphaltene concentration is 8.8 kg/m^3 . Asphaltene concentration was shown in Chapter 2 to have little effect on f_{insol} . Each group of solvents is discussed in detail below. Raw data for all the solvent systems discussed below is provided in Appendix B.

3.4.1 n-Alkane Homologous Series.

Predictions and experimental results for toluene with each of pentane, hexane, heptane, octane, and decane are presented in Figs. 3.1 to 3.5 respectively. In all cases the predicted fractional precipitation is within 0.05 of the experimental data and the predicted precipitation point is within 0.10 of the experimental value. As expected for non-polar solvents, both the single and three component solubility parameter predictions are comparable. Fig. 3.6 shows the δ_3 model prediction curves for the five systems. The predicted curves for heptane, octane and decane are nearly identical even though, as shown in Table 3.1, the solubility parameter and molar mass both increase along the homologous series. Increasing the solvent molar mass tends to increase the fraction of insoluble material, *i.e.*, shifts the solubility curve to the right. However, increasing the solvent solubility parameter has the opposite effect. The model correctly accounts for the compensating effects.

Andersen (12) found that the amount of asphaltene precipitate is greater when the asphaltenes are dissolved from solid form (solubility method) than when they are precipitated from a fully solubilized condition (precipitation method). In all our experiments, the same hysteresis is observed although the difference in fractional precipitation is small, usually less than 0.05. The hysteresis suggests that there is an extra step in the mechanics of solubilizing or precipitating the asphaltenes which is not yet accounted for in the theory.

In Figs. 3.1 to 3.5, it can be seen that near the precipitation point the predictions of f_{insol} are nearly linearly related to the volume fraction of toluene while the experimental insoluble mass fractions tail towards higher values of the toluene volume fraction. The tailing may occur because some asphaltenes which would otherwise be soluble, adsorb on the “solids” and are captured in the insoluble material. Another possibility is that the asphaltene solubility parameter is not related solely to molar mass. At each molar mass there may be a distribution of solubility parameters. Such a distribution could easily give rise to the tailing near the precipitation point seen in Figs. 3.1 to 3.6.

At this time, no attempt is made to predict the tailing effect. Instead, the solubility models are tested on a variety of solvent systems to determine if the models could be generalized beyond the toluene/hexane system. The measure of the quality of the predictions is taken to be the difference between predicted and experimental fractions of insoluble asphaltenes.

3.4.2 Branched Alkanes

Results for isopentane (2-methylbutane) and isooctane (2,2,4-trimethylpentane) each with toluene are given in Figs. 3.7 and 3.8. For the isopentane-toluene system, the procedure was altered because isopentane has a high vapor pressure (79.3 kPa) and the evaporation of the mixture overnight was significant. Therefore the mixture was left to come to equilibrium for one hour instead of overnight. Since isooctane has a low vapor pressure and takes a long time to evaporate, the precipitated asphaltenes were filtered instead of centrifuged. For both isopentane and isooctane, the predictions overestimate the fraction of insoluble asphaltenes; however, the predicted fractional precipitation is still reasonably close to the experimental data.

The polar and hydrogen bonding components of the branched alkane solubility parameters are zero; hence, the δ_1 and δ_3 model predictions should be nearly identical for the branched alkane/toluene systems. The predictions from each model for the

isopentane/toluene system are similar. However, the predictions for the isooctane/toluene system are not the same because the isooctane solubility parameters for the δ_1 and δ_3 models are different, as shown in Table 1. The isooctane solubility parameters are different because they are taken from different data sources. Hence, the disagreement in the predictions of the two models reflects the data sources rather the effect of using three component versus single component solubility parameters.

3.4.3 Aromatics

Results for nitrobenzene and t-butylbenzene each with hexane are shown in Figs. 3.9 and 3.10. Nitrobenzene and t-butylbenzene both have low vapor pressures so again the precipitated asphaltene were filtered rather than centrifuged. For the t-butylbenzene/hexane system, the solvents are relatively non-polar and both the δ_1 and δ_3 models predict the fractional precipitation quite accurately. However, nitrobenzene is quite polar as is reflected in the difference between the δ_1 and δ_3 model predictions for the nitrobenzene/hexane system. As expected, the δ_3 model is more accurate and predicts the fractional precipitation to within 0.05. Since the dispersion forces dominate in the nitrobenzene/hexane mixtures, the δ_1 model still predicts the data reasonably well.

3.4.4 Cyclic Compounds

Results for decalin (decahydronaphthalene) and cyclohexane each with hexane are presented in Figs. 3.11 and 3.12, respectively. Decalin has a low vapor pressure so the precipitated asphaltene were filtered rather than centrifuged. Decalin, $C_{10}H_{18}$, is structurally equivalent to two cyclohexane rings attached along one side. For the decalin/hexane system, both models predict the experimental data well, only slightly underestimating the fractional precipitation. However, the quality of the predictions is much poorer for the cyclohexane/hexane system. Both models predict complete solubility of asphaltene in a mixture of 75% cyclohexane and 25% hexane. In fact, 30% of the asphaltene are insoluble in pure cyclohexane. Predicted fractional precipitation deviates from experimental data quite significantly.

To test that the experimental data represent the equilibrium condition, a solubility experiment was conducted with a five day interval between mixing and centrifuging instead of the usual one day interval. There was no difference in the results. As a further check, the solubility experiments were repeated at a lower concentration of asphaltenes, 4.4 kg/m^3 . As shown in Fig. 3.12, there is little difference from the results at 8.8 kg/m^3 of asphaltenes. Hence, the experimental data appears to be valid and the discrepancy must arise from the solubility models. The reason for the model failure may lie in the cyclic nature of the solvent. There is some evidence that the entropy of mixing between cyclic and linear molecules does not follow the form used in the Flory-Huggins term. (13) Unfortunately, this hypothesis does not explain why the predictions are successful for decalin, also a cyclic compound. However, the hypothesis cannot be tested further until the entropy of mixing between cyclic and linear molecules is better understood. In any case, a modified version of the theory is necessary to deal with cyclic compounds.

3.4.5 Dichloromethane, 1-Hexene

Dichloromethane and 1-hexene are of interest because they have quite different chemical properties than the solvents to which the solubility models were tuned, toluene and hexane. Therefore, the two solvents are good test cases for the generality of the models. Results for dichloromethane with hexane are shown in Fig. 3.13. The results for toluene with 1-hexene are presented in Fig. 3.14. For the dichloromethane/hexane system, both models slightly underestimate the fractional precipitation. As expected for the slightly polar solvent, the δ_3 model is more accurate. For the toluene/1-hexene system, both models predict the fractional precipitation equally well. In all cases, the predictions are quite accurate.

3.4.6 Polar Solvents

Polar solvents are expected to be the most difficult to model and the solvents for which the δ_3 model is more appropriate. Results for acetone and methanol each with toluene are shown in Figs. 3.15 and 3.16. The δ_1 model predicts complete solubility of asphaltene in acetone and therefore there is no δ_1 prediction curve on Fig. 3.15. As

expected, the δ_1 model is unsuccessful in predicting solubility in polar solvents. The δ_3 model is superior but provides, at best, qualitative predictions.

3.5 Conclusions

The solubility of Athabasca asphaltenes in variety of organic solvents is determined using a solid-liquid equilibrium calculation based on Scatchard-Hildebrand solubility theory with a Flory-Huggins entropy of mixing. The necessary input for the calculation is the feed composition and the molar volumes and solubility parameters of the components. Previously determined molar mass distribution and property correlations are used to calculate the necessary asphaltene input. The solvent properties are obtained from published data. Both single solubility parameter and three component solubility parameter models are tested.

Both the δ_1 and δ_3 models successfully predicted the solubility of asphaltene in a variety of non-polar and slightly polar solvents, including normal alkanes, branched alkanes, aromatics, dichloromethane, 1-hexene and decalin. The models were unable to accurately predict asphaltene solubility in cyclohexane/hexane mixtures. The model failure may arise because the entropy of mixing between cyclic and linear molecules does not conform to the Flory-Huggins term. Once the mixing of cyclic and linear molecules is better understood, it may be possible to adapt the solubility theory to cyclic compounds.

The δ_3 model predicted the solubility of asphaltenes in slightly polar compounds better than the δ_1 model. For highly polar solvents, the δ_1 model failed while the δ_3 model predicted the experimental data, at best, qualitatively. Hence, the three component solubility parameter improves the predictions but is not adequate to describe the solubility of asphaltene in highly polar solvents. Nonetheless, the solid-liquid equilibrium method is suitable for predicting the solubility of asphaltenes in a broad range of non-polar and slightly polar solvents.

3.6 References

1. Cimino, R.S.; Corraera, S.; Sacomani, P.A.; Spa, E.; Carniani, C., "Thermodynamic Modeling for Prediction of Asphaltene Deposition in Live Oils," *SPE Int. Symp. Oilfield Chemistry*, San Antonio (Feb.1995).
2. Kowalewski, I.; Vandenbrouke, M.; Huc, A.Y., *Energy & Fuels*, **10**, (1996), 97.
3. Hirschberg, A.; deJong, L.N.J.; Schipper, B.A.; Meijer, J.G., *SPEJ*, **24**, (1984), 283.
4. Kawanaka, S.; Park, S.J.; Mansoori, G.A., *SPE Res. Eng.*, **5**, (1991), 185.
5. Ferworn, K.A.; Svrcek, W.Y., "Thermodynamic and Kinetic Studies of Asphaltene Deposition from Bitumens," *Proc. Can. Chem. Eng. Conf.*, Calgary (Oct. 1994).
6. Thomas, F.B.; Bennion, D.B.; Bennion, D.W.; Hunter, B.E., *J. Cnd. Petr. Tech.*, **31(1)**, (1992), 22.
7. Rassamdana, H.B.; Dabir, B.; Nematy, M.; Farhani, M.; Sahimi, M., *AIChE J.*, **42**, (1996), 10.
8. Mitchell, D.L.; Speight, J.G., *Fuel*, **52**, (1973), 149.
9. Wiehe, I.A., *Fuel Sci. Technol. Intl.*, **14**, (1996), 289.
10. Barton, A.M.F., *CRC Handbook of Solubility Parameters and Other Cohesion Parameters*, CRC Press, Boca Raton, FL., 1983.
11. Andersen, S.I., *Fuel Sci. Technol. Intl.*, **10**, (1992), 1743.
12. Andersen, S.I.; Stenby, E.H., "Hysteresis in Asphaltene Precipitation and Redissolution," *Proc. Can. Chem. Eng. Conf.*, Calgary (Oct. 1994).
13. Xu, R.; Leonard, J.; Bui, V.T., "Comparative Behaviors between Cyclic and Linear Oligomers in Solution," *Proc. Can. Chem. Eng. Conf.*, Kingston (Sept. 1996).
14. Weast, R.C., "CRC Handbook of Chemistry and Physics", 59th Ed., CRC Press, Boca Raton, FL., 1978-79.

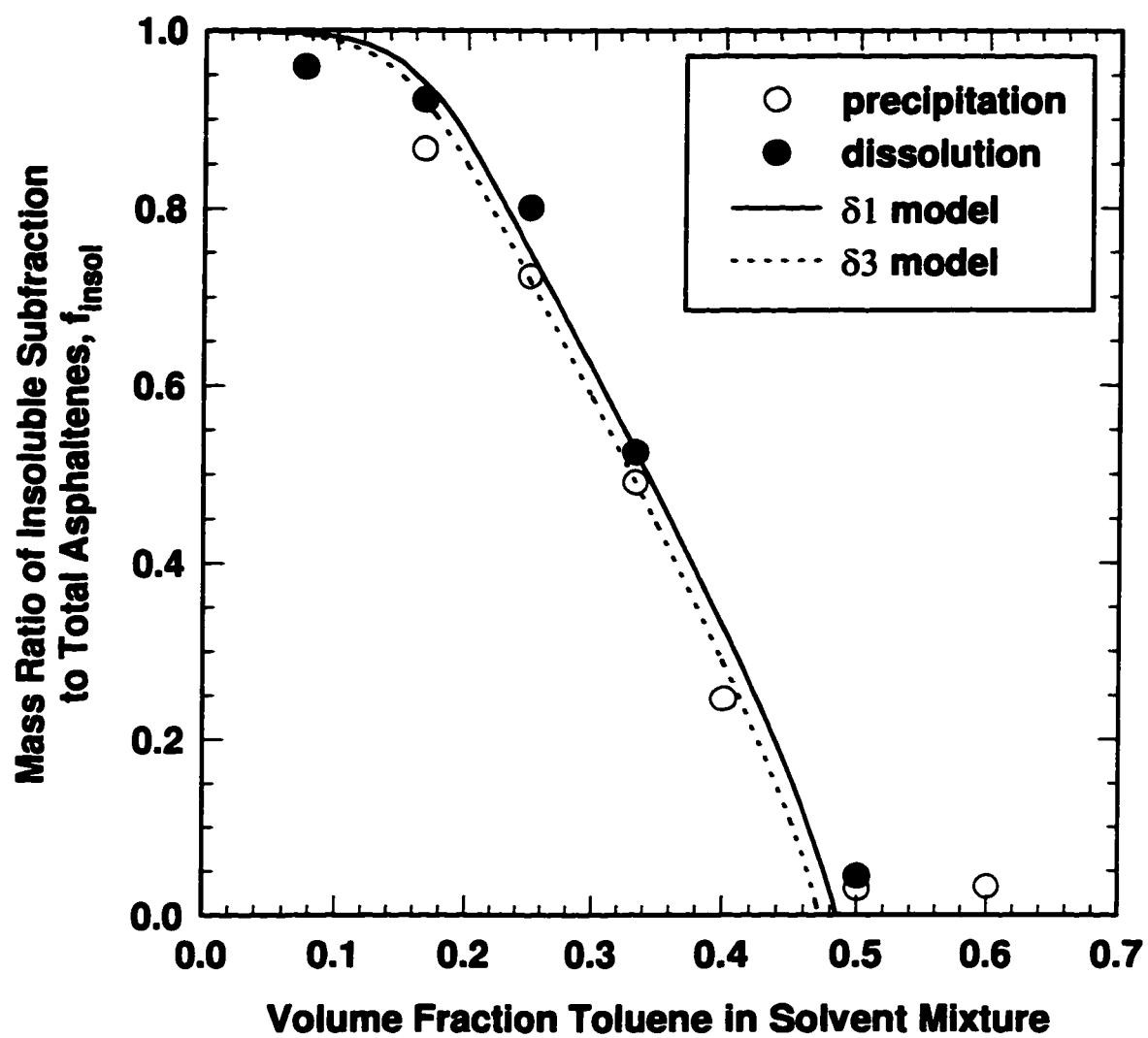


Figure 3.1: Solubility of asphaltenes in solutions of toluene and n-pentane.

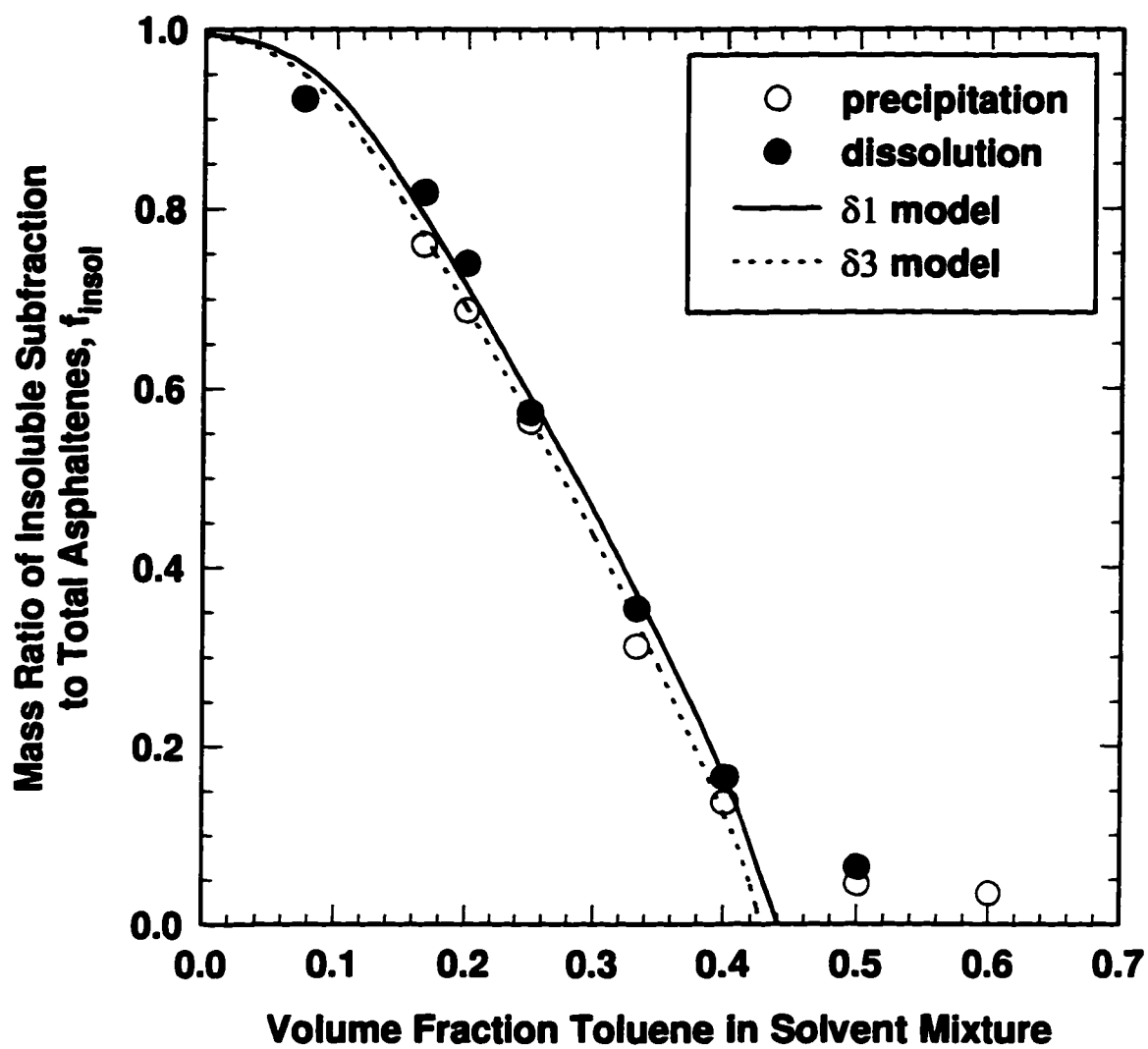


Figure 3.2: Solubility of asphaltenes in solutions of toluene and n-hexane.

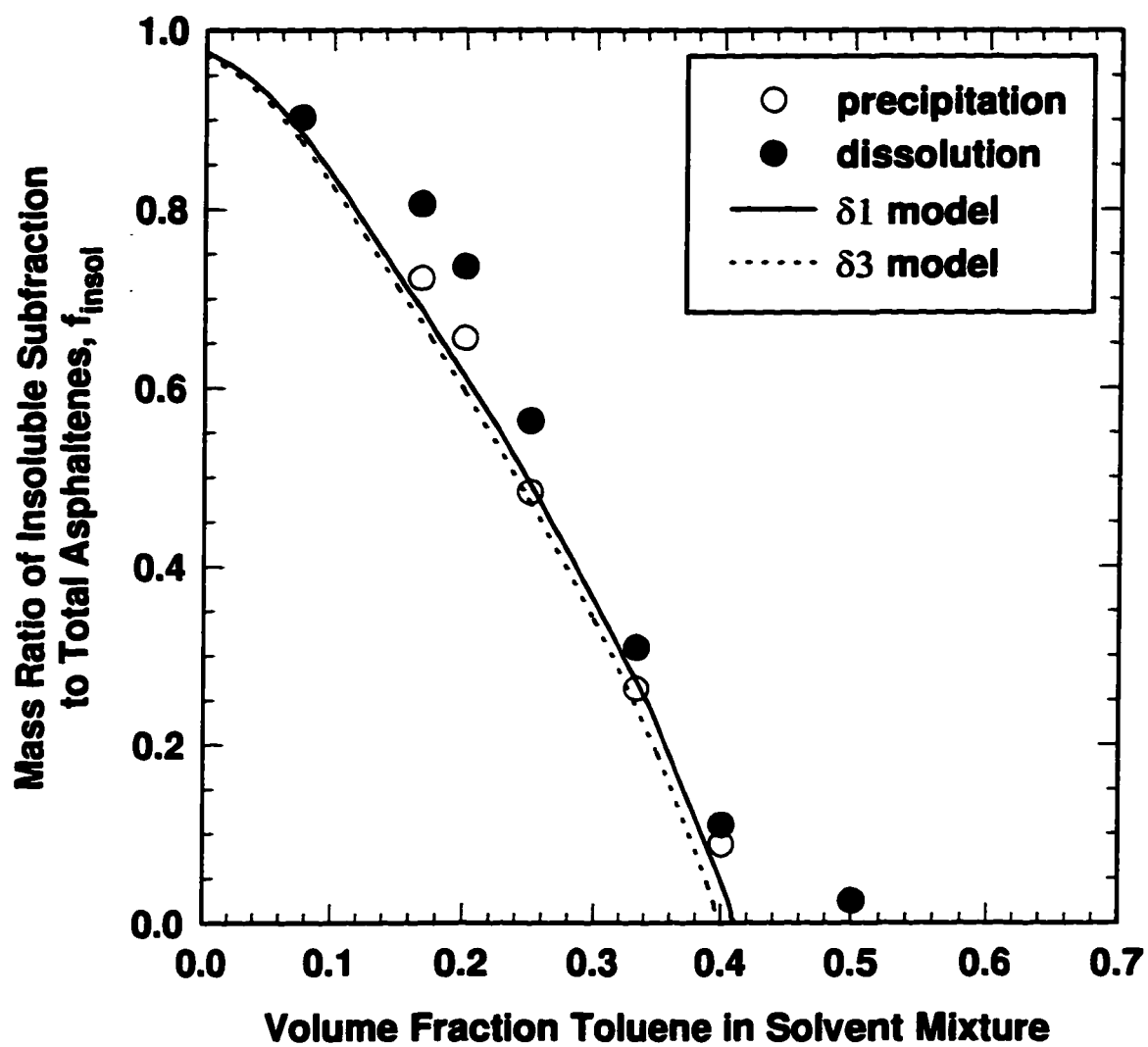


Figure 3.3: Solubility of asphaltenes in solutions of toluene and n-heptane.

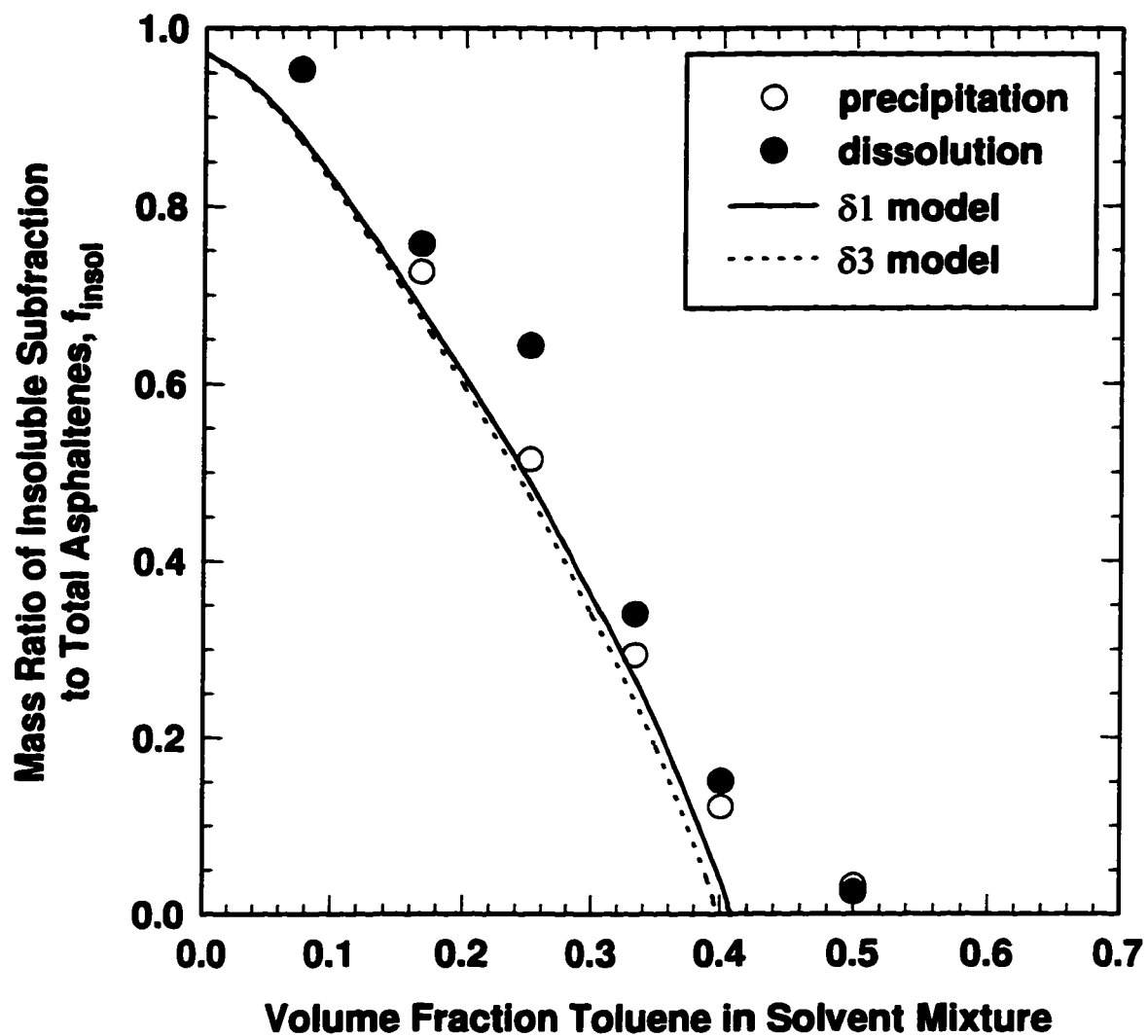


Figure 3.4: Solubility of asphaltenes in solutions of toluene and n-octane.

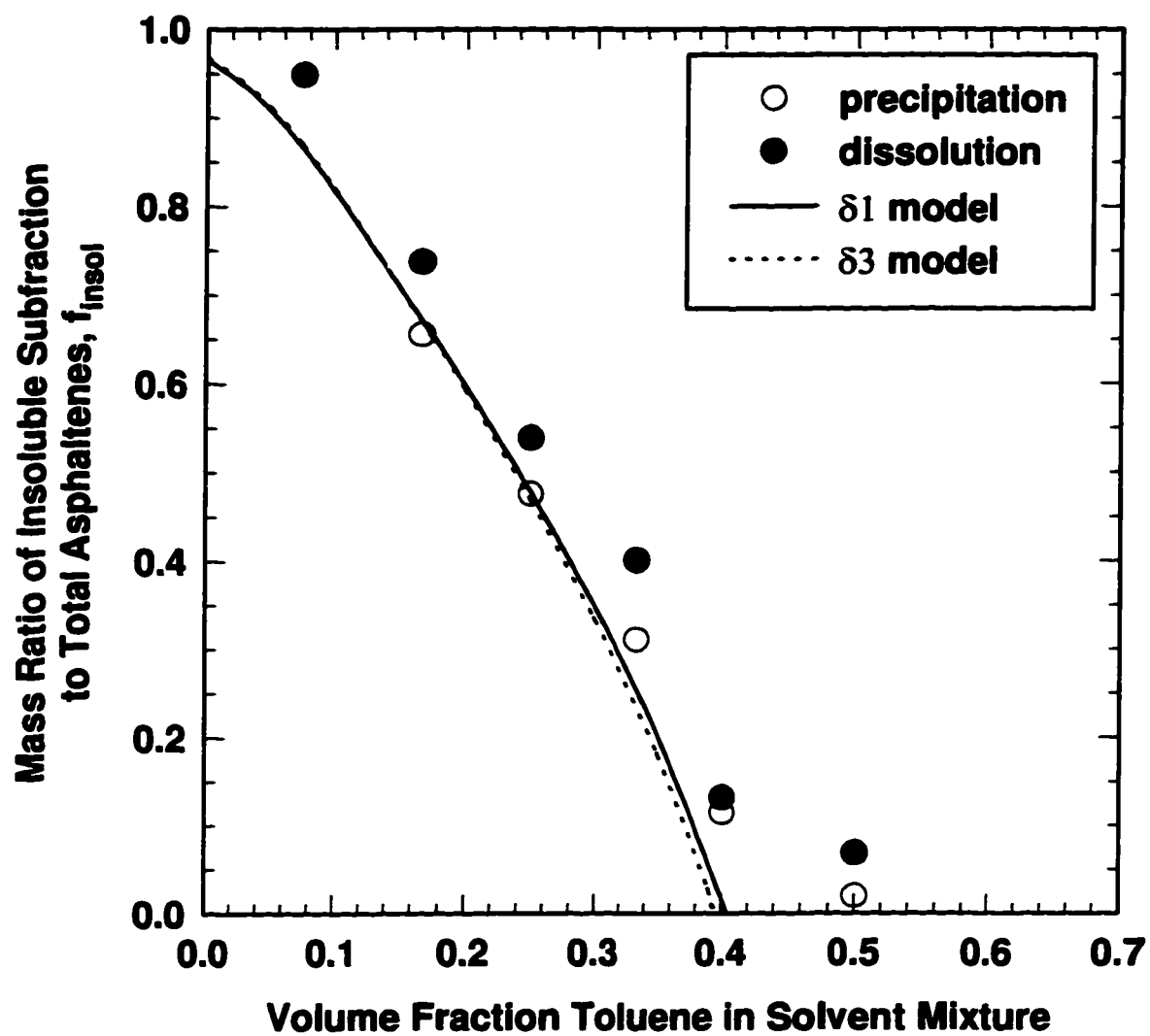


Figure 3.5: Solubility of asphaltenes in solutions of toluene and n-decane.

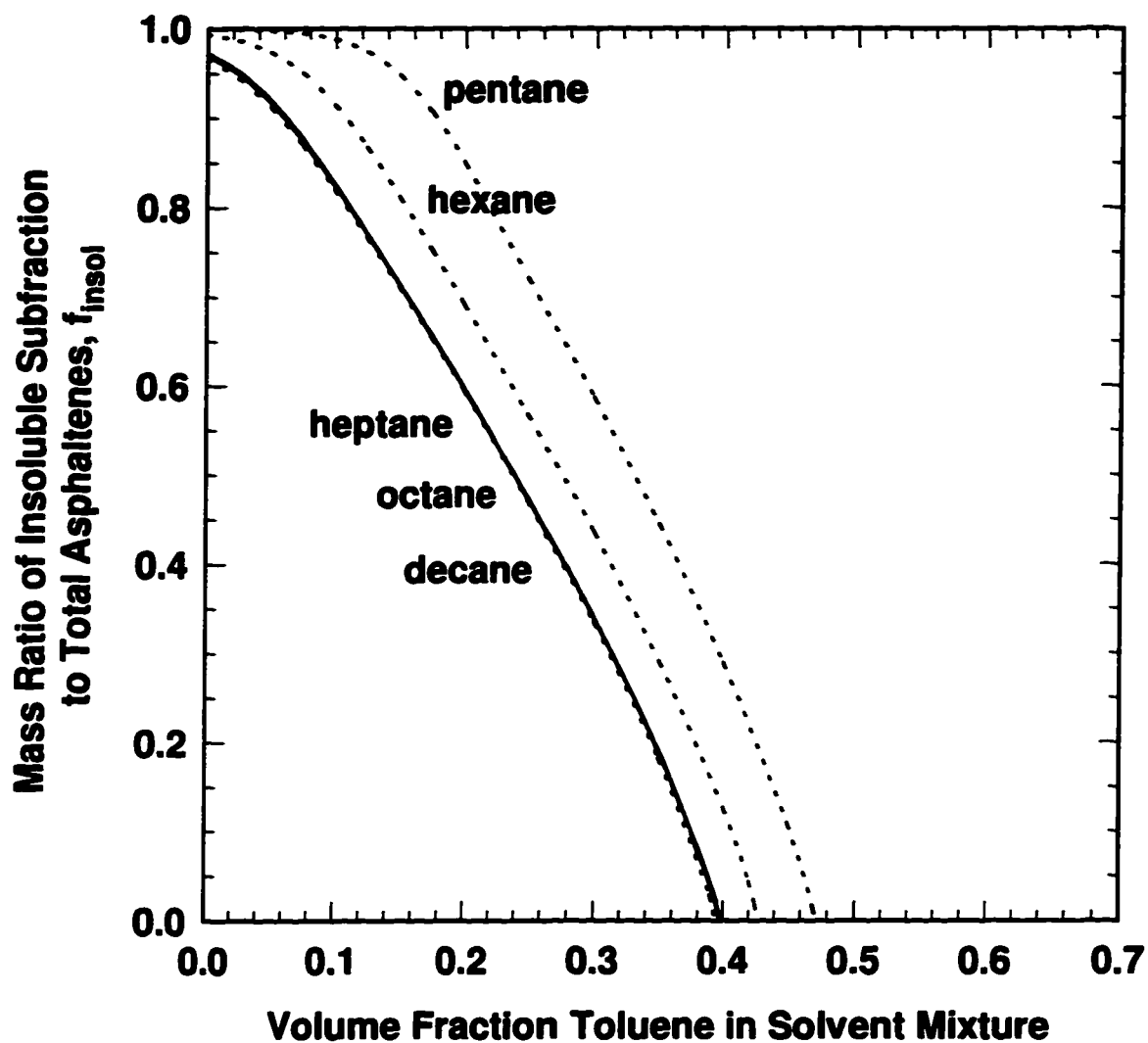


Figure 3.6: Predicted solubility of asphaltenes in solutions of toluene and each of the n-alkanes (C_5 - C_8 , C_{10}).

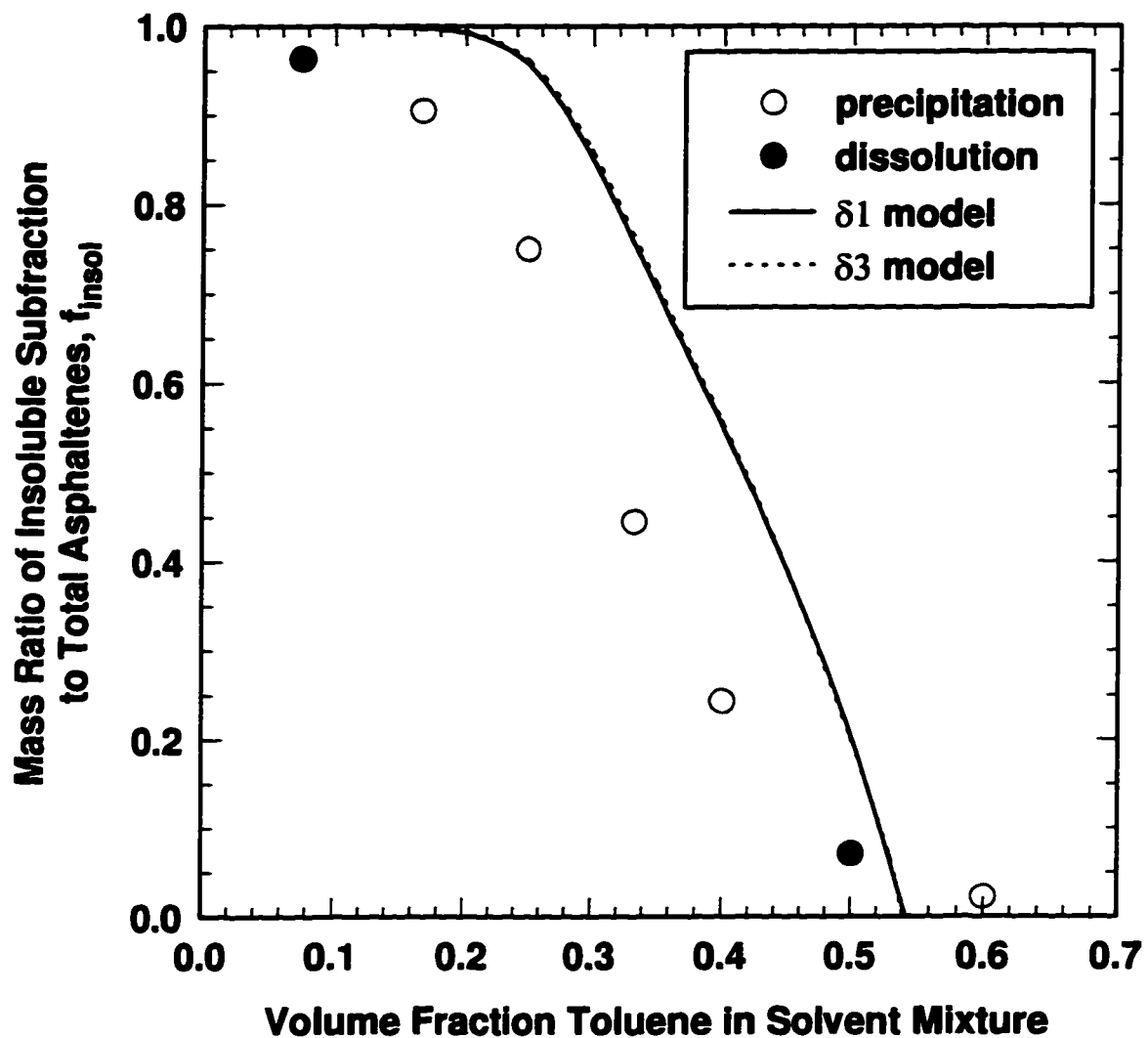


Figure 3.7: Solubility of asphaltenes in solutions of toluene and isopentane.

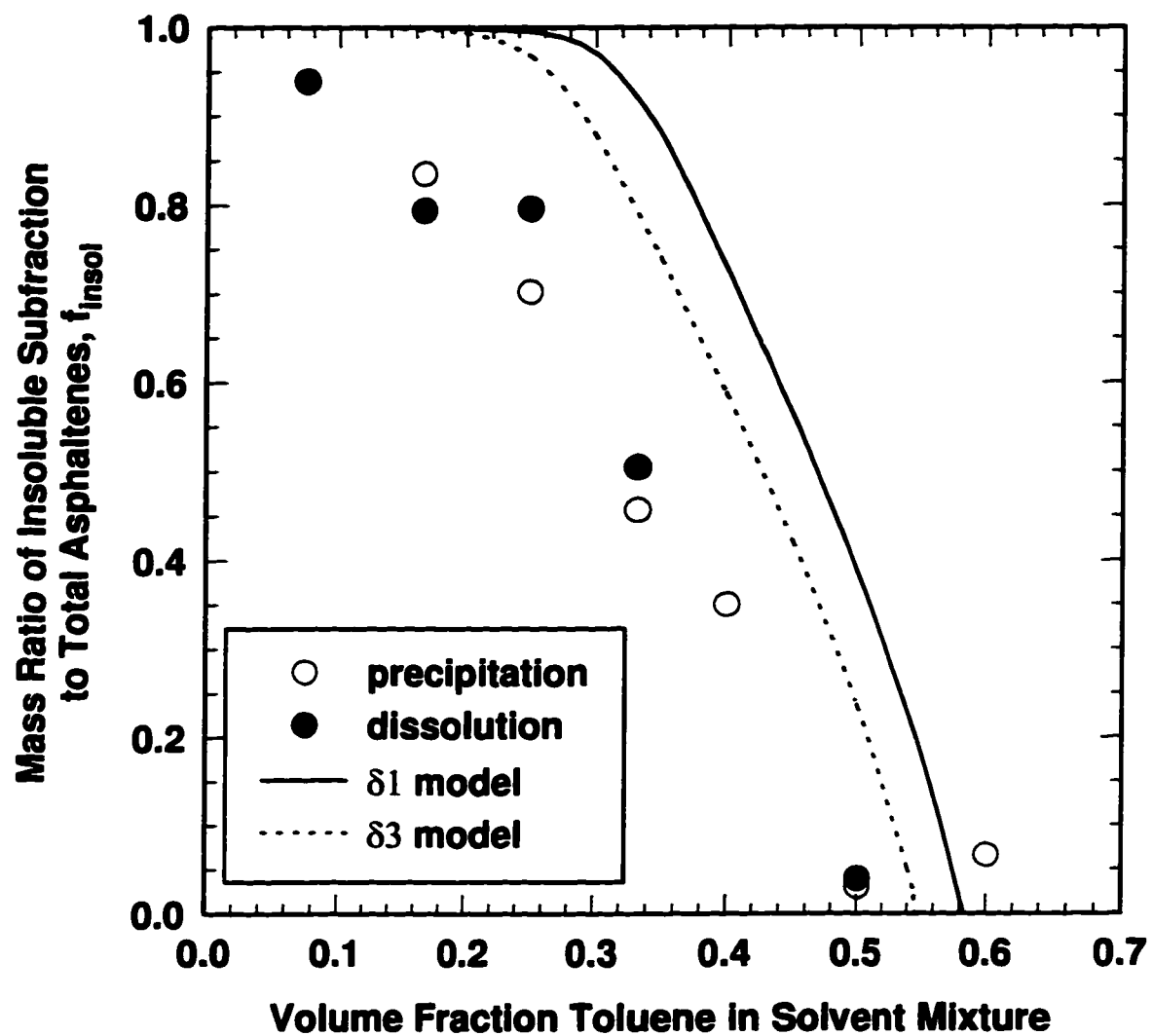


Figure 3.8: Solubility of asphaltenes in solutions of toluene and isooctane.

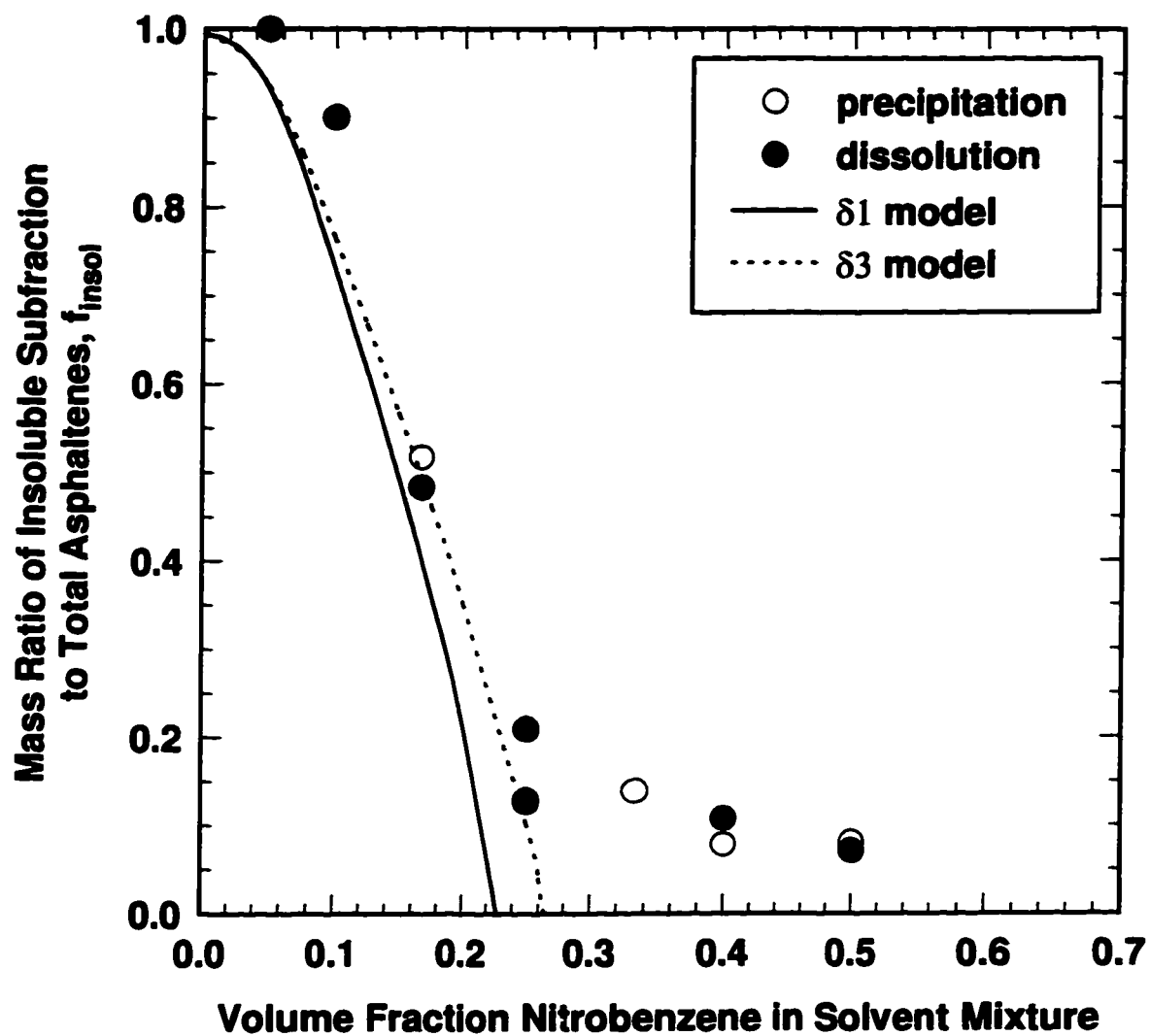


Figure 3.9: Solubility of asphaltenes in solutions of nitrobenzene and hexane.

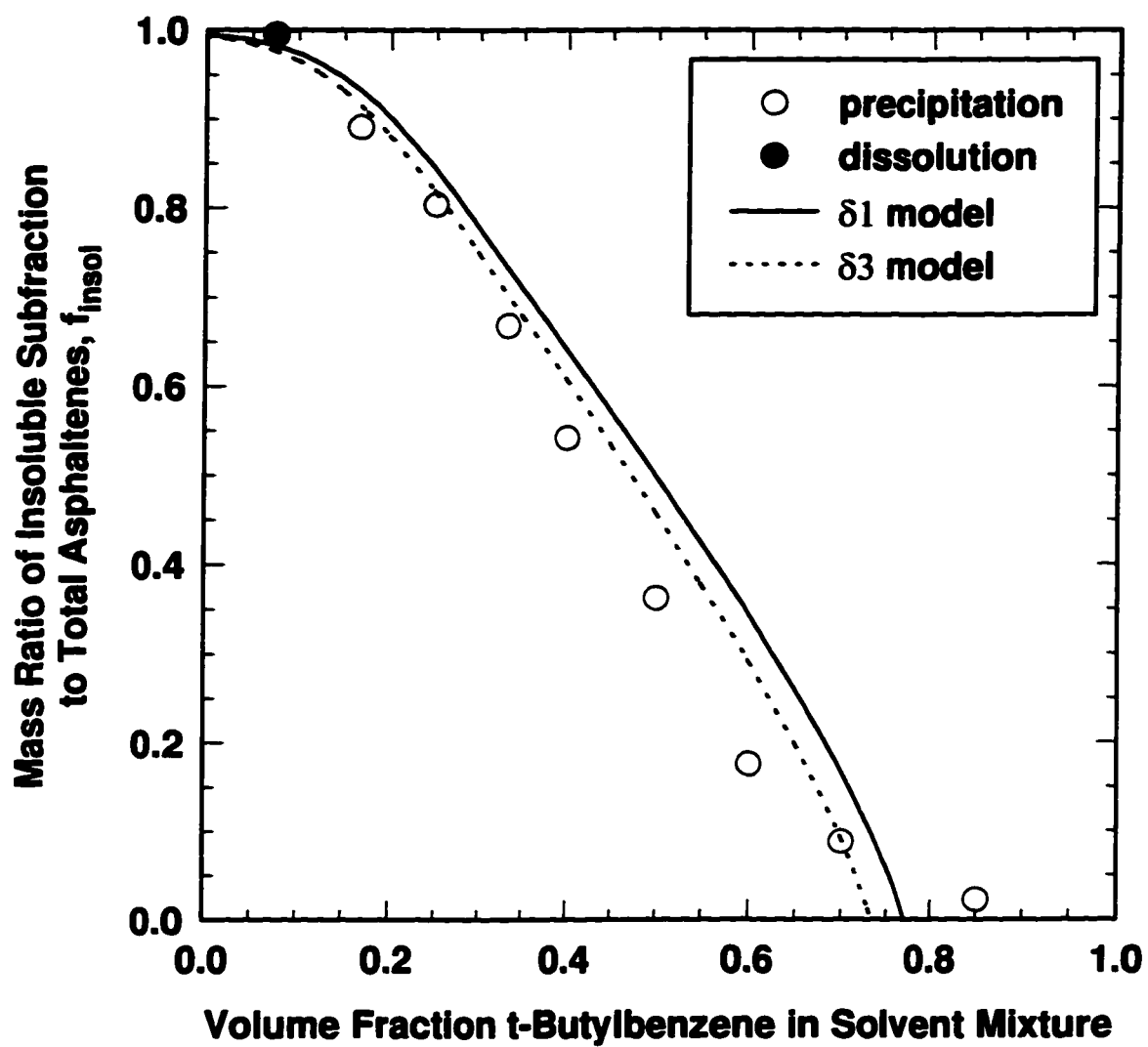


Figure 3.10: Solubility of asphaltenes in solutions of t-butylbenzene and hexane.

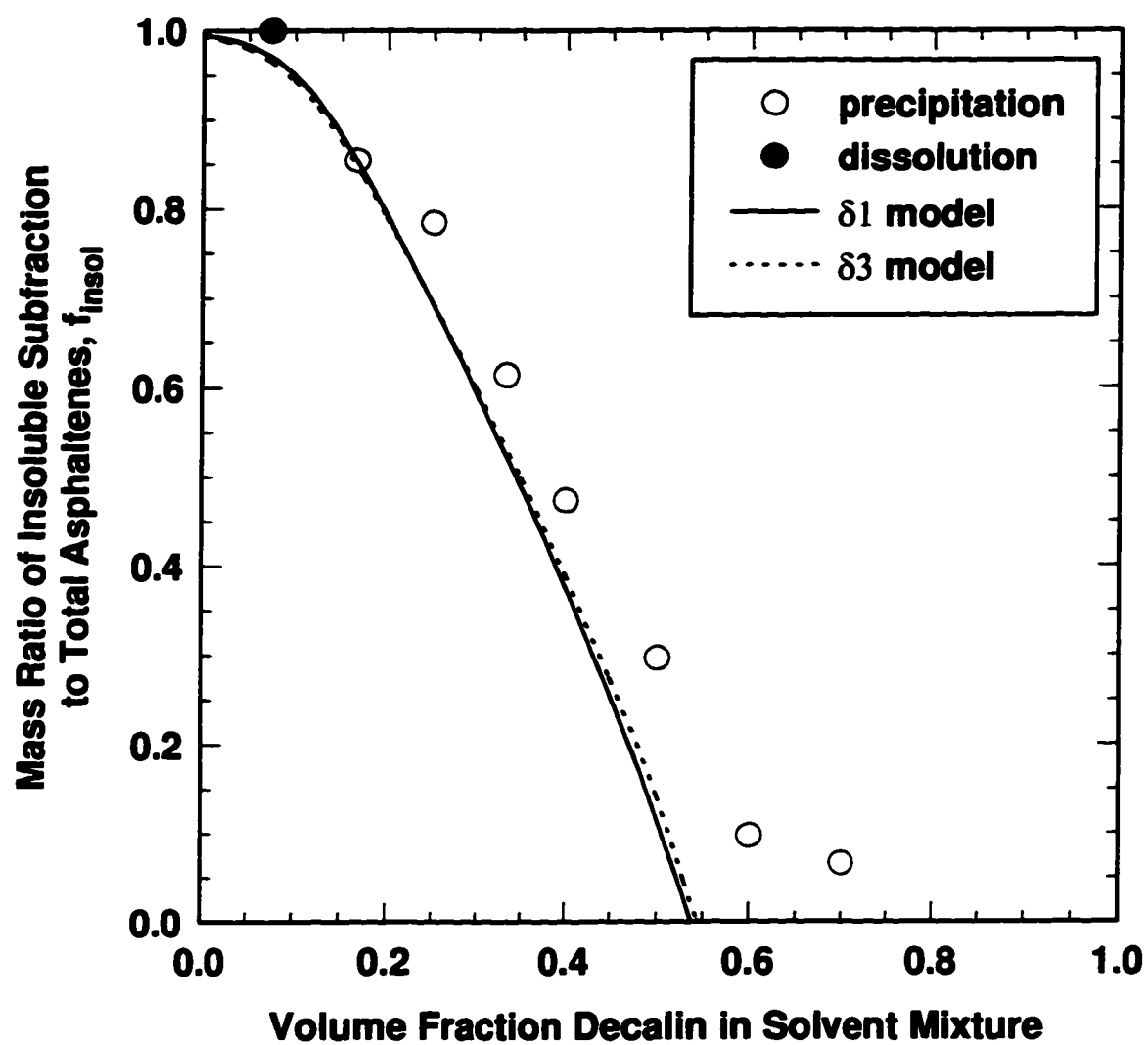


Figure 3.11: Solubility of asphaltenes in solutions of decalin and hexane.

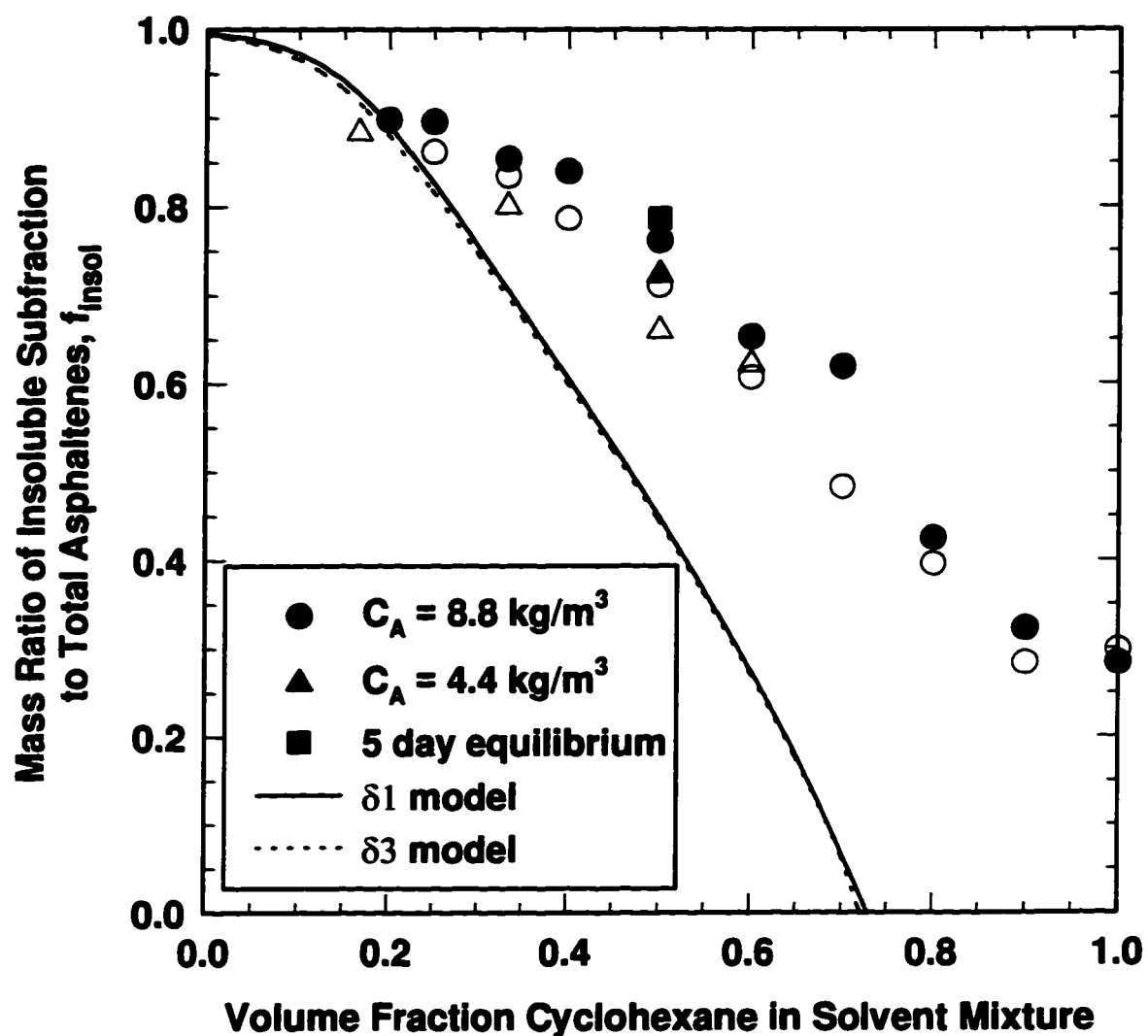


Figure 3.12: Solubility of asphaltenes in solutions of cyclohexane and hexane, (open symbols) - precipitation, (closed symbols) - dissolution

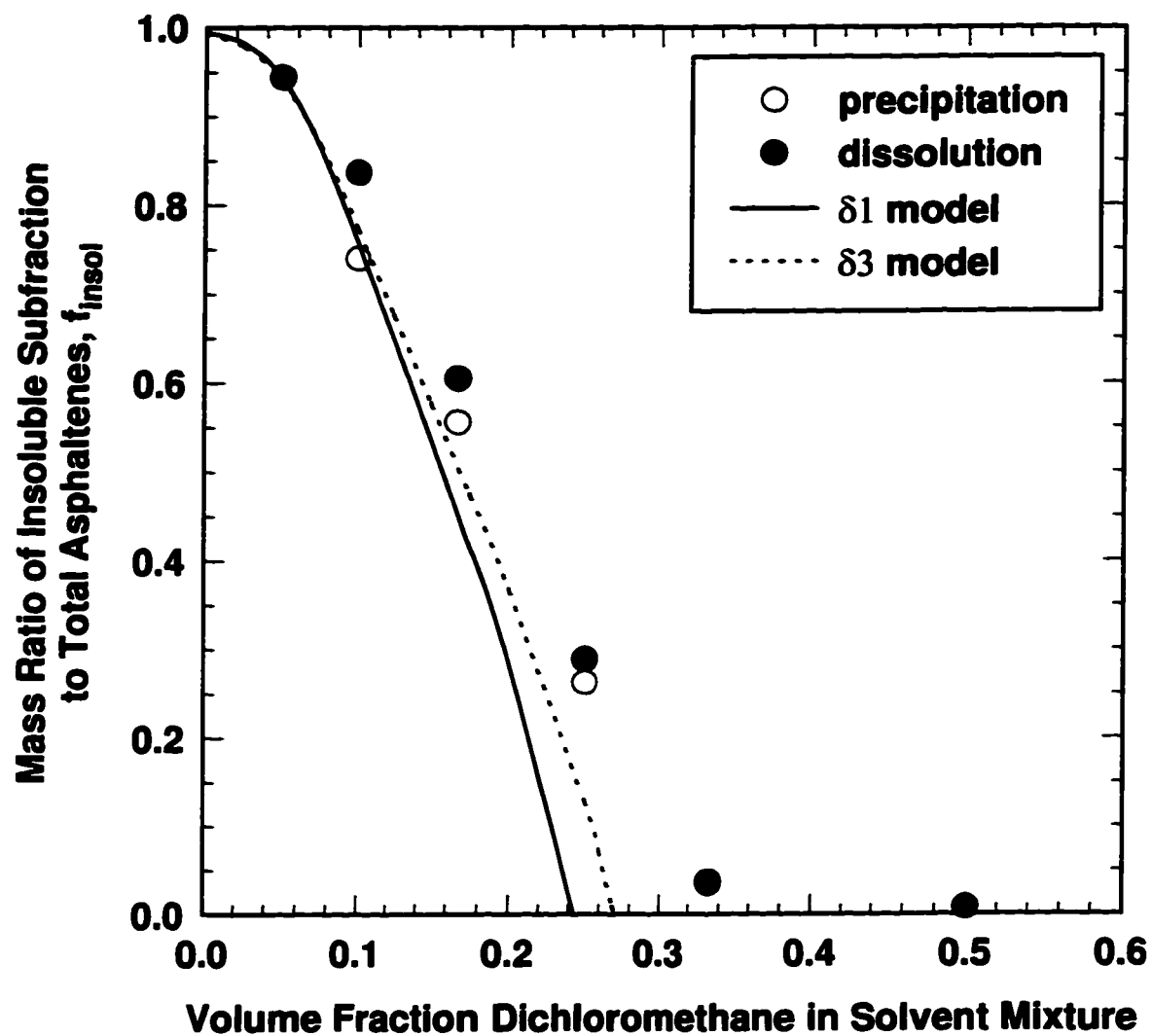


Figure 3.13: Solubility of asphaltenes in solutions of dichloromethane and hexane.

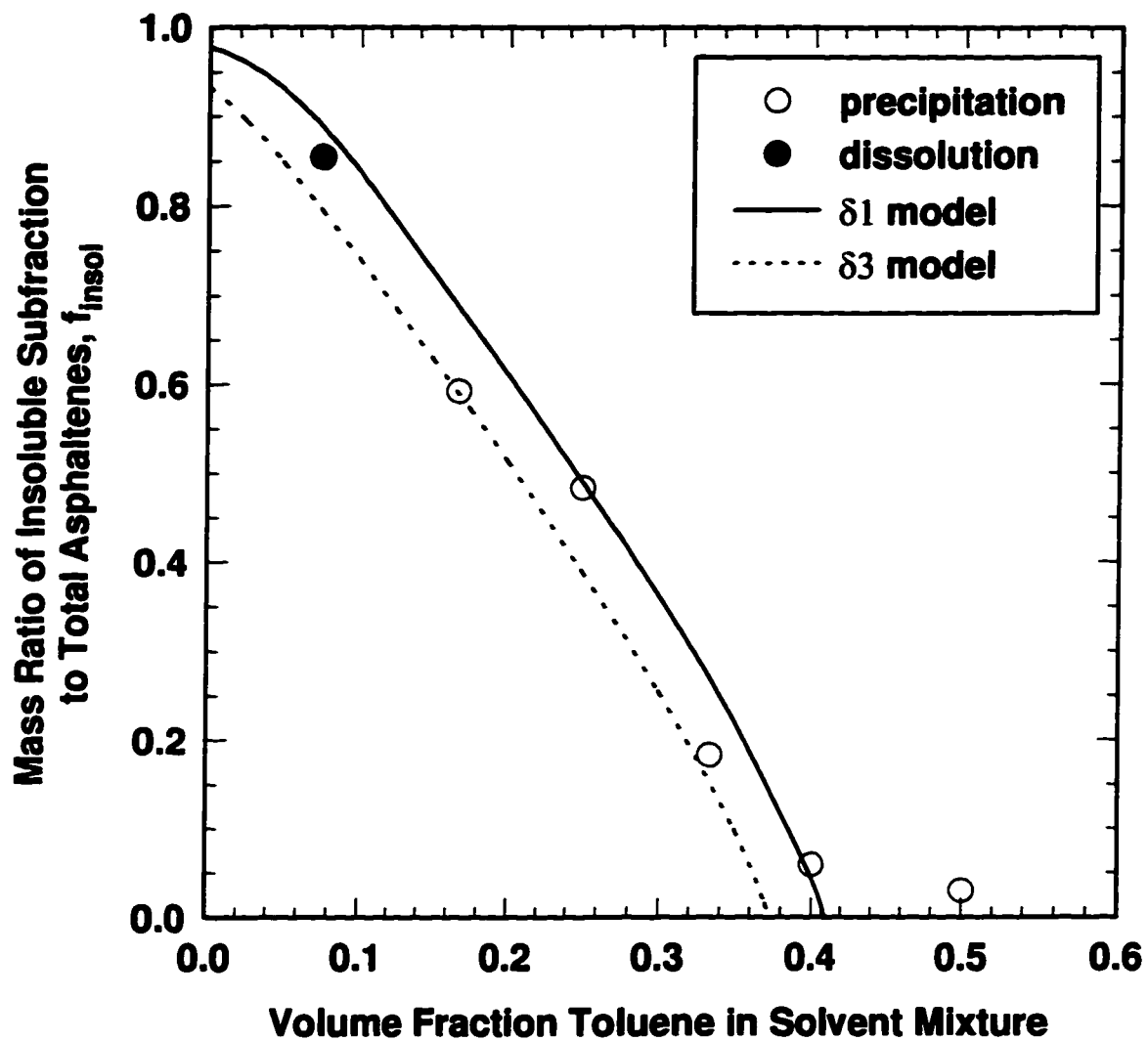


Figure 3.14: Solubility of asphaltenes in solutions of 1-hexene and toluene.

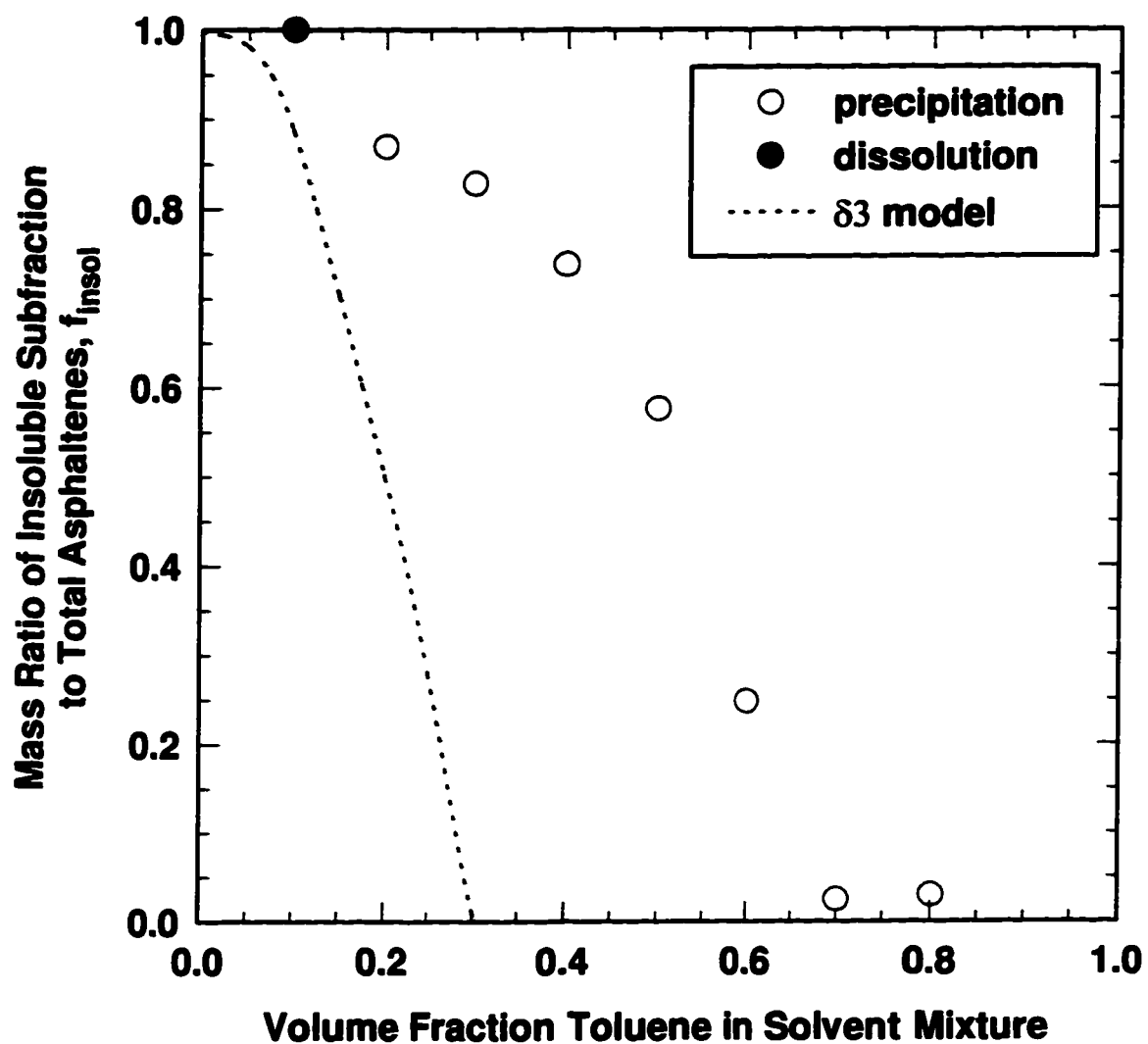


Figure 3.15: Solubility of asphaltenes in solutions of acetone and toluene.

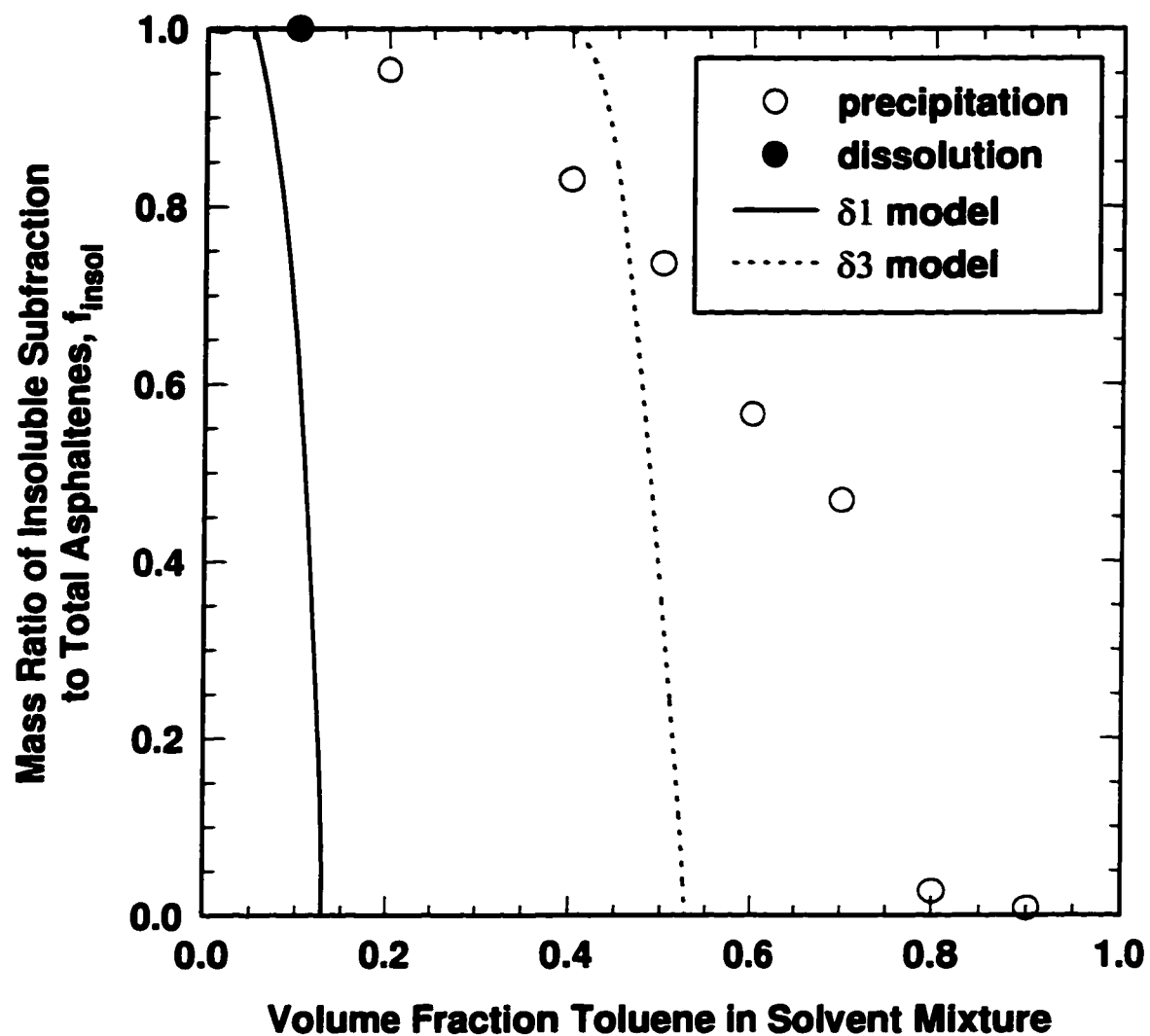


Figure 3.16: Solubility of asphaltenes in solutions of methanol and toluene.

Chapter 4

THE STABILIZATION OF WATER-IN-OIL EMULSIONS BY ASPHALTENES

4.1 Introduction

Water-in-crude oil emulsions are of interest to the oil industry for two reasons. First, water-in-crude oil emulsions can form in hydrocarbon reservoirs or in production facilities during extraction or cleaning. The emulsified water adds significant volume to the crude oil, increasing the cost of transportation and refining. Second, water-in-crude oil emulsions can form in oceanic oil spills. The emulsions are very stable and the oil in the emulsions is difficult to recover, leading to greater environmental damage. In order to devise an optimum treatment for water-in-oil emulsions, it is helpful to understand how they are stabilized.

Asphaltenes are commonly identified as the agent responsible for stabilizing water-in-crude oil emulsions. Asphaltenes are the fraction of a crude oil soluble in toluene yet insoluble in alkanes, typically pentane or heptane. Hence, asphaltenes are a solubility class and contain a wide variety of chemical species. Asphaltenes are also known to self-associate and form colloids or micelles (1-3). Here, an asphaltene colloid is defined as a submicron particle stabilized by resins or other aromatic species. Therefore, asphaltenes may exist as molecules, micelles, colloids or precipitated solid particles in any given oil. It is not known which asphaltene phase stabilizes emulsions.

Each asphaltene phase is a plausible candidate for the emulsion stabilizer. Asphaltene molecules are large polyaromatic hydrocarbons with molar masses ranging from 1,000 to 10,000 g/mol. They contain many heteroatom functional groups, including some acids and bases (4). Some of the functional groups are hydrophilic while the hydrocarbon structure of asphaltenes is hydrophobic. Hence, asphaltenes can be surface active and

may stabilize emulsions as a molecular surfactant. However, Eley *et al.* (5) found that the stability of water-in-crude oil emulsions is related to the asphaltene precipitation point. This observation suggests that asphaltenes on the verge of precipitation may stabilize emulsions. Asphaltenes near their precipitation point are likely to adsorb more strongly on an interface than fully soluble asphaltenes. More strongly adsorbed molecules are more difficult to displace from an interface and more likely to stabilize an emulsion. Other experiments suggest that particulate asphaltenes stabilize emulsions. Fine particles are observed on water-crude oil interfaces in electron micrographs (6). In addition, rheological studies indicate that water/crude oil interfaces contain particles (7,8). These methods do not indicate whether the particles are colloids, micelles or precipitated solids.

The choice of treatment for an emulsion depends on the nature of the material on the interface. Hence, it is useful to determine which asphaltene phase(s) adsorbs on the interface. Unfortunately, it is difficult to isolate the effects of the asphaltenes in a crude oil because crude oils are such complex mixtures. An alternative is to examine water-in-hydrocarbon emulsions where the hydrocarbon consists of toluene, hexane and asphaltenes. Toluene and hexane mixtures are chosen as the hydrocarbon continuous phase because, by definition, the full range of asphaltene solubility is observed in the mixtures.

The form of asphaltene that stabilizes the emulsions can be determined by comparing emulsions prepared with asphaltenes at different solvent conditions. For example, an emulsion prepared with fully solubilized asphaltenes might be stable while one prepared from insoluble asphaltenes might be unstable. More exact comparisons are made by determining what proportion of the asphaltenes adsorb on the interface in different solvent conditions. The amount of asphaltenes that adsorb on the interface is related to the Sauter mean diameter of the emulsion, a measurable quantity. Comparisons of the Sauter mean diameters reveal not only what phase of the asphaltenes stabilize emulsions but also provide qualitative data about the adsorption of asphaltenes on the water/hydrocarbon interface.

4.2 Experimental Method

4.2.1 Materials

The asphaltenes used in the experiments were extracted from Syncrude coker feed Athabasca bitumen (bitumen that has been treated to remove sand and water and is ready for upgrading). These asphaltenes contain “solids” which make up 6.3 wt% of the asphaltenes, (see Section 2.4). The “solids” include fine clays, ash and some adsorbed hydrocarbons and are insoluble in toluene. The “solids” form part of the first material to precipitate and hence are always part of the insoluble portion of an asphaltenes-solids mixture.

Asphaltene-solids were extracted from the bitumen with a 40:1 volume ratio of heptane to bitumen. The mixture was stirred for four hours and left to settle overnight. The supernatant liquid was removed and the remaining precipitate was further washed with heptane at a 4:1 heptane:bitumen volume ratio, stirred for one hour and left to settle for four hours. The final mixture was filtered and the remaining asphaltenes dried at ambient conditions until there was no further change in mass. The asphaltene-solids recovered with this method make up approximately 14.5% of the original bitumen.

Asphaltene-solids may be further divided into soluble and insoluble subfractions. The fractionation was achieved by dissolving the asphaltene-solids in a solvent (toluene) then adding a precipitator (hexane). The ratio of toluene to hexane was controlled to obtain the desired split between soluble and insoluble subfractions. The solution was stirred in a sonic mixer for five minutes and then centrifuged on a desktop centrifuge at 3400 rpm (1300 g) for five minutes. To recover the insoluble subfraction, the supernatant was poured off and the undissolved asphaltenes-solids dried until there was no further change in mass. The soluble asphaltenes were recovered in the supernatant and the entire supernatant diluted with a known hexane/toluene mixture as needed to make up the desired emulsions.

4.2.2 Preparation of Emulsions

To prepare an emulsion, a known amount of asphaltene-solids or asphaltene-solids subfraction was dissolved in toluene. Hexane was added after the asphaltenes were dissolved and the solution stirred in a sonic mixer for five minutes. The solution was transferred to a commercial blender and, while the blender was running, a known volume of water was added. After the water was added, blending continued for five minutes at low speed. The emulsion was then transferred to a jar where it creamed and separated into a continuous phase (on top) and a concentrated emulsion layer (on bottom), usually within five minutes. After one hour, some continuous phase and a drop of emulsion were placed onto a hanging drop slide. A slip cover was placed on the sample and four sets of two photographs were taken through a Carl Zeiss Jena microscope. The pictures of the droplets were developed, printed and then traced onto transparencies and counted using a Buehler Omnimet Image Analyzer. Example photographs of asphaltene stabilized water-in-oil emulsions with mean drop diameters of 8, 21 and 38 microns are reproduced in Plate 4.1. The range of mean diameters in Plate 4.1 spans the range of diameters encountered in the experiments discussed here.

All the emulsion experiments were conducted at asphaltene concentrations below the cmc. In Chapter 2, the cmc was shown to be greater than 40 kg/m^3 in toluene/hexane solutions. Here emulsions were prepared with asphaltene concentrations of 2 kg/m^3 or less. Since the emulsions were prepared below the cmc, only the effect of soluble molecular asphaltenes, near precipitation point asphaltenes and solid asphaltene particles could be examined.

4.3 Theory

The experimental data presented later in Section 4.4 indicates that asphaltenes stabilize emulsions as molecular surfactants. However, not all of the asphaltene species necessarily act as surfactants (are surface active). It is useful to determine what fraction of the soluble asphaltenes is surface active in different conditions. An expression relating the surface active fraction of asphaltenes to the Sauter mean diameter of the emulsion and

other measurable quantities is developed below. We start with the volume and surface area of the dispersed phase in the emulsion. Water is the dispersed phase in this case. The water drops do not necessarily have a uniform diameter; hence, the total volume of water, V_w , is related to the distribution of drop diameters.

$$V_w = \frac{\pi N}{6} \sum \hat{F}_i d_i^3 \quad (4.1)$$

The total surface area of emulsion is the surface area of the water drops, A_w , and is related to the distribution of drop diameters by

$$A_w = \pi N \sum \hat{F}_i d_i^2 \quad (4.2)$$

Here, N is the total number of drops, \hat{F}_i , is the drop number frequency and d_i is the diameter of drop i . An expression relating the surface area of the emulsion to the Sauter mean diameter, d_{32} , is found by combining Eqs. 4.1 and 4.2 and is given by

$$A_w = \frac{6V_w}{d_{32}} \quad (4.3)$$

where d_{32} is defined as

$$d_{32} = \frac{\sum \hat{F}_i d_i^3}{\sum \hat{F}_i d_i^2} \quad (4.4)$$

The next step is to express the emulsion surface area in terms of the mass of asphaltenes on the interface. The mass of asphaltenes on the interface, m_I , is the product of the volume and density, ρ_A , of the asphaltenes on the interface. If the drops are covered with a monolayer of asphaltene molecules, the volume of asphaltenes on the interface is the product of the surface area of the emulsion and the monolayer thickness, t_A . The

relationship of the mass of asphaltenes on the interface to the surface area of the emulsion is given by

$$m_I = \rho_A A_W t_A = \frac{6\rho_A t_A V_W}{d_{32}} \quad (4.5)$$

The second part of Eq. 4.5 is obtained by substituting Eq. 4.3 for A_W . The mass of the asphaltenes on the interface can also be expressed in terms of the concentration of asphaltenes in the continuous phase before emulsification, C_A^o .

$$m_I = f_I^* C_A^o V_O \quad (4.6)$$

Here, f_I^* is the mass ratio of asphaltenes on the interface to total asphaltene-solids and V_O is the total volume of the continuous oil phase. Now, another expression for the Sauter mean diameter is found by combining Eqs. 4.5 and 4.6 and it is given by

$$d_{32} = \frac{6\rho_A t_A V_W}{f_I^* C_A^o V_O} = \frac{6\rho_A t_A \phi_W}{f_I^* C_A^o (1 - \phi_W)} \quad (4.7)$$

where ϕ_W is the volume fraction of water in the emulsion. All the terms in Eq. 4.7 are known or measurable except for f_I^* . However, experimental data in Section 3.4 indicate that f_I^* is a function of asphaltene concentration. Hence, it is necessary to determine the concentration dependence to develop a predictive equation for the Sauter mean diameter.

The maximum fraction of asphaltene that is able to adsorb on the interface, f_I^{max} is the fraction of asphaltenes that is both soluble and surface active in a given solution. It is given by

$$f_I^{max} = f_a f_{sol} \quad (4.8)$$

where f_a and f_{sol}^* are the mass ratio of the surface active to soluble asphaltenes and the mass ratio of the soluble to total asphaltene-solids, respectively. Not all of the soluble surface active asphaltenes necessarily adsorb on the interface. It is reasonable to assume that an equilibrium concentration of surface active asphaltenes, C_a^{eq} , remains in solution in the continuous phase. Hence, the mass fraction of asphaltenes that adsorbs on the interface is given by

$$f_i^* = f_a f_{sol}^* - \frac{C_a^{eq}}{C_A^o} \quad (4.9)$$

A more convenient expression for d_{32} is found when Eq. 4.9 is substituted into Eq. 4.7:

$$d_{32} = \frac{6\rho_A t_A \left(\frac{\phi_w}{1 - \phi_w} \right)}{f_a f_{sol}^* C_A^o - C_a^{eq}} \quad (4.10)$$

Eq. 4.10 consists of known or measurable quantities except for f_a and C_a^{eq} . The experimental results presented in the next section show that both f_a and C_a^{eq} are constant in a given solvent. Their values can be calculated from experimental measurements of d_{32} at various asphaltenes concentrations and water volume fractions.

4.4 Results and Discussion

The objective of the research presented below is to determine what part of the asphaltene-solids stabilizes water-in-toluene/hexane emulsions. No direct measurements of the asphaltenes on the interface are made. Rather, the fraction of asphaltenes responsible for stabilizing emulsions is inferred from three sets of experiments. The first set of experiments relates to the role of the insoluble asphaltenes in stabilizing emulsions. The second set of experiments deals with asphaltenes as molecular surfactants. Finally, the effect of the solvent on the stabilization of emulsions by asphaltenes is examined. The

change in the amount of asphaltene adsorbed on the interface with a change in solvent reveals some qualitative details on the nature of asphaltene surfactant behavior.

Note that to avoid confusion, the “solids” are not referred to in the following discussion. However, they are a part of the insoluble asphaltene fractions in all the experiments presented here.

4.4.1 Experimental Design

The asphaltenes are a mixture of soluble and insoluble fractions in toluene/hexane mixtures with a hexane volume fractions greater than 50% (see Chapter 2). The partition between soluble and insoluble phases is shown on the hypothetical molar mass distribution of the asphaltenes given in Fig. 4.1. The relative proportion of the two fractions depends on the solvent that forms the continuous phase. The solubility theory and experiments presented in Chapter 2 indicate that the highest molar mass material precipitates first. Hence, the insoluble fraction shown on Fig. 4.1 makes up the top end of the molar mass distribution. The asphaltenes that stabilize the emulsion may be solid particles from the insoluble fraction, molecules on the verge of precipitation from the part of the molar mass distribution at the boundary of the two phases, or surface active asphaltenes from the soluble fraction.

It is difficult to determine what part of the asphaltenes adsorb on the interface when an emulsion is made from a two phase mixture of asphaltenes. However, the fraction of the asphaltenes that stabilizes the emulsions can be found by examining how the amount of adsorbed asphaltenes changes as the ratio of soluble to insoluble asphaltenes changes. The amount of asphaltenes adsorbed on the interface is inversely proportional to the Sauter mean diameter of the emulsion, as shown by Eq. 4.3. An increase in Sauter mean diameter indicates a decrease in surface area and therefore a decrease in the amount of asphaltenes on the interface. So, for example, if the Sauter mean diameter increases as the amount of soluble asphaltenes decreases, the soluble asphaltenes must contribute to the stability of the emulsion.

To make the desired comparisons, it is necessary to prepare emulsions from asphaltenes with different ratios of soluble to insoluble subfractions. The ratio of soluble to insoluble asphaltenes is a function of the solvent conditions and of the molar mass distribution of the asphaltenes. Changing the solvent conditions may affect more than the ratio of soluble to insoluble asphaltenes. For instance, the asphaltenes may adsorb on the interface more strongly in one solvent than in another. Hence, a more accurate comparison is possible with emulsions stabilized in the same solvent by asphaltenes consisting of different molar mass distributions.

The molar mass distribution of the asphaltene sample can be controlled by pretreating the asphaltenes in a solution of a given volume ratio of toluene to hexane. The original asphaltene sample is split into soluble and insoluble subfractions with known molar mass distributions. The characteristics of the subfractions are discussed in Chapter 2 and the molar mass distributions of hypothetical pretreated asphaltene subfractions are given in Fig 4.1. An emulsion is prepared from either the soluble or the insoluble subfraction of the pretreated asphaltenes. At emulsion conditions, the subfraction has a different ratio of soluble to insoluble asphaltenes than the original asphaltene sample. In the example given in Fig 4.1, the pretreated soluble fraction contains no insoluble asphaltenes at emulsion conditions. On the other hand, the pretreated insoluble fraction has a higher ratio of insoluble to soluble asphaltenes than the original sample.

The experimental objective is to measure the Sauter mean diameter of emulsions prepared from asphaltene subfractions in a given toluene/hexane mixture. However, one must be sure that the Sauter mean diameter is not affected by the mixing conditions. If some asphaltenes fail to reach the interface because the interface is saturated, then misleading results would ensue. The potential problem was avoided by limiting the asphaltene concentration to the point that insufficient asphaltenes were available to completely cover the surface area generated in the blender. At such low concentrations and low surface

coverages, the adsorption of asphaltenes on the interface is favored and an equilibrium is reached where most of the asphaltenes reside on the interface.

A Sauter mean diameter measured during blending at low asphaltene concentrations is also misleading because the interface is only partially covered by the asphaltenes. However, once blending ceases, the droplets quickly coalesce until their surfaces are completely covered. For example, the drop size distribution given in Fig. 4.2 was measured 1.5 hours after blending ceased. The mean diameter of the emulsion is 24.2 microns. The blender creates water droplets of approximately 5-10 microns. Clearly, the emulsion has destabilized either through coalescence or Ostwald ripening. There is strong evidence suggesting that Ostwald ripening occurs in these emulsions and it is presented in Chapter 5. However, Ostwald ripening causes little change in the Sauter mean diameter in the short run. The Sauter mean diameter of the emulsion presented in Fig. 4.3 increases by only 1% in 24 hours. Hence, after blending stops, the droplets appear to grow by coalescence until the surfaces are completely covered by asphaltenes. Further growth occurs only by Ostwald ripening.

The Sauter mean diameters used to determine the fraction of asphaltene on the interface were measured between 1 and 2 hours. No evidence of coalescence was observed more than 5 minutes after blending, while the effects of Ostwald ripening are not apparent for at least 24 hours. An interval of 1 to 2 hours between blending and the drop diameter measurement minimizes the potential for either insufficient coalescence or significant Ostwald ripening to affect the drop diameters.

Note that some asphaltenes desorb during coalescence. The desorption was visible in many cases as the hydrocarbon phase darkened continuously for a minute or two after blending ceased. The desorption occurs because the surface coverage rises as the drops coalesce. The equilibrium between the asphaltenes on the surface and in solution shifts to the solution side at higher surface coverage. Hence, some asphaltenes desorb until the new equilibrium is reached. The desorption continues until coalescence ceases. It is not

certain why the coalescence ceases. However, it is likely that the asphaltenes interact with each other on the surface as surface coverages increase. The interaction may prevent further desorption. In any case, the experimental measurements reflect the equilibrium after coalescence.

4.4.2 Role of Solid Asphaltenes

The first set of experiments was designed to measure the effect of removing insoluble asphaltenes on the Sauter mean diameter of water-in-hydrocarbon emulsions. Emulsions were prepared from a sequence of pretreated asphaltenes where greater and greater portions of the least soluble asphaltenes were removed prior to making the emulsions. The volumes of toluene, hexane and water and the mass of the initial untreated asphaltene were all held constant for each set of experiments. A volume ratio of toluene to hexane of 5 to 1 was selected because a significant portion of the asphaltenes is insoluble in that solvent mixture. A water volume fraction of 0.25 was chosen to obtain a sufficient volume of emulsion.

Asphaltene subfractions were obtained by pretreating a fixed mass of asphaltenes. The untreated mass of asphaltenes was sufficient to make up a predetermined concentration of asphaltenes in the hydrocarbon phase prior to emulsification, C_A^o . The subfraction of the asphaltenes that precipitated in the pretreatment toluene/hexane mixture, f'_{insol} , was removed. The remaining soluble material, $C_A^o f'_{sol}$, was used to make up the emulsion. f'_{sol} and f'_{insol} are, respectively, the mass ratios of soluble to total asphaltenes and of insoluble to total asphaltenes at the pretreatment conditions. For example, an untreated sample has an f'_{sol} of unity and a sample where 40% of the asphaltenes were precipitated has an f'_{sol} of 0.60.

The Sauter mean diameters of emulsions prepared from asphaltenes with the precipitated material removed are shown in Fig. 4.4. Two sets of experiments were performed: the first at an initial untreated asphaltene concentration of 1.0 kg/m^3 ; and the second at 1.5 kg/m^3 . In both cases, there is no change in Sauter mean diameter until f'_{sol} drops below a

critical value, f_{sol}^c , of 0.63. However, the Sauter mean diameter increases rapidly as f'_{sol} decreases below 0.63. The increase in Sauter mean diameter means that some of the material responsible for stabilizing the emulsion has been removed. Hence, only the asphaltenes that fall in the range $f'_{sol} < 0.63$ act to stabilize water-in-hydrocarbon emulsions with a 5 to 1 volume ratio of hexane to toluene. *The least soluble asphaltenes of $f'_{sol} > 0.63$ do not appear to participate in stabilizing the emulsions.*

Similar experiments were conducted for water-in-hydrocarbon emulsions with various hexane to toluene ratios. The Sauter mean diameters for emulsions with 3 to 1 and 3 to 2 volume ratios of hexane to toluene are shown in Figs. 4.5 and 4.6, respectively. A critical mass ratio of soluble to total asphaltenes is evident in Fig 4.5 but is not evident in Fig. 4.6. The small region from $f_{sol}^c > 0.94$ contains the “solids” from the asphaltene-solids. The solids are the first material to precipitate and do not appear to participate in stabilizing the emulsions. The values of f_{sol}^c for each hexane to toluene ratio are listed in Table 4.1.

Table 4.1: A comparison of f_{sol}^c to f_{sol}^* at various hexane to toluene ratios.

| ϕ_H/ϕ_T | f_{sol}^c | f_{sol}^* at a C_A of 1 kg/m ³ |
|-----------------|-------------------|--|
| 5 | 0.63 | 0.33 |
| 3 | 0.80 | 0.49 |
| 1.5 | 0.94 ^a | 0.90 |

a) theoretical value - 6% of the untreated asphaltenes are “solids” (see p. 129)

The existence of an f_{sol}^c and the increase in f_{sol}^c as the hexane to toluene ratio increases both suggest that f_{sol}^c marks the boundary between the solid and liquid asphaltene phases. First, the asphaltenes in the group bounded by f_{sol}^c and 1 are the least soluble asphaltenes, the asphaltenes most likely to be solid phase. Second, the fraction of asphaltenes that

falls into that category decreases as the hexane to toluene ratio increases, *i.e.*, as the toluene content increases. The fraction of insoluble asphaltenes is also known to decrease as the toluene content increases. The predicted mass ratio of soluble to total asphaltene-solids, f_{sol}^* , at an asphaltene concentration of 1 kg/m³ is given in Table 4.1 for comparison. The predictions were made with the model developed in Chapter 2. While the absolute values of f_{sol}^c and f_{sol}^* do not agree, the trend with the hexane to toluene ratio is similar.

The above observations suggest that some or all of the soluble asphaltenes adsorb on the interface but none of the insoluble or solid phase asphaltenes do. A plausible model of the distribution of the asphaltenes during emulsification is illustrated in Fig. 4.7. The soluble asphaltenes are in equilibrium with the interfacial asphaltenes and the insoluble asphaltenes. The fraction of the asphaltenes that is insoluble is a function of the concentration and composition of the non-adsorbed asphaltenes and the volume ratio of hexane to toluene. However, the concentration and composition of the non-adsorbed asphaltenes depend on the surface area of the emulsion. The greater the surface area, the lower the asphaltene coverage and the more asphaltenes tend to adsorb from solution. The change in asphaltene concentration and composition during emulsification explains why the values of f_{sol}^c and f_{sol}^* presented in Table 4.1 are not identical.

4.4.3 Asphaltenes as a Molecular Surfactant

The results presented in the previous section provide circumstantial evidence that insoluble, “solid” asphaltenes do not participate in stabilizing the emulsions. What about the near precipitation point asphaltenes? Consider Fig. 4.6. The precipitation point, the boundary between the liquid and solid asphaltene phases, is observed at an f_{sol}^* of 0.94. And yet stable emulsions are observed even when 60% of the asphaltenes were removed in pretreatment. In other words, asphaltenes far from the precipitation point are capable of stabilizing the emulsions. Hence, our working hypothesis is that asphaltenes act as molecular surfactants and surface active asphaltenes are distributed throughout the soluble asphaltenes.

The hypothesis is tested by comparing predictions from Eq. 4.10 with experimental data. Eq. 4.10 was derived in Section 4.3 to predict the Sauter mean diameter of emulsions stabilized by asphaltenes acting as molecular surfactants. All but two of the variables in Eq. 4.10 are known or measurable. The density of the asphaltenes, ρ_A , and the thickness of the asphaltene monolayer, t_A , were determined in Chapter 2. The density varies only slightly with asphaltene composition. For convenience, only an average asphaltene density of 1160 kg/m^3 is used here. The asphaltene monolayer thickness estimated in Chapter 2 is 1.18 nm . The water volume fraction, ϕ_W , and the concentration of the asphaltenes in the solvent prior to emulsification, C_A^o , are measured quantities. The mass ratio of soluble to total asphaltenes, f_{sol}^* , is assumed to equal f_{sol}^c , a measured quantity. Only the mass ratio of surface active to total asphaltene-solids, f_a , and the equilibrium concentration of surface active asphaltenes, C_a^{eq} , are unknown.

In this section, Eq. 4.10 is tested over the broadest possible range of data. If the equation fits the data, the hypothesis that asphaltenes stabilize emulsions as a molecular surfactant is substantiated. To test the equation, the effect of varying ϕ_W , C_A^o , and f_{sol}^* on the Sauter mean diameter, d_{32} , was measured for emulsions with a 5 to 1 volume ratio of toluene to hexane. The previously discussed effect of pretreating asphaltenes to remove the highest molar mass material is also considered.

The effect of varying ϕ_W and C_A^o on d_{32} is shown in Fig. 4.8. Untreated asphaltenes samples are used in all cases so that f_{sol}^* has a constant value of 0.63. In Fig. 4.8, the volume fraction term is included in the y-axis so that all the data collapses onto a single curve. Emulsions with water volume fractions of 0.20, 0.25, 0.44 and 0.40 were examined over a range of initial asphaltene concentrations of 0.25 to 2 kg/m^3 . The emulsions became unstable at concentrations below 0.25 kg/m^3 . At concentrations greater than 2 kg/m^3 , the emulsion drop sizes were influenced by the mixing conditions. Eq. 4.10 fits the entire range of data very well. The particular values of f_a and C_a^{eq} that were found to fit the data are discussed later.

The effect of varying f_{sol}^* on d_{32} is shown in Fig. 4.9. All the emulsions in Fig. 4.9 were prepared with a water volume fraction of 0.25 and an initial asphaltene concentration of 1 kg/m³. For each data point, a mass of asphaltenes was pretreated in a mixture of toluene and hexane. The volume ratio of toluene to hexane was adjusted to obtain a desired mass ratio of insoluble to total asphaltenes, f'_{insol} . The precipitated asphaltenes were recovered and dried. Emulsions were prepared with the procedure described in Section 4.2 with an initial concentration of 1 kg/m³ of the precipitated subfraction. The value of f_{sol}^* for each emulsion was calculated with the following expression:

$$f_{sol}^* = 1 - \frac{1 - f_{sol}^c}{f'_{insol}} \quad (4.11)$$

Recall, f_{sol}^c is 0.63 for emulsions with a 5 to 1 volume ratio of hexane to toluene. Hence, soluble material is available to stabilize the emulsions in all precipitated subfractions that exceed 37 wt% of the original asphaltene sample.

The fitted Sauter mean diameters in Fig. 4.9 agree well with the experimental data except where f_{sol}^* approaches zero. Stable emulsions are observed at an f_{sol}^* of zero although unstable emulsions are predicted for $f_{sol}^* < 0.15$. The discrepancy is likely caused by experimental error. It is difficult to perform a perfect separation when the precipitated asphaltenes are recovered from the toluene/hexane mixture during pretreatment. As a result, the precipitate contains small quantities of trapped soluble asphaltenes. Soluble asphaltenes making up as little as 5% of the asphaltene subfraction are sufficient to account for the observations as f_{sol}^* approaches zero.

The data presented in Fig. 4.4 also provide a test of Eq. 4.10. Recall that for Fig. 4.4, the soluble asphaltenes from the pretreatment were used to prepare the emulsions. Here, C_A^o is the concentration of asphaltenes prior to emulsification for an untreated sample. The

effective concentration is $f'_{sol}C_A^o$. Hence, the effective values of f^*_{sol} required to solve Eq. 4.10 are given by:

$$\begin{aligned} f^*_{sol} &= f'_{sol}, & 0 \leq f'_{sol} \leq f^c_{sol} \\ f^*_{sol} &= f^c_{sol}, & f'_{sol} \geq f^c_{sol} \end{aligned} \quad (4.12)$$

Eq. 4.12 was employed to solve Eq. 4.10 and the results are plotted on Fig. 4.4. The fitted Sauter mean diameters agree very well with the experimental data.

The data from Figs. 4.4, 4.8 and 4.9 is combined in Fig. 4.10. The fitted parameters, $f_a = 0.38$ and $C_a^{eq} = 0.033 \text{ kg/m}^3$ were obtained from a linear regression of the data. A linear equation can be obtained by rearranging Eq. 4.10 as follows:

$$f_a (f^*_{sol} C_A^o) - C_a^{eq} = \frac{6\rho_A^t \phi_W}{d_{32}(1 - \phi_W)} \quad (4.13)$$

The data of Fig. 4.10 are plotted on the appropriate linear coordinates in Fig. 4.11. The fitted parameters and standard deviations from the linear regression are given in Table 4.2. The near unity values of the correlation coefficients indicate a good quality fit.

Table 4.2: Fitted estimates of f_a and C_a^{eq} at various hexane:toluene ratios.

| ϕ_H/ϕ_T | f_a | Std. Dev. of f_a | C_a^{eq} | Std. Dev. of C_a^{eq} | Corr. Coeff. |
|-----------------|-------|-----------------------|------------|----------------------------|-----------------|
| 5 | 0.383 | 0.019 | 0.033 | 0.010 | 0.933 |
| 3 | 0.288 | 0.014 | 0.028 | 0.011 | 0.983 |
| 1.5 | 0.231 | 0.018 | 0.012 | 0.014 | 0.958 |
| 1 | 0.187 | 0.017 | 0.008 | 0.015 | 0.953 |
| 0.25 | 0.152 | 0.015 | 0.009 | 0.015 | 0.964 |

The quality of the fit tends to support the hypothesis that asphaltenes act as molecular surfactants when stabilizing emulsions. However, the value of 0.383 found for f_a suggests that not all but really a fraction of the soluble asphaltenes is responsible for stabilizing the emulsion. The result is not surprising when one considers the large variety of molecular species that make up the asphaltenes. Asphaltenes have been shown to include acidic, basic, amphoteric and neutral species (4). Furthermore, asphaltenes range broadly in molar mass and molecular structure. Hence, a wide range in surface activity is likely within the asphaltenes. It appears that only the soluble surface active asphaltenes act to stabilize emulsions.

4.4.4 The Effect of the Hexane:Toluene Ratio

Similar experiments were conducted for asphaltene stabilized emulsions in toluene/hexane solvents of various volume ratios of hexane to toluene, ϕ_H/ϕ_T . The data for hexane to toluene ratios of 3, 1.5, 1 and 0.25 are plotted on the appropriate linear coordinates in Figs 4.12 - 4.15, respectively. In almost all cases, Eq. 4.10 fitted the data very well. The fitted parameters for each solvent system are listed in Table 4.2.

Eq. 4.10 seems to break down at low toluene to hexane ratios when large fractions of precipitate are removed prior to emulsification. The experimental Sauter mean diameters of some soluble subfractions are significantly greater than predicted in Fig. 4.14 for a 1 to 1 volume ratio of hexane to toluene. Smaller deviations are also visible in Fig. 4.6 for a volume ratio of 1.5. This type of experiment was not performed for the 0.25 volume ratio. The deviations occur when there is a substantial difference between the molar mass of the soluble treated and untreated asphaltenes. For example, in Fig. 4.6, the soluble untreated asphaltenes include the entire asphaltene molar mass distribution. The treated samples that deviate from the fitted line include only 50 wt% of the asphaltenes and that 50% includes only the lowest asphaltene molar masses. In contrast, consider the data for a 5 to 1 volume ratio of hexane to toluene in Fig 4.4. The soluble untreated asphaltenes only include the lightest 70 wt% of the asphaltene molar mass distribution. Hence, the

difference in molar mass between the soluble treated and untreated asphaltenes is relatively small. In this case, no deviation occurs.

The molar mass dependence suggests that the fraction of surface active asphaltenes decreases slightly with a decrease in molar mass. A decrease in f_a leads to an increase in d_{32} and hence the experimental data deviates from the prediction. The change in the surface active fraction is small enough that it is only apparent when samples with very different molar masses are compared. Asphaltene solubility is related to molar mass and the dependence of f_a on molar mass may reflect a solubility effect. This concept is discussed in more detail later.

Effect of the hexane:toluene ratio on f_a : The value of f_a decreases exponentially as the volume fraction of toluene in the solvent mixture increases. The values are plotted in Fig. 4.16. While the fraction of surface active asphaltenes decreases, it does not diminish to zero. Stable emulsions are obtained even in solvents, such as toluene, where all of the asphaltenes are soluble. Once again, neither insoluble nor near precipitation point asphaltenes are required to obtain stable water-in-oil emulsions.

The change in f_a with ϕ_T may be caused by a change in the molar mass of the soluble asphaltenes or by a change in asphaltene surface activity. However, the predicted effect of the change in molar mass is the opposite to what is observed. As the volume fraction of toluene increases, asphaltenes of higher molar mass become soluble and the average molar mass of the soluble subfraction increases. As discussed previously, the higher molar mass asphaltenes contain a higher fraction of surface active material. Hence, the value of f_a is expected to increase as the volume fraction of toluene increases. Since the value of f_a decreases with an increase in ϕ_T , asphaltene surface activity must be affected by the hexane:toluene ratio.

The surface activity of a surfactant is a function of the hydrophilic and hydrophobic interactions of the surfactant with the water and oil phases. The polyaromatic skeleton of

asphaltene molecules is so hydrophobic that asphaltenes are insoluble in water. Their surface activity arises from the attraction between their heteroatom structural elements and the water. The stronger that attraction relative to the attraction between the polyaromatic skeleton and the hydrocarbon phase, the more strongly an asphaltene molecule adsorbs on the interface and the more effective a surfactant it becomes. When the toluene content of the hydrocarbon phase increases, the attraction between the hydrocarbon phase and the asphaltene skeleton increases and the asphaltenes become less surface active. Since the asphaltenes are a mixture of components with a variety of surface activities, some asphaltenes remain strongly surface active while others in effect become too weak a surfactant to be considered surface active.

The surface activity of the asphaltenes can be represented by a distribution of adsorption coefficients. The definition of the adsorption coefficient is best illustrated through the Langmuir adsorption isotherm. The adsorption of a mixture of surfactants on an interface can sometimes be modeled with this isotherm (9). Furthermore, in many cases, asphaltenes adsorb on solid surfaces according to the Langmuir isotherm (10,11). The Langmuir adsorption isotherm of a mixture of surfactants is given by

$$\theta = \sum \theta_i = \frac{\sum k_i C_{ai}^{eq}}{1 + \sum k_i C_{ai}^{eq}} \quad (4.14)$$

Here, θ is the fractional surface coverage, k is the adsorption coefficient and the subscript i denotes the i^{th} asphaltene species. A strong surfactant has a higher adsorption coefficient and occupies a larger fraction of the interface than a weak surfactant. Note that the distribution of adsorption coefficients is not necessarily related to the molar mass distribution.

The effect of the solvent on asphaltene surface activity is illustrated in Fig. 4.17. The asphaltenes are represented by a broad range of adsorption coefficients. Some species adsorb so weakly that they are, in effect, non-surface active. Others are irreversibly

bound to the interface. A threshold adsorption coefficient, k_c , is defined to arbitrarily separate the surface active and non-surface active asphaltenes. Adsorption coefficients below the threshold are considered non-surface active. The position of the distribution of adsorption coefficients relative to k_c depends on the solvent. In the examples given in Fig. 4.17, approximately 50% of the asphaltenes are surface active in the poor solvent. The entire distribution curve shifts to lower adsorption coefficients in the good solvent because the attraction between the solvent and the asphaltene hydrocarbon skeleton increases. The relative amount of asphaltenes above k_c decreases in this example to approximately 30%. The explanation illustrated in Fig. 4.17 is qualitative but it describes the results plotted in Fig. 4.16.

In summary, the dependence of f_a on the hexane:toluene ratio indicates that asphaltene solubility influences the surface activity of the asphaltenes. The influence likely arises through the interaction between the solvent and the hydrocarbon skeleton of the asphaltene molecules. The effect of the hexane:toluene ratio dominates the effect of the asphaltene molar mass. Nonetheless, the molar mass dependence of f_a is consistent with this interpretation. The lower molar mass molecules are more soluble and less likely to be strong surfactants. Hence, the value of f_a is expected to decrease as the molar mass decreases, just as was observed. This concept is similar to the idea that near precipitation point asphaltenes are responsible for stabilizing emulsions. However, the effect is fairly small and some asphaltenes far from the precipitation point are still able to stabilize the emulsions.

Effect of the hexane:toluene ratio on C_a^{eq} : The values of C_a^{eq} given in Table 4.2 are all near zero relative to the initial soluble surface active asphaltene concentrations. In other words, the vast majority of the surface active asphaltenes adsorbs on the interface. The low relative values of C_a^{eq} cast doubt on their accuracy. Consider Figs. 4.11 to 4.15. A very small difference in the measured values could lead to large changes in the intercept from which C_a^{eq} is calculated. The high standard deviations of the C_a^{eq} in Table 4.2 reflect the large relative error. Any interpretation of the C_a^{eq} values is risky because the

potential error is so great. Furthermore, some knowledge of the distribution of asphaltene adsorption coefficients is necessary to interpret the equilibrium concentration results. Therefore, no analysis is attempted here.

The Effect of Solvent on f_i^* : Consider Eq. 4.9. At low C_a^{eq} , f_i^* is approximately equal to the product $f_a f_{sol}^*$. Hence, the fraction of asphaltenes that stabilizes the emulsions is generally constant for a given hexane:toluene ratio. However, the value of f_i^* may vary at very low asphaltene concentrations or when very different asphaltene molar mass are considered. The estimated values of f_i^* are summarized at different volume fractions of toluene in Table 4.3. In a poor solvent, a higher fraction of asphaltenes are surface active but a higher fraction are insoluble. Hence, the fraction of asphaltenes that adsorbs on the interface is a complex function of asphaltene solubility. For toluene/hexane mixtures, the values of f_i^* are nearly constant at toluene volume fractions less than 40% but drop substantially as the toluene content increases above 40 vol%.

Table 4.3: The fraction of asphaltene-solids that stabilize water-in-toluene/hexane emulsions as a function of toluene content.

| ϕ_T | f_i^* |
|----------|---------|
| 0.17 | 0.24 |
| 0.25 | 0.23 |
| 0.40 | 0.22 |
| 0.50 | 0.18 |
| 0.80 | 0.14 |

4.5 Conclusions

Below the cmc, asphaltenes can stabilize water-in-oil emulsions in one of three possible forms: solid particles; near precipitation point molecules; and molecular surfactants.

Measurements of the Sauter mean diameter of water-in-toluene/hexane emulsions

stabilized by different asphaltene subfractions were employed to determine what fraction of the asphaltenes stabilized the emulsions. The removal of insoluble asphaltenes had no effect on the interfacial area stabilized by the asphaltenes. Furthermore, asphaltenes far from the precipitation point were capable of stabilizing emulsions. Hence, asphaltenes appear to act as molecular surfactants.

An expression was derived to calculate the Sauter mean diameter of emulsions stabilized by asphaltenes acting as molecular surfactants. The expression successfully fitted the experimental data over a broad range of water volume fractions, asphaltene concentrations and asphaltene solubilities. The quality of the fit supports the concept that asphaltenes act as molecular surfactants.

Only soluble asphaltenes can act to stabilize emulsions, but not all soluble asphaltenes are surface active. The mass ratio of surface active to soluble asphaltenes depends on the degree of solubility. The mass ratio of surface active to soluble asphaltenes decreases in a good solvent (low hexane:toluene ratio) and decreases as the asphaltene molar mass decreases. Low molar mass asphaltenes are more soluble than high molar mass ones. Hence, more soluble asphaltene molecules are less surface active.

Solubility controls the amount of asphaltenes that adsorbs on an interface in two opposing ways. Only soluble, surface active asphaltenes stabilize the emulsions. The supply of soluble asphaltenes increases in good solvents (low hexane:toluene ratios). However, since the more soluble asphaltene molecules are less surface active, the proportion of surface active asphaltenes decreases in good solvents. In general, a small fraction of the asphaltenes stabilizes the emulsions in good solvents.

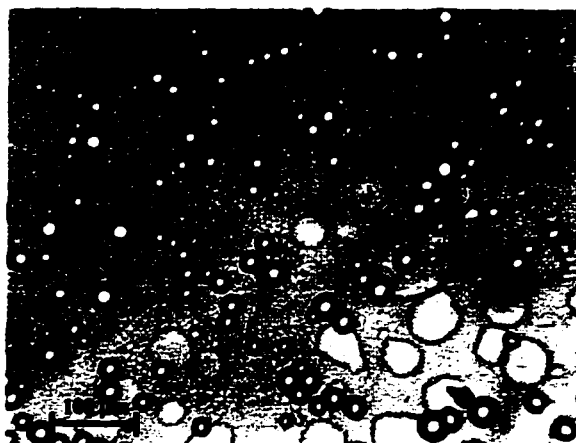
4.5 References

1. Sheu, E.Y., Storm, D.A., De Tar, M.M., *J. Non-Crystalline Solids*, **131-133**, (1991), 341.
2. Dickie, J.P., and Yen, T.F., *Anal. Chem.*, **39**, (1967), 1847.

3. Cimino, R., Corraera, S., Del Bianco, A., in "Asphaltenes Fundamentals and Applications", Ed. E.Y. Sheu and O.C. Mullins, Plenum Press, New York, 1995, p. 97.
4. Speight, J.G., in "Asphaltenes and Asphalts, 1", Ed. T.F. Yen and G.V. Chilingarian, Elsevier Science, Amsterdam, 1994, p. 7.
5. Eley, D.D., Hey, M.J., and Symonds, J.D., *Colloids Surfaces.*, **32**, (1988), 87.
6. Eley, D.D., Hey, M.J., and Symonds, J.D., and Willison, J.H.M., *J. Colloid Interface Sci.*, **54**, (1976), 462.
7. Eley, D.D., Hey, M.J., and Lee, M.A., *Colloids Surfaces A*, **24**, (1987), 173.
8. Acevedo, S., Escobar, G., Gutiérrez, L.B., and Rivas, H., *Colloids Surfaces A*, **71**, (1993), 65.
9. Yarranton, H.W., and Masliyah, J.H., *J. Phys. Chem.*, **100**, (1996), 1786.
10. Kokal, S., Tang, T., Schramm, L., and Sayegh, S., *Colloids Surfaces A*, **95**, (1995), 253.
11. González, G., and Moreira, M.B.C., in "Asphaltenes and Asphalts, 1", Ed. T.F. Yen and G.V. Chilingarian, Elsevier Science, Amsterdam, 1994, p. 207.



a) $\phi_H/\phi_T = 5$, $\phi_W = 0.25$, $C_A^0 = 1.5 \text{ kg/m}^3$, $d_{10} = 8.0 \text{ μm}$



b) $\phi_H/\phi_T = 5$, $\phi_W = 0.40$, $C_A^0 = 1.0 \text{ kg/m}^3$, $d_{10} = 21.1 \text{ μm}$



c) $\phi_H/\phi_T = 5$, $\phi_W = 0.40$, $C_A^0 = 0.4 \text{ kg/m}^3$, $d_{10} = 38.0 \text{ μm}$

Plate 4.1: Asphaltene Stabilized Water-in-Toluene/Hexane Emulsions

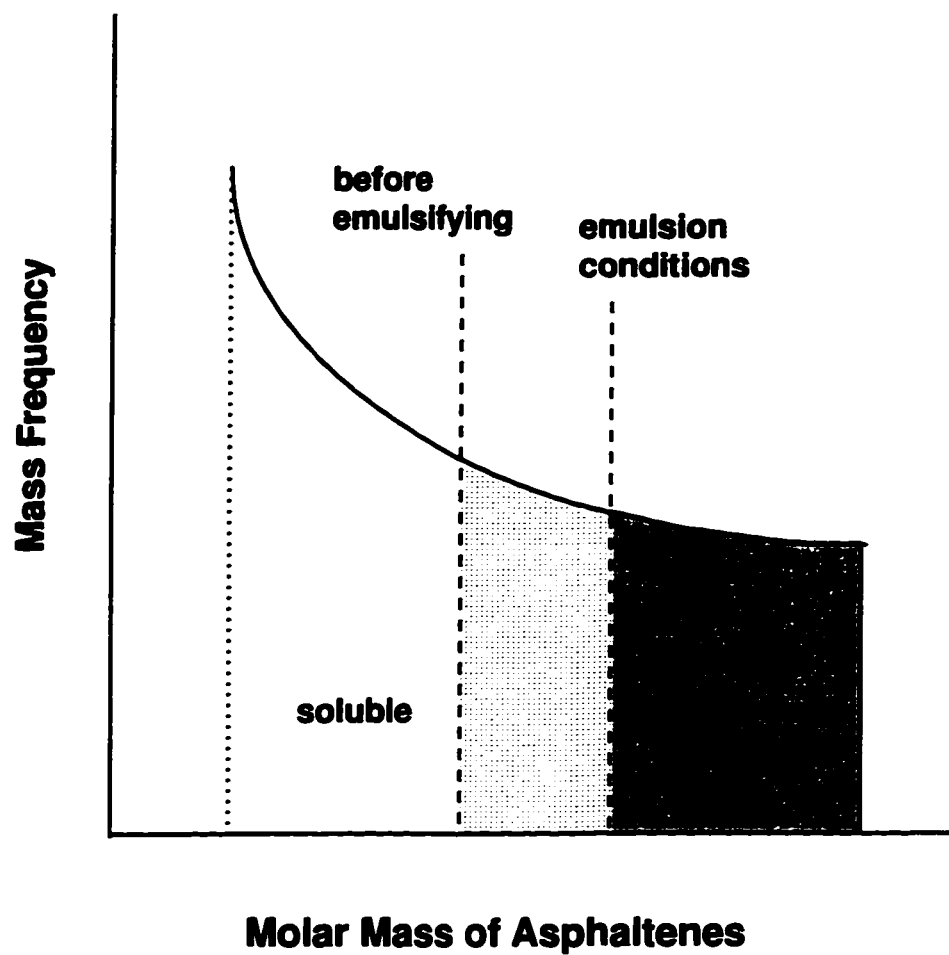


Figure 4.1: The fractionation of the asphaltene molar mass distribution by solubility.

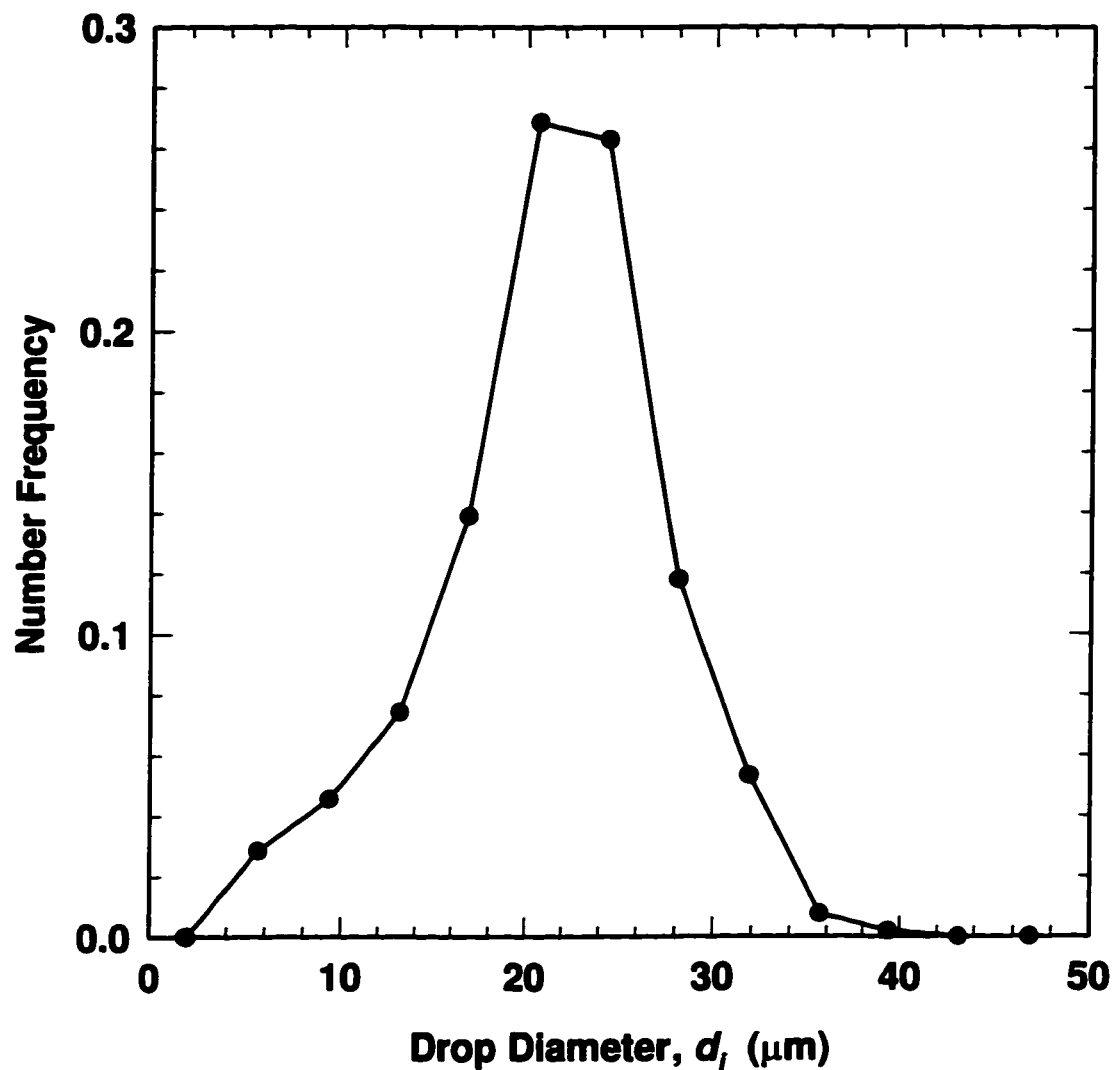


Figure 4.2: Drop size distribution of an asphaltene stabilized water-in-toluene/hexane emulsion measured 1.5 hours after blending.

($\phi_H/\phi_T = 5$, $\phi_W = 0.40$, $C_A^0 = 1.00 \text{ kg/m}^3$)

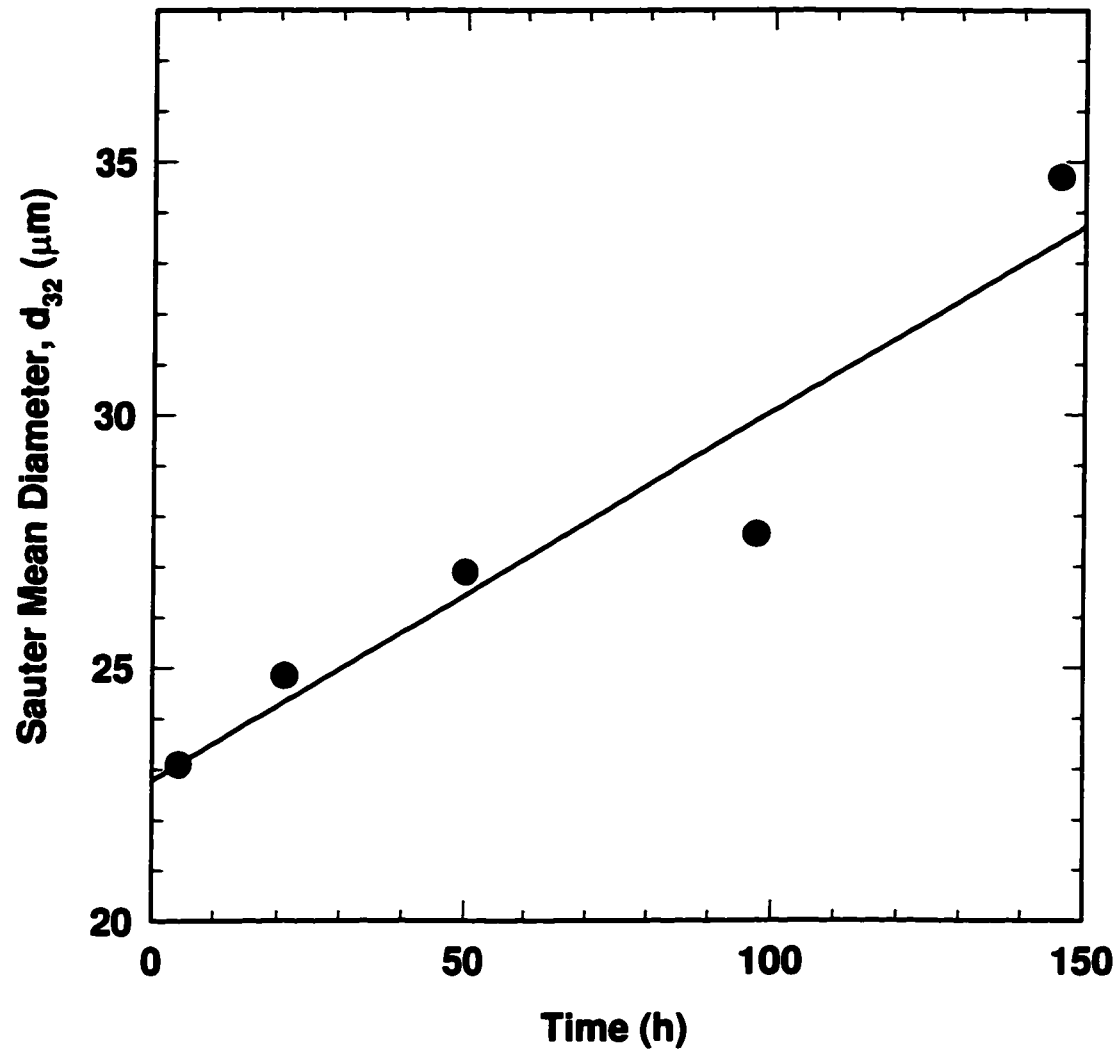


Figure 4.3: Growth with time of the Sauter mean diameter of an asphaltene stabilized water-in-toluene/hexane emulsion. ($\phi_T/\phi_H = 5$, $\phi_W = 0.40$, $C_A^0 = 1.00 \text{ kg/m}^3$)

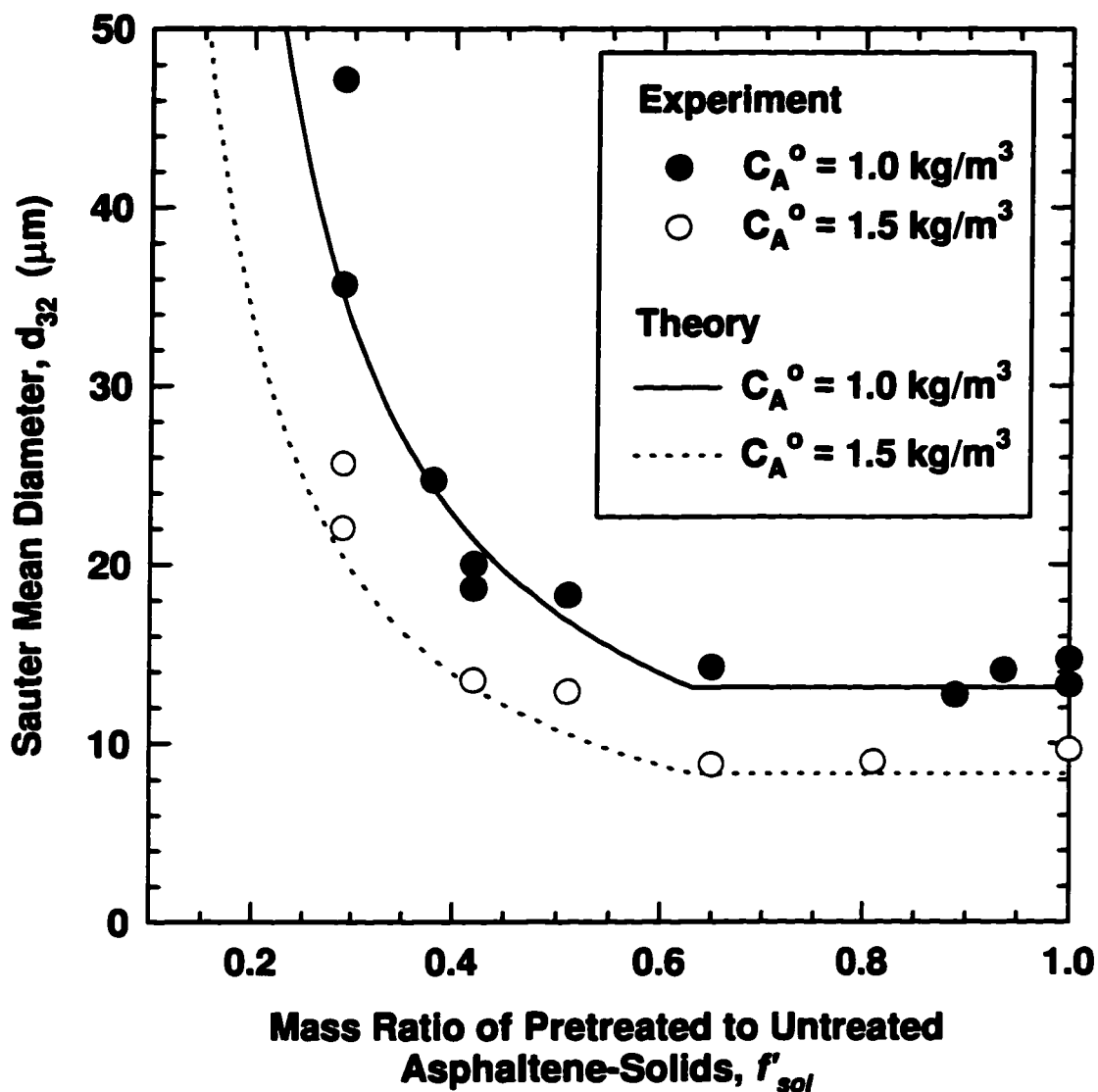


Figure 4.4: Change in the Sauter mean diameter of asphaltene stabilized water-in-toluene/hexane emulsions when the highest molar mass asphaltenes are removed before emulsification. ($\phi_H/\phi_T = 5$ and $\phi_W = 0.25$)

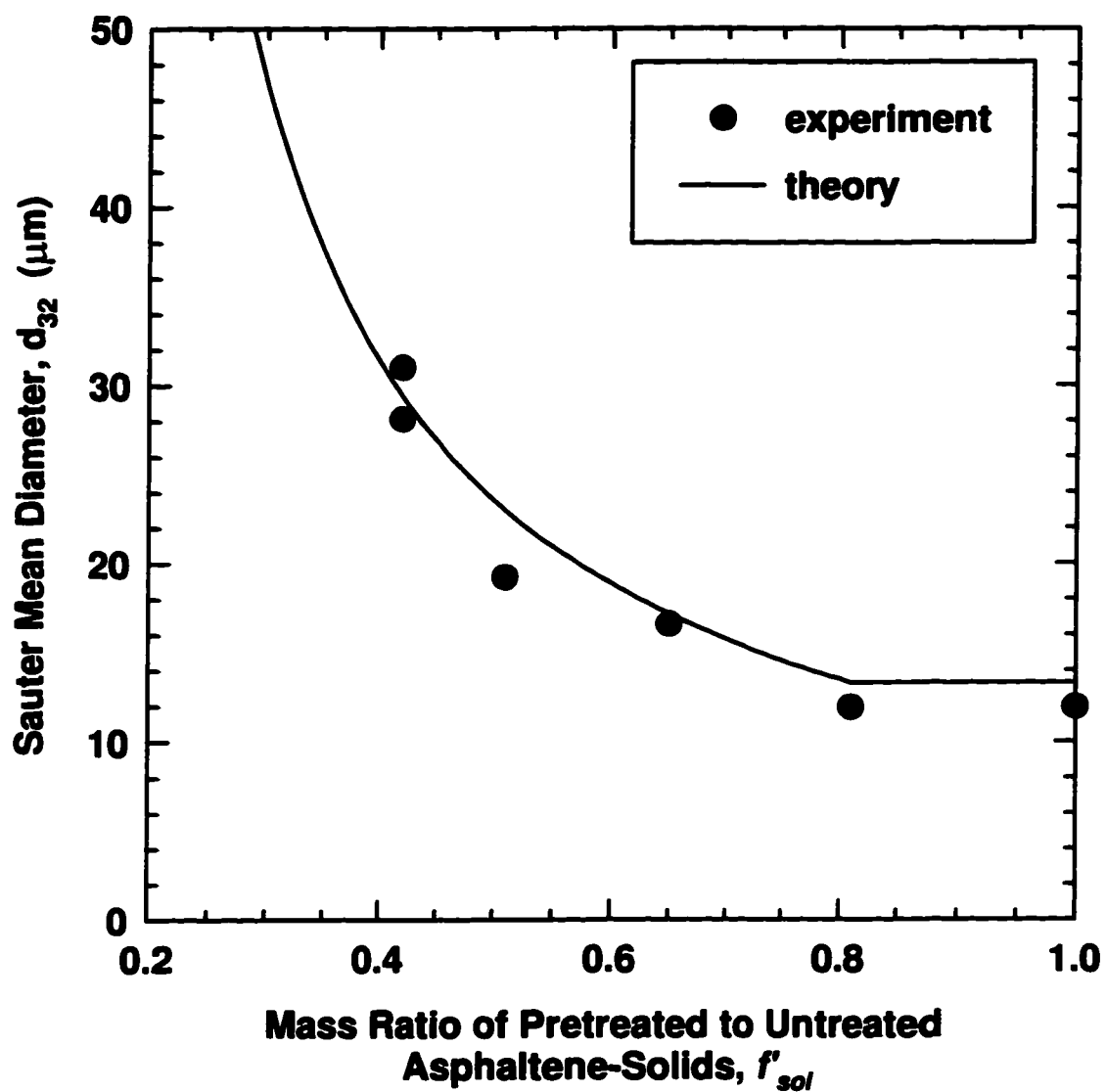


Figure 4.5: Change in the Sauter mean diameter of asphaltene stabilized water-in-toluene/hexane oil emulsions when the highest molar mass asphaltenes are removed before emulsification. ($\phi_H/\phi_T = 3$, $\phi_W = 0.25$, $C_A^0 = 1.00 \text{ kg/m}^3$)

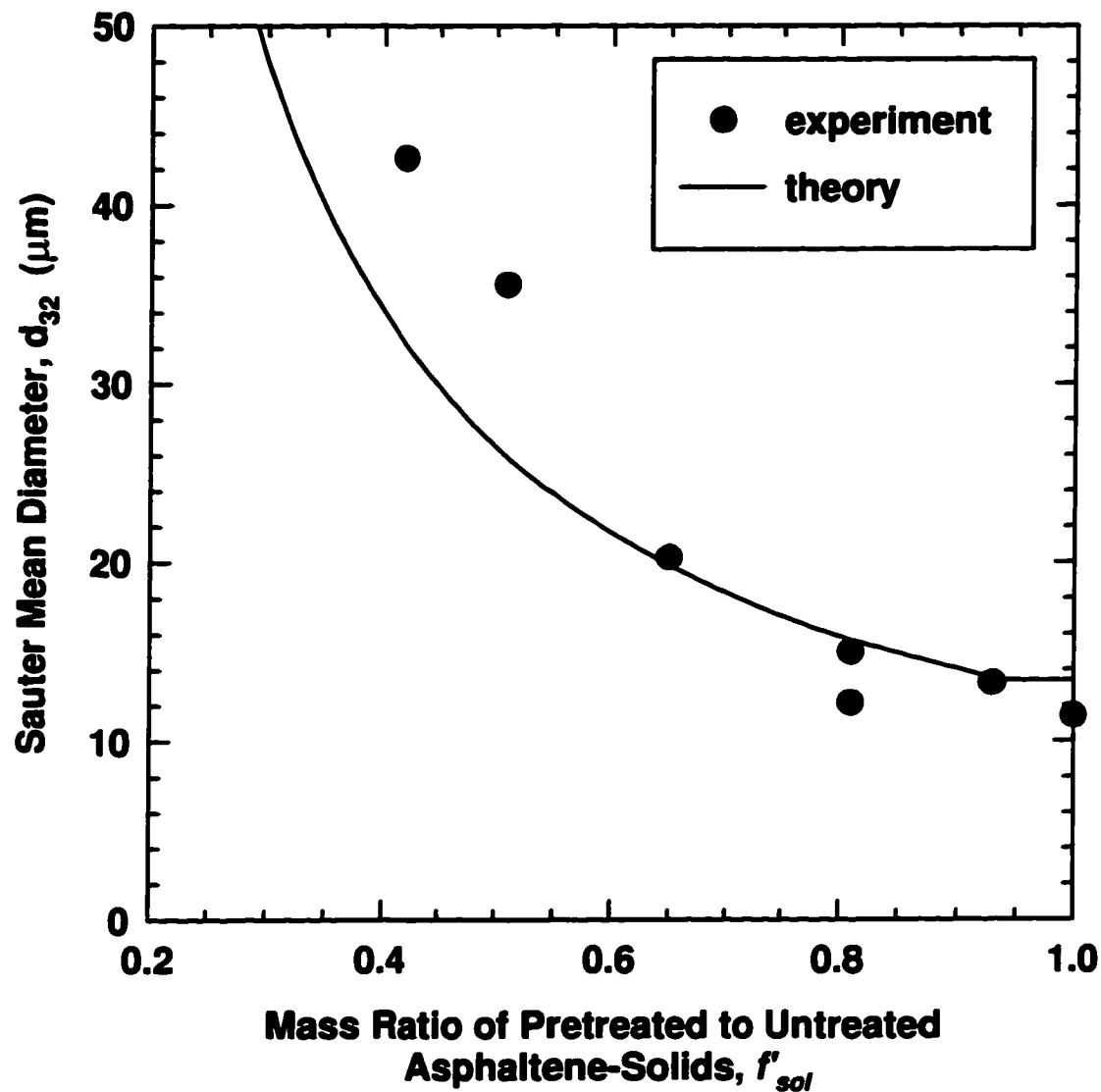
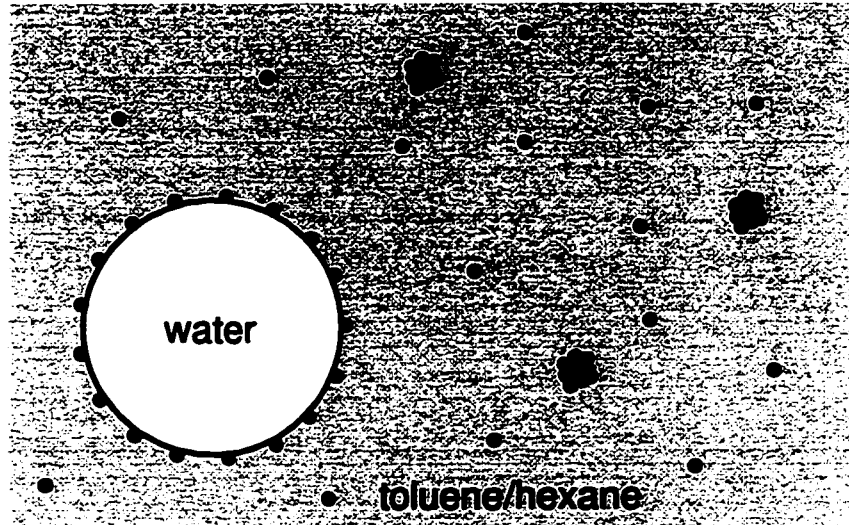


Figure 4.6: Change in the Sauter mean diameter of asphaltene stabilized water-in-toluene/hexane emulsions when the highest molar mass asphaltenes are removed before emulsification. ($\phi_H/\phi_T=1.5$, $\phi_W=0.25$, $C_A^0=1.00$ kg/m³)



- soluble asphaltene molecule
- insoluble asphaltene aggregate



Figure 4.7: Equilibrium relations between asphaltenes in an emulsion.

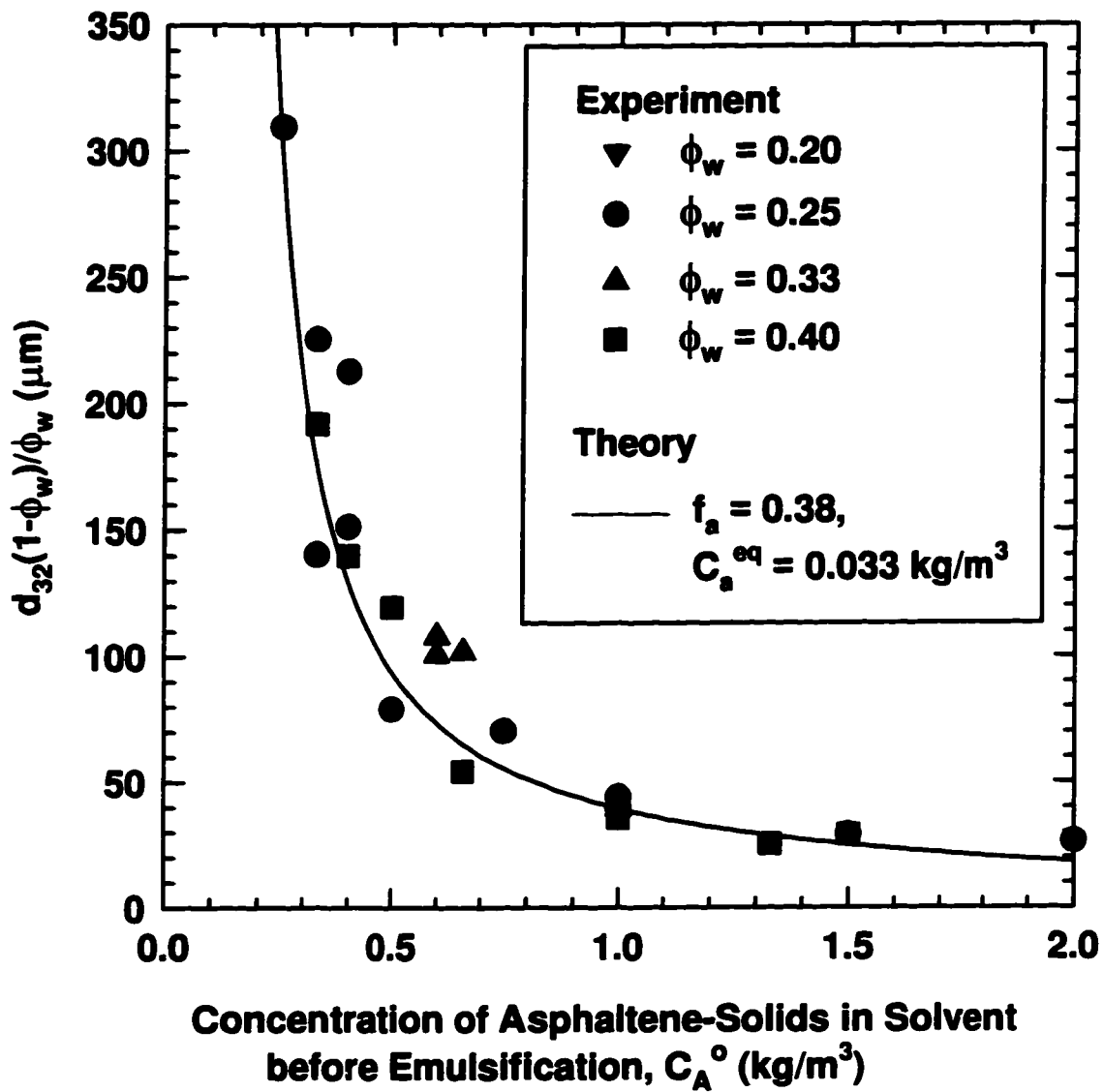


Figure 4.8: Effect of water volume fraction and asphaltene concentration on the Sauter mean diameter of asphaltene stabilized water-in-toluene/hexane emulsions. ($\phi_H/\phi_T = 5$ and $f_{sol}^* = 0.63$)

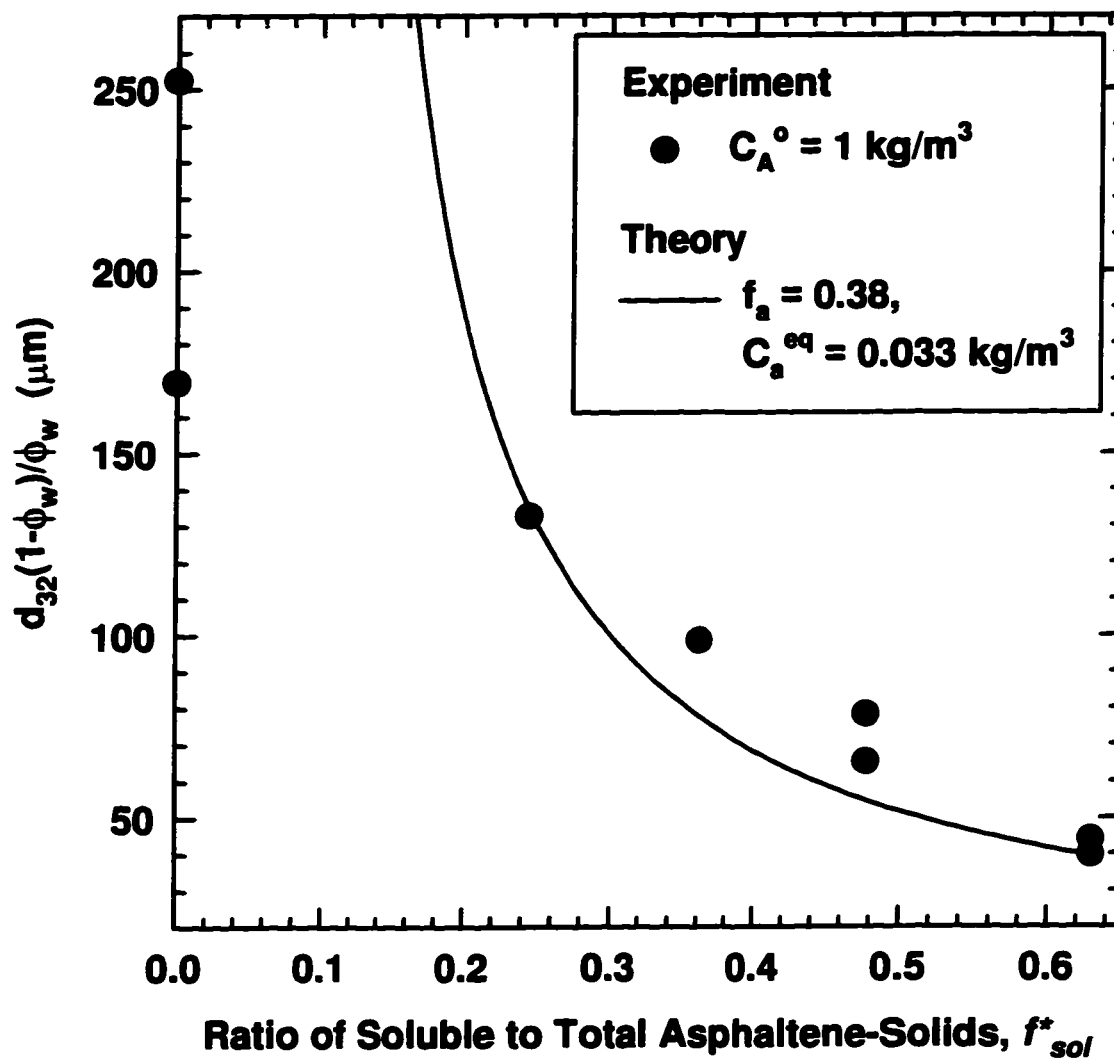


Figure 4.9: Effect of f_{sol}^* on the Sauter mean diameter of asphaltene stabilized water-in-toluene/hexane emulsions. ($\phi_H/\phi_T = 5$ and $\phi_W = 0.25$)

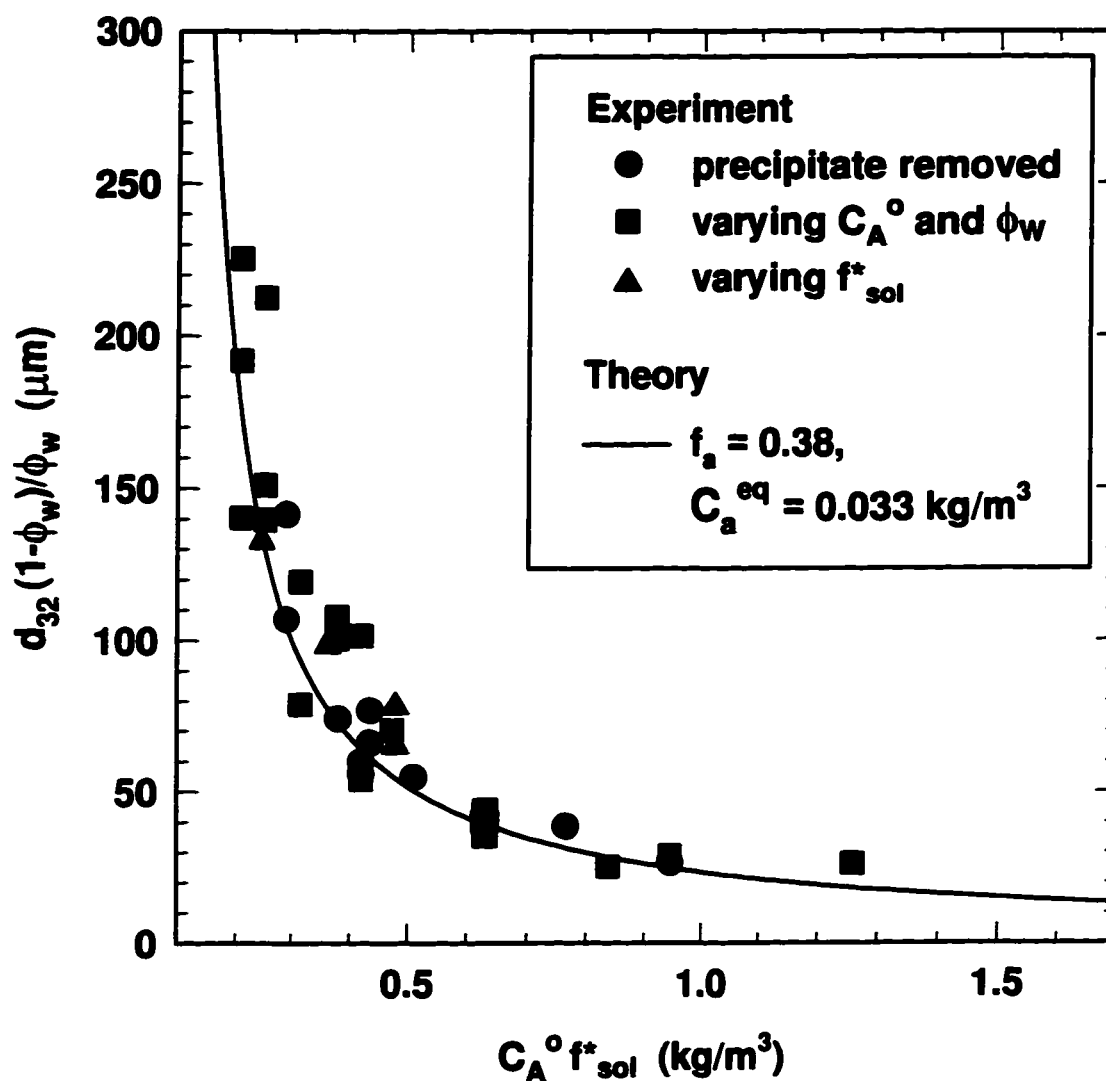


Figure 4.10: Predicted and experimental Sauter mean diameters of asphaltene stabilized water-in-toluene/hexane emulsions with a 5:1 volume ratio of hexane to toluene. ($0.20 < \phi_w < 0.40$, $0.25 < C_A^0 < 2.00 \text{ kg/m}^3$, $0.24 < f_{sol}^* < 0.63$)

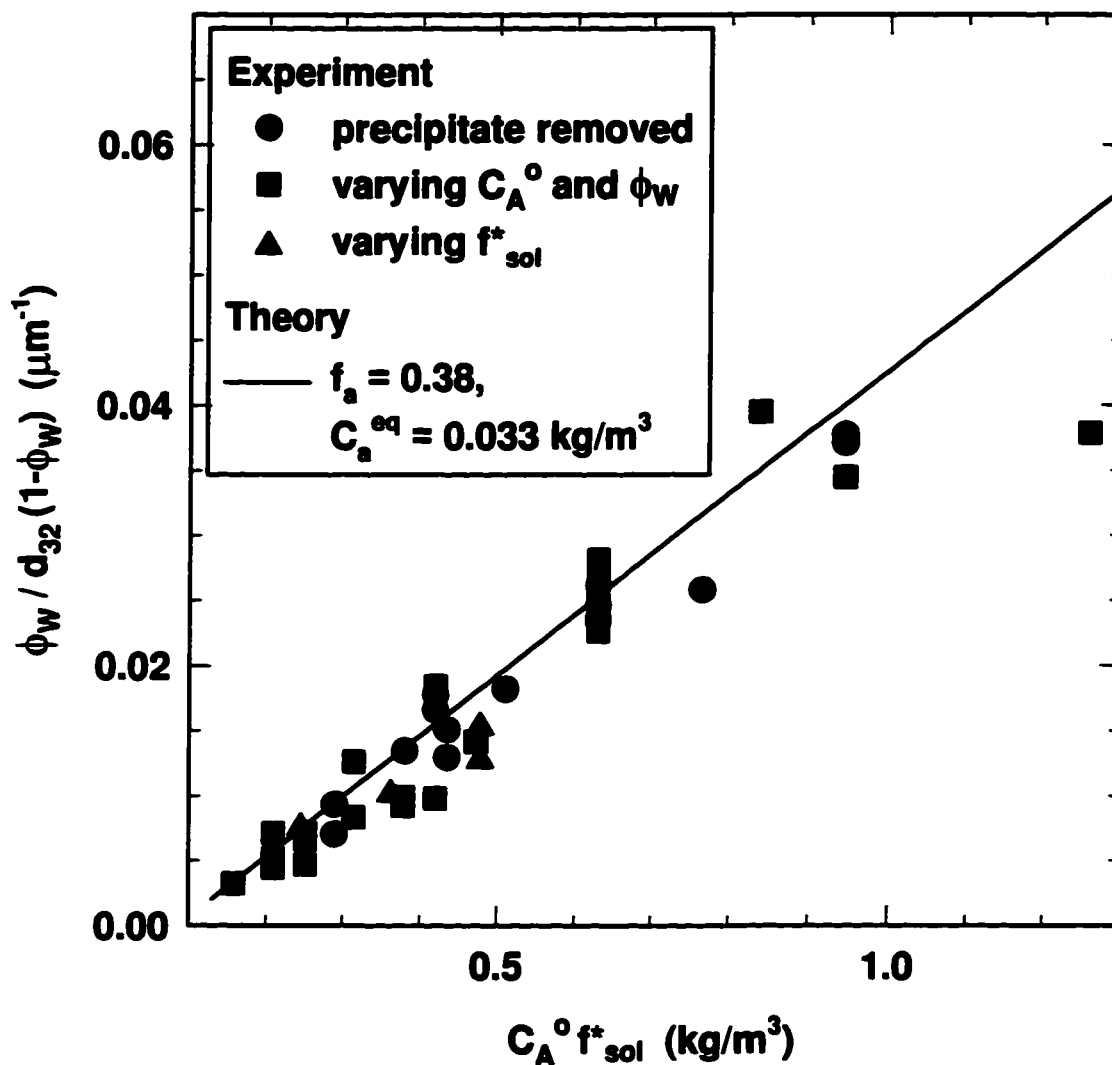


Figure 4.11: Inverse Sauter mean diameter versus the concentration of soluble asphaltenes in asphaltene stabilized water-in-toluene/hexane emulsions with a 5:1 volume ratio of hexane:toluene.

($0.20 < \phi_W < 0.40$, $0.25 < C_A^0 < 2.00 \text{ kg}/\text{m}^3$, $0.24 < f_{\text{sol}}^* < 0.63$)

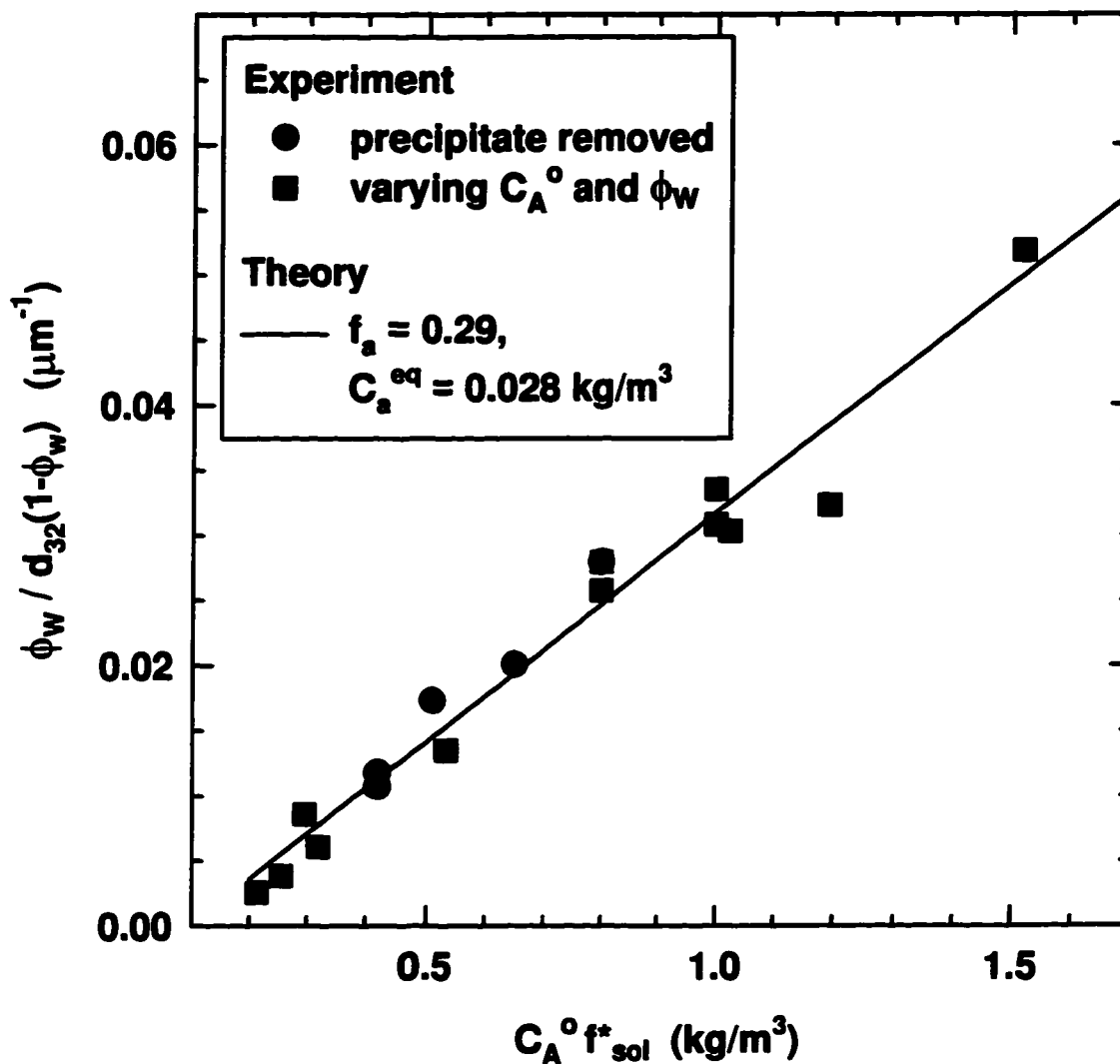


Figure 4.12: Inverse Sauter mean diameter versus the concentration of soluble asphaltenes in asphaltene stabilized water-in-toluene/hexane emulsions with a 3:1 volume ratio of hexane:toluene.
 $(0.25 < \phi_w < 0.40, 0.27 < C_A^0 < 1.90 \text{ kg}/\text{m}^3, 0.4 < f_{\text{sol}}^* < 0.8)$

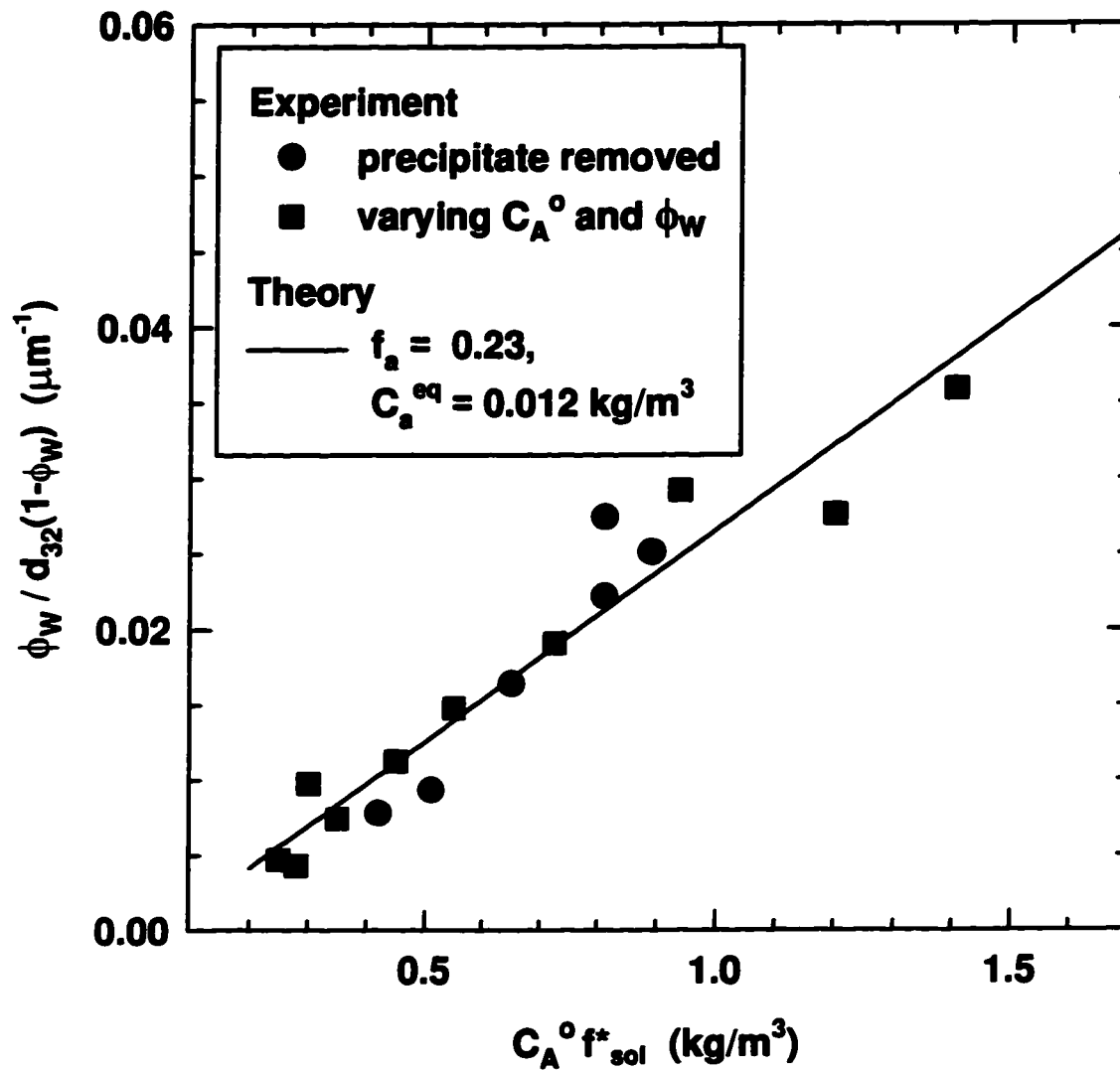


Figure 4.13: Inverse Sauter mean diameter versus the concentration of soluble asphaltenes in asphaltene stabilized water-in-toluene/hexane emulsions with a 3:2 volume ratio of hexane:toluene.

($0.25 < \phi_w < 0.40$, $0.27 < C_A^o < 1.50 \text{ kg}/\text{m}^3$, $0.4 < f_{sol}^* < 0.94$)

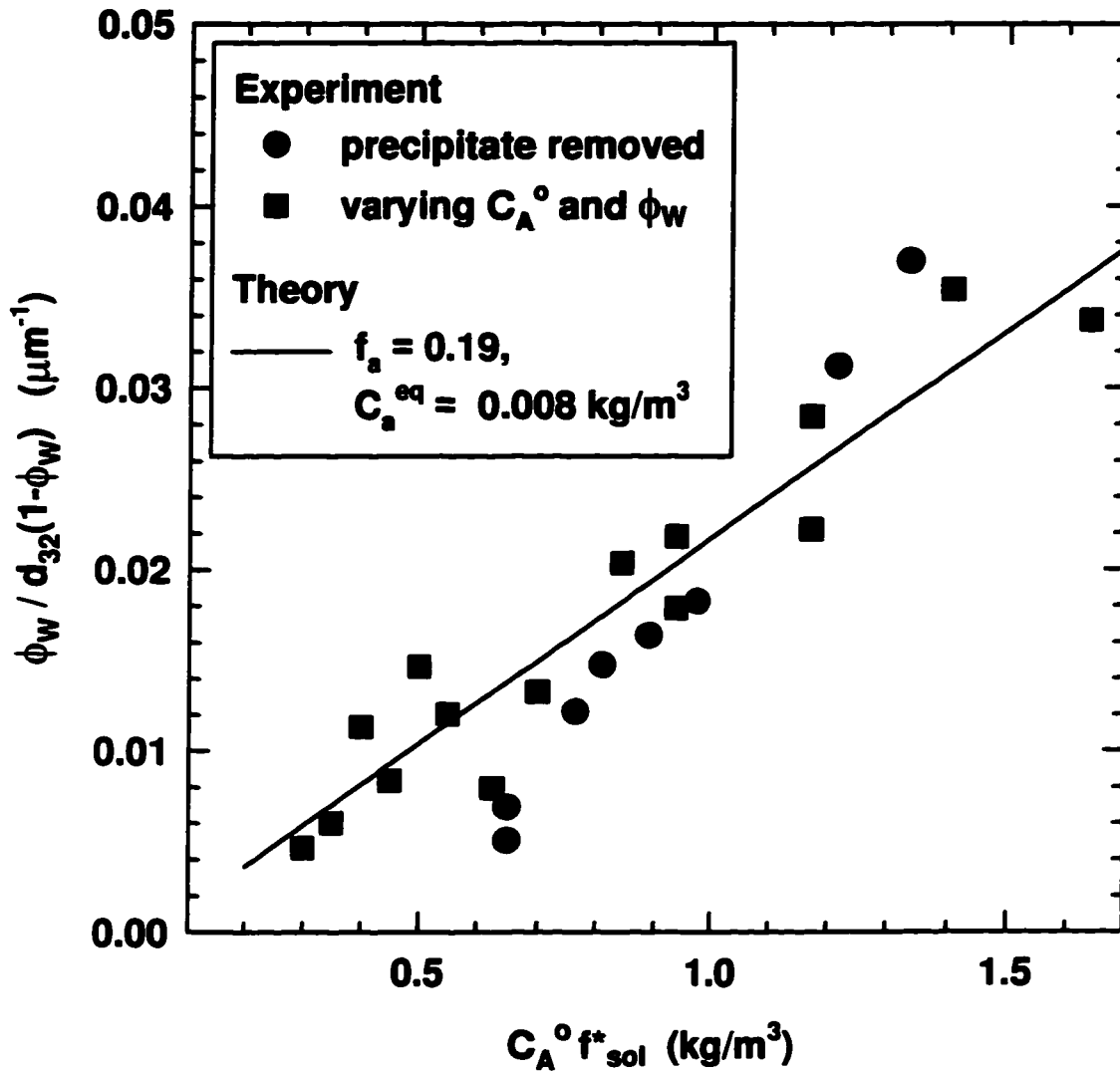


Figure 4.14: Inverse Sauter mean diameter versus the concentration of soluble asphaltenes in asphaltene stabilized water-in-toluene/hexane emulsions with a 1:1 volume ratio of hexane:toluene.

($0.25 < \phi_w < 0.40$, $0.32 < C_A^o < 1.75 \text{ kg}/\text{m}^3$, $0.55 < f_{sol}^* < 0.94$)

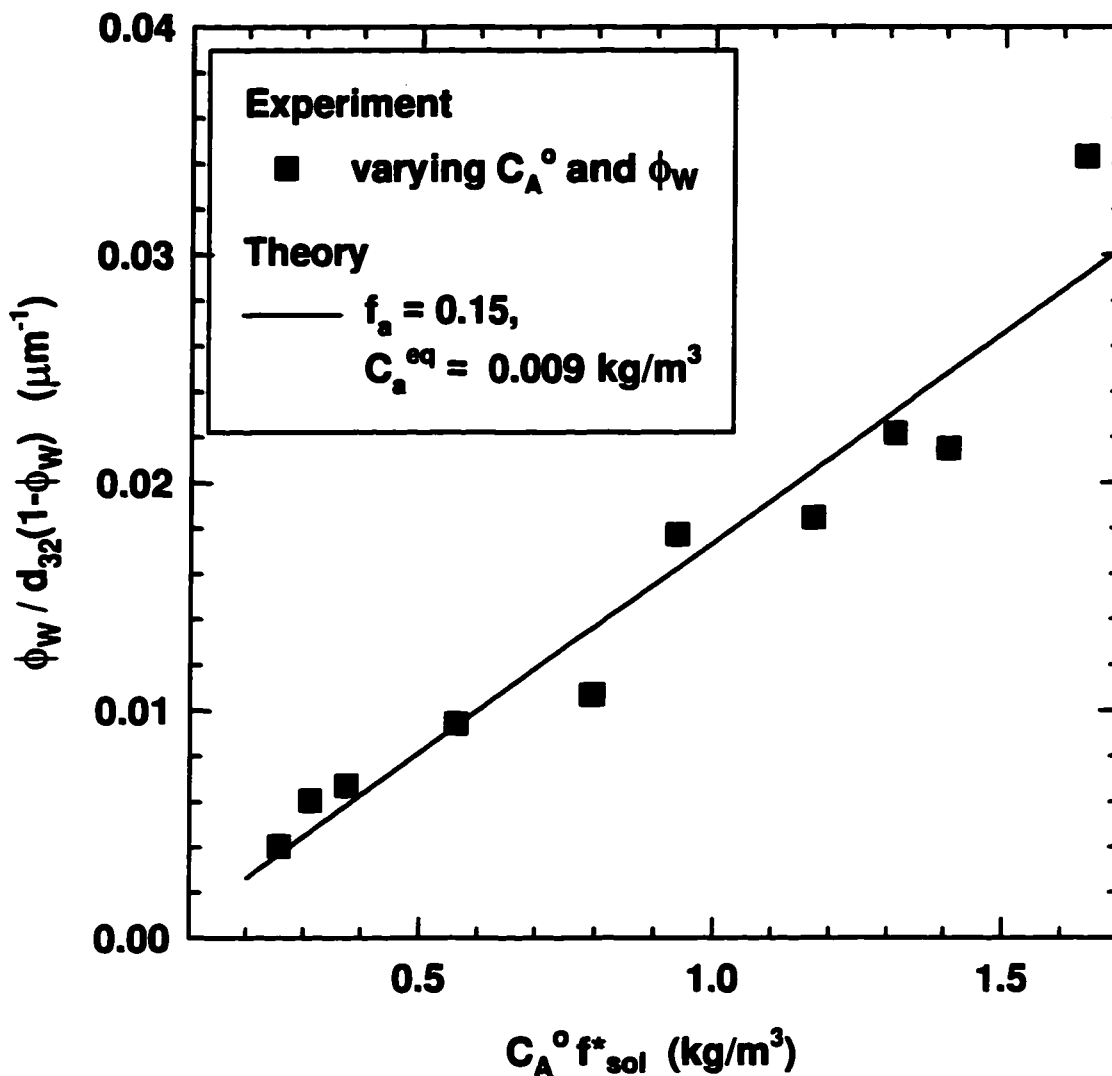


Figure 4.15: Inverse Sauter mean diameter versus the concentration of soluble asphaltenes in asphaltene stabilized water-in-toluene/hexane emulsions with a 1:4 volume ratio of hexane:toluene.

($0.25 < \phi_w < 0.40$, $0.28 < C_A^o < 1.75 \text{ kg}/\text{m}^3$, $f_{sol}^* = 0.94$)

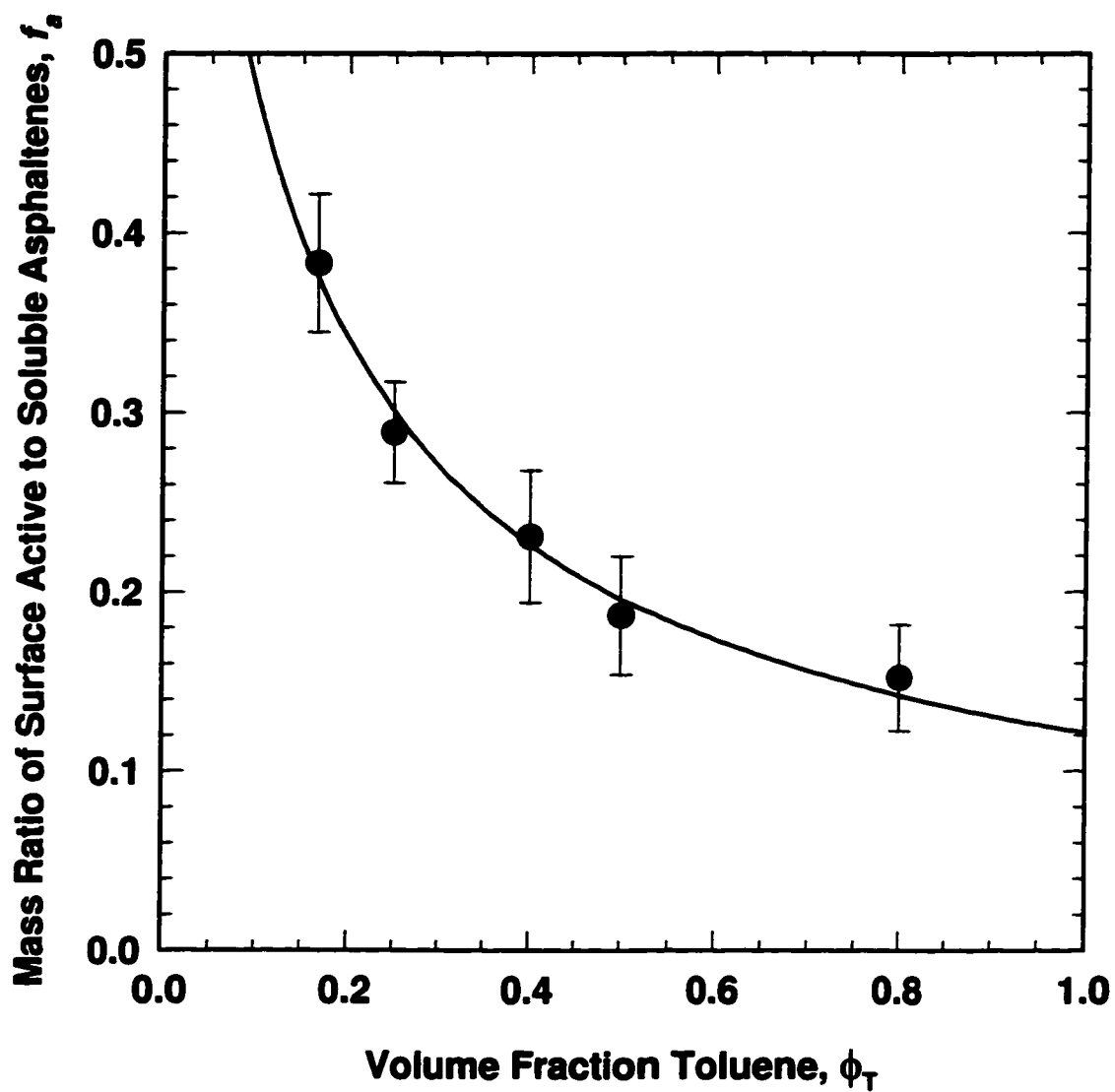


Figure 4.16: The effect of solvent composition on the mass ratio of surface active to soluble asphaltenes.

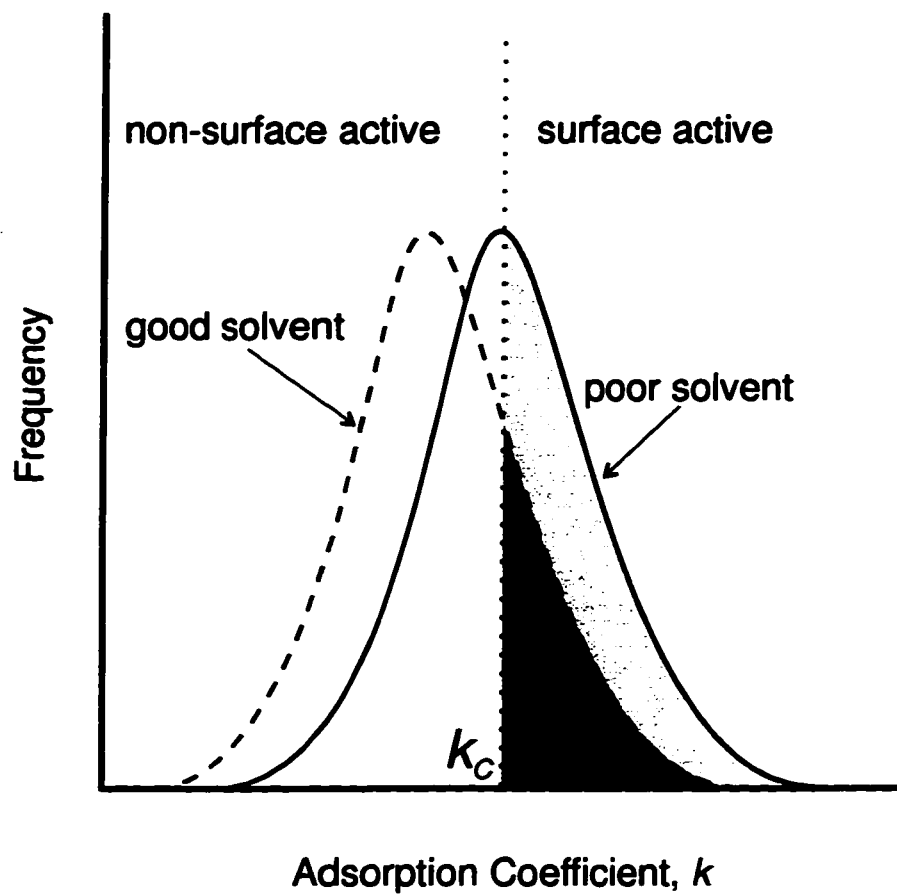


Figure 4.17: The effect of the solvent on a hypothetical distribution of asphaltene adsorption coefficients.

Chapter 5

OSTWALD RIPENING OF ASPHALTENE STABILIZED WATER-IN-TOLUENE/HEXANE EMULSIONS

In this chapter, experimental measurements of the drop size distributions are employed to determine whether asphaltene stabilized water-in-toluene/hexane emulsions destabilize through coalescence or Ostwald ripening. The original intention was to model the destabilization process with an appropriate theory. However, the emulsions destabilized in a manner not previously observed but similar to Ostwald ripening. The shrinkage of droplets that occurs with Ostwald ripening appeared to be retarded. The retardation suggests that the asphaltenes can form an impermeable membrane on the interface. Testing this hypotheses is beyond the scope of this thesis but recommendations for further studies are made and the first step in numerically modeling the destabilization is undertaken in Chapter 6.

5.1 Introduction

Emulsions consist of two liquid phases where one phase (the dispersed phase) is dispersed in the other (the continuous phase) in the form of droplets. An emulsion where the dispersed phase remains intact and fully dispersed is deemed stable. Emulsions can destabilize in several ways including creaming, flocculation, coalescence and Ostwald ripening. Creaming and flocculation involve a spatial rearrangement of the dispersed phase droplets. They do not directly lead to phase separation. Coalescence and Ostwald ripening involve a change in the drop size distribution. Coalescence ultimately results in complete phase separation. In principle, Ostwald ripening can also lead directly to phase separation. However, in practice, ripening leads to the formation of large droplets that coalesce more readily than small droplets. Hence, pure coalescence and Ostwald ripening

coupled with coalescence are processes that ultimately can cause emulsions to separate into distinct phases.

In general, coalescence is more commonly observed than Ostwald ripening but it is not known which process occurs in water-in-crude oil emulsions (1). It is useful to determine which process dominates because the rate of growth of the mean drop diameter and the shape of the drop size distribution for each process are different. Hence, the long term behavior and stability of an emulsion undergoing coalescence may differ significantly from a similar emulsion undergoing Ostwald ripening.

Unfortunately, it is not easy to examine water-in-crude oil emulsions directly because the continuous oil phase is usually opaque. However, water-in-toluene/hexane/asphaltene emulsions can serve as a substitute. Asphaltenes are commonly believed to stabilize water-in-oil emulsions and asphaltenes in solutions of toluene and hexane have previously been employed as model oils (2,3). One can manipulate the asphaltene concentration in the model oil to obtain nearly transparent solutions. Hence, one can measure the drop size distribution over time using optical microscopy. Here, this approach is used to determine whether asphaltene stabilized water-in-toluene/hexane emulsions destabilize through coalescence or Ostwald ripening.

5.2 Experimental Method

Asphaltenes were extracted from Syncrude coker feed bitumen with the methods described in Chapter 2. The results presented in the following section are for asphaltene-solids although, for convenience, only asphaltenes are referred to. Note that it was shown in Chapter 4 that the solids do not participate in stabilizing water-in-toluene/hexane emulsions. The emulsions were prepared and drop size distributions measured employing the techniques discussed in Chapter 4.

The emulsions examined here are creamed and samples were drawn from the center of the creamed layer for all measurements. The location of the sampling point can be a

source of error because in some cases the drop size distribution varies with the height of the cream. For example, Bhakta and Ruckenstein (13) showed that the rate of coalescence of concentrated emulsions is strongly affected by drainage and therefore depends on the vertical position within the cream. The Sauter mean diameters measured at four different depths in an asphaltene stabilized water-in-toluene/hexane emulsion are shown in Fig. 5.1. The data show some random scatter but there is little or no correlation to depth for at least the bottom three quarters of the emulsion. The drops at the very top of the emulsion appear to grow more slowly perhaps because they have fewer contacts with other water droplets. In any case, samples drawn from the center of the cream are representative of the majority of the emulsion.

5.3 Results and Discussion

Several types of average diameter are discussed below and, for convenience, are defined here. They are: the mean diameter, d_{10} , given by

$$d_{10} = \sum \hat{F}_i d_i \quad (5.1)$$

the Sauter mean diameter, d_{32} , given by

$$d_{32} = \frac{\sum \hat{F}_i d_i^3}{\sum \hat{F}_i d_i^2} \quad (5.2)$$

and the cube root of the mean cubic diameter, $(d_{30})^{1/3}$, given by

$$d_{30}^{1/3} = \left(\sum \hat{F}_i d_i^3 \right)^{1/3} \quad (5.3)$$

Here, \hat{F}_i is the number frequency and d_i is the diameter of the i^{th} emulsion droplet. Note that d_{30} is proportional to the mean volume, V_{10} , given by:

$$V_{10} = \sum \hat{F}_i V_i = \frac{\pi}{6} \sum \hat{F}_i d_i^3 \quad (5.4)$$

where V_i is the volume of the i^{th} emulsion droplet. We shall see that the mean diameter is the appropriate diameter to consider for Ostwald ripening whereas the cube root mean volume is appropriate for coalescence. The Sauter mean diameter is inversely related to the surface area of an emulsion. The exact relationship is given by Eq. 4.3:

$$d_{32} = \frac{6V_W}{A_W} \quad (4.3)$$

where V_W is the volume of the dispersed water phase and A_W is the total surface area of the water droplets. The Sauter mean diameter is a useful measure for tracking the stability of an emulsion because any form of instability results in a decrease in the surface area of an emulsion. Hence, for unstable emulsions, d_{32} must increase with time.

5.3.1 Coalescence and Ostwald Ripening Theory

Both the shape of the drop size distribution and the mean drop size change when an emulsion destabilizes through coalescence or Ostwald ripening. With coalescence, the mean drop volume, V_{10} , and therefore d_{30} , increase linearly with time. With standard Ostwald ripening, the cube of the mean drop diameter, d_{10}^3 , increases linearly with time. In some cases, the ripening can be retarded and the drop size distributions and change in mean diameter can depart from the standard prediction. Retarded ripening is discussed in more detail later. In most cases, measuring the growth rate (expressed as either the change in d_{30} or the change in d_{10}^3 with time) is a useful way to assess the stability of an emulsion. However, the growth rate cannot easily be used to distinguish between coalescence and ripening. The two processes are distinguished by the shape of the drop size distribution they produce over time. The growth rate and drop size distribution caused by each process are discussed below.

Coalescence: Coalescence is the merger of two droplets when they come into close contact and it is discussed in some detail by Tadros and Vincent (4). The rate of coalescence is governed by the number of contacts between droplets and the probability that a contact will result in coalescence. Smoluchowski (5) first described the rate at which droplets come into contact in a dispersion under Brownian motion:

$$\left(\frac{N}{V}\right) = \frac{\left(\frac{N}{V}\right)_o}{1 + k_B \left(\frac{N}{V}\right)_o t} \quad (5.5)$$

Here, (N/V) is the number concentration of droplets, $(N/V)_o$ is the initial number concentration of droplets, and t is time. k_B is the collision rate constant and, for contact through Brownian motion, it is given by

$$k_B = \frac{4kT}{3\mu_c} \quad (5.6)$$

where k is the Boltzmann constant, T is temperature and μ_c is the viscosity of the continuous phase. An expression for the mean drop volume, V_{10} , is obtained by combining Eqs. 5.5 and 5.6 and recognizing that $(N/V) = \phi_d/V_{10}$, where ϕ_d is the volume fraction of the dispersed phase. The expression is given by:

$$V_{10} = V_{10}^o + \frac{4\phi_d kTt}{3\mu_c} \quad (5.7)$$

The rate at which the mean drop volume changes is given by the differential of Eq. 5.7:

$$\frac{dV_{10}}{dt} = \frac{4\phi_d kT}{3\mu_c} \quad (5.8)$$

Eq. 5.8 describes the rate at which the mean volume changes when every collision results in coalescence. However, not every collision necessarily leads to coalescence. When two droplets approach, the continuous phase between them is forced out until only a thin film remains. If the film ruptures, the droplets coalesce. Otherwise, they may remain together in an aggregate or separate into individual drops. The probability of film rupture depends on the physical properties of the film and the material adsorbed on the interface. Davies and Rideal (6) represented the resistance to rupture as an energy barrier to coalescence and modified Eq. 5.8 as follows:

$$\frac{dV_{10}}{dt} = \frac{\pi d(d_{30})}{6dt} = \frac{4\phi_d kT}{3\mu_c} \exp\left\{\frac{-\Delta G_{coal}}{kT}\right\} \quad (5.9)$$

Eq. 5.9 shows that the mean drop volume (or d_{30}) increases at a constant rate. More sophisticated coalescence models employ numerical techniques to follow the behavior of the entire drop size distribution. Both shear induced (7,8) and Brownian motion induced coalescence have been examined (7,9). In general, a linear relationship of mean drop volume to time holds true. Numerical and experimental results also show that the drop size distribution during coalescence reaches a self-preserving form. Wright and Ramkrishna (7) observed such a self preserving form experimentally for coalescence in zero shear of a benzene/carbon tetrachloride in water emulsion. The change in time of their reported drop size distribution is provided as an example in Fig. 5.2a. The distribution is plotted against the drop diameter in order to compare with the Ostwald ripening distribution discussed later. Note that no initial distribution is given; rather, the change over time of an established coalescence distribution is illustrated.

The distribution given in Fig. 5.2a is not necessarily valid for all emulsions undergoing coalescence. Implicit in Eq. 5.9 and in Fig. 5.2a is the assumption that the ΔG_{coal} term (a form of collision efficiency) is independent of time or drop size. However, in some cases, surfactant builds up on the surfaces of droplets that have undergone coalescence and experienced a reduction in surface area. The surfactant build up can increase the

energy barrier to coalescence and reduce the collision efficiency. Hence, as time progresses larger droplets may exhibit lower collision efficiencies than smaller droplets. As a result, the evolution of the drop size distribution may depart from that given in Fig. 5.2a. An accumulation of larger droplets may occur giving rise to a distribution that resemble the Ostwald ripening case presented in Fig. 5.2b. Nonetheless, a critical difference between Ostwald ripening and coalescence remains: with coalescence only larger droplets are created while with Ostwald ripening (as will be discussed later) both smaller and larger droplets are created. Hence, the appearance of smaller droplets is good indicator for Ostwald ripening.

Ostwald Ripening: Ostwald ripening refers to mass transfer between particles or drops of different curvature through their surrounding continuous medium. The concentration of the dispersed phase material at the surface of a drop is inversely related to the radius of curvature. Hence, a small drop has a high surface concentration relative to a large drop giving rise to a concentration gradient of the dispersed phase material in the continuous phase. Mass is transferred along the concentration gradient from small drops to large drops. In other words, when Ostwald ripening occurs, small drops shrink and ultimately disappear while large drops grow at their expense, eventually leading to phase separation.

Lifshitz and Slyozov and, independently, Wagner (LSW) first developed an analytical solution for Ostwald ripening in infinitely dilute dispersions (10,11). The LSW technique is discussed in greater detail in Chapter 6. The technique shows that, after sufficient time, the Ostwald ripening process enters a stationary state where the cube of the mean drop radius increases linearly with time and the shape of the drop size distribution normalized by the mean radius is invariant with time. The growth rate is given by

$$\frac{da_{10}^3}{dt} = \frac{d(d_{10}^3)}{8dt} = \frac{8\sigma Dv_d \phi_\infty}{9RT} \quad (5.10)$$

where a_{10} is the mean drop radius, σ is the interfacial tension between the dispersed and continuous phases, D is the diffusivity of the dispersed phase material in the continuous phase, v_d is the molar volume of the continuous phase, ϕ_∞ is the solubility of the dispersed phase material in the continuous phase expressed as a volume fraction, and R is the universal gas constant. Here the cube of the mean diameter (see Eq. 5.1) increases linearly with time as compared to coalescence where the mean cubic diameter (see Eq. 5.3) increases linearly with time.

The shape of the normalized drop size distribution established during Ostwald ripening is given by

$$\hat{F}(v) = \frac{81v^2 \exp\left\{1 + \frac{1}{2v/3 - 1}\right\}}{32^{1/3}(v+3)^{2/3}(1.5-v)^{1/3}} \quad 0 \leq v \leq 1.5 \quad (5.11)$$

$$\hat{F}(v) = 0 \quad v \geq 1.5$$

Here, $\hat{F}(v)$ is the number frequency of drops of size v , where v is the ratio of the drop radius to the mean drop radius. Eqs. 5.10 and 5.11 only apply to infinitely dilute emulsions. The effect of finite dispersed phase volumes is discussed in Chapter 6. At finite dispersed phase volume fractions, the shape of the drop size distribution is slightly different than the infinitely dilute case. The growth rate is faster but still linearly related to time. Hence, Eqs. 5.10 and 5.11 are suitable for qualitative comparisons of emulsions.

The change of the drop size distribution given by Eq. 5.11 with time is shown in Fig. 5.2b. The distribution is plotted against the drop diameter. Note that the distributions are for established ripening and no initial distribution is given. The shape of the established distribution is different than the established coalescence drop distribution shown in Fig. 5.2a. The ripening distribution contains a significant number of drops of near zero radius because any droplet below the mean radius eventually shrinks to zero radius. Coalescence, on the other hand, always results in larger droplets and the entire drop size

distribution gradually shifts to larger diameters. Hence, in most cases, the type of instability an emulsion experiences can be determined by comparing the drop size distribution to the ideal curves presented in Fig. 5.2. One notable exception is an emulsion that destabilizes through retarded ripening.

Retarded Ostwald Ripening: Retarded ripening occurs when the shrinkage of smaller droplets is slowed or arrested. In this case, the growth of a small fraction of large droplets and an accumulation of small droplets is observed. For example, Kabal'nov *et al.* (12) demonstrated that, in theory, retarded ripening occurs when the dispersed phase consists of two components one of which is insoluble in the continuous phase. As the droplets shrink, the concentration of the insoluble component increases inside the droplets, creating a chemical potential that acts against the outward diffusion of the soluble component. The size distributions predicted by Kabal'nov *et al.* are given in Fig. 5.3. Note that other mechanisms can also cause retardation, for example changes in the properties of an interfacial membrane upon contraction. The exact shape of the drop size distributions and the change in mean diameter depend on the mechanism responsible for slowing the shrinkage of the droplets. If the observed drop size distributions of an emulsion do not match the coalescence and standard ripening cases presented in Fig. 5.2, then retarded ripening should be considered.

5.3.2 The Stability of Water-in-Hydrocarbon Emulsions

In the following experiments, the continuous hydrocarbon phase of the emulsions consists of toluene, hexane and asphaltenes. The drop size distributions of the emulsions are measured over time and three types of average diameter are determined: the mean diameter, d_{10} , the Sauter mean diameter, d_{32} , and the cube root of the mean cubic diameter, $(d_{30})^{1/3}$, given in Eqs. 5.1, 5.2 and 5.3, respectively. The drop size distributions are compared with the predicted distributions for coalescence and Ostwald ripening given in Figs. 5.2a and 5.2b, respectively. The cube root of the mean cubic diameters are compared with those predicted for coalescence by Eq. 5.9 and the mean diameters are compared with those predicted for Ostwald ripening by Eq. 5.10. Since a good match

between the measured distributions and the predictions given in Fig. 5.2 is not observed, the drop size distributions are also compared with those predicted for retarded ripening and given in Fig. 5.3.

The change in the shape of the drop diameter frequency distribution over time for a typical asphaltene stabilized emulsion is given in Fig. 5.4. In this case, the water volume fraction of the emulsion, ϕ_w , is 25 %. The remainder of the emulsion is a toluene, hexane and asphaltene mixture with a volume ratio of hexane to toluene, ϕ_H/ϕ_T , of 5 and an initial asphaltene concentration, C_A^0 , of 0.50 kg/m^3 . The change over time of the three types of average diameter for the same emulsion is shown in Fig. 5.5.

The drop size distributions in Fig. 5.4 resemble neither the coalescence distributions in Fig 5.2a nor the Ostwald ripening distributions in Fig. 5.2b. Both coalescence and Ostwald ripening cause the mean and peak of the drop size distributions to increase with time. The peak of the observed distributions shown in Fig. 5.4 shifts to smaller rather than larger drop diameters. In fact, the distributions resemble those of Fig. 5.3, the retarded ripening case.

Now consider the average diameters of Fig. 5.5. The experimental values of d_{30} and $(d_{10})^3$ are fitted by coalescence theory (Eq. 5.9) and ripening theory (Eq. 5.10), respectively. The coalescence theory appears to fit the data well but the good fit is misleading. The significant feature of Fig. 5.5 is that the mean diameter is invariant with time while the Sauter mean diameter increases. An invariant mean diameter indicates that coalescence does not take place. Coalescence can only lead to the formation of larger drops and hence the mean diameter must increase with time. An invariant mean diameter also would normally indicate that no ripening is occurring. And yet, the Sauter mean diameter is increasing, indicating that the emulsion is destabilizing. Therefore, the emulsions destabilize through a process other than coalescence or standard ripening.

Taken together Figs. 5.3 and 5.4 indicate that retarded Ostwald ripening is acting on the asphaltene stabilized emulsions. The distributions in Fig. 5.3 indicate that small droplets are forming and accumulating as larger droplets grow. The process decreases the surface area of the emulsion and therefore the Sauter mean diameter increases. As will be discussed later, the increase in d_{32} is fitted linearly for convenience. The mean diameter does not necessarily increase because the contribution of the relatively few large droplets is balanced by the contribution of many small droplets.

5.3.3 The Effect of Composition on Emulsion Stability

The effect of composition on drop size distribution was examined to: (a) confirm that the observed destabilization is not unique; (b) confirm that ripening takes place; and (c) provide data for future testing of models of the modified ripening process. The ripening behavior was observed over a broad range of asphaltene concentrations, hexane to toluene ratios and water volume fractions. The change in the mean and Sauter mean diameters were fitted linearly for the purposes of comparison. The cube root mean volume was not examined because it is not relevant to a ripening process. The linear fit parameters for the change in d_{10} and d_{32} with time are summarized in Table 5.1.

Before discussing the results, some experimental error must be considered. In some cases, the smallest drops pass below the detection limit of optical microscopy. For instance, consider the emulsion of $\phi_H/\phi_T = 5$, $\phi_W = 0.25$, and $C_A^o = 2.00 \text{ kg/m}^3$. Drop size distributions for this emulsion are given in Fig. 5.6. In this case, the initial drop size distribution lies close to the minimum size detectable with optical microscopy. It is likely that the smallest droplets are too small to be observed and are not accounted for correctly in the drop size distributions. Hence, the calculated mean diameter can be overestimated as more droplets pass below the detection limit. It is for this reason that the mean diameter of this emulsion appears to increase with time.

The experimental error is also significant for the emulsions of $\phi_H/\phi_T = 0$; *i.e.*, emulsions with a pure-toluene/asphaltene continuous phase. The error in the emulsion growth rate

(the change in d_{32} with time) is in the order of 50%. The error may arise from the breadth of the drop size distribution or from the relatively fast rate of ripening. The drop size distributions for one example are shown in Fig. 5.7. A very broad distribution is established within the first hour after the emulsion was prepared. It is difficult to accurately measure such a distribution. Furthermore, d_{32} increases most rapidly for the $\phi_H/\phi_T = 0$ emulsions. Hence, some droplets may shrink below the detection limit sooner than in emulsions with higher hexane content. Despite the large measurement error, the emulsion growth rates measured for the $\phi_H/\phi_T = 0$ emulsions are consistent with the rates measured for emulsions with higher hexane content.

Table 5.1: Fitted d_{10} and d_{32} for asphaltene stabilized water-in-toluene/hexane emulsions.

| ϕ_H/ϕ_T | ϕ_W | C_A^o (kg/m ³) | d_{10}^o (μm) | $\frac{d(d_{10})}{dt}$ ($\mu\text{m/hr}$) | d_{32}^o (μm) | $\frac{d(d_{32})}{dt}$ ($\mu\text{m/hr}$) |
|-----------------|-------------------|---------------------------------|---------------------------------|--|---------------------------------|--|
| 5 | 0.25 | 0.50 | 22.0±2.1 | -0.006±0.013 | 27.4±2.9 | 0.097±0.019 |
| 5 | 0.25 | 1.00 | 12.3±1.4 | 0.006±0.010 | 15.3±4.0 | 0.094±0.028 |
| 5 | 0.25 | 2.00 | 9.6±2.8 | 0.066±0.034 | 11.5±4.0 | 0.124±0.049 |
| 5 | 0.40 | 0.67 | 32.5±1.6 | -0.012±0.006 | 34.1±4.4 | 0.062±0.017 |
| 5 | 0.40 | 1.00 | 18.4±2.3 | 0.006±0.010 | 25.1±11 | 0.080±0.048 |
| 5 | 0.40 ^a | 1.00 | 21.2±2.3 | 0.006±0.014 | 29.3±7.6 | 0.096±0.047 |
| 5 | 0.40 | 1.33 | 14.8±1.3 | 0.002±0.006 | 19.3±4.0 | 0.067±0.018 |
| 3 | 0.25 | 1.00 | 12.4±3.8 | 0.007±0.025 | 16.3±4.9 | 0.080±0.033 |
| 1.5 | 0.25 | 1.00 | 9.9±1.8 | 0.029±0.013 | 15.8±8.1 | 0.128±0.061 |
| 1 | 0.25 | 1.00 | 13.4±1.3 | 0.006±0.016 | 18.6±4.7 | 0.189±0.040 |
| 0 | 0.40 | 1.33 | 25.6±4.7 | 0.048±0.060 | 45.3±10 | 0.308±0.161 |
| 0 | 0.40 | 2.00 | 15.9±1.5 | -0.012±0.020 | 24.7±3.5 | 0.140±0.045 |

a ultrafiltered deionized “pure” water

The results presented in Table 5.1 show that the same pattern of retarded ripening occurs for all the emulsions considered. In all cases, the Sauter mean diameter increases with time. And in all cases except the previously noted exception, the mean diameter is invariant with time. Further evidence that the observed behavior is a form of ripening is found by considering the change in growth rate as the hexane:toluene ratio changes. The emulsion growth rate during Ostwald ripening is expected to increase as the toluene content of the continuous phase increases. Eq. 5.10 shows that the emulsion growth rate for ripening increases as the interfacial tension, σ , between the water and the continuous phase increases and as the diffusivity, D , and solubility of water in the continuous phase, ϕ_{∞} , increase. The values of σ , D and ϕ_{∞} in toluene and hexane are listed in Table 5.2. Neither the diffusivity nor the interfacial tension for asphaltene stabilized interfaces varies significantly in the different solvents. However, the solubility of water is higher in toluene. Hence, the growth rate is expected to increase as the toluene content of the continuous phase increases.

Table 5.2: Interfacial tension, diffusivity and solubility of water in toluene and hexane.

| Property @ 20 °C | in Toluene | in Hexane |
|--------------------------------------|---------------------|---------------------|
| σ (mN/m) ^a | 35.8 | 50.1 |
| σ (mN/m) ^b | 25 | 28 |
| D (m ² /s) ^c | $1.7 \cdot 10^{-9}$ | $1.6 \cdot 10^{-9}$ |
| ϕ_{∞} ^d | 0.013 | 0.004 |

a ref. 14

b IFT for asphaltene/toluene/hexane mixtures with an asphaltene concentration of 1 wt%. The result for hexane is in a hexane/toluene mixture of 20 vol% toluene. (present work - Appendix A)

c calculated employing the method given in ref. 15

d ref. 16

The emulsion growth rates given in Table 5.1 clearly increase as the volume fraction of toluene in the continuous phase, ϕ_T , increases. The growth rate is plotted against ϕ_T in Fig. 5.8. All the data in Fig. 5.8 except at $\phi_T = 1$ was determined from emulsions with $\phi_W = 0.25$ and $C_A^o = 1.00 \text{ kg/m}^3$. The data at $\phi_T = 1$ was determined from an emulsion with $\phi_W = 0.40$ and $C_A^o = 1.00 \text{ kg/m}^3$. The increase of d_{32} with time, the invariant mean diameter, and the increase of the emulsion growth rate as the toluene content of the continuous phase increases all confirm that a form of Ostwald ripening is taking place where the shrinkage of the droplets is retarded.

5.3.4 Modified Ostwald Ripening Models

The evidence presented in Section 5.3.3 suggests that a modified form of Ostwald ripening occurs in asphaltene stabilized water-in-hydrocarbon emulsions. The shrinkage of smaller droplets that accelerates in standard ripening is retarded in these emulsions. It is of interest to understand the physics behind the retardation and model the effect. A full analysis is beyond the scope of the thesis but some hypotheses are discussed below.

As discussed previously, a retardation of drop shrinkage can occur if the dispersed phase contains a component that is insoluble in the continuous phase. It is possible that the deionized water used to make up the emulsions is contaminated and that the contaminant is insoluble in the hydrocarbon phase. Two emulsions were prepared to test this idea: one from deionized water; one from deionized ultrafiltered “pure” water obtained from Fisher Chemicals. Both emulsions were prepared with a ϕ_W of 0.40, a ϕ_H/ϕ_T of 5 and a C_A^o of 1.00 kg/m^3 . The drop size distributions for the deionized and pure water emulsions are given in Figs. 5.9a and 5.9b, respectively. The change in the mean and Sauter mean diameters over time are compared in Fig. 5.10. The results are all within experimental error. Hence, the water used to make up the emulsion had no bearing on the stability of the emulsion. Since the modified ripening process occurs with a pure water sample, the retardation is not caused by a two component dispersed phase.

The retardation of the ripening may be caused by an interfacial effect. Standard Ostwald ripening is governed by the diffusion of the dispersed phase material through the continuous phase. However, the material adsorbed on the interface can form a barrier to mass transfer. It is necessary to return to the derivation of the Ostwald ripening equations to see how adsorbed interfacial material affects the ripening rate. Ostwald ripening theory is reviewed in Chapter 6. For present purposes, consider the differential equation for the change in an individual drop radius with time during Ostwald ripening at finite dispersed phase volume fractions:

$$\frac{da}{dt} = D\phi_{\infty}\alpha \frac{(a+\delta)}{a^2\delta} \left(\frac{a}{a_c} - 1 \right) \quad (6.6)$$

Here a is the radius of a given drop, $\alpha = 2\sigma\nu/RT$, and a_c is the critical drop radius. Note that the critical drop radius is identical to the mean radius for infinitely dilute emulsions. δ is an average separation distance between droplets and is a function of the dispersed phase volume fraction. The corresponding differential equation when an interfacial barrier is present is derived in Appendix C and is given by:

$$\frac{da}{dt} = \frac{D\phi_{\infty}\alpha}{\eta} \frac{(a+\delta)}{a^2\delta} \left(\frac{a}{a_c} - 1 \right) \quad (5.11)$$

where

$$\eta = 1 + \frac{(a+\delta)\delta_l D}{a\delta D_l} \quad (5.12)$$

Here, δ_l is the thickness of the material on the interface and D_l is the diffusivity of the dispersed phase material through the interface. The thickness of the interfacial membrane is very small relative to the drop radius. Therefore, the value of η only becomes significant when the ratio D/D_l is small; that is, when the interfacial membrane has a low

diffusivity to the dispersed phase. Hence, the ripening rate, da/dt , decreases when the diffusivity through the interface is low and η is large.

The retardation in the ripening rate as the droplets shrink may be caused by a decrease in diffusivity through the interface of shrunken droplets. A change in diffusivity could be caused by a change in the properties of the asphaltenes adsorbed on the interface. Once asphaltenes adsorb on the interface, the interaction forces between the asphaltenes molecules may trap the asphaltenes on the interface. In other words, the asphaltenes may adsorb irreversibly and form a membrane on the surface. There are several ways a membrane can act to slow the ripening rate. Two examples are considered.

In the first case, assume that the volume of the asphaltene membrane is constant. Hence, when the droplet shrinks, the membrane thickens. Diffusion is slower through a thicker membrane. Therefore, as a droplet shrinks, its surface presents a larger barrier to diffusion and the rate of shrinkage slows. The overall effect is similar to that observed for a two component dispersed phase emulsion. The thickness of the membrane is a function of the initial thickness and drop radius and the drop radius at the time of interest. The relationship is given by

$$\delta_t = \left(\frac{a_o}{a} \right)^2 \delta_t^o \quad (5.13)$$

A new expression for η is obtained by substituting Eq. 5.13 into Eq. 5.12 and it is given by

$$\eta = 1 + \frac{(a + \delta)a_o^2 \delta_t^o D}{a^3 \delta D_t} \quad (5.14)$$

Eq. 5.14 shows that as the drop radius decreases, the value of η increases and therefore ripening is retarded.

The previous hypothesis requires that the volume of the membrane remains constant. An alternative approach is to assume that the asphaltene molecules are forced into closer contact as the droplet shrinks. In this case, the density of the membrane increases and its volume decreases. The denser membrane would likely exhibit lower diffusivity to water and possibly lower interfacial tension. A decrease in interfacial tension is apparent in experiments where some of the water in a droplet stabilized by asphaltenes is removed (17). The surface of the droplet wrinkles and collapses like a deflated balloon. When interfacial tension is high, a smooth surface is maintained in order to minimize surface energy. The observed wrinkling indicates that interfacial tension is low. Hence, both diffusivity and interfacial tension may decrease as a droplet shrinks. If this hypothesis is correct, the change in the diffusivity and interfacial tension are related to the change in surface area of the droplet. The ripening equations appropriate for this theory are given by

$$\frac{da}{dt} = \frac{D\phi_{\infty}\alpha_o}{\eta} \left(\frac{a+\delta}{a^2\delta} \right) \left(\frac{a}{a_c} - 1 \right) \quad (5.15)$$

where

$$\eta = \frac{\sigma_o}{\sigma} \left[1 + \frac{(a+\delta)\delta_l D}{a\delta D_l} \right] \quad (5.16)$$

Here $\alpha_o = 2\sigma_o v/RT$ and σ and D_l are unknown functions of $(a/a_c)^2$. Both σ and D_l decrease as the drop shrinks, increasing the value of η and slowing the ripening rate.

The proposed hypotheses can be tested with further experiments and by numerically modeling the modified Ostwald ripening process governed by Eqs. 5.11 and 5.14 or by Eqs. 5.15 and 5.16. Further experiments are beyond the scope of this thesis but some

numerical modeling was performed. The simpler case of Ostwald ripening without the membrane barrier is considered in Chapter 6. The complete model is left for future work.

5.4 Conclusions

The stability of water-in-toluene/hexane/asphaltene emulsions was examined by measuring the drop size distributions over time. Small droplets were observed to accumulate over time while larger drops appeared. The mean drop diameter of the emulsions remained constant while the Sauter mean diameter increased with time. The growth rate of the Sauter mean diameter increased as the toluene content of the toluene/hexane continuous phase increased.

The emulsions appear to destabilize through a form of Ostwald ripening where the shrinkage of the droplets is retarded. The drop shrinkage may be slowed by the thickening of a membrane of asphaltene molecules adsorbed irreversibly on the interface. A thicker membrane forms a greater barrier to diffusion. Alternatively, the retardation may arise from a decrease in diffusivity and interfacial tension as the membrane contracts. Models for both modified ripening processes were posed but can only be tested with a numerical model and further experiments.

5.5 References

1. Pal, R., *AIChE J.*, **42**, (1996), 3181.
2. Eley, D.D., Hey, M.J., and Lee, M.A., *Colloids Surfaces A*, **24**, (1987), 173.
3. Førdedal, H., Midttun, Ø., Sjöblom, J., Kvalheim, O.M., Schildberg, Y., Volle, J-L., *J. Colloid Interface Sci.*, **182**, (1996), 117.
4. Tadros, T.F. and Vincent, B., in "Encyclopedia of Emulsion Technology", Vol. 1, Ed. P. Becher, Marcel Dekker, Inc., New York, 1983, p.129.
5. von Smoluchowski, M., *Z. Phys. Chem.*, **92**, (1917), 129.
6. Davies, J.T., and Rideal, E.K., "Interfacial Phenomena", Academic Press, New York, 1961.
7. Wright, H., and Ramkrishna, D., *AIChE J.*, **40**, (1994), 767.

8. Mousa, H., and van de Ven, T.G.M., *Colloids Surfaces A*, **95**, (1995), 221.
9. Wang, C.S., and Friedlander, S.K., *J. Colloid Interface Sci.*, **24**, (1967), 170.
10. Lifshitz, I.M., Slyozov, V.V., *J. Phys. Chem. Solids*, **19**(1/2), 1961, 35.
11. Wagner, C., *Ber. Bunsenges Phys.Chem.*, **65**, 1961, 581.
12. Kabal'nov, A.S., Pertzov, A.V., Shchukin, E.D., *Colloids Surfaces A*, **24**, (1987), 19.
13. Bhakta, A., and Ruckenstein, E., *Langmuir*, **11**, (1995), 4642.
14. Li, B., and Fu, J., *J. Chem. Eng. Data*, **37**, (1992), 172.
15. Danner, R.P., and Daubert, T.E., Method 10G-1 in "Manual for Predicting Chemical Process Design Data", AIChE, New York, 1983.
16. Sørensen, J.M., Arlt, W., "Liquid-Liquid Equilibrium Data Collection, Binary Systems", Dechema Chemistry Data Series, Vol. V(1), Dechema, 1979.
17. Yeung, T., Department of Chemical and Materials Engineering, University of Alberta, 1997.

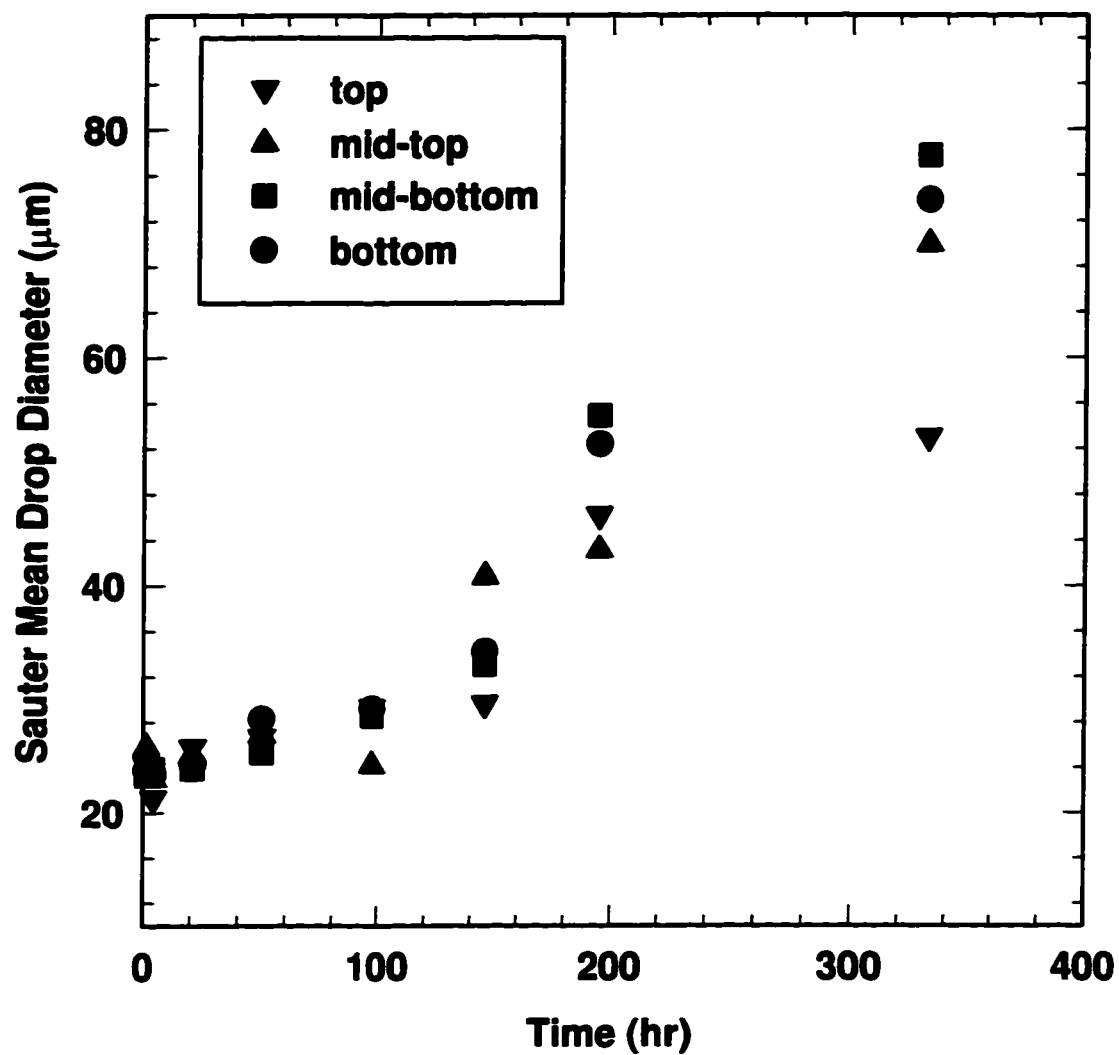


Figure 5.1: Effect of emulsion height on the measured Sauter mean diameter of an asphaltene stabilized water-in-toluene/hexane emulsion.

($\phi_T/\phi_H = 5$, $\phi_W = 0.40$, $C_A^0 = 1.00 \text{ kg/m}^3$)

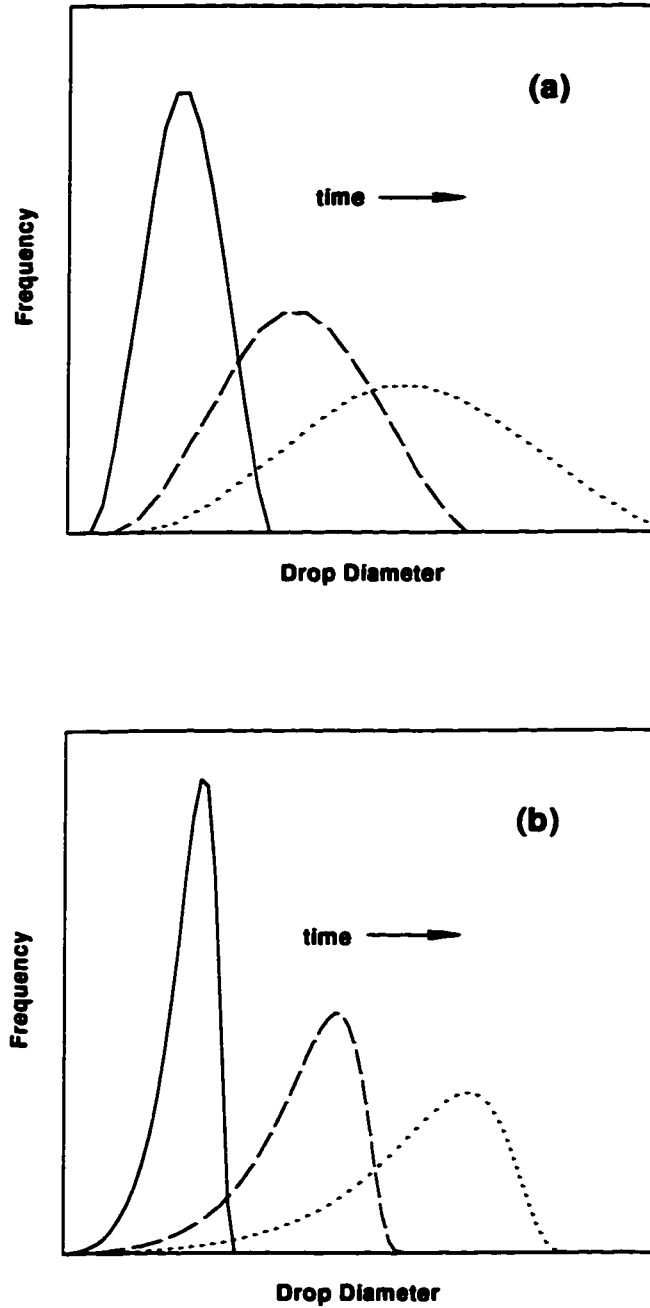


Figure 5.2: The change over time of the self preserving drop size distributions of an emulsion destabilizing through: a) coalescence, b) Ostwald ripening.

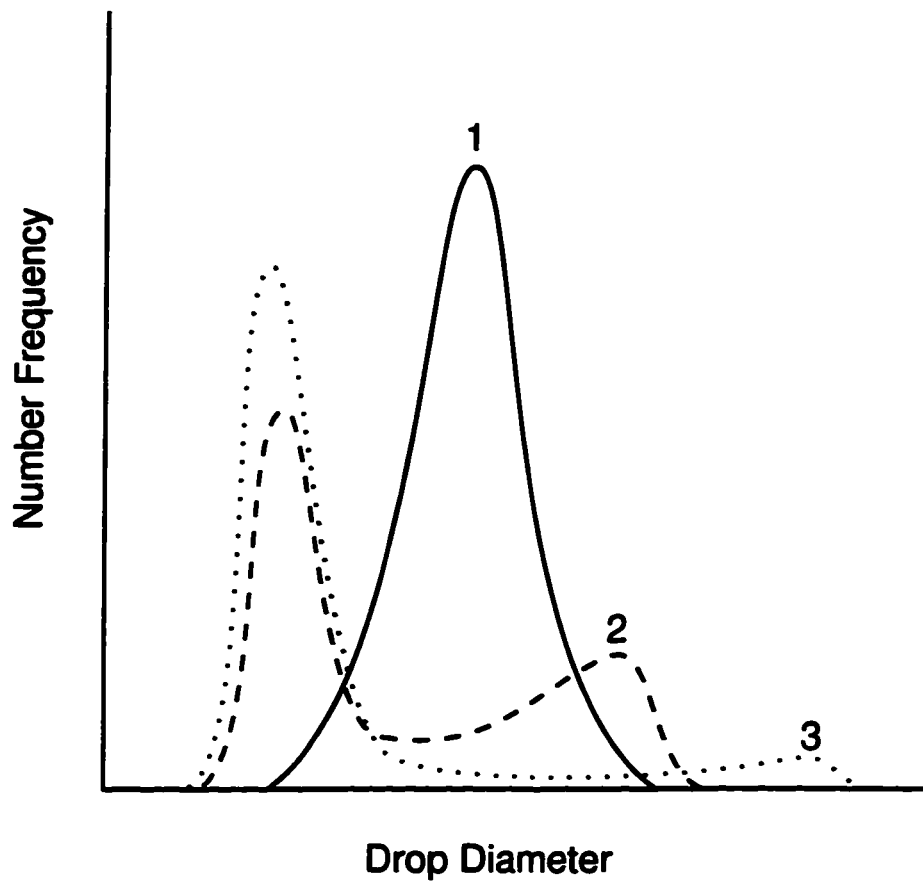


Figure 5.3: Evolution of the drop size distribution for Ostwald ripening in emulsions with a two component dispersed phase (12). 1. initial distribution, 2,3. distributions after ripening has occurred

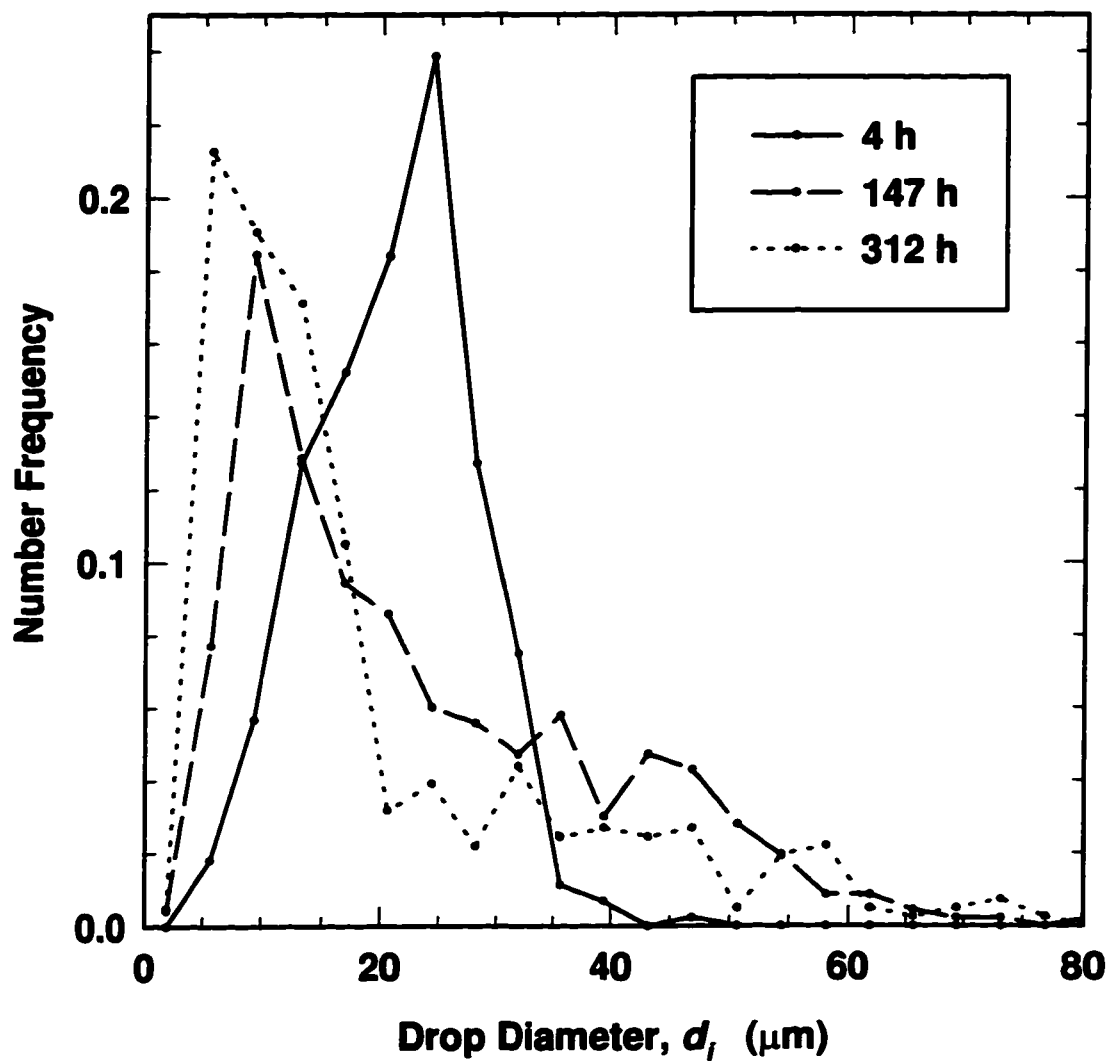


Figure 5.4: Change in drop size distribution over time of an asphaltene stabilized water-in-toluene/hexane emulsion. ($\phi_H/\phi_T = 5$, $\phi_W = 0.25$, $C_A^0 = 0.50 \text{ kg/m}^3$)

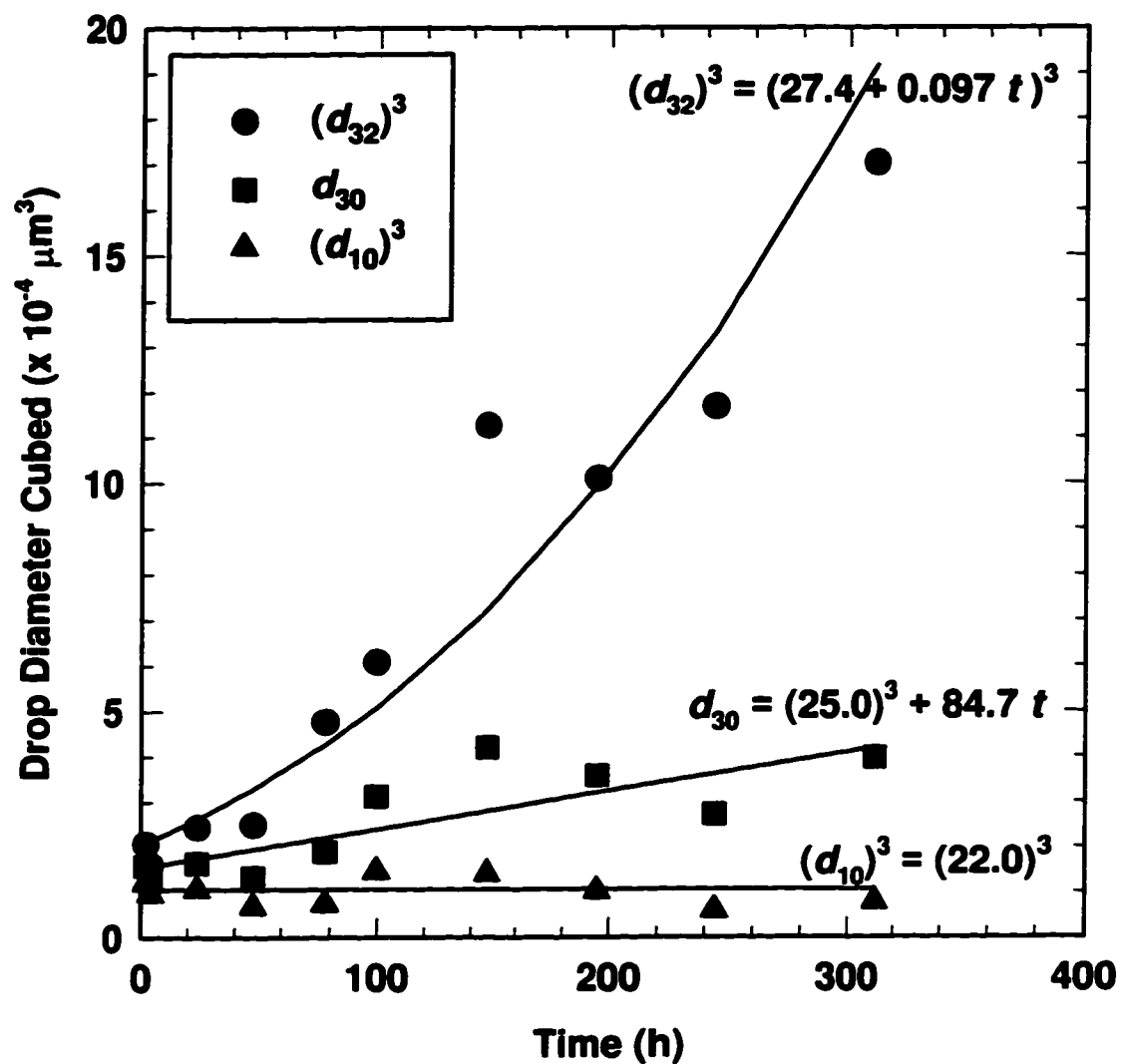


Figure 5.5: Change in average drop diameters over time of an asphaltene stabilized water-in-toluene/hexane emulsion. ($\phi_T/\phi_H = 5$, $\phi_W = 0.25$, $C_A^0 = 0.50 \text{ kg/m}^3$)

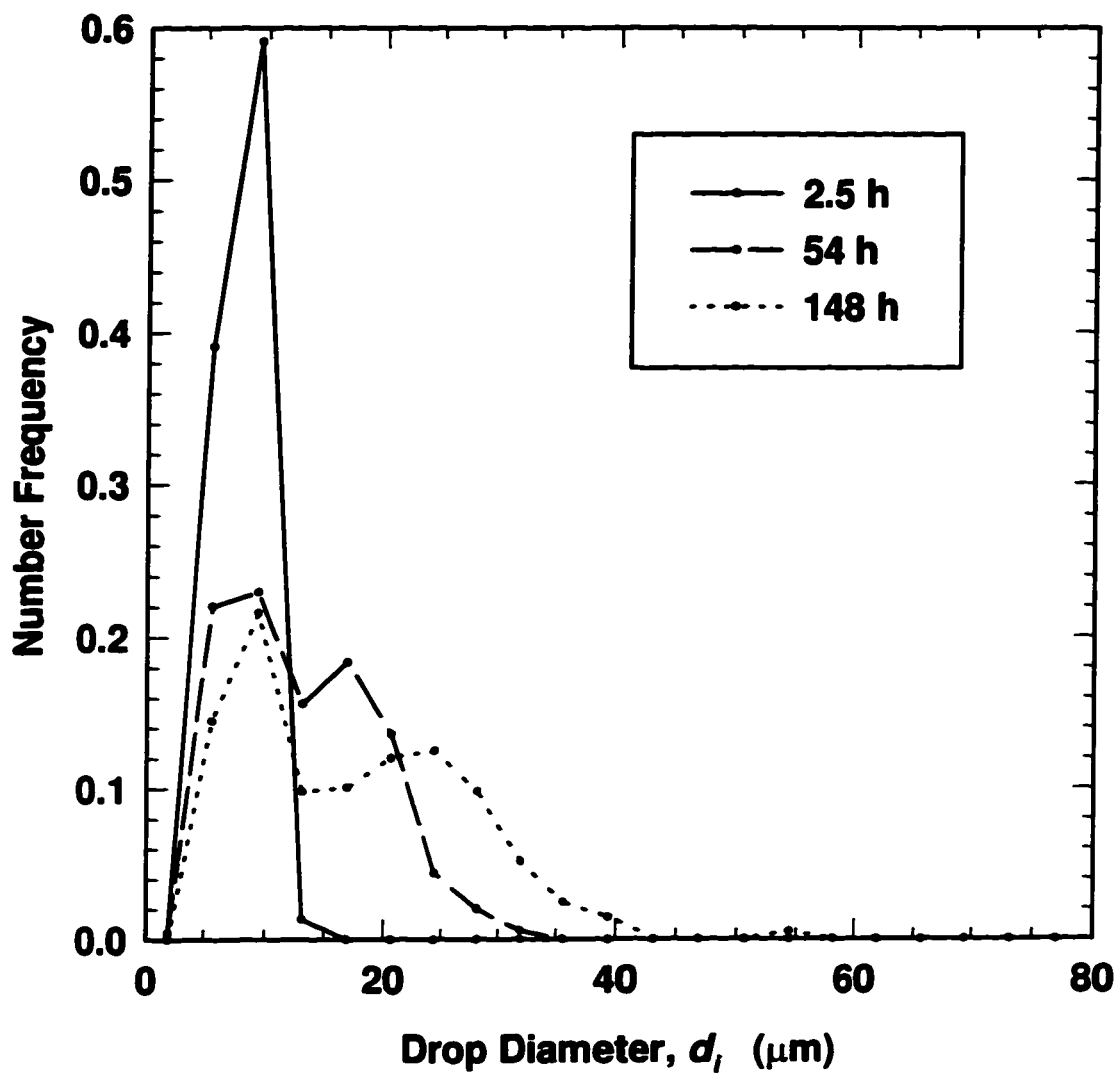


Figure 5.6: Change in drop size distribution over time of an asphaltene stabilized water-toluene/hexane emulsion. ($\phi_H/\phi_T = 5$, $\phi_W = 0.25$, $C_A^0 = 2.00 \text{ kg/m}^3$)

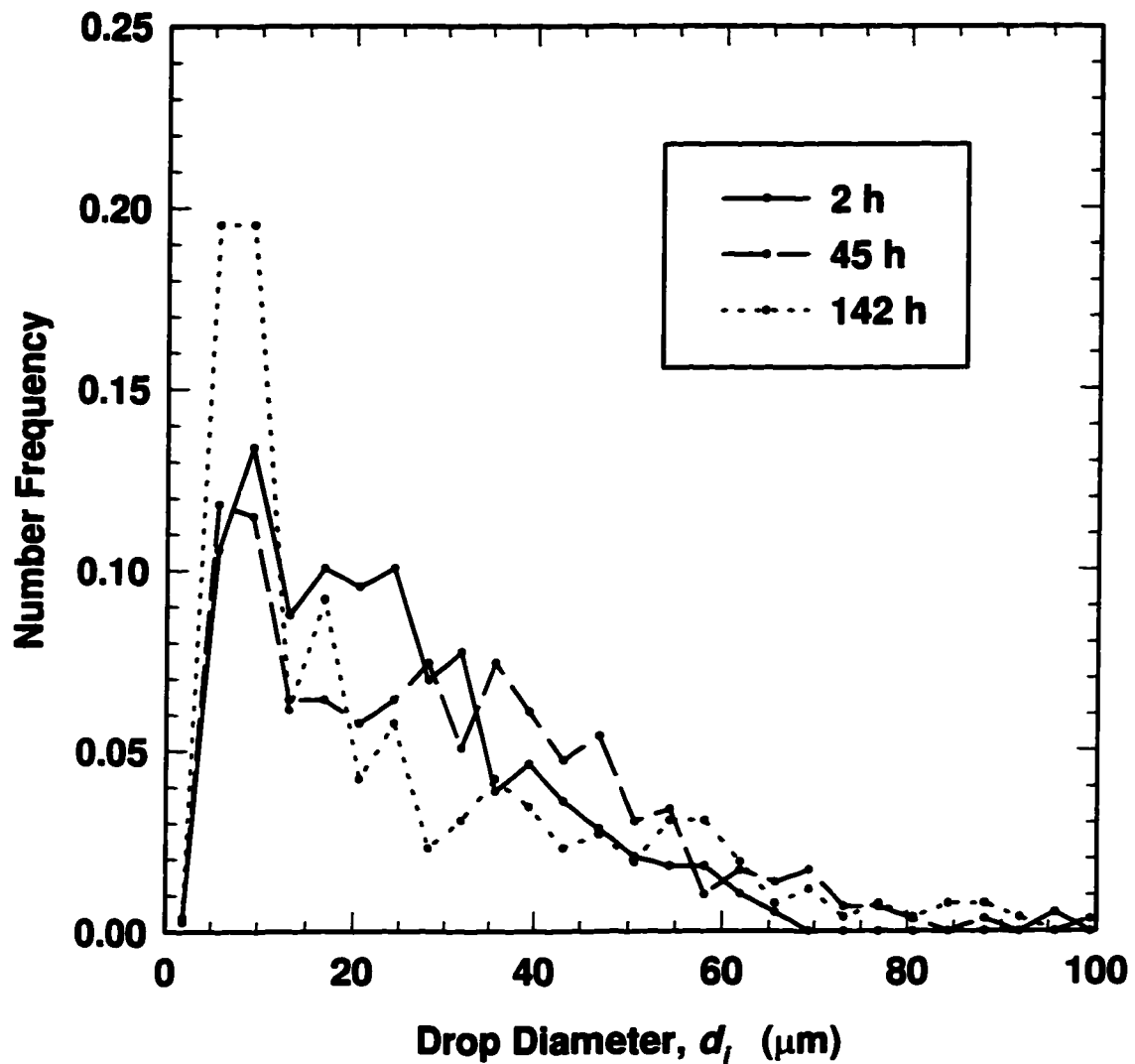


Figure 5.7: Change in drop size distribution over time of an asphaltene stabilized water-in-toluene/hexane emulsion. ($\phi_H/\phi_T = 0$, $\phi_W = 0.40$, $C_A^0 = 1.33 \text{ kg/m}^3$)

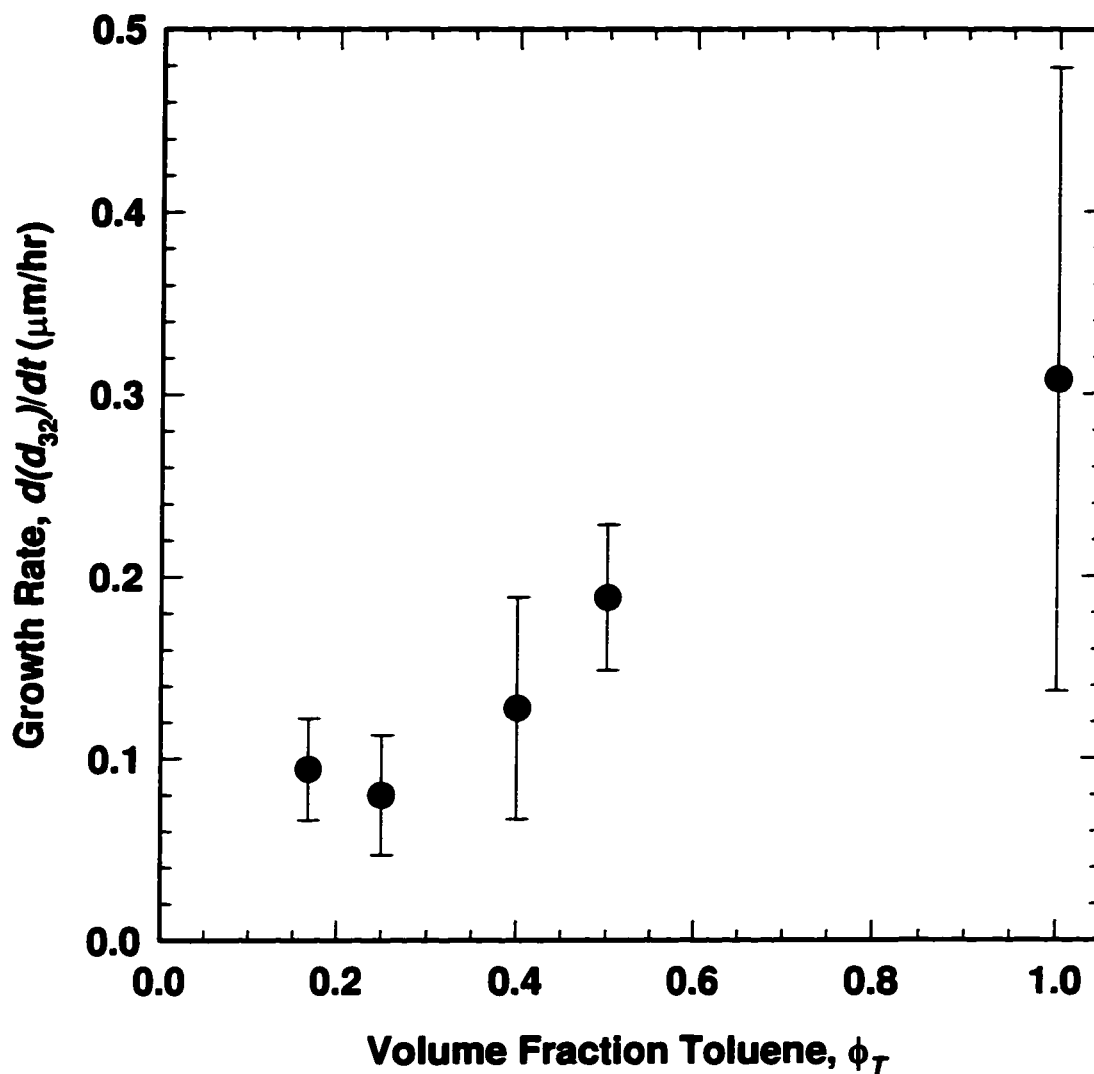


Figure 5.8: Growth rate of the Sauter mean diameter of asphaltene stabilized water-in-toluene/hexane emulsions versus the toluene content of the continuous phase. ($\phi_W = 0.25$, $C_A^0 = 1.00 \text{ kg/m}^3$)

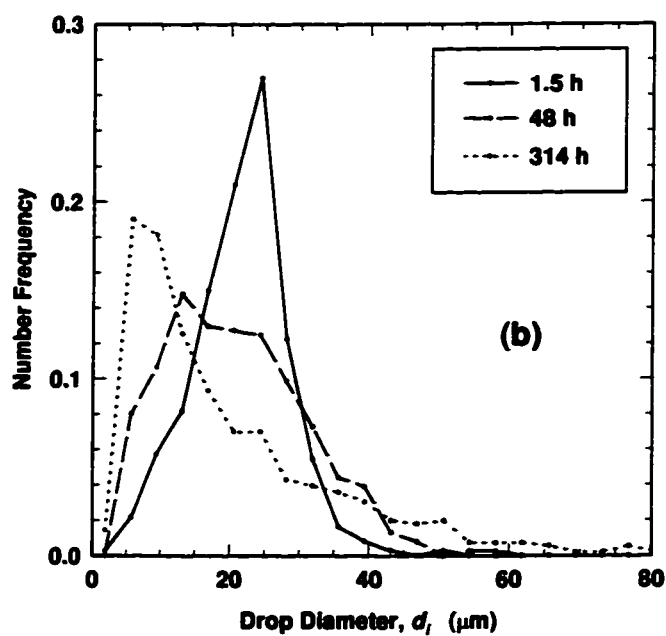
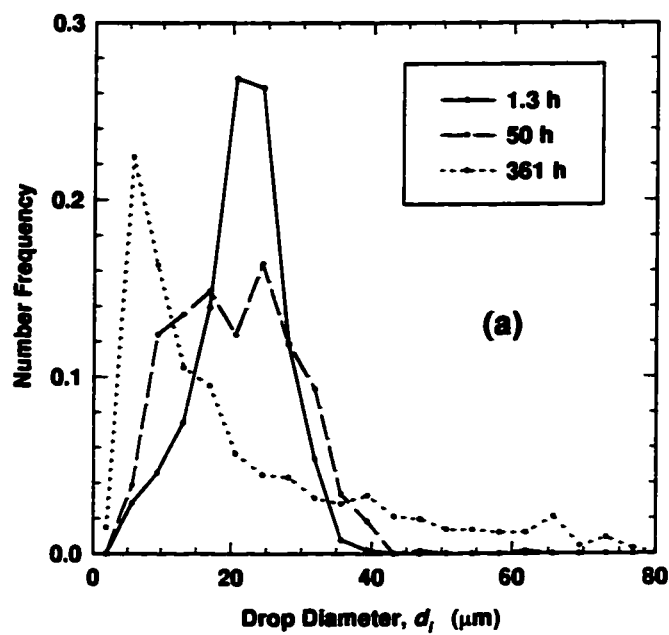


Figure 5.9: Change in drop size distribution over time of two asphaltene stabilized water-in-toluene/hexane emulsions: a) deionized water, b) deionized ultrafiltered water. ($\phi_H/\phi_T = 5$, $\phi_W = 0.40$, $C_A^0 = 1.00 \text{ kg/m}^3$)

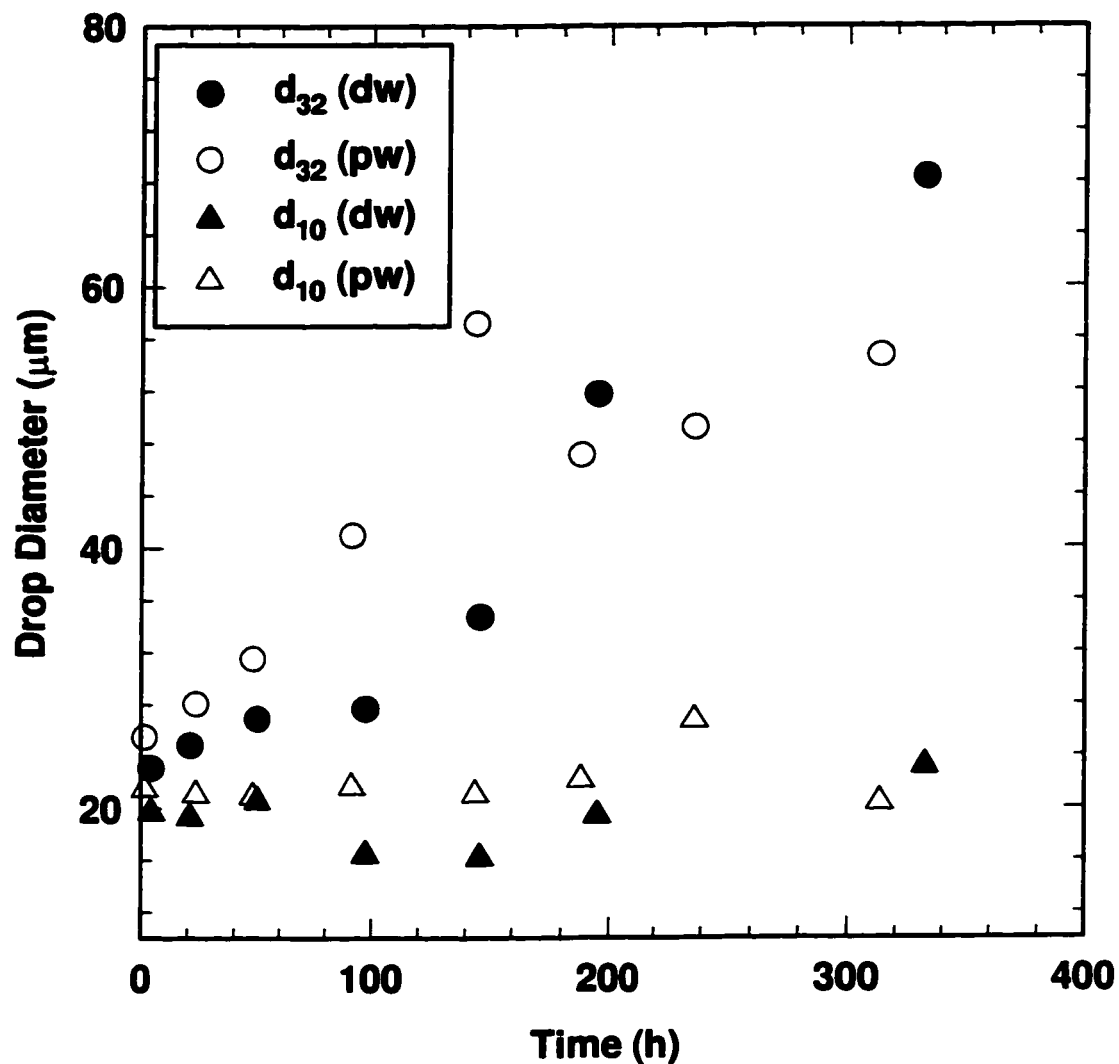


Figure 5.10: Change in drop diameter over time of two asphaltene stabilized water-in-toluene/hexane emulsions: one of deionized water (dw); one of pure water (pw). ($\phi_T/\phi_H = 5$, $\phi_W = 0.40$, $C_A^0 = 1.00 \text{ kg/m}^3$)

Chapter 6

NUMERICAL SIMULATION OF OSTWALD RIPENING IN EMULSIONS [†]

6.1 Introduction

A dispersion may degrade in many ways, for example, through aggregation, creaming, coalescence and Ostwald ripening. Only coalescence and Ostwald ripening involve a change in the drop size distribution and can result in complete phase separation.

Coalescence is more common and has been studied in detail (1). Ostwald ripening has only received attention in the past 15 years and is of interest in the preparation of metal alloys (2) and artificial blood substitutes (3). Ostwald ripening refers to mass transfer between particles or drops of different curvature through their surrounding continuous medium. The concentration of the dispersed phase material at the surface of a drop is inversely related to the radius of curvature. Hence, a small drop has a high surface concentration relative to a large drop giving rise to a concentration gradient of the dispersed phase material in the continuous phase. Mass is transferred along the concentration gradient from small drops to large drops. In other words, when Ostwald ripening occurs, small drops shrink and ultimately disappear while large drops grow at their expense, eventually leading to phase separation.

Lifshitz and Slyozov and, independently, Wagner (LSW) first developed an analytical solution for Ostwald ripening in infinitely dilute dispersions (4,5). The LSW technique showed that, after sufficient time, the Ostwald ripening process enters a stationary state where the cube of the mean drop radius increases linearly with time and the shape of the drop size distribution normalized by the mean radius is invariant with time.

Experimental measurements of Ostwald ripening are relatively few, particularly for

[†] Accepted in part in: *J. Colloid Interface Sci.*, August 1997.

emulsions, but experiments conducted at low dispersed phase volume fractions generally confirm the predictions of the LSW technique (6,7). However, the measured size distributions for emulsions with higher volume fractions of dispersed phase tend to be broader than predicted by theory and the absolute growth rate, *i.e.* the change in the cube of the mean radius with time, tends to be faster than predicted (8). Recent work has focused on determining the effect of the dispersed phase volume fraction on the ripening process (2,9-11).

In general, the effect of the dispersed phase volume fraction has been handled by tracking the location of each drop and determining the local environment through the contribution of source/sink terms for each drop (8). This approach is constrained to a limited number of drops but various statistical techniques have been used to overcome the deficiency (9,11). In all cases, the predicted drop size distributions and the change in the cube of the mean radius with time are in better agreement with experimental observations than are predictions from the LSW technique. As yet, few predictions have been made for finite dispersed phase volume fractions greater than 30%. However, concentrated emulsions with dispersed phase volume fractions as high as 70% can undergo Ostwald ripening, *e.g.*, a creamed emulsion that does not coalesce. Hence, it is desirable to extend the solution of the ripening problem to higher dispersed phase volume fractions.

Marqusee and Ross (MR) have used a different analytical technique to examine Ostwald ripening in the infinitely dilute case and in an interfacially controlled diffusion case. The latter case is equivalent to Ostwald ripening in an infinitely concentrated emulsion where the continuous phase in effect exists as a thin interface around the drops. Predictions from the MR technique confirm that the cube of the mean radius increases linearly with time for infinitely dilute emulsions but indicate that the square, not the cube, of the mean radius increases linearly with time for infinitely concentrated emulsions (12). By extending the numerical solutions to higher dispersed phase concentrations, one can test the MR technique and find a form of the growth rate expression that is valid for dispersed phase volume fractions ranging from 0 to 1.

In this chapter, an approach is developed for modeling ripening at finite dispersed phase volume fractions using a number frequency distribution of drop radii rather than employing a discrete number of drops. The effect of volume fraction is accounted for by a local environment related to the separation distance between the drops. The non-linear differential equations that arise from ripening theory are solved in an explicit numerical scheme. The numerical solutions are compared with the LSW and MR techniques for the infinitely dilute and concentrated cases, respectively. Predictions at various dispersed phase volume fractions are compared with published data and the power law for the mean radius growth rate is examined across the full range of dispersed phase concentration.

6.2 Theory

In this section, the differential equations governing Ostwald ripening are developed for the general case of a finite dispersed phase volume fraction and for the special cases of an infinitely dilute and an infinitely concentrated emulsion. As discussed previously, Ostwald ripening arises from the mass transfer between drops and the continuous phase. The change in radius of a sphere resulting from mass transfer can be expressed as follows (8,13),

$$\frac{da}{dt} = \frac{arD}{a^2(r-a)}(\phi_c - \phi_s) \quad (6.1)$$

where t is time, D is the diffusivity and, as shown in Fig. 6.1, a is the radius of the sphere, and r is the boundary radius for mass transfer. ϕ_c and ϕ_s are the volume fractions of the dispersed phase material in the continuous phase and at the surface of a drop, respectively. The surface concentration of a drop, in terms of volume fraction, is related to solubility by the Kelvin equation (14),

$$\phi_s = \phi_\infty \exp\left\{\frac{2\sigma v_d}{RTa}\right\} \cong \phi_\infty \left(1 + \frac{2\sigma v_d}{RTa}\right) \quad (6.2)$$

where ϕ_∞ is the solubility of the dispersed phase material in the continuous phase expressed as a volume fraction, σ is the interfacial tension between the two phases, v_d is the molar volume of the dispersed phase, R is the universal gas constant and T is temperature. The first order approximation of the exponential term is employed because $2\sigma v_d/RTa$ is generally much less than unity. Eq. 6.3 indicates that for a drop of finite radius, a , the concentration of the dispersed phase material at the surface of the drop exceeds the solubility of the dispersed material in the continuous phase. Hence, the continuous phase becomes supersaturated and ϕ_c exceeds ϕ_∞ by some fraction, θ ,

$$\phi_c = \phi_\infty(1 + \theta) \quad (6.3)$$

After substituting Eqs. 6.2 and 6.3 into Eq. 6.1 and some manipulation, one obtains the following equation,

$$\frac{da}{dt} = \frac{rD\phi_\infty\alpha}{a^2(r-a)} \left(\frac{a}{a_c} - 1 \right) \quad (6.4)$$

Here, $\alpha = 2\sigma v_d/RT$ and a_c , the critical radius, is defined as α/θ . From Eq. 6.4, the characteristic behavior of Ostwald ripening is apparent, that is, for drops with a radius exceeding the critical radius ($a/a_c > 1$), da/dt is positive and the drops grow. Conversely, drops with a radius below the critical radius ($a/a_c < 1$) shrink. The infinitely dilute form of Eq. 6.4 used in the LSW technique is found as r approaches infinity,

$$\frac{da}{dt} = \frac{D\phi_\infty\alpha}{a^2} \left(\frac{a}{a_c} - 1 \right) \quad (6.5)$$

To find the infinitely concentrated form of Eq. 6.4, it is simplest to recast the equation in terms of the separation distance between the drops, 2δ , where $\delta = r - a$. Note that the

mass transfer boundary is assumed to lie exactly between the drops. Eq. 6.4 then becomes

$$\frac{da}{dt} = D\phi_{\infty}\alpha \frac{(a+\delta)}{a^2\delta} \left(\frac{a}{a_c} - 1 \right) \quad (6.6)$$

and the infinitely concentrated limit of Eq. 6.6 is found as δ approaches zero,

$$\frac{da}{dt} = \frac{D\phi_{\infty}\alpha}{a\delta} \left(\frac{a}{a_c} - 1 \right) \quad (6.7)$$

Eq. 6.6 is the general form of the ripening equation and is applicable at any volume fraction of the dispersed phase. To relate the separation distance between drops to the dispersed phase volume fraction, we use an approach similar to the cell model for hindered settling (15) and assume that the continuous phase is distributed around each drop in the form of a concentric shell of thickness δ , as shown in Fig. 6.1. Then the volumes of the dispersed phase and the emulsion can be expressed in terms of the number of drops:

$$V_d = N \frac{4\pi}{3} \sum \hat{F}_i a_i^3 \quad (6.8)$$

$$V_t = N \frac{4\pi}{3} \sum \hat{F}_i (a_i + \delta)^3 \quad (6.9)$$

where V_d and V_t are the volumes of the dispersed phase and the emulsion respectively, N is the number of drops and \hat{F}_i is the number frequency of the drops with radius a_i . Recall that $V_d = \phi_d V_t$, where ϕ_d is the volume fraction of the dispersed phase. Hence, Eqs. 6.8 and 6.9 can be combined to give

$$\phi_d = \frac{\sum \hat{F}_i a_i^3}{\sum \hat{F}_i (a_i + \delta)^3} \quad (6.10)$$

Note, that as $\phi_d \rightarrow 0$, $\delta \rightarrow \infty$, and as $\phi_d \rightarrow 1$, $\delta \rightarrow 0$. In other words, as expected, the infinitely dilute and infinitely concentrated cases are equivalent to infinite and zero separation distances, respectively. The half-separation distance, δ , is assumed to be identical for all drops regardless of their size and represents an average dimension. Hence, a weakness of the cell model approach is that the effect of different local environments within the dispersion cannot be accounted for. To solve the ripening problem at a finite dispersed phase volume fraction, the half-separation distance, δ , is found from Eq. 6.10 and then used to solve Eq. 6.6. The special cases of an infinitely dilute and an infinitely concentrated emulsion are solved from the simplified Eqs. 6.5 and 6.7 respectively.

6.3 Numerical Method

6.3.1 Ripening Equations

The differential equations developed in the previous section are non-linear because a_c and δ are functions of time. While analytical approximations were used to solve the infinitely dilute and infinitely concentrated cases (4,5), the general case including the effect of the dispersed phase volume fraction must be solved numerically. An explicit numerical scheme is sufficient to solve the problem. In this approach, a_c and δ are held constant for each time step, linearizing the ripening equations and allowing for direct integration. The discrete forms of the exact analytical solutions are given for the infinitely dilute case, Eq. 6.5,

$$\frac{a_c}{2} \left([a_i^{j+1}]^2 - [a_i^j]^2 \right) + a_c^2 (a_i^{j+1} - a_i^j) + a_c^3 \ln \left\{ \frac{a_i^{j+1} - a_c}{a_i^j - a_c} \right\} = k_o \Delta t \quad (6.11)$$

the infinitely concentrated case, Eq. 6.7,

$$a_c(a_i^{j+1} - a_i^j) + a_c^2 \ln \left\{ \frac{a_i^{j+1} - a_c}{a_i^j - a_c} \right\} = \frac{k_o}{\delta} \Delta t \quad (6.12)$$

and the general case, Eq. 6.6,

$$\delta a_c \left[(a_i^{j+1} - a_i^j) - \frac{\delta^2}{a_c + \delta} \ln \left\{ \frac{a_i^{j+1} + \delta}{a_i^j + \delta} \right\} + \frac{a_c^2}{a_c + \delta} \ln \left\{ \frac{a_i^{j+1} - a_c}{a_i^j - a_c} \right\} \right] = k_o \Delta t \quad (6.13)$$

Here, a_i^j and a_i^{j+1} are the radii of a drop at the start and end of the time step, respectively, with $k_o = D\phi_\infty\alpha$. Note, that as $\delta \rightarrow 0$, Eq. 6.13 reduces to Eq. 6.12 and as $\delta \rightarrow \infty$, Eq. 6.13 approaches Eq. 6.11.

6.3.2 Critical Radius

To solve the ripening equations we must be able to determine a_c and δ at each time step. The average half-separation distance can be calculated from Eq. 6.10. The critical radius for the infinitely dilute case has been shown to equal the mean radius (4,5). However, the relationship of the critical radius to dispersed phase volume fraction is unknown. To model such a relationship, we again picture the dispersion as a collection of drops, each surrounded by a shell of continuous phase. The concentration of the dispersed phase in the medium may then be expressed as

$$\phi_c = \frac{\sum f_i g(a_i, \delta) \phi_{ci}}{\sum f_i g(a_i, \delta)} \quad (6.14)$$

where

$$g(a_i, \delta) = (a_i + \delta)^3 - a_i^3 \quad (6.15)$$

Now, as $\delta \rightarrow 0$, $\phi_{ci} \rightarrow \phi_{si}$ and as $\delta \rightarrow \infty$, $\phi_{ci} \rightarrow \phi_\infty$. The simplest function relating ϕ_{ci} to δ that satisfies the preceding limits is given by,

$$\phi_{ci} = \phi_{si} + h(a_i, \delta)\phi_{\infty} \quad (6.16)$$

where $h(a_i, \delta)$ is a bridging function between the infinitely concentrated and infinitely dilute concentrations. Rearranging Eq. 6.1, for the i^{th} drop, one can write,

$$\phi_{ci} = \phi_{si} + \frac{a_i \delta}{D(a_i + \delta)} \left[\frac{da_i}{dt} \right] \quad (6.17)$$

An expression for the derivative, da_i/dt , at infinite dilution is found by rearranging Eq. 6.5,

$$\left[\frac{da_i}{dt} \right]_{\infty} = \frac{D\phi_{\infty}\alpha}{a_i} \left(\frac{1}{a_{c\infty}} - \frac{1}{a_i} \right) \quad (6.18)$$

where $a_{c\infty}$ is the critical radius at infinite dilution. The LSW technique showed that the critical radius at infinite dilution is identical to the mean radius, a_{10} (4,5). Replacing $a_{c\infty}$ with a_{10} and substituting Eq. 6.18 into Eq. 6.17, one obtains

$$\phi_{\infty} = \phi_{si} + \frac{\alpha\delta\phi_{\infty}}{a_i + \delta} \left(\frac{1}{a_{10}} - \frac{1}{a_i} \right) \quad (6.19)$$

Now, by comparing Eq. 6.19 with Eq. 6.16, it is apparent that the bridging function must have the following form

$$h(a_i, \delta) = \frac{\alpha\delta}{a_i + \delta} \left(\frac{1}{a_{10}} - \frac{1}{a_i} \right) \quad (6.20)$$

ϕ_c can be expressed as follows by making use of Eqs. 6.3, 6.14, 6.16 and 6.20:

$$\phi_c = \frac{\sum f_i g(a_i, \delta) \left[1 + \frac{\alpha}{a_i} + \frac{\alpha \delta}{a_i + \delta} \left(\frac{1}{a_{10}} - \frac{1}{a_i} \right) \right] \phi_\infty}{\sum f_i g(a_i, \delta)} \quad (6.21)$$

The ϕ_c in Eq. 6.21 represents the average dispersed phase volume fraction at the mass transfer boundary, $r = a + \delta$. Hence, it represents a hypothetical average local environment for mass transfer from any drop and the effect of different local environments within the same dispersion is not accounted for. Now, recalling that $\theta = (\phi_c/\phi_\infty) - 1$ and that $a_c = \alpha/\theta$, an expression for the critical radius as a function of the dispersed phase volume fraction can be obtained from Eq. 6.21.

$$a_c = \frac{\sum f_i [(a_i + \delta)^3 - a_i^3]}{\sum f_i [(a_i + \delta)^3 - a_i^3] \left[\frac{1}{a_i} + \frac{\delta}{a_i + \delta} \left(\frac{1}{a_{10}} - \frac{1}{a_i} \right) \right]} \quad (6.22)$$

As will be shown later, Eq. 6.22 provides estimates of a_c that lead to a minimum material balance error in the numerical simulations. Interestingly, for an infinitely concentrated emulsion, the critical radius, a_{c0} , is the ratio of the mean square radius to the mean radius, a_{21} . Hence, the critical radius appears to vary from a_{10} to a_{21} as the dispersed phase volume fraction varies from 0 to 1. Allowing for the variation of a_c is a significant departure from other approaches where the critical radius is assumed to be the mean radius at all values of the dispersed phase volume fraction (8).

6.3.3 Frequency Distribution

The theory presented up to this point is sufficiently developed to track the size of individual drops with time. In previous approaches, the growth or shrinkage of a reasonably large number of drops was calculated. The procedure was repeated for many groups of drops with different initial size distributions and statistical techniques were used to combine the calculated distributions from each group in order to evaluate the

average drop size distribution and growth rate (10,11). To use a frequency distribution, the equations developed for individual drops must be employed to predict changes in the whole distribution. First, it is necessary to define the distribution. As shown in Fig. 6.2, the plot of the number frequency of drop radii is divided into equal intervals where the number frequency of each interval, \hat{F}_i , is defined as follows,

$$\hat{F}_i = \int_{a_i}^{a_{i+1}} \left[\frac{d\hat{f}}{da} \right] da_i \quad (6.23)$$

where \hat{f} is the cumulative number frequency. To obtain the simplest form of \hat{F}_i , we assume that the slope of the frequency distribution over each interval is constant, *i.e.*, $(d\hat{f}/da)_i = z_i$, where z_i is a constant. Then, at the start of a time step,

$$f_i^j = z_i^j (a_{i+1}^j - a_i^j) \quad (6.24)$$

Now to illustrate how the change in the frequency distribution is determined after each time step, consider an arbitrary interval, i , with boundaries a_i and a_{i+1} as shown in Fig. 6.2. Assume that the interval falls below the critical radius and therefore lies in a region of the distribution where all drops are shrinking. Hence, over the time step, some drops with radii greater than a_{i+1} will shrink until they fall into the interval and some drops of radii greater than a_i will shrink until they fall below the interval. Let a_b and a_{b+1} be the radii of the drops that in time Δt shrink to radii a_i and a_{i+1} respectively. In time Δt , no drops with radius greater than a_{b+1} will enter interval i and all of the drops of radius less than a_b will shrink to below interval i . Then, the number of drops in interval i at time $t+\Delta t$ must equal the number of drops between a_b and a_{b+1} at time t .

$$\hat{F}_i^{j+1} = z_p^j (a_{p+1}^j - a_b^j) + \sum_{k=p+1}^q z_k^j (a_{k+1}^j - a_k^j) + z_q^j (a_{b+1}^j - a_q^j) \quad (6.25)$$

where p , q and k denote the interval containing a_b , the interval containing a_{b+1} and the intervals in between, respectively. For this calculation, the number frequency is equivalent to the number of drops in the interval. If some drops shrink to zero radius and hence disappear, the total number of drops will change and the sum of \hat{F}_i^{j+1} will not equal unity. Therefore, the frequency distribution must be normalized after each time step to sum to unity. The sum before normalization, when the number frequency is still equivalent to the number of drops, can be used to find the material balance error after each time step. The error is given by,

$$err = \frac{4\pi}{3} \left(\sum \hat{F}_i^{j+1} a_i^3 - \sum \hat{F}_i^j a_i^3 \right) \quad (6.26)$$

6.3.4 Numerical Procedure

All the necessary equations to set up the numerical routine have been developed but one significant source of error must yet be dealt with. Assume, for example, that the radius of the largest drop, a_L , lies near the lower end of the highest non-zero interval on the frequency distribution. The frequency for the interval then should only apply to the fraction of the interval from the lower boundary to a_L . However, in the numerical procedure, the frequency is assumed to encompass the whole interval. Consequently, the radius of the largest drop is artificially increased to the radius of the upper boundary of the interval. In this way, significant error can propagate at the upper end of the frequency distribution. To avoid the problem of error accumulation, the exact radius of the largest drop is calculated at each time step and its position in the largest non-zero interval is determined exactly.

The numerical procedure for each time step, starting with a known number frequency distribution of drop radii, \hat{F}_i^j , is as follows:

- calculate z_i^j from Eq. 6.24
- calculate δ and a_c from Eqs. 6.10 and 6.22 respectively

- calculate a_b^j and a_{b+1}^j for each interval using Eq. 6.11, 6.12 or 6.13 for the infinitely dilute, infinitely concentrated and general cases, respectively
- find the position of a_L in the highest non-zero interval
- calculate \hat{F}_i^{j+1} from Eq. 6.25.
- find the material balance error from Eq. 6.26
- normalize \hat{F}_i^{j+1}

For all cases, a flat initial size distribution was used with $0 < a_i < 80$, $\Delta a = a_{i+1} - a_i = 0.5$ and $\hat{F}_i^o = 1/80$ for $i = 1 \dots 80$ and $\hat{F}_i^o = 0$ for $i = 80 \dots 160$. Considering the form of Eqs. 6.11 to 6.13, the time step was defined as $\Delta\tau = k_o\Delta t$ for the general and infinitely dilute cases and $\Delta\tau' = k_o\Delta t/\delta$ for the infinitely concentrated case. As will be seen later, these choices of time step are useful for examining the growth rates. Note that, although τ is in volume units, it is a measure of time because k_o is independent of time. In order to control the numerical error, a value of $\Delta\tau$ was chosen such that the total material balance error was less than 2% over each completed simulation. The input for all the numerical simulations presented here are summarized in Table 6.1.

Table 6.1: Simulation input parameters.

| ϕ_d | δ^o | a_c^o | τ | τ' |
|----------|------------|---------|--------|---------|
| 0 | ∞ | 20.00 | 10 | - |
| 0.01 | 95.8 | 20.20 | 5 | - |
| 0.25 | 16.7 | 21.98 | 1 | - |
| 0.50 | 7.57 | 23.51 | 0.5 | - |
| 0.75 | 2.98 | 25.05 | 0.2 | - |
| 0.99 | 0.100 | 26.60 | 0.01 | 0.1 |
| 1 | 0 | 26.67 | - | 0.1 |

6.4 Results and Discussion

6.4.1 Infinitely Dilute Case

As discussed previously, the stationary state frequency distribution and growth rate for the infinitely dilute case as $\tau \rightarrow \infty$ were predicted by the LSW technique. The predictions are given by:

$$\hat{F}_\infty(u) = \frac{81eu^2 \exp\left\{\frac{1}{2u/3 - 1}\right\}}{32^{1/3}(u+3)^{7/3}(1.5-u)^{11/3}}, \quad 0 \leq u \leq 1.5 \quad (6.27)$$

$$\hat{F}_\infty(u) = 0, \quad u > 1.5$$

and

$$\frac{da_{10}^3}{d\tau} = \frac{4}{9} \quad (6.28)$$

where $u = a_i/a_c$ is the reduced radius and $\hat{F}_\infty(u)$ denotes the stationary state number frequency distribution.

The numerically predicted frequency distributions at different times are shown in Fig. 6.3. The initially flat distribution grows with time until it reaches the characteristic shape of Ostwald ripening. When the cumulative frequency distributions are plotted against the appropriate reduced coordinate, u , it is clear that the numerical solutions reach and stay at the LSW stationary state solution as shown in Fig. 6.4. Figure 6.5, a plot of the cube of the mean radius against τ , shows that the linear stationary state region is attained after the initial mean drop size doubles. The final stationary slope is 0.442, or 3.978/9, within 0.5% of the value of 4/9 predicted by the LSW technique.

6.4.2 Infinitely Concentrated Case

The stationary state frequency distribution and growth rate for the infinitely concentrated case were predicted by Marqusee and Ross (12). Their predictions, transformed into functions of the reduced radius, $\nu = a/a_{10}$, are given by:

$$\hat{F}_{\infty}(\nu) = \frac{686.3\nu \exp\left\{\frac{3}{4\nu/9 - 1}\right\}}{(2.25 - \nu)^5}, \quad 0 \leq \nu \leq 2.25 \quad (6.29)$$

$$\hat{F}_{\infty}(\nu) = 0, \quad \nu > 2.25$$

and

$$\frac{da_{10}^2}{d\tau'} = \frac{32}{81} \quad (6.30)$$

The numerically predicted frequency distributions at different times are shown in Fig. 6.6. As expected, the ultimate frequency distributions are broader than the infinitely dilute case given in Fig. 6.3. Like the infinitely dilute case, the numerical predictions reach a stationary state solution, as shown in Fig. 6.7 where the cumulative frequency distributions are plotted against the reduced radius, u . The numerically calculated cumulative frequency distribution is compared to the MR prediction in Fig. 6.8. The stationary state frequency distribution from the numerical model is somewhat narrower than that from the MR technique but is significantly closer to the MR prediction than the prediction for the infinitely dilute case, also shown on Fig. 6.8.

Since the MR predictions of the frequency distribution employ the reduced radius, ν , whereas the numerical predictions are based the reduced radius u , it is not immediately apparent if the predictions can be directly compared as they were on Fig. 6.8. However, the numerical results indicate that, once the stationary state is reached, the mean radius is

directly proportional to the critical radius and therefore v is directly proportional to u . Hence, it is valid to transform one reduced radius to the other.

A plot of the square of the critical radius against τ' is given in Fig. 6.9. As with the infinitely dilute case, a linear stationary state is attained after the initial mean drop size doubles but it is the square of the critical radius that increases linearly with τ' . Since the mean radius is proportionate to the critical radius and τ' is a measure of time, the prediction from the MR technique that the square of the mean radius is linearly related to time is confirmed. From the numerical results, the final stationary slope in terms of a_c^2 is 0.381 and the ratio of a_{10} to a_c is 0.910. Therefore, the stationary slope in terms of a_{10}^2 is 0.315, or 25.5/81, within 18 % of the value of 32/81 predicted by the MR technique.

The numerically predicted frequency distribution and growth rate are only qualitatively in agreement with the MR predictions. The MR technique employs a truncated power law series to relate the frequency distribution of drop radii to time and hence the differences between the numerical and the MR predictions may arise from the effects of higher order terms in the power law series that are not accounted for in the analytical approach. We have confidence in the numerical predictions because they match predictions from the LSW technique almost exactly, they predict the same form of growth rate as the MR technique and, as will be shown later, they predict the effect of the dispersed phase volume fraction on the frequency distribution very well.

6.4.3 General Case

Before proceeding with the general case, it is necessary to test the validity of the proposed relationship between a_c and δ , as given in Eq. 6.22. A correct prediction of a_c is necessary to satisfy the conservation of mass and, therefore, the predicted values of a_c should minimize the material balance error. To illustrate the connection between a_c and the material balance error, consider that the larger the predicted value of a_c the more drops there are with radii less than a_c and the more drops that shrink. Hence, if a_c is predicted too high, too many drops are predicted to shrink and too few to grow and a

negative material balance error ensues. Similarly, if a_c is predicted too low, a positive material balance error results. Consequently, if Eq. 6.22 predicts a_c correctly, the material balance error should equal zero.

Numerical predictions were made for $\phi_d = 0.01, 0.25, 0.50, 0.75$ and 0.99 and the material balance error for a single time step was determined at different values of a_c and compared with the error at the predicted value of a_c . As shown on Fig. 6.10, the material balance error reaches a minimum within 2.5% of the predicted value of a_c . There is a slight positive material balance error at the predicted a_c because the value of a_c is fixed at the start of each time step when, in reality, it should increase during the time step. Nonetheless, Eq. 6.22 clearly predicts the critical radius correctly.

In Fig. 6.11, the numerically determined cumulative frequency distributions at $\phi_d = 0.01, 0.50$ and 0.99 are compared with published experimental data. As expected, the predicted frequency distributions broaden as the dispersed phase volume fraction increases. However, the difference between the frequency distributions from infinitely dilute to infinitely concentrated dispersions is relatively small. Therefore, only one intermediate case, at $\phi_d = 0.50$, is shown. Experimental data at $\phi_d = 0.10$ and 0.32 closely match the predictions for $\phi_d = 0.01$ and 0.50 respectively. Considering the difficulty in obtaining accurate experimental distributions over such broad ranges of drop radii, the agreement between predictions and experimental data is very good.

6.4.4 Growth Rate Expression

At this point, the main advantage of the numerical approach presented here is that it is simple to implement and does not rely on statistical techniques to obtain a solution. However, now we can examine the growth rate across the full range of dispersed phase concentration and find a growth rate expression that is solely a function of ϕ_d . Given that the growth rate expression must conform to the limiting cases of Eqs. 6.28 and 6.30, and noting that δ is a constant in the limiting cases, a general growth rate expression of the following form is considered,

$$\frac{d(\delta^n a_c^{3-n})}{d\tau} = \beta \quad (6.31)$$

where the growth rate, β , and the exponent, n , are functions of ϕ_d . To be consistent with Eqs. 6.28 and 6.30, n must vary between 0 at infinite dilution and 1 at infinite concentration. When n is set to ϕ_d , Eq. 6.31 agrees very well with the numerical data over the entire range of dispersed phase volume fractions. An example, at $\phi_d = 0.5$, is shown in Fig. 6.12.

While Eq. 6.31 is valid for the entire range of dispersed phase volume fractions, it depends on a_c and δ both of which are unwieldy functions of the frequency distribution. To simplify the equation, we relate δ to a_c and a_c to a_{10} . As shown in Figs. 6.13a and 6.13b respectively, δ is directly proportional to a_c and a_c is in turn directly proportional to a_{10} . When the substitutions $n = \phi_d$, $\delta = b a_c$ and $a_{10} = c a_c$ (where b and c are proportionality constants) are made in Eq. 6.31, one obtains

$$\frac{da_{10}^3}{d\tau} = \frac{c^3 \beta}{b^{\phi_d}} = \beta' \quad (6.32)$$

Eq. 6.32 confirms that, as found with other numerical techniques (9-11), the change in the cube of the mean radius with time is a function of the dispersed phase volume fraction only. Values of β' obtained from the numerical simulations are plotted against ϕ_d in Fig. 6.14. We can observe from Fig. 6.14 that above $\phi_d = 0.9$ the growth rate increases rapidly, approaching infinity as ϕ_d approaches 1. The exponential increase in growth rate at high dispersed phase volume fractions is consistent with the physics of mass transfer through a thin layer of continuous phase. Hence, at $\phi_d > 0.9$, and in all cases where a poorly permeable interface limits diffusion, it is more appropriate to use a rate expression of the form given by the MR technique, Eq. 6.30. Since, in practice, the dispersed phase volume fraction of creamed emulsions undergoing Ostwald ripening will not exceed 0.8,

the growth rate given by Eq. 6.32 is suitable for the full range of practically realizable emulsions. However, at this point, the values of β' must be determined numerically.

6.4.5 Approximate Method For Predicting Growth Rate

Since a significant amount of CPU time is required to determine each value of β' , it is desirable to find a universally fitted expression relating β' to ϕ_d . The shape of the curve relating β' to ϕ_d in Fig. 6.14 is difficult to fit as is. However, the parameters, β , b^{ϕ_d} , and c , that comprise β' are relatively easy to fit and their respective curve fits are given in Figs. 6.15a-c. The equations for each curve fit are given below,

$$\beta = 1.445 - 3.751(\phi_d - 0.4959)^2 \quad (6.33)$$

$$b^{\phi_d} = 1.041(1 - \phi_d) + 0.09055 \sin\{2\pi\phi_d\} \quad (6.34)$$

$$c = 0.9993 - 0.08982\phi_d - 0.001754 \sin\{2\pi\phi_d\} \quad (6.35)$$

The approximate growth rate of any emulsion can be determined without using a numerical simulation by simply substituting Eqs. 6.33 to 6.35 into Eq. 6.32. The approximate growth rates are compared with the full numerical predictions on Fig. 6.14.

In addition, the values of β' can be converted into correction factors to the LSW growth law given by Eq. 6.28,

$$K = \frac{9\beta'}{4} = \frac{9c^3\beta}{4b^{\phi_d}} \quad (6.36)$$

The correction factors are the ratio of the growth rate at a finite dispersed phase volume fraction to the growth rate at infinite dilution, $K = \beta'(\phi_d)/\beta'(0)$. Correction factors from the full numerical solution and from the approximate method are shown in Fig. 6.16 and compared with correction factors determined numerically by Enomoto et al. (11).

Enomoto et al. showed that their correction factors are consistent with results from

several other numerical approaches for the range of dispersed phase volume fractions considered, $\phi_d \leq 0.3$. The correction factors from our approach and Enomoto's agree well at $\phi_d < 0.2$ but there is appreciable deviation at the data point at $\phi_d = 0.3$. Experimental data at $\phi_d = 0.1$ (3) are consistent with both sets of correction factors. Unfortunately, there is no experimental data for concentrated emulsions with which to compare the correction factor predictions. However, Kang and Yoon (16) measured growth rates for the coarsening of cobalt grains in liquid copper at high volume fractions of cobalt, ϕ_d ranging from 0.34 to 0.55. The absolute theoretical growth rates cannot be calculated because the values of the diffusivity in the copper/cobalt system were not known precisely. However, the ratio of the predicted growth rates at different ϕ_d can be calculated and compared with the experimental data as shown in Table 6.2. The predictions from Eq. 6.36 agree very well with Kang and Yoon's experimental data.

Table 6.2: Growth rates of cobalt grains in liquid copper.

| ϕ_d | Experimental ^a $\beta'(\phi_d)/\beta'(0.34)$ | Predicted ^b $\beta'(\phi_d)/\beta'(0.34)$ |
|----------|--|---|
| 0.34 | 1 | 1 |
| 0.42 | 1.34 | 1.21 |
| 0.55 | 1.83 | 1.74 |

a source: ref. 15

b source: Eq. 6.36

6.5 CONCLUSIONS

Ostwald ripening at finite dispersed phase volumes was modeled successfully using linearized analytical solutions of the ripening equations and an explicit numerical routine. The routine incorporated a number frequency distribution of drop radii rather than using a discrete number of drops. The effect of volume fraction was accounted for by using half the average separation distance between drops as a mass transfer boundary. The

numerical predictions for infinitely dilute systems match the LSW predictions almost exactly. The numerical predictions are in qualitative agreement with predictions from the MR technique for infinitely concentrated systems.

The numerical model was applied to the full range of dispersed phase concentrations and successfully predicted cumulative frequency distributions for the range of available experimental data at dispersed phase volume fractions between 0 and 0.3. The critical radius was found to vary between the mean radius, a_{10} , and the a_{21} radius as the dispersed phase volume fraction varied between 0 and 1. Despite the variation in critical radius, the growth rate could be related to the cube of the mean radius at any dispersed phase volume fraction.

A simple expression, depending solely on the dispersed phase volume fraction, was developed to predict the growth rate, da_{10}^3 / dt , at any dispersed phase volume fraction. Correction factors to the LSW growth law were determined for $0 \leq \phi_d \leq 1$. The correction factors agree well with previously published correction factors at $\phi_d < 0.2$ but have higher values, *i.e.* predict faster growth rates, at higher dispersed phase volume fractions. While we found no experimental data for concentrated emulsions, data is available for concentrated solid dispersions. The predicted correction factors agree well with experimental data for the precipitation of cobalt in liquid copper at $0.34 \leq \phi_d \leq 0.55$.

6.6 References

1. Tadros, T.F., Vincent, B., *Encyclopedia of Emulsion Technology*, Vol. 1, Ed. P. Becher, Marcel Dekker, New York, 1983.
2. Davies, C.K.L., Nash, P., Stevens, R.N., *Acta Metall.*, **28**, 1980, 179.
3. Kabalnov, A.S., Makarov, K.N., Pertzov, A.V., Shchukin, E.D., *J. Coll. Interf. Sci.*, **138**(1), 1990, 98.
4. Lifshitz, I.M., Slyozov, V.V., *J. Phys. Chem. Solids*, **19**(1/2), 1961, 35.
5. Wagner, C., *Ber. Bunsenges. Phys. Chem.*, **65**, 1961, 581.
6. Taylor, P., *Coll. Surf. A*, **99**, 1995, 175.

7. Kabalnov, A.S., Pertzov, A.V., Shchukin, E.D., *J. Coll. Interf. Sci.*, **118**(2), 1987, 590.
8. Kabalnov, A.S., Shchukin, E.D., *Adv. Coll. Interf. Sci.*, **38**, 1992, 69.
9. Ardell, A.J., *Acta Metall.*, **20**, 1972, 61.
10. Voorhees, P.W., Glicksman, M.E., *Acta Metall.*, **32**(11), 1984, 2001.
11. Enomoto, Y., Kawasaki, K., Tokutama, M., *Acta Metall.*, **35**(4), 1987, 907.
12. Marqusee, J.A., Ross, J., *J. Chem. Phys.*, **79**(1), 1983, 373.
13. Lifshitz, E.M., Pitaevskii, L.P., "Physical Kinetics," Vol. 10 of L.D. Landau and E.M. Lifshitz Course of Theoretical Physics, Pergamon Press, Oxford, 1981.
14. Thomson, W. (Lord Kelvin), *Proc. Royal Soc., Edinburgh*, **7**, 1871, 63.
15. Happel, J., Brenner, H., "Low Reynolds number hydrodynamics", Kluwer Academic Publishers, 2nd Ed., Dordrecht (1991), p 387.
16. Kang, C.H., Yoon, D.N., *Metall. Trans. A*, **12A**, 1981, 65.

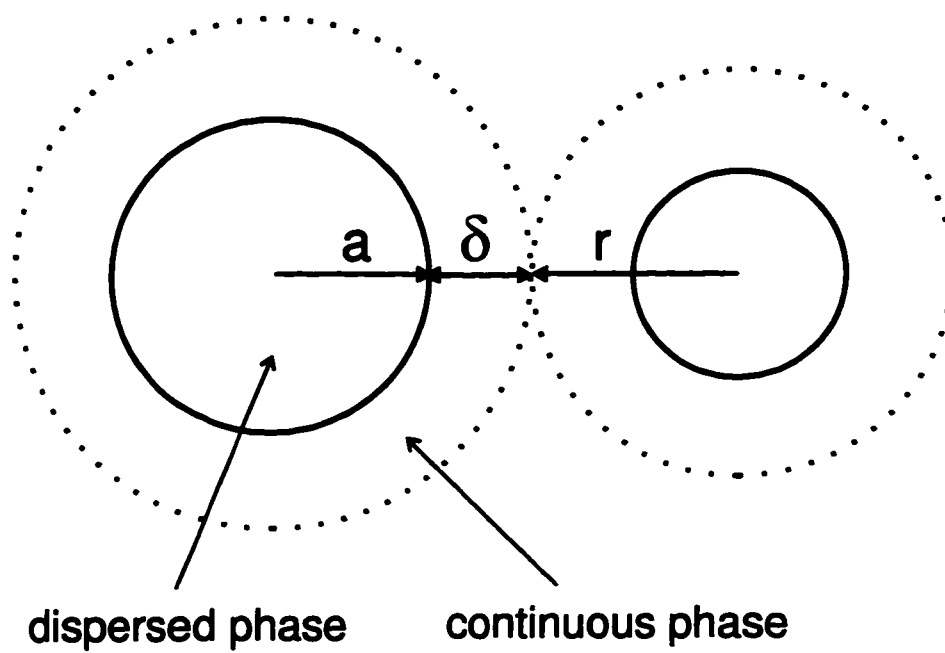


Figure 6.1: Cell model of a dispersion.

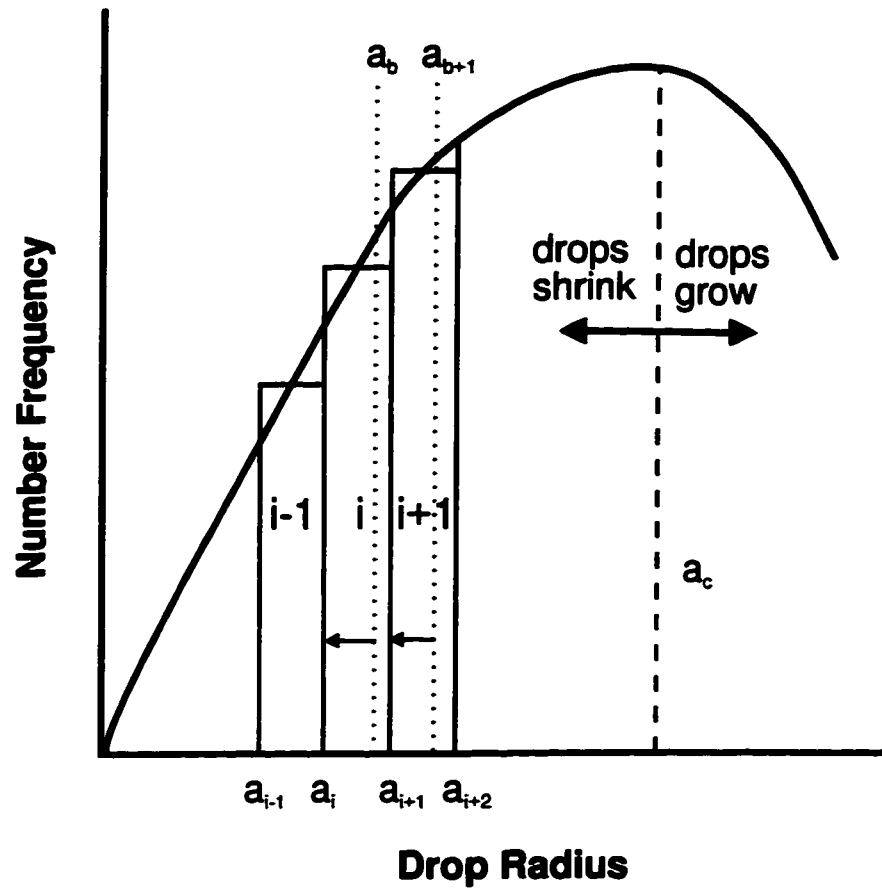


Figure 6.2: Discretization of number frequency interval.

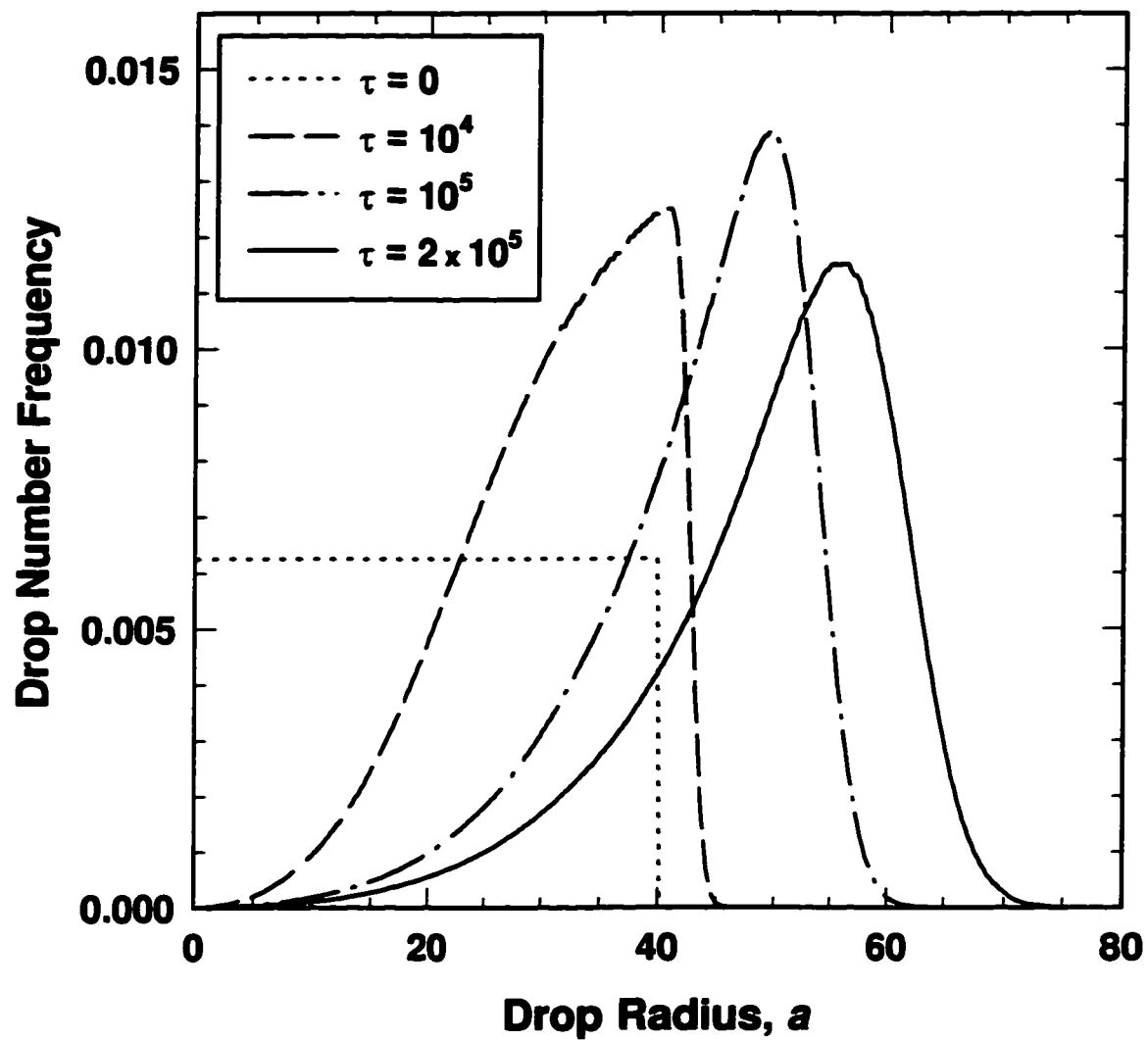


Figure 6.3: Number frequency distribution of drop radii for an infinitely dilute system.

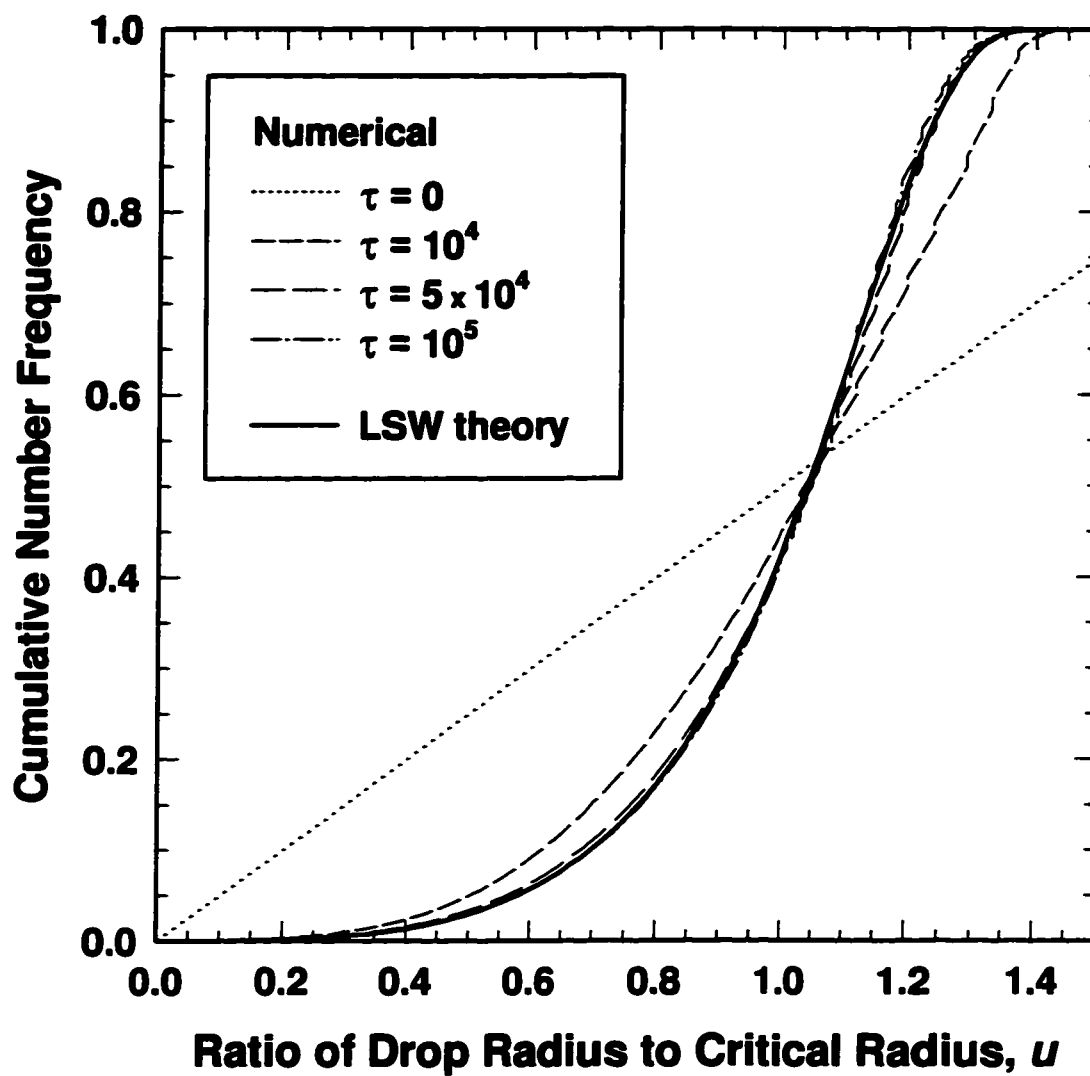


Figure 6.4: Cumulative number frequency distribution of drop radii for an infinitely dilute system.

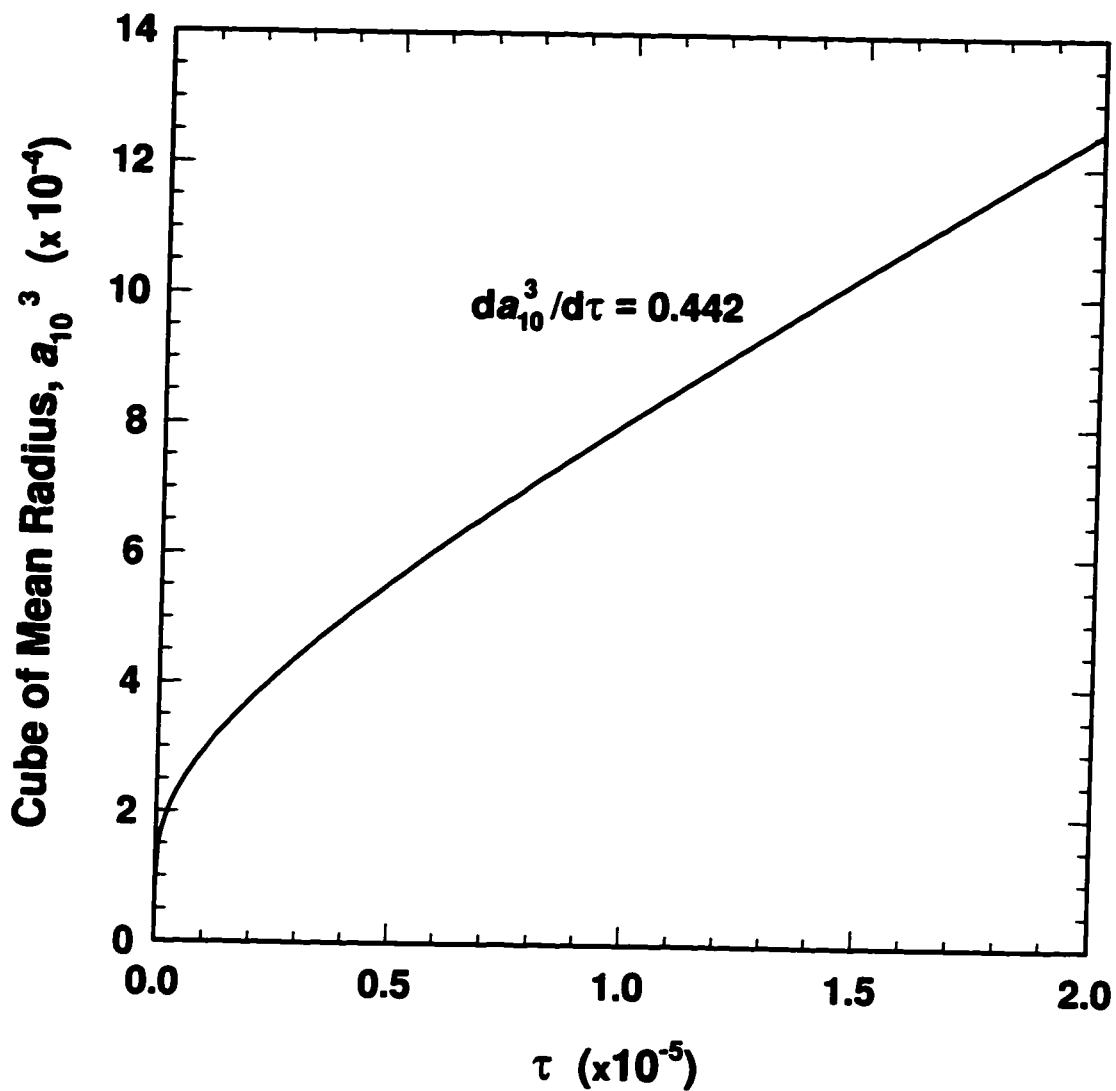


Figure 6.5: Cube of the mean radius versus τ for an infinitely dilute system.

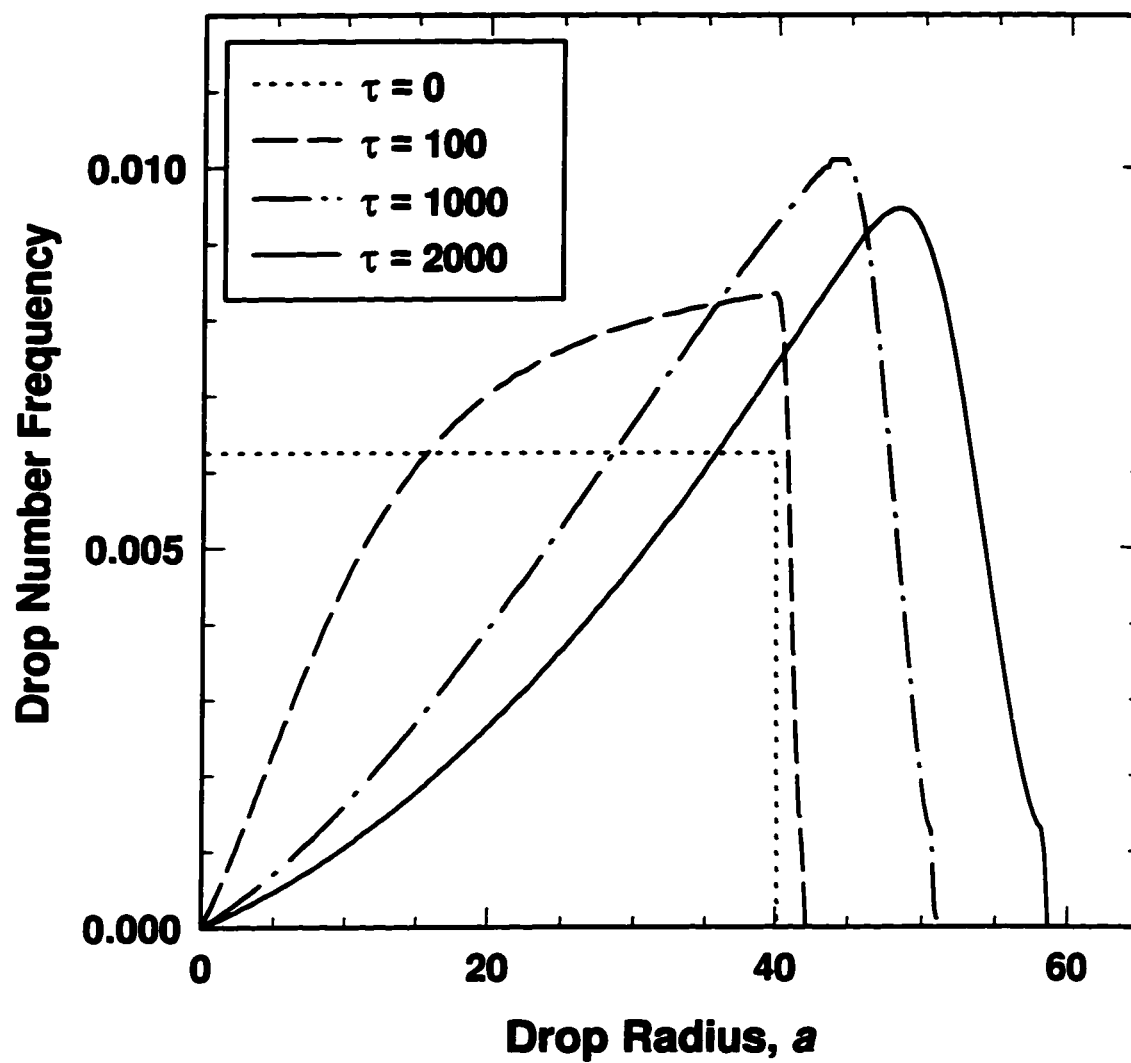


Figure 6.6: Number frequency distribution of drop radii for an infinitely concentrated system.

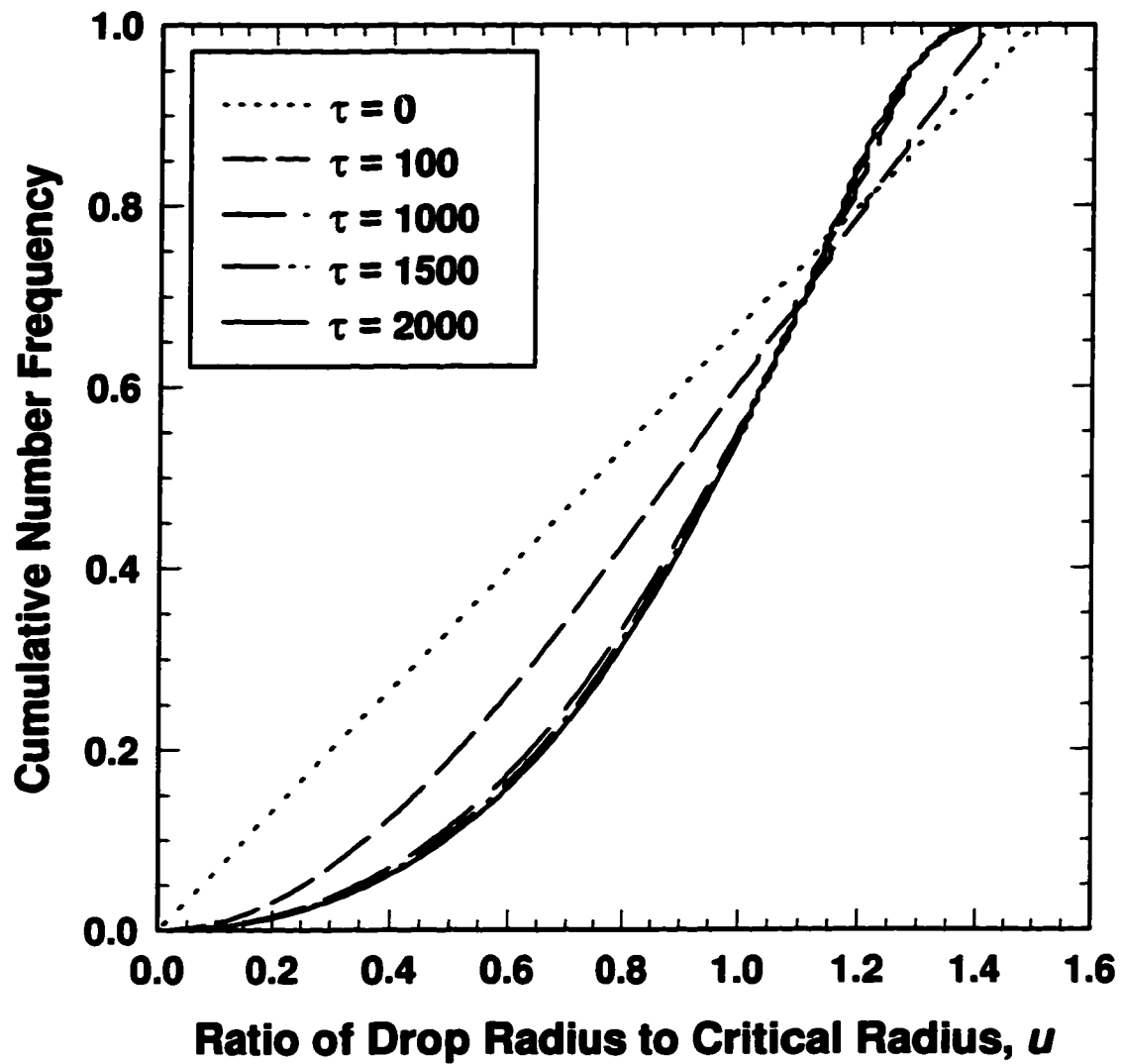


Figure 6.7: Cumulative number frequency distribution of drop radii for an infinitely concentrated system.

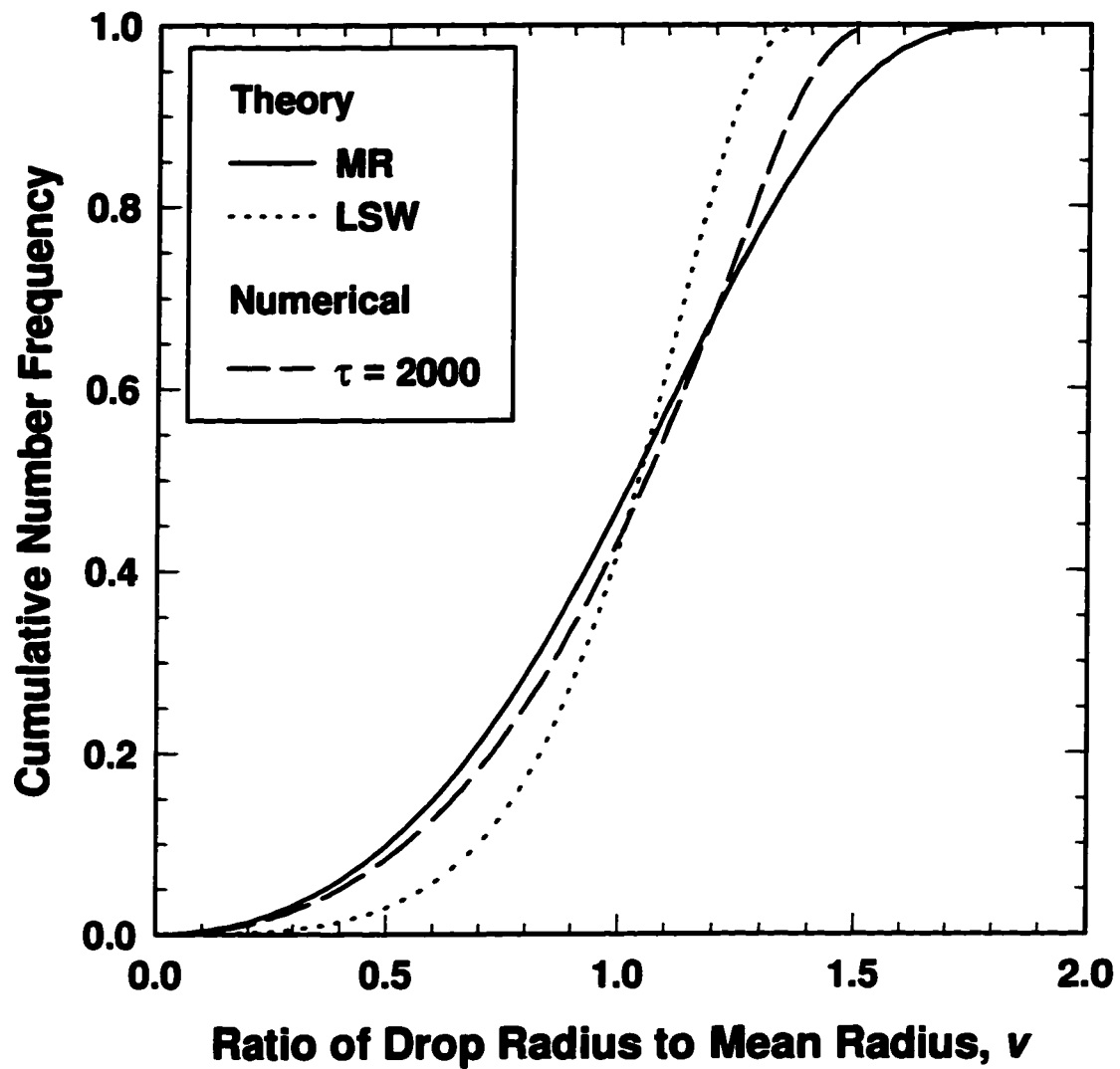


Figure 6.8: Numerical and MR predictions of the cumulative number frequency of drop radii for an infinitely concentrated system.

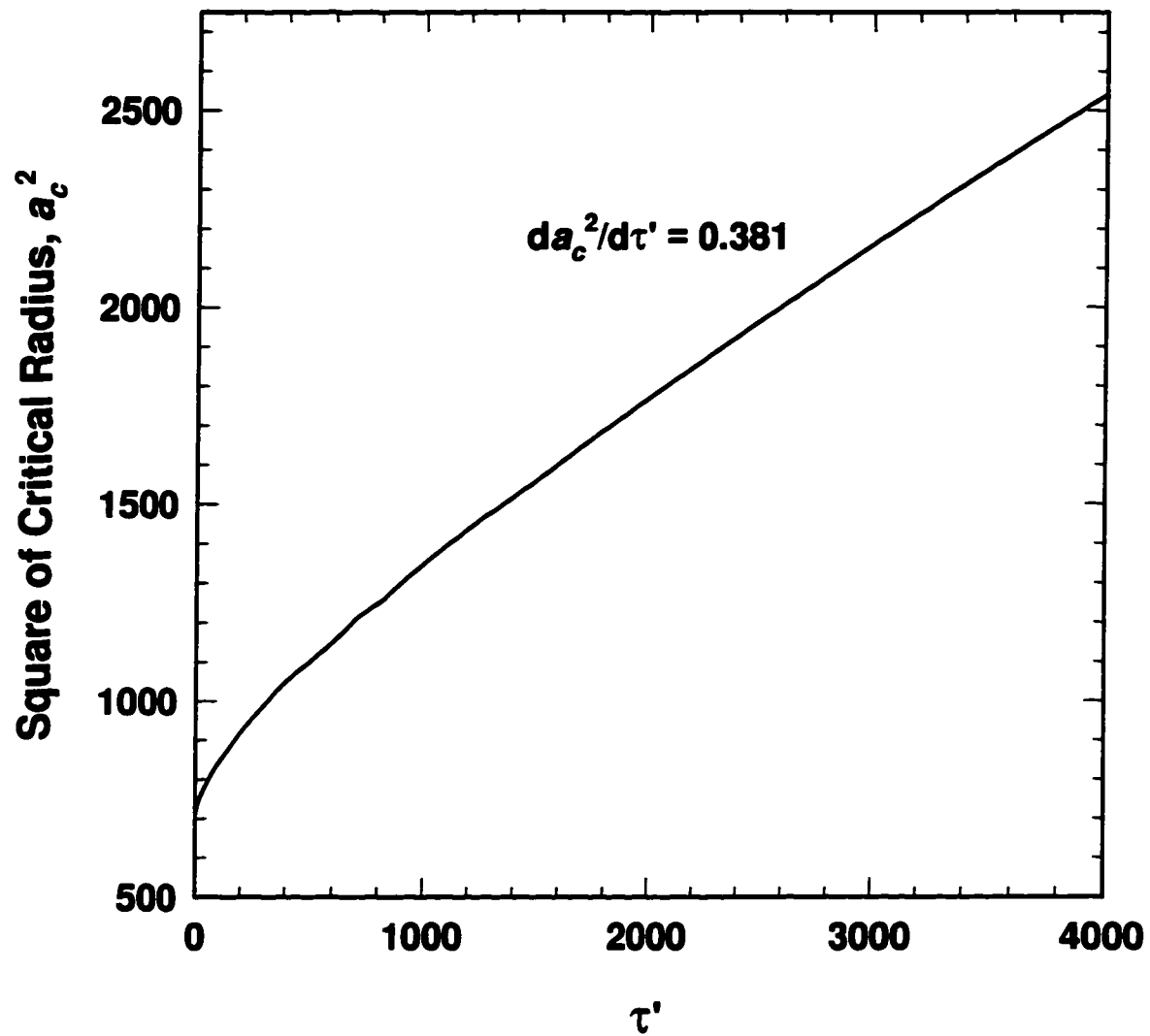


Figure 6.9: Square of the critical radius versus τ' for an infinitely concentrated system.

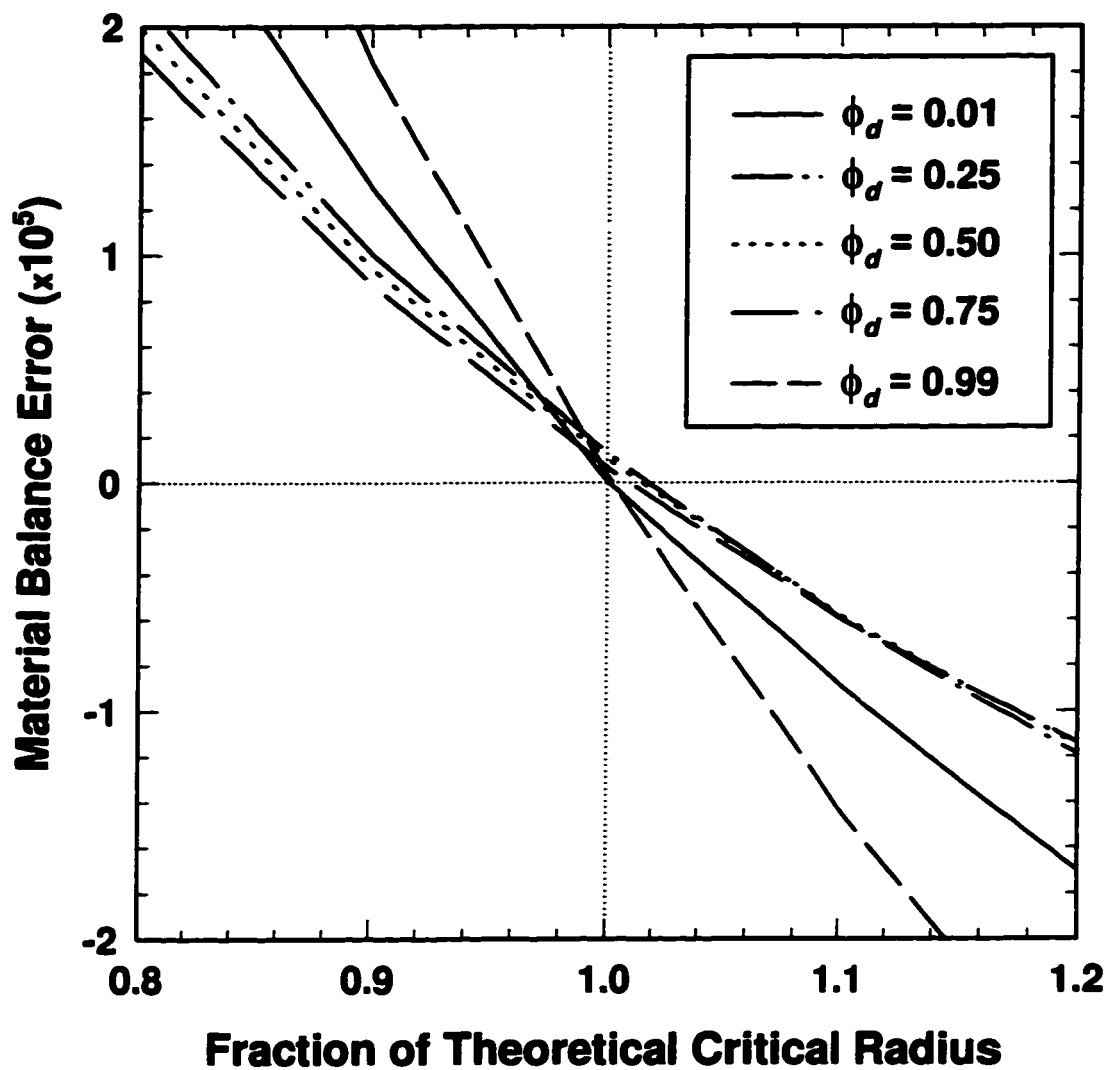


Figure 6.10: Computed material balance error as a function of the critical radius.

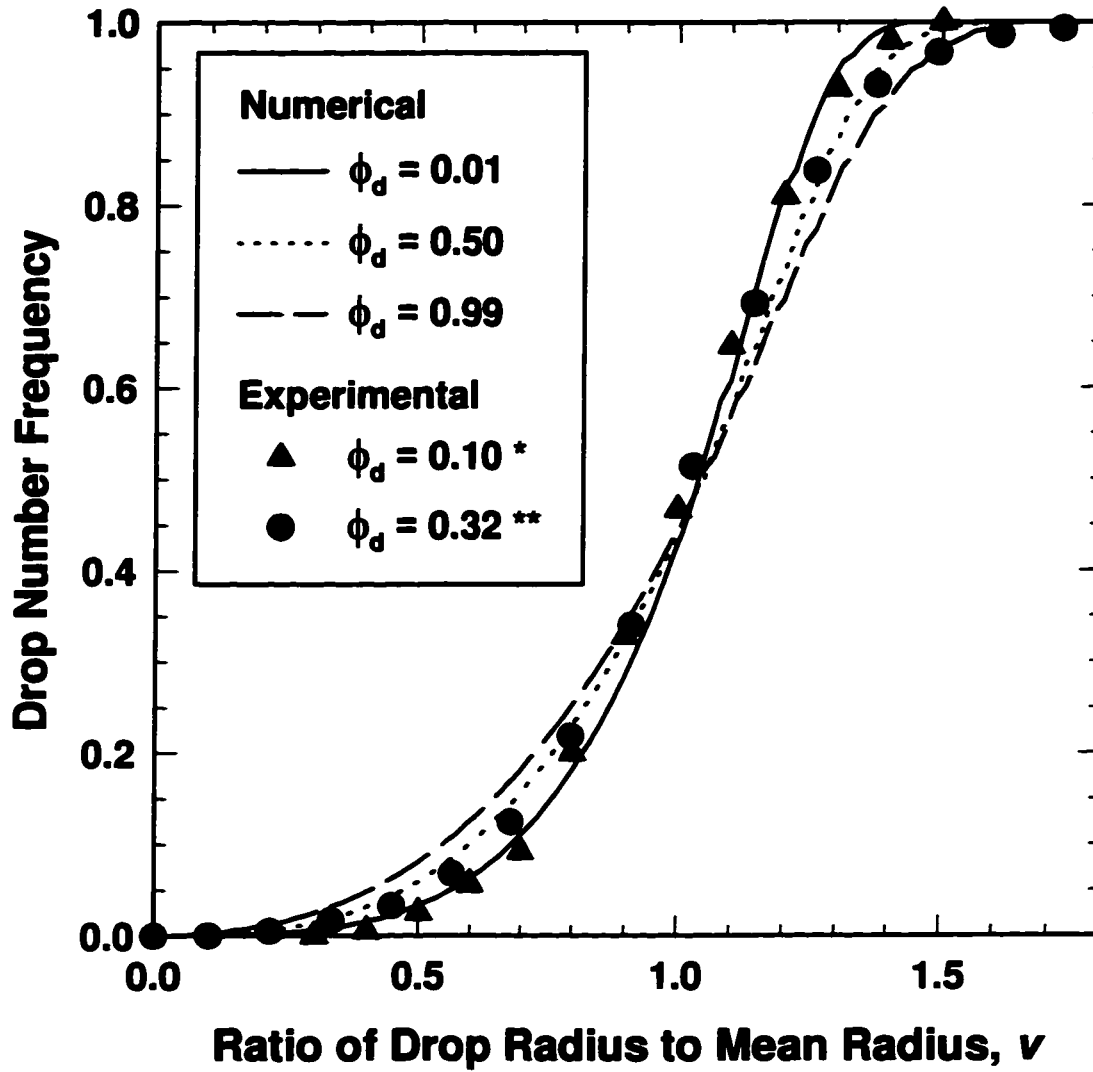


Figure 6.11: Comparison of numerically predicted and experimental cumulative frequency distributions (* ref. 11, ** ref. 2).

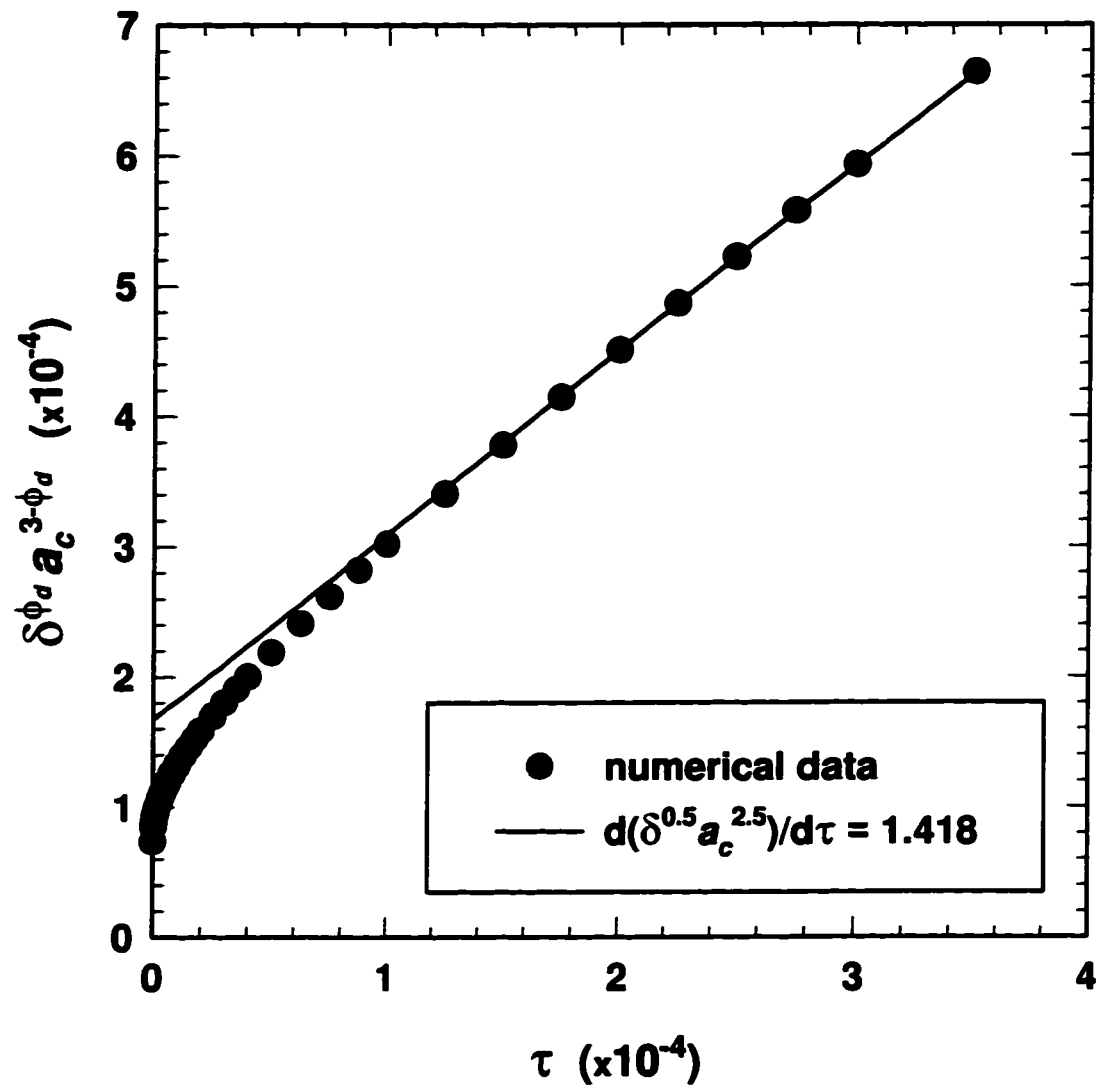


Figure 6.12: Growth rate for a system with a dispersed phase volume fraction 0.5.

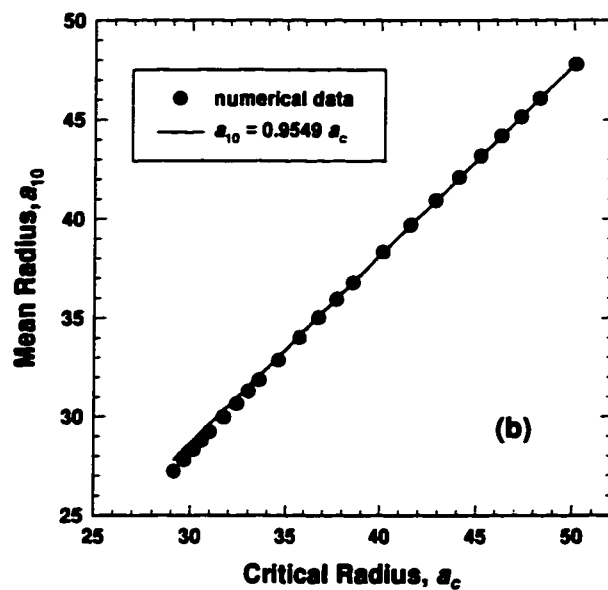
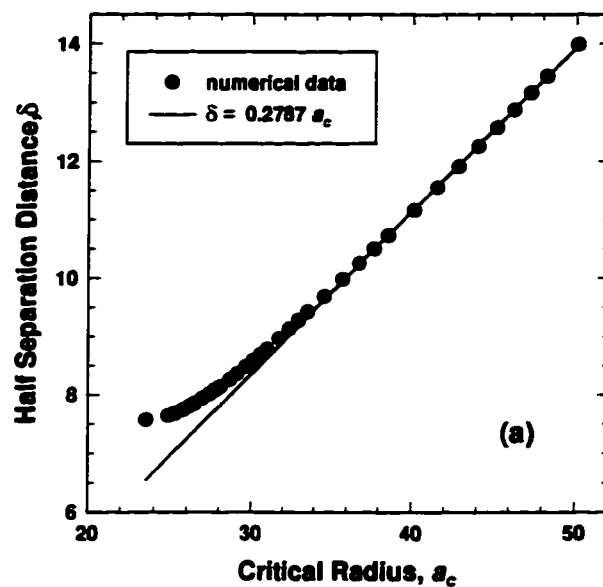


Figure 6.13: System with a dispersed phase volume fraction of 0.5. a) half separation distance versus critical radius
b) mean radius versus critical radius

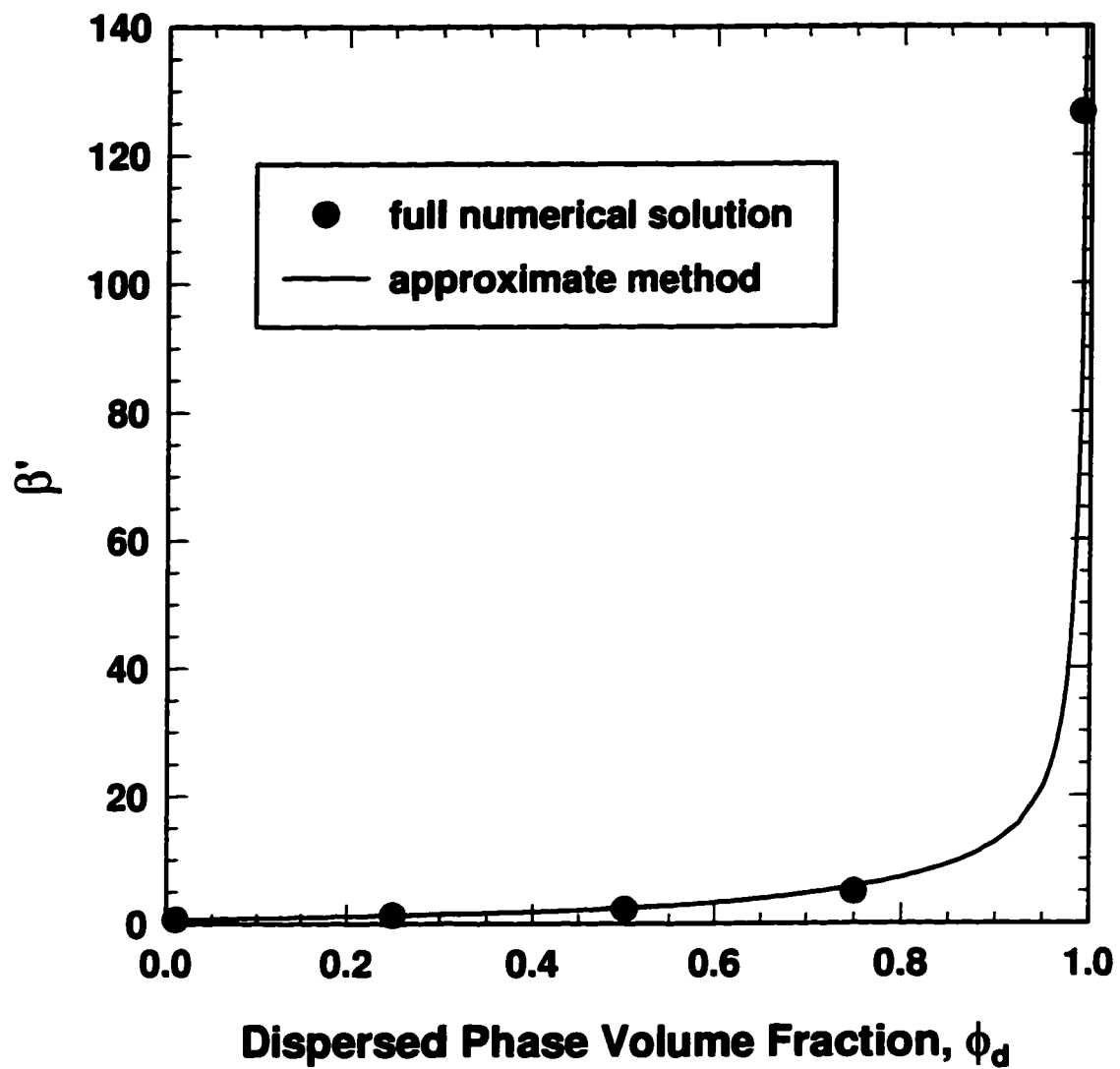


Figure 6.14: Growth rate, β' , for all dispersed phase volume fractions.

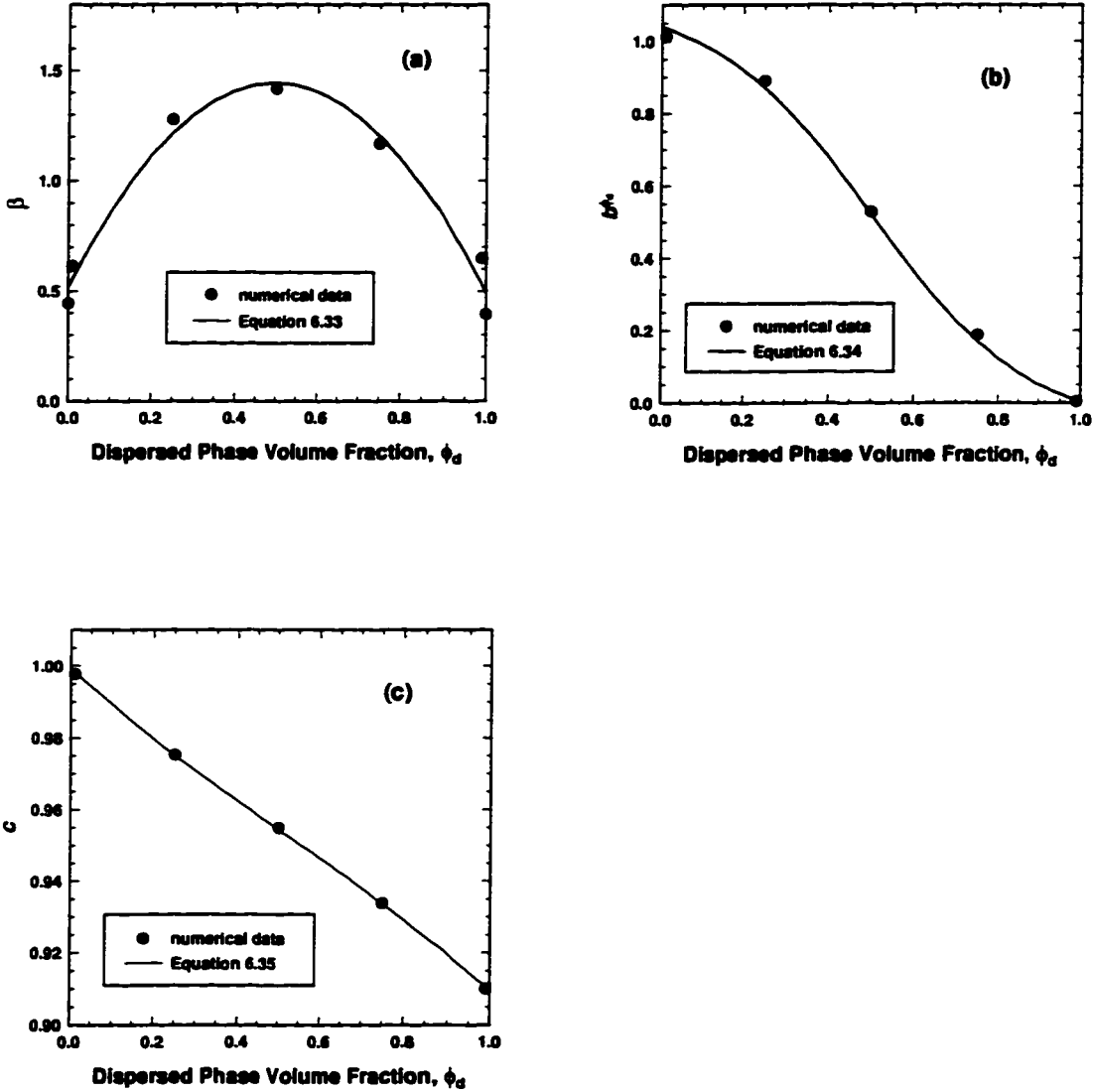


Figure 6.15: Curve fits for: a) the growth rate, β ; b) the proportionality constant, b ; c) the proportionality constant, c .

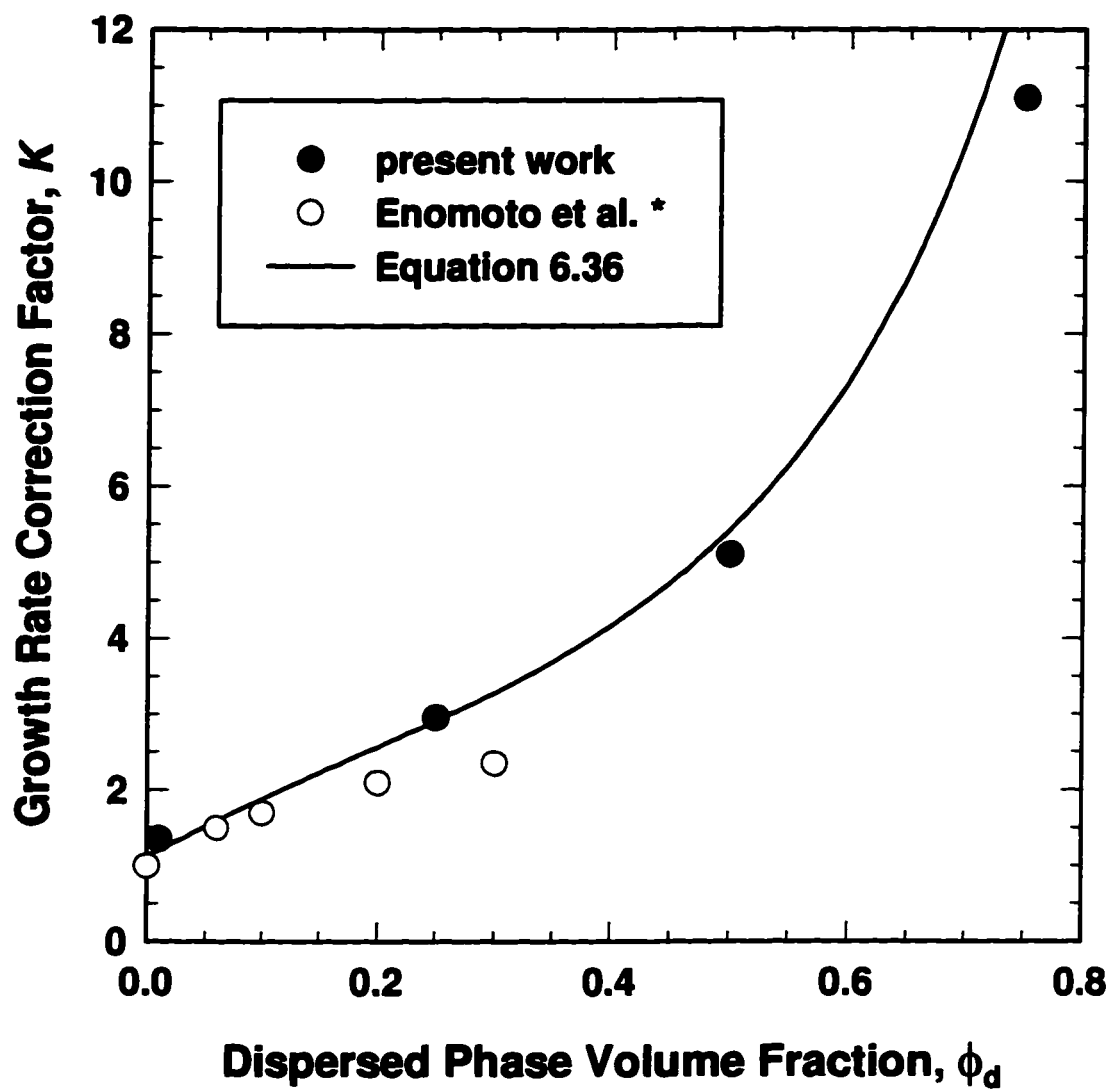


Figure 6.16: Growth rate correction factor for dispersed phase volume fractions less than 0.80 (* ref. 11).

Chapter 7

CONCLUSIONS AND RECOMMENDATIONS

Three objectives for the thesis were set out in Chapter 1:

1. Measure and predict the solubility of asphaltenes in toluene/hexane mixtures.
2. Determine what phase of the asphaltenes adsorbs on the interface of water-in-hexane/toluene emulsions.
3. Examine the stability of water-in-hexane/toluene emulsions stabilized by asphaltenes.

The conclusions and recommendations arrived at for each objective are considered in turn. The implications for emulsion treatment are also discussed.

7.1 Asphaltene Solubility

The solubility of asphaltenes was measured in toluene/hexane solutions and several other organic solvent mixtures. Sufficiently low asphaltene concentrations were prepared to avoid the formation of micelles. Hence, a solid/liquid equilibrium calculation could be employed to predict the solubility of the asphaltenes. The solid-liquid calculation requires a feed composition and equilibrium ratios for each component. The asphaltenes were treated as a multicomponent mixture of asphaltene subfractions, each with a different molar mass and equilibrium ratio.

The equilibrium ratios for the equilibrium calculation were determined from Scatchard-Hildebrand theory with a Flory-Huggins entropy of mixing term. The asphaltenes were assumed to precipitate as a solubilized (swollen) polymer. The molar volumes and solubility parameters of the asphaltenes are required to apply the solubility theory. Both

the molar volume and the solubility parameter were correlated to the molar mass of the asphaltenes with the use of experimental measurements of asphaltene density. The molar mass distribution of the asphaltenes was determined from interfacial tension and vapor pressure osmometry measurements.

The thermodynamic solubility model contained one unknown physical property, the change in the asphaltene heat of vaporization as the molar mass changes. A value for the term was estimated by fitting the model prediction to the experimental data for the toluene/hexane solvent system. The completed model successfully predicted the solubility of asphaltenes in a variety of non-polar or slightly polar organic solvents. The model provided poor predictions for highly polar solvents and, curiously, for cyclohexane as well. It is generally recognized that Scatchard-Hildebrand theory does not apply well to polar solvents. However, the reason for the failure to predict asphaltene solubility in cyclohexane is not certain.

Despite some limitations, the thermodynamic model performed well for many solvent systems. The model provides sufficient understanding of asphaltene solubility to interpret the emulsion stabilization experiments discussed later. It would be extremely useful to extend the model to the conditions experienced in the oil industry, such as, high temperature and pressure, high asphaltene concentration and crude oil solvents. To extend the model, solubility experiments could be conducted with asphaltenes from different sources at different temperatures and pressures. The solvent properties of crude oils need to be tested and correlations developed based on easily obtained crude oil properties, such as the solubility class fractions (SARA). Finally and perhaps of greatest interest and challenge, the formation and effect on solubility of asphaltenes micelles has yet to be examined.

The structure of the asphaltenes micelles and even of precipitated asphaltenes is not well understood. Several colloidal and micellar theories have been advanced but experimental evidence is limited and contradictory. Since the asphaltene structure is unknown, all

solubility theories rest on uncertain assumptions. Hence, experiments to elucidate the asphaltene structure are a necessary complement to asphaltene solubility work. Perhaps further clues could be obtained by examining asphaltenes in solvents where asphaltene micelles are known to exist, for instance, pyridine. Measurements of heats of fusion and micellization can indicate the nature of any phase change. Andersen and Birdi have performed calorimetry experiments for the asphaltene heat of micellization above the cmc in toluene (1). The heats of fusion could be examined by calorimetry as well.

7.2 Asphaltenes Adsorption on a Water/Hydrocarbon Interface

The fraction of asphaltenes responsible for stabilizing water-in-oil emulsions was determined by measuring the surface area of the stable emulsions. The emulsions were prepared from asphaltene subfractions each with a different proportion of soluble to insoluble asphaltenes. Sufficiently low asphaltene concentrations were employed to prevent the formation of micelles. Therefore, the asphaltene phases available to stabilize the emulsion were precipitated particles or soluble molecules. The experiments demonstrated that the surface area stabilized was proportional to the amount of soluble asphaltenes. The amount of precipitate had no effect on the emulsion surface area. Hence, asphaltenes appear to stabilize emulsions as a molecular surfactant.

Stabilized surface areas were determined over a wide range of asphaltene concentrations, water volume fractions and hexane:toluene ratios. Only a fraction of the soluble asphaltene were found to be surface active. The mass ratio of surface active to soluble asphaltenes, f_a , depends on the hexane:toluene volume ratio. The value of f_a increases as the hexane:toluene ratio increases. However, surface active asphaltenes were observed for all soluble asphaltene subfractions and hence throughout the asphaltenes molar mass distribution.

The interpretation that only part of the asphaltenes is surface active is consistent with the concept of asphaltenes as a mixture of many molecular species of various molar masses and elemental composition. Some of those species have been shown to be acidic, basic or

amphoteric (2). Very likely, these are the surface active species. The group of surface active species is probably a mixture of molecules with a broad range of surface activities. The change in surface activity in different solvents reflects the variety of surface activities. The change in the surface active fraction likely results from the change in the balance of hydrophilic and hydrophobic forces between the asphaltene molecules and the water and hydrocarbon phases. In a good organic solvent, the asphaltenes are less strongly bound to the interface and the less surface active species become, in effect, non-surface active.

The conclusions about the asphaltenes surface activity are inferred from the emulsion surface area measurements. It would be useful to obtain confirmation through more direct measurements of the asphaltene properties. For instance, the asphaltenes on the interface could be isolated and analyzed for their acidic, basic and amphoteric (non-neutral) content as well as their molar mass. If the conclusions about asphaltene surface activity are correct, the adsorbed asphaltenes are expected to consist of primarily non-neutral species with a broad range of molar mass.

7.3 Stability of Water-in-Toluene/Hexane/Asphaltene Emulsions

The drop size distributions of asphaltene stabilized water-in-toluene/hexane emulsions were measured over time. The mean diameter and Sauter mean diameter were calculated for each distribution. Over time, smaller droplets appeared accumulated while large droplets grew. The mean diameter was invariant with time while the Sauter mean diameter increased.

The increase in the Sauter mean diameter indicates that the emulsion surface area decreasing; *i.e.*, the emulsion is destabilizing. There are only two forms of instability that result in a change in drop size distribution: coalescence and Ostwald ripening. The appearance of small droplets is inconsistent with coalescence but does occur with Ostwald ripening. However, the invariant mean diameter and the accumulation of small droplets are inconsistent with standard Ostwald ripening. In standard ripening the smaller

droplets continue shrinking until they disappear. The observed accumulation of small droplets in the asphaltene stabilized emulsions suggests that shrinkage is retarded.

The cause of the shrinkage retardation is unknown. Two possible explanations for the retardation are: a thickening of the asphaltene interfacial membrane; or a change in the diffusivity through the membrane and the interfacial tension between the membrane and the water. In either case, some of the asphaltenes must be irreversibly adsorbed on the interface. In the former hypothesis, the volume of the membrane remains constant as the droplet shrinks. The thickening membrane presents a greater barrier to the diffusion of water from the droplet. In the latter case, the membrane contracts along with the droplet increasing its density but decreasing the diffusivity and interfacial tension. A decrease in diffusivity and interfacial tension retards the ripening rate. At present, the explanations for the observed drop size distributions are speculative. More information can be obtained by examining pairs or small numbers of droplets over time under a microscope. The occurrence and retardation of Ostwald ripening could then be confirmed directly. Once a hypothesis for the retarded ripening process is developed, it can be tested employing the numerical model presented in Chapter 6.

7.4 Implications for Treating the Oil Sands Emulsion

The emulsion experiments presented in this thesis confirm that asphaltenes are capable of stabilizing water-in-toluene/hexane emulsions. The asphaltenes appear to act as molecular surfactants and form a strong membrane on the interface. The asphaltene stabilized emulsions are qualitatively similar to the oil sands emulsion (the water-in-oil emulsions formed in the oil sands process). For instance, the oil sands emulsion tends to flocculate in aliphatic solvents but is resistant to coalescence in both aliphatic and aromatic solvents even when centrifuged (3). The same behavior was observed for the asphaltene stabilized water-in-toluene/hexane emulsions. The similarities in behavior do not prove that asphaltenes are responsible for stabilizing the oil sands emulsions. However, the similarities confirm that asphaltenes are a leading candidate as the

stabilizer. Therefore, it is useful to consider treatments for breaking asphaltene stabilized emulsions.

7.4.1 Mechanical Treatments

Mechanical treatments attempt to concentrate an emulsion and force close contact between droplets in order to accelerate coalescence. Filtering, centrifuging and electrostatic aggregation are examples of mechanical treatments. The occurrence of Ostwald ripening and the strength of the asphaltene interfacial membrane are a problem for most mechanical treatments. Simply concentrating the emulsions may not be sufficient to induce coalescence, especially between the accumulated small droplets. The asphaltene membrane on droplets that have shrunk through retarded Ostwald ripening must be very rigid to prevent the droplets from shrinking further. Such a rigid membrane could easily prevent coalescence even between droplets that are in close contact. Indeed, the oil sands emulsion that survives centrifuging may well consist of these shrunken drops.

Mechanical treatments that disrupt the membrane are more likely to be successful. For instance, treating the emulsion in high shear may rupture the membrane and permit coalescence. However, the shear conditions must be controlled so that the droplets that coalesce are not broken into smaller droplets. If both coalescence and breakage occur, the emulsion may persist. A possible alternative to careful control of the shear conditions is to change the solvent to one in which the asphaltenes are insoluble, such as an aliphatic solvent. The asphaltene membrane is likely to be very rigid in an aliphatic solvent. Furthermore, the asphaltene cannot easily migrate through the continuous phase. Hence, when droplets are broken in high shear the membrane may not reform to completely cover the surface. In such conditions, coalescence is favored over breakage.

Another mechanical means of disrupting the membrane is to strip off the continuous phase. The asphaltene stabilized emulsions were observed to be unstable in air. Very likely, as the continuous toluene/hexane phase evaporated into the air, the asphaltenes on

the interface solidified and could no longer stabilize the emulsion. Hence, any device that efficiently strips off the continuous phase is likely to be an effective treatment for asphaltene stabilized emulsions.

7.4.2 Chemical Treatments

Chemical treatments change the chemical environment of the emulsion in order to induce coalescence. Adding a solvent or surfactant are examples of chemical treatments.

Adding a solvent can destabilize an emulsion by causing surface active material to desorb from the interface. However, a significant proportion of the asphaltenes are surface active even in aromatic solvents. Hence, adding a solvent is not likely to completely break asphaltene stabilized emulsions. On the other hand, aliphatic solvents can be used to flocculate and separate dilute water-in-oil emulsions as a first step in treatment. And, as discussed previously, an aliphatic solvent can be used to assist a mechanical emulsion treatment.

Adding a surfactant is a very common method for treating emulsions. The surfactant is designed to replace the emulsion stabilizer on the interface and allow the emulsion to coalesce. Hence, a surfactant is chosen that is more surface active than the asphaltenes but small enough so as not to form a barrier to coalescence itself. However, there are several pitfalls to employing surfactants. The surfactant can lead to the formation of an inverse oil-in-water emulsion and/or the formation of mixed surfactant-asphaltene micelles. Both an inverse emulsion and the formation of mixed micelles can prevent a clean separation of the oil and water. Finally, the surfactant can be costly and is itself a potential contaminant that may need to be recovered after treating the emulsion.

Nonetheless, the addition of an appropriate surfactant is an effective treatment for many emulsions.

7.4.3 Recommended Treatments

Treatments that disrupt the interface are the most likely to succeed for an asphaltene stabilized emulsion. Conventional mechanical treatments can serve to concentrate the

emulsion or the same result can be achieved with the addition of an aliphatic solvent. The most effective means for breaking the emulsions have yet to be investigated. Two promising research avenues are: high shear treatments of the emulsions in aliphatic solvents; and treatment by the addition of a surfactant.

7.5 References

1. Andersen, S.I., and Birdi, K.S., *J. Colloid Interface Sci.*, **142**, (1991), 497.
2. Bestougeff, M.A., Byramjee, R.J., in "Asphaltenes and Asphalts, 1", Ed. T.F. Yen and G.V. Chilingarian, Elsevier Science, Amsterdam, 1994, p. 67.
3. Long, Y., Tipman, R.N., Tran, T., "Studies on Water, Chloride and Solids Removal from Froth to Enhance Diluted Bitumen Quality", Syncrude Research Monthly Report, Syncrude Canada Ltd., November 1994.

Appendix A

MEASUREMENT OF ASPHALTENE PHYSICAL PROPERTIES

A.1 Density

Densities were measured with an Anton Paar DMA 45 density meter calibrated with demineralized water and toluene. Density measurements with this instrument are generally accurate to $\pm 0.03 \text{ kg/m}^3$.

Densities are calculated from the density meter readings with the following equation (1),

$$\rho = \frac{R_{dm}^2 - B_{dm}}{A_{dm}} \quad (\text{A.1})$$

where ρ is the density (g/cm^3), R_{dm} is the meter reading and A_{dm} (cm^3/g) and B_{dm} are coefficients that are determined from calibration with two pure components. The calibration equations for A_{dm} and B_{dm} are given by

$$A_{dm} = \frac{R_{dm1}^2 - R_{dm2}^2}{\rho_2 - \rho_1} \quad (\text{A.2})$$

and

$$B_{dm} = R_{dm1}^2 - A_{dm}\rho_1 \quad (\text{A.3})$$

where the subscripts 1 and 2 denote the pure components used for the calibration. Densities were measured for mixtures of asphaltene and toluene with asphaltene concentrations ranging from 2 to 10 kg/m^3 . In the first set of data, the “solids” were not separated from the asphaltenes prior to taking the measurements. The raw data and calculated densities for asphaltene-solids/toluene mixtures using asphaltene subfractions precipitated from

toluene/hexane solutions of 0.00, 0.20, 0.25, and 0.33 volume fraction toluene are given in Tables A.1 to A.4 respectively. The mixture specific volumes are plotted against asphaltene mass fraction for the same respective asphaltene subfractions in Figures A.1 to A.4.

For the second set of data, the “solids” were precipitated from the asphaltenes prior to obtaining the asphaltene subfractions, i.e., the density measurements are for “solids”-free asphaltenes. The raw data and calculated densities for asphaltene-solids/toluene mixtures using asphaltene subfractions precipitated from toluene/hexane solutions of 0.00, 0.20, 0.25, and 0.33 volume fraction toluene are given in Tables A.5 to A.8 respectively. The mixture specific volumes are plotted against asphaltene mass fraction for the same respective asphaltene subfractions in Figures A.5 to A.8 respectively.

The slopes and intercepts from Figs. A.1 to A.8 were used to determine the density of the asphaltene subfractions as discussed in Section 2.4.2. The asphaltene density was calculated using Eq. 2.9 and 2.10 for the asphaltene/toluene mixtures and asphaltene-solids/toluene mixtures respectively. The calculated densities are listed in Table 2.1.

A.2 Interfacial Tension

A.2.1 Method

Interfacial tensions of oil over demineralized water were measured with a Fisher deNouy ring tensiometer accurate to ± 0.5 mN/m. For each measurement, the platinum ring was placed in the water, the organic phase was added dropwise to the water surface and the two phase system left to equilibrate for the desired length of time before the ring was pulled through the interface. Before each measurement, the surface tension of the water was checked and, after each measurement, the ring was cleaned in toluene and any traces of hydrocarbon burned off. All measurements were corrected for the solvent density using an equation (2) based on the Harkins and Jordan tables (3) and given by,

$$\frac{\sigma}{\sigma_m} = 0.7250 + \left(\frac{0.01452\sigma_m}{p_r^2 \Delta\rho} + 0.04534 - \frac{1.679}{\xi_r} \right)^{1/2} \quad (\text{A.4})$$

where σ_m and σ are the measured and corrected interfacial tensions (mN/m) respectively, p_r is the circumference of the platinum ring (cm), ξ_r is the ratio of the radius of the ring to the radius of the wire and $\Delta\rho$ is the density difference between the two phases (g/cm^3). In this case, p_r is 5.995 cm and ξ_r is 53.2.

All measurements were taken at 22 °C. Surface tensions and interfacial tensions versus water for several systems are compared with literature values in Table A.9. The experimental values were measured after 1 minute. The corrected values are consistently 2-3 mN/m below published values for similar substances. The reason for the discrepancy is not clear but may arise from errors in the correction factor equation, impurities in the solvent or most likely from the technique of the experimenter. For example, Nianxi Yan and Harvey Yarranton repeatedly measured water surface tensions of 75 and 76 mN/m respectively on the same sample. Fortunately the discrepancy is systematic and affects the absolute values of the interfacial tension but not the slope of the interfacial tension versus a given component, e.g. asphaltene. Since the slope of interfacial tension was the only result of interest, the source of error was not pursued further.

Interfacial tension changes with time as some mixing occurs between the two phases after contact and, in multicomponent systems, the composition at the interface changes until equilibrium is reached. To determine how long the systems of interest take to reach equilibrium, interfacial tensions were measured for mixtures of toluene and hexane over water. Raw and corrected data are given in Tables A.10 and A.11 respectively. After 1 hour, the interfacial tension does not change significantly. Interfacial tension as a function of composition is plotted in Figure A.9. Clearly, interfacial tension decreases some 2-3 mN/m until equilibrium is reached. If the equilibrium values are compared with literature values the difference is in the order of 5 mN/m. Such a large difference indicates that the systems are contaminated or that the literature values may not represent

true equilibrium conditions. The discrepancy appears to be systematic and the slope of interfacial tension versus asphaltene composition determined from this method agrees well with literature data as discussed in Section 2.4.3. Therefore, the matter was not pursued further.

Similar time dependent behavior was observed by Sheu et al (7) in interfacial tension measurements of asphaltene/toluene over 1 N NaOH solutions as shown in Fig. A.10. The interfacial tensions decreased to within 5-15 % of the equilibrium value after 1 hour and to within 1% after two hours . Ideally, two hours should be allowed for the systems to reach equilibrium. However, in our experiments, evaporation of the solvent is a consideration and the experiments should be conducted in the minimum time possible to achieve consistent results. Therefore, an error of approximately 10% was accepted and the systems were left for 1 hour to reach equilibrium.

A.2.2 Results

Raw and corrected data for the interfacial tension after 1 hour of asphaltene-solids/toluene/hexane solutions over water are given in Tables A.12 and A.13 respectively. The corrected data are plotted for asphaltene in toluene/hexane mixtures of 20, 25, 33, 40 and 50 vol% toluene in Figs. A.11 to A.15 respectively. The slopes from these figures were used to calculate the molar mass of the asphaltenes as discussed in Section 2.4.3. The data used to examine the effect of precipitate on measured interfacial tension is provided in Table A.14.

The asphaltenes used in all the preceding measurements, except those in Table A.14, were part of a single extraction from bitumen where the recovered asphaltene made up 14.5% of the bitumen. The asphaltenes used to obtain the data in Table A.14 came from an extracted sample that made up 13% of the bitumen. In Fig A.16, the interfacial tension of asphaltenes from the two different extractions in a toluene/hexane solution of 25 vol% toluene over water are compared and a slight difference in slope is apparent. The asphaltenes from the two extractions likely have slightly different molar mass

distributions leading to different slopes on the interfacial tension plot. The small difference highlights the importance of using consistent samples.

Interfacial tension measurements of asphaltene in 1,2-dichlorobenzene and in cyclohexane are given in Tables A.15 and A.16 respectively. The corrected data of Table A.16 is plotted in Fig. A.17. The interfacial tension of asphaltene/1,2-dichlorobenzene over water does not vary with asphaltene concentration indicating the presence of micelles. The presence of micelles may influence vapor pressure osmometry determinations of asphaltene molar mass and will be discussed in more detail in Section A.3.1. Fig. A.17 shows that the interfacial tension of asphaltene/cyclohexane over water is linearly related to the log of the asphaltene concentration and therefore there are no micelles over the concentration range examined.

It is interesting to note that the slope on Fig. A.17 corresponds to an asphaltene molar mass of 2246 g/mol using the methods of Section 2.4.3. Note that 70 wt% of the asphaltenes are soluble in pure cyclohexane. The molar mass in cyclohexane is 68% of the value of approximately 3300 g/mol determined in toluene at an f_{sol} of 0.70. While the measurements were taken using asphaltenes from different extractions, the discrepancy is large enough to suggest that asphaltenes are solubilized differently in different solvents. For example, the asphaltenes may form monomers in one solvent and dimers in another. Alternatively, the asphaltene molecules may form complexes with the solvent and the measured molar masses may be the masses of the complexes rather than the molecules and therefore are a function of the solvent as well as the asphaltene. In either case, the molar mass distribution determined in Chapter 2 may only be valid for some solvents.

A.3 Vapor Pressure Osmometry

A.3.1 Theory

Vapor pressure osmometry is based on the difference in vapor pressure between a pure solvent and a dilute solution of the component of interest and the solvent (8). Two thermistors are sealed in a vessel containing the saturated vapor of the solvent. A drop of

pure solvent is placed on one thermistor and a drop of the dilute solution on the other. The vapor pressure of the solution is lower than that of the solvent and solvent condenses from the surrounding saturated vapor. The heat released from the condensing solvent warms the drop of solution until its vapor pressure matches that of the surroundings. For dilute solutions, the temperature difference between the two thermistors is related to the concentration and molar mass of the solute as follows,

$$\Delta T = \left(\frac{RT^2 M_m}{1000 \rho_m \Delta H_m^{vap}} \right) \frac{C}{M} \quad (\text{A.5})$$

where ΔT is the temperature difference between the thermistors (K), R is the universal gas constant, (J/mol K), T is the temperature, (K), M_m is the molar mass of the solvent, (g/mol), ΔH_m^{vap} is the molar heat of vaporization, (J/mol), C is the concentration of the solute (kg/m^3) and M is the molar mass of the solute, (g/mol). For small temperature differences, the temperature difference between the thermistors is proportional to the resistance. Hence, Eq. A.5 can be replaced by

$$\Delta R_{vpo} = \frac{K_{vpo} C}{M} \quad (\text{A.6})$$

where R_{vpo} is resistance and K_{vpo} is a constant determined from calibration. The above described theory does not account for heat losses through radiation and conduction. However, the heat losses are independent of the solute concentration and molar mass in the dilute conditions and can be accounted for in the calibration.

As long as there is no molecular association of the solute, i.e. no formation of micelles, molar mass is independent of concentration. If micelles are formed the resistivity will be proportional to the non-associated solute concentration rather than the total solute concentration. Above the critical micelle concentration, the non-associated solute concentration is constant and so is the resistivity. Hence, considering Eq. A.6, molar mass

will appear to increase linearly with solute concentration. In fact, this behavior has been observed for asphaltenes in 1,2-dichlorobenzene at low temperature (9). Therefore, molar masses are usually measured at several solute concentrations in order to determine if micelles are present.

A.3.2 Results

Molar masses were determined with a Westcan Instrument Inc. Model 232A vapor pressure osmometer calibrated with benzil. Measurements were taken in toluene and 1,2-dichlorobenzene. Asphaltene molar masses in toluene were determined at 50 °C for a concentration range of 1.5 to 4.5 gram asphaltene per litre toluene. Measurements of the molar mass of asphaltene-solids and solids-free asphaltenes in toluene are given in Tables A.17 and A.18 respectively. Molar mass is independent of asphaltene concentration for the range of concentrations examined indicating that no micelles are present. Similar results were obtained for asphaltenes in benzene (10). Both vapor pressure osmometry and interfacial tension measurements demonstrate that asphaltenes do not form micelles in toluene at concentrations up to 40 kg/m³ for temperatures between 22 and 50 °C.

Interfacial tension measurements in Section A.2.2 indicate that asphaltenes form micelles in 1,2-dichlorobenzene at 22 °C. VPO measurements of asphaltene in 1,2-dichlorobenzene in the literature (9) confirm the presence of micelles at low temperature but show that the micelles are not present at 120 °C, Fig. A.18. On Fig. 1.18, the measured molar masses at 70 and 129 °C converge at a near zero asphaltene concentration. Similarly, the interfacial tensions of asphaltene in 1,2-dichlorobenzene are constant down to an asphaltene concentration of 0.044 kg/m³ or 0.003 wt%. In other words, micelles form in 1,2-dichlorobenzene at very low asphaltene concentrations at temperatures below 70 °C. However, there are no micelles and hence asphaltene VPO molar mass is independent of concentration in 1,2-dichlorobenzene at 120 °C. Therefore, in that solvent, a single measurement at 120 °C was taken for each sample. The results are given in Table A.19.

As discussed in Section 2.4.3, the measured molar mass in 1,2-dichlorobenzene is 2.2 times smaller than that measured in toluene. Since there is no micellization in either system the difference must be caused by some other factor. However, at present no hypotheses fit the facts. For example, dimerization or similar asphaltene interactions should exhibit a concentration dependence, yet there is none. Asphaltenes may form complexes with the solvent but the number of complexes equals the number of asphaltene molecules. Therefore, the ratio of C/M in Eq. A.5 is identical for complexes and asphaltene molecules. Hence, as long as the asphaltene concentration is used in the calculation then the asphaltene molar mass is determined even if complexes have formed. Finally, Eq. 1.5 is based on an ideal solution and any departures from ideality may affect the temperature change and the measured molar mass. However, the measurements are made at extremely dilute conditions and any non-ideality should be negligible. At this time, there is no satisfactory explanation for the discrepancies in measured molar mass. Consequently, as with the molar masses calculated from interfacial tension measurements, the VPO determined molar masses may only be valid for some solvents.

A.4 Asphaltene Sample Storage and Oxidation

The asphaltenes precipitated from the Athabasca bitumen were stored in glass jars in air. There is some concern that the precipitated asphaltenes can oxidize and exhibit properties differing from those of the asphaltenes in the original oil. While no attempt was made to prevent contact with air in the experiments presented in this thesis, the results are consistent with those observed for asphaltenes recovered and stored under nitrogen. For example, the measured interfacial tension of nitrogen stored Ratawi vacuum residue in toluene over water has been found to range from 27-31 mN/m at residue concentrations from 0.2 to 0.9 kg/m³ (11). The range of values measured here for Athabasca asphaltenes at identical conditions was 27-29 mN/m. Considering that the asphaltenes came from different sources, the agreement is very good. In addition, the surface area of an average asphaltene molecule derived from the slope of a surface tension versus log asphaltene concentration plot was 4.5 nm² for nitrogen stored Ratawi asphaltenes in pyridine (12). The surface area for air stored Athabasca asphaltenes found from interfacial tension

measurements in toluene over water was 4.75 nm^2 . Clearly, oxidation does not appear to affect the interfacial tension of asphaltene solvent systems.

The interfacial tension of asphaltenes in solvents is likely governed by the relative proportions and structure of the heteroatoms and the hydrocarbon skeleton of the asphaltene molecules. Therefore, interfacial tension may be expected to be sensitive to the oxidation state of the asphaltenes and should be a good indicator if the oxidation is changing the asphaltene properties. In the experiments presented here, oxidation does not appear to be a factor.

A.5 UV Measurements of Asphaltene Concentration

All the measurements of asphaltene concentration in this thesis were obtained gravimetrically. In some cases, it was not possible to measure a concentration of interest gravimetrically, for example, the concentration of asphaltenes in solution after emulsification. UV absorbance is an alternative technique for measuring the concentration of a solute. The amount of ultraviolet light absorbed by a dilute solution is related to the concentration of the solute by Beer's Law (13):

$$\frac{I}{I_o} = \exp\{-K_{uv}C\} \quad (\text{A.7})$$

Here, I_o is the incident light intensity, I is the intensity of the light that passes through the sample, K_{uv} is the absorption coefficient for the sample at a specific wavelength of light and C is the concentration of the solute. K_{uv} is found by calibration. For convenience, Eq. A.7 is usually expressed as follows:

$$A_{uv} = K_{uv}C \quad (\text{A.8})$$

where $A_{uv} = -\ln(I/I_0)$ is the absorbance. In principle, once the calibration equation is determined, the concentration of the solute can be found simply by measuring its absorbance.

The UV technique was tested on solutions of asphaltene-solids in toluene and a suitable calibration was obtained at a wavelength of 800 nm. The calibration is shown in Fig. A.19. The good calibration is a promising start. However, for this technique to be useful for our work, it must provide consistent results for solutions of asphaltene-solids in toluene and hexane and for solutions in contact with water.

First consider solutions of toluene and hexane. The absorbance of hexane and toluene are within 0.002 of each other at 800 nm. Hence, the toluene calibration curve should apply to the toluene/hexane solutions as long as the asphaltenes show the same properties in both solutions. As we saw in Chapter 2, the asphaltenes soluble in the toluene hexane mixtures may have quite a different molar mass distribution from asphaltenes in toluene. The uv absorbance may change as the molar mass distribution changes. Therefore, the calibration must be tested for asphaltene-solids in toluene/hexane mixtures.

Solutions of asphaltene in toluene and hexane were prepared and the precipitated asphaltenes removed by centrifugation. The amount of precipitate was measured and the concentration of the asphaltenes in solution determined from the difference between the mass of precipitate and the original mass of asphaltenes. Then the uv absorbance in the supernatant was measured. The uv absorbance in toluene/hexane solutions decreased over 15-30 minutes to an equilibrium value. The decrease in absorbance is likely caused by the small fraction of insoluble asphaltenes left in the supernatant settling from the solution. The equilibrium value is reported in Table A.20. The absorbance in toluene solutions was constant. The concentrations determined from the uv absorbance are compared with the gravimetric measurements in Table A.20 for two solutions. The predicted concentrations are low by approximately 0.3 kg/m^3 or 30%.

The error may arise from the different asphaltene molar mass distribution in each solvent mixture. Another explanation may be the effect of the “solids” in the asphaltene-solids on the measured uv absorbance. The presence of solids increases the observed absorbance. It was shown in Chapter 2 that the “solids” are precipitated out in toluene/hexane mixtures but remain in solution in toluene. The constant absorbance in toluene solutions confirms that the “solids” are not settling. Hence, the calibration curve applies to asphaltene-solids but the measurements in toluene/hexane solutions are for solids-free asphaltenes. The predicted concentrations are expected to be too high.

A new calibration curve for solids-free asphaltenes in toluene could be found and tested on toluene/hexane mixtures. However, the approach was abandoned because the presence of water also affected the measured uv absorbance. A 1 kg/m³ solution of asphaltenes in toluene was placed in contact with water for an hour. Then the absorbance of a sample of the water contacted toluene solution was measured. The measured absorbance is compared with the calibration curve on Fig. A.19. The absorbance of the water contacted sample is substantially higher than the predicted absorbance for a water-free sample. Water is slightly soluble in toluene and the increase in absorbance may arise from the small amount of water in solution.

A.6 References

1. DMA 02C Instruction Manual, Digital Precision Density Meter, Anton Paar, A-8054 Graz, Austria, Europe.
2. Fisher Scientific surface tensiometer manual.
3. Harkins, W.D., and Jordan, H.F., *J. Amer. Chem. Soc.*, **52**, (1930), 1751.
4. Adamson, A.W., “Physical Chemistry of Surfaces”, 2nd Ed., Interscience Publishers, John Wiley & Sons, 1967, p57.
5. Ross, S., and Patterson, R.E., *J. Chem. Eng. Data*, **24**, (1979), 111.
6. Li, B., and Fu, J., *J. Chem. Eng. Data*, **37**, (1992), 172.
7. Sheu, E.Y., De Tar, M.M., and Storm, D.A., *Fuel*, **71**, (1992), 1277.
8. Burge, D.E., “Molecular Weight Measurements by Osmometry”, Reprint June 1977 Issue of American Laboratory.

9. Wiehe, I., *Ind. Eng. Chem. Res.*, **31**, (1992), 530.
10. Moschopedis, S.E., Fryer, J.F., and Speight, J.G., *Fuel*, **55**, (1976), 227.
11. Sheu, E.Y., Storm, D.A., and Shields, M.B., *Fuel*, **74**, (1995), 1475.
12. Taylor, S.E., *Fuel*, **71**, (1992), 1338.
13. Shimadzu Corp. UV-160 Instruction Manual, Kyoto Japan.

Table A.1: Density of asphaltene-solids/toluene mixtures using entire asphaltene fraction.

| | | | |
|--------------------------------------|---------|------------------------|---------|
| toluene density (g/cm ³) | 0.867 | A (cm ³ /g) | 13.9125 |
| water density (g/cm ³) | 0.99704 | B | 16.8790 |
| R _{dm} for pure toluene | 5.3797 | | |
| R _{dm} for pure water | 5.5453 | Temp. (°C) | 25.8 |

| Asph. Conc. (kg/m ³) | Asph. Mass (g) | Solvent Volume (cm ³) | Solvent Mass (g) | Asph. Mass Fr. | R _{dm} | Calculated Density (g/cm ³) | Specific Volume (cm ³ /g) |
|----------------------------------|----------------|-----------------------------------|------------------|----------------|-----------------|---|--------------------------------------|
| 0 | 0.00 | | | 0.00000 | 5.3797 | 0.86700 | 1.1534 |
| 2 | 0.08 | 40 | 34.68 | 0.00230 | 5.3804 | 0.86754 | 1.1527 |
| 4 | 0.16 | 40 | 34.68 | 0.00459 | 5.3811 | 0.86808 | 1.1520 |
| 6 | 0.12 | 20 | 17.34 | 0.00687 | 5.3818 | 0.86862 | 1.1512 |
| 8 | 0.16 | 20 | 17.34 | 0.00914 | 5.3824 | 0.86909 | 1.1506 |
| 10 | 0.20 | 20 | 17.34 | 0.01140 | 5.3830 | 0.86955 | 1.1500 |

Table A.2: Density of asphaltene-solids/toluene mixtures using asphaltene subfraction precipitated in hextol of 20 vol% toluene.

| | | | |
|--------------------------------------|---------|------------------------|---------|
| toluene density (g/cm ³) | 0.867 | A (cm ³ /g) | 13.9042 |
| water density (g/cm ³) | 0.99704 | B | 16.8873 |
| R _{dm} for pure toluene | 5.3798 | | |
| R _{dm} for pure water | 5.5453 | Temp. (°C) | 25.7 |

| Asph. Conc. (kg/m ³) | Asph. Mass (g) | Solvent Volume (cm ³) | Solvent Mass (g) | Asph. Mass Fr. | R _{dm} | Calculated Density (g/cm ³) | Specific Volume (cm ³ /g) |
|----------------------------------|----------------|-----------------------------------|------------------|----------------|-----------------|---|--------------------------------------|
| 0 | 0.00 | | | 0.00000 | 5.3798 | 0.86708 | 1.1533 |
| 2 | 0.08 | 40 | 34.68 | 0.00230 | 5.3805 | 0.86762 | 1.1526 |
| 4 | 0.16 | 40 | 34.68 | 0.00459 | 5.3812 | 0.86816 | 1.1519 |
| 6 | 0.12 | 20 | 17.34 | 0.00687 | 5.3818 | 0.86862 | 1.1512 |
| 8 | 0.16 | 20 | 17.34 | 0.00914 | 5.3825 | 0.86917 | 1.1505 |
| 10 | 0.20 | 20 | 17.34 | 0.01140 | 5.3832 | 0.86971 | 1.1498 |

Table A.3: Density of asphaltene-solids/toluene mixtures using asphaltene subfraction precipitated in hextol of 25 vol% toluene.

| | | | |
|--------------------------------------|---------|------------------------|---------|
| toluene density (g/cm ³) | 0.867 | A (cm ³ /g) | 13.8957 |
| water density (g/cm ³) | 0.99704 | B | 16.8947 |
| R _{dm} for pure toluene | 5.3798 | | |
| R _{dm} for pure water | 5.5452 | Temp. (°C) | 25.7 |

| Asph. Conc. (kg/m ³) | Asph. Mass (g) | Solvent Volume (cm ³) | Solvent Mass (g) | Asph. Mass Fr. | R _{dm} | Calculated Density (g/cm ³) | Specific Volume (cm ³ /g) |
|----------------------------------|----------------|-----------------------------------|------------------|----------------|-----------------|---|--------------------------------------|
| 0 | 0.00 | | | 0.00000 | 5.3798 | 0.86700 | 1.1534 |
| 2 | 0.08 | 40 | 34.68 | 0.00230 | 5.3805 | 0.86754 | 1.1527 |
| 4 | 0.16 | 40 | 34.68 | 0.00459 | 5.3812 | 0.86808 | 1.1520 |
| 6 | 0.12 | 20 | 17.34 | 0.00687 | 5.3820 | 0.86870 | 1.1511 |
| 8 | 0.16 | 20 | 17.34 | 0.00914 | 5.3827 | 0.86925 | 1.1504 |
| 10 | 0.20 | 20 | 17.34 | 0.01140 | 5.3835 | 0.86987 | 1.1496 |

Table A.4: Density of asphaltene-solids/toluene mixtures using asphaltene subfraction precipitated in hextol of 33 vol% toluene.

| | | | |
|--------------------------------------|---------|------------------------|---------|
| toluene density (g/cm ³) | 0.867 | A (cm ³ /g) | 13.9040 |
| water density (g/cm ³) | 0.99704 | B | 16.8864 |
| R _{dm} for pure toluene | 5.3797 | | |
| R _{dm} for pure water | 5.5452 | Temp. (°C) | 25.8 |

| Asph. Conc. (kg/m ³) | Asph. Mass (g) | Solvent Volume (cm ³) | Solvent Mass (g) | Asph. Mass Fr. | R _{dm} | Calculated Density (g/cm ³) | Specific Volume (cm ³ /g) |
|----------------------------------|----------------|-----------------------------------|------------------|----------------|-----------------|---|--------------------------------------|
| 0 | 0.00 | | | 0.00000 | 5.3797 | 1.71303 | 0.5838 |
| 2 | 0.08 | 40 | 34.70 | 0.00230 | 5.3805 | 1.71354 | 0.5836 |
| 4 | 0.16 | 40 | 34.70 | 0.00459 | 5.3812 | 1.71399 | 0.5834 |
| 6 | 0.12 | 20 | 17.35 | 0.00687 | 5.3820 | 1.71450 | 0.5833 |
| 8 | 0.16 | 20 | 17.35 | 0.00914 | 5.3827 | 1.71494 | 0.5831 |
| 10 | 0.20 | 20 | 17.35 | 0.01140 | 5.3836 | 1.71552 | 0.5829 |

Table A.5: Density of asphaltene/toluene mixtures using entire asphaltene fraction.

| | | | |
|--------------------------------------|---------|------------------------|---------|
| toluene density (g/cm ³) | 0.867 | A (cm ³ /g) | 13.8877 |
| water density (g/cm ³) | 0.99704 | B | 16.9038 |
| R _{dm} for pure toluene | 5.3800 | | |
| R _{dm} for pure water | 5.5453 | Temp. (°C) | 25.7 |

| Asph. Conc. (kg/m ³) | Asph. Mass (g) | Solvent Volume (cm ³) | Solvent Mass (g) | Asph. Mass Fr. | R _{dm} | Calculated Density (g/cm ³) | Specific Volume (cm ³ /g) |
|----------------------------------|----------------|-----------------------------------|------------------|----------------|-----------------|---|--------------------------------------|
| 0 | 0.00 | | | 0.00000 | 5.3800 | 0.86700 | 1.1534 |
| 2 | 0.08 | 40 | 34.68 | 0.00230 | 5.3806 | 0.86746 | 1.1528 |
| 4 | 0.16 | 40 | 34.68 | 0.00459 | 5.3812 | 0.86793 | 1.1522 |
| 6 | 0.12 | 20 | 17.34 | 0.00687 | 5.3819 | 0.86847 | 1.1514 |
| 8 | 0.16 | 20 | 17.34 | 0.00914 | 5.3825 | 0.86894 | 1.1508 |
| 10 | 0.20 | 20 | 17.34 | 0.01140 | 5.3832 | 0.86948 | 1.1501 |

Table A.6: Density of asphaltene/toluene mixtures using asphaltene subfraction precipitated in hextol of 20 vol% toluene.

| | | | |
|--------------------------------------|---------|------------------------|---------|
| toluene density (g/cm ³) | 0.867 | A (cm ³ /g) | 13.9042 |
| water density (g/cm ³) | 0.99704 | B | 16.8873 |
| R _{dm} for pure toluene | 5.3798 | | |
| R _{dm} for pure water | 5.5453 | Temp. (°C) | 25.7 |

| Asph. Conc. (kg/m ³) | Asph. Mass (g) | Solvent Volume (cm ³) | Solvent Mass (g) | Asph. Mass Fr. | R _{dm} | Calculated Density (g/cm ³) | Specific Volume (cm ³ /g) |
|----------------------------------|----------------|-----------------------------------|------------------|----------------|-----------------|---|--------------------------------------|
| 0 | 0.00 | | | 0.00000 | 5.3798 | 1.71217 | 0.5841 |
| 2 | 0.08 | 40 | 34.70 | 0.00230 | 5.3805 | 1.71262 | 0.5839 |
| 4 | 0.16 | 40 | 34.70 | 0.00459 | 5.3812 | 1.71307 | 0.5837 |
| 6 | 0.12 | 20 | 17.35 | 0.00687 | 5.3818 | 1.71345 | 0.5836 |
| 8 | 0.16 | 20 | 17.35 | 0.00914 | 5.3825 | 1.71389 | 0.5835 |
| 10 | 0.20 | 20 | 17.35 | 0.01140 | 5.3831 | 1.71428 | 0.5833 |

Table A.7: Density of asphaltene/toluene mixtures using asphaltene subfraction precipitated in hextol of 25 vol% toluene.

| | | | |
|--------------------------------------|---------|------------------------|---------|
| toluene density (g/cm ³) | 0.867 | A (cm ³ /g) | 13.9042 |
| water density (g/cm ³) | 0.99704 | B | 16.8873 |
| R _{dm} for pure toluene | 5.3798 | | |
| R _{dm} for pure water | 5.5453 | Temp. (°C) | 25.7 |

| Asph. Conc. (kg/m ³) | Asph. Mass (g) | Solvent Volume (cm ³) | Solvent Mass (g) | Asph. Mass Fr. | R _{dm} | Calculated Density (g/cm ³) | Specific Volume (cm ³ /g) |
|----------------------------------|----------------|-----------------------------------|------------------|----------------|-----------------|---|--------------------------------------|
| 0 | 0.00 | | | 0.00000 | 5.3798 | 0.86700 | 1.1534 |
| 2 | 0.08 | 40 | 34.68 | 0.00230 | 5.3805 | 0.86754 | 1.1527 |
| 4 | 0.16 | 40 | 34.68 | 0.00459 | 5.3812 | 0.86808 | 1.1520 |
| 6 | 0.12 | 20 | 17.34 | 0.00687 | 5.3819 | 0.86863 | 1.1512 |
| 8 | 0.16 | 20 | 17.34 | 0.00914 | 5.3824 | 0.86901 | 1.1507 |
| 10 | 0.20 | 20 | 17.34 | 0.01140 | 5.3831 | 0.86955 | 1.1500 |

Table A.8: Density of asphaltene/toluene mixtures using asphaltene subfraction precipitated in hextol of 33 vol% toluene.

| | | | |
|--------------------------------------|---------|------------------------|---------|
| toluene density (g/cm ³) | 0.867 | A (cm ³ /g) | 13.9042 |
| water density (g/cm ³) | 0.99704 | B | 16.8873 |
| R _{dm} for pure toluene | 5.3798 | | |
| R _{dm} for pure water | 5.5453 | Temp. (°C) | 25.8 |

| Asph. Conc. (kg/m ³) | Asph. Mass (g) | Solvent Volume (cm ³) | Solvent Mass (g) | Asph. Mass Fr. | R _{dm} | Calculated Density (g/cm ³) | Specific Volume (cm ³ /g) |
|----------------------------------|----------------|-----------------------------------|------------------|----------------|-----------------|---|--------------------------------------|
| 0 | 0.00 | | | 0.00000 | 5.3798 | 1.71385 | 0.5835 |
| 2 | 0.08 | 40 | 34.70 | 0.00230 | 5.3805 | 1.71429 | 0.5833 |
| 4 | 0.16 | 40 | 34.70 | 0.00459 | 5.3812 | 1.71474 | 0.5832 |
| 6 | 0.12 | 20 | 17.35 | 0.00687 | 5.3819 | 1.71519 | 0.5830 |
| 8 | 0.16 | 20 | 17.35 | 0.00914 | 5.3826 | 1.71563 | 0.5829 |
| 10 | 0.20 | 20 | 17.35 | 0.01140 | 5.3836 | 1.71627 | 0.5827 |

Table A.9: Surface and interfacial tension measurements of various two component systems.

| System | Interfacial Tension (mN/m) | | |
|--------------------------|----------------------------------|-----------------------------------|----------------------|
| | present work (22 °C) raw data | present work (22 °C) corrected | literature (20°C) |
| water/air | 75.00 | 70.12 | 72.75 ^a |
| benzene/air | - | - | 28.88 ^a |
| toluene/air | 30.50 | 27.22 | - |
| n-hexane/air | 21.50 | 19.12 | 18.1 ^b |
| n-heptane/air | 21.00 | 18.62 | - |
| benzene/water | - | - | 34.0 ^c |
| toluene/water | 32.75 | 34.77 | 35.8 ^c |
| hexane/water | 48.25 | 47.83 | 50.1 ^c |
| cyclohexane/water | 46.50 | 48.97 | 50.0 ^c |
| 1,2dichlorobenzene/water | 31.50 | 30.25 | - |

a - ref. 4.

b - ref. 5.

c - ref. 6.

Table A.10: Interfacial tension measurements of toluene/hexane mixtures over water - raw data.

| Time (min) | Toluene | | | Interfacial Tension (mN/m) | | | | | | Hexane | | |
|---------------|---------|---------|---------|----------------------------|--------------------|--------------------|--------------------|--------------------|--------------------|--------------------|--------------------|--------|
| | Toluene | Toluene | Toluene | HexTol 80% tol. | HexTol 60% tol. | HexTol 60% tol. | HexTol 40% tol. | HexTol 20% tol. | HexTol 10% tol. | HexTol 20% tol. | HexTol 10% tol. | Hexane |
| 1 | 32.50 | 33.00 | 32.50 | 33.75 | 35.50 | 36.00 | 38.50 | 42.00 | 44.50 | 48.25 | | |
| 10 | 31.25 | - | - | 32.50 | 34.50 | 33.75 | 35.75 | - | 43.25 | 47.50 | | |
| 15 | - | 32.00 | 31.50 | - | - | - | - | - | - | - | | |
| 20 | 30.25 | - | - | 31.00 | 33.50 | 33.00 | 34.00 | 37.75 | 41.50 | 46.50 | | |
| 30 | 29.75 | 31.50 | 31.25 | 30.50 | 32.50 | 32.00 | 33.50 | 36.75 | 40.50 | 46.00 | | |
| 45 | 29.25 | 31.25 | 30.75 | 30.50 | 32.00 | 31.50 | 32.75 | 36.00 | 39.75 | 45.50 | | |
| 60 | 29.00 | 31.00 | 30.75 | 31.00 | 31.50 | 31.25 | 32.75 | 35.75 | 39.00 | 45.00 | | |
| 90 | - | 31.00 | - | - | - | - | - | - | - | - | | |
| 150 | - | 31.00 | - | - | - | - | - | - | - | - | | |

Table A.11: Interfacial tension measurements of toluene/hexane mixtures over water - corrected data.

| Time (min) | Toluene | | | Interfacial Tension (mN/m) | | | | | | Hexane | | |
|---------------|---------|---------|---------|----------------------------|--------------------|--------------------|--------------------|--------------------|--------------------|--------------------|--------------------|--------|
| | Toluene | Toluene | Toluene | HexTol 80% tol. | HexTol 60% tol. | HexTol 60% tol. | HexTol 40% tol. | HexTol 20% tol. | HexTol 10% tol. | HexTol 20% tol. | HexTol 10% tol. | Hexane |
| 1 | 34.46 | 35.07 | 34.46 | 34.70 | 35.79 | 36.35 | 38.39 | 41.60 | 44.03 | 47.83 | | |
| 10 | 32.96 | - | - | 33.26 | 34.66 | 33.82 | 35.36 | - | 42.66 | 47.01 | | |
| 15 | - | 33.86 | 33.26 | - | - | - | - | - | - | - | | |
| 20 | 31.76 | - | - | 31.54 | 33.55 | 32.99 | 33.45 | 36.97 | 40.76 | 45.92 | | |
| 30 | 31.17 | 33.26 | 32.96 | 30.97 | 32.43 | 31.88 | 32.91 | 35.89 | 39.68 | 45.37 | | |
| 45 | 30.58 | 32.96 | 32.36 | 30.97 | 31.88 | 31.33 | 32.10 | 35.09 | 38.87 | 44.83 | | |
| 60 | 30.28 | 32.66 | 32.36 | 31.54 | 31.33 | 31.05 | 32.10 | 34.82 | 38.06 | 44.28 | | |
| 90 | - | 32.66 | - | - | - | - | - | - | - | - | | |
| 150 | - | 32.66 | - | - | - | - | - | - | - | - | | |

Table A.12: Interfacial tension measurements of asphaltene-solids in toluene/hexane solvent mixtures over water - raw data.

| Asph. Conc. (C _A) (kg/m ³) | ln(C _A) | Interfacial Tension (mN/m) | | | | Toluene | Toluene Toluene ^a | |
|--|---------------------|----------------------------|--------------------|--------------------|--------------------|---------|---------------------------------|-------|
| | | HexTol 20% tol. | HexTol 25% tol. | HexTol 33% tol. | HexTol 40% tol. | | | |
| 0.0044 | -5.4262 | 33.25 | 33.50 | 32.50 | 32.50 | 31.75 | 30.75 | - |
| 0.0088 | -4.7330 | 33.00 | - | - | 31.25 | - | - | - |
| 0.0088 | -4.7330 | 32.00 | 32.75 | 31.75 | 31.75 | 31.00 | 30.00 | - |
| 0.0176 | -4.0399 | 31.50 | 31.75 | 30.75 | 31.25 | 30.25 | 29.75 | - |
| 0.0440 | -3.1236 | 29.50 | 30.50 | 30.25 | 30.00 | 29.25 | 28.75 | 29.00 |
| 0.0880 | -2.4304 | 28.50 | 29.50 | 29.25 | 29.25 | 28.75 | 28.00 | 28.75 |
| 0.1760 | -1.7373 | 27.75 | 28.50 | 28.75 | 28.50 | 28.25 | 27.75 | 28.50 |
| 0.4400 | -0.8210 | 27.25 | 27.75 | 27.75 | 28.25 | 27.75 | 26.75 | 28.25 |
| 0.8800 | -0.1278 | 26.25 | 27.50 | 27.00 | 27.25 | 27.00 | 26.75 | 27.50 |
| 1.7600 | 0.5653 | 25.50 | 26.50 | 26.25 | 27.00 | 26.25 | 26.00 | 27.25 |
| 2.3000 | 0.8329 | 26.50 | - | - | - | - | - | - |
| 3.0000 | 1.0986 | 27.50 | - | - | - | - | - | - |
| 4.4000 | 1.4816 | 27.50 | 26.50 | 25.75 | 26.25 | 25.50 | 25.50 | 27.00 |
| 6.0000 | 1.7918 | - | 27.50 | 26.50 | - | - | - | - |
| 8.8000 | 2.1748 | 27.50 | 28.25 | 27.50 | 26.00 | 24.75 | 25.00 | 26.75 |
| 17.6000 | 2.8679 | - | 28.50 | 27.75 | 26.75 | 24.50 | 24.50 | 26.50 |
| 25.0000 | 3.2189 | - | - | - | - | 23.75 | - | - |
| 44.0000 | 3.7842 | - | - | - | - | 22.75 | 23.50 | - |

a - using asphaltene fraction precipitated from bitumen with a 4:1 volume ratio of heptane:bitumen

Table A.13: Interfacial tension measurements of asphaltene-solids in toluene/hexane solvent mixtures over water - corrected data.

| Asph. Conc. (C _A) (kg/m ³) | ln(C _A) | HexTol | | | Interfacial Tension (mN/m) | | | | | Toluene | Toluene ^a |
|--|---------------------|----------|----------|----------|----------------------------|----------|----------|----------|----------|---------|----------------------|
| | | 20% tol. | 25% tol. | 33% tol. | 33% tol. | 40% tol. | 40% tol. | 50% tol. | 50% tol. | | |
| 0.0044 | -5.4262 | 32.16 | 32.53 | 31.65 | 31.83 | 31.29 | 32.36 | - | - | - | - |
| 0.0088 | -4.7330 | 31.89 | - | - | 30.48 | - | - | - | - | - | - |
| 0.0088 | -4.7330 | 30.84 | 31.74 | 30.85 | 31.02 | 30.48 | 31.47 | - | - | - | - |
| 0.0176 | -4.0399 | 30.31 | 30.68 | 29.79 | 30.48 | 29.66 | 31.17 | - | - | - | - |
| 0.0440 | -3.1236 | 28.22 | 29.36 | 29.26 | 29.15 | 28.59 | 29.99 | 30.28 | - | - | - |
| 0.0880 | -2.4304 | 27.18 | 28.31 | 28.20 | 28.35 | 28.05 | 29.10 | 29.99 | 30.28 | - | - |
| 0.1760 | -1.7373 | 26.40 | 27.26 | 27.67 | 27.55 | 27.51 | 28.81 | 29.69 | 29.69 | - | - |
| 0.4400 | -0.8210 | 25.88 | 26.48 | 26.62 | 27.29 | 26.98 | 27.64 | 29.40 | 29.40 | - | - |
| 0.8800 | -0.1278 | 24.85 | 26.22 | 25.84 | 26.23 | 26.18 | 27.64 | 28.52 | 28.52 | - | - |
| 1.7600 | 0.5653 | 24.09 | 25.19 | 25.06 | 25.97 | 25.38 | 26.77 | 28.22 | 28.22 | - | - |
| 2.3000 | 0.8329 | 25.11 | - | - | - | - | - | - | - | - | - |
| 3.0000 | 1.0986 | 26.14 | - | - | - | - | - | - | - | - | - |
| 4.4000 | 1.4816 | 26.14 | 25.19 | 24.54 | 25.18 | 24.59 | 26.19 | 27.93 | 27.93 | - | - |
| 6.0000 | 1.7918 | - | 26.22 | 25.32 | - | - | - | - | - | - | - |
| 8.8000 | 2.1748 | 26.14 | 27.00 | 26.36 | 24.92 | 23.80 | 25.61 | 27.64 | 27.64 | - | - |
| 17.6000 | 2.8679 | - | 27.26 | 26.62 | 25.71 | 23.54 | 25.04 | 27.35 | 27.35 | - | - |
| 25.0000 | 3.2189 | - | - | - | - | 22.75 | - | - | - | - | - |
| 44.0000 | 3.7842 | - | - | - | - | 21.71 | 23.90 | - | - | - | - |

a - using asphaltene fraction precipitated from bitumen with a 4:1 volume ratio of heptane:bitumen

Table A.14: Interfacial tension measurements of asphaltene-solids in toluene/hexane solvent mixture of 25 vol% toluene over water.

| Asph. Conc. (C_A) (kg/m^3) | Interfacial Tension (mN/m) | | | |
|---|----------------------------|-----------|---------------------|-----------|
| | precipitate present | | precipitate removed | |
| | raw data | corrected | raw data | corrected |
| 0.0176 | 30.25 | 29.09 | 30.00 | 28.83 |
| 0.0440 | - | - | 29.25 | 28.05 |
| 0.0880 | 28.75 | 27.52 | - | - |
| 0.1760 | - | - | 28.25 | 27.00 |
| 0.4400 | 28.00 | 26.74 | 27.25 | 25.96 |
| 0.8800 | 27.00 | 25.70 | - | - |
| 0.8800 | 27.25 | 25.96 | - | - |
| 1.7600 | 26.00 | 24.67 | 25.50 | 24.16 |
| 4.4000 | 27.50 | 26.22 | 24.75 | 23.39 |
| 4.4000 | 26.50 | 25.19 | - | - |
| 8.8000 | 27.50 | 26.22 | 25.00 | 23.64 |
| 17.6000 | - | - | 23.75 | 22.37 |

Table A.15: Interfacial tension measurements of asphaltene-solids in 1,2-dichlorobenzene over water.

| Asph. Conc. (C_A) (kg/m^3) | Interfacial Tension (mN/m) precipitate present | |
|---|---|-----------|
| | raw data | corrected |
| 0.0000 | 31.50 | 30.25 |
| 0.0440 | 29.75 | 28.42 |
| 0.0880 | 29.50 | 28.16 |
| 0.0880 | 29.50 | 28.16 |
| 0.1760 | 29.50 | 28.16 |
| 0.1760 | 29.25 | 27.90 |
| 0.8800 | 29.50 | 28.16 |

Table A.16: Interfacial tension measurements of asphaltene-solids in cyclohexane over water.

| Asph. Conc. (C_A) (kg/m^3) | Interfacial Tension (mN/m) precipitate removed | |
|---|---|-----------|
| | raw data | corrected |
| 0.00 | 46.5 | 48.97 |
| 0.10 | 29.4 | 29.27 |
| 0.25 | 28.7 | 28.50 |
| 0.50 | 28.0 | 27.73 |
| 0.50 | 27.2 | 26.85 |
| 1.00 | 26.6 | 26.20 |
| 2.50 | 25.0 | 24.46 |
| 3.50 | 24.4 | 23.82 |
| 5.00 | 24.0 | 23.39 |
| 7.50 | 24.1 | 23.50 |
| 10.00 | 23.7 | 23.07 |
| 20.00 | 23.5 | 22.85 |

Table A.17: Vapor pressure osmometry measurements of the molar mass of asphaltene-solids in toluene at 50 °C.

$$K_{vpo} = 37755.2 \text{ m}^3/\text{kmol}$$

| Entire Asphaltene-Solids Fraction | | | Asphaltene-Solids Precipitated from hextol of 20 vol% toluene | | |
|-----------------------------------|------------|-------------------------|---|------------|-------------------------|
| Asph. Conc. (kg/m ³) | ΔR | Asph. Mol. Mass (g/mol) | Asph. Conc. (kg/m ³) | ΔR | Asph. Mol. Mass (g/mol) |
| 1.944 | 31.74 | 2312 | 1.837 | 7.73 | 8968 |
| 3.169 | 48.32 | 2476 | 3.150 | 13.98 | 8503 |
| 3.426 | 64.34 | 2010 | 4.587 | 20.13 | 8600 |
| 4.517 | 58.22 | 2929 | | | |

| Asphaltene-Solids Precipitated from hextol of 25 vol% toluene | | | Asphaltene-Solids Precipitated from hextol of 33 vol% toluene | | |
|---|------------|-------------------------|---|------------|-------------------------|
| Asph. Conc. (kg/m ³) | ΔR | Asph. Mol. Mass (g/mol) | Asph. Conc. (kg/m ³) | ΔR | Asph. Mol. Mass (g/mol) |
| 2.121 | 9.94 | 8050 | 1.498 | 5.91 | 9558 |
| 2.519 | 12.09 | 7866 | 2.175 | 9.04 | 9076 |
| 3.05 | 15.09 | 7627 | 2.821 | 9.98 | 10665 |

Table A.18: Vapor pressure osmometry measurements of the molar mass of asphaltenes in toluene at 50 °C.

$$K_{vpo} = 40737.7 \text{ m}^3/\text{kmol}$$

| Entire Asphaltene Fraction | | | Asphaltenes Precipitated from hextol of 20 vol% toluene | | |
|----------------------------------|------------|-------------------------|---|------------|-------------------------|
| Asph. Conc. (kg/m ³) | ΔR | Asph. Mol. Mass (g/mol) | Asph. Conc. (kg/m ³) | ΔR | Asph. Mol. Mass (g/mol) |
| 1.941 | 22.20 | 3562 | 1.600 | 13.40 | 4864 |
| 3.044 | 47.05 | 2636 | 1.926 | 14.65 | 5356 |
| 4.092 | 65.40 | 2549 | 2.170 | 18.45 | 4791 |
| | | | 3.047 | 19.20 | 6465 |
| | | | 3.186 | 18.40 | 7054 |

| Asphaltenes Precipitated from hextol of 25 vol% toluene | | | Asphaltenes Precipitated from hextol of 33 vol% toluene | | |
|---|------------|-------------------------|---|------------|-------------------------|
| Asph. Conc. (kg/m ³) | ΔR | Asph. Mol. Mass (g/mol) | Asph. Conc. (kg/m ³) | ΔR | Asph. Mol. Mass (g/mol) |
| 1.965 | 12.15 | 6588 | 1.948 | 11.15 | 7117 |
| 3.120 | 19.65 | 6468 | 2.896 | 18.20 | 6482 |

Table A.19: Vapor pressure osmometry measurements of the molar mass of asphaltene-solids in 1,2-dichlorobenzene at 120 °C.

| Asphaltene Sample | Asph. Mol. Mass (g/mol) |
|--|-------------------------|
| Entire fraction | 2570 |
| Precipitate from hextol of 17 vol% toluene | 6003 |
| Precipitate from hextol of 20 vol% toluene | 3821 |
| Precipitate from hextol of 20 vol% toluene | 3784 |
| Precipitate from hextol of 25 vol% toluene | 3656 |
| Precipitate from hextol of 33 vol% toluene | 4358 |

Table A.20: Comparison of asphaltene concentration determined gravimetrically and from uv absorbance.

| Supernatant | Gravimetric | ----- Ultraviolet ----- | |
|---|-----------------------------------|-------------------------|----------------------------|
| | Conc. (±0.004 kg/m ³) | Absorbance | Conc. (kg/m ³) |
| 4:1 hexane:toluene - solubility method | 0.58 | 0.143 | 0.22 |
| 4:1 hexane:toluene - precipitation method | 0.78 | 0.321 | 0.50 |
| 2:1 hexane:toluene - solubility method | 1.25 | 0.590 | 0.92 |
| 2:1 hexane:toluene - precipitation method | 1.39 | 0.839 | 1.31 |

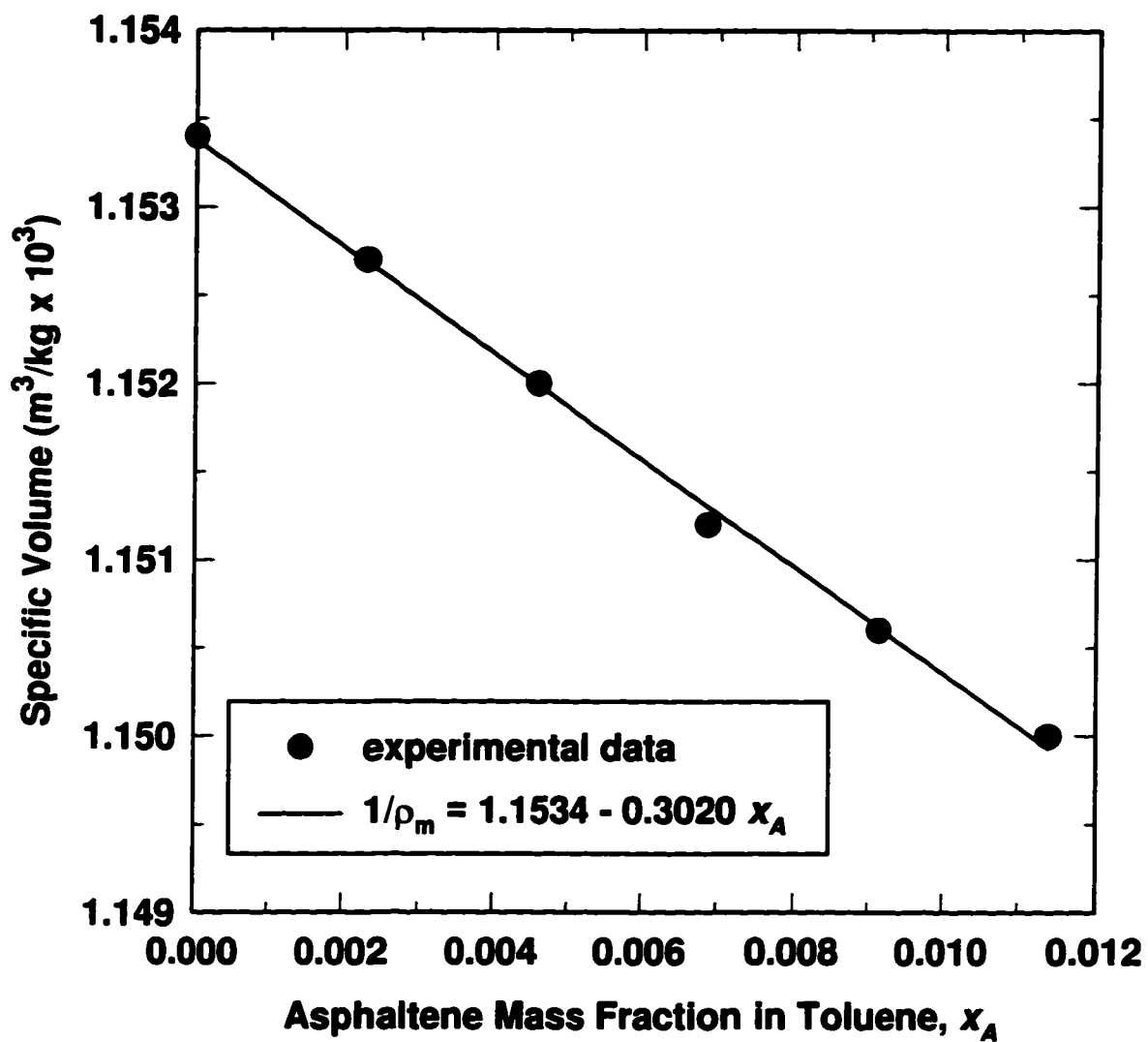


Figure A.1: Specific volume of asphaltene-solids/toluene mixtures using entire asphaltene fraction.

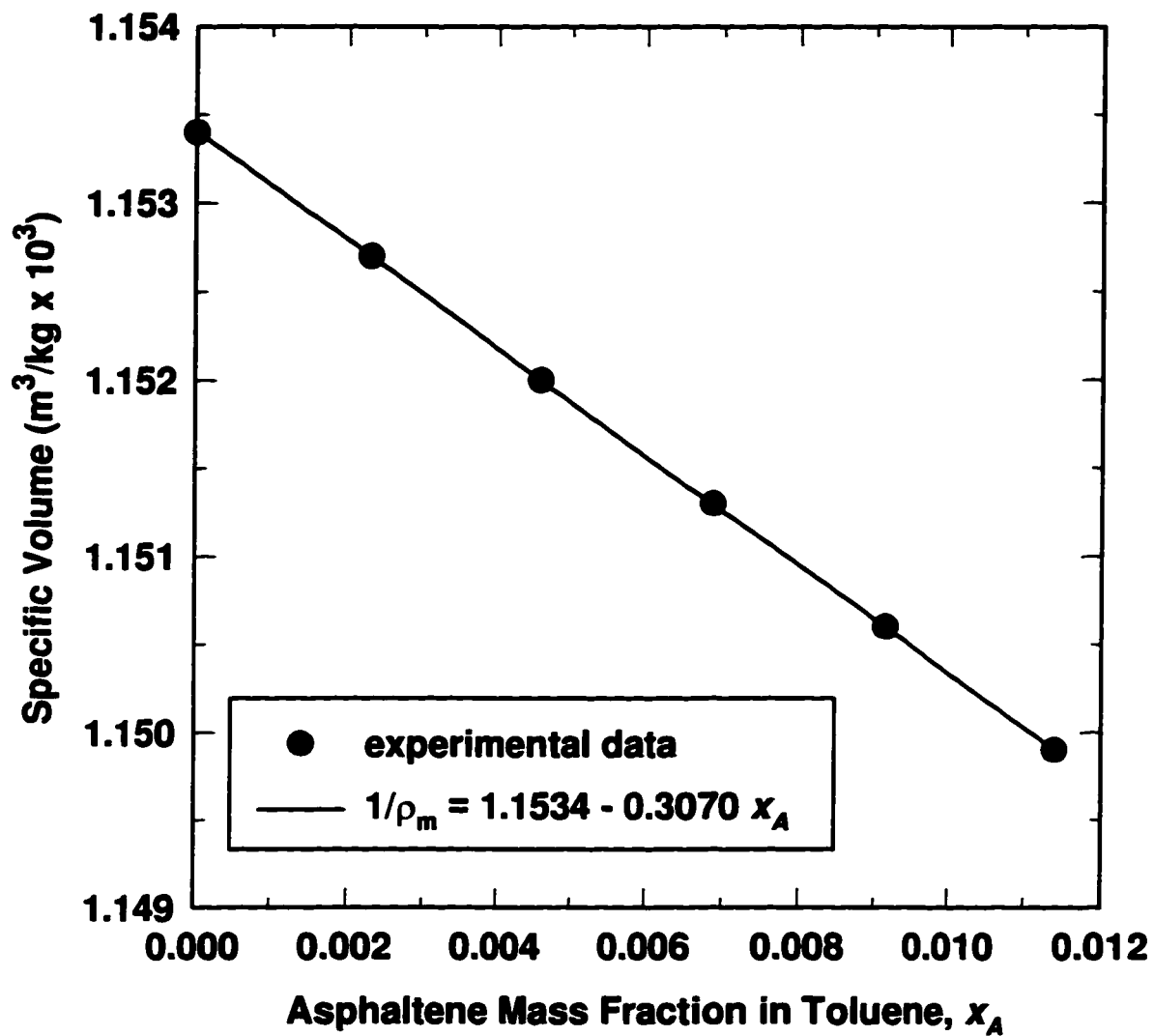


Figure A.2: Specific volume of asphaltene-solids/toluene mixtures using asphaltene subfraction precipitated from toluene/hexane solutions of 20 vol% toluene.

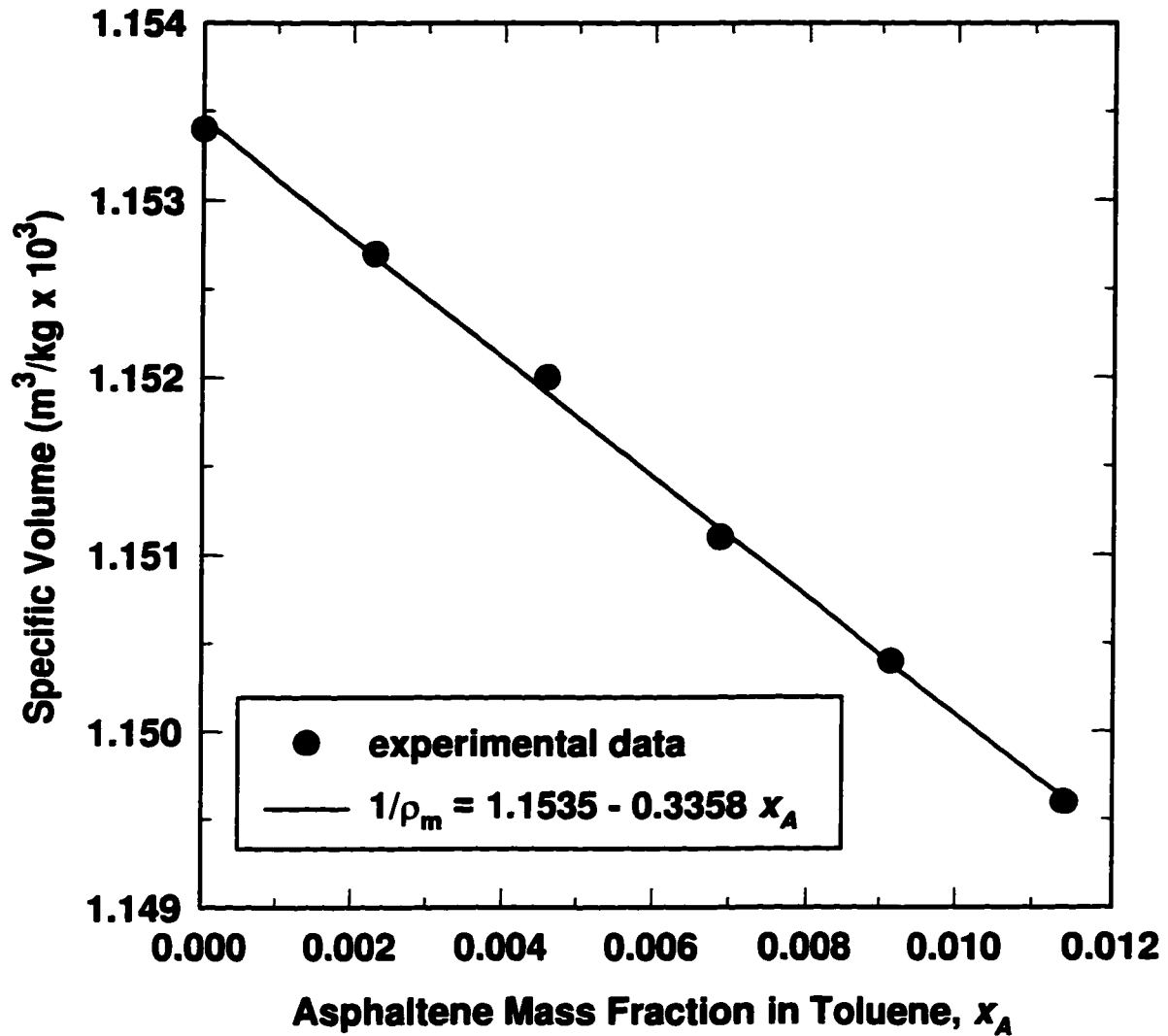


Figure A.3: Specific volume of asphaltene-solids/toluene mixtures using asphaltene subfraction precipitated from toluene/hexane solutions of 25 vol% toluene.

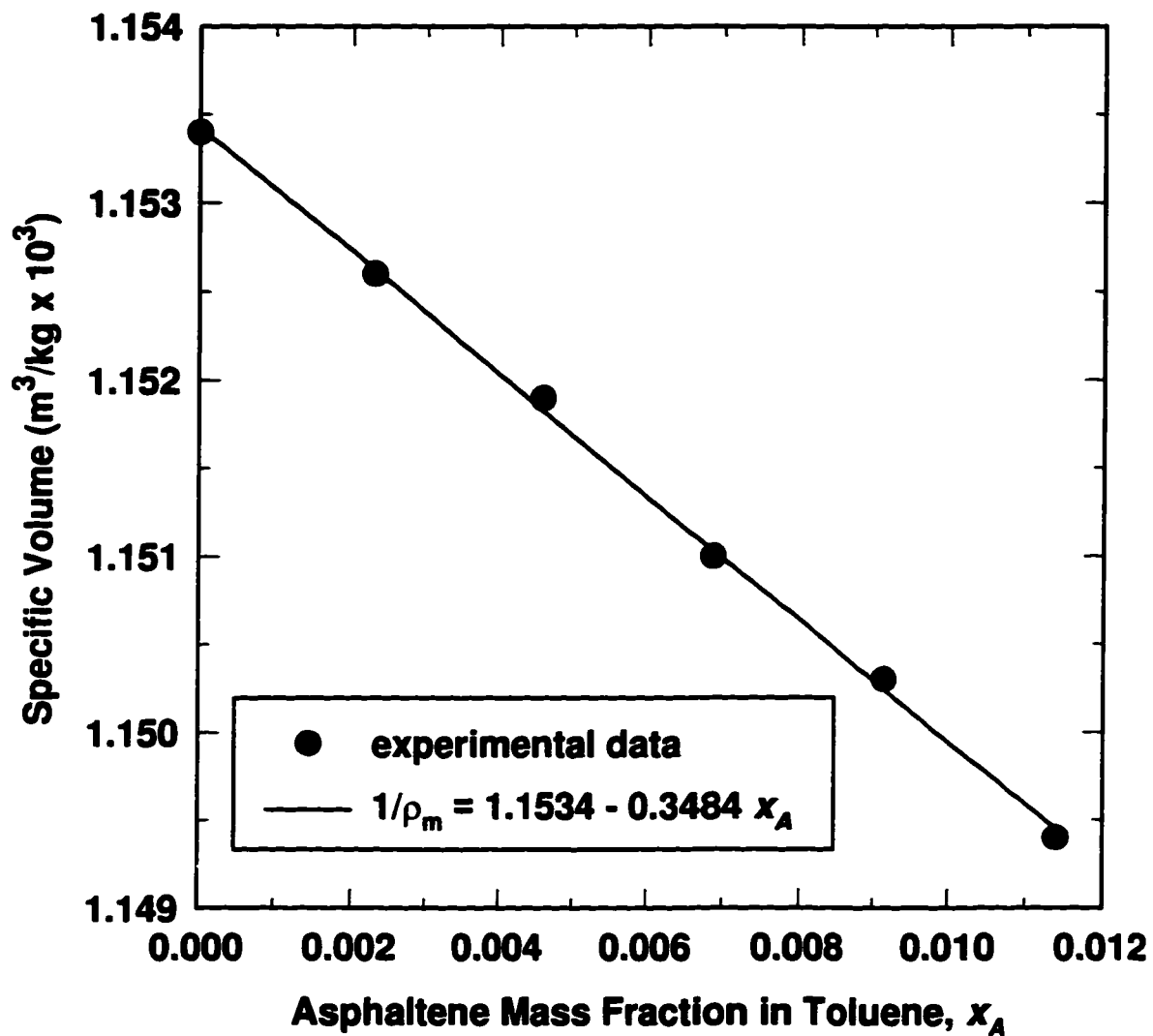


Figure A.4: Specific volume of asphaltene-solids/toluene mixtures using asphaltene subfraction precipitated from toluene/hexane solutions of 33 vol% toluene.

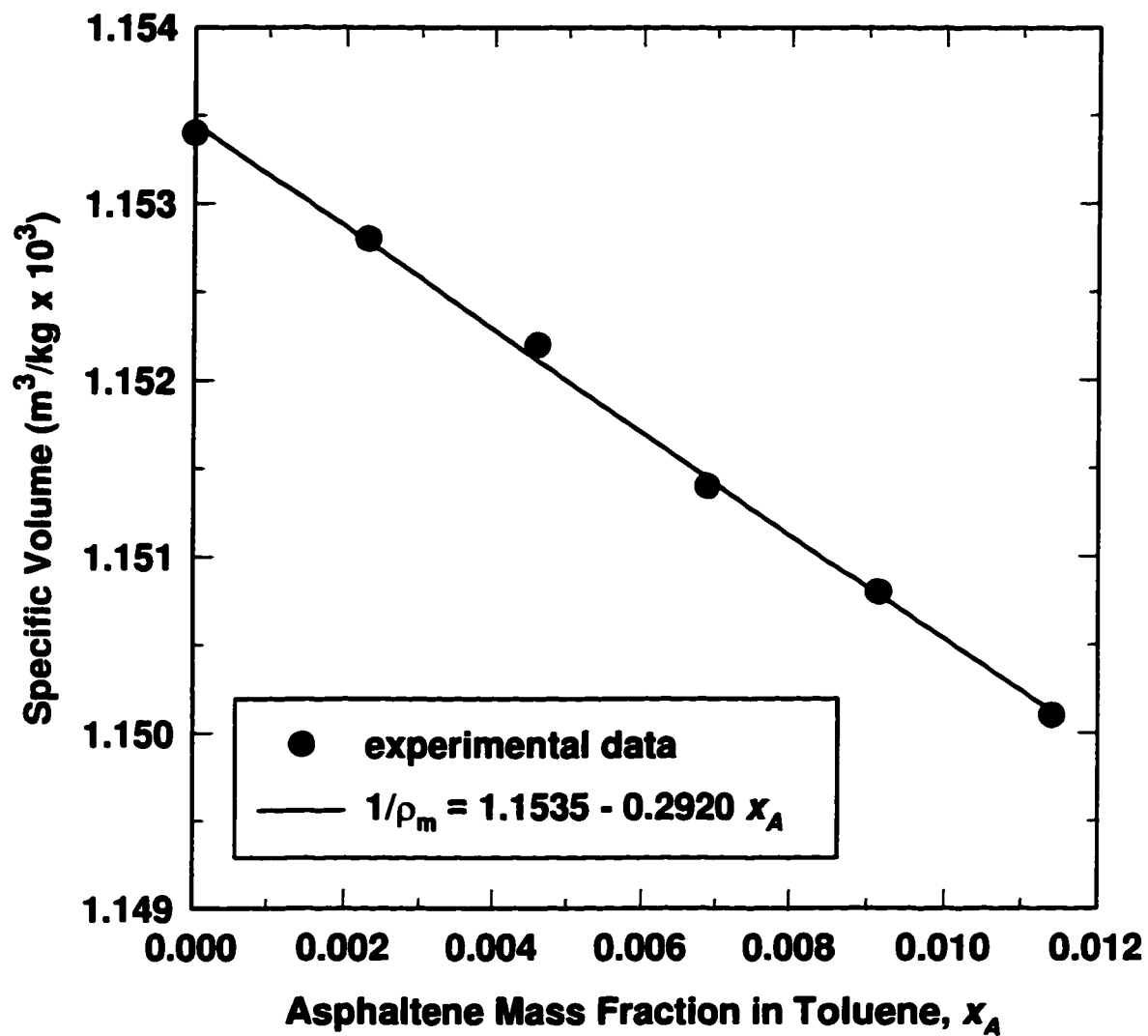


Figure A.5: Specific volume of asphaltene-toluene mixtures using entire asphaltene fraction.

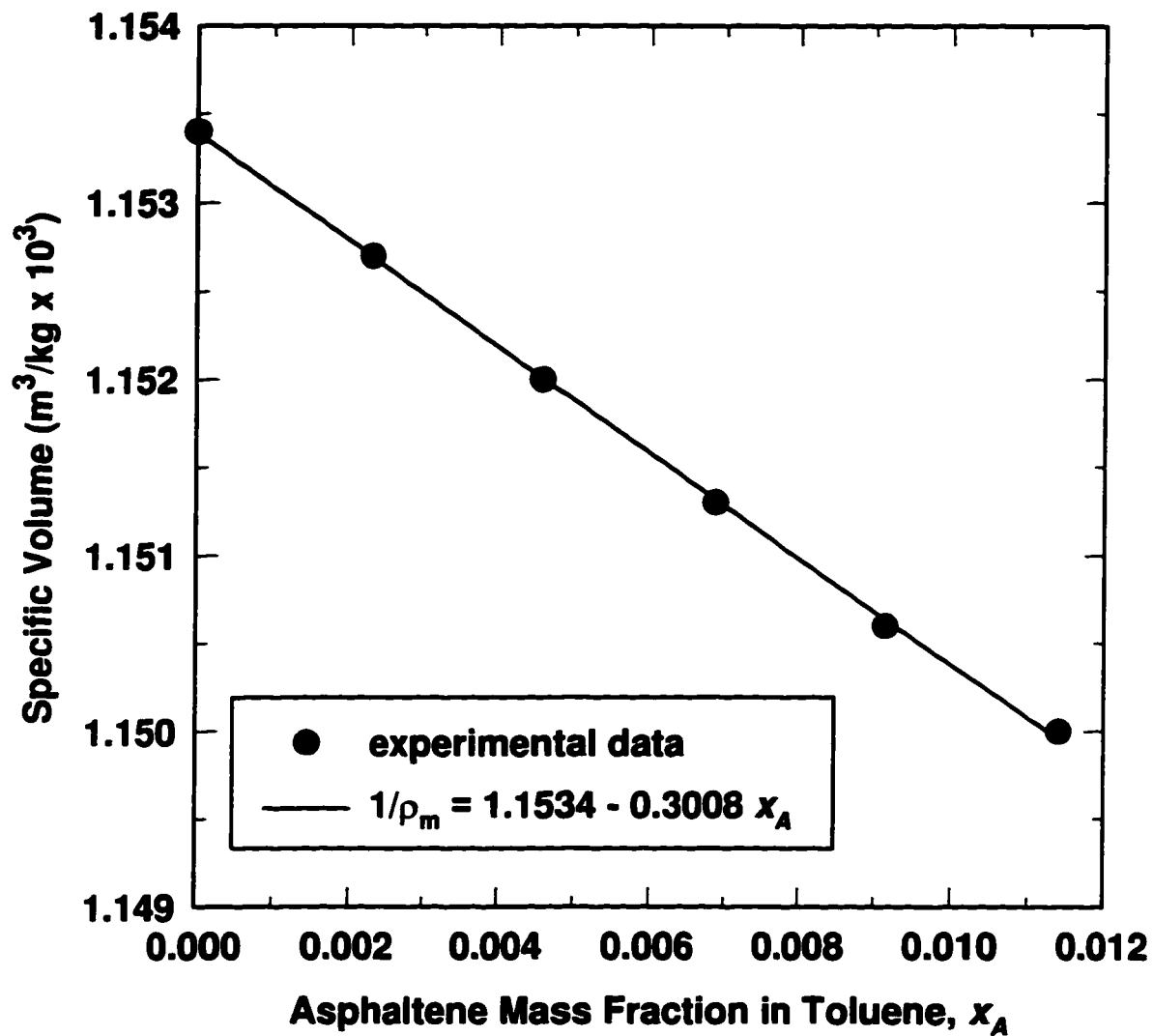


Figure A.6: Specific volume of asphaltene/toluene mixtures using asphaltene subfraction precipitated from toluene/hexane solutions of 20 vol% toluene.

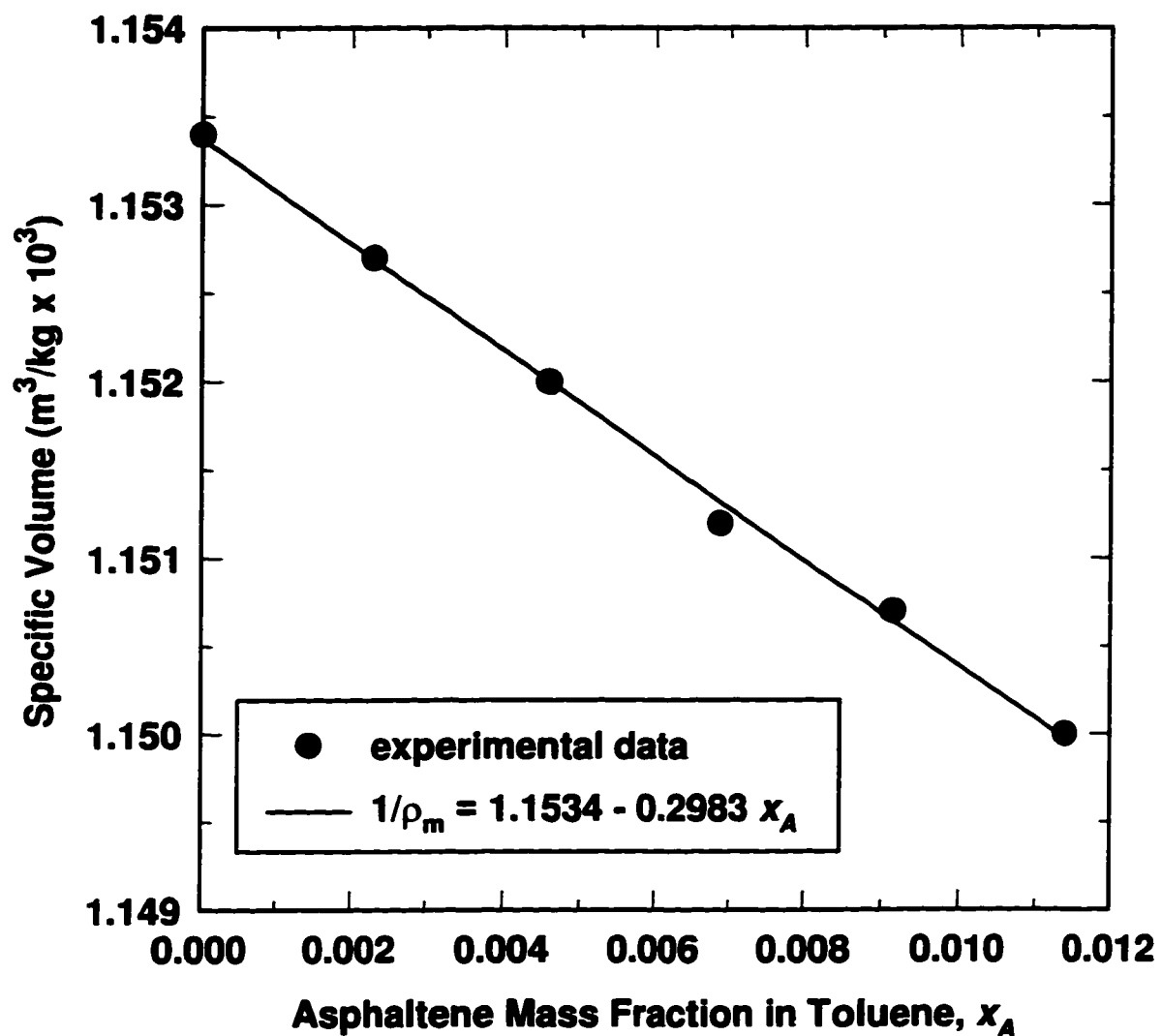


Figure A.7: Specific volume of asphaltene/toluene mixtures using asphaltene subfraction precipitated from toluene/hexane solutions of 25 vol% toluene.

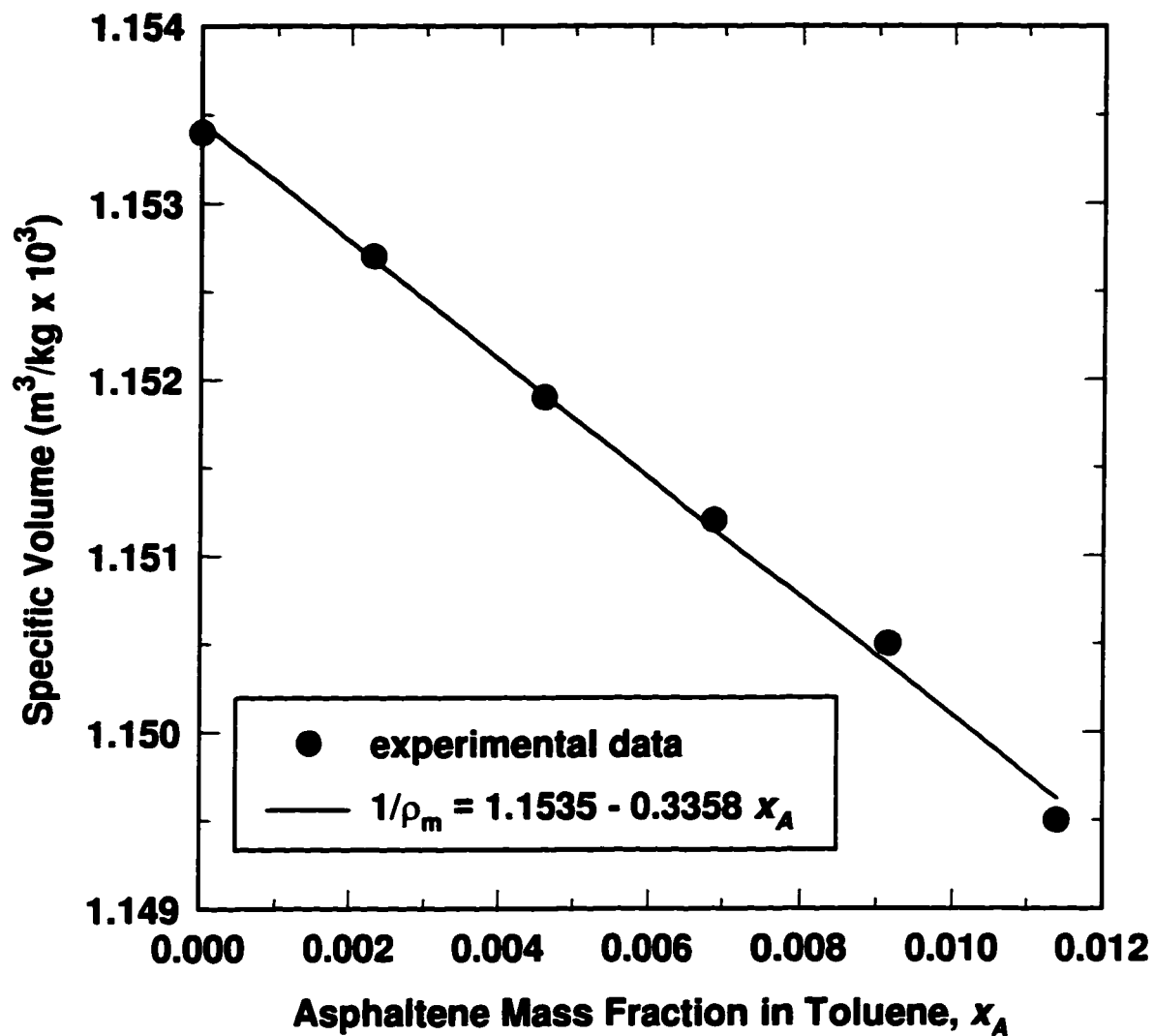


Figure A.8: Specific volume of asphaltene/toluene mixtures using asphaltene subfraction precipitated from toluene/hexane solutions of 33 vol% toluene.

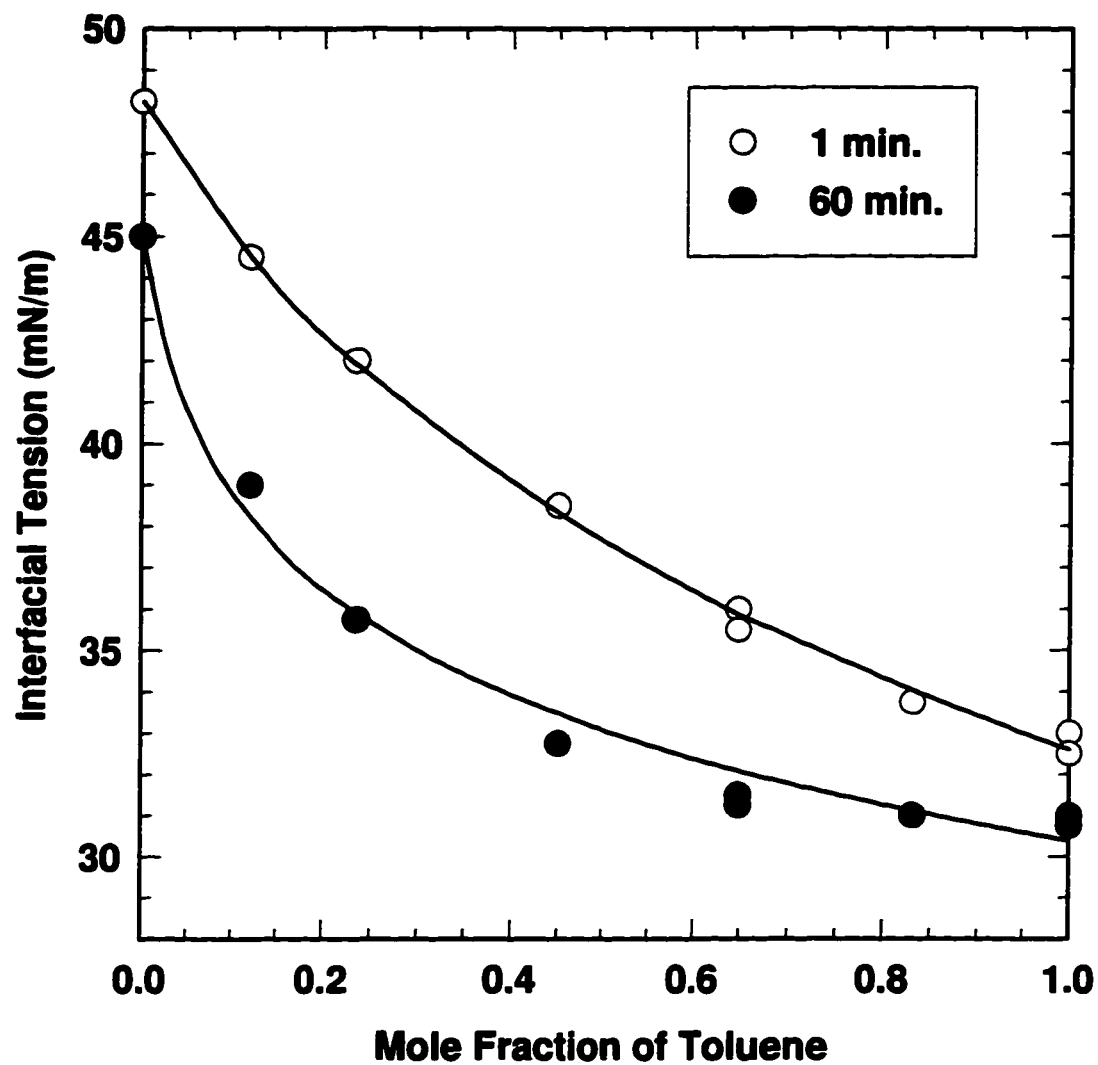


Figure A.9: Interfacial tension of solutions of toluene and hexane over water.

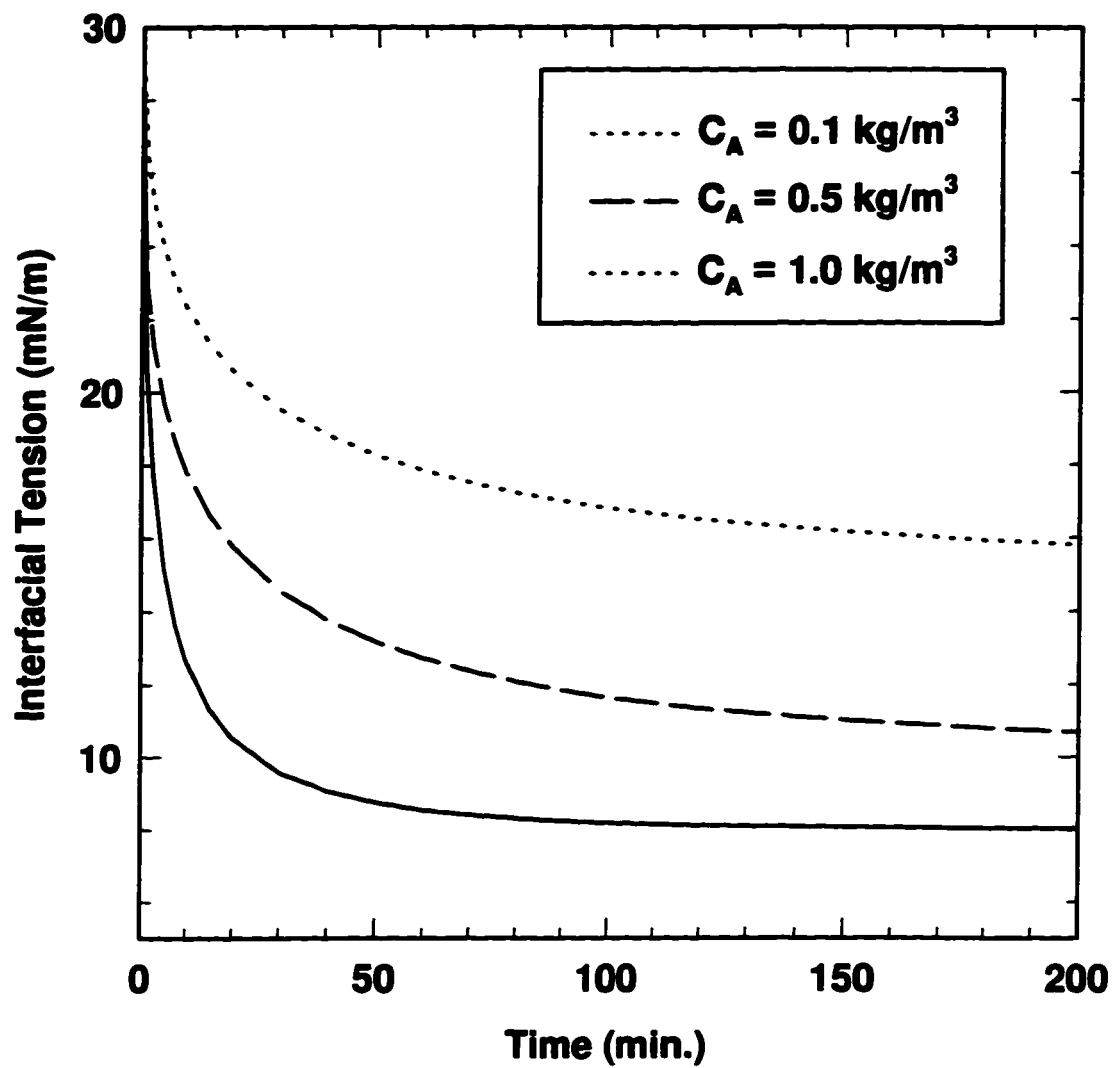


Figure A.10: Dynamic interfacial tension of asphaltene/toluene against 1 N NaOH (adapted from ref. 7).

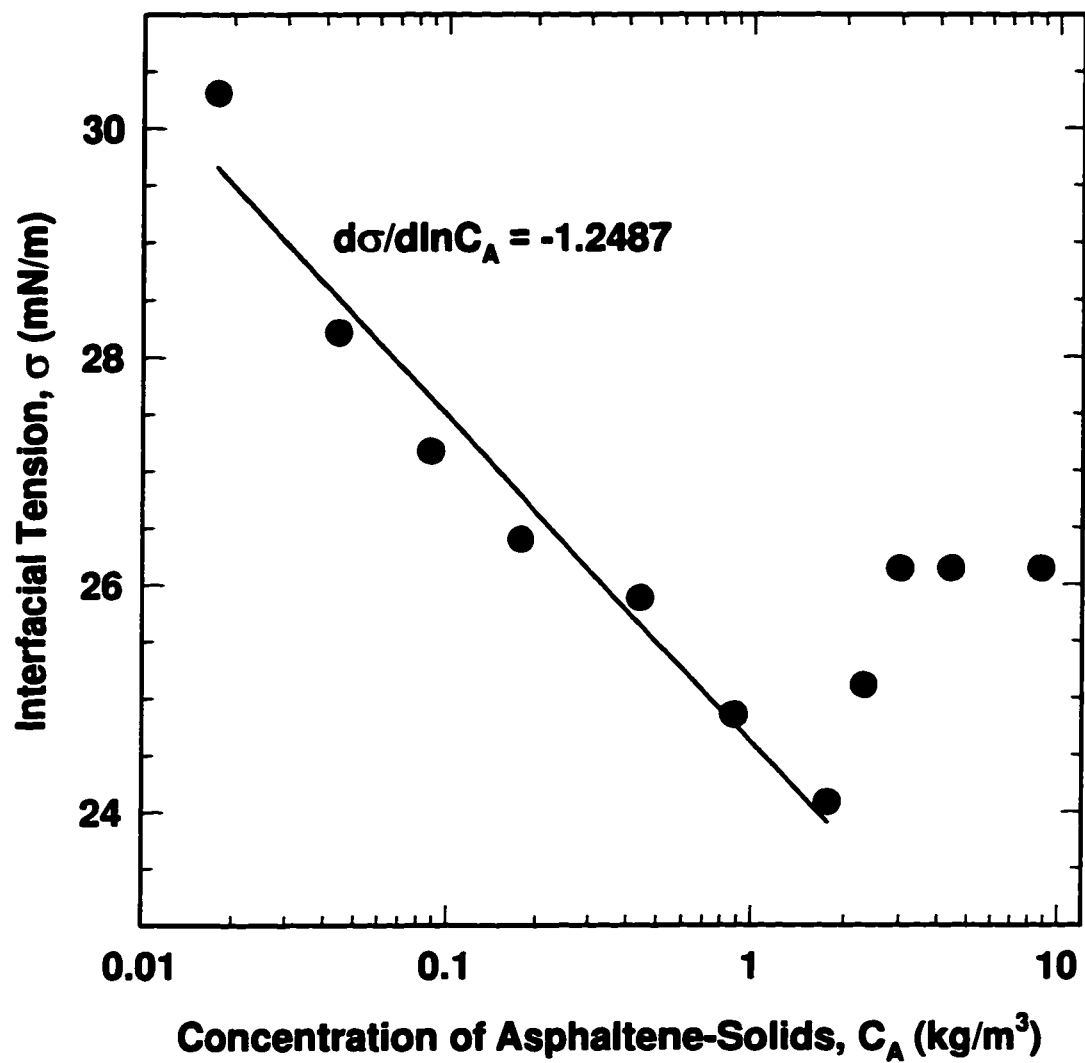


Figure A.11: Interfacial tension of asphaltene-solids in a toluene/hexane solution of 20 vol% toluene.

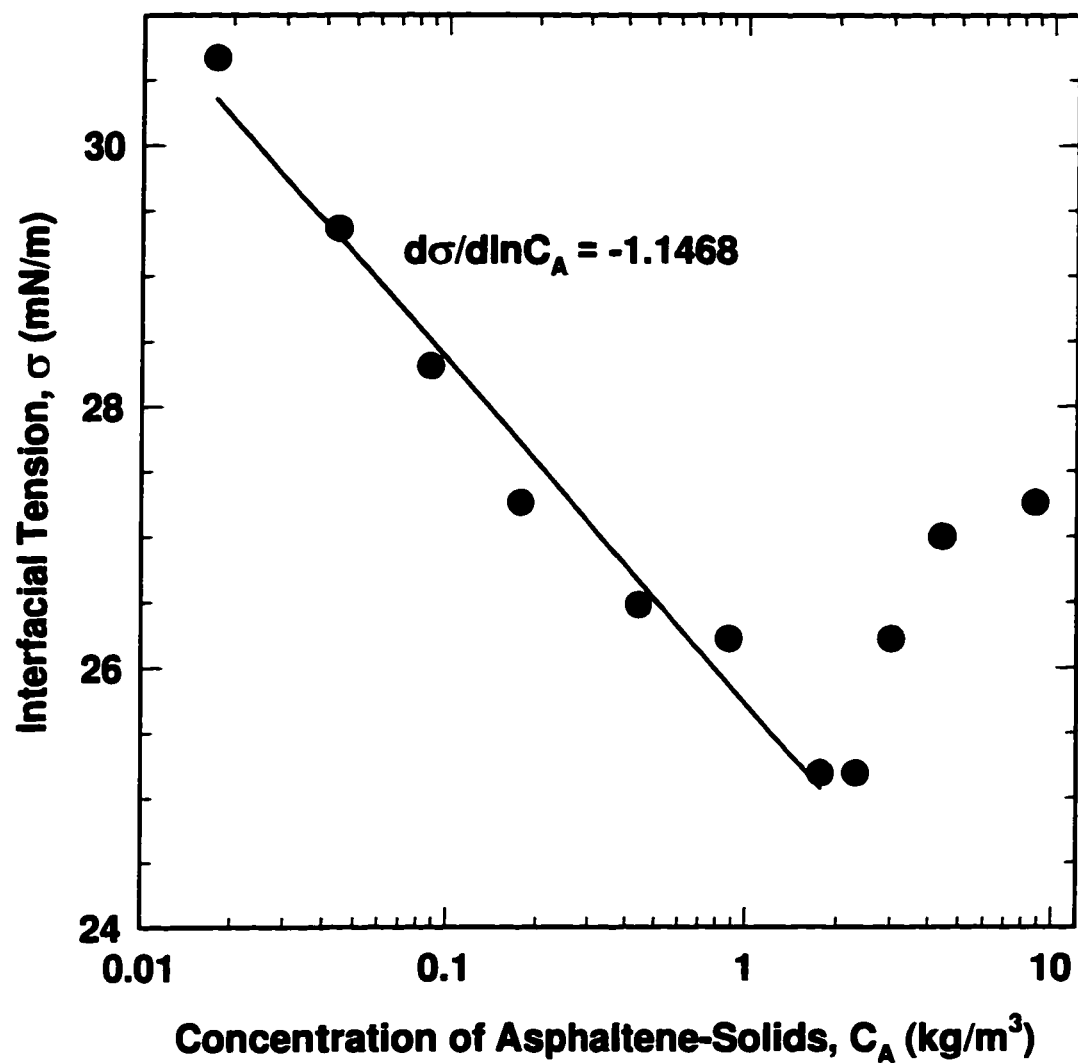


Figure A.12: Interfacial tension of asphaltene-solids in a toluene/hexane solution of 25 vol% toluene.

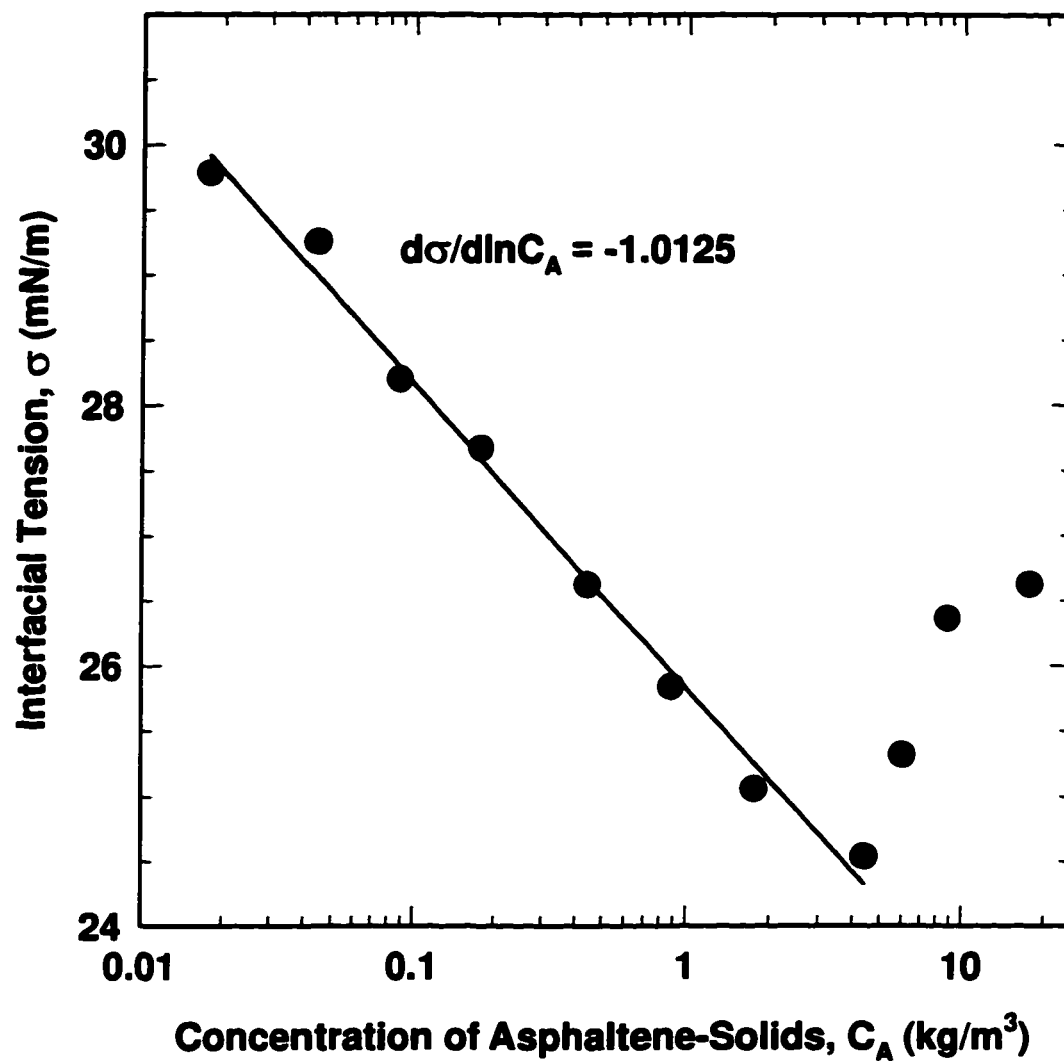


Figure A.13: Interfacial tension of asphaltene-solids in a toluene/hexane solution of 33 vol% toluene.

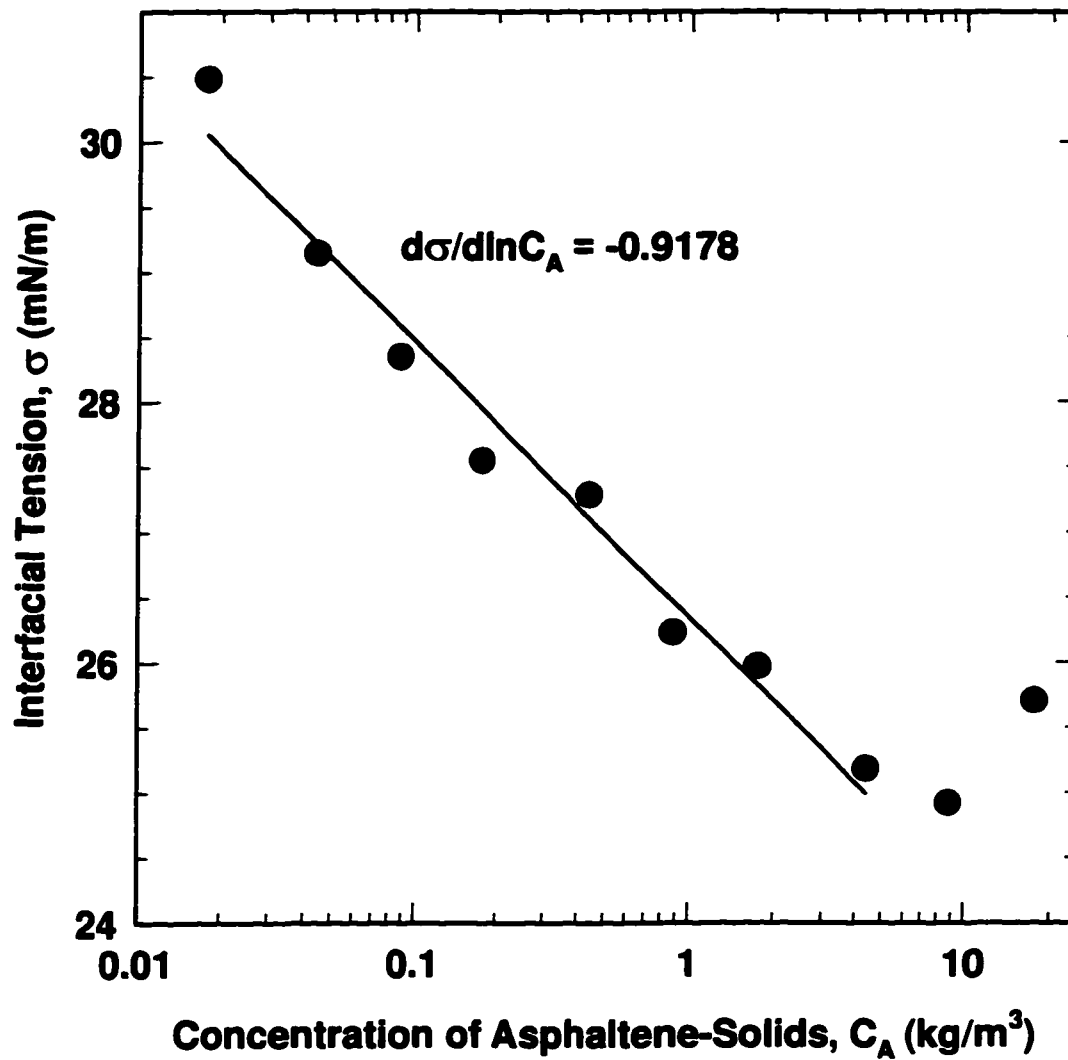


Figure A.14: Interfacial tension of asphaltene-solids in a toluene/hexane solution of 40 vol% toluene.

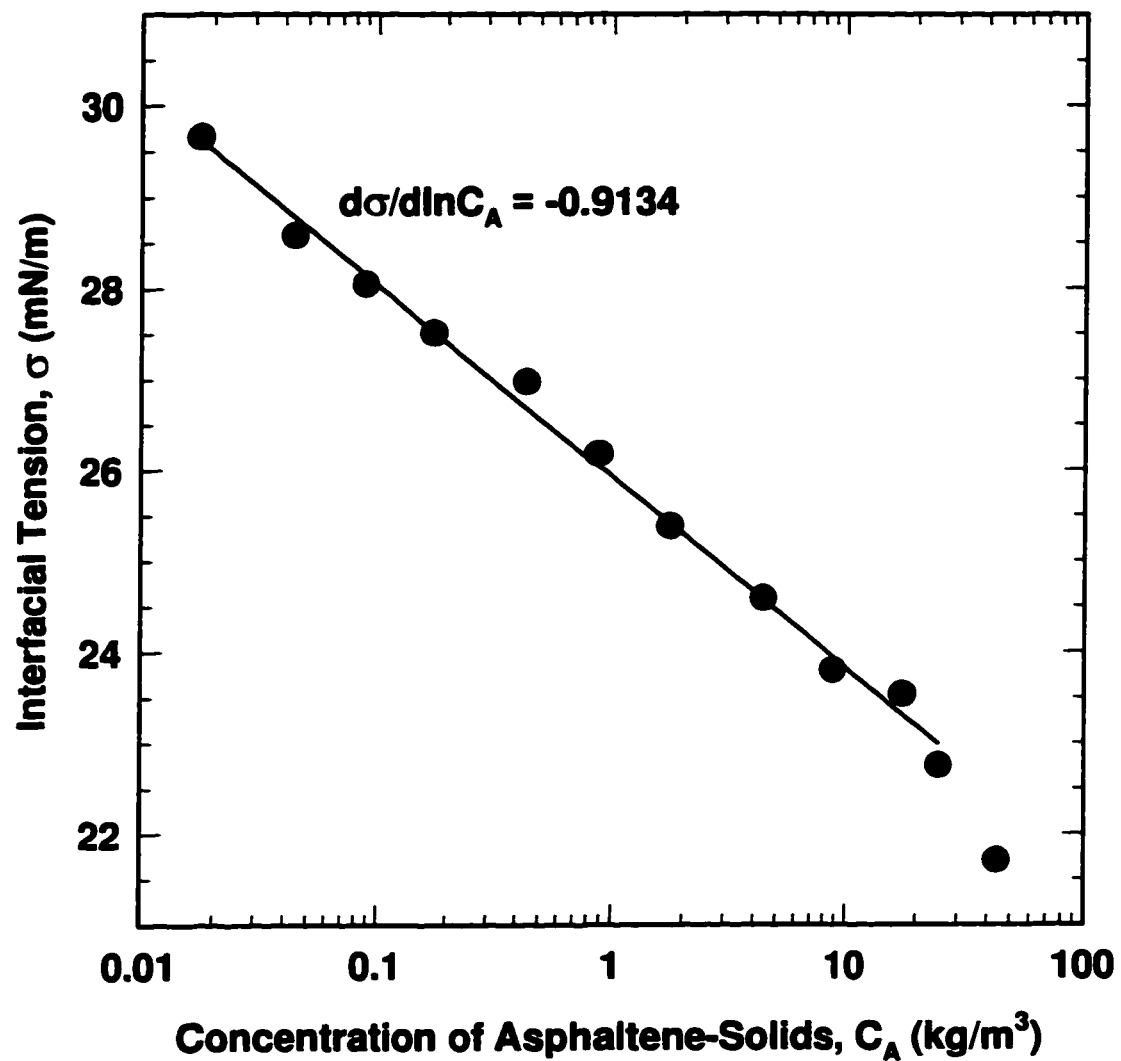


Figure A.15: Interfacial tension of asphaltene-solids in a toluene/hexane solution of 50 vol% toluene.

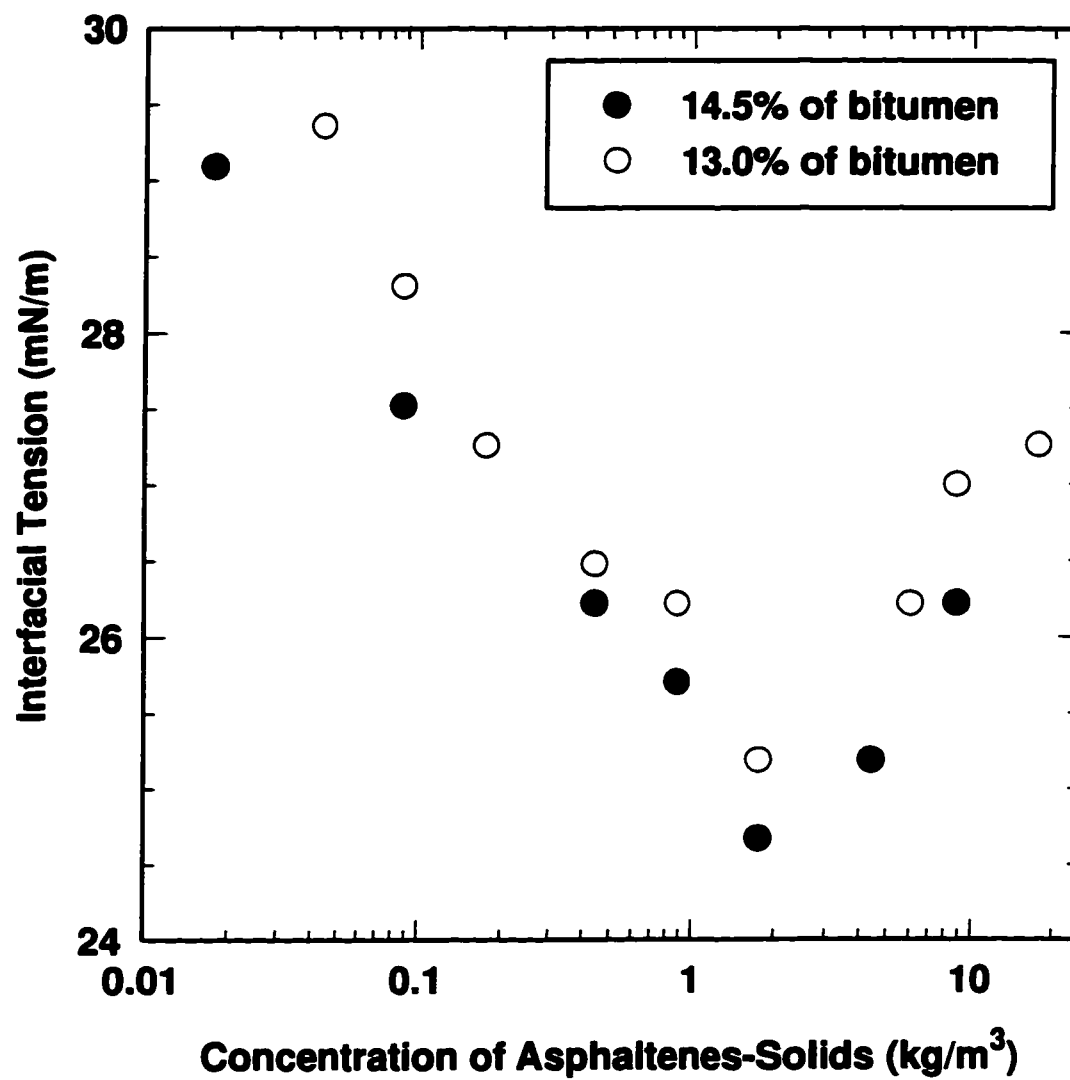


Figure A.16: Interfacial tensions of asphaltene-solids from different extractions in a toluene-hexane solution of 25 vol% toluene over water.

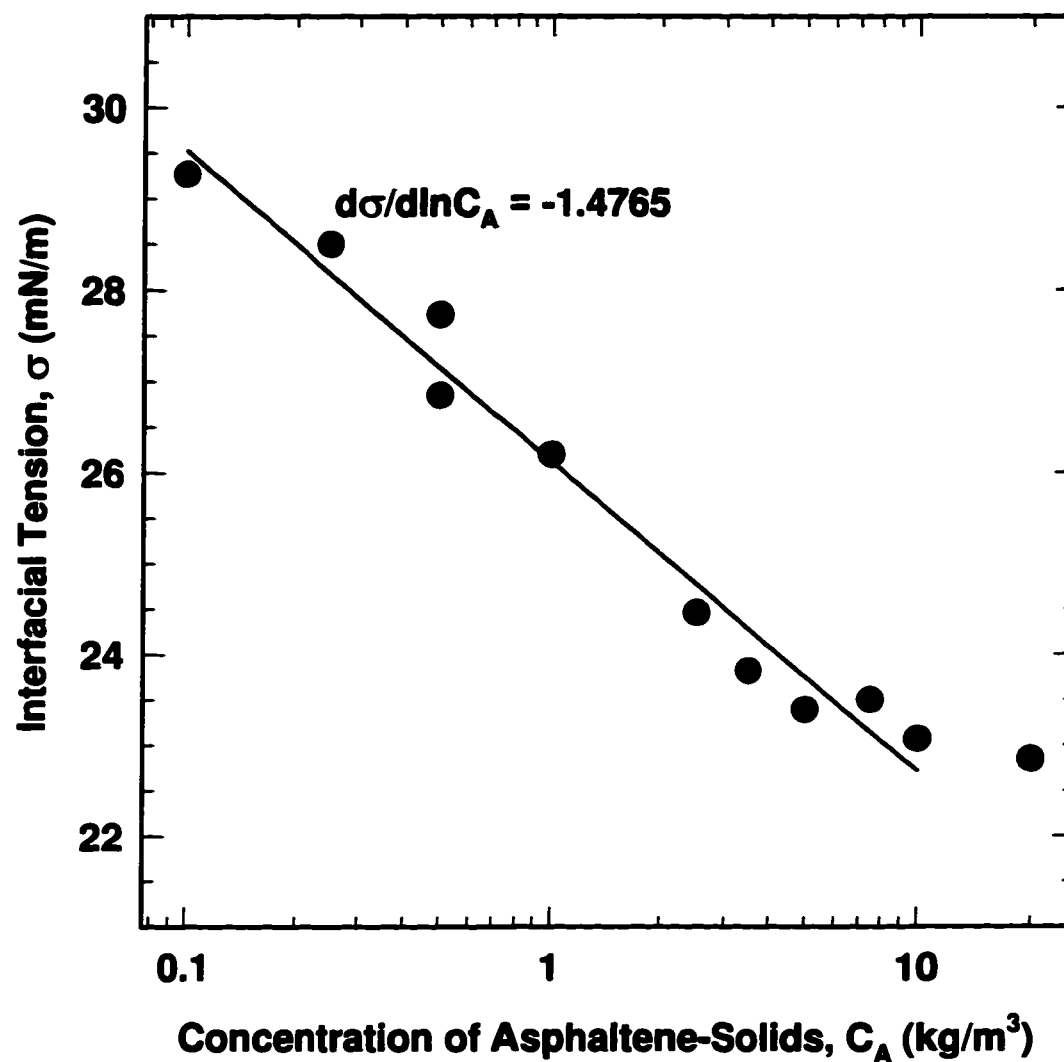


Figure A.17: Interfacial tension of asphaltene-solids in cyclohexane (precipitate removed).

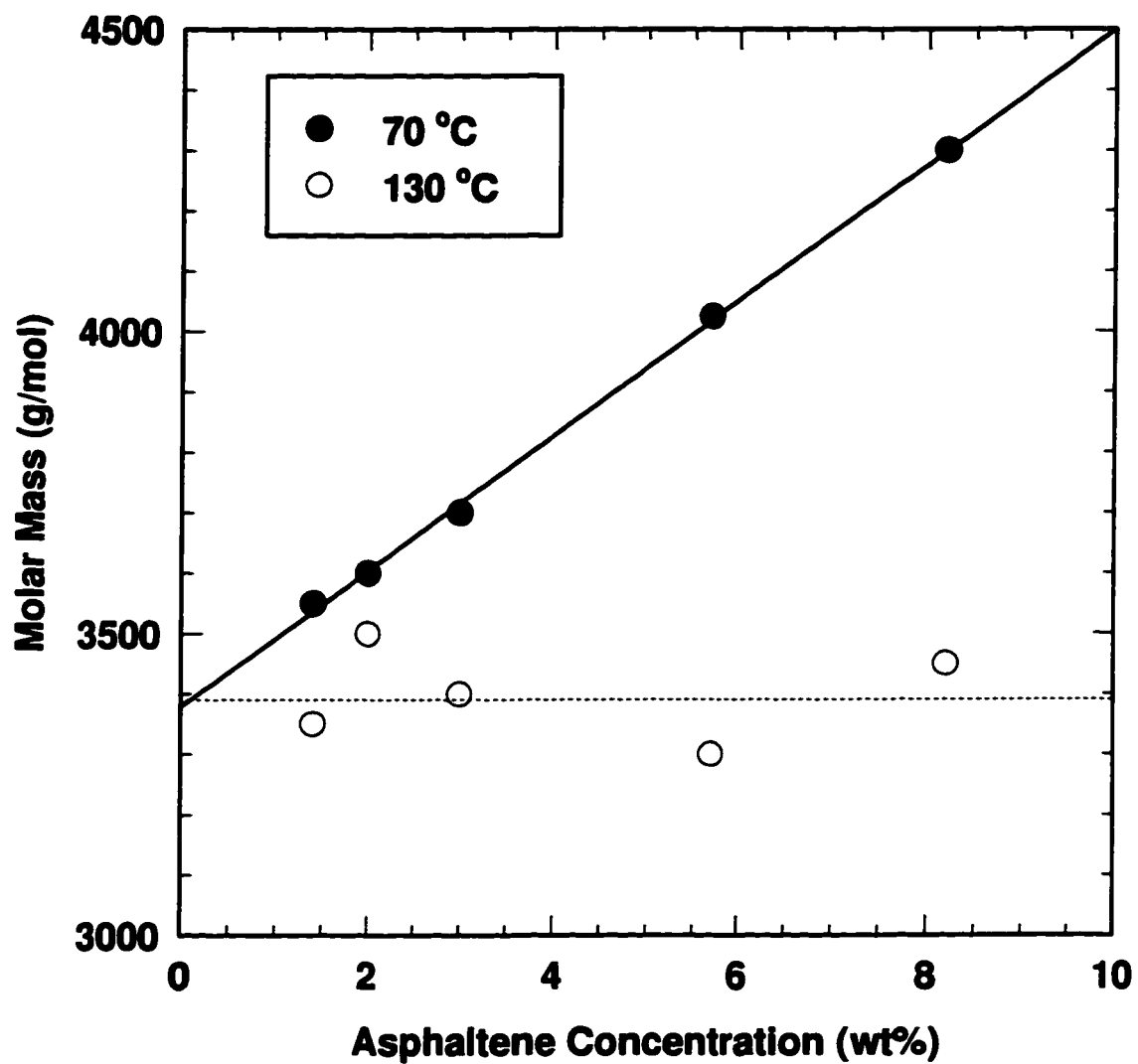


Figure A.18: Effect of asphaltene concentration on molar mass measured by vpo in 1,2-dichlorobenzene (9).

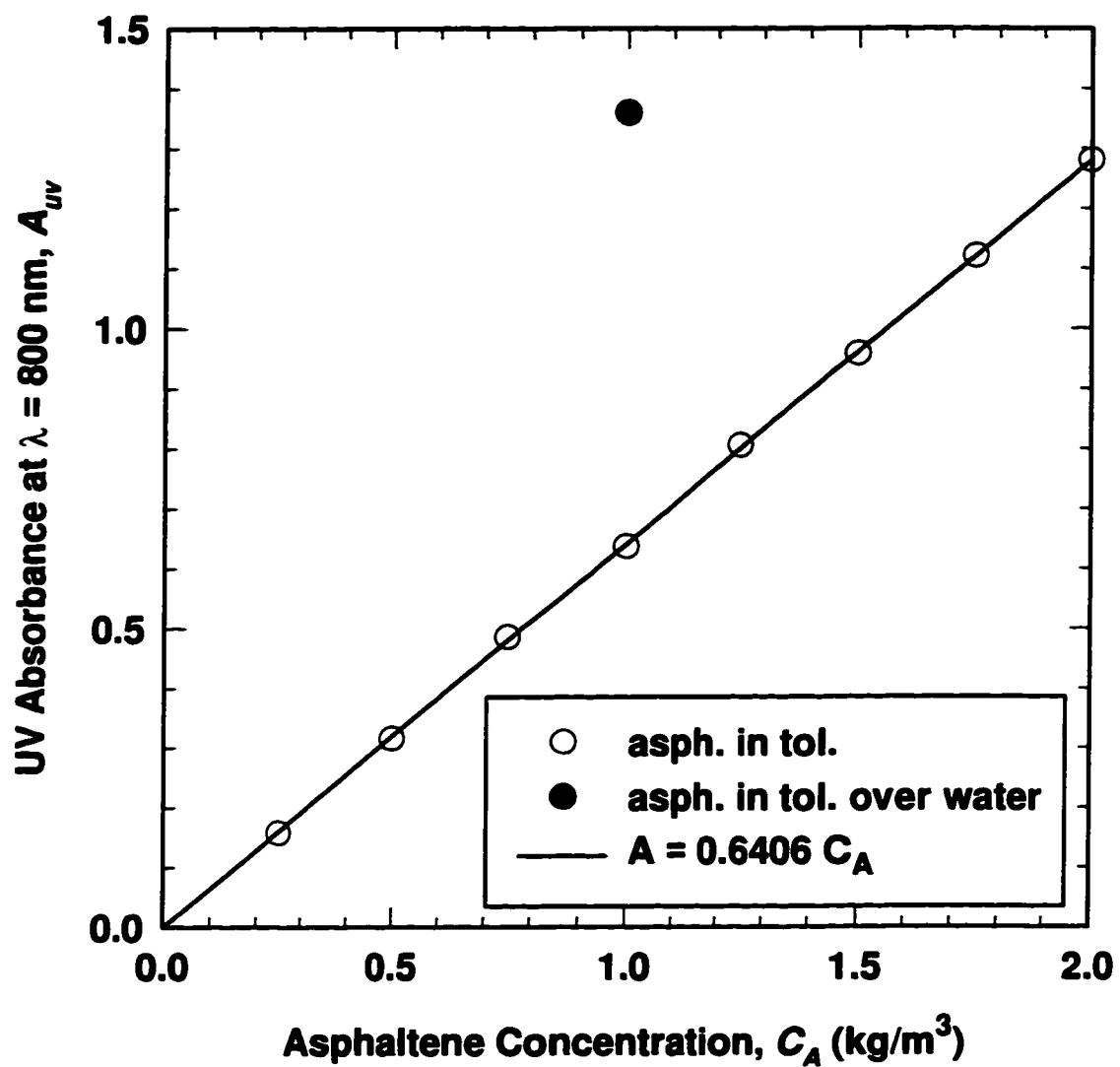


Figure A.19: Calibration curve for asphaltene concentration from UV absorbance at 800 nm.

Appendix B

ASPHALTENE MOLAR MASS DISTRIBUTION AND SOLUBILITY - ADDITIONAL MATERIAL

B.1 Number and Mass Average Molar Mass

The molar masses determined from interfacial tension measurements and from vapor pressure osmometry are number averaged molar masses. However, the predicted asphaltene molar masses are given in terms of a mass frequency distribution. A number average molar mass can be related to mass frequency as follows:

$$\bar{M} = \frac{\int M d\hat{f}}{\int d\hat{f}} = \frac{\int df}{\int \frac{df}{M}} \quad (\text{B.1})$$

where M is the molar mass of a single component, \bar{M} is the number averaged molar mass, f is the cumulative mass frequency and \hat{f} is the cumulative number frequency. The relationship of the cumulative mass frequency to molar mass in the asphaltenes is given by Eq. 2.11:

$$\frac{df_i}{dM_i} = \text{constant} (1 + \alpha_M \exp\{-\beta_M M_i\}) \quad (2.11)$$

where α_M and β_M have values of 50.63 and 0.00165 mol/g, respectively and are used to fit the molar mass distribution. M_i is the molar mass of the i^{th} asphaltene component and f_i is the cumulative mass frequency up to the i^{th} asphaltene component. Substituting Eq. 2.11 into Eq. B.1, the asphaltene number averaged molar mass can be expressed in terms of the asphaltene molar mass distribution,

$$\bar{M} = \frac{\int [1 + \alpha_M \exp\{-\beta_M M_i\}] dM_i}{\int \frac{1 + \alpha_M \exp\{-\beta_M M_i\}}{M_i} dM_i} \quad (\text{B.2})$$

Similarly, the mass average molar mass, \bar{M}_m , is given by,

$$\bar{M}_m = \frac{\int M df}{\int df} \quad (\text{B.3})$$

Eq. B.3 can be solved analytically giving the following expression:

$$\bar{M}_m = \frac{0.5(M_2^2 - M_1^2) - \frac{\alpha_M}{\beta_M} (M_2 e^{-\beta_M M_2} - M_1 e^{-\beta_M M_1}) + \frac{\alpha_M}{\beta_M^2} (e^{-\beta_M M_2} - e^{-\beta_M M_1})}{M_2 - M_1 - \frac{\alpha_M}{\beta_M} (e^{-\beta_M M_2} - e^{-\beta_M M_1})} \quad (\text{B.4})$$

The number and mass average molar masses of the asphaltene extracted from Athabasca bitumen and making up 14.5% of the mass of the bitumen are 3920 and 4860 g/mol, respectively. The polydispersity, or ratio of the mass to number average molar mass, of the asphaltenes is 1.24.

B.2 Solubility

The solids content of asphaltenes precipitated from toluene/hexane solutions of 0, 20, 25 and 33 vol% toluene are given in Table B.1. As discussed in Section 2.4, the data are consistent with a solids content of 6.3% in the entire asphaltene fraction. The solids-free asphaltene solubilities used in Chapters 2 and 3 were calculated from the measured asphaltene-solids solubility data with the following relationship,

$$f_{insol} = \frac{f_{insol}^* - 0.063}{1 - 0.063} \quad (\text{B.5})$$

The asphaltene-solids solubilities in toluene/hexane solvent mixtures measured with the solubility and precipitation methods, described in Section 2.2.2, are given in Tables B.2 and B.3, respectively. Asphaltene-solids solubilities in toluene mixed with the following solvents, n-pentane, n-heptane, n-octane, n-decane, isopentane, isooctane, acetone, methanol and 1-hexene are given in Tables B.4 to B.12, respectively. Asphaltene-solids solubilities in hexane mixed with the following solvents, dichloromethane, t-butylbenzene, nitrobenzene, cyclohexane, and decalin are given in Tables B.13 to B.17, respectively.

There is little literature data for the solubility of asphaltenes in solvents. Most experiments are concerned with the precipitation of asphaltenes from crude oils upon the addition of a poor solvent. However, there is data available for Boscan and Kuwait asphaltenes (1,2). The measured solubilities for Boscan and Kuwait asphaltene-solids in toluene/hexane mixtures are compared with the present work on Athabasca asphaltene-solids in Fig B.1. In all three cases, the solubility method described in Section 2.2.2 was employed; that is, the asphaltenes were dissolved in a premixed solvent mixture. Considering that the asphaltenes were obtained from different sources and likely have different molar mass distributions and solids content, the agreement is quite good.

The effect of temperature on the solubility of Boscan and Kuwait asphaltenes was also measured (2,3). The data is plotted in Fig. B.2 where the total asphaltenes are considered to be the amount of asphaltenes that precipitate at 25 °C. Two methods were employed to obtain the data: asphaltenes were precipitated from crude oil upon the addition of heptane; and the precipitated asphaltenes were redissolved in a toluene/heptane mixture of 20 vol% toluene. Predictions from the model developed in Chapter 2 are compared to the experimental results in Fig. B.2. Note the effect of temperature on the solvent solubility parameters was determined from Eq. B.12 (see Section B.3.1). The predicted effect of temperature on asphaltene solubility matches the Kuwait data very well. The

Boscan data deviates somewhat from the predicted trend. Again, considering the possible differences in molar mass distribution and solids content, the prediction is quite good.

B.3 Derivations

B.3.1 Scatchard-Hildebrand Theory

The activity coefficient for a given component can be calculated from the partial molar energy of mixing and the partial molar entropy of mixing. Scatchard-Hildebrand theory (4,5) provides a method for calculating the partial molar energy of mixing for a given component. The theory is built upon three major assumptions:

1. the interaction energy of molecular pairs is additive
2. the molecules are randomly distributed
3. there is no volume change upon mixing

With these assumptions, an expression for the molar internal energy of a mixture, U_{mix} (J/mol), can be derived for a two component system and it is given by (1),

$$-U_{mix} = \frac{\varepsilon_{11}v_1^2\hat{x}_1^2 + 2\varepsilon_{12}v_1v_2\hat{x}_1\hat{x}_2 + \varepsilon_{22}v_2^2\hat{x}_2^2}{v_1\hat{x}_1 + v_2\hat{x}_2} \quad (\text{B.6})$$

where v_1 and v_2 are the volumes (m^3/mol) and \hat{x}_1 and \hat{x}_2 are the mole fractions of components 1 and 2, respectively. The term ε_{ij} is the cohesive energy density, (J/m^3), *i.e.*, the molecular interaction energy between components i and j . For a pure component the cohesive energy density is defined as

$$\varepsilon_{ii} = \frac{\Delta U_i^{vap}}{v_i} \quad (\text{B.7})$$

where ΔU_i^{vap} is the molar internal energy of vaporization (J/mol) of component i . The cohesive energy density between two unlike molecules must be estimated as will be discussed later. For convenience, Eq. B.6 is converted to a volume fraction basis,

$$-U_{mix} = (v_1 x_1 + v_2 x_2) (\epsilon_{11} \phi_1^2 + 2\epsilon_{12} \phi_1 \phi_2 + \epsilon_{22} \phi_2^2) \quad (\text{B.8})$$

Here, ϕ_1 and ϕ_2 are the volume fractions of components 1 and 2, respectively. Now the change in molar internal energy upon mixing, ΔU_{mix} , is the difference between the molar internal energy of the mixture and of the pure components.

$$\begin{aligned} \Delta U_{mix} &= U_{mix} - U_1 x_1 - U_2 x_2 \\ &= (v_1 \hat{x}_1 + v_2 \hat{x}_2) (\epsilon_{11} + \epsilon_{22} - 2\epsilon_{12}) \phi_1 \phi_2 \end{aligned} \quad (\text{B.9})$$

The ϵ_{12} interaction energy can be estimated but is usually assumed to be the geometric mean of the pure component interaction energies, $\epsilon_{12} = (\epsilon_{11} \epsilon_{22})^{1/2}$. When the geometric mean is substituted into Eq. B.9, the equation simplifies to

$$\Delta U_{mix} = (v_1 \hat{x}_1 + v_2 \hat{x}_2) (\epsilon_{11}^{1/2} - \epsilon_{22}^{1/2})^2 \phi_1 \phi_2 \quad (\text{B.10})$$

For simplicity, a solubility parameter, δ ($\text{Pa}^{1/2}$), is introduced where $\delta_i = \epsilon_i^{1/2}$, and Eq. B.10 is further reduced to,

$$\Delta U_{mix} = (v_1 \hat{x}_1 + v_2 \hat{x}_2) (\delta_1 - \delta_2)^2 \phi_1 \phi_2 \quad (\text{B.11})$$

Note that, from its definition, the solubility parameter can be calculated from the molar heat of vaporization, ΔH_i^{vap} (J/mol). The expression for the ideal case is given by,

$$\delta_i = \left(\frac{\Delta U_i^{vap}}{v_i} \right)^{1/2} = \left(\frac{\Delta H_i^{vap} - RT}{v_i} \right)^{1/2} \quad (\text{B.12})$$

where R is the universal gas constant (J/mol K) and T is temperature (K).

Now, the partial molar energy of mixing for component i , \bar{U}_i (J/mol), is defined as the partial derivative of the internal energy of mixing with respect to the moles of component i , n_i ,

$$\bar{U}_i = \frac{\partial \Delta \hat{U}_{mix}}{\partial n_i} \quad (\text{B.13})$$

Therefore, to solve for the partial molar energy of mixing, Eq. B.11 must be recast in terms of moles rather than volume fractions.

$$\Delta \hat{U}_{mix} = (v_1 n_1 + v_2 n_2) (\delta_1 - \delta_2)^2 \frac{v_1 v_2 n_1 n_2}{(v_1 n_1 + v_2 n_2)^2} \quad (\text{B.14})$$

where $\Delta \hat{U}_{mix}$ is the internal energy of mixing (J). The derivation of Eq. B.13 is performed and the result converted back to volume fractions to obtain the partial molar energy of mixing. It is given by,

$$\bar{U}_i = v_i \phi_j^2 (\delta_i - \delta_j)^2 \quad (\text{B.15})$$

Now that the partial molar internal energy of mixing is known, the partial molar free energy of mixing and the activity coefficient can be determined. Recall the fundamental thermodynamic relations,

$$\bar{G}_i = \bar{H}_i - T\bar{S}_i \quad (\text{B.16})$$

$$\bar{U}_i = \bar{H}_i - P\bar{V}_i \quad (\text{B.17})$$

where T and P are temperature and pressure and \bar{G}_i , \bar{H}_i , \bar{S}_i and \bar{V}_i are, respectively, the partial molar free energy, enthalpy, entropy and volume of mixing of component i .

However, the assumption that there is no volume change upon mixing means that \bar{V}_i is zero and hence

$$\bar{G}_i = \bar{U}_i - T\bar{S}_i \quad (\text{B.18})$$

The activity of component i , \hat{a}_i , is defined as

$$\hat{a}_i = \exp\left\{\frac{\bar{G}_i}{RT}\right\} \quad (\text{B.19})$$

and the activity of component i can also be expressed as

$$\hat{a}_i = \frac{f_i^l}{f_i^o} = \frac{\hat{x}_i \gamma_i f_i^{ol}}{f_i^o} \quad (\text{B.20})$$

Here, f_i^l is the fugacity in the liquid phase, f_i^o is an arbitrary reference standard state fugacity, f_i^{ol} is the standard state fugacity of the pure component and γ_i is the activity coefficient, all of component i . The reference standard state fugacity is usually chosen to be the fugacity of the pure component in the liquid phase. With this assumption, Eq. B.20 reduces to

$$\hat{a}_i = \hat{x}_i \gamma_i \quad (\text{B.21})$$

Eqs. B.18, B.19 and B.21 are combined to obtain the following:

$$\ln\{\hat{x}_i\gamma_i\} = \frac{\bar{U}_i - T\bar{S}_i}{RT} \quad (\text{B.22})$$

The partial molar internal energy is given by Eq. B.15 and for ideal systems the partial molar entropy is given by

$$\bar{S}_i = -R \ln \hat{x}_i \quad (\text{B.23})$$

Eqs. B.15 and B.23 are substituted into B.22, to obtain an expression for the activity coefficient in a two component system. The expression is given by

$$\gamma_1 = \exp\left\{\frac{v_1\phi_2^2(\delta_1 - \delta_2)^2}{RT}\right\} \quad (\text{B.24})$$

Eq. 24 gives the activity coefficient from standard Scatchard-Hildebrand theory. For the mixing of large molecules, the partial molar entropy of mixing can be estimated with Flory-Huggins theory and, for a two component system, is given by

$$\bar{S}_1 = -R \left[\ln \phi_1 + \phi_2 \left(1 - \frac{v_1}{v_2} \right) \right] \quad (\text{B.25})$$

Eqs. B.15 and B.25 are substituted into Eq. B.22 to obtain the following:

$$\gamma_1 = \exp\left\{\ln \frac{\phi_1}{\hat{x}_1} + \phi_2 \left(1 - \frac{v_1}{v_2} \right) + \frac{v_1\phi_2^2(\delta_1 - \delta_2)^2}{RT}\right\} \quad (\text{B.26})$$

Eq. B.26 is the general solution for the activity coefficient of a large molecule. In dilute solutions, where $\phi_2 \approx 1$, $\hat{x}_2 \approx 1$ and $\phi_1 \approx \hat{x}_1 v_1 / \hat{x}_2 v_2$, Eq. B.26 reduces to

$$\gamma_1 = \exp \left\{ \ln \frac{v_1}{v_2} + \left(1 - \frac{v_1}{v_2} \right) + \frac{v_1 (\delta_1 - \delta_2)^2}{RT} \right\} \quad (\text{B.27})$$

Eqs. B.26 and B.27 were derived for two component mixtures. For multicomponent mixtures, all the components except the component of interest are lumped together and an average molar volume and solubility parameter are determined for the mixture. Eq. B.27 is modified as follows

$$\gamma_1 = \exp \left\{ \ln \frac{v_1}{v_m} + \left(1 - \frac{v_1}{v_m} \right) + \frac{v_1 (\delta_1 - \delta_m)^2}{RT} \right\} \quad (\text{B.28})$$

where

$$v_m = \sum \hat{x}_i v_i \quad (\text{B.29})$$

and

$$\delta_m = \sum \phi_i \delta_i \quad (\text{B.30})$$

B.4.2 Solid-Liquid Equilibrium Calculation

Consider the total mole and component mole balances for a feed stream separating into a “solid” precipitate and a liquid,

$$n_F = n_{SP} + n_L \quad (\text{B.31})$$

$$\hat{z}_i n_F = \hat{x}_i^s n_{SP} + \hat{x}_i^l n_L \quad (\text{B.32})$$

Here, n_F , n_L and n_{SP} are the moles of feed, liquid and solid, respectively, and \hat{z}_i , \hat{x}_i^l and \hat{x}_i^s are the mole fractions of component i in the feed, liquid and solid, respectively. When Eq. B.31 is substituted into B.32, the following expression for the mole fraction of component i in the solid phase is found:

$$\hat{x}_i^s = \frac{\hat{z}_i(1 + \alpha_{SL})}{\frac{1}{K_i} + \alpha_{SL}} \quad (\text{B.33})$$

where the equilibrium ratio, K_i , is defined as $K_i = \hat{x}_i^s / \hat{x}_i^l$, and the solid-liquid ratio, α_{SL} is defined as $\alpha_{SL} = n_{SP}/n_L$. Now the solid phase mole fractions must sum to unity. The summation of Eq. B.33 is given by

$$\sum x_i^s = \sum \frac{z_i K_i (1 + \alpha_{SL})}{1 + K_i \alpha_{SL}} = 1 \quad (\text{B.34})$$

If the feed composition and equilibrium ratios are known, the solid-liquid ratio can be calculated from Eq. B.34. The mole ratio of the solid to the feed is $\alpha_{SL}/(1 + \alpha_{SL})$. If the solid phase is entirely comprised of asphaltenes, then the mole ratio of solid asphaltenes to total asphaltenes is given by:

$$\hat{f}_{insol} = \frac{\alpha_{SL}}{\hat{z}_A (1 + \alpha_{SL})} \quad (\text{B.35})$$

where \hat{z}_A is the mole fraction of all the asphaltenes in the feed. Similarly, the mass ratio of solid asphaltenes to total asphaltenes is given by,

$$f_{insol} = \frac{\alpha_{SL} \sum \hat{x}_i^s M_i}{z_A (1 + \alpha_{SL}) \sum \hat{z}_i M_i} \quad (\text{B.36})$$

where z_A is the mass fraction of all the asphaltenes in the feed.

B.4 Computer Programs

Solubility and other computer calculations were carried out on MATLAB[®]. The routines and subroutines written for the calculations are printed out at the end of the appendix. A brief index is given below.

| | |
|------------|---|
| fsolasph.m | asphaltene solid-liquid equilibrium calculation in two phase region |
| sptasph.m | find solvent mix at which first asphaltene molecule precipitates |
| kvalasph.m | find equilibrium ratios for asphaltene subfractions |
| solvprop.m | input file for solvent properties |
| asphprop.m | input file for asphaltene properties |
| mwdist1.m | generate discretized asphaltene molar mass distribution |
| bisct.m | subroutine used to calculate asphaltene molar mass |
| mavgh.m | find number average molar mass of heaviest asphaltene subfraction |
| mavgl.m | find number average molar mass of lightest asphaltene subfraction |
| mint.m | subroutine used in average molar mass calculation |
| pavgh.m | find average density of heaviest asphaltene subfraction |
| pavgl.m | find average density of lightest asphaltene subfraction |
| pint.m | subroutine used in average density calculation |

B.5 References

1. Andersen, S.I., and Stenby, E.H., "Hysteresis in Asphaltene Precipitation and Redissolution", *Proc. Can. Chem. Eng. Conf.*, Calgary, 1994.
2. Andersen, S.I., and Stenby, E.H., *Fuel Sci. Technol. Intl.*, **14**, (1996), 261.
3. Andersen, S.I., *Fuel Sci. Technol. Intl.*, **12**, (1994), 51.
4. Prausnitz, J.M., R.N. Lichtenthaler and E.G. de Azevedo, "Molecular Thermodynamics of Fluid-Phase Equilibria", 2nd Ed., Prentice-Hall, Inc., Englewood Cliffs, New Jersey (1986).
5. Barton, A.M.F., "CRC Handbook of Solubility Parameters and Other Cohesion Parameters", CRC Press, Boca Raton, Fl. (1983).

Table B.1: Solids content of asphaltene-solids precipitated from toluene/hexane solutions.

| vol% tol. | mass fr. solids |
|-----------|--------------------|
| 0 | 0.064 |
| 0 | 0.068 |
| 20 | 0.083 |
| 25 | 0.111 |
| 33 | 0.149 |

Table B.2: Solubility of asphaltene-solids in toluene/hexane mixtures - solubility method.

| Asph. Conc. (kg/m ³) | Mass Ratio of Insoluble to Total Asphaltenes in Toluene/Hexane Mixtures | | | | | | |
|--|---|----------|----------|----------|----------|----------|----------|
| | 7.5 % tol. | 17% tol. | 20% tol. | 25% tol. | 33% tol. | 40% tol. | 50% tol. |
| 1.76 | - | - | 0.709 | 0.595 | 0.373 | 0.223 | 0.101 |
| 4.4 | - | - | 0.741 | 0.609 | 0.368 | 0.214 | 0.109 |
| 8.8 | 0.927 | 0.830 | 0.755 | 0.6 | 0.395 | 0.218 | 0.123 |
| 17.6 | - | - | 0.759 | 0.613 | 0.391 | 0.186 | 0.091 |

Table B.3: Solubility of asphaltene-solids in toluene/hexane mixtures - precipitation method.

| Asph. Conc. (kg/m ³) | Mass Ratio of Insoluble to Total Asphaltene-Solids in Toluene/Hexane Mixtures | | | | | | |
|--|---|----------|----------|----------|----------|----------|----------|
| | 17% tol. | 20% tol. | 25% tol. | 33% tol. | 40% tol. | 50% tol. | 60% tol. |
| 1.76 | - | 0.609 | 0.495 | 0.305 | 0.173 | 0.100 | - |
| 4.4 | - | 0.691 | 0.545 | 0.350 | 0.209 | 0.105 | - |
| 8.8 | 0.775 | 0.707 | 0.591 | 0.355 | 0.191 | 0.105 | 0.09550 |
| 17.6 | - | 0.727 | 0.591 | 0.382 | 0.180 | 0.093 | - |

Table B.4: Solubility of asphaltene-solids in toluene/pentane mixtures.

| Vol. Fr. Toluene | f_{insol} Solubility Method | f_{insol} Precipitation Method |
|---------------------|--|---|
| 0.075 | 0.961 | - |
| 0.167 | 0.927 | 0.875 |
| 0.250 | 0.814 | 0.741 |
| 0.330 | 0.555 | 0.523 |
| 0.400 | - | 0.293 |
| 0.500 | 0.105 | 0.091 |
| 0.600 | - | 0.093 |

Table B.5: Solubility of asphaltene-solids in toluene/heptane mixtures.

| Vol. Fr. Toluene | f_{insol} Solubility Method | f_{insol} Precipitation Method |
|---------------------|--|---|
| 0.075 | 0.909 | - |
| 0.167 | 0.816 | 0.741 |
| 0.200 | 0.752 | 0.677 |
| 0.250 | 0.591 | 0.516 |
| 0.330 | 0.352 | 0.309 |
| 0.400 | 0.166 | 0.145 |
| 0.500 | 0.086 | 0.086 |

Table B.6: Solubility of asphaltene-solids in toluene/octane mixtures.

| Vol. Fr. Toluene | f_{insol} Solubility Method | f_{insol} Precipitation Method |
|---------------------|--|---|
| 0.075 | 0.957 | - |
| 0.167 | 0.773 | 0.743 |
| 0.250 | 0.666 | 0.545 |
| 0.330 | 0.382 | 0.339 |
| 0.400 | 0.205 | 0.177 |
| 0.500 | 0.086 | 0.093 |

Table B.7: Solubility of asphaltene-solids in toluene/decane mixtures.

| Vol. Fr. Toluene | f_{insol} Solubility Method | f_{insol} Precipitation Method |
|---------------------|--|---|
| 0.075 | 0.952 | - |
| 0.167 | 0.755 | 0.677 |
| 0.250 | 0.568 | 0.509 |
| 0.330 | 0.439 | 0.355 |
| 0.400 | 0.186 | 0.170 |
| 0.500 | 0.093 | 0.082 |

Table B.8: Solubility of asphaltene-solids in toluene/isopentane mixtures ^a.

| Vol. Fr. Toluene | f_{insol} Solubility Method | f_{insol} Precipitation Method |
|---------------------|--|---|
| 0.075 | 0.966 | - |
| 0.167 | - | 0.911 |
| 0.250 | - | 0.766 |
| 0.330 | - | 0.480 |
| 0.400 | - | 0.291 |
| 0.500 | 0.130 | 0.130 |
| 0.600 | - | 0.084 |

Table B.9: Solubility of asphaltene-solids in toluene/isooctane mixtures.

| Vol. Fr. Toluene | f_{insol} Solubility Method | f_{insol} Precipitation Method |
|---------------------|--|---|
| 0.075 | 0.943 | - |
| 0.167 | 0.807 | 0.845 |
| 0.250 | 0.809 | 0.720 |
| 0.330 | 0.536 | 0.491 |
| 0.400 | - | 0.391 ^b |
| 0.500 | 0.100 | 0.909 ^b |
| 0.600 | - | 0.125 ^b |

a - left 1 hour to reach equilibrium

b - used filter paper to dry precipitate

Table B.10: Solubility of asphaltene-solids in toluene/acetone mixtures.

| Vol. Fr. Toluene | f_{insol} Solubility Method | f_{insol} Precipitation Method |
|---------------------|-------------------------------------|--|
| 0.100 | 1.000 | - |
| 0.200 | - | 0.877 |
| 0.300 | - | 0.839 |
| 0.400 | - | 0.755 |
| 0.500 | - | 0.602 |
| 0.600 | - | 0.295 |
| 0.700 | - | 0.086 |
| 0.800 | - | 0.091 |

Table B.11: Solubility of asphaltene-solids in toluene/methanol mixtures.

| Vol. Fr. Toluene | f_{insol} Solubility Method | f_{insol} Precipitation Method |
|---------------------|-------------------------------------|--|
| 0.100 | 1.000 | - |
| 0.200 | - | 0.957 |
| 0.400 | - | 0.841 |
| 0.500 | - | 0.752 |
| 0.600 | - | 0.593 |
| 0.700 | - | 0.502 |
| 0.800 | - | 0.089 |
| 0.900 | - | 0.071 |

Table B.12: Solubility of asphaltene-solids in toluene/1-hexene mixtures.

| Vol. Fr. Toluene | f_{insol} Solubility Method | f_{insol} Precipitation Method |
|---------------------|--|---|
| 0.075 | 0.864 | - |
| 0.167 | - | 0.593 |
| 0.250 | - | 0.483 |
| 0.330 | - | 0.183 |
| 0.400 | - | 0.059 |
| 0.500 | - | 0.030 |

Table B.13: Solubility of asphaltene-solids in dichloromethane/hexane mixtures.

| Vol. Fr. dcm | f_{insol} Solubility Method | f_{insol} Precipitation Method |
|-----------------|--|---|
| 0.050 | 0.952 | - |
| 0.100 | 0.848 | 0.757 |
| 0.167 | 0.630 | 0.584 |
| 0.250 | 0.334 | 0.309 |
| 0.330 | 0.098 | 0.095 |
| 0.500 | 0.071 | 0.071 |

Table B.14: Solubility of asphaltene-solids in t-butylbenzene/hexane mixtures ^a.

| Vol. Fr. tbutylbenz. | f_{insol} Solubility Method | f_{insol} Precipitation Method |
|-------------------------|--|---|
| 0.075 | 0.995 | - |
| 0.167 | - | 0.898 |
| 0.250 | - | 0.816 |
| 0.330 | - | 0.689 |
| 0.400 | - | 0.464 |
| 0.400 | - | 0.571 |
| 0.500 | - | 0.402 |
| 0.600 | - | 0.227 |
| 0.700 | - | 0.145 |
| 0.850 | - | 0.084 |

Table B.15: Solubility of asphaltene-solids in nitrobenzene/hexane mixtures.

| Vol. Fr. nitrobenzene | f_{insol} Solubility Method | f_{insol} Precipitation Method |
|--------------------------|--|---|
| 0.050 | 1.000 | - ^a |
| 0.100 | 0.961 | ^a |
| 0.167 | 0.516 | 0.548 |
| 0.250 | 0.182 | 0.184 |
| 0.250 | 0.259 | ^a |
| 0.330 | | 0.193 ^a |
| 0.400 | 0.163 | 0.136 ^a |
| 0.500 | 0.130 | 0.139 |

a - filter paper used to dry precipitate

Table B.16: Solubility of asphaltene-solids in cyclohexane/hexane mixtures.

| Vol. Fr. cyclohexane | $f_{\text{insol}} (C_A = 8.8 \text{ kg/m}^3)$ | | $f_{\text{insol}} (C_A = 4.4 \text{ kg/m}^3)$ | |
|-------------------------|---|-------------------------|---|-------------------------|
| | Solubility Method | Precipitation Method | Solubility Method | Precipitation Method |
| 0.167 | - | - | - | 0.898 |
| 0.200 | 0.905 | 0.905 | - | - |
| 0.250 | 0.902 | 0.870 | - | - |
| 0.330 | 0.864 | 0.845 | - | 0.814 |
| 0.400 | 0.850 | 0.800 | - | - |
| 0.500 | 0.777 | 0.730 | 0.741 | 0.682 |
| 0.500 | 0.800 | 0.787 | - | - |
| 0.600 | 0.675 | 0.632 | - | 0.645 |
| 0.700 | 0.643 | 0.516 | - | - |
| 0.800 | 0.461 | 0.434 | - | - |
| 0.900 | 0.366 | 0.330 | - | - |
| 1.000 | 0.330 | 0.343 | - | - |

Table B.17: Solubility of asphaltene-solids in decalin/hexane mixtures ^b.

| Vol. Fr. decalin | f_{insol} Solubility Method | f_{insol} Precipitation Method |
|---------------------|--|---|
| 0.075 | 1.000 | - |
| 0.167 | - | 0.564 |
| 0.250 | - | 0.798 |
| 0.330 | - | 0.639 |
| 0.400 | - | 0.507 |
| 0.500 | - | 0.341 |
| 0.600 | - | 0.155 |
| 0.700 | - | 0.125 |

a - left 5 days to reach equilibrium

b - filter paper used to dry precipitate

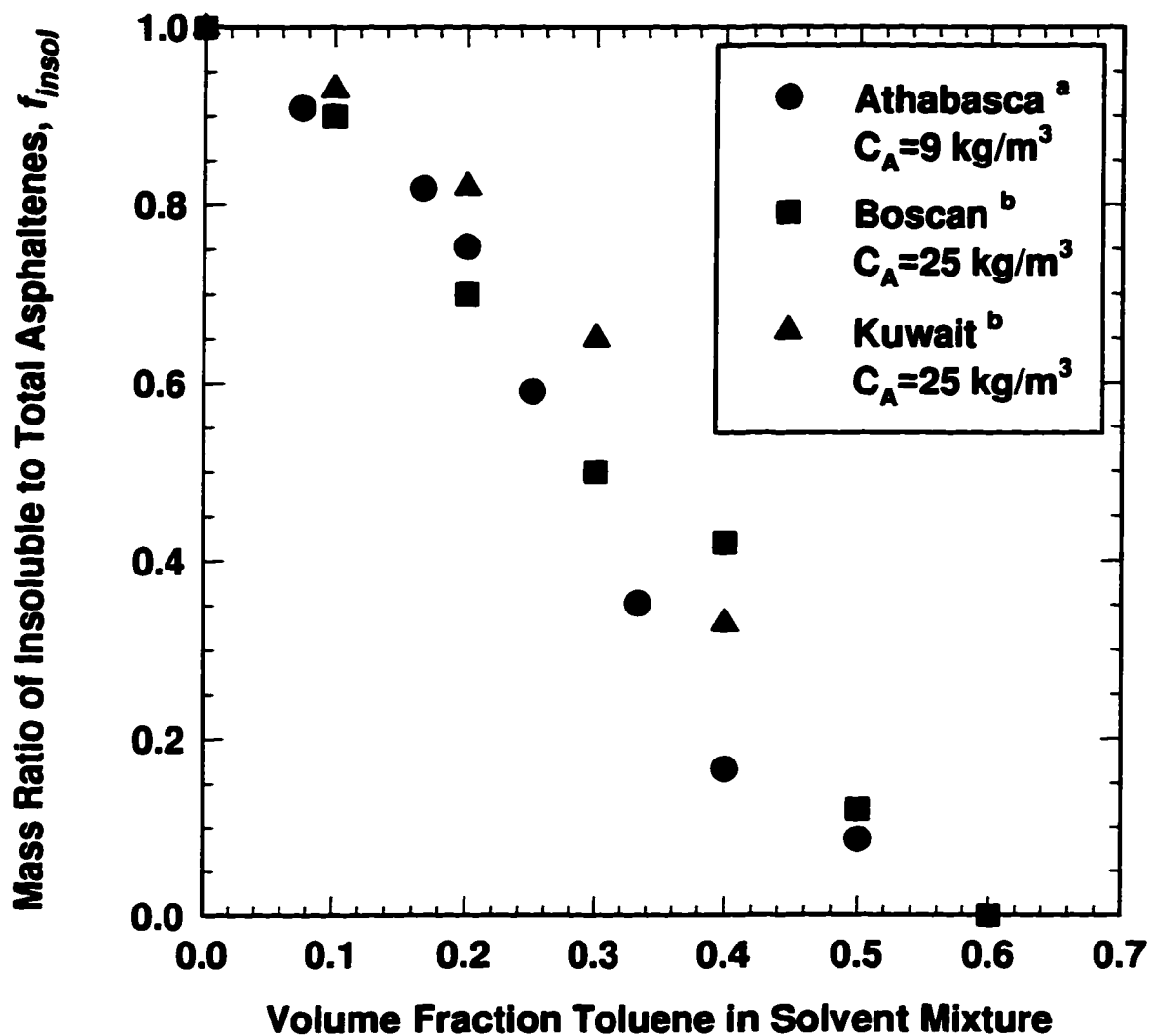


Figure B.1: Solubility of asphaltene-solids from various sources in solutions of toluene and heptane. (a) present work, (b) ref. (1,2)

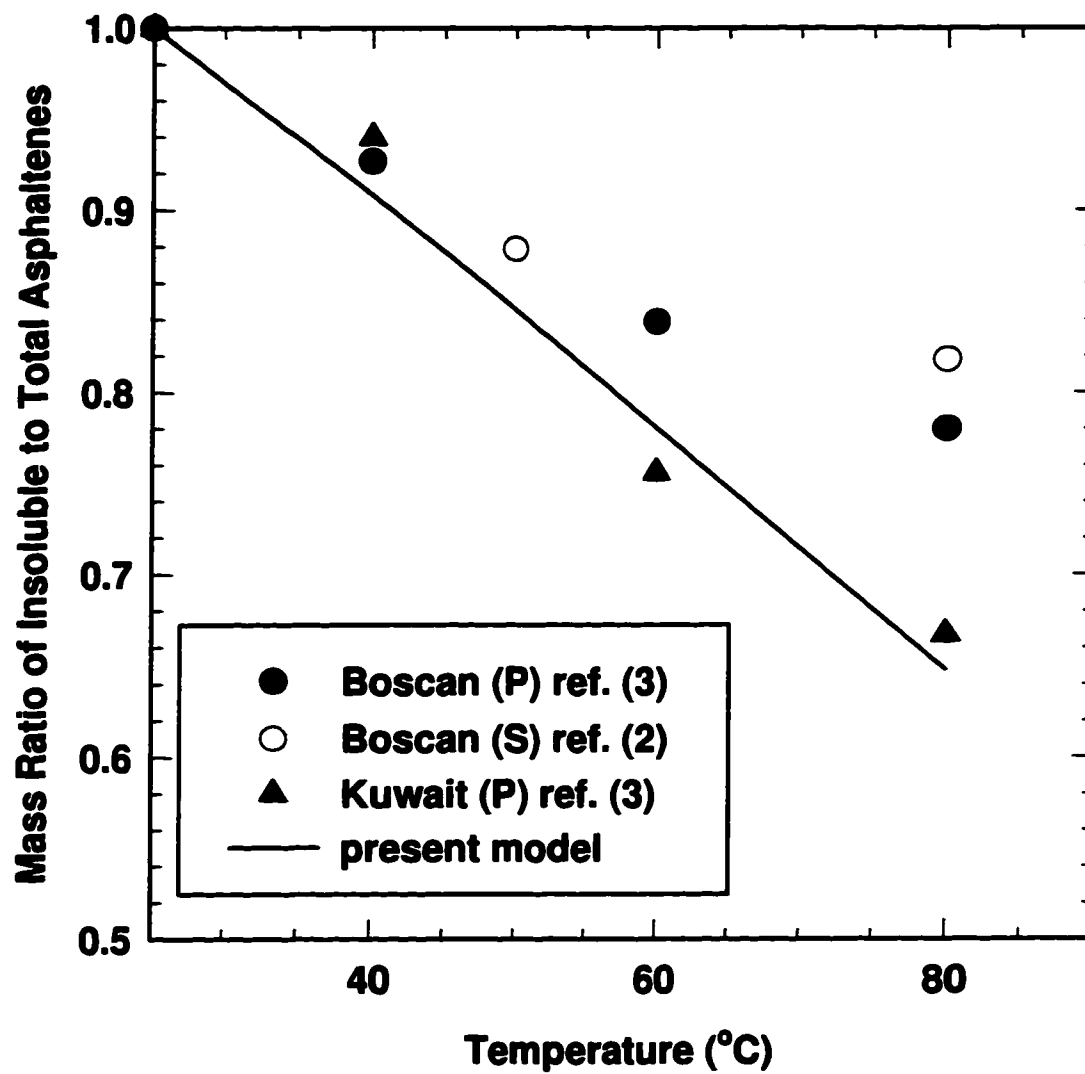


Figure B.2: Effect of temperature on asphaltene-solids solubility. (P) precipitated from crude, (S) redissolved in solvent


```

function [fsol,fsolm,slr] = fsolasph(phi1,ca,xa,mwa)
% function [fsol,fsolm,slr] = fsolasph(phi1,ca,xa,mwa)
% subroutines: kvalasph.m, solvprop.m
% solid-liquid equilibrium calculation using equilibrium ratios calculated with
% Scatchard-Hildebrandt/Flory-Huggins expression and Hansen solubility parameters
% feed: two component solvent and low concentration of asphaltene
% solvent specified by volume fractions (phi1)
% asphaltene given in subfractions of different molar mass (xa, mwa)
%
% fsol   = equilibrium mass ratio of solid to total asphaltenes
% fsolm  = equilibrium mole ratio of solid to total asphaltenes
% phi1   = volume fr. component 1
% ca     = concentration asphaltene (g/cc)
% xa     = vector: mass ratio of asph subfraction to total asphaltenes
% mwa    = vector: molar mass of asph subfraction (g/mol)
% comp 1 = good solvent
% comp 2 = poor solvent
% comp a = asphaltene

% find equilibrium ratios for asphaltene, (k),
% vector of mass fr. of asphaltene subfractions in feed, (xa1),
% and mole fractions of all components in feed, (xm1,xm2,xma)
n=length(xa);
[xm1,xm2,xma,xa1,k]=kvalasph(phi1,ca,xa,mwa);

% solid liquid equilibrium iterative calculation
% solve for solid liquid mole ratio, (slr)
tol=.0001;
test=1;
slr1=1e-20;
slr2=1;
while test>tol
    slrn=exp((log(slr1)+log(slr2))/2);
    for i=1:n
        xms(i)=xma(i)*k(i)*(1+slrn)/(1+k(i)*slrn);
    end
    sum1=sum(xms);
    if sum1>1
        slr1=slrn;
    else
        slr2=slrn;
    end
    test=abs(1-sum1);
end
slr=slrn;

% read in molar masses of solvent components, (mw1, mw2)
[temp,d1,d2,mw1,mw2,sd1,sd2,sp1,sp2,sh1,sh2]=solvprop;

% solve for mole ratio of solid to total asphaltenes, (fsolm)
fsolm=slr/(1+slr)/sum(xma);

% solve for mass ratio of solid to total asphaltenes, (fsol)

```

```

for i=1:n
    xs(i)=xms(i)*slr/(1+slr)*mwa(i);    % vector: solid asph subfr. per mole feed
    mwf(i)=xma(i)*mwa(i);              % vector: molar mass of asph subfr in feed
end
mwft=sum(mwf)+xm1*mw1+xm2*mw2; % molar mass of feed
fsol=sum(xs)/sum(xa1)/mwft;

```

function phi1 = sptasph(ca,xa,mwa)

```

% function phi1 = sptasph(ca,xa,mwa)
% solid point of asphaltene as function of solvent mix
% phi1 = volume fr. comp 1
% ca = concentration asphaltene (g/cc)
% xa = vector: mass ratio of asph subfraction to total asphaltenes
% mwa = vector: molar mass of asph subfraction (g/mol)
% comp 1 = toluene
% comp 2 = hexane
% comp a = asphaltene

```

```

n=length(xa);
tol=.001;
test=1;
phig1=1;
phig2=0;

```

```

while test>tol
    phin=(phig1+phig2)/2;
    [xm1,xm2,xma,xa1,k]=kvalasph(phin,ca,xa,mwa);
    sum=k*xma;
    tn=log(sum);
    if tn<0
        phig1=phin;
    else
        phig2=phin;
    end
    test=abs(1-sum);
end
phi1=phin;

```

```

end

```

function [xm1,xm2,xma,xa1,k] = kvalasph(phi1,ca,xa,mwa)

```

% function [xm1,xm2,xma,xa1,k] = kvalasph(phi1,ca,xa,mwa)
% subroutines: asphprop.m, solvprop.m
% calculate equilibrium ratios for asphaltene subfractions
% using Scatchard-Hildebrand/Flory-Huggins theory
% feed: two component solvent and low concentration of asphaltene
% solvent specified by volume fractions (phi1)
% asphaltene given in subfractions of different molar mass (xa, mwa)
%
% phi1 = volume fr. component 1

```

```

% ca      = concentration asphaltene (g/cc)
% xa      = vector: mass ratio of asph subfraction to total asphaltenes
% mwa     = vector: molar mass of asph subfraction (g/mol)
% xm1     = mole fraction of comp. 1 in feed
% xm2     = mole fraction of comp. 2 in feed
% xma     = vector: mole fr. asph. subfractions in feed
% xa1     = vector: mass fr. asph. subfractions in feed
% k       = vector: equilibrium ratio (solid/liquid) for asph. subfraction
% comp 1  = good solvent
% comp 2  = poor solvent
% comp a  = asphaltene

n=length(xa);

% read in solvent and asphaltene properties
[temp,d1,d2,mw1,mw2,sd1,sd2,sp1,sp2,sh1,sh2]=solvprop;
[ds1p,dint,us1pd,us1pp,us1ph,deltah]=asphprop;

% calculate solvent mixture properties
phi2=1-phi1;
dmix=phi1*d1+phi2*d2;           % solution density (g/cc)
vmix=1/(phi1*d1/mw1+phi2*d2/mw2); % solution sp. vol. (cc/mol)
smixd=phi1*sd1+phi2*sd2;       % solution dispersion sol. par. (MPa^.5)
smixp=phi1*sp1+phi2*sp2;       % solution polar sol. par. (MPa^.5)
smixh=phi1*sh1+phi2*sh2;       % solution h-bonding sol. par. (MPa^.5)

% calculate mass fractions
x1=d1*phi1/dmix;                % mass fr comp 1 before asph added
x2=1-x1;
xat=ca/dmix;                     % total asph mass fr. in feed
xsum=x1+x2+xat;
x1=x1/xsum;                       % mass fr comp 1 in feed
x2=x2/xsum;
xa=xa*xat/xsum;                  % mass fr asph subfractions in feed
xa1=xa;

% calculate mole fractions and K-values
xom1=x1/mw1;
xom2=x2/mw2;
xomasum=0;
for i=1:n;
    xoma(i)=xa(i)/mwa(i);
    xomasum=xoma(i)+xomasum;
end
xomsum=xom1+xom2+xomasum;
xm1=xom1/xomsum;
xm2=xom2/xomsum;
for i=1:n
    xma(i)=xoma(i)/xomsum;
    da=ds1p*mwa(i)+dint;
    va=mwa(i)/da;
    sad=(us1pd*da)^.5;
    sap=(us1pp*da)^.5;
    sah=(us1ph*da)^.5;
    dels=(sad-smixd)^2+0.15*((sap-smixp)^2+(sah-smixh)^2);

```

```

k(i)=va/vmix*exp(deltah+1-va/vmix+va/8.314/temp*(dels));
end
end

```

```

function [temp,d1,d2,mw1,mw2,sd1,sd2,sp1,sp2,sh1,sh2]=solvprop
% input solvent properties for solid-liquid equilibrium calculation
% two component solvent, Hansen solubility parameters

```

```

temp=295;      % temperature (K)
d1=.867;      % density of comp. 1 (g/cc)
d2=0.659;    % density of comp. 2 (g/cc)
mw1=92;      % molar mass of comp. 1 (g/mol)
mw2=86;      % molar mass of comp. 2 (g/mol)
sd1=18;      % dispersion sol. parameter of comp. 1 (MPa^0.5)
sd2=14.9;    % dispersion sol. parameter of comp. 2 (MPa^0.5)
sp1=1.4;     % polar sol. parameter of comp. 1 (MPa^0.5)
sp2=0;       % polar sol. parameter of comp. 2 (MPa^0.5)
sh1=2;       % h-bonding sol. parameter of comp. 1 (MPa^0.5)
sh2=0;       % h-bonding sol. parameter of comp. 2 (MPa^0.5)

```

```
end
```

```

function [dslp,dint,uslpd,uslpp,uslph,deltah]=asphprop
% input asphaltene properties for solid-liquid equilibrium calculation
% inputs are coefficients for Yarranton/Masliyah asphaltene property correlations
% hansen solubility parameters
% density = dint + dslp*(molar mass)
% sol. parameter = (uslp*density)^0.5

```

```

dslp=1.7e-5;   % mol/cc
dint=1.08;     % g/cc
psi1=0.01;
psi3=4;
uslpd=355;    % J/g
uslpp=psi1*uslpd;
uslph=psi3*uslpp;
deltah=0;     % heat of fusion, J/mol
end

```

```

function [x,mw]=mwdist1(mwl,mwh,n)
% function [x,mw]=mwdist1(mwl,mwh,n)
% subroutine bisct.m
% generate molar mass distribution of asphaltenes for use in solubility model
% average molar mass for intervals of dx=1/n
% assumes cumx linear/exponential fn of mw
% x = mass ratio of asph. subfraction to total asphaltenes
% mw = molar mass of asph. subfraction

```

```

dx=1/n;
f(1)=dx/2;
for i=2:n+1
    x(i-1)=dx;
    f(i)=f(i-1)+dx;    % cumulative mass frequency
    ft=f(i);
    mw(i-1)=bisct(mwl,mwh,ft);
end

```

function m = bisct(ml,mh,f)

```

%function m = bisct(ml,mh,f)
% calculate molar mass of asph. subfractions using linear/exp distribution
% ml = lower limit of molar mass distribution
% mh = upper limit of molar mass distribution
% f = vector: mass ratio of asph. subfraction to total asphaltenes
% m = molar mass at f

```

```

b=50.625;
c=.00165;

```

```

a=mh-ml-b/c*(exp(-c*mh)-exp(-c*ml));
tol=.00001;
m1=ml;
m2=mh;
fg=1;
while abs(fg)>tol
    mg=(m1+m2)/2;
    fg = f-(mg-ml-b/c*(exp(-c*mg)-exp(-c*ml)))/a;
    if fg<0
        m2=mg;
    else
        m1=mg;
    end
end
m=mg;

```

function mb=mavgh(f)

```

% function mb=mavgh(f)
% subroutine: bisct.m, mwprop.m, mint.m
% f = cumulative mass ratio of highest molar mass asph subfractions to total asphaltene
% mb = number average molar mass of asphaltene subfractions in the range f to 1

```

```

[ml,mh,b,c]=mwprop;

```

```

% find molar mass of asphaltene molecule that corresponds to f in the cum. freq. distribution
m=bisct(ml,mh,f);

```

```

% solve for number average molar mass
mnum=mh-m-b/c*(exp(-c*mh)-exp(-c*m));
mden=quad('mint',m,mh);

```

```
mb=mnum/mden;
end
```

function mb=mavgl(f)

```
% function mb=mavgl(f)
% subroutine: bisct.m, mwprop.m, mint.m
% f = cumulative mass ratio of lowest molar mass asph subfractions to total asphaltene
% mb = number average molar mass of asphaltene subfractions in the range 0 to f
```

```
[ml,mh,b,c]=mwprop;
```

```
% find molar mass of asphaltene molecule that corresponds to f in the cum. freq. distribution
m=bisct(ml,mh,f);
```

```
% solve for number average molar mass
mnum=m-ml-b/c*(exp(-c*m)-exp(-c*ml));
mden=quad('mint',ml,m);
mb=mnum/mden;
end
```

function md=mint(m)

```
% function md=mint(m)
% subroutine: mwprop.m
% denominator for average molar mass calculation
```

```
[ml,mh,b,c]=mwprop;
```

```
md=(1+b.*exp(-c.*m))./m;
```

function pb=pavgh(f)

```
% function pb=pavgh(f)
% subroutine bisct.m, mwprop.m, pint.m
% f = cumulative mass ratio of highest molar mass asph. subfractions to total asphaltene
% pb = average density of asphaltene subfraction in range f to 1
```

```
[ml,mh,b,c]=mwprop;
```

```
% find molar mass of asph. molecule that corresponds to f in cum. freq. distribution
m=bisct(ml,mh,f);
```

```
% solve for average density
pnum=mh-m-b/c*(exp(-c*mh)-exp(-c*m));
pden=quad('pint',m,mh);
pb=pnum/pden;
end
```

function pb=pavgl(f)

```
% function pb=pavgl(f)
% subroutine: bisct.m, mwprop.m, pint.m
% f = cumulative mass ratio of lowest molar mass asph. subfractions to total asphaltene
% pb = average density of asphaltene subfraction in range 0 to f
```

```
[ml,mh,b,c]=mwprop;
```

```
% find molar mass of asph. molecule that corresponds to f in cum. freq. distribution
m=bisct(ml,mh,f);
```

```
% solve for average density
pnum=m-ml-b/c*(exp(-c*m)-exp(-c*ml));
pden=quad('pint',ml,m);
pb=pnum/pden;
end
```

function pd=pint(m)

```
% function pd=pint(m)
% subroutine: mwprop.m, densprop.m
% denominator of average density calculation
```

```
[ml,mh,b,c]=mwprop;
[pa,pb]=densprop;
```

```
pd=(1+b.*exp(-c.*m))/(1+pb.*m)/pa;
```

function [mwl,mwh,b,c]=mwprop

```
% function [mwl,mwh,b,c]=mwprop
% limits and coefficients for asph. molar mass distribution
```

```
mwl=2000;      % lowest molar mass
mwh=8500;     % highest molar mass
b=50.625;    % preexponential coeff.
c=.00165;    % exponential coeff.
end
```

function [pa,pb]=densprop

```
% function [pa,pb]=densprop
% coefficients relating density to molar mass
% density=pa*(1+pb*M)
```

```
pa=1.08;
pb=1.7e-5/pa;
```

```
end
```

Appendix C

ASPHALTENE STABILIZED WATER-IN-OIL EMULSIONS - ADDITIONAL MATERIAL

C.1 Drop Size Distributions

Drop size distributions were measured with the methods described in Chapter 4. The initial (1 hr after emulsification) mean drop diameter, mean drop volume and Sauter mean diameter were calculated from the drop size distributions. The mean drop volumes are converted to a diameter, $(d_{30})^{1/3}$ where

$$d_{30} = \sum \hat{F}_i d_i^3 \quad (\text{C.1})$$

Here \hat{F}_i is the drop number frequency and d_i is the diameter of the i^{th} droplet. The average diameters are summarized in Tables C.1 to C.6 for emulsions with volume ratios of hexane to toluene of 5, 3, 1.5, 1, 0.25 and 0, respectively.

The change in the drop size distribution over time was also measured for several emulsions, including a range of asphaltene concentrations, water volume fractions and hexane to toluene ratios. The measured distributions are shown in Figs. C.1 to C.13. In all cases, an accumulation of small droplets was observed while some large droplets also appeared. The ultimate distributions are log normal in appearance. Note that the same behavior was observed for the case where precipitated asphaltenes were removed in pretreatment (Fig. C.13).

The change in the mean diameters over time for the distributions presented in Figs. C.1 to C.13 are shown in Figs. C.14 to C.26, respectively. The mean diameters are nearly invariant with time whereas the Sauter mean diameters seem to increase linearly with time. The fitted initial diameters and changes in diameter over time are also shown on

the figures. The emulsion where the precipitated asphaltenes were removed in pretreatment (Fig. C.26) can be compared with an emulsion prepared with untreated asphaltenes at exactly the same conditions (Fig. C.15). The initial diameters are slightly lower for the treated asphaltenes. The changes in the mean and Sauter mean diameters over time for treated and untreated asphaltenes are the same within experimental error. Hence, the stability of the emulsions is not affected by removing the highest molar mass asphaltenes. The same conclusion was reached in Chapter 4.

C.2 Ostwald Ripening Through an Interfacial Membrane

Ostwald ripening through an interfacial membrane can be derived in a similar manner to heat transfer through concentric spheres. We start from the general equation for mass transfer from a sphere, Eq. 6.1. Eq. 6.1 can be rewritten for diffusion from a membrane covered sphere as follows:

$$\frac{dV}{dt} = \frac{4\pi}{3} \frac{da^3}{dt} = \frac{4\pi(a + \delta_l)rD}{r - (a + \delta_l)} (\phi_c - \phi_{so}) \quad (\text{C.2})$$

Here dV/dt is the volume flux from the sphere, a is the drop radius, t is time, r is the diffusion boundary radius, δ_l is the membrane thickness, and D is the diffusivity of the dispersed phase material in the continuous phase. ϕ_c and ϕ_{so} are the volume fractions of the dispersed phase material in the continuous phase and the outside of the droplet membrane, respectively. Similarly, the mass transfer rate through the membrane is given by

$$\frac{dV}{dt} = \frac{4\pi}{3} \frac{da^3}{dt} = \frac{4\pi a(a + \delta_l)D_l}{\delta_l} (\phi_{so} - \phi_{si}) \quad (\text{C.3})$$

where ϕ_{si} is the volume fraction of the dispersed phase material at the inside surface of the membrane. D_l is the diffusivity of the dispersed phase material in the membrane. Now

$\delta_l \ll a$ and $r = a + \delta$ where δ is half the separation distance between droplets. Hence, Eqs. C.2 and C.3 reduce to the following respective expressions:

$$\frac{dV}{dt} = \frac{4\pi a(a + \delta)D}{\delta} (\phi_c - \phi_{so}) \quad (\text{C.4})$$

$$\frac{dV}{dt} = \frac{4\pi a^2 D_l}{\delta_l} (\phi_{so} - \phi_{si}) \quad (\text{C.5})$$

We can eliminate ϕ_{so} from consideration by combining and rearranging Eqs. C.4 and C.5. The new expression for the volume flux is given by

$$\frac{dV}{dt} = \frac{(\phi_c - \phi_{si})}{\frac{\delta}{4\pi a(a + \delta)D} + \frac{\delta_l}{4\pi a^2 D_l}} \quad (\text{C.6})$$

Eq. C.6 is the same as given by Kabal'nov *et al.* (1). The rest of the derivation is the same as for the standard Ostwald ripening case discussed in Chapter 6. The resulting expression for the derivative of the drop radius with time is given by

$$\frac{da}{dt} = \frac{\phi_{\infty} \alpha}{\frac{a\delta}{(a + \delta)D} + \frac{\delta_l}{D_l}} \left(\frac{1}{a^2} \right) \left(\frac{a}{a_c} - 1 \right) \quad (\text{C.7})$$

Here ϕ_{∞} is the solubility of the dispersed phase material in the continuous phase expressed as a volume fraction, and a_c is the critical radius. Also, $\alpha = 2\sigma v_d / RT$ where σ is interfacial tension, v_d is the molar volume of the dispersed phase material, R is the universal as constant and T is temperature. Eq. C.7 can be rearranged into the following form:

$$\frac{da}{dt} = \frac{D\phi_{\infty}\alpha}{\eta} \left(\frac{a+\delta}{a^2\delta} \right) \left(\frac{a}{a_c} - 1 \right) \quad (\text{C.8})$$

where

$$\eta = 1 + \frac{(a+\delta)\delta_l D}{a\delta D_l} \quad (\text{C.9})$$

Here η expresses the departure from standard ripening when an interfacial membrane exists.

C.3 Computer Programs

Ostwald ripening calculations were carried out on MATLAB[®]. The routines and subroutines written for the calculations are printed out at the end of the appendix. There are three groups of programs: a) for infinitely dilute solutions; b) for infinitely concentrated solutions; c) for finite volume fractions. Only the program “ostcnt.m” is common to all three groups. A brief index is given below.

ostcnt.m control loop

Group 1: infinitely dilute

acrit.m solves ripening equations for a single time step
afmov.m determines the radius of the largest drop at time t+dt
fnext.m controls single iteration of the ripening calculation

Group 2: infinitely concentrated

acrit1.m solves ripening equations for a single time step
afmov1.m determines the radius of the largest drop at time t+dt
fnext1.m controls single iteration of the ripening calculation

Group 3: finite dispersed phase volume fraction

| | |
|----------|---|
| ac.m | calculate critical radius for a given drop size distribution |
| acrit2.m | solves ripening equations for a single time step |
| afmov2.m | determines the radius of the largest drop at time t+dt |
| dcalc.m | subroutine to calculate average half separation distance between drops |
| dcalc1.m | calculate average half separation distance between drops for a given drop size distribution |
| fnext2.m | controls single iteration of the ripening calculation |

C.4 References

1. Kabal'nov, A.S., Shchukin, E.D., *Adv. Colloid Interface Sci.*, **38**, (1992), 69.

Table C.1: Average initial drop size for asphaltene stabilized water-in-toluene/hexane emulsions, $\phi_H/\phi_T = 5$

| Pretreatment | ϕ_w | C_A^o (kg/m ³) | d_{10} (μm) | $(d_{30})^{1/3}$ (μm) | d_{32} (μm) |
|----------------------------|----------|---------------------------------|-------------------------------|---------------------------------------|-------------------------------|
| none | 0.20 | 1.00 | 8.41 | 8.78 | 9.16 |
| none | 0.25 | 0.25 | 45.00 | 68.12 | 103.15 |
| none | 0.25 | 0.33 | 18.37 | 30.40 | 46.79 |
| none | 0.25 | 0.33 | 41.75 | 56.25 | 75.11 |
| none | 0.25 | 0.40 | 18.76 | 37.88 | 70.86 |
| none | 0.25 | 0.40 | 30.59 | 39.13 | 50.40 |
| none | 0.25 | 0.50 | 22.94 | 25.13 | 27.46 |
| none | 0.25 | 0.75 | 18.74 | 20.97 | 23.46 |
| none | 0.25 | 1.00 | 12.98 | 13.84 | 14.72 |
| none | 0.25 | 1.00 | 11.09 | 12.17 | 13.29 |
| none | 0.25 | 1.50 | 8.00 | 8.79 | 9.67 |
| none | 0.25 | 2.00 | 7.93 | 8.37 | 8.81 |
| none | 0.33 | 0.60 | 26.05 | 36.17 | 50.30 |
| none | 0.33 | 0.60 | 38.48 | 45.90 | 53.96 |
| none | 0.33 | 0.67 | 24.65 | 36.11 | 50.83 |
| none * | 0.33 | 1.00 | 15.01 | 17.29 | 19.77 |
| none | 0.40 | 0.33 | 58.34 | 86.62 | 127.91 |
| none | 0.40 | 0.40 | 38.04 | 61.21 | 93.15 |
| none | 0.40 | 0.50 | 36.85 | 55.79 | 79.66 |
| none | 0.40 | 0.67 | 32.20 | 34.22 | 36.11 |
| none | 0.40 | 1.00 | 21.14 | 22.68 | 24.20 |
| none | 0.40 | 1.00 | 21.23 | 22.80 | 24.30 |
| none - pure water | 0.40 | 1.00 | 21.08 | 24.59 | 28.06 |
| none | 0.40 | 1.33 | 14.80 | 15.84 | 16.87 |
| toluene - ppt removed | 0.25 | 1.00 | 12.05 | 13.08 | 14.10 |
| 1:1 hextol - ppt removed * | 0.25 | 1.00 | 10.70 | 11.71 | 12.73 |
| 3:2 hextol - ppt removed | 0.25 | 1.50 | 7.58 | 8.27 | 8.99 |
| 2:1 hextol - ppt removed | 0.25 | 1.00 | 12.82 | 13.56 | 14.25 |
| 2:1 hextol - ppt removed | 0.25 | 1.50 | 8.91 | 9.81 | 10.76 |
| 5:2 hextol - ppt removed | 0.25 | 1.00 | 13.70 | 15.86 | 18.30 |
| 5:2 hextol - ppt removed | 0.25 | 1.50 | 10.34 | 11.59 | 12.91 |
| 3:1 hextol - ppt removed * | 0.25 | 1.00 | 15.52 | 17.03 | 18.70 |
| 3:1 hextol - ppt removed | 0.25 | 1.00 | 16.92 | 18.34 | 20.04 |
| 3:1 hextol - ppt removed | 0.25 | 1.50 | 13.40 | 15.04 | 16.77 |
| 7:2 hextol - ppt removed | 0.25 | 1.00 | 25.50 | 29.93 | 34.95 |
| 4:1 hextol - ppt removed | 0.25 | 1.00 | 21.27 | 28.10 | 35.96 |
| 4:1 hextol - ppt removed | 0.25 | 1.00 | 22.16 | 31.98 | 47.19 |
| 4:1 hextol - ppt removed | 0.25 | 1.50 | 16.00 | 18.85 | 22.06 |
| 4:1 hextol - ppt removed | 0.25 | 1.50 | 18.37 | 21.85 | 25.67 |
| 2:1 hextol - ppt used | 0.25 | 1.00 | 44.50 | 50.76 | 56.48 |
| 2:1 hextol - ppt used | 0.25 | 1.00 | 69.42 | 76.60 | 84.13 |
| 5:2 hextol - ppt used | 0.25 | 1.00 | 40.42 | 42.44 | 44.25 |
| 3:1 hextol - ppt used | 0.25 | 1.00 | 23.69 | 27.96 | 32.85 |
| 4:1 hextol - ppt used | 0.25 | 1.00 | 21.93 | 23.83 | 26.09 |
| 4:1 hextol - ppt used | 0.25 | 1.00 | 15.74 | 18.40 | 21.76 |

* only one sample measured

Table C.2: Average initial drop size for asphaltene stabilized water-in-toluene/hexane emulsions, $\phi_H/\phi_T = 3$

| Pretreatment | ϕ_w | C_A^0 (kg/m ³) | d_{10} (μm) | $(d_{30})^{1/3}$ (μm) | d_{32} (μm) |
|--------------------------|----------|---------------------------------|-------------------------------|---------------------------------------|-------------------------------|
| none | 0.25 | 0.27 | 54.69 | 85.33 | 130.61 |
| none | 0.25 | 0.32 | 44.71 | 61.57 | 86.81 |
| none | 0.25 | 0.37 | 27.65 | 32.72 | 38.68 |
| none | 0.25 | 0.40 | 27.44 | 38.47 | 54.66 |
| none | 0.25 | 1.00 | 9.70 | 10.78 | 11.93 |
| none | 0.25 | 1.25 | 8.61 | 9.26 | 9.95 |
| none | 0.33 | 0.66 | 25.04 | 30.29 | 37.02 |
| none | 0.40 | 1.00 | 19.71 | 22.72 | 25.90 |
| none | 0.40 | 1.25 | 17.08 | 19.22 | 21.64 |
| none | 0.40 | 1.28 | 17.85 | 19.82 | 22.00 |
| none | 0.40 | 1.49 | 17.14 | 18.83 | 20.64 |
| none | 0.40 | 1.90 | 10.98 | 11.89 | 12.86 |
| 3:2 hextol - ppt removed | 0.25 | 1.00 | 9.99 | 10.90 | 11.92 |
| 2:1 hextol - ppt removed | 0.25 | 1.00 | 13.42 | 14.97 | 16.58 |
| 5:2 hextol - ppt removed | 0.25 | 1.00 | 13.17 | 15.89 | 19.23 |
| 3:1 hextol - ppt removed | 0.25 | 1.00 | 19.86 | 24.85 | 31.02 |
| 3:1 hextol - ppt removed | 0.25 | 1.00 | 18.94 | 23.09 | 28.12 |

* only one sample measured

Table C.3: Average initial drop size for asphaltene stabilized water-in-toluene/hexane emulsions, $\phi_H/\phi_T = 1.5$

| Pretreatment | ϕ_w | C_A^0 (kg/m ³) | d_{10} (μm) | $(d_{30})^{1/3}$ (μm) | d_{32} (μm) |
|--------------------------|----------|---------------------------------|-------------------------------|---------------------------------------|-------------------------------|
| none | 0.25 | 0.27 | 41.79 | 54.96 | 70.68 |
| none | 0.25 | 0.30 | 50.38 | 62.65 | 77.31 |
| none | 0.25 | 0.32 | 25.40 | 29.49 | 34.05 |
| none | 0.25 | 0.37 | 31.87 | 37.38 | 44.74 |
| none | 0.25 | 0.48 | 21.35 | 25.38 | 29.57 |
| none | 0.25 | 0.59 | 18.40 | 20.44 | 22.53 |
| none | 0.25 | 1.00 | 8.70 | 10.00 | 11.41 |
| none | 0.40 | 0.77 | 27.33 | 31.07 | 34.90 |
| none | 0.40 | 1.28 | 20.30 | 22.20 | 24.11 |
| none | 0.40 | 1.50 | 13.98 | 16.12 | 18.55 |
| 1:1 hextol - ppt removed | 0.25 | 1.00 | 10.32 | 11.70 | 13.26 |
| 3:2 hextol - ppt removed | 0.25 | 1.00 | 9.26 | 10.62 | 12.14 |
| 3:2 hextol - ppt removed | 0.25 | 1.00 | 11.12 | 12.90 | 14.99 |
| 2:1 hextol - ppt removed | 0.25 | 1.00 | 14.36 | 17.14 | 20.27 |
| 5:2 hextol - ppt removed | 0.25 | 1.00 | 17.47 | 24.68 | 35.57 |
| 3:1 hextol - ppt removed | 0.25 | 1.00 | 15.18 | 24.90 | 42.63 |

* only one sample measured

Table C.4: Average initial drop size for asphaltene stabilized water-in-toluene/hexane emulsions, $\phi_H/\phi_T = 1$.

| Pretreatment | ϕ_w | C_A^o (kg/m ³) | d_{10} (μm) | $(d_{30})^{1/3}$ (μm) | d_{32} (μm) |
|--------------------------|----------|---------------------------------|-------------------------------|---------------------------------------|-------------------------------|
| none | 0.25 | 0.32 | 45.00 | 57.57 | 72.03 |
| none | 0.25 | 0.37 | 40.46 | 47.68 | 55.43 |
| none | 0.25 | 0.43 | 24.35 | 26.92 | 29.42 |
| none | 0.25 | 0.48 | 33.26 | 36.58 | 39.85 |
| none | 0.25 | 0.53 | 19.19 | 20.95 | 22.73 |
| none | 0.25 | 0.59 | 19.51 | 23.08 | 27.72 |
| none | 0.25 | 0.77 | 20.31 | 22.72 | 25.11 |
| none | 0.25 | 1.00 | 11.18 | 13.13 | 15.27 |
| none | 0.25 | 1.25 | 9.26 | 10.44 | 11.72 |
| none | 0.25 | 1.50 | 7.96 | 8.66 | 9.41 |
| none | 0.33 | 0.67 | 23.38 | 37.77 | 63.05 |
| none | 0.40 | 0.90 | 23.52 | 27.87 | 32.75 |
| none | 0.40 | 1.00 | 18.28 | 26.11 | 37.31 |
| none | 0.40 | 1.25 | 17.57 | 22.90 | 30.02 |
| none | 0.40 | 1.75 | 14.88 | 17.14 | 19.77 |
| 1:1 hextol - ppt removed | 0.25 | 1.00 | 11.41 | 15.18 | 20.36 |
| 1:1 hextol - ppt removed | 0.25 | 1.50 | 7.32 | 8.12 | 9.01 |
| 3:2 hextol - ppt removed | 0.25 | 1.00 | 13.79 | 17.66 | 22.58 |
| 3:2 hextol - ppt removed | 0.25 | 1.50 | 8.00 | 9.20 | 10.68 |
| 2:1 hextol - ppt removed | 0.25 | 1.00 | 12.31 | 22.86 | 48.43 |
| 2:1 hextol - ppt removed | 0.25 | 1.00 | 23.70 | 39.15 | 66.08 |
| 2:1 hextol - ppt removed | 0.25 | 1.50 | 9.36 | 12.74 | 18.25 |
| 5:2 hextol - ppt removed | 0.25 | 1.50 | 9.95 | 15.73 | 27.39 |

* only one sample measured

Table C.5: Average initial drop size for asphaltene stabilized water-in-toluene/hexane emulsions, $\phi_H/\phi_T = 0.25$.

| Pretreatment | ϕ_w | C_A^o (kg/m ³) | d_{10} (μm) | $(d_{30})^{1/3}$ (μm) | d_{32} (μm) |
|--------------|----------|---------------------------------|-------------------------------|---------------------------------------|-------------------------------|
| none | 0.25 | 0.28 | 29.79 | 48.87 | 82.05 |
| none | 0.25 | 0.33 | 28.47 | 40.40 | 54.95 |
| none | 0.25 | 0.40 | 24.36 | 35.13 | 49.69 |
| none | 0.25 | 0.60 | 24.17 | 29.67 | 35.35 |
| none | 0.25 | 0.85 | 11.08 | 18.44 | 31.15 |
| none | 0.25 | 1.00 | 9.28 | 13.08 | 18.78 |
| none | 0.40 | 1.25 | 19.87 | 27.05 | 36.11 |
| none | 0.40 | 1.40 | 18.00 | 23.32 | 30.03 |
| none | 0.40 | 1.50 | 15.23 | 21.98 | 30.99 |
| none | 0.40 | 1.75 | 12.75 | 15.84 | 19.42 |

Table C.6: Average initial drop size for asphaltene stabilized water-in-toluene/hexane emulsions, $\phi_H/\phi_T = 0$.

| Pretreatment | ϕ_w | C_A^o (kg/m ³) | d_{10} (μm) | $(d_{30})^{1/3}$ (μm) | d_{32} (μm) |
|--------------|----------|---------------------------------|-------------------------------|---------------------------------------|-------------------------------|
| none | 0.25 | 0.50 | 11.26 | 21.06 | 39.96 |
| none | 0.25 | 1.00 | 16.53 | 20.95 | 26.20 |
| none | 0.25 | 1.00 | 9.76 | 14.71 | 21.46 |
| none | 0.25 | 1.67 | 8.35 | 12.11 | 18.31 |
| none | 0.40 | 1.33 | 24.17 | 32.73 | 42.82 |
| none | 0.40 | 2.00 | 12.80 | 15.70 | 18.73 |
| none | 0.40 | 2.00 | 14.82 | 17.80 | 21.14 |

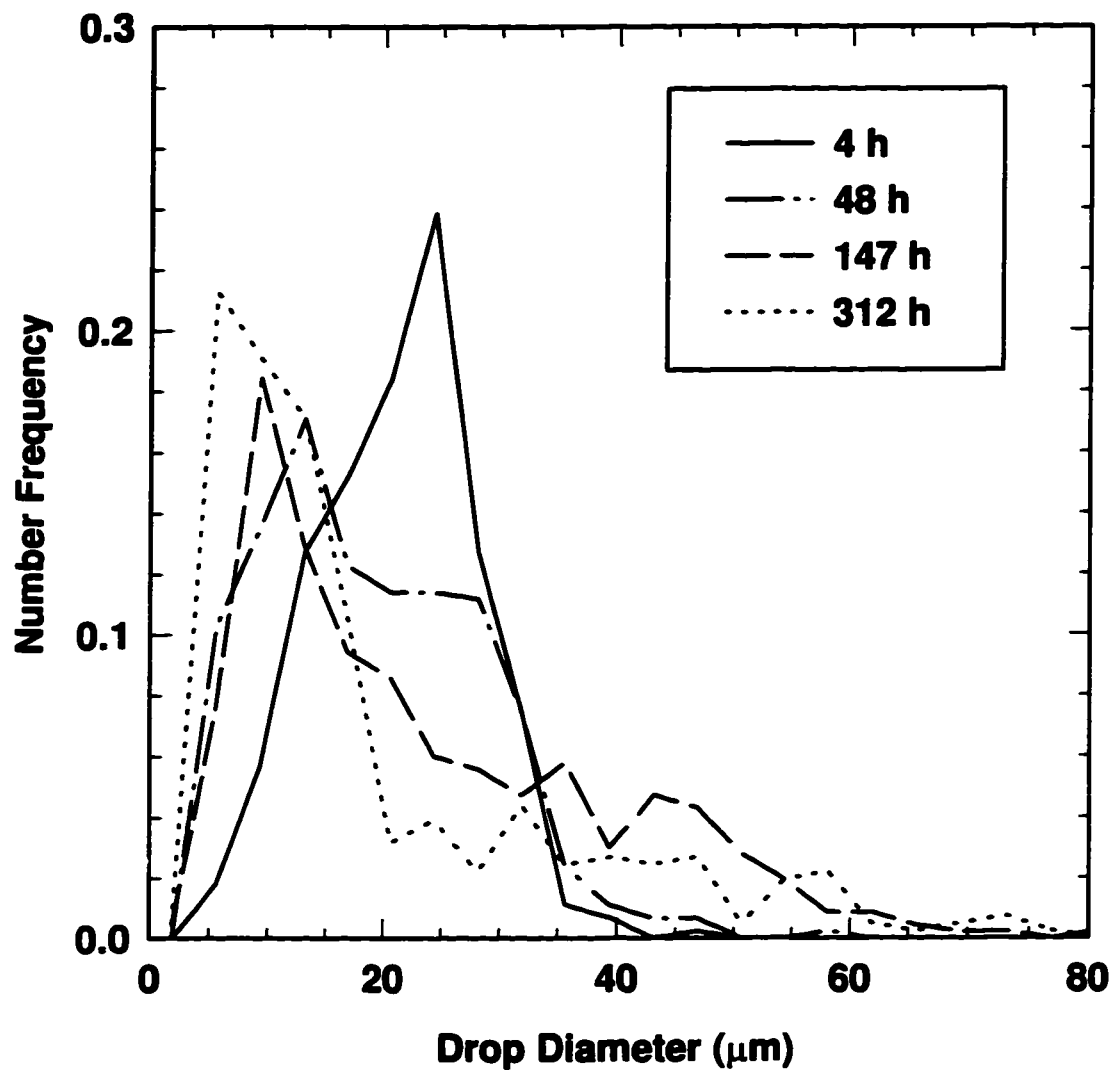


Figure C.1: Change in drop size distribution with time for an asphaltene stabilized water-in-toluene/hexane emulsion. ($\phi_H/\phi_T = 5$, $\phi_W = 0.25$, $C_A^0 = 0.50 \text{ kg/m}^3$)

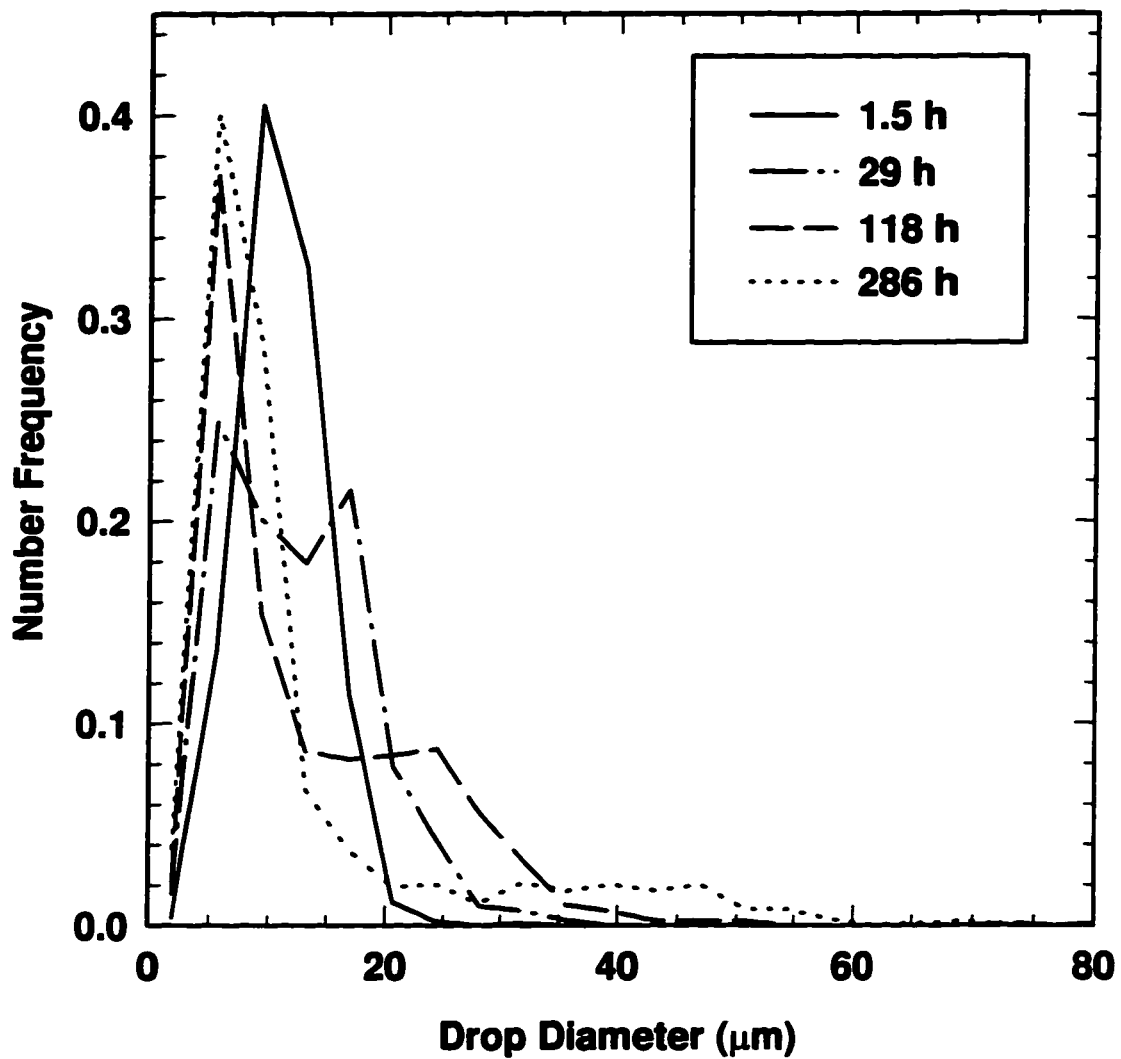


Figure C.2: Change in drop size distribution over time for an asphaltene stabilized water-in-toluene/hexane emulsion. ($\phi_H/\phi_T = 5$, $\phi_W = 0.25$, $C_A^0 = 1.00 \text{ kg/m}^3$)

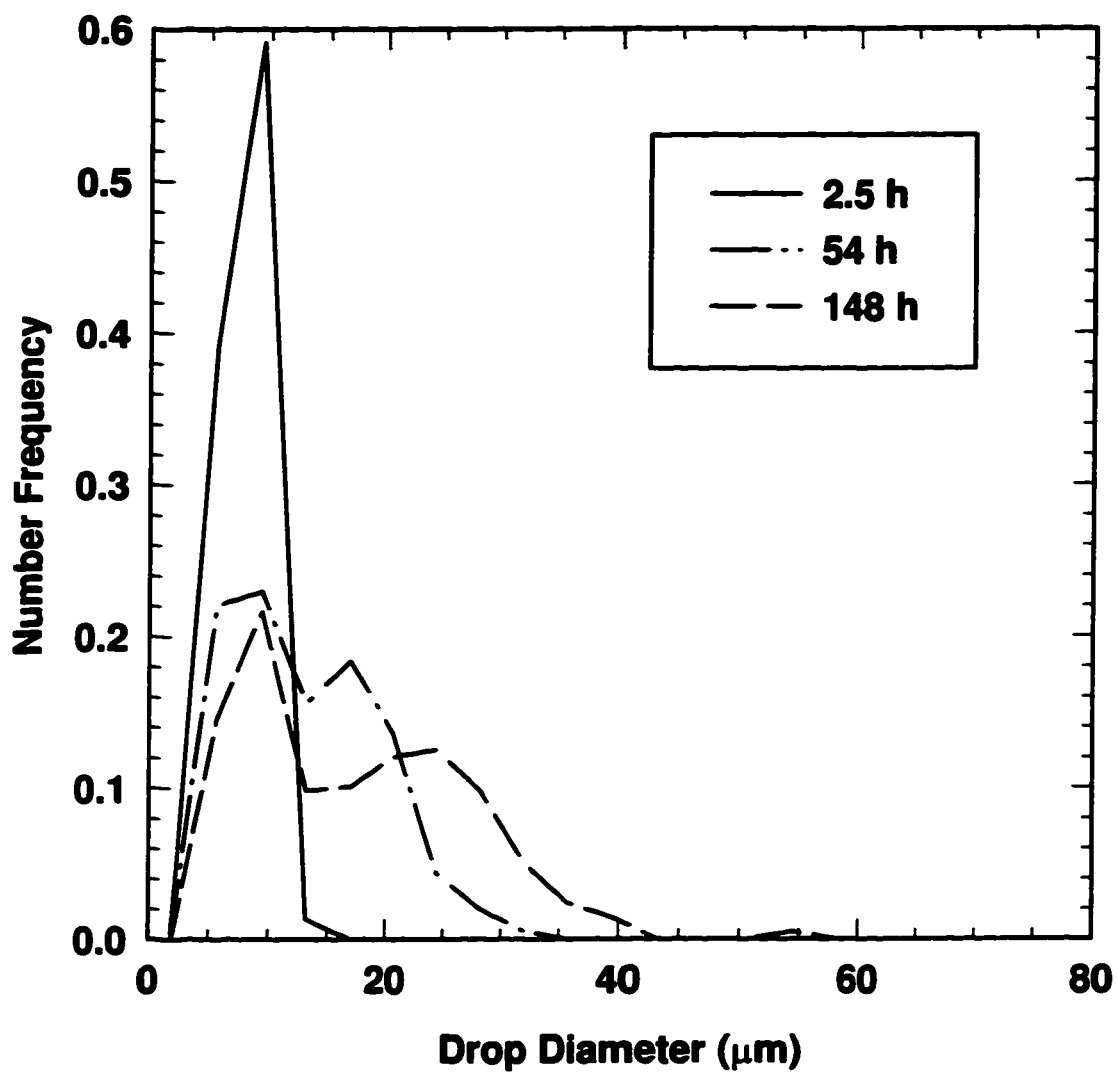


Figure C.3: Change in drop size distribution over time for an asphaltene stabilized water-in-toluene/hexane emulsion. ($\phi_H/\phi_T = 5$, $\phi_W = 0.25$, $C_A^0 = 2.00 \text{ kg/m}^3$)

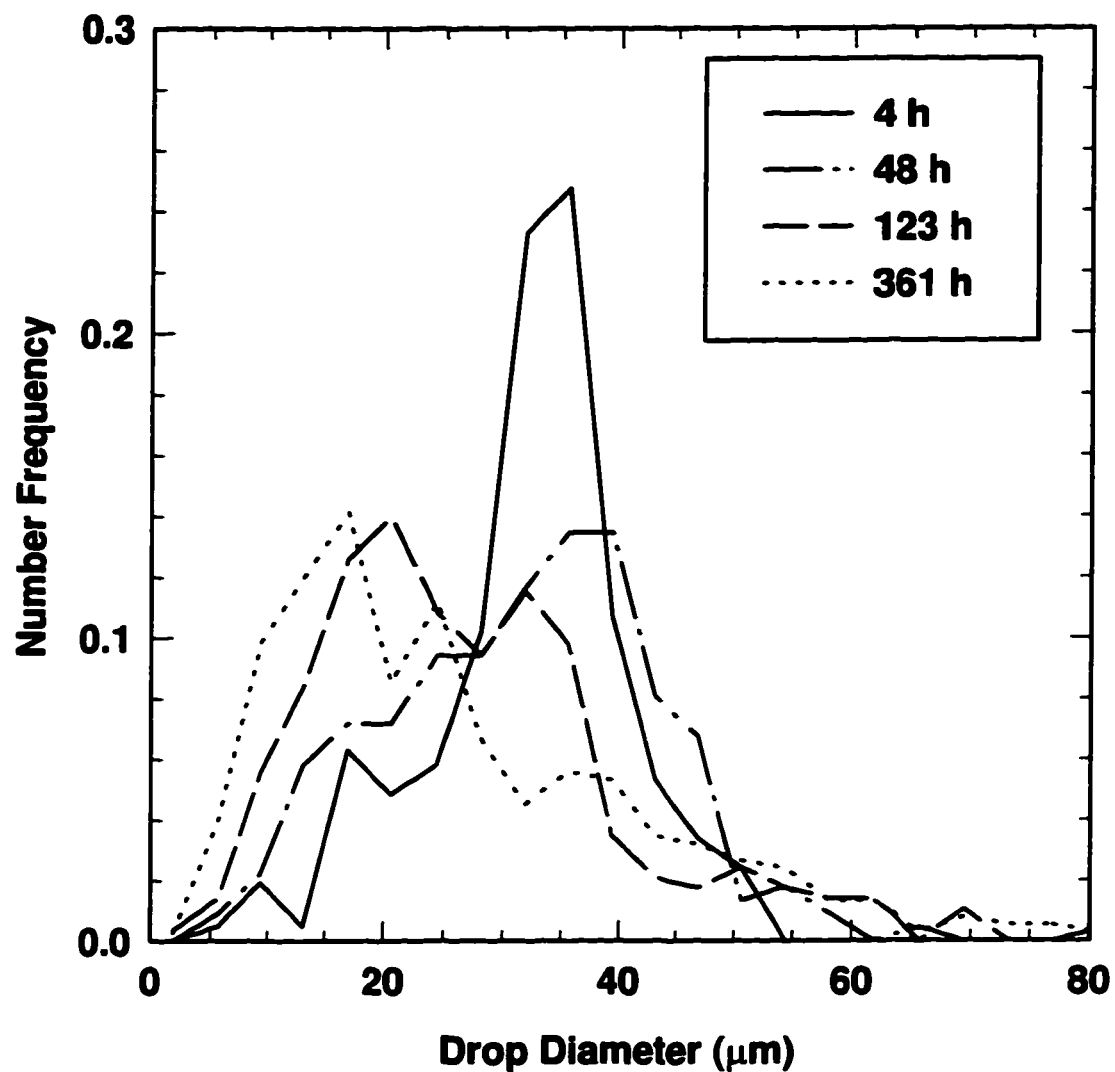


Figure C.4: Change in drop size distribution over time for an asphaltene stabilized water-in-toluene/hexane emulsion. ($\phi_H/\phi_T = 5$, $\phi_W = 0.40$, $C_A^0 = 0.67 \text{ kg/m}^3$)

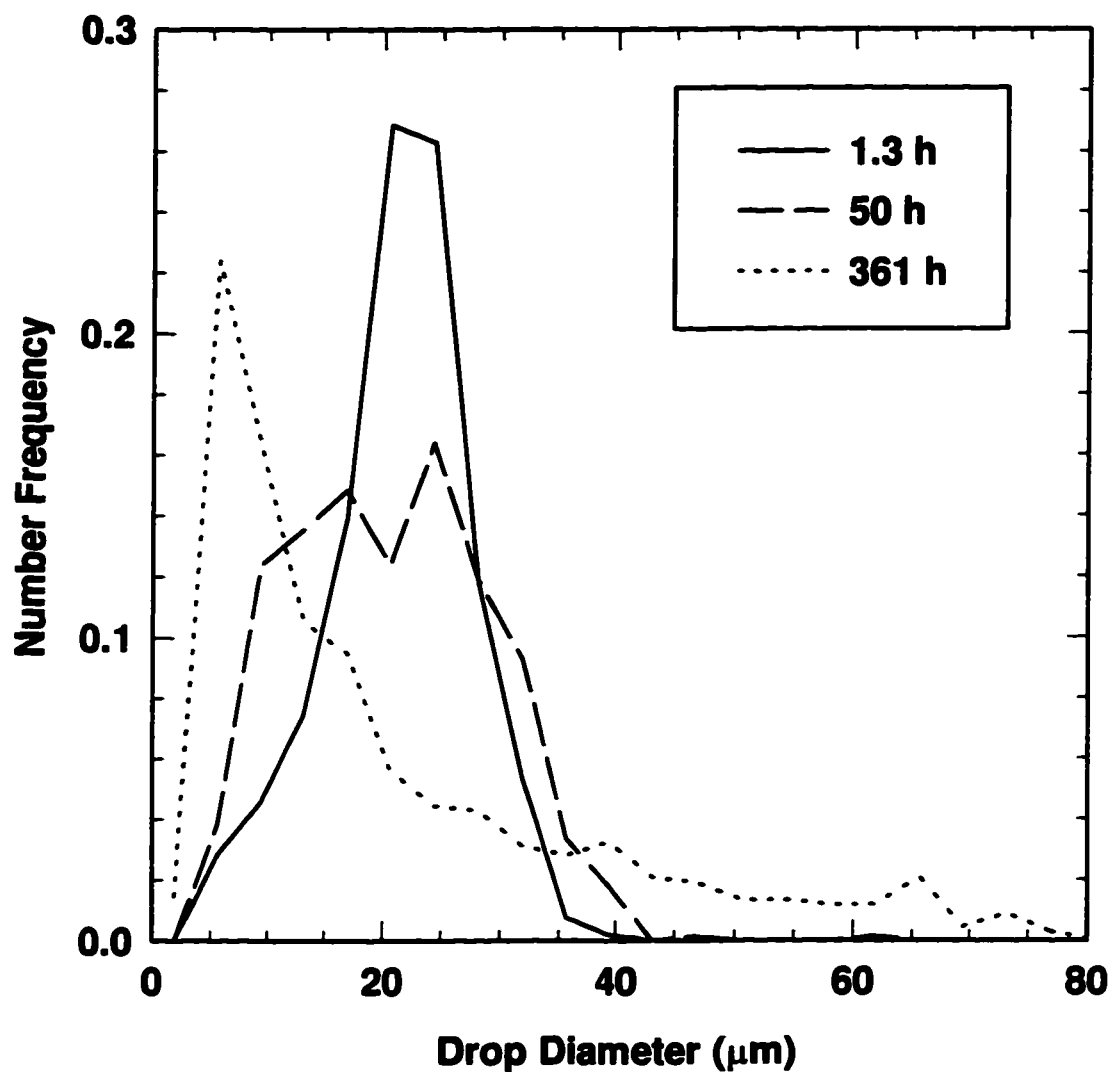


Figure C.5: Change in drop size distribution over time for an asphaltene stabilized water-in-toluene/hexane emulsion. ($\phi_H/\phi_T = 5$, $\phi_W = 0.40$, $C_A^0 = 1.00 \text{ kg/m}^3$)

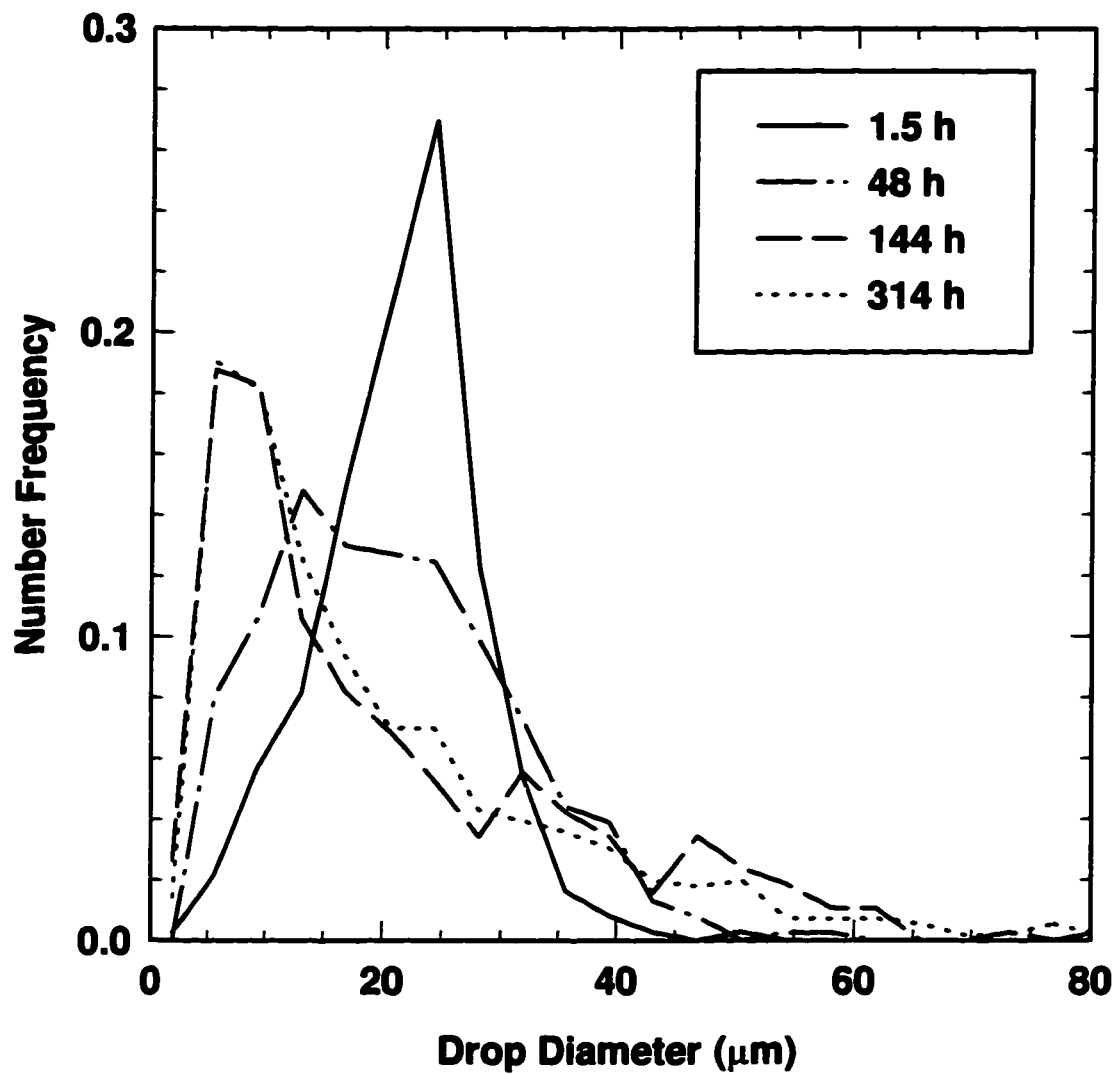


Figure C.6: Change in drop size distribution over time for an asphaltene stabilized water-in-toluene/hexane emulsion - deionized ultrafiltered water.

($\phi_H/\phi_T = 5$, $\phi_W = 0.40$, $C_A^0 = 1.00 \text{ kg/m}^3$)

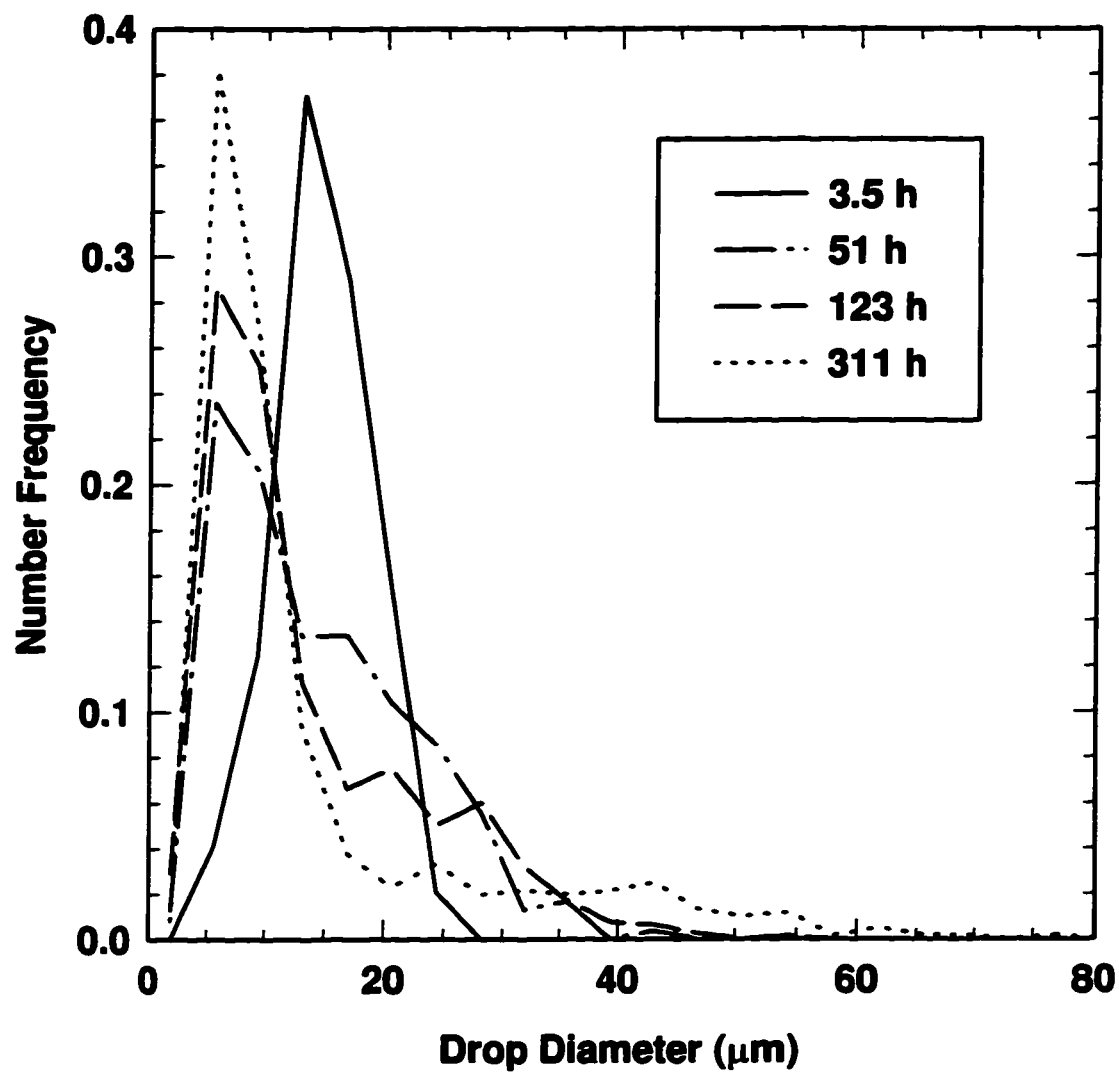


Figure C.7: Change in drop size distribution over time of an asphaltene stabilized water-in-toluene/hexane emulsion. ($\phi_H/\phi_T = 5$, $\phi_W = 0.40$, $C_A^0 = 1.33 \text{ kg/m}^3$)

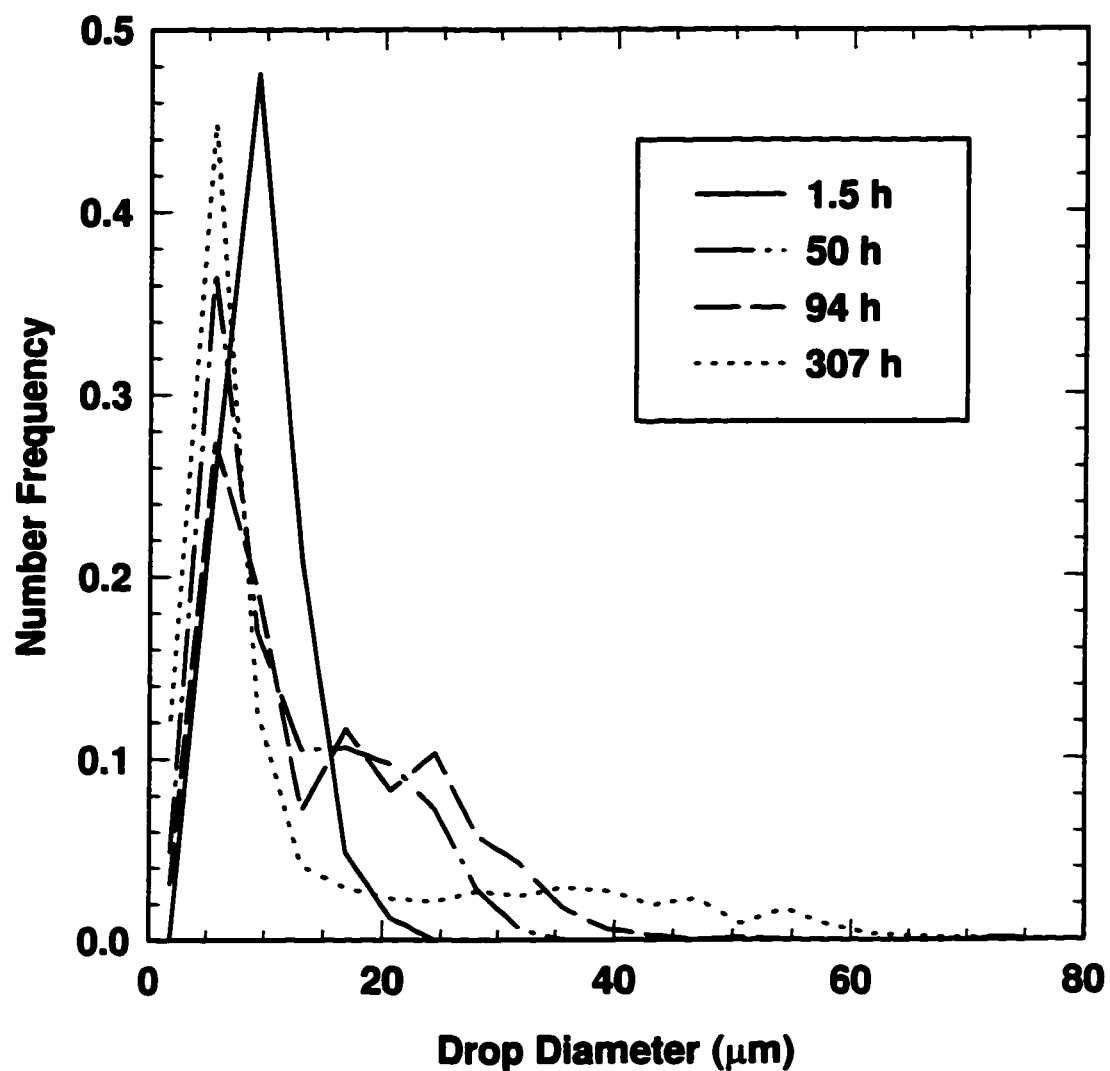


Figure C.8: Change in drop size distribution over time of an asphaltene stabilized water-in-toluene/hexane emulsion. ($\phi_H/\phi_T = 3$, $\phi_W = 0.25$, $C_A^0 = 1.00 \text{ kg/m}^3$)

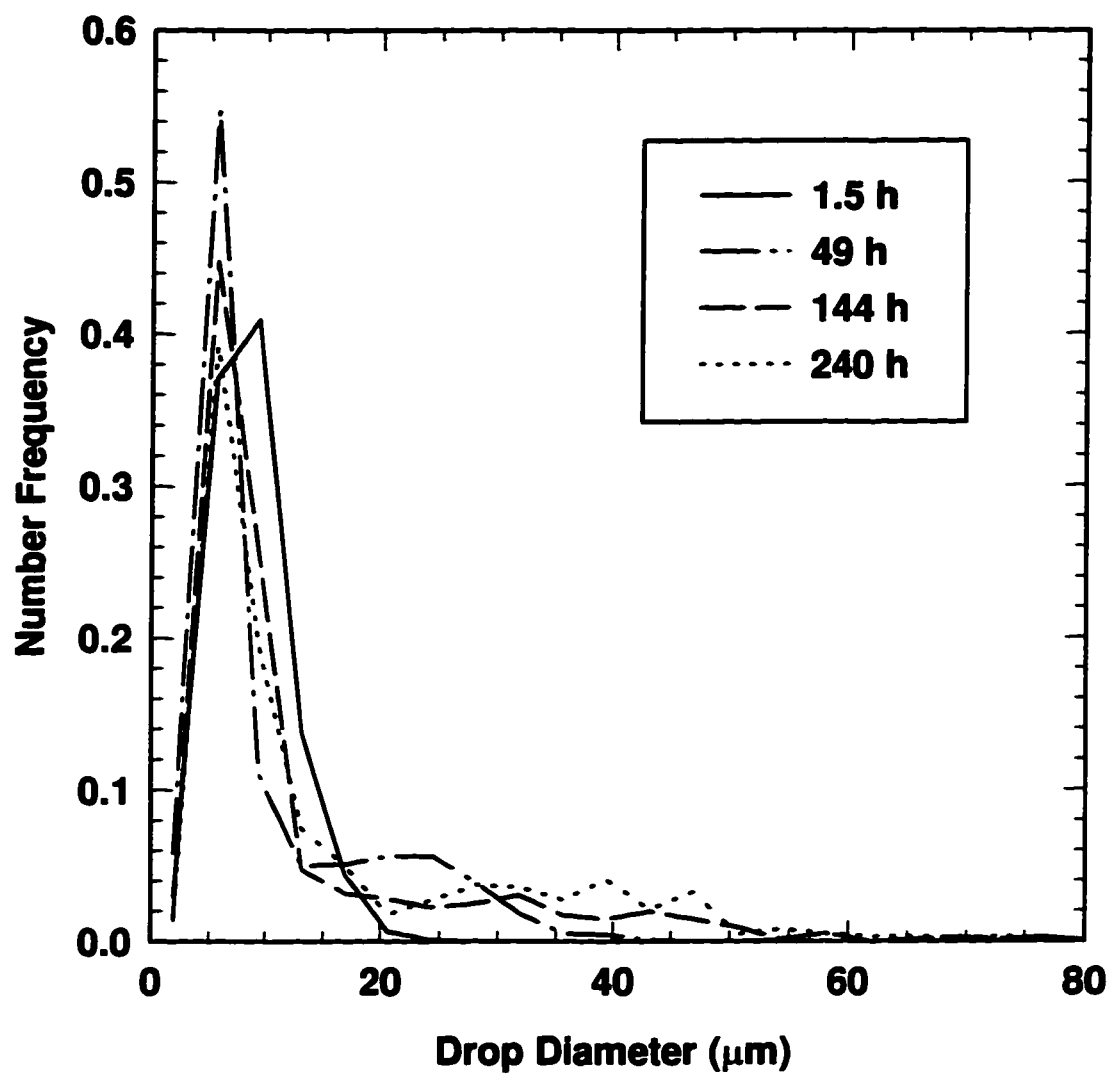


Figure C.9: Change in drop size distribution over time of an asphaltene stabilized water-in-toluene/hexane emulsion. ($\phi_H/\phi_T = 1.5$, $\phi_W = 0.25$, $C_A^0 = 1.00 \text{ kg/m}^3$)

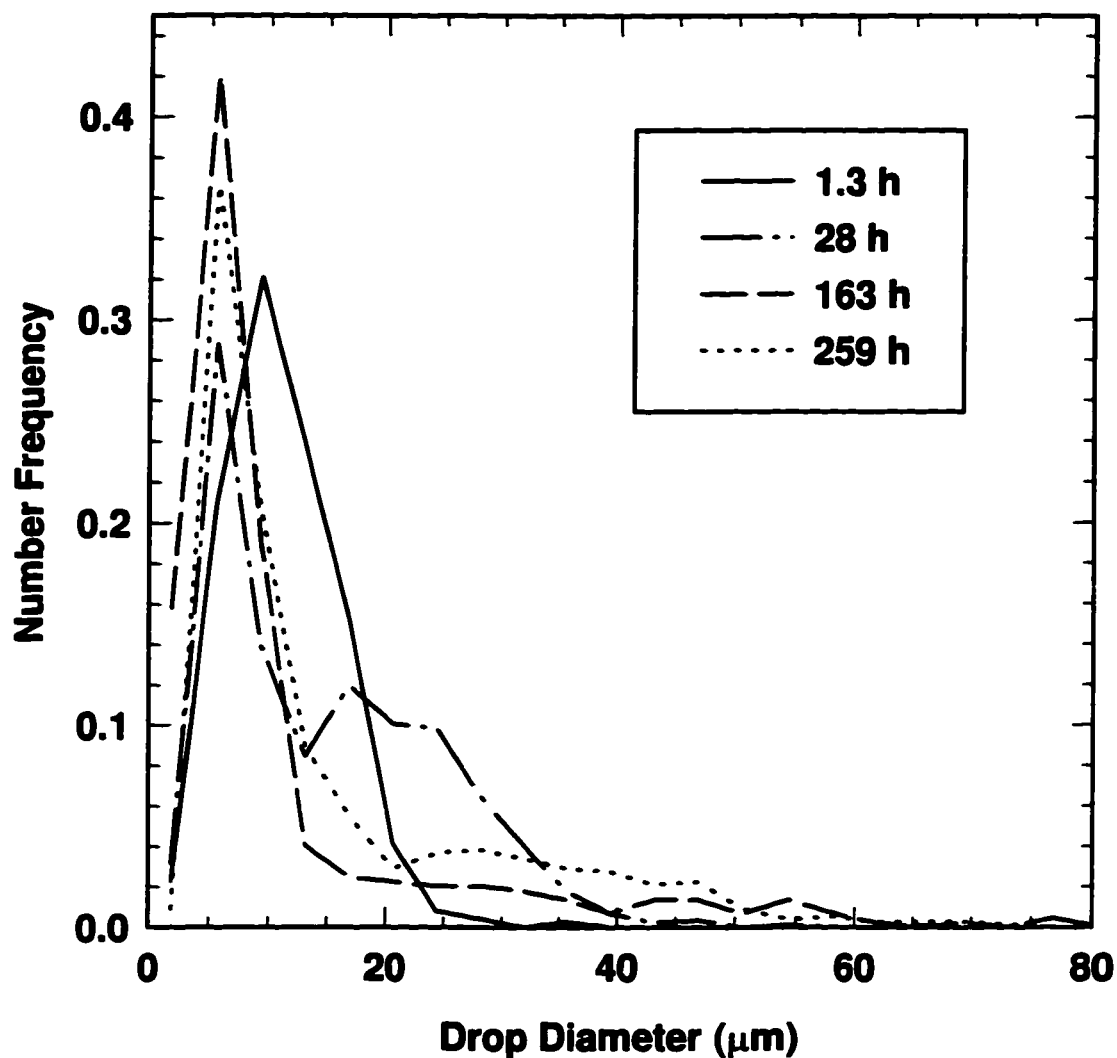


Figure C.10: Change in drop size distribution over time of an asphaltene stabilized water-in-toluene/hexane emulsion. ($\phi_H/\phi_T = 1$, $\phi_W = 0.25$, $C_A^0 = 1.00 \text{ kg/m}^3$)

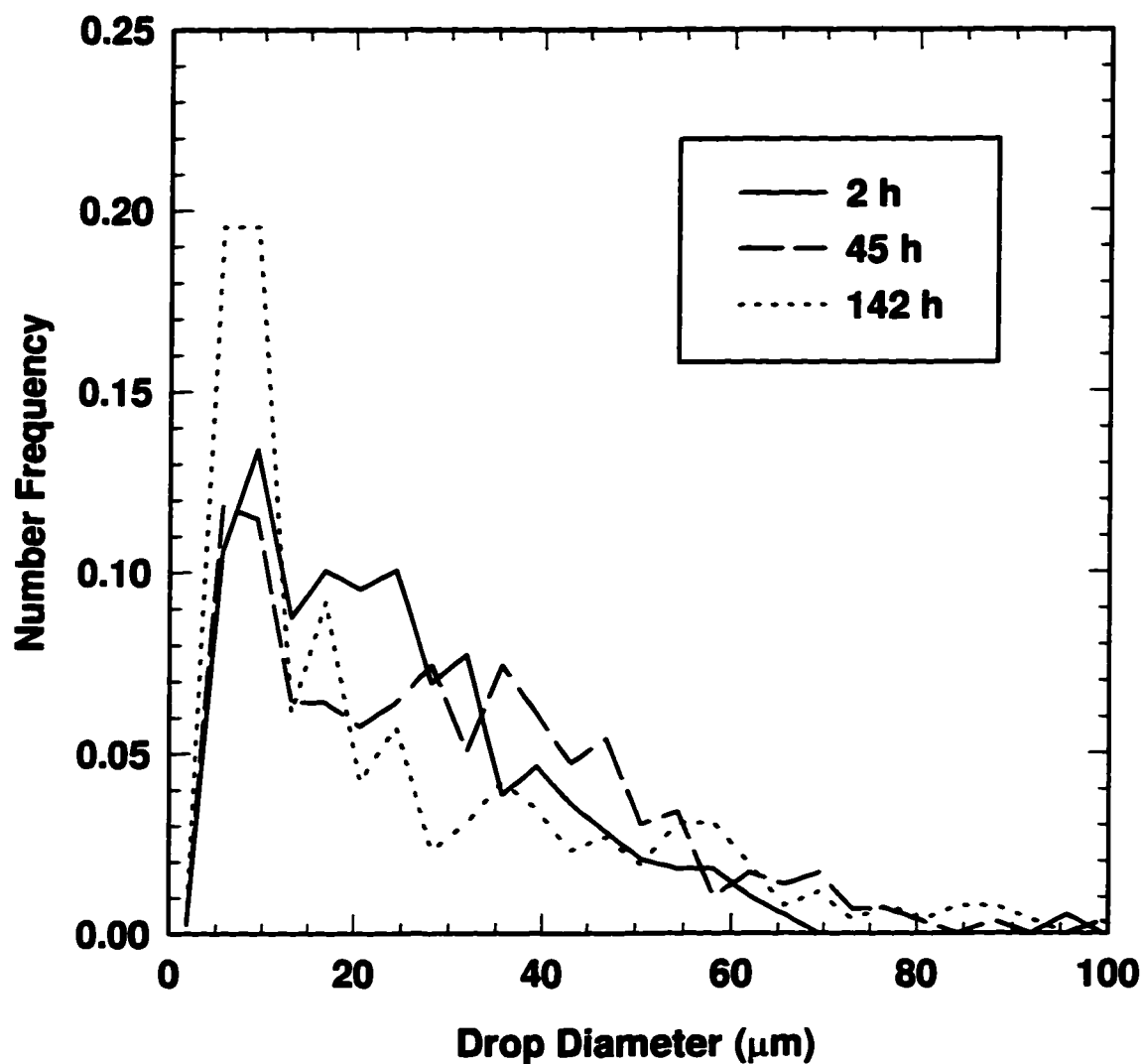


Figure C.11: Change in drop size distribution over time of an asphaltene stabilized water-in-toluene/hexane emulsion. ($\phi_H/\phi_T = 0$, $\phi_W = 0.40$, $C_A^0 = 1.33 \text{ kg/m}^3$)

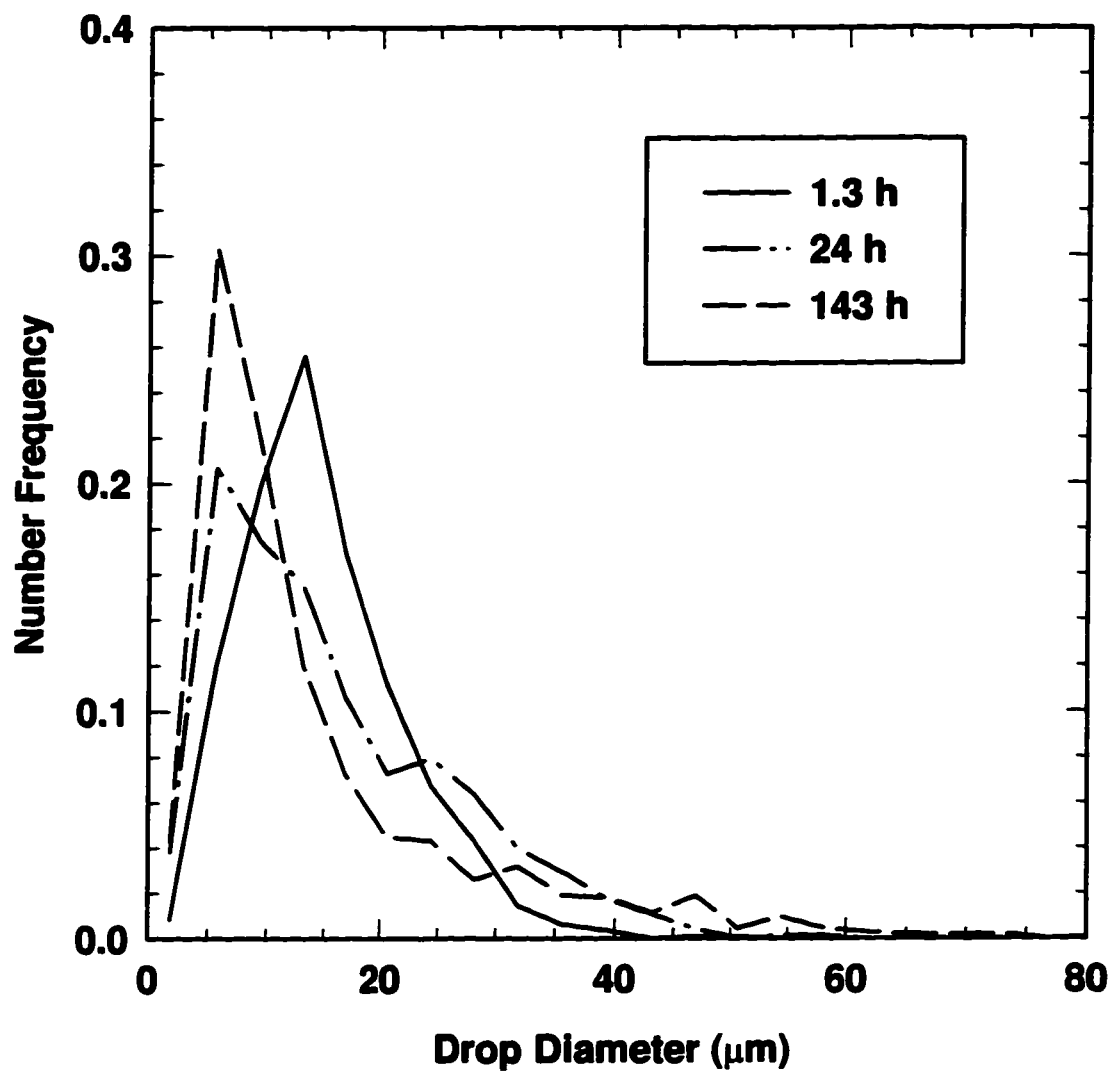


Figure C.12: Change in drop size distribution over time of an asphaltene stabilized water-in-toluene/hexane emulsion. ($\phi_H/\phi_T = 0$, $\phi_W = 0.40$, $C_A^0 = 2.00 \text{ kg/m}^3$)

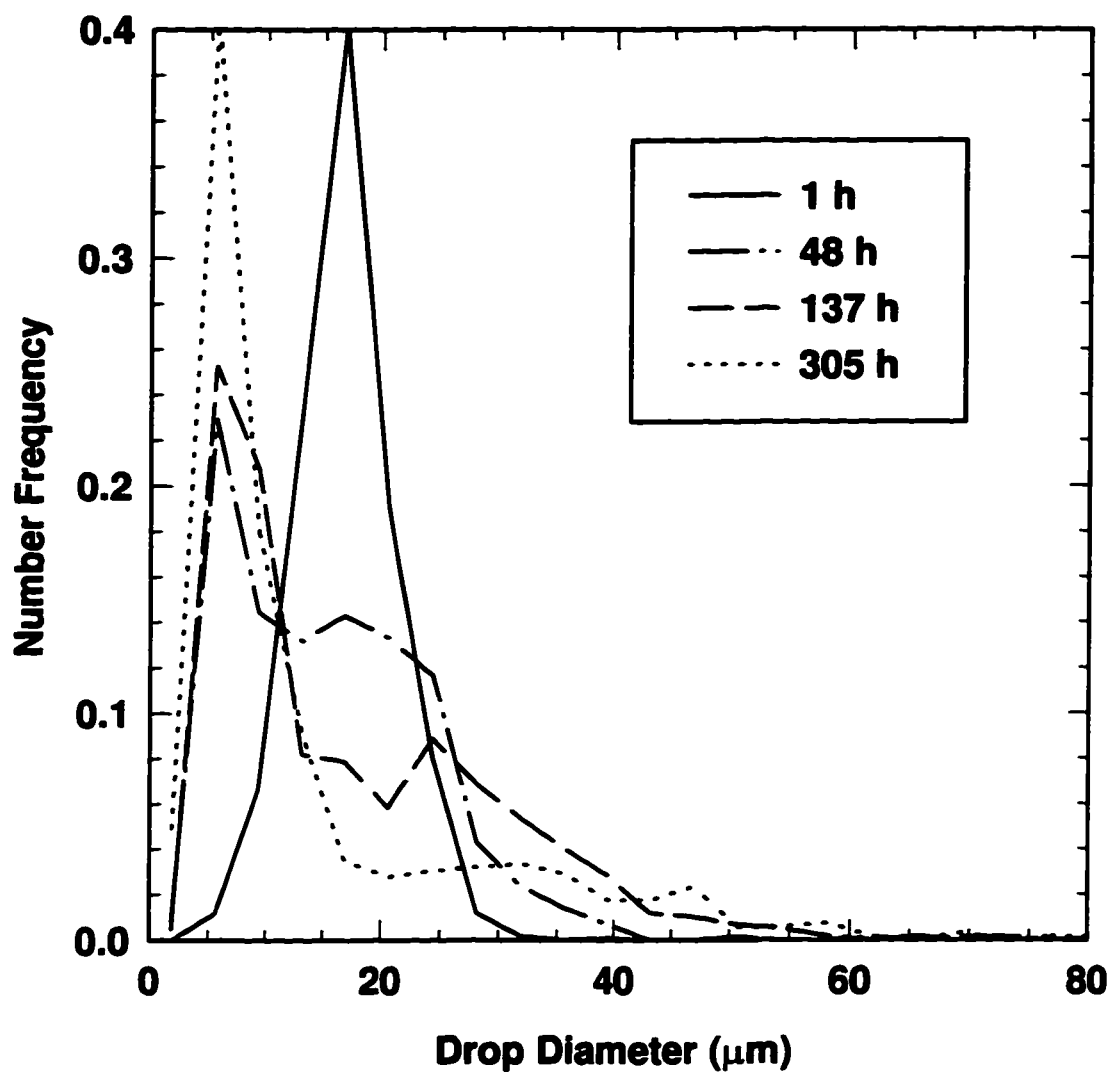


Figure C.13: Change in drop size distribution over time of an asphaltene stabilized water-in-toluene/hexane emulsion - pretreated in 3:1 hex:tol, precipitate removed. ($\phi_H/\phi_T = 5$, $\phi_W = 0.25$, $C_A^0 = 1.00 \text{ kg/m}^3$)

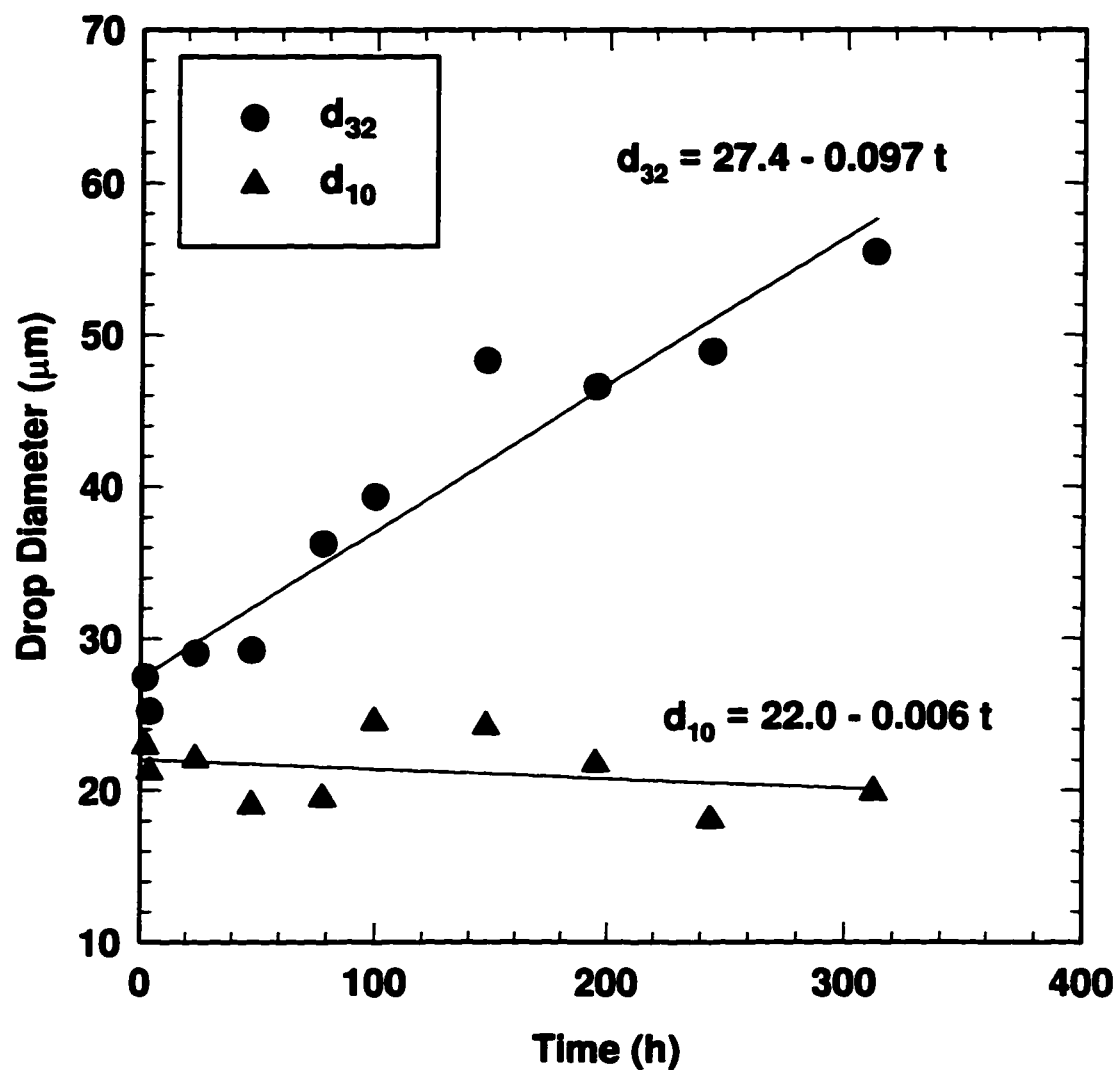


Figure C.14: Change in drop diameter over time of an asphaltene stabilized water-in-toluene/hexane emulsion. ($\phi_H/\phi_T = 5$, $\phi_W = 0.25$, $C_A^0 = 0.50 \text{ kg/m}^3$)

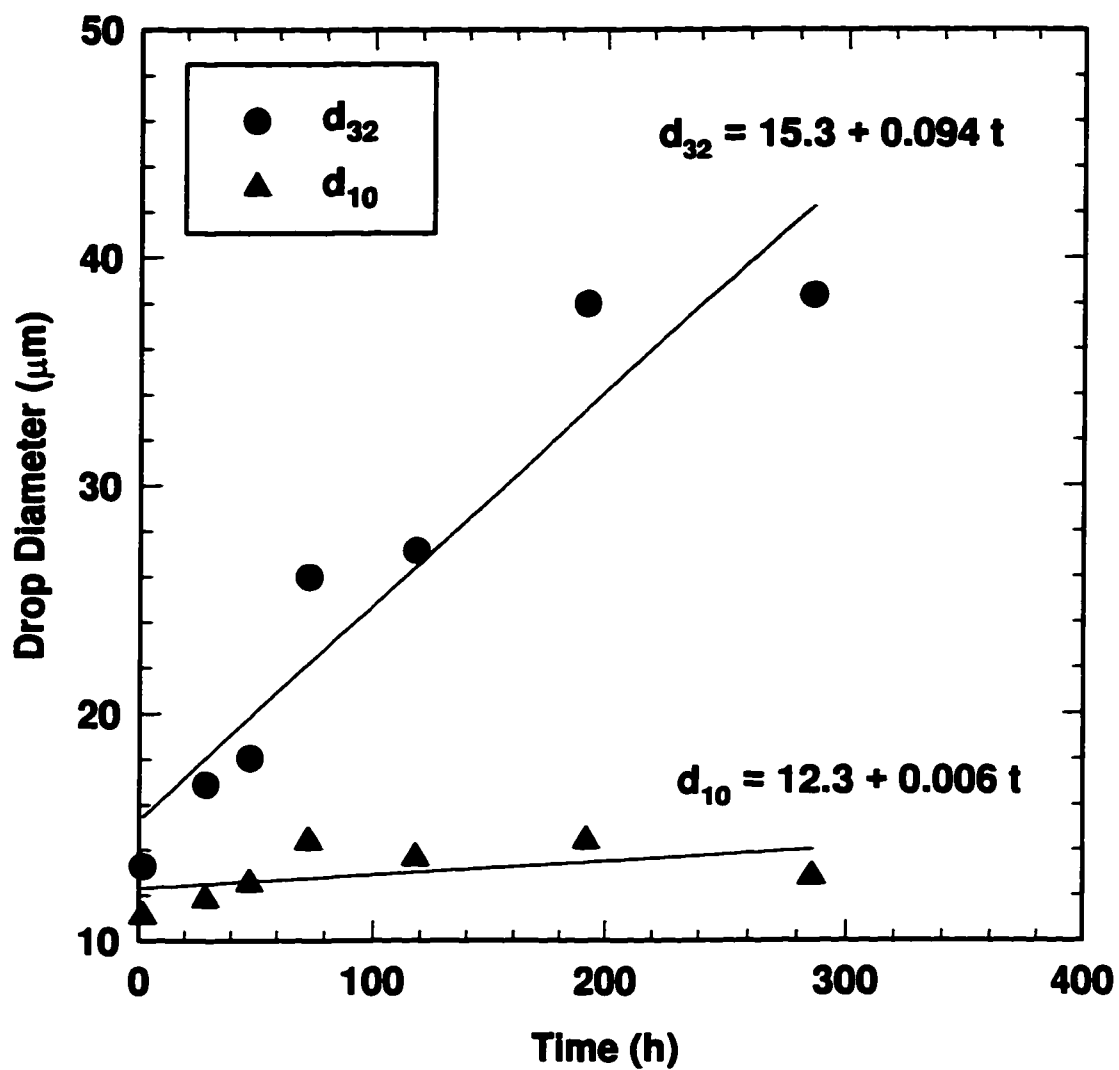


Figure C.15: Change in drop diameter over time of an asphaltene stabilized water-in-toluene/hexane emulsion. ($\phi_H/\phi_T = 5$, $\phi_W = 0.25$, $C_A^0 = 1.00 \text{ kg/m}^3$)

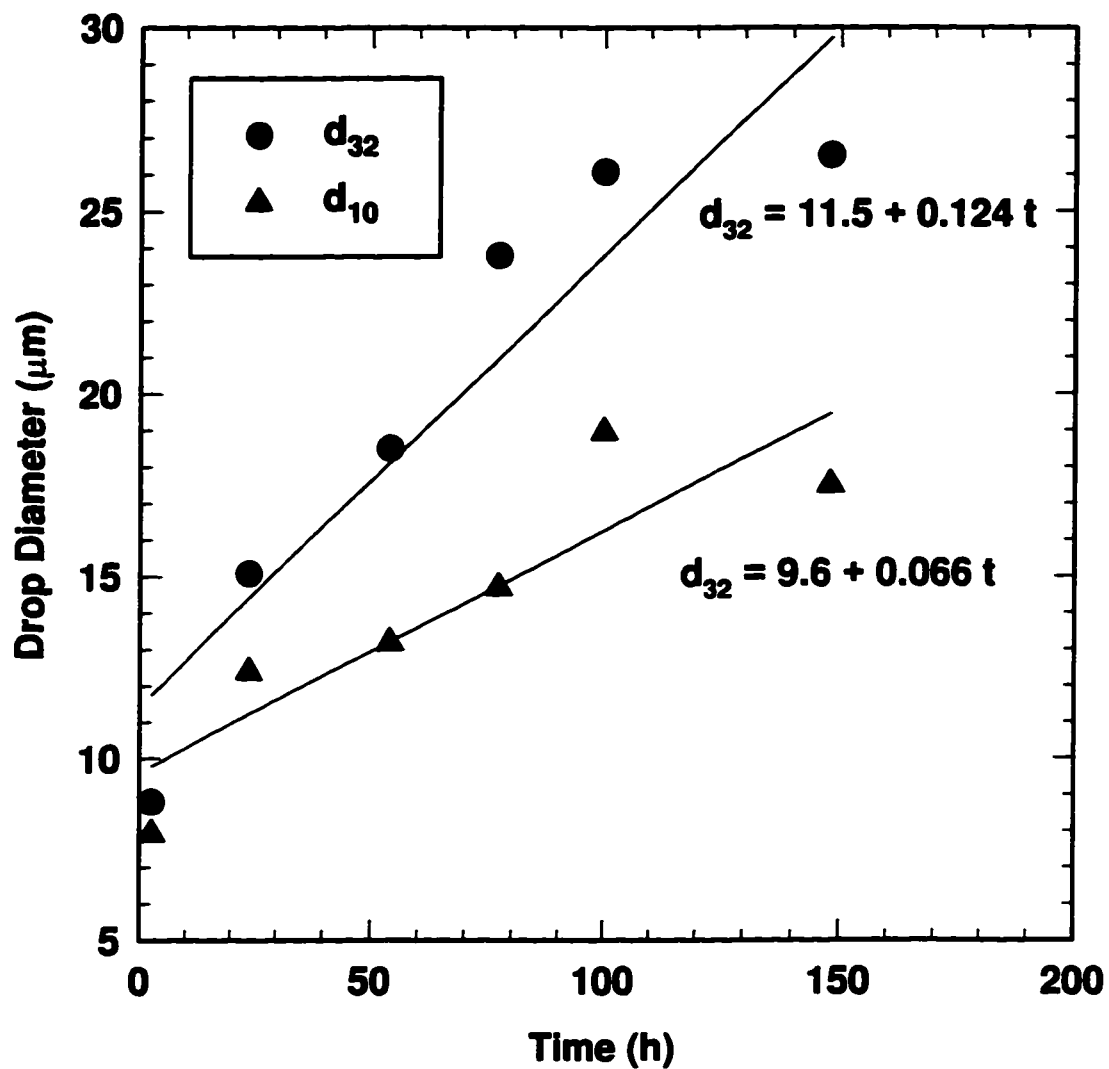


Figure C.16: Change in drop diameter over time of an asphaltene stabilized water-in-toluene/hexane emulsion. ($\phi_H/\phi_T = 5$, $\phi_W = 0.25$, $C_A^0 = 2.00 \text{ kg/m}^3$)

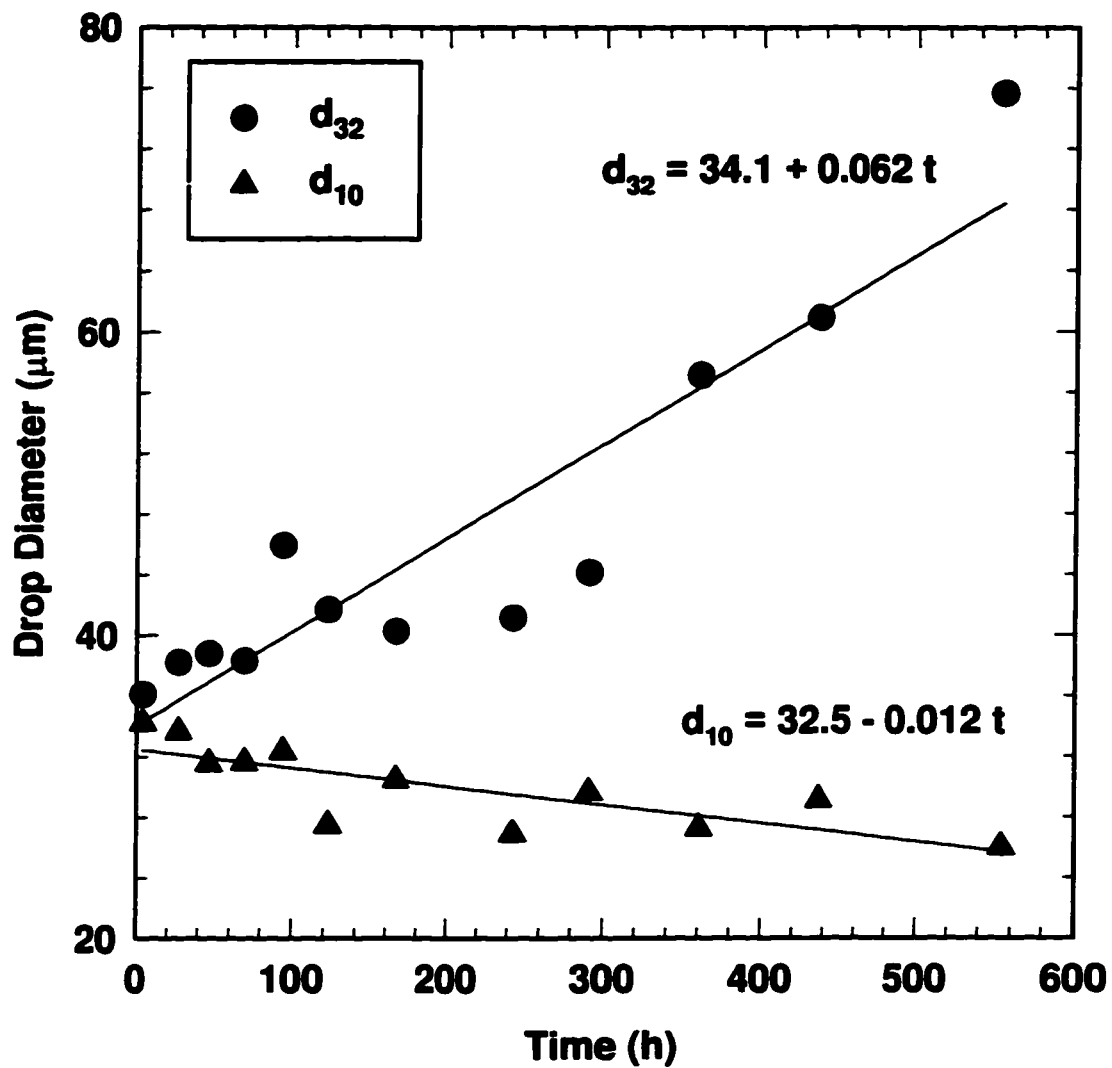


Figure C.17: Change in drop diameter over time of an asphaltene stabilized water-in-toluene/hexane emulsion. ($\phi_H/\phi_T = 5$, $\phi_W = 0.40$, $C_A^0 = 0.67 \text{ kg/m}^3$)

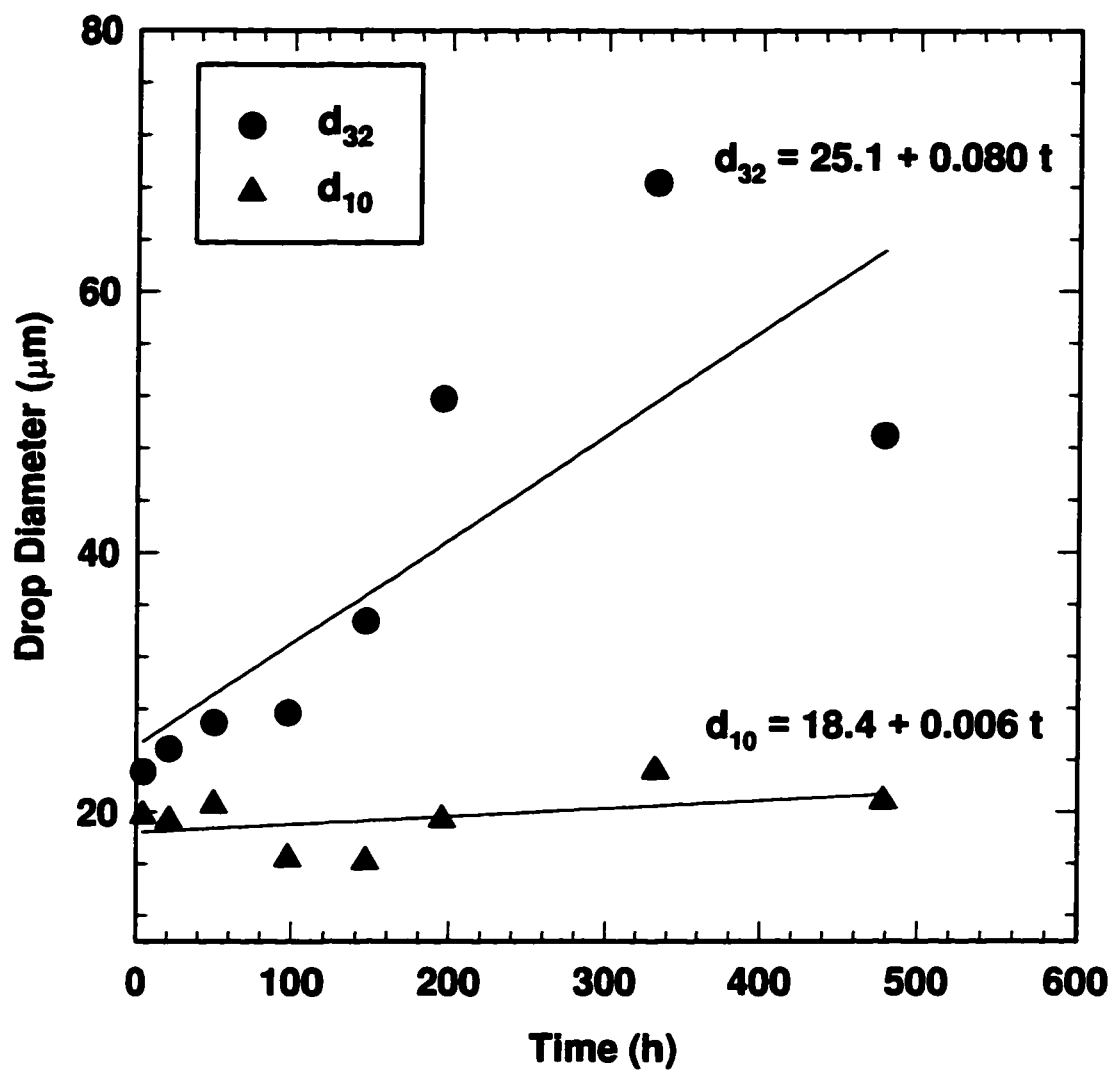


Figure C.18: Change in drop diameter over time of an asphaltene stabilized water-in-toluene/hexane emulsion. ($\phi_H/\phi_T = 5$, $\phi_W = 0.40$, $C_A^0 = 1.00 \text{ kg/m}^3$)

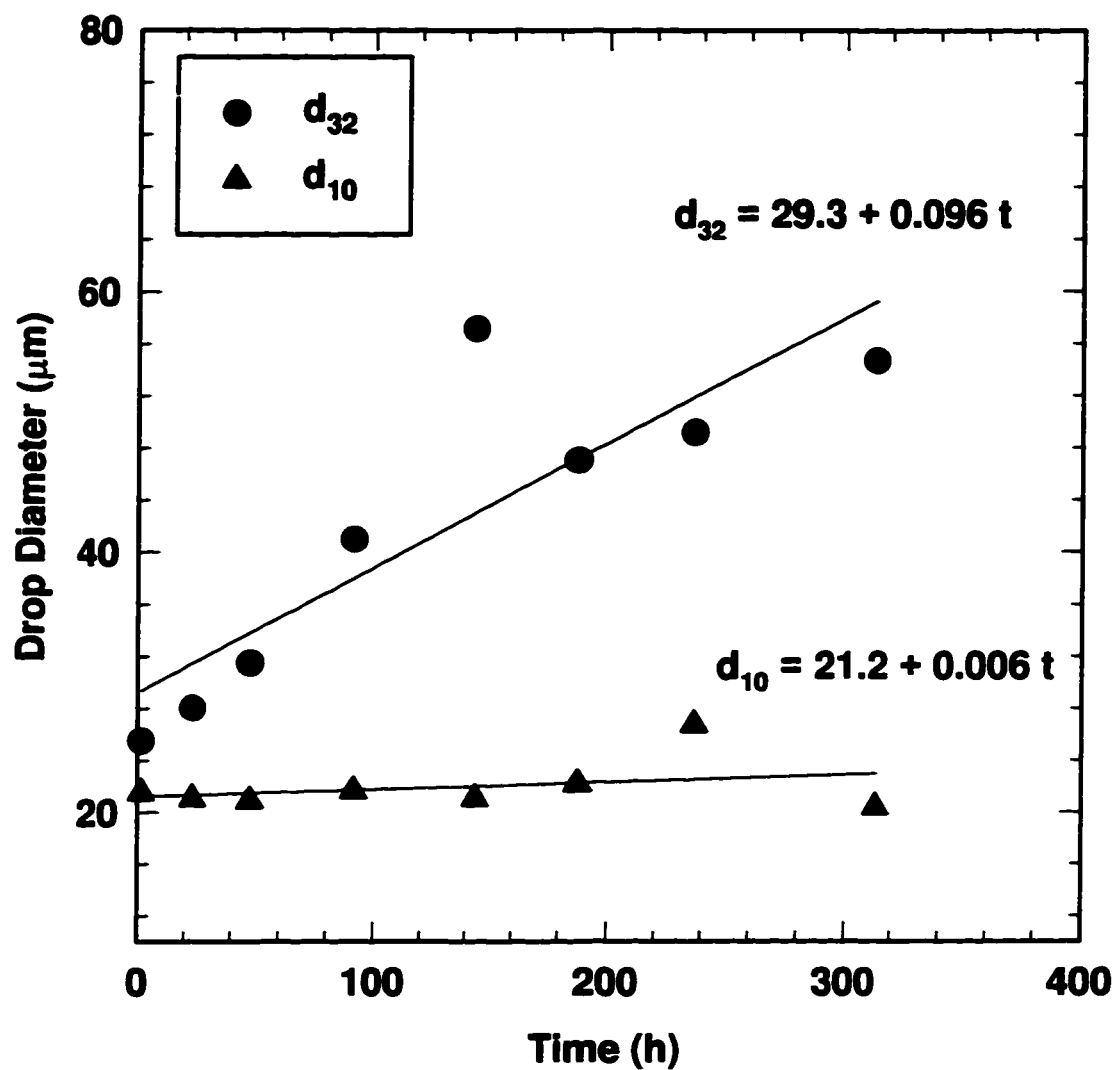


Figure C.19: Change in drop diameter over time of an asphaltene stabilized water-in-toluene/hexane emulsion - deionized, ultrafiltered water.

$$(\phi_H/\phi_T = 5, \phi_W = 0.40, C_A^o = 1.00 \text{ kg/m}^3)$$

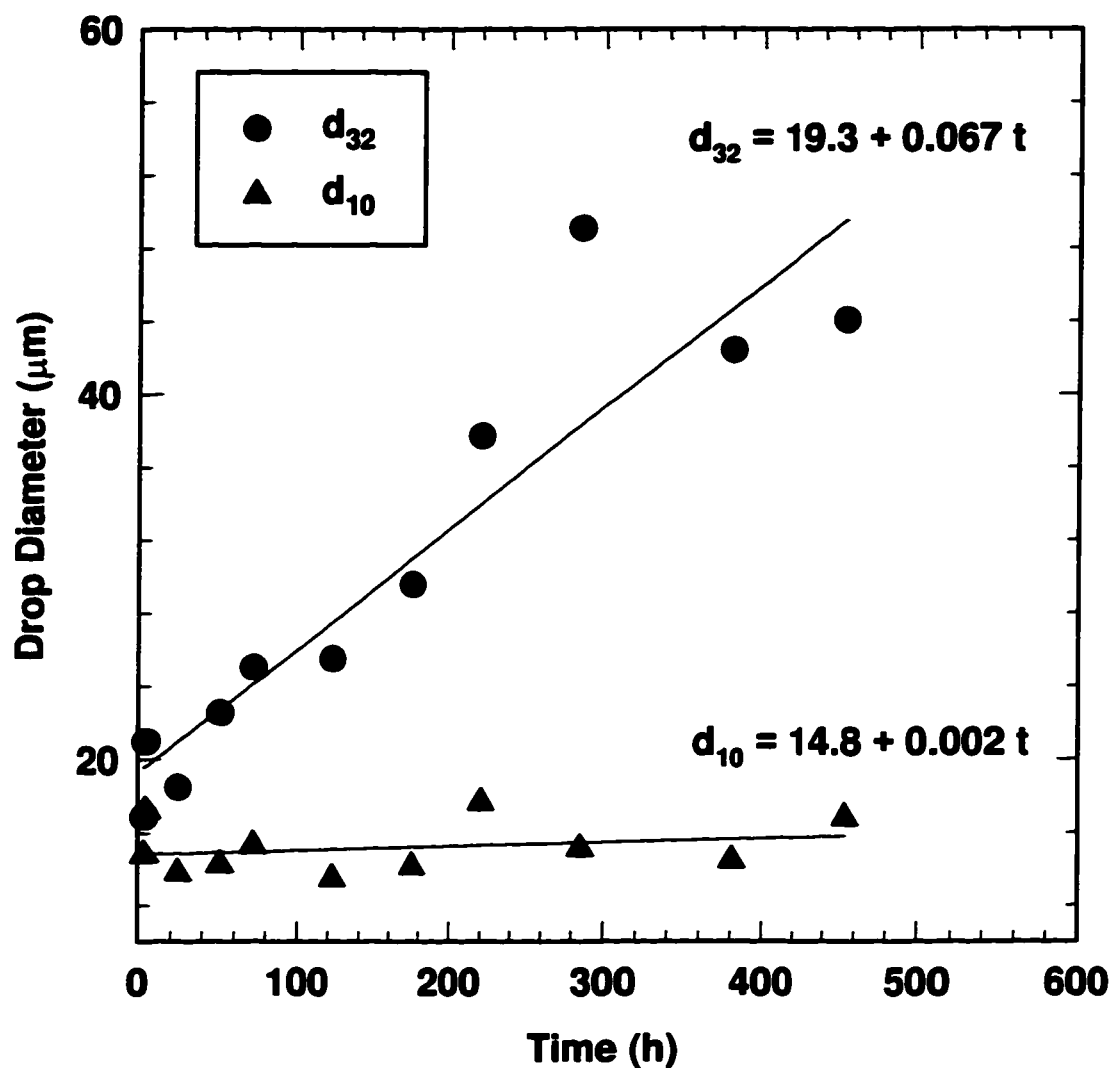


Figure C.20: Change in drop diameter over time of an asphaltene stabilized water-in-toluene/hexane emulsion. ($\phi_H/\phi_T = 5$, $\phi_W = 0.40$, $C_A^0 = 1.33 \text{ kg/m}^3$)

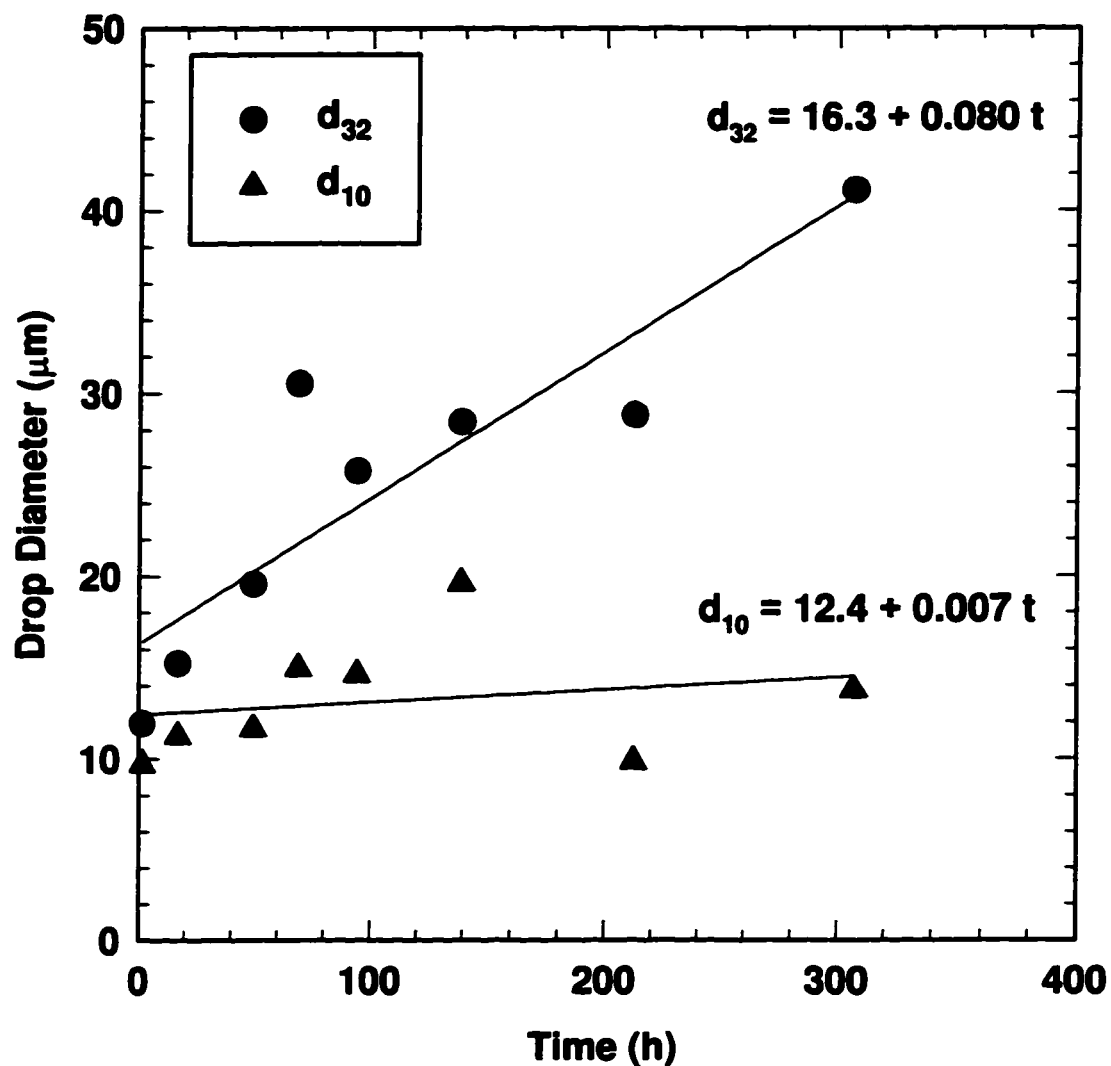


Figure C.21: Change in drop diameter over time of an asphaltene stabilized water-in-toluene/hexane emulsion. ($\phi_H/\phi_T = 3$, $\phi_W = 0.25$, $C_A^0 = 1.00 \text{ kg/m}^3$)

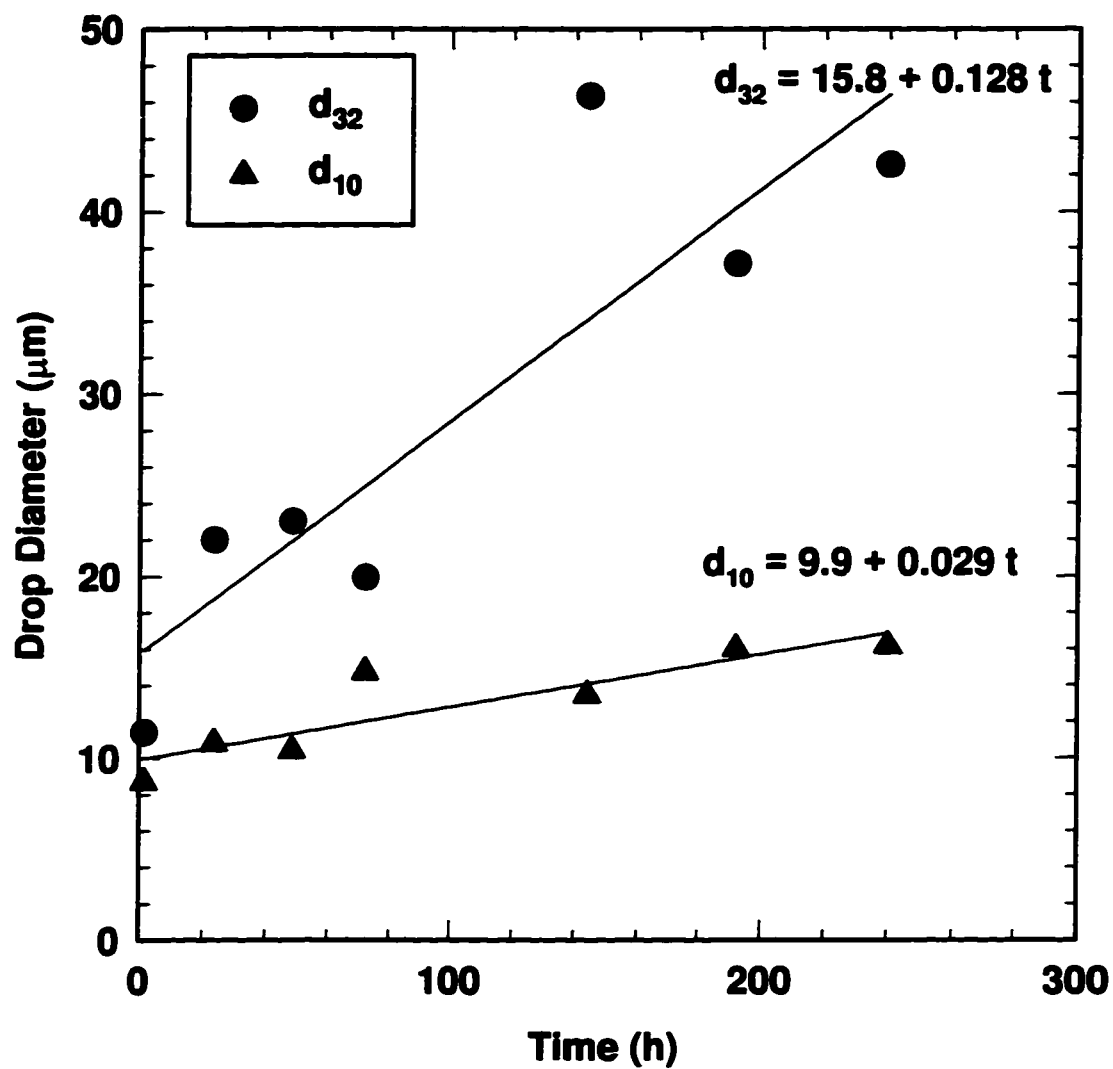


Figure C.22: Change in drop diameter over time of an asphaltene stabilized water-in-toluene/hexane emulsion. ($\phi_H/\phi_T = 1.5$, $\phi_W = 0.25$, $C_A^0 = 1.00 \text{ kg/m}^3$)

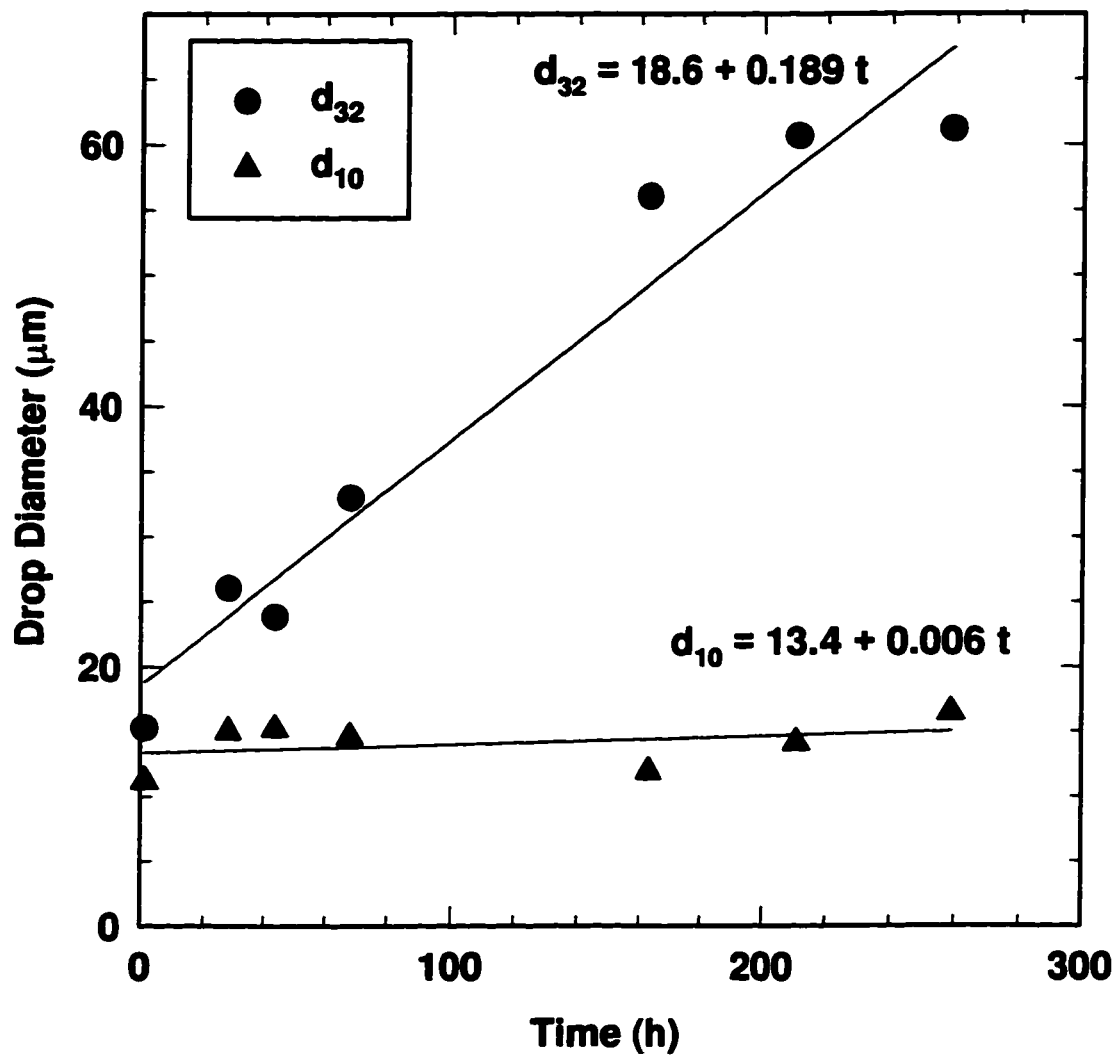


Figure C.23: Change in drop diameter over time of an asphaltene stabilized water-in-toluene/hexane emulsion. ($\phi_H/\phi_T = 1$, $\phi_W = 0.25$, $C_A^0 = 1.00 \text{ kg/m}^3$)

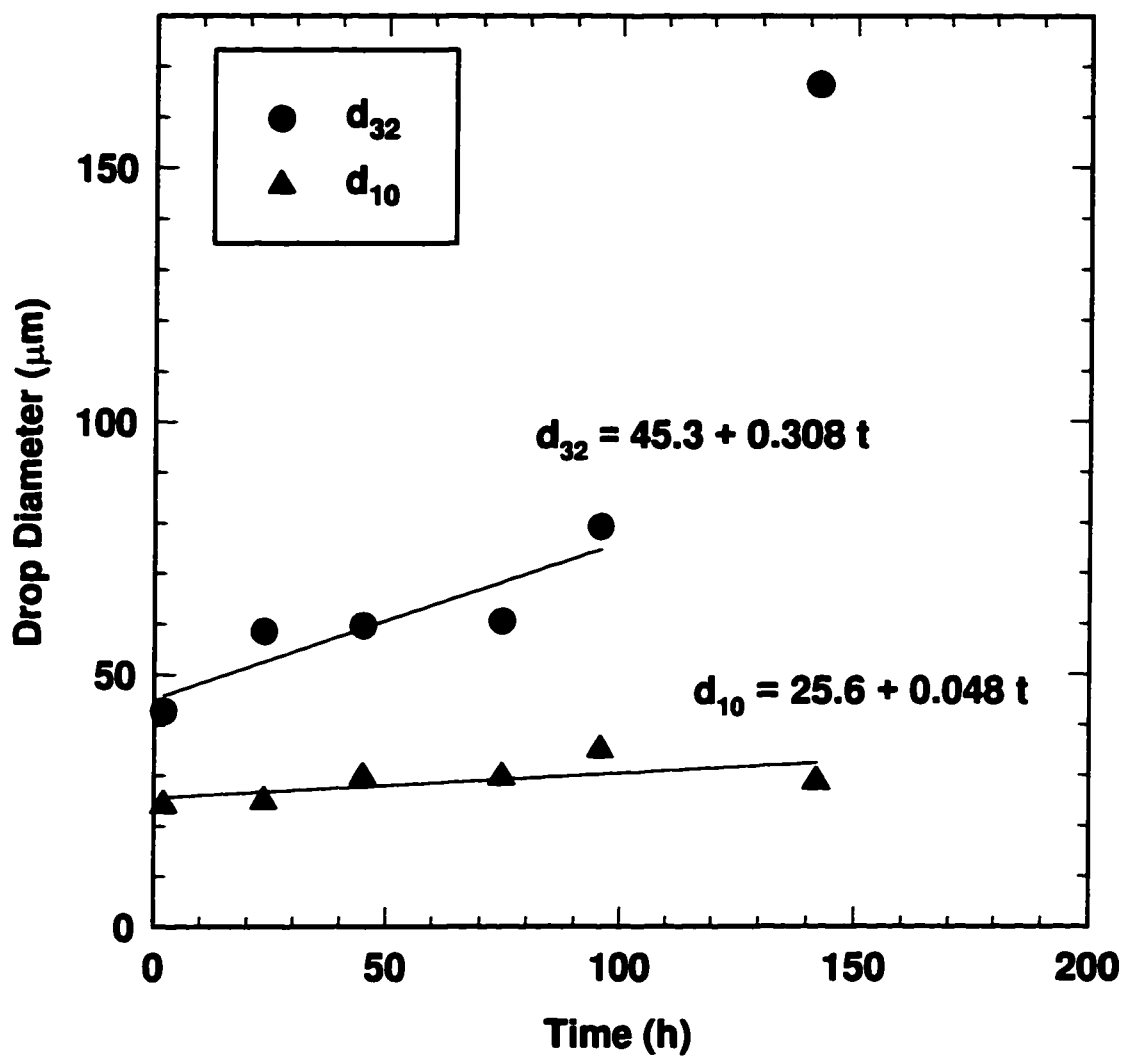


Figure C.24: Change in drop diameter over time of an asphaltene stabilized water-in-toluene/hexane emulsion. ($\phi_H/\phi_T = 0$, $\phi_W = 0.40$, $C_A^0 = 1.33 \text{ kg/m}^3$)

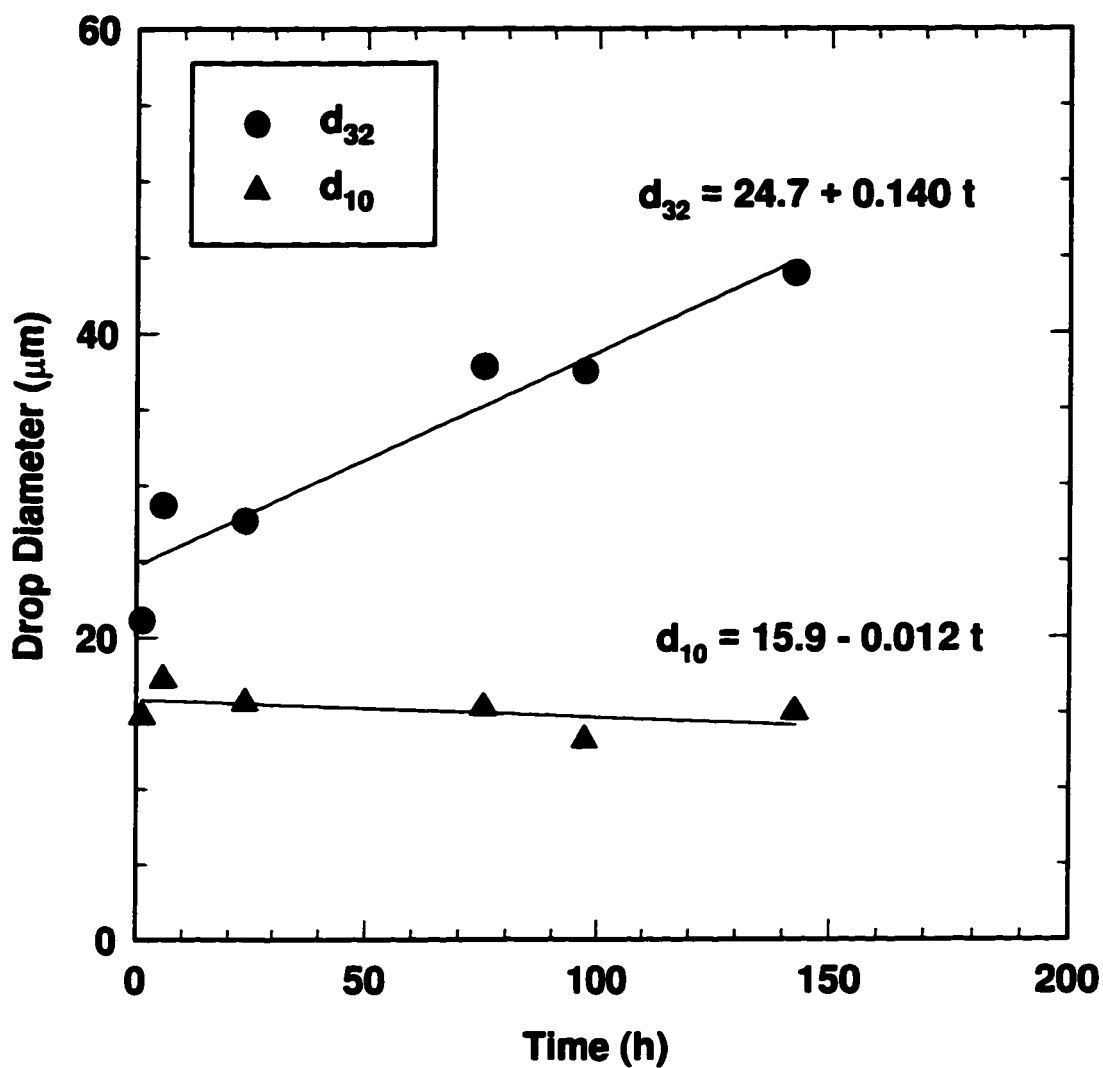


Figure C.25: Change in drop diameter over time of an asphaltene stabilized water-in-toluene/hexane emulsion. ($\phi_H/\phi_T = 0$, $\phi_W = 0.40$, $C_A^0 = 2.00 \text{ kg/m}^3$)

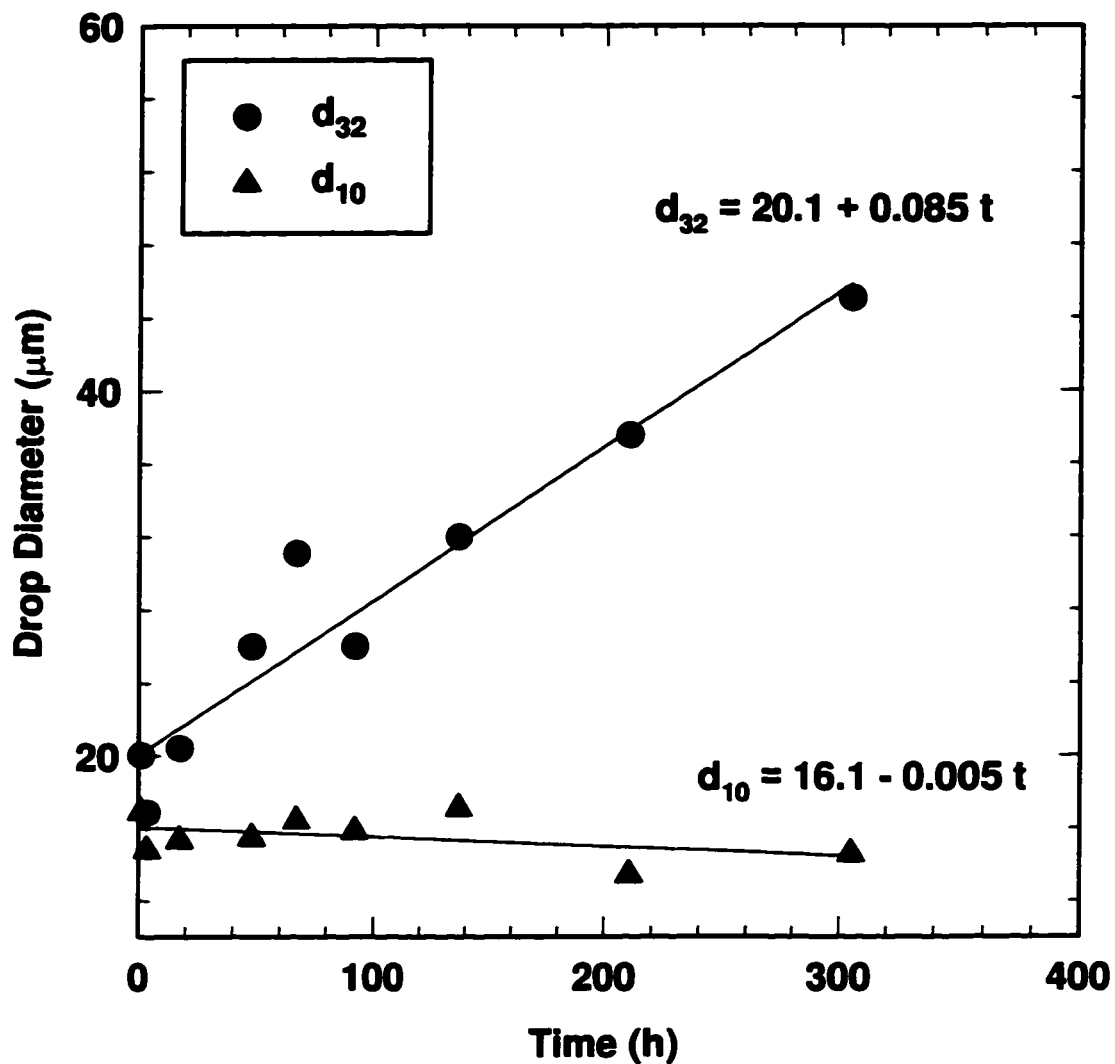


Figure C.26: Change in drop diameter over time of an asphaltene stabilized water-in-toluene/hexane emulsion - pretreated in 3:1 hex:tol - precipitate removed.

$$(\phi_H/\phi_T = 5, \phi_W = 0.25, C_A^0 = 1.00 \text{ kg/m}^3)$$

```

function [fdn,t,verr]=ostcnt(fd,dint,ko,nstep,dt)
%function [fdn,t,verr]=ostcnt(fd,dint,ko,nstep,dt)
% Ostwald ripening for infinitely dilute solution
% control loop

% ac    = critical radius
% acn   = critical radius at time t+dt
% af    = radius of largest drop
% afn   = radius of largest drop at time t+dt
% dint  = width of drop radius frequency interval
% dt    = time step
% fd    = initial drop radius frequency distribution
% fdn   = drop radius frequency distribution at time t+dt
% ko    = Ostwald ripening constant
% nstep = number of time steps in control loop
% t     = nstep*dt = time at end of loop
% verr  = fractional material balance error at end of loop

m=length(fd);
t=0;
verrcm=0;
fdn=fd;

% find largest drop size
for i=1:m-1
    if fd(i)>0 & fd(i+1)==0, af=i*dint; end
end

% find cumulative volume balance error
for i=1:nstep
    [fdn,verr,af]=fnext(fdn,dint,ko,dt,af);
    verrcm=verrcm+verr;
    t=t+dt;
    fdn=fdn/sum(fdn);
end

% find fractional cumulative volume balance error
suml=0;
for i=1:m
    v(i)=((i-.5)*dint)^3;
    suml=suml+v(i)*fd(i);
end
verr=verrcm/suml;

function acint=acrit(a1,ac,dint,ko,dt)
%function acint=acrit(a1,ac,dint,ko,dt)
% Ostwald ripening for infinitely dilute solution
% subroutine to find radius which changes in size to radius a1 in time dt
% uses bisection method on integrated solution of ripening equations

% ac    = critical radius
% acint = radius at time t
% a1    = radius at time t+dt, also interval boundary radius

```

```

% dint = width of drop radius frequency interval
% dt   = time step
% ko   = Ostwald ripening constant

tol=.0001;
test=tol+1;
a2=a1-dint/2;

% use bisection method on integrated solution of Ostwald ripening eqn's
% "ac" is held constant over time step

if ac>a1-dint/2
    acig1=a2;
    acig2=ac;
    while abs(test)>tol
        acig=(acig1+acig2)/2;
        tmp=(a2/ac-1)^2-(acig/ac-1)^2+4/ac*(a2-acig)+2*log((ac-a2)/(ac-acig));
        test=ko*dt-ac^3/2*tmp;
        if test>0
            acig1=acig;
        else
            acig2=acig;
        end
    end
    acint=acig;
else
    acig1=ac;
    acig2=a2;
    while abs(test)>tol
        acig=(acig1+acig2)/2;
        tmp=(a2/ac-1)^2-(acig/ac-1)^2+4/ac*(a2-acig)+2*log((a2-ac)/(acig-ac));
        test=ko*dt-ac^3/2*tmp;
        if test<0
            acig1=acig;
        else
            acig2=acig;
        end
    end
    acint=acig;
end

function afn=afmov(af,ac,dint,ko,dt)
%function afn=afmov(af,ac,dint,ko,dt)
% Ostwald ripening for infinitely dilute solution
% subroutine to find size of the largest drop at time t+dt
% uses bisection method on integral solution of ripening equations

% ac   = critical radius
% af   = radius of largest drop
% afn  = radius of largest drop at time t+dt
% dint = width of drop radius frequency interval
% dt   = time step
% ko   = Ostwald ripening constant

```


end

% adjust frequency distribution: if acint(4) moves to radius "0" and acint(5)
 % moves to radius "0+dint", then the frequency of the drops now the interval
 % "0 to dint" is the integral of b.df from acint(4) to acint(5)
 % i.e. sum (b(i)*(ab(i+1)-ab(i))) over the appropriate intervals

```
for i=1:me
  ac1=aci(i);
  ac2=aci(i+1);
  ilow=fix(ac1/dint)+1;
  ihi=fix(ac2/dint)+2;
  if ihi>m, ihi=m; end
  dfd(i)=0;
  for j=ilow:ihi
    ab1=ab(j);
    ab2=ab(j+1);
    if ac2>=ab2,
      if ac1<=ab1 & (ac1-dint)<ab1,
        dfd(i)=dfd(i)+b(j)*(ab2-ab1);
      elseif ac1>ab1 & (ac1-dint)<ab1,
        dfd(i)=dfd(i)+b(j)*(ab2-ac1);
      else
        dfd(i)=dfd(i);
      end
    end
  else
    if ac1<=ab1 & (ac2+dint)>ab2,
      dfd(i)=dfd(i)+b(j)*(ac2-ab1);
    elseif ac1>ab1 & (ac2+dint)>ab2,
      dfd(i)=dfd(i)+b(j)*(ac2-ac1);
    else
      dfd(i)=dfd(i);
    end
  end
end
end
end
```

% special tracking of largest particle to prevent propagation of error
 % to larger dropsizes and hence the necessity for large fd vectors

```
ac1=aci(me+1);
ac2=aci(me+2);
ab1=ab(me);
ab2=ab(me+1);
if af<ac2,
  dfd(me+1)=b(me-1)*(ab1-ac1)+b(me)*(ab2-ab1);
  dfd(me+2)=0;
  afn=afmov(af,ac,dint,ko,dt);
else
  dfd(me+1)=b(me-1)*(ab1-ac1)+b(me)*(ab2-ab1)*(ac2-ab1)/(af-ab1);
  if af==ac2,
    dfd(me+2)=0;
    afn=ab2;
  else
    dfd(me+2)=b(me)*(ab2-ab1)*(af-ac2)/(af-ab1);
```

```

    afn=afmov(af,ac,dint,ko,dt);
end
end
if me+2<=m,
    for i=me+3:m+1
        dfd(i)=0;
    end
end

% material balance error for iteration
vsum1=0;
vsum2=0;
for i=1:m
    fdn(i)=dfd(i+1);
    vsum1=vsum1+fdn(i)*amid(i)^3;           % volume of drops at t
    vsum2=vsum2+fdn(i)*amid(i)^3;         % volume of drops at t+dt
end
verr=(vsum2-vsum1);                       % total volume error for iteration

```

function acint=acrit1(a1,ac,dint,ko,dt)

```

%function acint=acrit1(a1,ac,dint,ko,dt)
% Ostwald ripening for infinitely concentrated solution
% subroutine to find radius which changes in size to radius a1 in time dt
% uses bisection method on integrated solution of ripening equations

% ac    = critical radius
% acint = radius at time t
% a1    = radius at time t+dt, also interval boundary radius
% dint  = width of drop radius frequency interval
% dt    = time step
% ko    = Ostwald ripening constant

tol=.0001;
test=tol+1;
a2=a1-dint/2;

% use bisection method on integrated solution of Ostwald ripening eqn's
% "ac" is held constant over time step

if ac>a1-dint/2
    acig1=a2;
    acig2=ac;
    while abs(test)>tol
        acig=(acig1+acig2)/2;
        tmp=1/ac*(a2-acig)+log((ac-a2)/(ac-acig));
        test=ko*dt-ac^2*tmp;
        if test>0
            acig1=acig;
        else
            acig2=acig;
        end
    end
end
acint=acig;

```



```

else
  acig1=ac;
  acig2=a2;
  while abs(test)>tol
    acig=(acig1+acig2)/2;
    tmp=1/ac*(a2-acig)+log((a2-ac)/(acig-ac));
    test=ko*dt-ac^2*tmp;
    if test<0
      acig1=acig;
    else
      acig2=acig;
    end
  end
  acint=acig;
end

```

function afn=afmov1(af,ac,dint,ko,dt)

```

%function afn=afmov1(af,ac,dint,ko,dt)
% Ostwald ripening for infinitely concentrated solution
% subroutine to find size of the largest drop at time t+dt
% uses bisection method on integral solution of ripening equations

```

```

% ac    = critical radius
% af    = radius of largest drop
% afn   = radius of largest drop at time t+dt
% dint  = width of drop radius frequency interval
% dt    = time step
% ko    = Ostwald ripening constant

```

```

tol=.0001;
test=tol+1;

```

```

acig1=af;
acig2=af+5*dint;
while abs(test)>tol
  acig=(acig1+acig2)/2;
  tmp=1/ac*(acig-af)+log((acig-ac)/(af-ac));
  test=ko*dt-ac^2*tmp;
  if test>0
    acig1=acig;
  else
    acig2=acig;
  end
end
afn=acig;

```

function [fdn,verr,afn]=fnext1(fd,dint,ko,dt,af)

```

% function [fdn,verr,afn]=fnext1(fd,dint,ko,dt,af)
% Ostwald ripening for infinitely concentrated solution
% single iteration of Ostwald ripening calculation
% ac    = critical radius
% af    = radius of largest drop

```

```

% afn  = radius of largest drop at time t+dt
% dint = width of drop radius frequency interval
% dt   = time step
% fd   = initial drop radius frequency distribution
% fdn  = drop radius frequency distribution at time t+dt
% ko   = Ostwald ripening constant
% verr = fractional material balance error at end of loop

m=length(fd);
b=fd/dint; % b=vector of slope of interval drop frequency
ac2=0;
ac1=0;
for i=1:m
    amid(i)=(i-.5)*dint; % midpoint of interval
    ac2=ac2+fd(i)*amid(i)^2;
    ac1=ac1+amid(i)*fd(i);
    if i<m,
        if fd(i)>0 & fd(i+1)==0, me=i; end % me = end of distribution
    end
end
ac=ac2/ac1;

% in time, dt, a drop of radius, acint(i), changes in size to
% the radius of the lower boundary of the interval i
aci(1)=0;
for i=1:me+2
    if (ac+.0001*dint)>=((i+2)*dint) & (ac-.0001*dint)<=((i+2)*dint), ac=ac+0.0001*dint; end
    a1=(i-.5)*dint;
    acint=acrit(a1,ac,dint,ko,dt);
    aci(i+1)=acint;
    ab(i)=(i-1)*dint; % lower boundary of interval i
end

% adjust frequency distribution: if acint(4) moves to radius "0" and acint(5)
% moves to radius "0+dint", then the frequency of the drops now the interval
% "0 to dint" is the integral of b.df from acint(4) to acint(5)
% i.e. sum ( b(i)*(ab(i+1)-ab(i)) ) over the appropriate intervals
for i=1:me
    ac1=aci(i);
    ac2=aci(i+1);
    ilow=fix(ac1/dint)+1;
    ihi=fix(ac2/dint)+2;
    if ihi>m, ihi=m; end
    dfd(i)=0;
    for j=ilow:ihi
        ab1=ab(j);
        ab2=ab(j+1);
        if ac2>=ab2,
            if ac1<=ab1 & (ac1-dint)<ab1,
                dfd(i)=dfd(i)+b(j)*(ab2-ab1);
            elseif ac1>ab1 & (ac1-dint)<ab1,
                dfd(i)=dfd(i)+b(j)*(ab2-ac1);
            else
                dfd(i)=dfd(i);
            end
        end
    end
end

```

```

else
  if ac1<=ab1 & (ac2+dint)>ab2,
    dfd(i)=dfd(i)+b(j)*(ac2-ab1);
  elseif ac1>ab1 & (ac2+dint)>ab2,
    dfd(i)=dfd(i)+b(j)*(ac2-ac1);
  else
    dfd(i)=dfd(i);
  end
end
end
end

% special tracking of largest particle to prevent propagation of error
% to larger dropsizes and hence the necessity for large fd vectors
ac1=aci(me+1);
ac2=aci(me+2);
ab1=ab(me);
ab2=ab(me+1);
if af<ac2,
  dfd(me+1)=b(me-1)*(ab1-ac1)+b(me)*(ab2-ab1);
  dfd(me+2)=0;
  afn=afmov(af,ac,dint,ko,dt);
else
  dfd(me+1)=b(me-1)*(ab1-ac1)+b(me)*(ab2-ab1)*(ac2-ab1)/(af-ab1);
  if af==ac2,
    dfd(me+2)=0;
    afn=ab2;
  else
    dfd(me+2)=b(me)*(ab2-ab1)*(af-ac2)/(af-ab1);
    afn=afmov(af,ac,dint,ko,dt);
  end
end
end
if me+2<=m,
  for i=me+3:m+1
    dfd(i)=0;
  end
end

% material balance error for iteration
vsum1=0;
vsum2=0;
for i=1:m
  fdn(i)=dfd(i+1);
  vsum1=vsum1+fd(i)*amid(i)^3;           % volume of drops at t
  vsum2=vsum2+fdn(i)*amid(i)^3;         % volume of drops at t+dt
end
verr=(vsum2-vsum1);

```

function ac=acalc(fd,dint,phi)

```

% function ac=acalc(fd,dint,phi)
% Ostwald ripening for finite dispersed phase volume fractions
% calculate critical radius for a given drop size distribution

```

```

m=length(fd);

asum=0;
vsum=0;
for i=1:m
    a(i)=(i-.5)*dint;
    asum=asum+fd(i)*a(i);
    vsum=vsum+fd(i)*a(i)^3;
end

d=dcalc(fd,dint,phi,m,a,asum,vsum);

sum1=0;
sum2=0;
for i=1:m
    s1=fd(i)*(a(i)+d)^2;
    sum1=sum1+s1;
    sum2=sum2+s1*(1/a(i)+(1/asum-1/a(i))*d/(a(i)+d));
end

ac=sum1/sum2;

function acint=acrit2(a1,ac,dint,ko,dt,d)
% function acint=acrit2(a1,ac,dint,ko,dt,d)
% Ostwald ripening for finite dispersed phase volume fraction
% find radius which changes in size to radius a1 in time dt
% a1 = radius at time 0
% ac = critical radius
% acint = radius at time t
% d = half mean separation distance between drops
% dt = time step
% ko = Ostwald ripening constant

tol=.0001;
test=tol+1;
a2=a1-dint/2;

% use bisection method on integrated solution of Ostwald ripening eqn's
% "ac" and "d" are held constant over time step

if ac>a1-dint/2
    acig1=a2;
    acig2=ac;
    while abs(test)>tol
        acig=(acig1+acig2)/2;
        tmp=ac*(a2-acig)-ac*d^2/(ac+d)*log((a2+d)/(acig+d));
        tmp=tmp+ac^3/(ac+d)*log((ac-a2)/(ac-acig));
        test=ko*dt-d*tmp;
        if test>0
            acig1=acig;
        else
            acig2=acig;
        end
    end
end

```

```

end
acint=acig;
else
acig1=ac;
acig2=a2;
while abs(test)>tol
acig=(acig1+acig2)/2;
tmp=ac*(a2-acig)-ac*d^2/(ac+d)*log((a2+d)/(acig+d));
tmp=tmp+ac^3/(ac+d)*log((a2-ac)/(acig-ac));
test=ko*dt-d*tmp;
if test<0
acig1=acig;
else
acig2=acig;
end
end
acint=acig;
end

```

function afn=afmov2(af,ac,dint,ko,dt,d)

```

% function afn=afmov2(af,ac,dint,ko,dt,d)
% Ostwald ripening at finite dispersed phase volume fractions
% subroutine to find size of the largest drop at time t+dt
% uses bisection method on integral solution of ripening equations

% ac    = critical radius
% af    = radius of largest drop
% afn   = radius of largest drop at time t+dt
% d     = half mean separation distance between drops
% dint  = width of drop radius frequency interval
% dt    = time step
% ko    = Ostwald ripening constant

```

```

tol=.0001;
test=tol+1;

acig1=af;
acig2=af+5*dint;
while abs(test)>tol
acig=(acig1+acig2)/2;
tmp=ac*(acig-af)-ac*d^2/(ac+d)*log((acig+d)/(af+d));
tmp=tmp+ac^3/(ac+d)*log((acig-ac)/(af-ac));
test=ko*dt-d*tmp;
if test>0
acig1=acig;
else
acig2=acig;
end
end
afn=acig;

```

```
function d=dcalc(fd,dint,phi,n,a,am,v)
% function d=dcalc(fd,dint,phi,n,a,am,v)
% Ostwald ripening for finite dispersed phase volume fractions
% calculate average half separation distance between drops
% valid for  $1 > \phi > .0001$ 
```

```
% a = vector of drop radius interval midpoints
% am = mean radius of drops in interval
% dint = width of drop size interval
% fd = initial drop size frequency vector
% n = number of intervals
% phi = volume fraction of dispersed phase
% v = total volume of drops
```

```
dg1=0;
dg2=100*am;
```

```
test=1;
tol=.000001;
```

```
while abs(test)>tol,
    dg=(dg1+dg2)/2;
    sum1=0;
    for i=1:n
        sum1=sum1+(3*a(i)^2+3*a(i)*dg+dg^2)*dg*fd(i);
    end
    test=phi/(1-phi)-v/sum1;
    if test<0,
        dg1=dg;
    else
        dg2=dg;
    end
end
```

```
d=dg;
```

```
function d=dcalc1(fd,dint,phi)
% function d=dcalc1(fd,dint,phi)
% Ostwald ripening for finite dispersed phase volume fraction
% calculate half separation distance for a given drop size distribution
% valid for  $1 > \phi > .0001$ 
```

```
n=length(fd);
v=0;
am=0;
for i=1:n
    a(i)=dint*(i-.5);
    v=v+fd(i)*a(i)^3;
    am=am+fd(i)*a(i);
end
```

```
dg1=0;
dg2=100*am;
```

```

test=1;
tol=.000001;

while abs(test)>tol,
    dg=(dg1+dg2)/2;
    sum1=0;
    for i=1:n
        sum1=sum1+(3*a(i)^2+3*a(i)*dg+dg^2)*dg*fd(i);
    end
    test=phi/(1-phi)-v/sum1;
    if test<0,
        dg1=dg;
    else
        dg2=dg;
    end
end

d=dg;

```

function [fdn,verr,afn]=fnext2(fd,dint,ko,dt,af,phi)

```

% function [fdn,verr,afn]=fnext2(fd,dint,ko,dt,af,phi)
% single iteration of Ostwald ripening with volume fraction effect
% fd = initial drop size frequency vector
% fdn = drop size frequency vector at time t+dt
% dint = width of drop size interval
% ko = Ostwald ripening constant
% dt = time step
% af = initial radius of largest particle
% afn = radius of largest particle at time t+dt
% phi = volume fraction of drop phase

m=length(fd);
b=fd/dint; % b = vector of slope of interval drop frequency

% calculate critical radius
ac2=0;
ac1=0;
for i=1:m
    amid(i)=(i-.5)*dint; % midpoint of interval
    v(i)=fd(i)*amid(i)^3; % mean volume of drops in interval
    ac1=ac1+amid(i)*fd(i); % mean radius of drops in interval
    if i<m,
        if fd(i)>0 & fd(i+1)==0, me=i; end % me = end of distribution
    end
end
vsum=sum(v); % total volume of drops
d=dcalc(fd,dint,phi,m,amid,ac1,vsum); % find mean droplet separation

sum1=0;
sum2=0;
for i=1:m

```

```

s1=fd(i)*(amid(i)+d)^2;
sum1=sum1+s1;
sum2=sum2+s1*(1/amid(i)+(1/ac1-1/amid(i))*d/(amid(i)+d));
end
ac=sum1/sum2; % critical radius

% in time, dt, a drop of radius, acint(i), changes in size to
% the radius of the lower boundary of the interval i
aci(1)=0;
for i=1:me+2
if (ac+.0001*dint)>=((i+2)*dint) & (ac-.0001*dint)<=((i+2)*dint), ac=ac+0.0001*dint; end
a1=amid(i);
acint=acrit(a1,ac,dint,ko,dt,d);
aci(i+1)=acint;
ab(i)=(i-1)*dint; % lower boundary of interval i
end

% adjust frequency distribution: if acint(4) moves to radius "0" and acint(5)
% moves to radius "0+dint", then the frequency of the drops now the interval
% "0 to dint" is the integral of b.df from acint(4) to acint(5)
% i.e. sum ( b(i)*(ab(i+1)-ab(i)) ) over the appropriate intervals
for i=1:me
ac1=aci(i);
ac2=aci(i+1);
ilow=fix(ac1/dint)+1;
ihi=fix(ac2/dint)+2;
if ihi>m, ihi=m; end
dfd(i)=0;
for j=ilow:ihi
ab1=ab(j);
ab2=ab(j+1);
if ac2>=ab2,
if ac1<=ab1 & (ac1-dint)<ab1,
dfd(i)=dfd(i)+b(j)*(ab2-ab1);
elseif ac1>ab1 & (ac1-dint)<ab1,
dfd(i)=dfd(i)+b(j)*(ab2-ac1);
else
dfd(i)=dfd(i);
end
else
if ac1<=ab1 & (ac2+dint)>ab2,
dfd(i)=dfd(i)+b(j)*(ac2-ab1);
elseif ac1>ab1 & (ac2+dint)>ab2,
dfd(i)=dfd(i)+b(j)*(ac2-ac1);
else
dfd(i)=dfd(i);
end
end
end
end
end

% special tracking of largest particle to prevent propagation of error

```



```

% to larger dropsizes and hence the necessity for large fd vectors
ac1=aci(me+1);
ac2=aci(me+2);
ab1=ab(me);
ab2=ab(me+1);
if af<ac2,
    dfd(me+1)=b(me-1)*(ab1-ac1)+b(me)*(ab2-ab1);
    dfd(me+2)=0;
    afn=afmov(af,ac,dint,ko,dt,d);
else
    dfd(me+1)=b(me-1)*(ab1-ac1)+b(me)*(ab2-ab1)*(ac2-ab1)/(af-ab1);
    if af==ac2,
        dfd(me+2)=0;
        afn=ab2;
    else
        dfd(me+2)=b(me)*(ab2-ab1)*(af-ac2)/(af-ab1);
        afn=afmov(af,ac,dint,ko,dt,d);
    end
end

if me+2<=m,
    for i=me+3:m+1
        dfd(i)=0;
    end
end

% material balance error for iteration
vsum2=0;
for i=1:m
    fdn(i)=dfd(i+1);
    vsum2=vsum2+fdn(i)*amid(i)^3; % volume of drops at t+dt
end

verr=(vsum2-vsum); % total volume error for iteration

```